Auburn University

IR-97-04

SITE CHARACTERIZATION OF THE SPRING VILLA GEOTECHNICAL TEST SITE AND A COMPARISON OF STRENGTH AND STIFFNESS PARAMETERS FOR A PIEDMONT RESIDUAL SOIL

Prepared by

James L. Vinson, Graduate Research Assistant
Dan A. Brown, Associate Professor of Civil Engineering

Highway Research Center
Harbert Engineering Center
Auburn University, Alabama 36849-5337

November, 1997

SITE CHARACTERIZATION
OF THE
SPRING VILLA GEOTECHNICAL TEST SITE
AND
A COMPARISON OF STRENGTH AND
STIFFNESS PARAMETERS FOR A
PIEDMONT RESIDUAL SOIL

Prepared by

James L. Vinson, Graduate Research Assistant
Dan A. Brown, Associate Professor of Civil Engineering

November, 1997

ACKNOWLEDGEMENTS

The research reported in this document was conducted at Auburn University through the support of the Auburn University Highway Research Center. The property comprising the Spring Villa Geotechnical Test Site is composed of a portion of the site of the Pavement Test Facility and this property has been purchased with funding from Auburn University, the Auburn University Highway Research Center, and the National Center for Asphalt Technology at Auburn University. The site characterization and testing described in this report has been made possible by the financial and other contributions of the Morris-Shea Bridge Company, the Alabama Department of Transportation, the Federal Highway Administration, and the Auburn University Highway Research Center, and these contributions are gratefully acknowledged. Portions of the work described in this report have been conducted by or assisted by the following: Dr. Paul Mayne, Dr. Glenn Rix, Ms. Stephanie Mills, Ms. Gina Gates, and Mr. Yasser Hegazy of the Georgia Institute of Technology, Mr. Pedro Ruesta of the University of Florida, Williams Earth Sciences of Clearwater, Florida, and Christian Testing Laboratories of Montgomery, Alabama

The contents of this report reflect the views of the authors who are responsible for the facts and accuracy of the data presented. The contents do not necessarily reflect the official views or policies of the agencies listed.

SITE CHARACTERIZATION
OF THE
SPRING VILLA GEOTECHNICAL TEST SITE
AND
A COMPARISON OF STRENGTH AND
STIFFNESS PARAMETERS FOR A
PIEDMONT RESIDUAL SOIL

ABSTRACT:

A long term geotechnical research site has been established at a site consisting of Piedmont residual soil. This site represents (currently - 1997) a small portion roughly 10,000 square meters in area (about 1/4 acre) of a 320 acre site (1.3 sq. km) which is to be used as a pavement testing facility. The report which follows summarizes the geotechnical site characterization data which has been assembled to date, along with a comparison of strength and stiffness parameters derived from these data. The report is intended to serve as both a reference document on the soil characteristics for other geotechnical research at the site, and as a research report which compares different types of *in-situ* and laboratory measurements of the physical properties of the soils at this site.

The Piedmont soils are residual soils derived from in-place weathering of igneous and metamorphic rocks and tend to retain much of the parent rock structure, mineral alignment, and mineral segregation. These soils are commonly characterized as sandy silts or silty sands, and are nonhomogeneous and anisotropic. The area selected for the geotechnical research site exhibits relatively consistent characteristics across this limited area although the individual soil properties are highly variable across distances of a few centimeters. The geotechnical data presented in this report demonstrate some of the unique aspects of Piedmont residual soils.

The testing program includes data from the following:

- conventional soil borings with standard penetration testing (SPT)
- cone penetration soundings (CPT), including piezocone (PCPT)
- pressuremeter testing, including conventional Menard tests (PMT) and push-in type

pressuremeter tests using the cone pressuremeter (CPMT)

- flat dilatometer tests (DMT)
- Iowa borehole shear tests (BST)
- *in-situ* measurements of shear wave velocity obtained using crosshole measurements from borings (CHT) and downhole measurements using the seismic cone (SCPT) and seismic dilatometer (SDMT)
- laboratory triaxial testing of undisturbed samples from consolidated isotropically undrained triaxial tests (CIUC) to obtain effective stress strength parameters and stress strain behavior and unconsolidated undrained (UU) triaxial tests to obtain total stress strength parameters as might be typically measured using undisturbed samples
- routine water content, unit weight, grain size, atterberg limit, and other classification testing.

The results of this testing program provide a basis for comparison of strength and stiffness measurements obtained using a variety of different tools available to geotechnical engineers. These data also provide a basis for comparison of the many published correlations of strength and stiffness parameters from routine simple tests with those of a more sophisticated and expensive testing program. And finally, the geotechnical testing program provides a basis for understanding soil behavior and for comparing analytical models with respect to ongoing and future research in foundation testing and foundation performance at the site.

TABLE OF CONTENTS

LIST OF TABLES

LIST OF FIGURES

CHAPTER 1

INTRODUCTION

The Piedmont province is a geologic formation which extends from central Alabama across Georgia, the Carolinas, Virginia, and tapers into Maryland and Pennsylvania. The Piedmont is made up of residual soils derived from the weathering of ancient Precambrian igneous and metamorphic rocks. These residual soils have unique physical and mechanical properties because they retain the parent rock's relict structure, mineral alignment, and mineral segregation. They are commonly characterized as sandy silts/silty sands, nonhomogeneous and anisotropic since the degree of weathering tends to generally decrease with increasing depths. Horizontal at rest earth pressures are often unrelated to the vertical overburden pressure. Planes of weakness and high void ratios are also typical. Since these residual soils have many peculiar traits, their engineering behavior is quite different and sometimes contradictory to that of more commonly encountered sedimentary soils which are prevalent in many areas of the United States. The theories and empirical correlations developed for sedimentary soils often do not model Piedmont residual soils very well.

The Piedmont presently encompasses many rapidly growing manufacturing and commercial areas as well as major cities such as Atlanta, Charlotte, Baltimore, and

Philadelphia; however, until recently, little interest in the improvement of foundation design in the Piedmont had been expressed since this area had long been characterized by slow economic growth. Since mathematical models, design parameters, and empirical correlations developed for sedimentary soils often do a poor job of modelling Piedmont residual soils, foundation design in these developing areas has tended to be conservative and uneconomical; when the factor of safety increases, the cost of the foundation increases.

Many geotechnical tools (especially in-situ devices) of various complexity have recently been introduced to aid in the characterization of the physical and mechanical properties of soils. Some of these tools include the piezocone, flat dilatometer, cone-mounted pressuremeter, Iowa borehole shear, and hybrid tests (such as the seismic flat dilatometer) which make small- and large-strain measurements. However, at present there has been little mention in the literature of the various tests' usage in the Piedmont. Since these more recent techniques show promise of improved characterization of various soil properties such as strength and stiffness, a need for comparative studies between the different tests is evident.

A test site near Opelika, Alabama was purchased by Auburn University, the Auburn University Highway Research Center, and the National Center for Asphalt Technology for the future site of a pavement test facility. Within the bounds of this property, a portion of this land has been set aside for geotechnical research; this geotechnical testing area has been designated as the Spring Villa Test Site.

Spring Villa rests within the Piedmont province (Figure 1.1) and is predominantly micaceous sandy silts. In order to limit the effect of variable soil conditions on shallow

and deep foundation testing, less than one acre has been tested extensively since it was delineated through initial cone penetration testing (CPT) to be fairly homogeneous on a macroscopic scale. Through this foundation research, the need has arisen for characterizing the strength and stiffness parameters of this small area of the Spring Villa Test Site. A wide variety of soil characterization tests have been conducted prior to foundation construction ranging from highly specialized techniques such as the seismic piezocone penetration test (SCPT) to the common standard penetration test (SPT). From these tests' results, the physical and mechanical characteristics of the soil within the upper 15 meters have been evaluated and documented to assist ongoing and future foundation research.

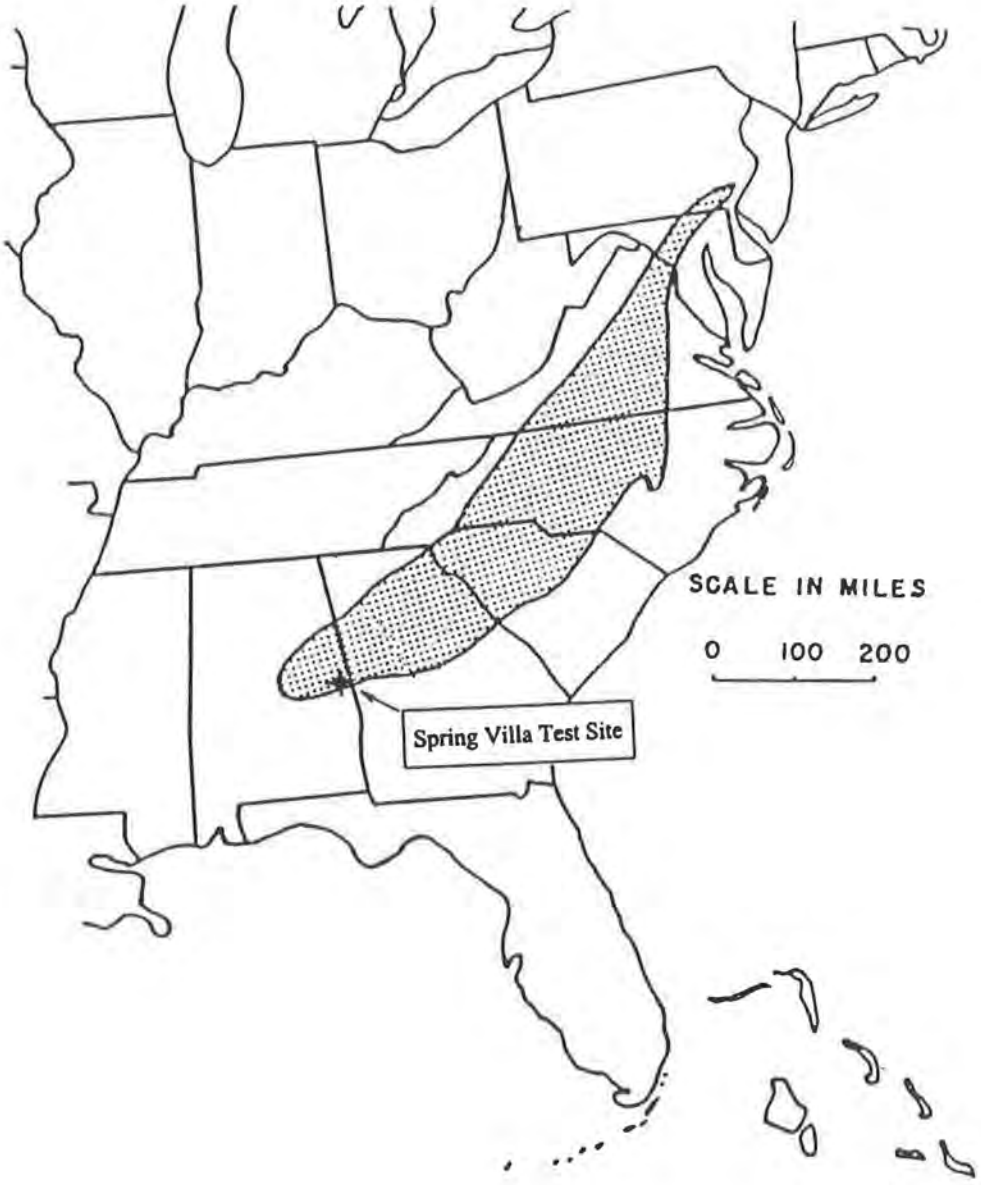

FIG. 1.1. - Location of Piedmont Province and Spring Villa Test Site.

CHAPTER 2

OBJECTIVES

This study was undertaken to achieve the following:

1. Document the physical geotechnical properties of the Spring Villa Test Site in order to assist in the analysis of ongoing and future research.
2. Investigate the unique characteristics of Piedmont residual soil and how these characteristics may affect the interpretation of various geotechnical tools' results.
3. Compare the strength and stiffness characteristics of the Piedmont residual soil at the Spring Villa Test Site by using a wide variety of laboratory and in-situ techniques.
4. Evaluate strength and stiffness correlations with simple geotechnical tools for this Piedmont residual soil.

CHAPTER 3

BACKGROUND OF PIEDMONT RESIDUAL SOILS

3.1 General

The Piedmont province is a geologic formation which extends from New Jersey southwest into Alabama and is bordered to the west by the Blue Ridge range of the Appalachian Mountains and to the east by the Atlantic Coastal Plain. (Figure 3.1.1) It is generally comprised of silty to sandy residual soils underlain by partially weathered rock. These residual soils are a result of chemical and physical in-place weathering of parent rock which consist of early Paleozoic age (or older) metamorphic and igneous rocks - primarily schists, gneisses, and granites (Sowers 1954).

Engineering behavior of piedmont residual soil is poorly understood. These soils retain the mineral segregation, mineral alignment, and stuctural defects of the parent rock because of the deep and irregular weathering which occurs without appreciable transportation (Sowers 1983). Residual soils are not subject to the mechanical sorting which occurs when a sediment is displaced by water or wind. These soils' anisotropic and nonhomogeneous nature create special difficulties in evaluating their engineering properties since more commonly used sediment behavior theories and correlations are not very applicable (Sowers 1963).

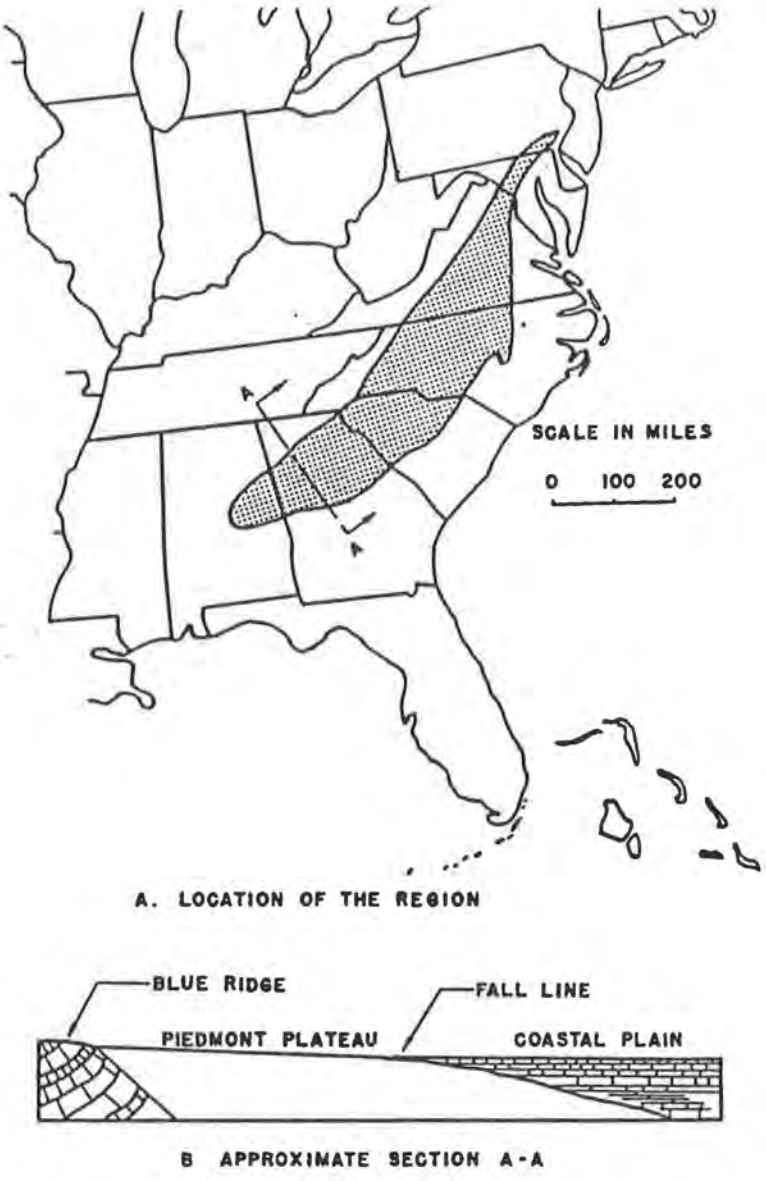

FIG. 3.1.1. - Location and Approximate Section of the Piedmont Region (Sowers 1954).

3.2 Soil Formation

Piedmont residual soils are a result of metamorphic or igneous parent rock being weathered in-place. These parent rocks were long ago subject to intense heat and/or pressure which caused the rock to become fluid; therefore, minerals became segregated into parallel bands or sheets. These bands are often swirled, contorted, crumpled, and/or twisted; they are sometimes mistaken as stratification. Upon being cooled, the rock was crystallized to form a complex fabric of tightly interbedded or interlocked grains. This crystalline structure, subjected to in-place weathering, is broken down to produce different soil zones which reflect varying degrees of weathering. Increased weathering is usually observed at decreasing depths below the ground surface (Sowers 1963).

Residual soils are products of chemical decomposition (i.e. weathering) of various complex aluminum silicate minerals of the original rock (Sowers 1983). The Piedmont is well-suited for rapid and deep weathering because of its warm, humid climate and gently sloping topography. The depth of weathering is also dependent upon the rock composition and upon the presence of cracks and fissures caused by the intrusion of younger igneous or basalt rock, faulting, and jointing of the parent rock (Sowers 1954). Those decomposition products which are soluble can be leached through these various rock crevices; depending upon the weathering environment of their place of deposition, either oxidation or reduction reactions can take place. The red colors prevalent in Piedmont soils are due to the oxidation of iron-bearing minerals (Sowers 1994). The depth and thickness of the residual soil blanket is extremely variable, but typical soil

depths range from 6 to 24 meters below the ground surface to the underlain parent rock formation (Sowers 1963).

3.3 Soil Profile

Although several residual soil profiles based on the degree of weathering have been suggested by various investigators such as Sowers (1954, 1963) and Deere and Patton (1971), a typical Piedmont soil can generally be divided into three zones : upper zone, intermediate zone, and partially weathered zone. See Figure 3.3.1 for some typical soil profiles. These zones, which represent different degrees of weathering, are not discrete strata; boundaries between zones are not well defined but are gradual in nature. Soil depth can be quite irregular due to more advanced weathering occuring at fractures or joints (Sowers 1954) Typical grain size curves and Atterberg limits of the different zones are presented on Figure 3.3.2.

The upper zone is usually 1 to 2.5 meters thick and is comprised of quartz, micas, clay minerals (usually of the kaolinite family), and iron oxides. This zone contains well-developed pedologic horizons and is at such an advanced stage of weathering that little evidence of the parent rock structure can be detected. It is also usually homogeneous and stiff; the stiffness is attributed to dessication and/or accumulation of soluble minerals which form weak cements. Grain size curves show a smooth gradation and large percentage of fines attributable to the extensive weathering. According to the Unified Soil Classification System (USCS), upper zone soils typically fall into the CL or CL-ML

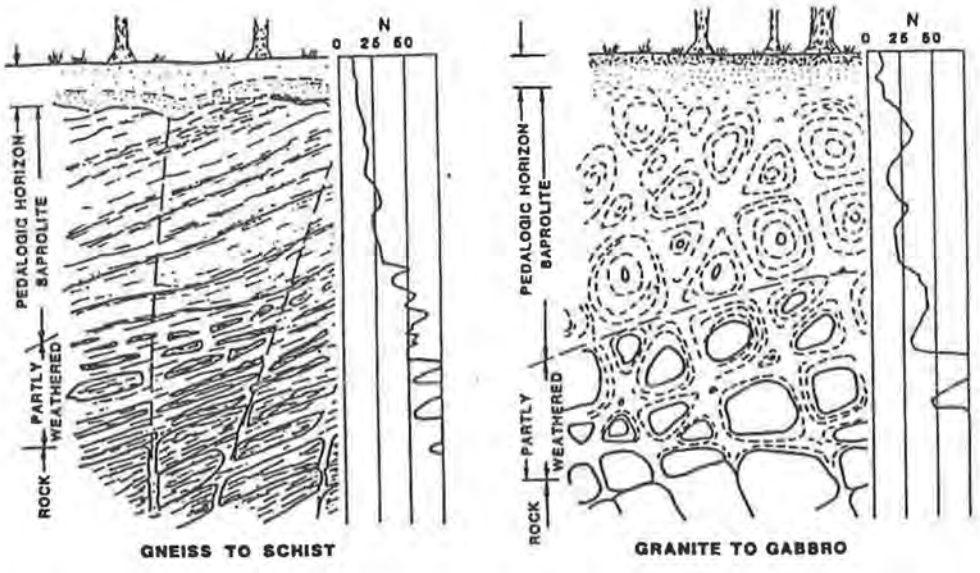

FIG. 3.3.1. - Typical Weathering Profiles in the Piedmont (Sowers 1994).

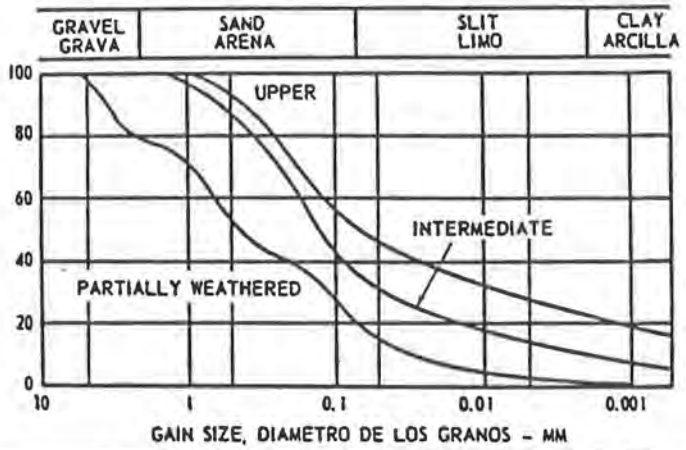

ZONE ZONA	LIQUID LIMIT LIMITE LIQUIDO	PLASTIC INDEX INDICE DE PL.	CLASSIFICATION-CLASIFICACION UNIFIED	 USBPR
UPPER	30-80	12-45	CL, CH	A-6, A-7
INTERMEDIATE	30-65	0-25	ML, MH	A-4, A-5
PART. WEATH	NON PLASTIC	NON PLASTIC	SM, GM	A-1, A-2

FIG. 3.3.2. - Typical Grain Size Curves and Atterberg Limits of Weathered Zones (Sowers 1963).

groups, with an occasional CH (Sowers 1963). Quite variable plasticity characteristics are common (Sowers 1954).

The intermediate zone, formed from incomplete weathering, is the most critical as far as foundation engineering is concerned because the upper zone is usually quite shallow and the partially weathered zone is stronger and sometimes quite deep. This zone is often called saprolite; this term is given for materials which are soil in texture but retain the appearance and structure of the parent rock (e.g. mineral bonding).

The saprolite is predominantly made up of quartz, clay minerals, partially weathered feldspars, and mica. The mica content has a large role in determining saprolite behavior. Mica contents typically vary from 5 to 25 percent; however, some bands may be 100 percent mica while others may have none. Mica does not tend to decompose as readily as feldspar. Also, the micas usually have planes of weakness due to the planes of cleavage being oriented parallel to banding. In addition, mica content is a major factor in determining a saprolite's void ratio. Higher mica content usually corresponds to a higher void ratio. Void ratios vary from 0.4 to 2 in the saprolite zone (Sowers 1963).

Saprolite grain size curves usually show a uniform to well-graded curve over sand sizes and a long flat curve over the fines range. The saprolite tends to have moderately high liquid limits but rather low plasticity indices. Accurate determination of the Atterberg limits is difficult because these soils do not readily flow in the liquid limit cup and the plastic limit threads are too spongy to roll easily (Sowers 1963). According to the USCS, saprolite soils are grouped as ML or SM. They can all be described as micaceous sandy silts or silty sands (Sowers 1954).

The partially weathered zone is a transition between the saprolite and less weathered rock (Sowers 1983). This zone is characterized by bands of intermediate zone sandy silts and silty sands separated by bands of relatively sound rock. The grain size curves are irregular with gravel, and sometimes boulder, sizes present. A small percentage of low plasticity fines is typical; this trait reflects the lesser weathering as compared to the zones above it. According to the UCS, this zone can vary from SM, GM, GW, GP, SW to SP or any combination thereof. (Sowers 1963)

3.4 Engineering Characteristics

3.4.1 Permeability

The coefficient of permeability varies greatly from one soil zone to the next. Generally, permeability is a function of the degree of weathering, size of weathering-resistant particles, and the patterns of fracture. Table 3.4.1 gives typical permeability ranges for each soil zone. Also, permeability is usually 2 to 4 times greater parallel, rather than perpendicular, to banding for saprolite soils (Sowers 1963).

Table 3.4.1. - Permeability of Weathered Zones (Sowers 1983).

Soil Zone	Permeability (cm/s)
Upper	10^{-3} to 10^{-7}
Saprolite	10^{-4} to 10^{-6}
Partially Weathered	10^{-1} to 10^{-5}
Rock	Impervious

3.4.2 Groundwater

The groundwater level is often complex and irregular in nature; however, the saprolite is usually pervious enough to allow for a normal gravity water table in the more humid areas of the Piedmont (Sowers 1985). The phreatic surface more or less parallels the surrounding topography, but irregularity arises from the anisotropic permeability in the saprolite and partially weathered zones. Groundwater levels tend to fluctuate several meters during the year due to rainfall variation (Sowers 1983).

3.4.3 Compressibility

Materials of the saprolite and partially weathered zones consolidate much like other soils subjected to a vertical pressure and lateral confinement. A partly saturated saprolite's time-rate of consolidation plot will show significant initial consolidation, clearly defined primary consolidation, and somewhat large secondary consolidation. This rapid consolidation behavior resembles that of partly saturated peat rather than saturated clays. The primary consolidation is greater than that seen in clays because of the high permeability of saprolite soils (Sowers 1983). Also, secondary consolidation, often a significant component of structural settlement, is relatively large like that of organic soils and tends to be related to mica content. Higher mica content corresponds with higher secondary compression (Sowers 1963).

Plots of stress vs. void ratio over the initial and primary consolidation range for saprolite soils are similar to those of undisturbed preconsolidated clays. Apparent preconsolidation loads are predicted for these soils, but no relationship appears to exist

between depth and preconsolidation stresses. The values of these preconsolidation stresses can vary erratically; this behavior probably reflects the residual mineral bonds and tectonic stresses that have been only partially relieved by the weathering process (Sowers 1983).

3.4.4 Shrinkage and Swelling

Volume changes of micaceous sandy silts and silty sands as a result of wetting and drying are similar to highly plastic clays even though saprolite soils have very low plasticities. Shrinkage and swelling appears due to mostly mechanical processes. Shrinkage involves the soil being compressed by capillary tension in the pore water as drying takes place, but unlike clays, these soils can expand when dried beyond the shrinkage limit because the capillary loss in the dry voids permits the quartz-mica framework to rebound to initial volume. Upon wetting, this framework expands because of reduced capillary tension, but upon swelling, unequal expansion can break the remaining mineral bonds (Sowers 1963).

3.4.5 Compaction

The upper and intermediate zone soils do not compact very well. Partially weathered zone soils are better construction materials, but they are typically too deep to be economically excavated. The maximum Standard Proctor dry density for compacted intermediate and partially weathered zone soils range from 1.25 g/cm^3 to 2.08 g/cm^3 with a median value near 1.55 g/cm^3. The optimum moisture contents can vary from 12 to 35

percent. Strengths of these soils compacted at or above 95 percent of the Standard Proctor maximum are better than what is expected from such low densities (Sowers 1963).

3.4.6 In-Situ Stresses

While sedimentary soils tend to have a constant proportion between horizontal and vertical soil pressures, Piedmont residual soils (except those derived from limestone) sometimes have horizontal stresses which are not related to the vertical stresses. Sowers (1963) noted that Piedmont soils tend to show preconsolidation to varying degrees and that the present overburden load seems to be unrelated. In fact, he reported that samples taken within a close proximity to one another, but from different mineral bands, can have greatly differing preconsolidation loads.

One possible reason for this phenomenon is that the retained tectonic strains from previous geologic evolutions are only partly relieved by weathering in the intermediate and partially weathered zones. It is quite common for horizontal pressures at shallow depths to greatly exceed vertical overburden; therefore, the coefficient of earth pressures at rest, K_o, often will exhibit decreases at increasing depths (Sowers 1985). Another hypothesis is that the volume changes due to weathering produces stress changes which are partially retained in the soil structure (Sowers 1963).

3.4.7 Shear Strength Characterization

The prediction of Piedmont residual soil shear strength is not a simple task due to the anisotropic, nonhomogeneous nature of this geology. Since contorted and swirled mineral bands are especially prevalent in the saprolite and partially weathered zones, strengths can vary a great deal from one location to the next; however, the shear strength within such bands is relatively constant. Also, the presence of cracks, joints, and/or faulting can help create a soil mass comprised of weak and strong areas due to uneven weathering. Therefore, a testing program involving a large number of triaxial shear tests is considered the most satisfactory method of characterizing shear strength (Sowers 1963).

Other strength tests besides triaxial shear have been conducted on residual soils such as unconfined compression, direct shear, and vane shear tests; however, these tests tend to be inaccurate in their strength predictions. Piedmont soils often fail along planes of weakness which cannot be predetermined by visual inspection; therefore, the direct shear test, which predetermines a failure surface, would tend to overpredict strength. Conversely, the unconfined compression test tends to underestimate strength because undrained shear strength of Piedmont soils increases with increasing confining pressure (Sowers 1963).

The triaxial shear test allows for a confining pressure to be applied and for this pressure to be adjusted to model different stress conditions; the failure surface is not predetermined. Consolidated-undrained (CU) triaxial shear tests are commonly

conducted, and consolidated-drained (CD) tests can be performed although testing times would generally take longer.

The Mohr-Coulomb failure envelope of saprolite soils generally consist of a straight line portion at confining pressures greater than a transition stress range, typically 100 to 200 kPa. Below this transition stress, the envelope exhibits a downward curvature until the true cohesion, or shear strength at zero confining pressure, is reached. Many saturated Piedmont soils exhibit true cohesion (Sowers 1983). Partially saturated soils tend to exhibit an apparent cohesion, but this characteristic is related to the negative pore water pressure and is indicative of true cohesion. True cohesion has been hypothesized to come from residual bonds of unweathered minerals and from bonding produced by precipitation of semi-soluble weathering products (Sowers 1985).

The internal angle of friction is thought to result from particle interlocking and true friction. Friction between particles decreases as a soil's void ratio increases; consequently, the friction angle decreases as well. Mica content plays a major role in determining the magnitude of a soil's void ratio; increases in mica percentage usually correspond to a higher void ratio. Sowers (1963) reported that the friction angle and void ratio relationship is much more pronounced than that between cohesion and void ratio, as presented in Figure 3.4.1. Also, increasing intensity of weathering causes a reduction in cohesion and angle of shearing resistance (Deere and Patton 1971).

Typical failure envelopes for undisturbed samples from saturated and partially saturated saprolite determined from CU triaxial tests are illustrated on Figure 3.4.2. The effective stress envelopes are larger than those for total stress conditions; however, the

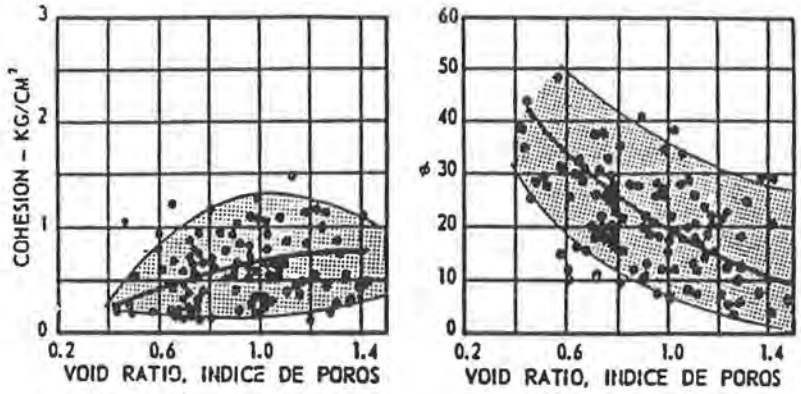

Note that upper half of each curve is partially saturated and lower half is saturated.

FIG. 3.4.1. - Total Stress Shear Strength Parameters' Relationship to Void Ratio in the Saprolite and Partially Weathered Zones (Sowers 1963).

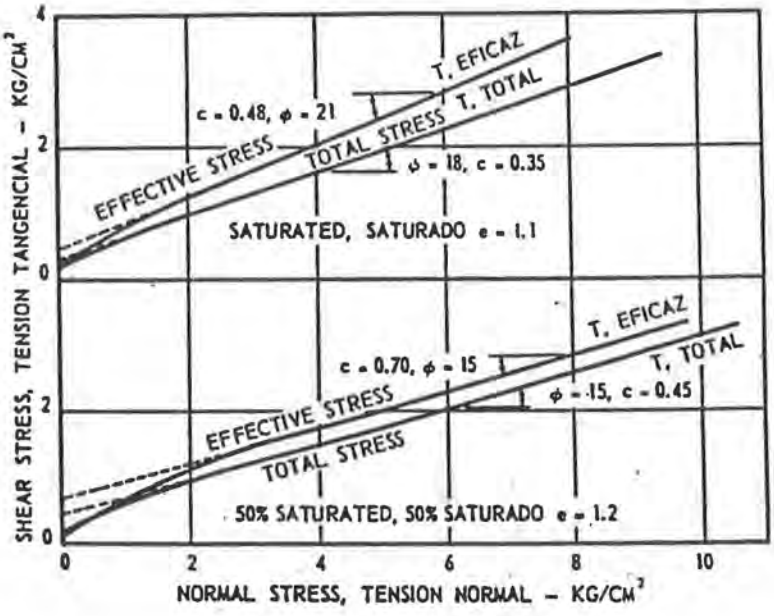

FIG. 3.4.2. - Typical Mohr Envelopes of Undisturbed Samples of Saprolite by CU Triaxial Tests (Sowers 1963).

differences are much less than what would be expected for a typical clay soil. Regardless of the stress state, the friction angle remains fairly constant for each level of saturation. The apparent and true cohesion values are much more variable (Sowers 1963). Various shear strength investigations in Piedmont soils have generally observed effective friction angles from 20 to 40 degrees and effective cohesion values between 0 to 70 kPa (Deere and Patton 1971; Sowers 1983; Harris and Mayne 1994).

3.4.8 Stiffness Characterization

Obtaining a good measure of soil stiffness is important in designing a sound, economical foundation. In Piedmont soils, sampling is oftentimes possible, so either laboratory or in situ testing methods are viable. For soils which are very stiff and/or have large rock fragments, in-situ methods are much more practical. In addition, laboratory testing introduces unavoidable sample disturbance which breaks weak bonds and allows stress release (Wang and Borden 1994).

Due to the heterogeneity of Piedmont soils, obtaining samples representative of overall soil conditions is difficult at best. Conventional one-dimensional laboratory consolidation test results and theory typically predict larger settlements than will occur (Barksdale et al. 1986). In fact, Sowers (1994) noted that settlements are typically 67% to 75% of that predicted by conventional lab testing. This common overprediction has led many to try in situ testing methods.

In-situ tests such as the pressuremeter and the flat dilatometer have been used to obtain soil stiffness parameters, especially where obtaining samples is difficult and quick

results are desired. In-situ tests also allow for a more encompassing investigation; more locations can be characterized for stiffness in order to evaluate a site's variability. The flat dilatometer has been reported to produce very similar settlement predictions to conventional oedometer testing (Mayne and Frost 1988). The pressuremeter is often claimed to be more accurate than the flat dilatometer or conventional lab testing (Martin 1977; Kahle 1983; Barksdale et al. 1986).

A discussion of soil stiffness must include soil's inherent non-linear stress-strain behavior. Seed and Idriss (1970) noted that secant shear modulus should be expressed as a function of a soil's induced shear strain; Piedmont soils are no exception. The decay pattern of normalized shear modulus with strain for Piedmont soils has been investigated at the North Carolina State University Research Farms near Selma, NC (Borden et al. 1994; Wang and Borden 1996). Figure 3.4.3 presents the normalized shear modulus vs. shearing strain for the residual soils at this site.

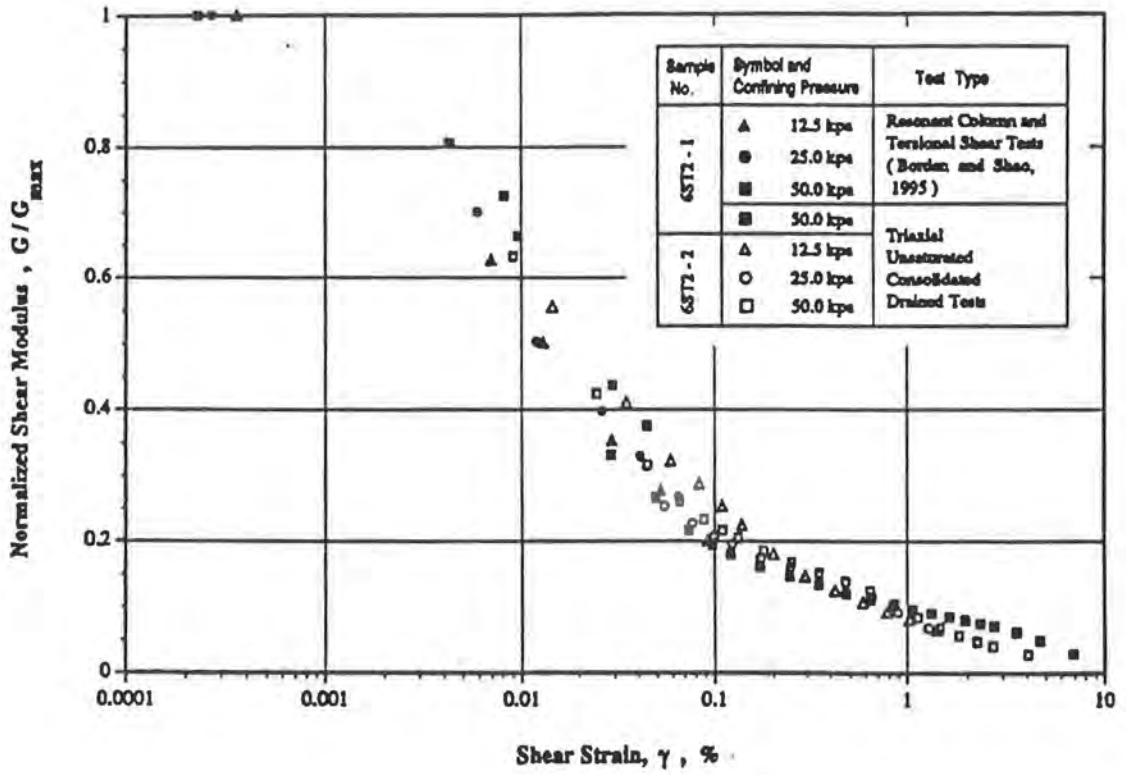

Figure 3.4.3. - Normalized Shear Modulus as Function of Shearing Strain for Selma, NC Site (Wang and Borden 1996).

CHAPTER 4

IN-SITU TESTING

4.1 Background of the Standard Penetration Test

4.1.1 General

The standard penetration test (SPT) is currently the most popular and economical in-situ testing device in North America. The SPT was developed around 1927, and the standardization of the testing methodology was begun in 1958 with the first version of ASTM D 1586. Its straightforward, relatively simple premise and robust nature have contributed to widespread SPT usage (Bowles 1996).

The SPT is basically comprised of driving a standard split-barrel sampler a distance of 460 mm into the soil at the bottom of a boring; the driving of the sampler is accomplished by a 63.5-kg hammer falling "free" from a height of 760 mm. The number of drops (or blows) of the hammer required to drive the sampler the last 305 mm is termed the N-value, which is a measure of penetration resistance.

Even though the SPT does not provide a direct measure of any mechanical property, it does provide soil property information through correlations which are especially useful to more routine geotechnical work. Since a disturbed sample is recovered, index tests such as grain size distribution, in situ water content determination,

and Atterberg limits can be conducted. Also, a site's general vertical and horizontal variability can be determined relatively quickly. In addition, correlations have been established to give predictions of shear strength, unit weight of cohesionless soils, pile friction, settlement of shallow foundations, soil liquefaction potential, and more.

4.1.2 Apparatus and Operation

The SPT is somewhat unique to geotechnical engineering because the hardware used in testing is not manufactured according to specifications set by users of the test's results; equipment development has largely been due to drill rig manufacturers and drilling contractors (Riggs 1986). Several equipment options are allowed by ASTM D 1586 as long as the basic premise of "a 63.5 kg weight falling free 760 mm" is fulfilled. The SPT apparatus is essentially comprised of the drilling equipment and the sampler driving system.

According to ASTM D 1586 (1984), the drilling equipment should provide a clean, open hole at the time of sampling to ensure that the test is performed on undisturbed soil. To this end, various drill bits and auger types are allowed with minor restraints on size. Sampling rods also have size and stiffness specifications. The split-barrel sampler has dimensions as shown in Figure 4.1.1.

The sampler driving system is made up of the hammer, anvil, and hammer drop system. Although the hammer mass is specified, hammer shape and type is not. The most common hammer type is the safety hammer; this and other commonly used

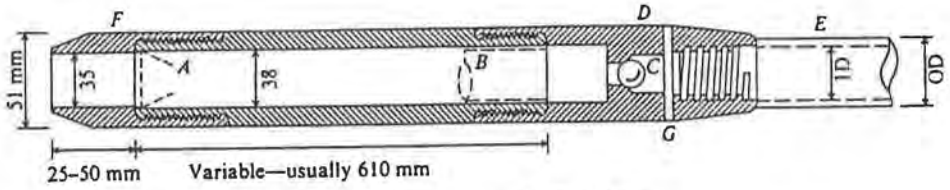

A—insert if used *B*—liner if used
C—ball check valve (provide suction on sample)
D—sampler-to-drill rod coupling
E—drill rod (A or AW)
F—drive shoe *G*—vent holes (used with *C*)

Drill rod sizes:

A: 41 OD × 29 ID mm	5.51 kg/m
AW: 44 OD × 32 ID mm	6.25 kg/m

FIG. 4.1.1. - Schematic of Standard Split Barrel Sampler (Bowles 1996).

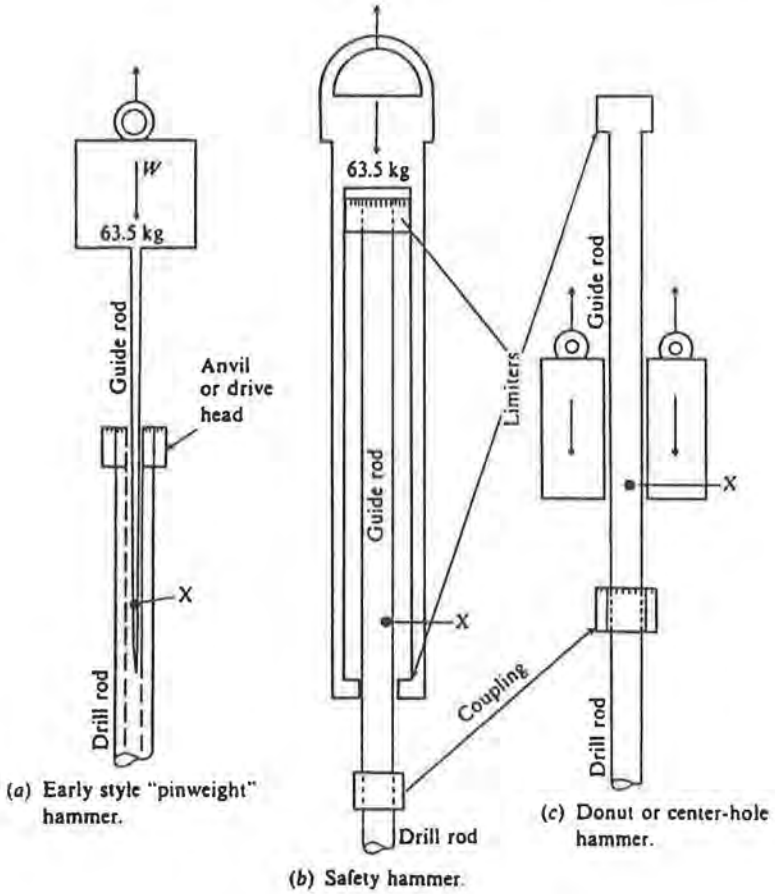

FIG. 4.1.2. - Schmematic Diagrams of Commonly Used Hammers (Bowles 1996).

hammers are shown in Figure 4.1.2. The anvil is required to provide steel to steel contact with the hammer, but no other anvil requirement is given. The hammer drop system can be either a rope-cathead, trip, semi-automatic or automatic type. Figure 4.1.3 shows an automatic hammer setup.

4.1.3 Testing Results

The SPT does not directly measure any soil property. Penetration resistance is monitored resulting in a blow count, or N-value, for each test depth. It has been observed that, both prior to and after ASTM standardization, SPT results are not reproducible (Bowles 1996). Many factors contribute to the variable nature of N-value measurement; each factor changes the amount of energy transmitted to the sampler (Bowles 1996; Riggs 1986; Kovacs et al. 1977).

Of the various hammer drop mechanisms, the most common method is by motor-driven cathead and manila rope. This method introduces human error since the operator must visually raise the hammer to a height of 760 mm above the drill rod and allow a "free" release of the rope. Such factors as the number of turns of the rope and the rope's condition can greatly vary the driving energy; in addition, the cathead speed is not specified in the ASTM specification.

A more recently developed hammer drop mechanism is the automatic hammer setup. This method is a totally mechanical system which limits the operator error compared to the motor-driven cathead and manila rope technique. Also, since this mechanism has less frictional resistance compared to any of the other techniques, more energy is

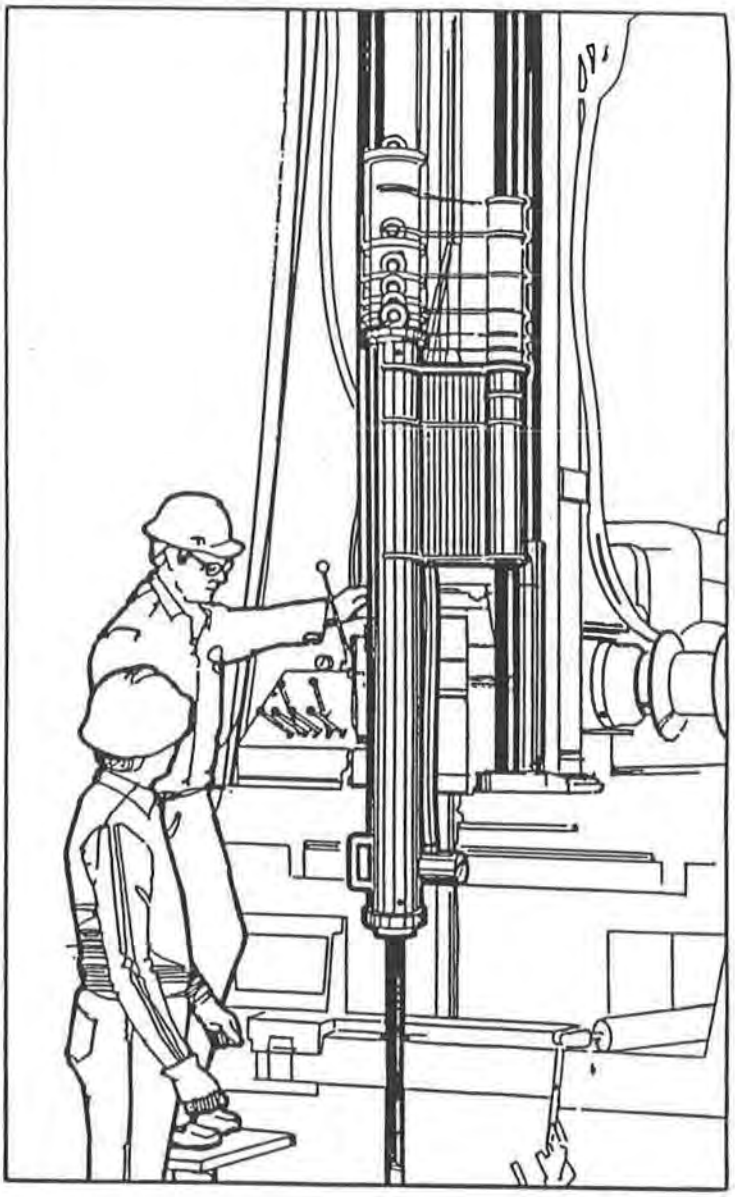

FIG. 4.1.3. - Automatic Hammer Setup (Riggs 1986).

delivered to the drill rod. Subsequently, N-values are usually lower than those determined using other hammer drop systems.

Friction is present in all mechanical driving systems; therefore, the energy delivered is only a percentage of the theoretical amount of a "free" fall of the hammer. Different hammers will deliver various amounts of energy. The relative tightness of the drill rods and the anvil shape used can also affect the delivered energy. Other factors which introduce variability include such things as using a warped driving shoe, pushing a rock with the sampler, and having a state of liquefaction at tests conducted near the ground water table. Also, sampler liner usage, drilling method, and drill rod lengths can have an effect on driving energies and, consequently, on N-values.

Overburden pressure, along with other variable testing factors such as hammer type, boring size, etc., can be accounted for by correction factors which either raise or lower measured N-values as follows

$$N_{CORR} = N \times C_N \times C_{ER} \times C_B \times C_S \times C_R$$

where N_{CORR} = corrected (or adjusted) N-value, N = uncorrected N-value, C_N = overburden factor, C_{ER} = energy ratio factor, C_B = borehole diameter factor, C_S = sampling method factor, and C_R = rod length factor. By applying these correction factors to the measured N-values, tests performed under different conditions are more correctly compared. However, it should be remembered that various authors (e.g. Riggs 1986; Skempton 1986) suggest different values for the correction factors mentioned above.

Even though different correction factors are available, overburden pressure and the energy of driving used are quite commonly accounted for; if tests are performed in a soil

deposit which has constant density over depth with everything else being equal, N-values taken at a great depth will be higher than those at a shallower depth. Also, if a correlation for a physical or mechanical soil property is established using a specific type of hammer, the use of a different hammer will require an adjustment of N-values by the measured or theoretical energy ratio between the two hammer types.

4.1.4 Usage in the Piedmont

One of the reasons that the SPT is widely used in the Piedmont is because it is sensitive to weak materials and robust enough to handle partially weathered rock (Sowers 1985). Sowers (1963) presented typical ranges for N-values in each zone of Piedmont soils. These values are presented in the table below along with data from the North Carolina State University Research Farm.

Table 4.1.1. - Reported Ranges of N-Values in Piedmont (Sowers 1963; Wang and Borden 1996).

	Sowers (1963)	Wang and Borden (1996)
Soil Zone	*N-Values Range*	*Observed N-Values*
Upper Zone	**5 to 50**	**10 to 37**
Intermediate Zone	**5 to 50**	**7 to 16**
Partially Weathered Zone	**> 50**	**10 to >100**

An investigation conducted on the Georgia Tech Campus in Atlanta, Georgia used several testing methods to predict effective friction angle of saprolite silty sands (Harris and Mayne 1994). The SPT prediction of effective friction angle by a method given by

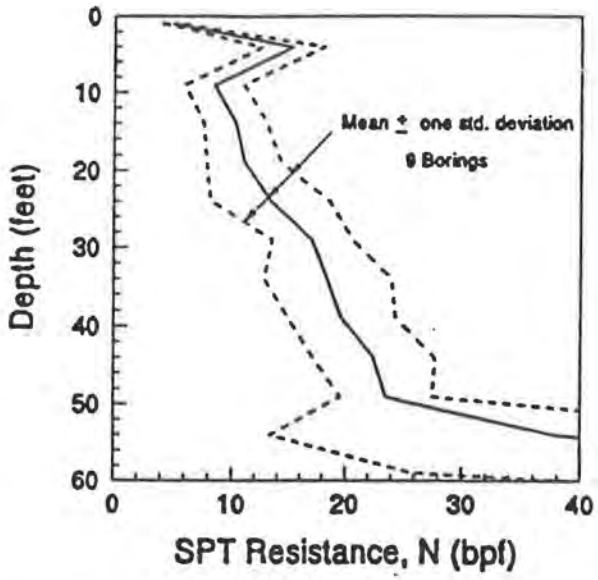

Figure 4.1.4. - SPT Results at Georgia Tech Campus (Harris and Mayne 1994).

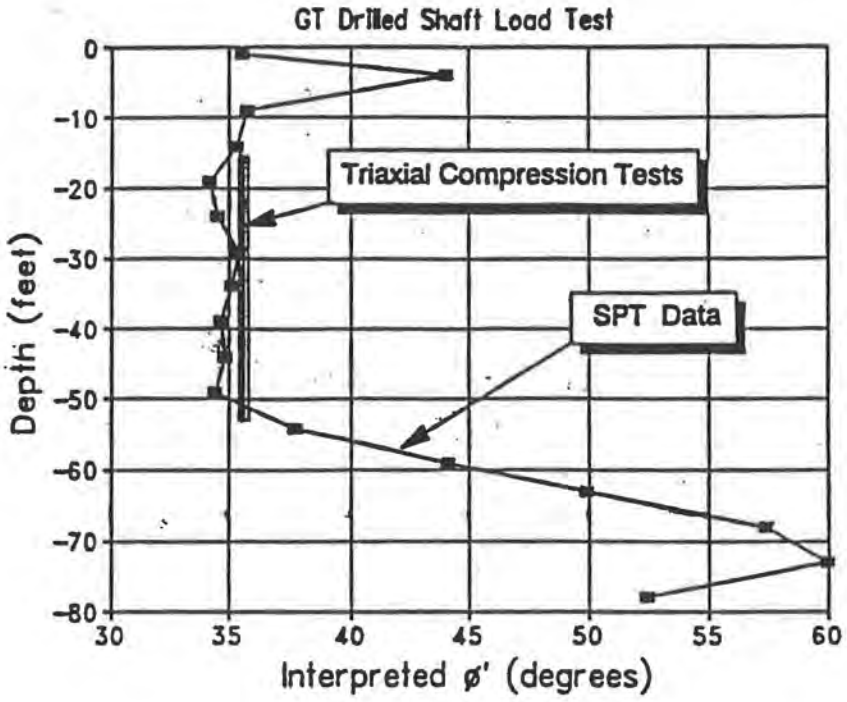

Figure 4.1.5. - Effective Friction Angle Predictions by SPT at Georgia Tech Campus (Harris and Mayne 1994).

Schmertmann (1975) agreed very well with isotropically consolidated-undrained triaxial compression tests. A plot of average N vs. depth can be seen in Figure 4.1.4, and Figure 4.1.5 shows a plot of predicted effective friction angle vs. depth by the SPT compared to back-calculated values.

4.2 Background of the Cone Penetration Test

4.2.1 General

The cone penetration test (CPT) was introduced in a form recognizable today by Barensten (1936). Since that time, various developments and technological advances have changed the type of cone used; mechanical cones have given way in recent times to the electric friction cone which measures friction resistance to penetration by transducers (Meigh 1987). The CPT, standardized by ASTM D 3441 (1986), has become a widely used test in most geologies excluding gravel and stiff clay deposits. Testing consists of pushing a standard cone into the ground at a rate of 10 to 20 mm/s and recording corresponding cone sleeve friction resistance (f_s), cone tip resistance (q_c), and sometimes pore pressure (u) over depth (Bowles 1996). The ratio of f_s to q_c expressed as a percentage is often reported and is termed the friction ratio (R_f). These CPT measurements can then be used in empirical correlations to predict a wide variety of soil properties including: soil type, effective friction angle of sands and clays, undrained shear

strength of clays, shear wave velocity, liquefaction potential, stress history, constrained modulus, and more (Mayne et al. 1995).

The CPT is typically used to determine soil type and profile, to interpolate ground conditions between control borings, and to evaluate engineering soil properties and probable foundation bearing capacity and settlement (Meigh 1987). The CPT is usually used in conjunction with borings and in-situ and/or laboratory testing. Since no sample is returned during testing, the CPT is seldom the only test used for building foundation investigations unless the geology is fairly uniform and local correlations have been established.

An important advantage of the CPT over other in-situ testing methods is that it can provide a virtually continuous record of soil conditions in a very short time period. Therefore, a site investigation can be done quickly and economically (Meigh 1987). The CPT has, in recent times, been incorporated with additional sensors which have increased versatility. Seismic-, resistivity-, natural gamma-, and chemical-cones have been especially attractive for geoenvironmental projects; the use of these cones allow expedient mapping of a contaminant site (Mayne et al. 1995).

4.2.2 Apparatus and Operation

The basic CPT apparatus generally consists of a thrust machine with reaction mass and a penetrometer with desired measurement and recording equipment. The thrust machine must provide a continuous stroke at a constant rate while the magnitude of the thrust varies. This requirement is usually accomplished by variously sized rigs which use

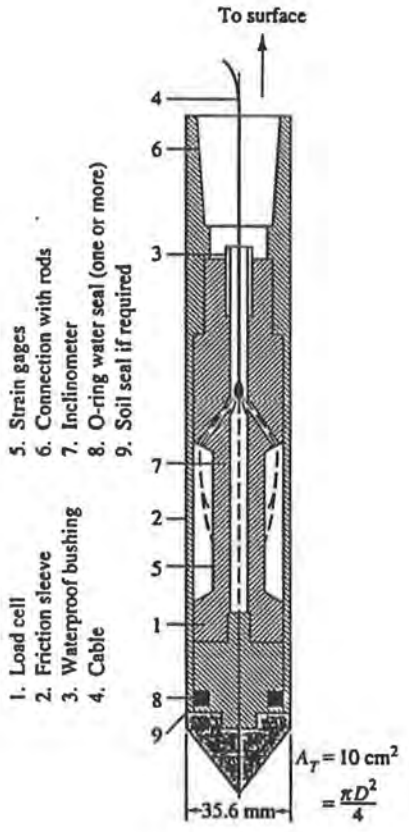

FIG. 4.2.1. - Cross-Section of Typical Electric Cone (Bowles 1996).

a hydraulic jacking system to advance steel push rods at the standard rate of 10 to 20 mm/s. These rigs have thrust capacities ranging from 20 to 300 kN and can be either truck-, trailer-, or track-mounted. The reaction mass aids in stabilizing the rig during rod insertion and is usually incorporated into the rig (Meigh 1987).

Penetrometers generally fall within two categories: mechanical and electric; both cone penetrometer types have been standardized for operation and dimension tolerances. In mechanical cone operation, the forces to mobilize tip and sleeve friction resistances are measured at the surface as they are applied through the sliding mechanism of inner and outer push rods. Electric cones are pushed into the ground by push rods, and the resistance forces are measured by electrical devices built into the tip and are relayed to the surface to a data acquisition system (Meigh 1987). In addition, a friction-reducer ring (a steel ring with larger diameter than the push rods) is often placed above the cone to reduce the thrust force necessary to overcome friction on the push rods. An electric cone cross-section is shown in Figure 4.2.1. The data acquisition system might include a portable computer, analog-digital converter, data storage media, and printer (Mayne et al. 1995).

Regardless of penetrometer type, routinely used cones have a 60° point angle, 35.7 mm diameter base, and a resulting projected tip area of 10 cm^2; the friction sleeve has the same outside diameter as the base diameter and a surface area of 150 cm^2. Different sized tips are sometimes used with only marginal effects on resistance for diameters between 5 and 15 cm (ASTM 1986).

Cones which are capable of monitoring pore pressures during cone penetration are called piezocones; these cones when combined with seismic testing capabilities provide a wealth of soil information over both small and large strains. Piezocones can also be used to perform pore pressure dissipation tests; this test gives an indication of soil type since the time rate of pore pressure dissipation is related to hydraulic conductivity and hence infers grain size and density. The porous elements used in piezocone testing are made of either flexible polypropylene, stainless steel, rigid ceramic, or stone. They can be positioned at various locations along the cone tip face or behind the tip. Each position has advantages and disadvantages depending upon geology investigated and use of piezocone results (Mayne et al. 1995).

4.2.3 Testing Results

The CPT does not directly measure any soil property; instead, resistance to penetration is measured. Piezocones also give a measure of pore pressure at the time of penetration; this pressure includes the ambient and excess pressures. Since electric cones use transducers to record friction resistance, frequent load cell calibration is recommended (Mayne et al. 1995).

Excessive wear can cause cone tip roughening to the point of not meeting the ASTM tolerances; this is especially prevalent in sandy soils. Another problem sometimes encountered is drift of the tip away from vertical alignment; this phenomenon is usually caused by the cone deflecting while pushed through a stiff lense or alongside an

obstruction such as a boulder. In order to monitor drift and to ensure drill rods do not bend excessively, an inclinometer can be installed within the cone.

During piezocone testing, the proper saturation of the porous element is critical to quality results. It should also be remembered that the element location affects the pore pressure measurement; the stress conditions are different at various locations along the cone (Mayne et al. 1995). If an interruption to penetration is encountered or the rate is not within standardized limits, test results will be suspect since friction resistance is related to the rate of cone penetration.

4.2.4 Usage in the Piedmont

As the CPT became more prominent in characterizing sedimentary deposits, it was thought that pushing the cone in the Piedmont would not be feasible since partially weathered rock can be at shallow depths and limit the depth of testing. Only after flat dilatometer testing proved successful in the Piedmont during the last decade has the CPT been routinely used. It was thought that stones might cause the cone to deflect greatly during insertion or possibly limit the depth of exploration; however, inclinometers can be used to ensure that cone travel is near vertical and that pushing will be stopped prior to damaging the cone. A typical CPT record at the Georgia Tech campus is shown in Figure 4.2.2. Correlations with CPT for effective friction angle prediction were used to evaluate their accuracy compared to triaxial testing; these correlations are presented in Figure 4.2.3.

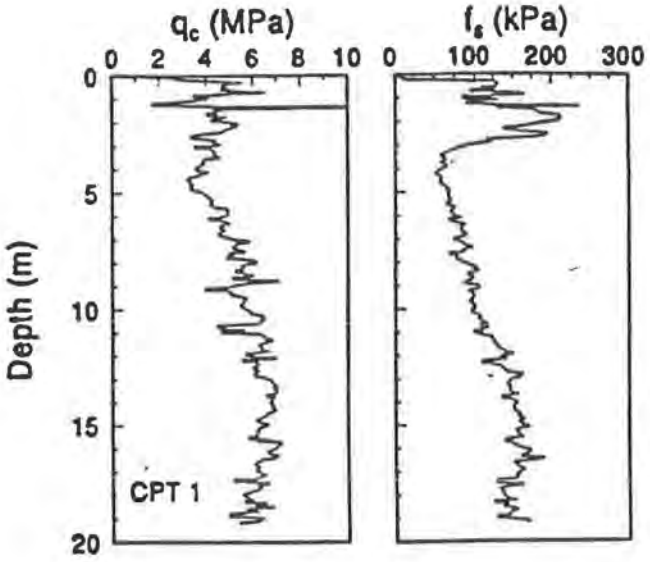

FIG. 4.2.2. - Typical Tip and Sleeve Friction Resistance at Georgia Tech Campus (Harris and Mayne 1994).

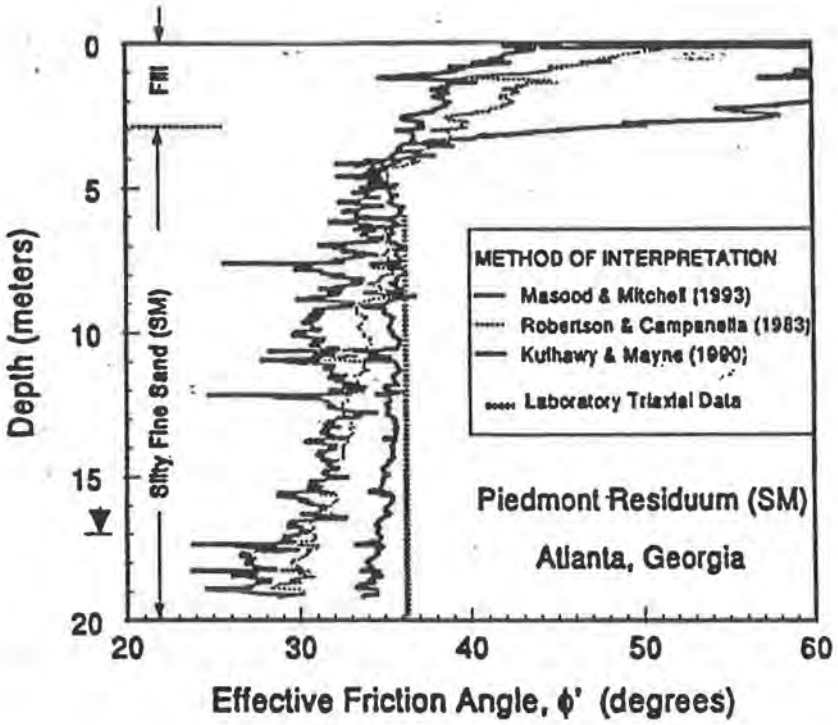

FIG. 4.2.3. - Effective Friction Angle Predictions by CPT Correlations at Georgia Tech Campus (Harris and Mayne 1994).

4.3 Background of the Pressuremeter Test

4.3.1 General

The pressuremeter (PM) test, first introduced by Louis Menard, involves the expansion of a long, cylindrical membrane installed into the ground (Mair and Wood 1987). Various categories of PMs are available such as Menard-type, self-boring, and pushed-in, but generally a PM can be defined as a cylindrical probe that has an .expandable, flexible membrane which applies a uniform pressure to the walls of a borehole (Clarke 1995; Mair and Wood 1987; Baguelin et al. 1978). It has become an in situ test with great versatility; parameters which can be deduced from PM tests include deformation modulus, undrained shear strength of clays and weak rocks, effective friction angle of sands and clays, angle of dilation, in situ horizontal earth pressure, and coefficient of horizontal consolidation.

The PM test's principal attraction is that, in theory, the test boundary conditions are controlled and well-defined. However, the degree of success in predicting soil properties is dependent upon proper installation of the PM and interpretation of the results and correlations used. Running a test involves first calibrating the PM, positioning it into a properly prepared hole, and measuring pressure and corresponding changes in volume of the expanding membrane until reaching full membrane expansion or yielding of the soil becomes disproportionately large (ASTM 1987). A common deviation from this basic test procedure involves an unload/reload cycle once the probe is sufficiently expanded in the soil cavity in order to examine the stiffness of undisturbed soil; the initial loading

stiffness is a property of the soil which was disturbed during probe placement. Although PM testing does not involve direct measurement of any soil property, a limit pressure, defined as the pressure reached when the soil cavity has been doubled in size, and the PM modulus, derived from the linear portion of the pressure vs. volume plot, can be used in various soil property correlations. Also, although different techniques accompany each PM type, the at rest horizontal earth pressure can be estimated from each (Briaud 1992).

4.3.2 Apparatus and Operation

PMs generally fall into three categories: Menard-type, self-boring, and pushed-in. Each type involves the same general testing procedures and volume/pressure measurement systems, but they differ primarily in size and method of probe positioning. Because of their differences, the geology or the level of accuracy required usually determines which probe is used. For example, the self-boring PM, which is uncommon to routine work, is thought to give a more accurate measure of the at-rest horizontal earth pressure because the probe is positioned with less disturbance than the other probe types.

The Menard-type PM is most commonly used. (Figure 4.3.1) Testing with this probe involves pre-forming a pocket in the soil slightly larger than the probe diameter at a depth of interest. Since expansion of the probe into the surrounding soil is rather small and even minor disturbance can greatly affect results, only certain drilling and sampling methods are allowed by ASTM D 4719 (1987) depending on soil type. These probes tend to have either a single measuring cell or a measuring cell located between two guard cells; the guard cells help ensure that the measuring cell will expand radially only. These

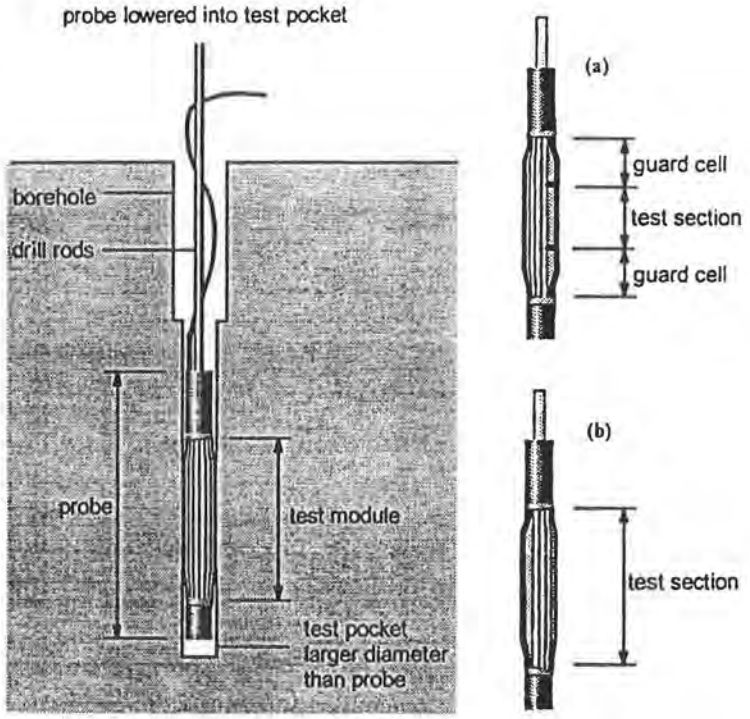

FIG. 4.3.1. - Types of Menard Pressuremeters : a.) a tricell probe; b.) a monocell probe (Clarke 1995).

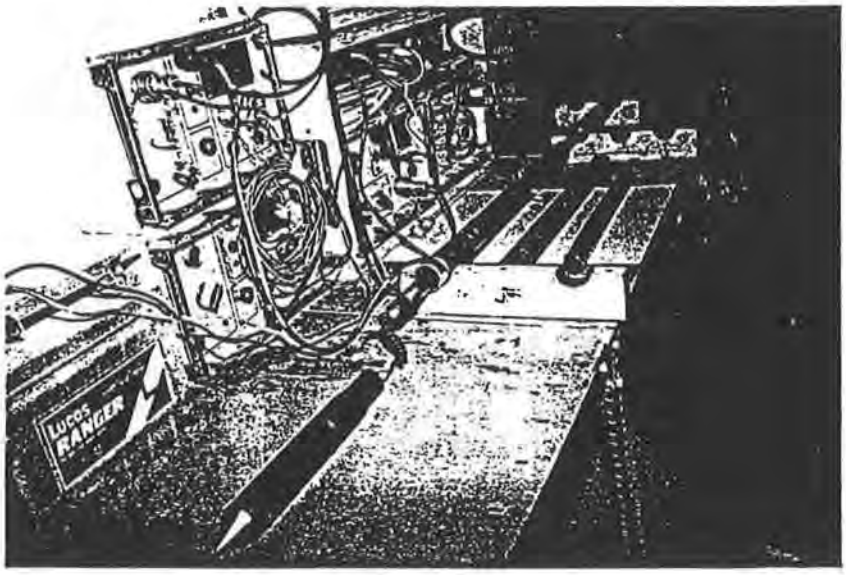

FIG. 4.3.2. - Cone Pressuremeter and Testing Equipment (Clarke 1995).

membranes are made of natural rubber and are sometimes protected on the outside by steel strips. Some common single cell probes have a sheath which runs the length of the expanding section and has a separate measuring cell within it which forms the guard cells. The sheath is expanded by gas pressure, and the measuring cell is expanded by water pressure (Clarke 1995).

The push-in PM, originally used in offshore testing, disturbs the soil upon insertion. The cone PM is one such type of push-in probe. (Figure 4.3.2) It allows the cone penetration test measurements to be made in addition to running PM tests at various depths; in order to obtain valid conventional cone data, cone PM tests (CPMT) are usually conducted at depths corresponding to locations where a push rod must be added. The probe is usually a monocell type, and oil is pressurized to expand the membrane (Clarke 1995).

4.3.3 Testing Results

Valuable information can be gained from the PM test, but several factors must be evaluated to ensure good results. The most critical factor is how well the hole is prepared; disturbance of the borehole is directly related to test results (ASTM 1987). Second, the PM evaluates soil stiffness horizontally; therefore, vertical stiffness may not be closely related to this measure in anisotropic, nonhomogeneous soils. Correlations are necessary for predicting soil properties since soil properties are directly measured only within the confines of the very restrictive boundary conditions of an ideal homogeneous, isotropic, elastic-plastic continuum. Care should be given when evaluating a correlation

because these predictions tend to be accurate only within the geology from which they were derived. Finally, regardless of probe type, proper probe calibration is almost as critical to accurate testing as good installation techniques. Calibrations take account of the following: expansion of the tubing running up the borehole to the surface from the probe, compression of the membrane under pressure, pressure needed to expand the membrane when not in soil, and instrument accuracy (Fair and Wood 1987).

4.4.4 Usage in the Piedmont

One reason why the PM test is being used in the Piedmont is because of the frequent difficulty in obtaining undisturbed samples for conventional consolidation testing and the lengthy time required for these tests, and the spacial variability of the soil and test results. Although the PM test does not totally overcome soil disturbance effects, it does tend to minimize them if the test is properly conducted. The PM test is also much quicker and costs nearly the same as consolidation testing. PM modulus is comparable to back-calculated foundation settlement values of elastic modulus (Barksdale et al. 1986; Martin 1977).

Barksdale et al. (1986) reported PM modulus values in the Piedmont ranging from 5,500 kPa to 28,000 kPa. Martin (1977) reported values from 16,000 kPa to 21,000 kPa. Case studies mentioned by Barksdale et al. (1986) include a hotel in Atlanta, Georgia and a water tank in Virginia. The water tank showed very similar settlements to those predicted by PM test data; the hotel's settlement was overpredicted using PM modulus on average by 25%.

4.4 Background of the Flat Dilatometer Test

4.4.1 General

The flat dilatometer test (DMT), introduced by Marchetti (1975), was initially used to determine in situ soil modulus for driven steel piles. The DMT has since been utilized as a semi-continuous soil stratigraphy and properties logging tool (Marchetti 1979, 1980). Soil properties which can be estimated through dilatometer testing include soil type, unit weight, coefficient of lateral earth pressure, undrained shear strength for clays, effective friction angle for sands, stress history, Young's modulus, and constrained modulus (Lacasse and Lunne 1988; Lutenegger 1988).

The DMT is relatively simple, robust, and operator-independent. Testing is comprised of vertical insertion of a stainless steel blade and expansion of the blade's steel membrane into the adjacent soil mass by regulated gas pressure. During a test the pressure required to begin membrane expansion (also termed lift-off pressure) and the pressure at full membrane expansion are taken as the A- and B-readings, respectively. DMT indexes are then calculated for use with various soil property correlations. The DMT does not directly measure any soil property and no sample is returned for index property testing and soil type verification; therefore, the DMT is often used in conjunction with other in situ and/or laboratory tests.

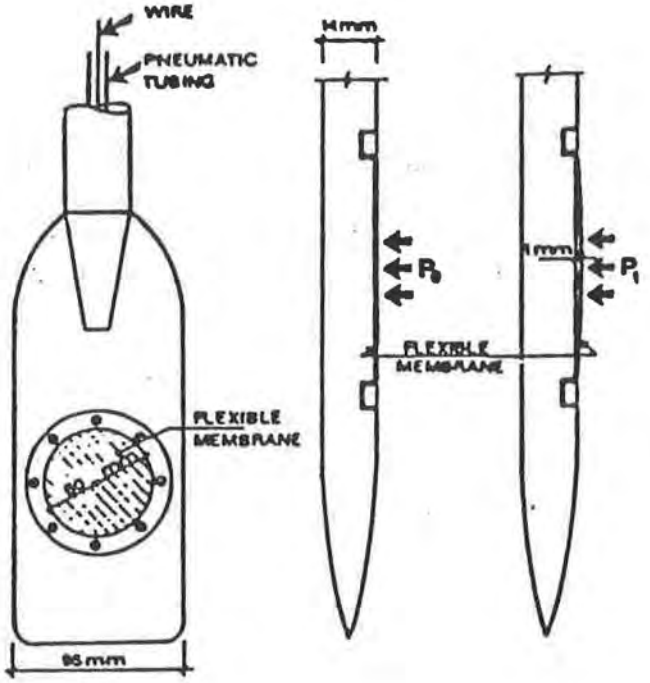

FIG. 4.4.1. - Marchetti Dilatometer (Lutenegger 1988).

4.4.2 Apparatus and Operation

The apparatus is comprised of a stainless steel blade fitted with an expandable steel membrane. The blade measures 95 mm wide, 220 mm long, and 14 mm thick. The membrane is of circular shape with a 60 mm diameter and is located on one face of the blade, as seen in Figure 4.4.1. The blade is typically pushed hydraulically to a testing depth, much like the pushing of a CPT cone, or can be driven through dense strata (Marchetti 1980).

Upon insertion, the steel membrane deflects inward due to lateral soil overburden pressure. To perform a test, a gas (typically nitrogen) is sent from a ground surface source down to the blade through pneumatic tubing to expand the membrane until it has moved from a flush position out 1.1 mm into the surrounding soil. The pneumatic tubing and an electrical wire run inside the push rods from the blade to the ground surface; the wire is part of the horizontal membrane displacement signaling mechanism. This mechanism allows the operator to record the A- and B-readings. Once the full expansion pressure is reached, the pressure is released so that the blade can be removed or advanced to a new test location.

4.4.3 Testing Results

The values obtained during flat dilatometer testing include the pressure readings for membrane lift-off and full expansion. The A- and B-readings are then adjusted for membrane stiffness and for zero offset of the pressure gauges. The corrected pressures are used empirically to define three dilatometer indices: material index (I_D), dilatometer

modulus index (E_D), and horizontal stress index (K_D). These indices are related to soil type, Young's modulus, and coefficient of earth pressure, respectively (Marchetti 1980).

Predicted soil properties must be carefully scrutinized because of several test-specific factors. First, the soil is subjected to complex strains during insertion of the dilatometer; blade insertion produces strain levels lower than that found in other in situ tests such as the cone penetration test. Although strain increments during membrane expansion are also relatively small, soil stiffness is affected by pre-straining, especially sensitive soils (Marchetti 1980). The dilatometer modulus is representative of intermediate- to high-strain soil stiffness (Lacasse and Lunne 1988). Secondly, the dilatometer measures horizontal soil characteristics; therefore, properties such as stiffness may be anisotropic and not be the same in the vertical direction. Finally, many correlations are based on soils without complex stress histories, cementation, etc.; consequently, soils which fall outside of geologies upon which these correlations were based would be expected to give erratic property predictions.

4.4.4 Usage in the Piedmont

The DMT has found use in structure settlement predictions in a variety of soils. Certain limitations, such as only being able to examine a soil's modulus at the in situ stress, do not allow for extremely accurate predictions; however, Schmertmann (1986) reported that accuracy is adequate for most practical purposes. Schmertmann found measured settlements in sands and silty sands to be slightly lower than DMT predictions.

Mayne and Frost (1988) reported several modulus prediction case studies of Piedmont soils in and around Washington, D.C. At one site in Virginia, the soil, derived primarily from schist and phyllite, classified as a fine silty sand (ML) and contained varying mica contents. Sixty-four DMTs produced a mean dilatometer modulus of 35 MPa. In addition, an observed correlation between dilatometer modulus and SPT resistance at various sites near Washington D.C. were given; this correlation bears a great similarity to the relation determined by Martin (1977) between PMT modulus and SPT resistance.

4.5 Background of the Iowa Borehole Shear Test

4.5.1 General

The Iowa borehole shear test (BST) is an in situ strength characterization test introduced by Handy (1967). To carry out a BST, a smooth hole is constructed and serrated plates are lowered to the depth of interest. The plates are then forced against the side of the borehole at a constant, known pressure. Time is allotted for the soil near the plates to consolidate and for all excess pore pressures in more granular soil deposits to dissipate. The plates are then pulled axially along the hole to induce shearing (Handy 1988). The maximum shear stress is noted and, as in conventional direct shear testing, a series of tests with increasing normal pressures are performed. The maximum shear stresses can then be plotted against the normal pressures to construct a Mohr-Coulomb

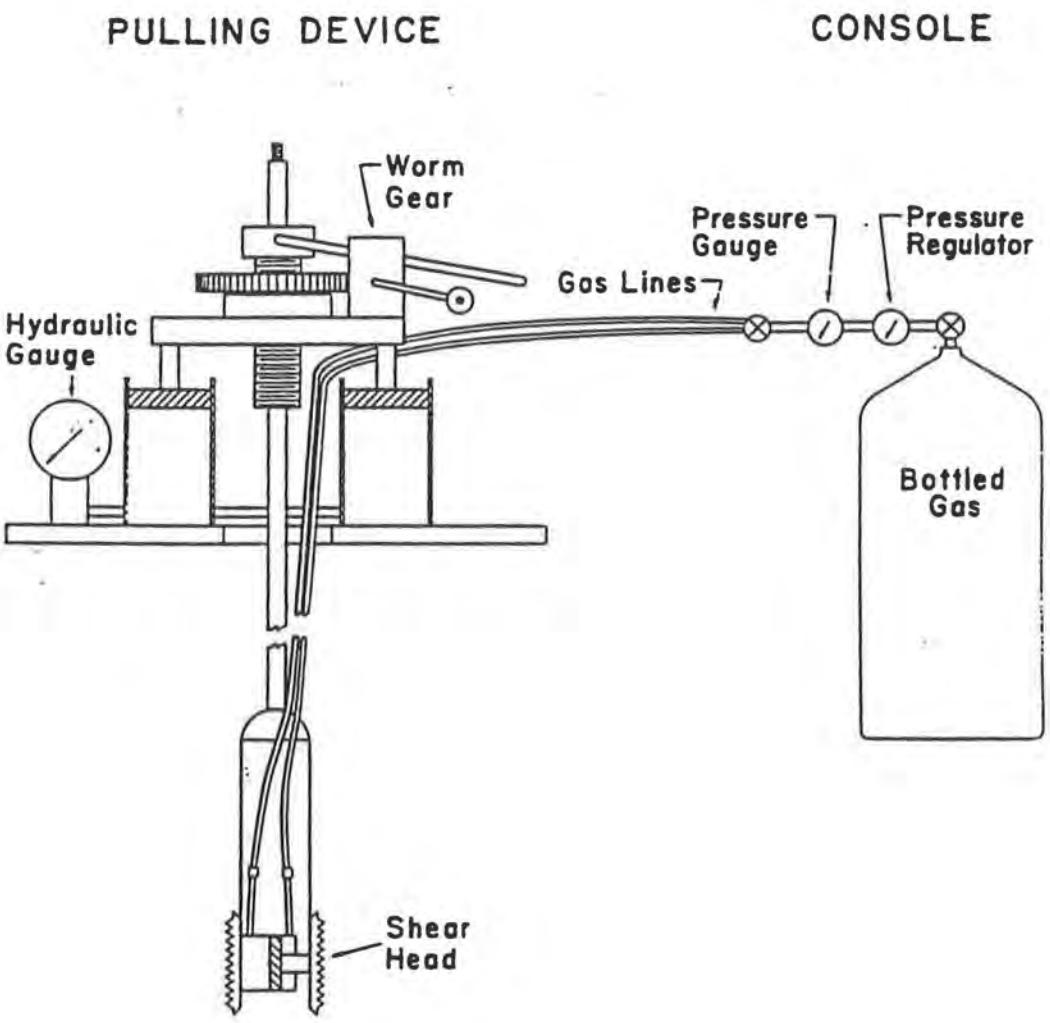

Figure 4.5.1. - Borehole Shear Device (Wineland 1975).

failure envelope, therefore allowing determination of the soil's cohesion and angle of shearing resistance.

4.5.2 Apparatus and Operation

The BST consists of three basic parts: shear head, pulling device, and console. These parts are shown in Figure 4.5.1. Although improvements have been made on early models, the key parts of the apparatus have not changed (Handy 1988).

The shear head typically consists of a gas operated piston or rolling diaphragm which expands the shear plates into the sides of a hole. The serrated plates are manufactured with a nominal surface area, teeth number, teeth shape, and teeth spacing. Studies such as the one done by Demartinecourt (1983) have evaluated the effects of using various sized shear plates on different soil types. The shearing head and pulling device are connected by steel pull rods which screw together end-to-end.

The pulling device components are attached to a plate which rests either on the ground surface or on top of a hollow stem auger left in place. A worm gear and screw arrangement are centered over an opening in the plate which allows the pull rods to pass. Two hydraulic cylinders and a hydraulic pressure gauge are also connected to the plate for the measurement of the shearing force. The crank is turned either by hand or electric motor to induce soil shearing (Wineland 1975).

The console is typically made up of a bottled gas supply (commonly carbon dioxide), a pressure regulator, and a pressure gauge. Therefore, the gas pressure supplied to the shear head can be monitored and regulated.

4.5.3 Testing Results

The BST is unique among in situ tests because it directly evaluates cohesion and friction angle much like a laboratory direct shear test. However, engineering judgement is required when considering the usefulness of the results. Excess pore pressure effects (i.e. drainage state of the test) can especially make proper test interpretation difficult.

Initially, it was thought that the BST measured total stress strength. However, as various investigative studies have been conducted, many BST's have compared very well with drained laboratory test results. At present, however, no procedure for determining the specific drainage state of many soils during a BST exists. For unsaturated soils or quick draining soils, proper interpretation is not very difficult, but for tests on saturated clays, excess pore pressures can be generated during the consolidation phase and/or the shearing phase of a test.

One of the attractions of using the BST is its reproducibility. Test procedures are relatively simple and, therefore, more operator-independent than many in situ tests. However, it is important to recognize common errors during BST testing so that poor results are not accepted. Some typical problems which occur during testing include poor seating of the shear plates in stiff soils, too large an initial normal pressure which limits the number of points obtainable on the failure envelope, and insufficient consolidation times producing stress states which do not fall on the failure envelope (Handy 1988). A disadvantage of the BST is that no soil sample is recovered; therefore, it would almost always be used to complement other testing methods.

4.5.4 General Usage and Application

The results from BST's have been compared with conventional laboratory testing of undisturbed samples, but no conclusive relationship between the two have been made primarily because strength measurements are a function of test procedure and conditions as well as soil type. For most reported case studies, the BST has been used in addition to laboratory strength testing and more conventional in situ tests.

Handy (1967) presented the comparison of BST to CU triaxial tests and direct shear tests for a sand, alluvial loam, and alluvial clay. A much larger study was conducted by the Kansas Highway Commission (Wineland 1975). Although the BST has not been widely used in Piedmont soils, a study by Lambrechts and Rixner (1981) compared the strength predictions of a silt and a varved silt at a cofferdam site in New Hampshire. In this specific case, the BST slightly underpredicted the friction angle as shown in Table 4.5.1.

The BST can been used in a variety of applications such as prediction of bearing capacity, pile capacity, and slope stability. Slope stability evaluations by the BST, especially of a failure surface within a thin soil strata, offers certain advantages over laboratory testing since strength is actually measured along the failure surface and conventional undisturbed sampling may be difficult. More accurate strength predictions of several slow moving active landslides have been claimed compared to laboratory testing (Solseng 1989;Little 1982).

Table 4.5.1. - Comparison of BST Shear Strength Results With Other Methods (Lambrechts and Rixner 1981).

Test Procedure	*Varved Silt*	*Silt*
CIUC Triaxial	$\varnothing = 33°$, c = 0	$\varnothing = 36°$, c = 0
Borehole Shear	$\varnothing = 29°$, c = 9.6 kPa to $\varnothing = 31°$, c = 3.4 kPa	$\varnothing = 32°$, c = 12.9 kPa to $\varnothing = 36°$, c = 11.5 kPa
Various CPT Interpretations	$\varnothing = 26°$ to 30°	$\varnothing = 28°$ to 34°

4.6 Background of Seismic Testing Methods

4.6.1 Introduction

Conventional borehole geophysical methods such as the crosshole test (CHT) and downhole test (DHT) provide an assessment of small-strain stiffness and liquefaction potential by measuring seismic body wave velocities as they travel through the soil. Laboratory tests such as the resonant column test can provide the same information, but in situ tests have the advantages of preserving soil fabric and aging characteristics and of testing soil under its anisotropic at rest earth pressures. The small-strain behavior of soil has been shown to be relevant to both static and dynamic problems (Burland 1989).

4.6.2 Seismic Waves

Seismic body waves include compression and shear waves, commonly referred to as P- and S-waves, respectively (Figure 4.6.1). Particle motion of compression waves is parallel to the direction of wave propagation; conversely, shear waves propagate

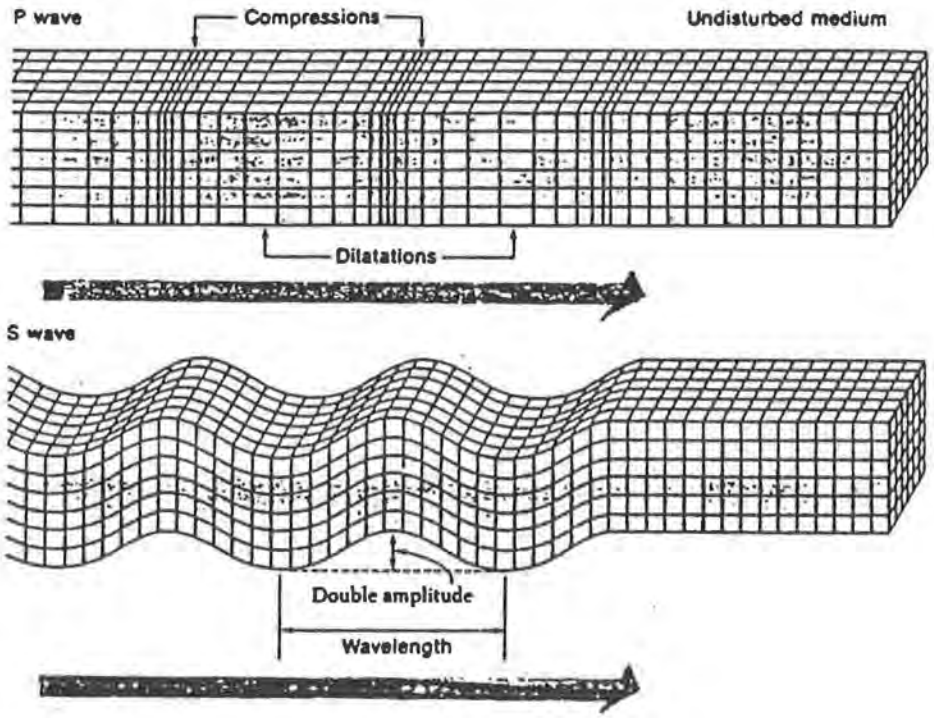

4.6.1. - Schematic of Compression and Shear Waves (Bolt 1976).

perpendicular to the direction of particle motion. Compression wave disturbance causes the medium it is travelling in to undergo a volume change; some material is compressed as some is dilated. Shear waves distort the medium, but no volume change occurs. P-waves travel faster than S-waves; however, S-waves are not greatly influenced by the degree of soil saturation since water provides no shearing resistance. P-waves are greatly affected by saturation levels; for a saturated soil, P-waves may be representative of the fluid and not the solids. P-wave velocities typically range from 210 to 760 m/s for dry soils, but for a saturated soil, velocities will be close to 1,525 m/s. S-wave velocities typically range from 120 to 430 m/s (Hoar and Stokoe 1978).

4.6.3 Crosshole Seismic Test

Crosshole tests have been accepted as the most reliable method for determining soil shear wave velocity (Gazetas 1991). Unlike downhole methods, the CHT allows for only the soil at the test depth to be considered in shear wave velocity measurement; therefore, a more refined knowledge of a site's stratification is possible. However, due to excessive test time and costs associated with preparation of a 3-borehole array, the CHT is not attractive for routine investigations.

In the preferred arrangement, three borings are made such that they are aligned 3 to 4.6 m apart center-to-center (Figure 4.6.2) These holes are cased with plastic pipe, and the casing is grouted in place to ensure good soil coupling. Upon grout curing, a wave source and two receivers are lowered to the same depth in the boreholes and clamped in place by either mechanical springs or by inflation of a rubber balloon with air. The wave

source can be positioned to generate shear waves polarized in the vertical or horizontal direction, and the wave travel times are measured by the two receivers. Upon fulfillment of ASTM D 4428 (1991) requirements, the wave velocities are then determined for a particular test depth by dividing the travel distance by the travel time between the two receivers.

The success of the CHT depends on several factors. The verticality and orientation of the holes must be determined so that correct wave travel distances are found for the wave velocity calculations. To aid in this, inclinometers are sometimes used to define the profile of the boreholes. Also, the source must be in good contact with the soil and rich in S-wave energy; otherwise, discerning first arrival times of both the P- and S-waves will be difficult at best. The receivers need to have adequate frequency response range; in addition, the correct orientation of the receivers greatly enhances the clarity of wave signal reception. The CHT can be conducted by using just two borings, but time errors due to triggering delays can adversely affect the computed wave velocities.

4.6.4 Downhole Seismic Methods

Downhole seismic testing tends to be more economical than crosshole testing. The downhole method requires only one borehole, one or more borehole receivers, trigger transducer, and surface-generating shear wave source. A typical setup can be seen in Figure 4.6.3. The borehole can be prepared with casing and grout in similar manner to the CHT.

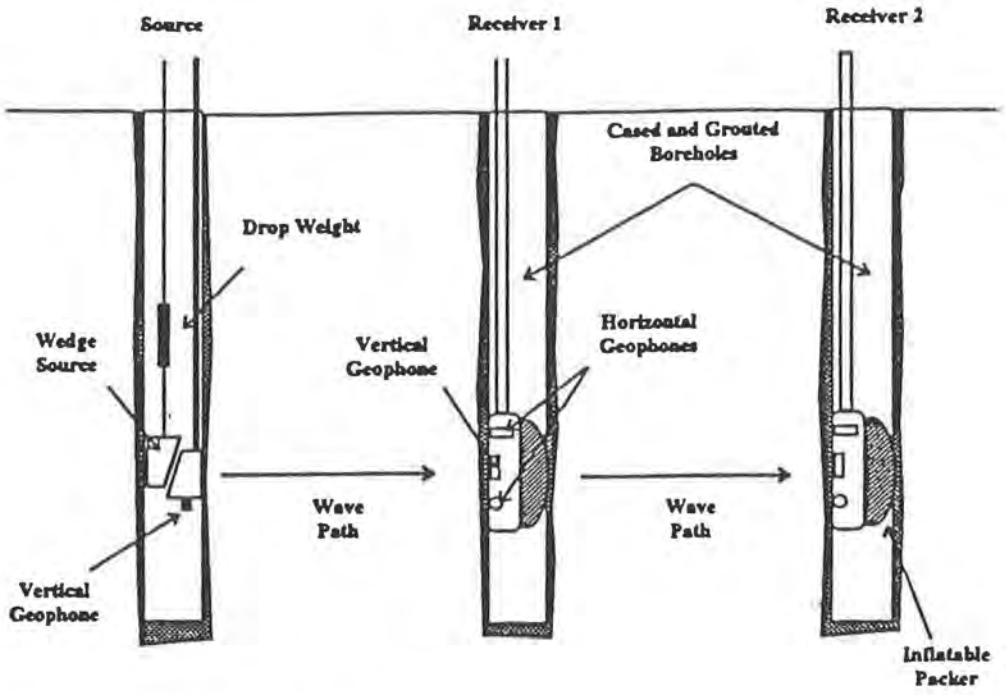

4.6.2. - Crosshole Test Setup (Kates 1996).

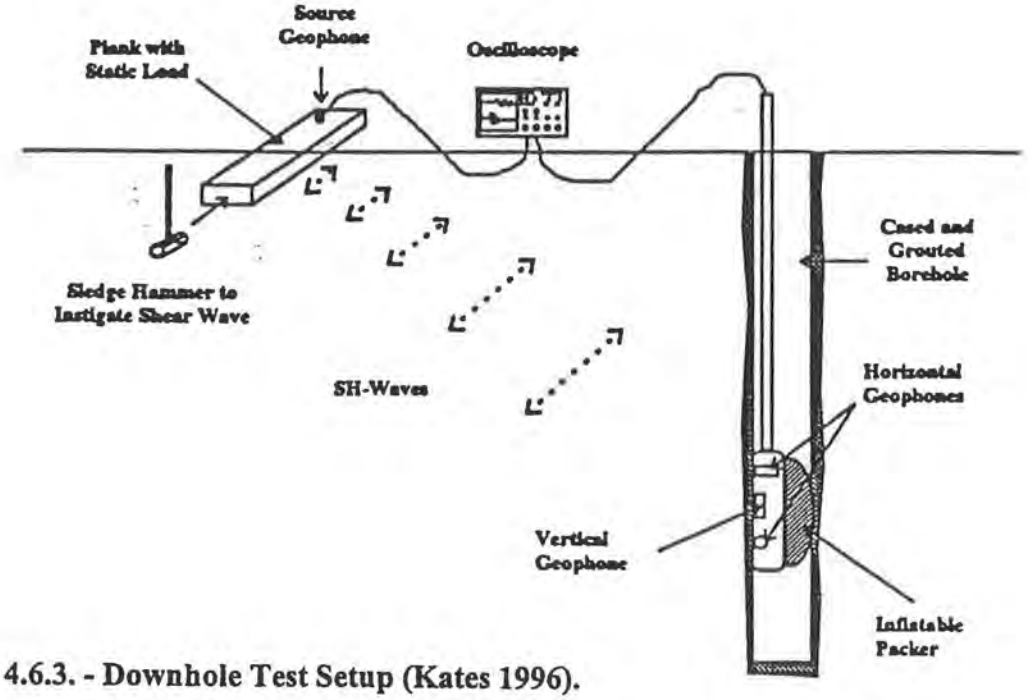

4.6.3. - Downhole Test Setup (Kates 1996).

A test is begun by lowering the borehole receiver to a desired depth and positioning it securely. The next step involves creating horizontally polarized shear waves. These waves are typically instigated by striking a vertically loaded plank, which is aligned perpendicular to the desired wave path, horizontally with a sledge hammer; proper plank orientation can greatly minimize compression wave disturbance. The trigger geophone is usually attached to the plank so that impulse start time can be measured. The travel time of the waves through the soil to the receiver is determined by a signal conditioner such as an oscilloscope.

Downhole methods allow for velocity measurements to be made by either the pseudo-interval or true-interval methods. The pseudo-interval shear wave velocity is found by taking the difference in travel distance at two consecutive test depths and dividing it by the difference in arrival time for the two depths. The true-interval method requires two receivers to be positioned a set distance apart; unlike the pseudo-interval method, the difference in initial receiver responses can be measured directly from a single impulse. Although the true-interval method is more expensive and complicated (two receivers and a multichannel oscilloscope are necessary), many potential problems with the pseudo-interval method, such as choosing a first arrival, triggering signal errors, and using multiple impulses instead of one, are eliminated.

4.6.5 Direct-Push Seismic Tests

By incorporating velocity transducers with direct-push probes such as the flat dilatometer and the cone penetrometer, small strain properties of the soil being tested can

be cost-effectively considered along with the respective test's traditional intermediate- to high-strain evaluations. These tests operate in a seismic downhole manner (Campanella et al. 1986; Hepton 1988). In addition, good soil to receiver contact is almost guaranteed due to the manner of probe insertion.

The seismic cone penetration test (SCPT) was introduced by Robertson et al. (1986) in order to determine in-situ shear wave velocity information to be used along with traditional CPT measurements. Since its inception, the SCPT has proven itself reliable in a number of soil types, and when coupled with piezocone capabilities (SPCPT), it is generally considered the premier soil logging tool. However, difficulty in penetrating cemented materials and dense cohesionless deposits can limit its use in certain geologies.

The seismic dilatometer test (SDMT) was first developed by Hepton (1988). His SDMT used two receivers mounted in the push rods one meter apart. The SDMT has some similar advantages and disadvantages compared to the SCPT; however, the SDMT is more simple and robust. A typical SDMT arrangement can be seen in Figure 4.6.4. The SDMT allows for wave travel time measurements to be made at any depth it can be pushed, but for the SCPT, these measurements are typically made at discrete increments corresponding to rod changes so that the other CPT measures are taken during a proper penetration rate.

4.6.6 Usage in the Piedmont

Several studies of Piedmont small-strain shear moduli have been conducted by North Carolina State University (NCSU). One such investigation involved taking Shelby tube

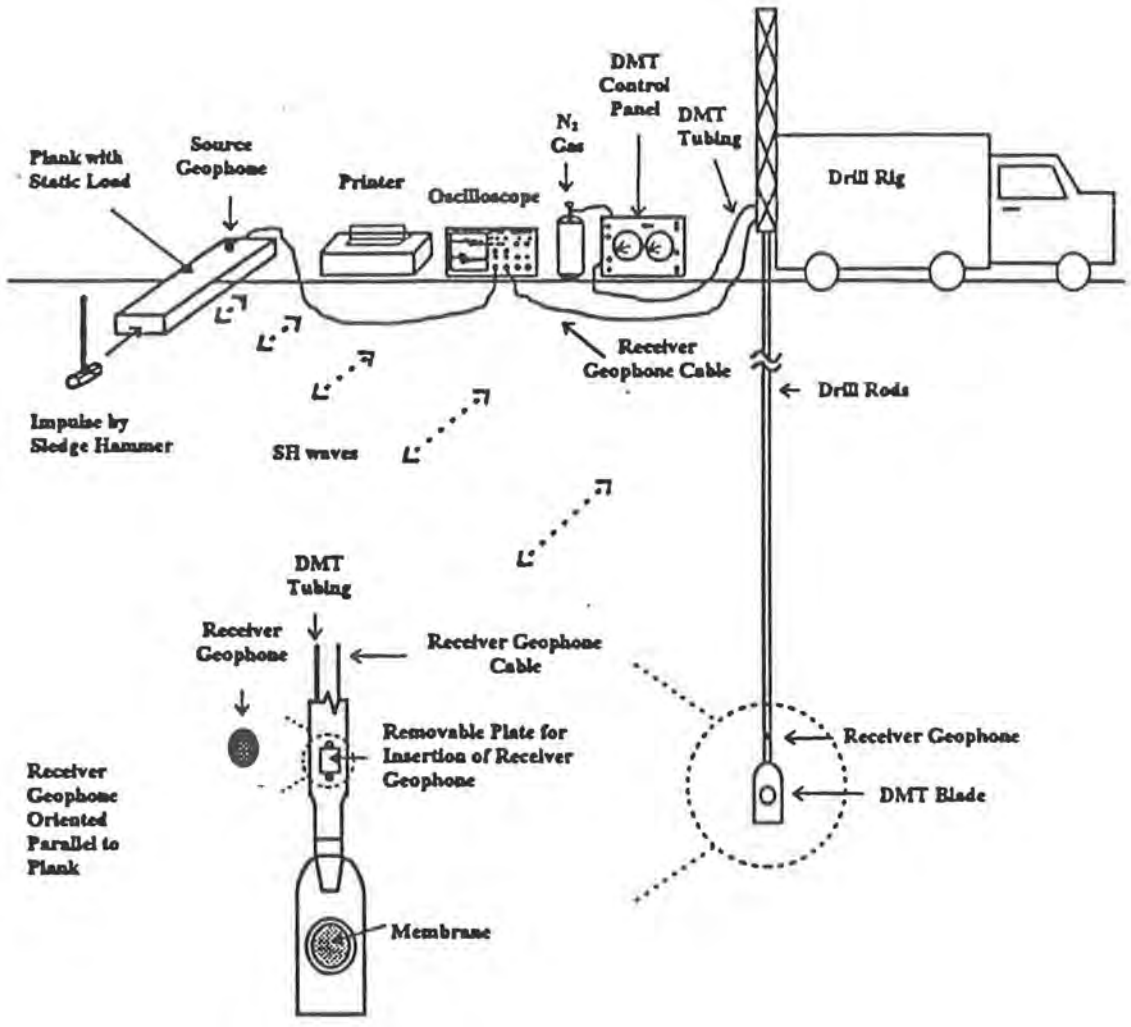

FIG. 4.6.4. - Seismic Dilatometer Test Setup (Kates 1996).

samples of saprolite from seven sites from depths of 1 to 5 meters. Resonant column testing was subsequently performed on these samples. For the same confining pressures, more granular samples produced higher modulus values. Small-strain shear moduli ranged from 25 to over 100 MPa (Borden et al. 1996). Another study by NCSU found the normalized shear modulus versus shearing strain curve of Piedmont soils from one research site to fall on the lower bound of the residual soils range given by Borden et al. (1994), as shown on Figure 10.1.2.

CHAPTER 5

LABORATORY TESTING

5.1 Introduction

Although laboratory soil testing has advanced in recent years, the conventional triaxial test is still "the" reference test for determining effective stress shear strengths. It is also quite frequently used to determine undrained shear strength. The triaxial test's popularity stems from the capability to control the all-around stress, consolidation, and shearing conditions on a sample. In addition to providing shear strength information, the triaxial test has been used successfully for several decades in providing insight into soil stress-strain relationships, consolidation, and permeability. Due to its widespread use, the particulars of triaxial testing are fairly well documented (e.g., Bishop and Henkel 1962), but as for any laboratory test, its effectiveness depends largely upon proper interpretation of results and the testing of samples which are of high quality and are representative of the soil deposit in question.

The triaxial test is one of the most common lab tests for several reasons. A state-of-the-art paper by Baldi et al. (1988) discusses several aspects of conventional triaxial testing. Some of the main advantages cited include the following:

1. relative simplicity of drainage control and pore pressure measurement
2. ability to apply principal stresses in known directions

3. ease of measuring axial and volumetric strains
4. use of cylindrical samples which are obtained from standard tube samples
5. equipment versatility for measuring different soil properties

The triaxial test is not without limitations, however. Some of these disadvantages include:

1. stress state limitations: only compression and extension testing; anisotropy and principal stress rotation cannot be investigated
2. even when test limitations such as rate effects and end restraint condition are ignored, reliance on experience for data interpretation prior to usage is necessary
3. relatively undisturbed samples required for meaningful testing
4. stress relief of samples due to sampling process (i.e. disturbance)

5.2 Test Types

Laboratory tests should model field conditions in order to produce meaningful results. To evaluate the shear strength of soils in cases of relatively quick loading (which cause transient pore pressures) the recovered soil specimen should be consolidated back its at rest earth pressures and no drainage should be allowed during shearing in order to gain the total stress (or short term) strength. Conversely, if the loading occurs slowly such that excess pore pressures are dissipated or if the stability of a foundation, embankment, etc. is questioned, the test should allow for drainage during shearing in order to determine the effective stress (or long term) strength.

The triaxial apparatus allows for two distinct testing phases - consolidation and shearing. If allowed, consolidation takes place after application of either anisotropic (such as K_o) or isotropic stresses to the soil sample as water from the sample is allowed to drain. Conditions of consolidation prior to shearing and drainage during application of the deviator stress differentiate the types of triaxial tests. They include the unconsolidated-undrained (UU) test, consolidated-undrained (CU) test, and consolidated-drained (CD) test.

The UU and CU tests can be used to find the maximum undrained shear strength (S_u) which is useful for a total stress analysis. The UU test does not involve consolidation of the sample prior to shearing; rather, a confining pressure is applied to the specimen prior to shearing without allowing drainage. The UU test includes a much faster rate of loading of the soil compared to the CU or CD tests because the change in pore pressures due to loading are not measured. Undrained testing assumes zero volume change during loading, but S_u is not a fundamental soil property and is related more to test conditions (e.g. Kulhawy and Mayne 1990). CU tests typically give higher values of S_u than do UU tests because the sample has been consolidated and this may mitigate some detrimental effects of sample disturbance. However, the UU and CU tests tend to more closely agree than do the predictions of the unconfined compression test (UC); the UC test is basically a UU test with no confining pressure applied (Chen and Kulhawy 1993). UU and UC tests are popular in practice because of their low cost and short testing time compared to other tests.

The CU and CD tests can be used to determine effective stress strength parameters as defined by Mohr-Coulomb failure criteria. The CD test gives effective stress strength

directly because the test is run slowly enough to prevent excess pore pressures and effective stresses are thus controlled; the CU test with pore pressure measurements can provide the same parameters. The CU test controls only total stresses, and effective stresses are computed using measured pore pressure changes. CU tests are typically conducted in considerably less time than CD tests since equalization of excess pore pressures occurs more quickly than drainage of the same. CU tests also give insight into the undrained behavior of soils as well as the effective stress strength parameters which might be used for long term conditions. Therefore, CU tests are much more common for commercial use when effective stress strength must be evaluated.

5.3 Apparatus and Operation

A typical test configuration is shown in Figure 5.3.1. The UU test procedure has been standardized by ASTM D 2850 (1982), and the CU test method has been standardized by ASTM D 4767 (1988). The CD test method and other testing details are described at length in the literature (e.g., Bishop and Henkel 1962; Holtz and Kovacs 1981).

5.4 K_o vs. Isotropic Consolidation

In situ stress conditions are typically anisotropic, but isotropic stress conditions are generally used in routine triaxial tests. Anisotropic consolidation near the at rest earth pressure ratio (K_o) would provide the most realistic testing conditions and best

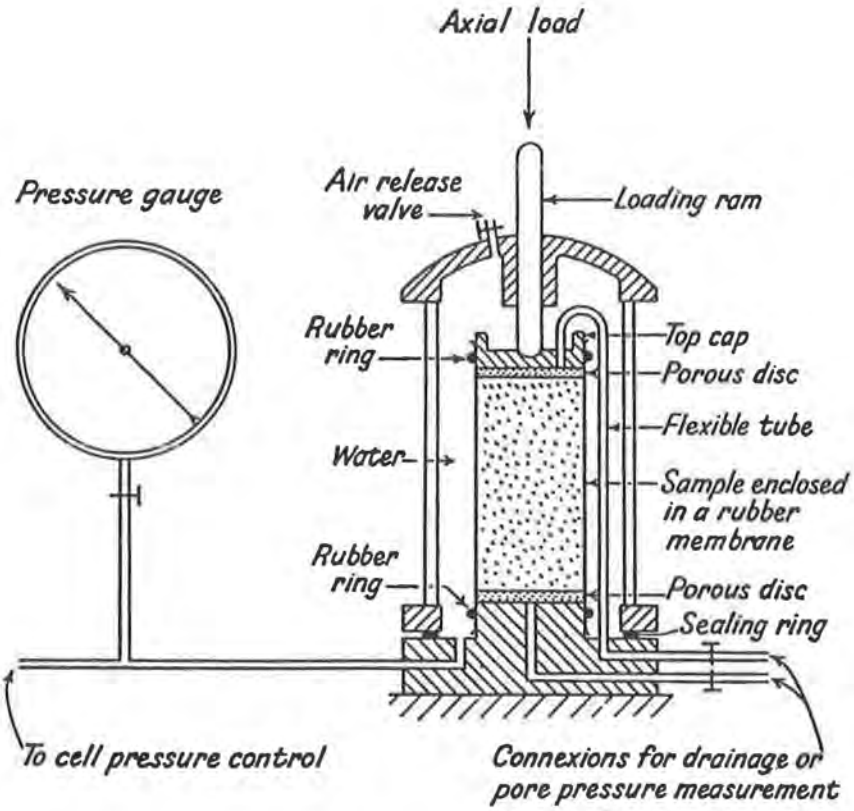

FIG. 5.3.1. - Schematic Layout of Triaxial Test (Bishop and Henkel 1962).

strength and stiffness estimates, but anisotropic consolidation requires complicated procedures and extra periods of time compared to isotropic consolidation.

Donaghe and Townsend (1978) reported that many investigators have both confirmed and denied the conclusions of previous researchers regarding the effect of consolidation ratio (K_c). In their study involving CU tests, they found that, regardless of K_c, effective friction angle did not vary when values to construct the failure envelope were taken at the maximum principal stress ratio. It was also reported that K_c had a major role in the stress-strain behavior; axial strains generally decreased with decreasing K_c. Finally, isotropic specimens produced higher S_u values than anisotropic specimens with the same vertical consolidation stress. The nature of the soil's anisotropy no doubt plays some role in the extent of soil property variation between isotropic and K_o consolidated samples.

5.5 Multi-Stage Testing

The multi-stage test involves using one soil sample to define a Mohr-Coulomb failure envelope. In principle, this method can be used with CU or CD testing. Since effective stress strength is almost linear over a considerable range of confining stresses for most soils, multi-stage testing is sometimes used when soil samples are scarce or nonhomogeneous such that obtaining a similar sample at the same depth is highly unlikely. Multi-stage testing also reduces overall testing time. Bishop and Henkel (1962) report that some loss in accuracy occurs in effective cohesion and friction angle prediction when using this technique. This testing principle should also be used

cautiously for strongly cemented soil because shearing beyond failure at any stage will greatly distort the soil structure (Saeedy and Mollah 1988).

Testing is comprised of shearing a single specimen to near failures at several elevated lateral pressures while measuring the corresponding deviator stresses at which these failures occur. Soranzo (1988) suggested that multi-stage testing should not be conducted if the expected peak shear stress is not expected for axial strains of at least 8%. Soranzo also reported very comparable results between conventional and multi-stage UU and CIUC tests on normally and overconsolidated cohesive soils.

5.6 Usage in the Piedmont

Sowers (1963) presented triaxial test results and noted the difficulty in characterizing soil strength and stiffness in Piedmont soils due to the inherent heterogeneity, especially in the saprolite and partially weathered zones. The spacial variation of minerals and twisted, contorted banding make the soil very nonhomogeneous over depth. As might be expected, great scatter in strength test data was observed by Sowers and Richardson (1983) after a large number of CU and CD tests were performed as shown in Figure 5.6.1. They noted that the average trend of saturated saprolite was that it does not exhibit true cohesion, but some samples did appear to.

Sowers (1963) also commented on the difficulty of obtaining truly undrained shear because of the relatively high permeabilities often encountered in the Piedmont. These high permeabilities allow CD tests to be performed somewhat rapidly when compared to tests on clayey soils.

Lambe and Heartz (1986) reported triaxial testing on samples from at a North Carolina State University research site which contained soils weathered from gneiss and schist bedrock. They noted that the soils were micaceous, nonplastic silts and had common residual soil characteristics such as slickensides, steeply dipping foliation, and quartz seams which made the trimming of shelby tube and block samples difficult. It was observed that in these samples, dipping foliation caused them to bend during isotropic consolidation and shearing to failure. This bending necessarily affects the uniformity of stresses and strains. In addition, uneven platen seating requires an extrapolation to zero for the deviator stress vs. axial strain curve; therefore, the stress-strain relationship and strength of the soil can be in error to varying degrees.

Multi-stage testing in Piedmont soils was also investigated by Lambe and Heartz (1986). One block sample was used to prepare three samples for conventional CIUD tests and one sample for multi-stage CIUD testing. During the first two stages, the multi-stage sample failed within 10% of the single stage tests run at the same consolidation pressure, but for the third stage, the multi-stage specimen bent badly and failed at 30% less strain than the corresponding single stage test.

The validity of multistage testing in Piedmont soils was inconclusive. However, variability of residual soils makes multistage testing an attractive alternative so that a complete failure envelope can be found for one specimen; in other words, the same material is being tested throughout as opposed to greatly differing samples taken a short distance apart. The triaxial test will remain a valuable tool for studying Piedmont residual soil behavior, but the characteristics of these soils will increase the variability of results when compared to sedimentary deposits.

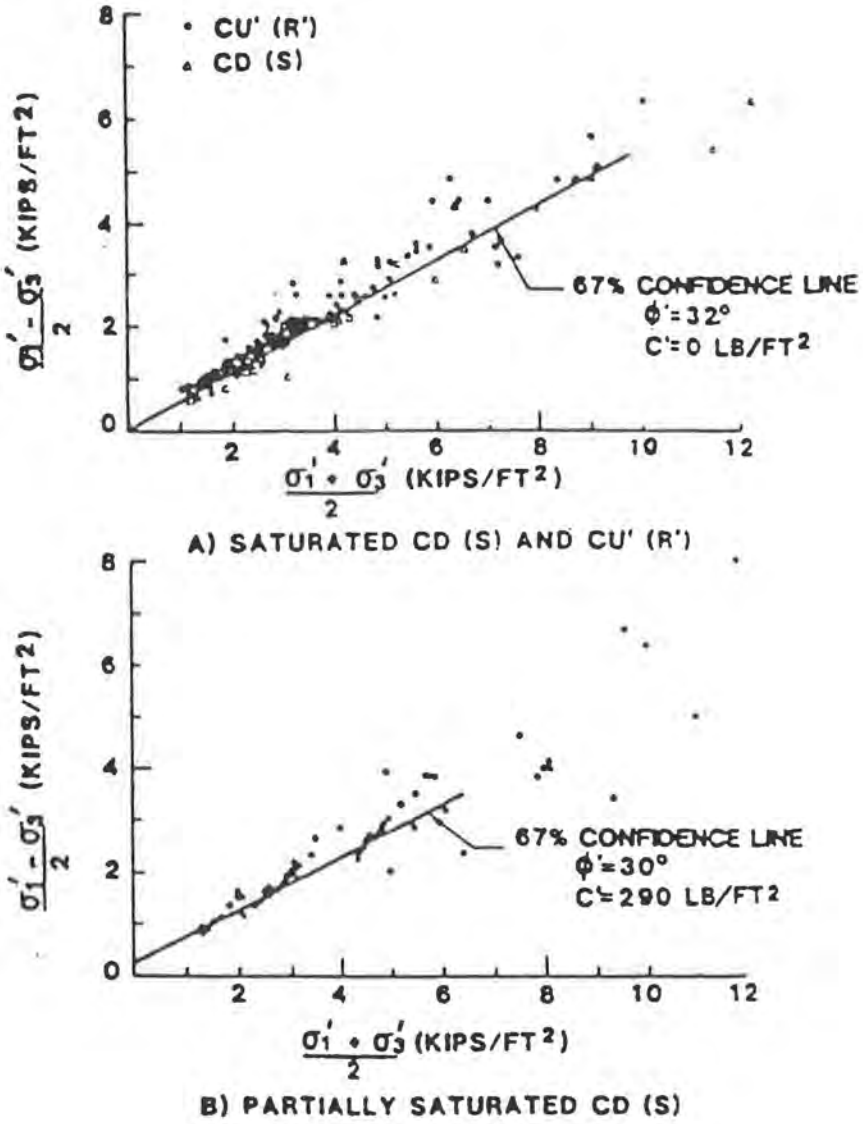

FIG. 5.6.1. - Saprolite Mohr-Coulomb Failure Envelopes : a.) Saturated Samples; b.) Partially Saturated Samples (Sowers 1983).

CHAPTER 6

SITE LOCATION AND TESTING PROGRAM

6.1 Site Location Maps

The maps in this chapter detail the location of the Spring Villa Test Site near Opelika in Lee County, Alabama. The site's general location in relation to major interstate and state highways and county roads near Opelika and Auburn, Alabama is given on Figure 6.1. Figure 6.2 provides the site's position relative to Lee County Road 151 which lies adjacent to the site. Surveyed cone penetration test (CPT) locations along with relative elevations in units of [feet] are shown in Figure 6.3. Finally, Figure 6.4 gives a detailed view of the concentrated test area where most in-situ testing and sampling for laboratory tests were performed. This area is denoted by the rectangle on Figure 6.3.

6.2 Testing Program Summary

The test program to characterize the Spring Villa Test Site began at the beginning of January 1996 after the site was generally cleared of brush and small trees. The various tests, the test locations, and the depth range of testing are listed in Table 6.1. The test locations mentioned in this table can be seen on Figure 6.3 or 6.4. It should be noted that all testing

included in this study was completed prior to drilled shaft construction which began in the spring of 1997.

Table 6.1. - Testing Program Summary.

Test Type	Locations	Depth Range (meters)
Isotropically Consolidated-Undrained Triaxial Compression (CIUC) Tests	B-2, B-5, B-7, B-8	4 to 15
Unconsolidated-Undrained Triaxial Compression (UU) Tests	B-2, B-5, B-6, B-7, B-8	1 to 3
Isotropically Consolidated-Drained Triaxial Compression (CIDC) Tests	B-8	10
Cone-mounted Pressuremeter Test (CPMT)	C-41, C-42, C-43, C-44	1 to 12
Menard Pressuremeter Test (PMT)	B-2, B-5	1 to 15
Flat Dilatometer Test (DMT)	AU1, AU2, AU3	< 1 to 8
Seismic Flat Dilatometer Test (SDMT)	AU1, AU2, AU3	< 1 to 8
Seismic Cone Penetration Test (SCPT)	C-41, C-42	< 1 to 15
Cone and Piezocone Penetration Test (CPT)	C-11, C-12, C-13, C-14, C-15, C-16, C-17, C-18, C-21, C-22, C-23, C-24, C-25, C-26, C-27, C-32, C-41, C-42, C-43, C-44	<1 to 25
Piezocone Pore Pressure Dissipation Test (PCPT)	C-23, C-43, C-44	7 to 17
Standard Penetration Test (SPT)	B-2, B-5	1 to 15
Crosshole Seismic Test (CHT)	Array #1 : B-1, B-2, B-3 Array #2 : B-4, B-5, B-6	<1 to 15
Iowa Borehole Shear Test (BST)	B-7, B-8	2 to 9

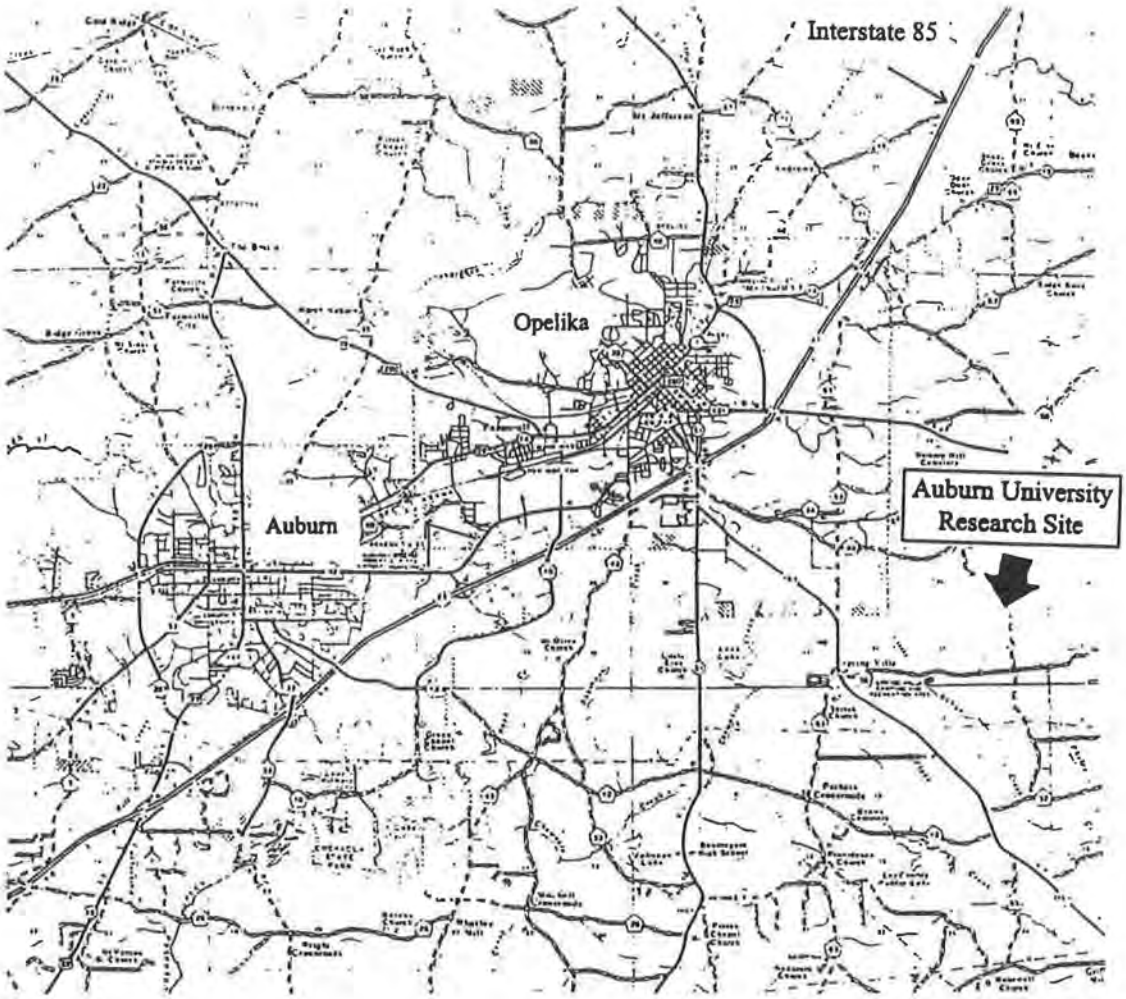

FIG. 6.1. - General Site Location Map.

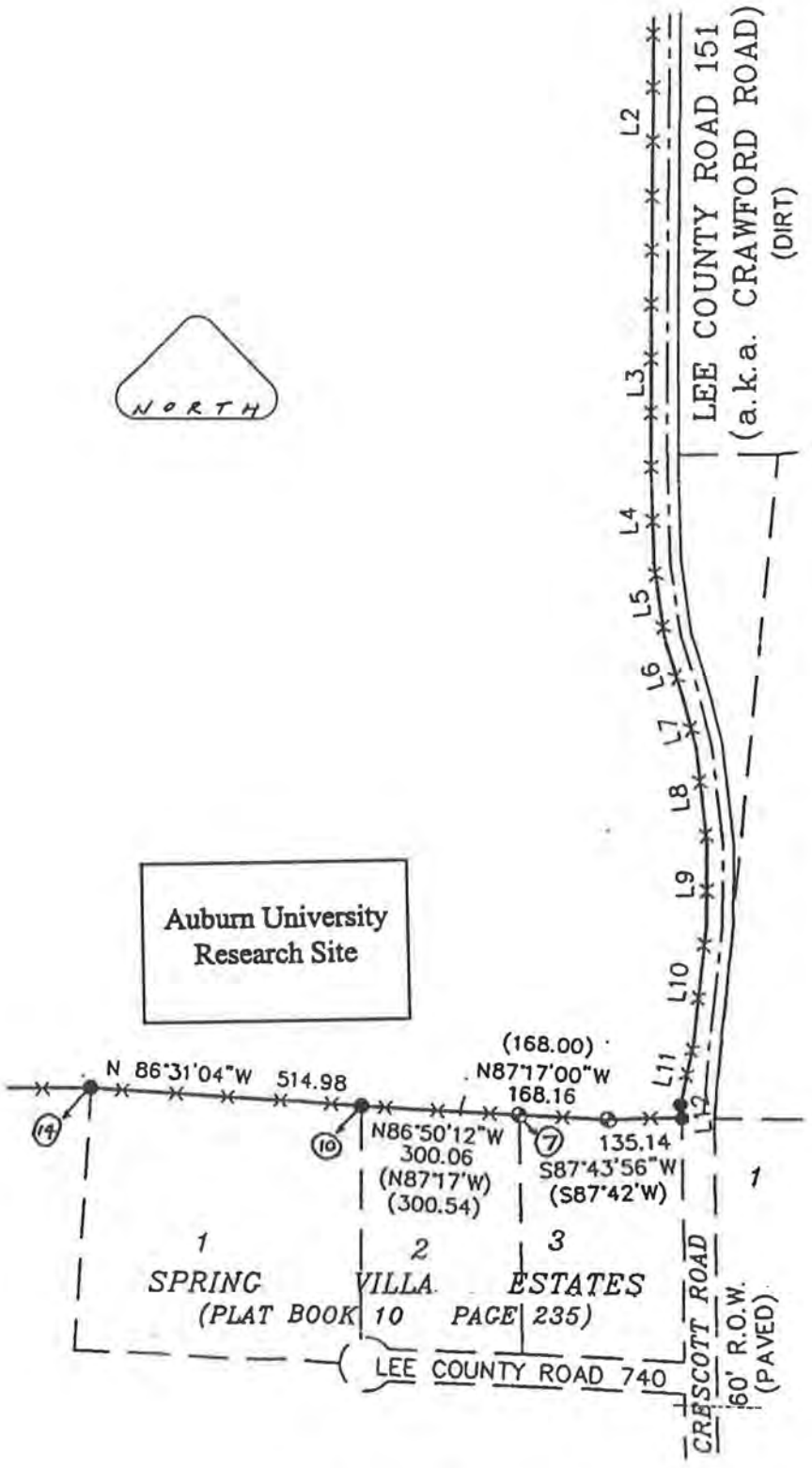

FIG. 6.2. - Specific Site Location Map.

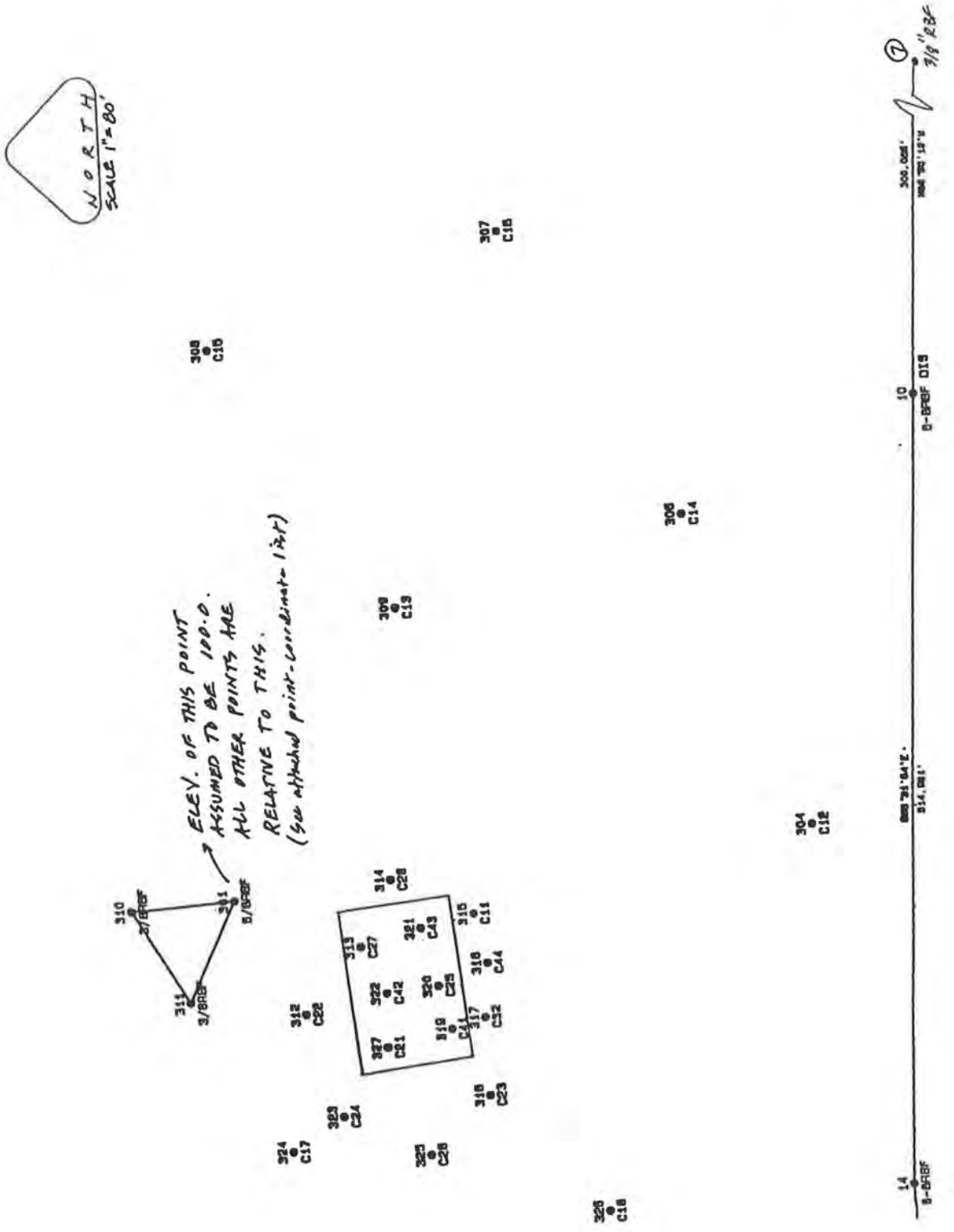

FIG. 6.3. - Survey Map of Cone Penetration Test Locations.

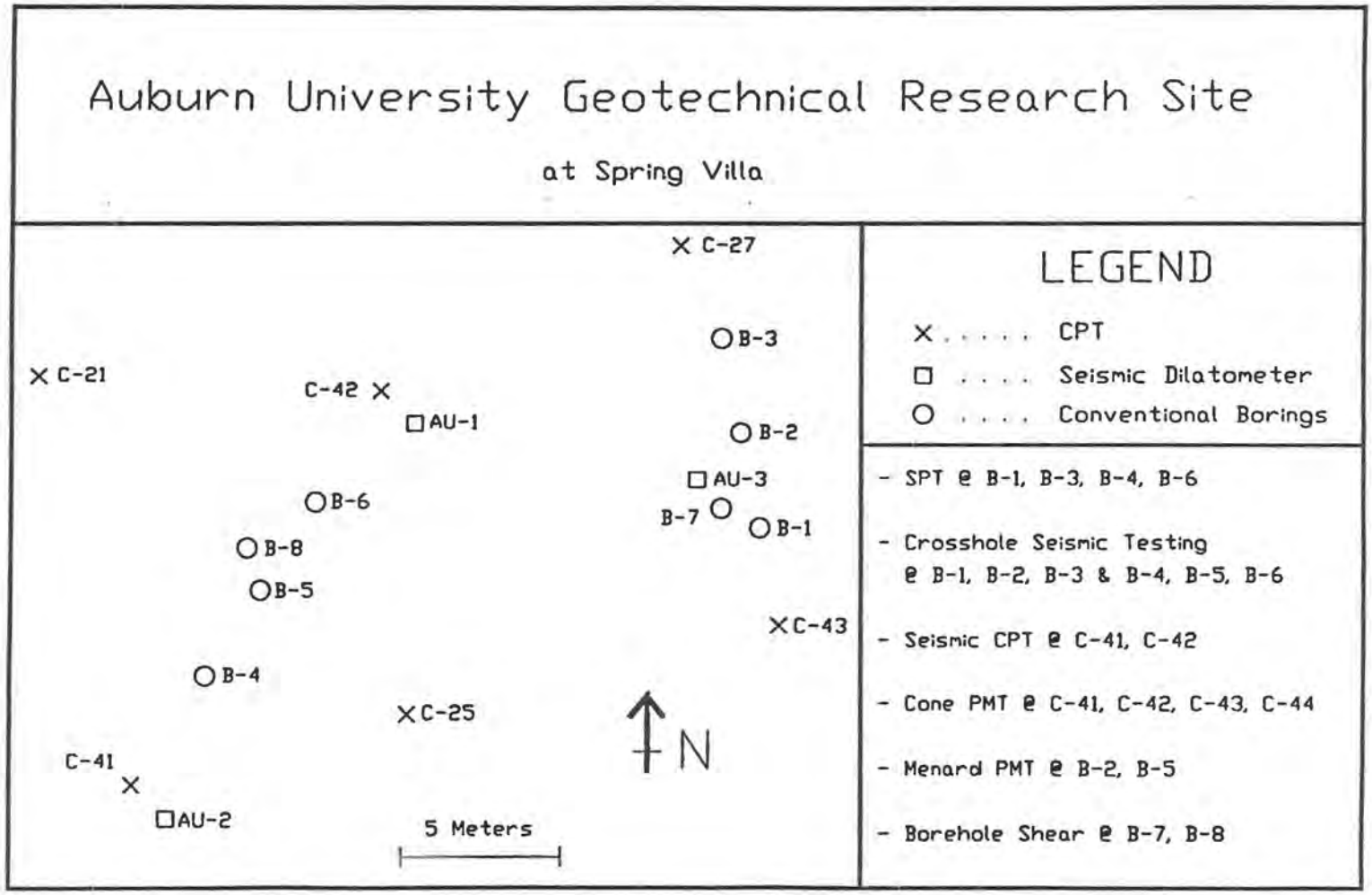

FIG. 6.4. - Detailed Map of Concentrated Testing Area.

CHAPTER 7

SITE GEOLOGY AND STRATIGRAPHY

7.1 Geology

Auburn University's Geotechnical Research Site at Spring Villa is located in the southwest portion of the Piedmont province. More specifically, the site resides in the Southern Piedmont, which was formed from Precambrian to Paleozic era high-grade metamorphic and igneous rocks; the residual soils are primarily of the Wacoochee Complex. The site geology can be further classified as being either Halawaka Schist or Phelps Creek Gneiss. The Halawaka Schist contains feldspathic muscovite-biotite schist and quartz-diorite gneiss; it can locally contain lenses of muscovite-graphite schist and amphibolite and is commonly cut by feldspathic veins and pegmatites. Phelps Creek Gneiss is made up of quartz monzonite to granite gneiss in dikes and sheets with wide migmatite zones at contacts (Osborne et al. 1988).

In addition, drilling logs from the various borings performed at the site note that most recovered soil samples were sandy and micacious. Quartz sand seams and weathered mica schist were also prevalent.

7.2 Stratigraphy Characterization by Index Testing

The site's stratigraphy has been characterized by conventional borings from which split-spoon samples from SPT and Shelby tube samples for triaxial testing were taken at various depths. Most of these samples were tested to determine the following index properties : in-situ water content, Atterberg limits, and grain size distribution (GSD). Figure 7.2.1 shows a summary of all samples where either in-situ water contents and/or Atterberg limits were determined. Figure 7.2.2 summarizes the GSD of all samples which were tested; a majority of the samples were analyzed solely by sieve analysis to the (-) # 200 sieve opening size. Table 7.2.1 presents three specific gravity values and these samples' depths. Figure 7.2.3 shows the variation in wet unit weight vs. depth as determined from trimmed triaxial samples. Individual boring plasticity profiles, GSD curves, sample classifications, and further explanations for the determination of physical properties, such as effective overburden pressure, which were used in the mechanical property correlations discussed in subsequent chapters are included in Appendix A.

Table 7.2.1. - Specific Gravity Results.

LOCATION	DEPTH	SPECIFIC GRAVITY
Boring B-7	6 meters	2.84
Boring B-7	8 meters	2.73
Boring B-7	10 meters	2.77

A summary of all index test data is shown in Table 7.2.2. From examination of the various index tests, the site shows the characteristic Piedmont residual soil profile. The upper zone extends to approximately 2 to 3 meters below the ground surface, and the saprolite zone extends below the upper zone to at least the greatest depth of sampling at

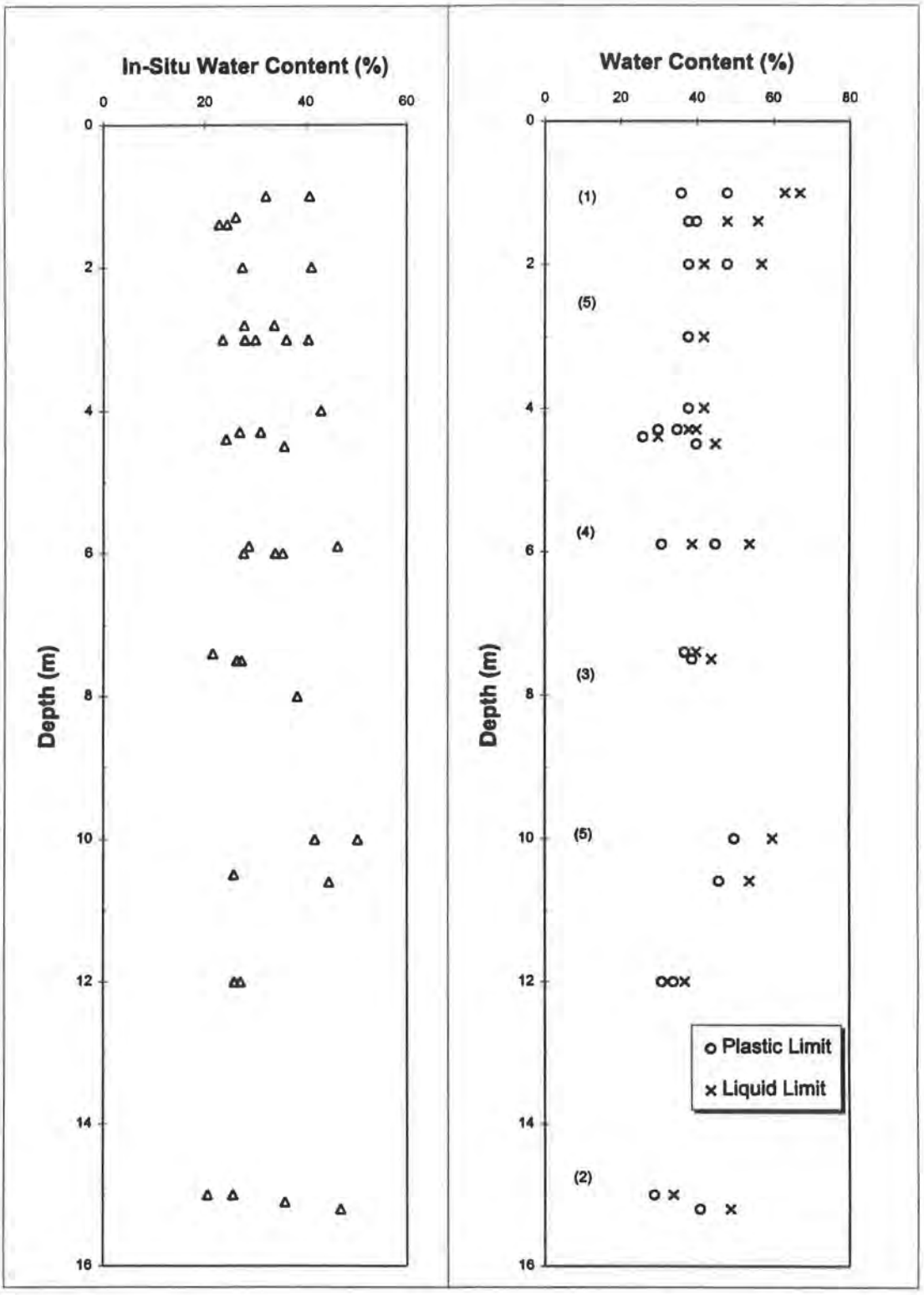

Note : Numbers in parentheses represent the number of samples which were nonplastic at that depth.

FIG. 7.2.1. - In-Situ Water Contents and Atterberg Limits.

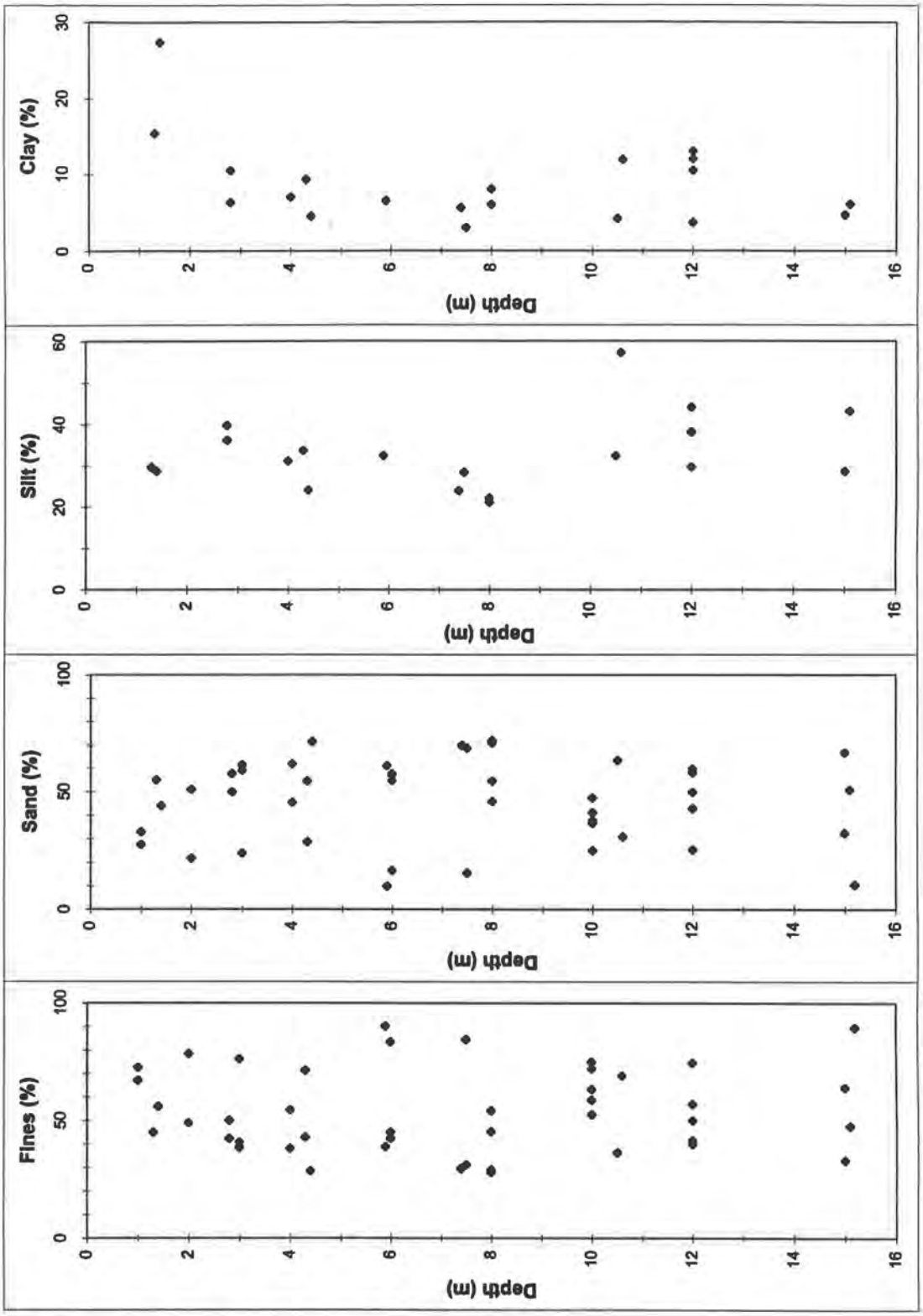

FIG. 7.2.2. - Particle Size Distribution Summary.

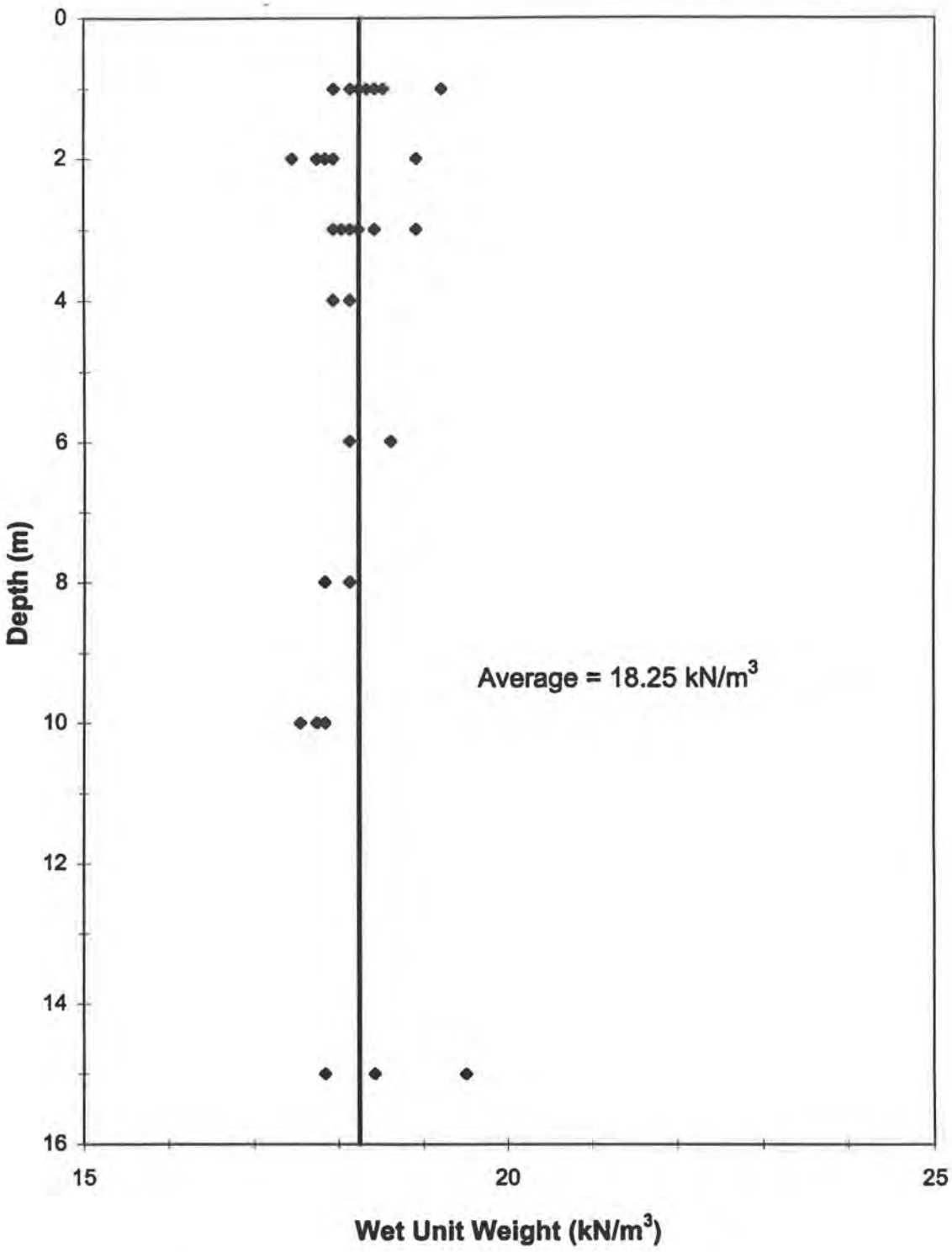

FIG. 7.2.3. - Wet Unit Weights from Trimmed Triaxial Samples.

Table 7.2.2. - Summary of Index Testing.

Index Property	Number of Tests	Average	Standard Deviation
Water Content (%)	64	34.0	7.5
Liquid Limit (%)*	22	46.3	10.0
Plastic Limit (%)*	22	38.1	6.5
Plasticity Index (%)*	22	8.2	5.9
Wet Unit Weight (kN/m^3)	35	18.25	0.51
Dry Unit Weight (kN/m^3)	35	13.32	0.89
Sand Content (%)	48	46.7	17.2
Silt Content (%)	22	33.0	8.4
Clay Content (%)	22	9.5	6.4

* 20 samples reported as "nonplastic" are not included in these values.

15 meters. Also, during the span of all testing, ground water table depths varied approximately between 2 and 4 meters.

Samples from the upper zone classified as either MH, ML, or SM according to the Unified Classification System (UCS); American Association of State Highway and Transportation Officials (AASHTO) classifications included A-4, A-5, and A-7-5 designations. The upper zone samples tended to show greater plasticity ranges than the deeper samples; in addition, the percentage of clay-sized particles was higher in the upper zone and remained basically constant over the saprolite zone.

The saprolite zone is composed of alternating UCS classifications of sandy silts (ML) and silty sands (SM) with an occasional MH; the corresponding AASHTO classifications were A-2-4, A-4, and A-5. The saprolite generally contained a higher percentage of nonplastic samples than the upper zone as would be expected for Piedmont soils.

The percentage of silt particles showed steady increase over depth; wide scatter was evident in the percentage of sand particles as the average value of percent passing remained relatively constant over depth at just below 50% as shown in Figure 7.2.1. Almost no gravel size particles were recovered in sampling for any depth. Wide scatter in plasticity and in-situ water content determination was also evident; in-situ water contents generally ranged from between 20% to 40% with an average of 34%. Wet unit weights exhibited rather large variation and were found to be between 17.5 and 19.5 kN/m^3. The variable nature of index testing of Piedmont soils, as reported by Sowers (1954, 1963), was clearly exhibited.

CHAPTER 8

SUMMARY OF TEST RESULTS

8.1 Standard Penetration Test

The Standard Penetration Test (SPT) was performed using an automatic hammer in borings B-1, B-3, B-4, and B-6; a plot of observed N-values for each boring is shown in Figure 8.1.1. The average N-values for the four borings are shown in Figure 8.1.2; the figure also shows the N-values plus or minus one standard deviation for the four tests. Table 8.1.1 shows the individual boring blow counts and corresponding test depths.

The first test was conducted in the upper soil zone; subsequent tests in the saprolite zone below the 2.8 meter depth generally resulted in increased N-values with increasing depth. The standard deviation was somewhat constant except for the tests between 12 and 15 meters; a substantial increase in comparative blow counts was observed in borings B-4 and B-6 at these depths. Perhaps a different mineral band runs through these depths at B-4 and B-6 compared to the other two borings since all borings showed general agreement at shallower depths.

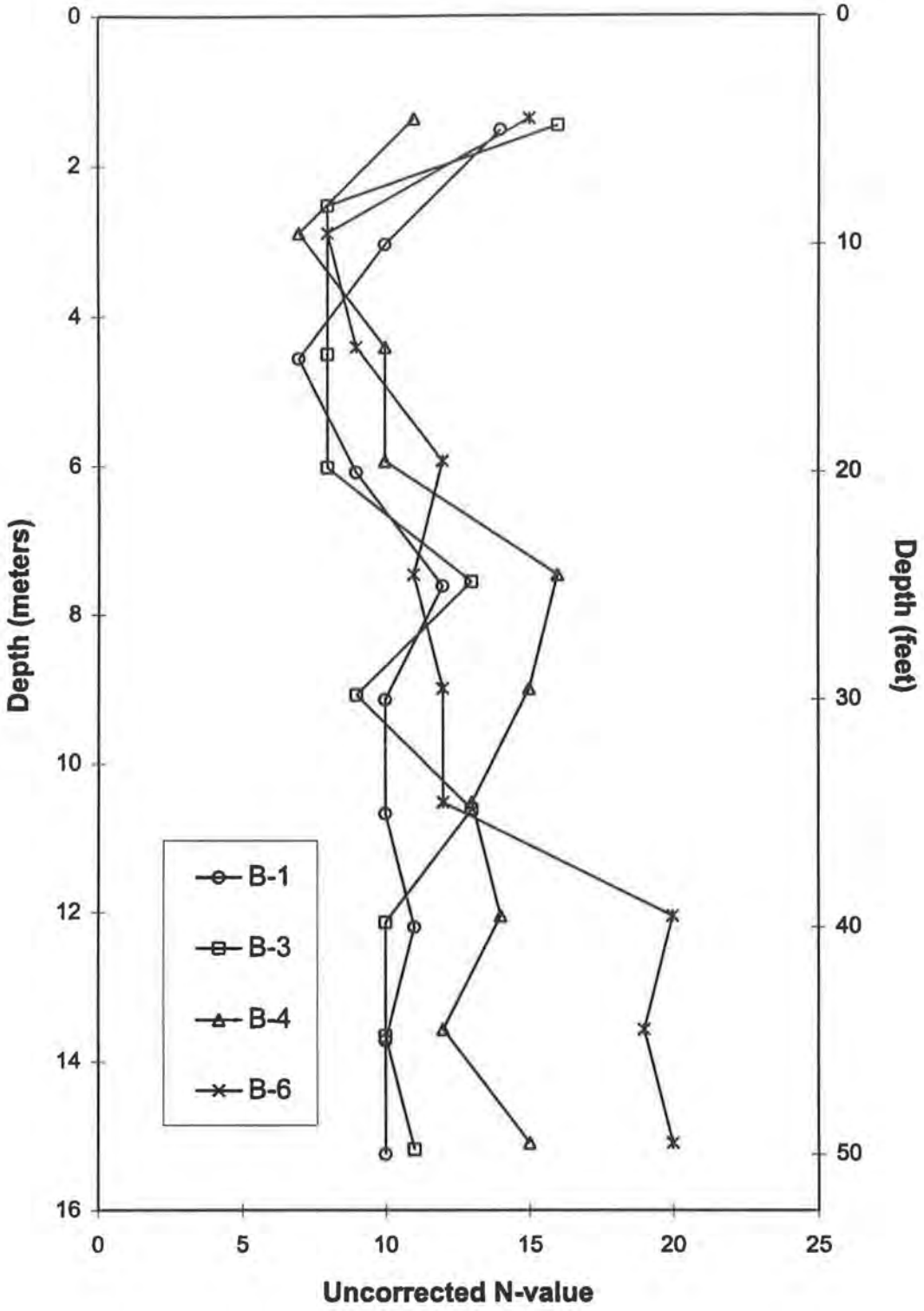

FIG. 8.1.1. - Summary of SPT Results.

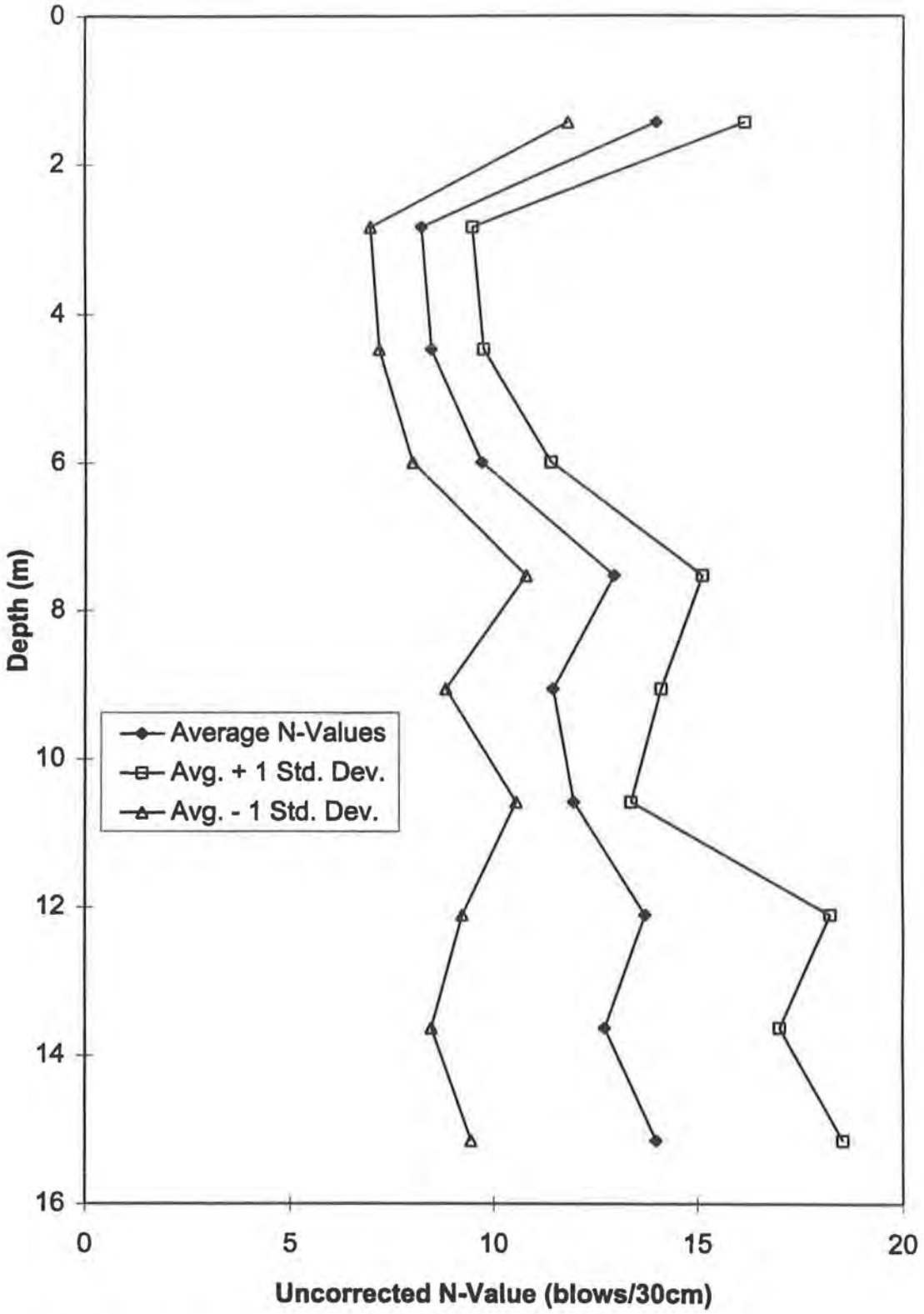

FIG. 8.1.2. - Average SPT Results.

Table 8.1.1. - Standard Penetration Test Results.

Boring :	B-1		B-3		B-4		B-6		Average Uncorrected N Values	Average Depth (m)	Standard Deviation of Uncorrected N Values	Avg. N + 1 St. Dev.	Avg. N - 1 St.Dev.
	N	meters	N	meters	N	meters	N	meters					
	14	1.5	16	1.5	11	1.4	15	1.4	14.0	1.4	2.16	16.2	11.8
	10	3.0	8	2.5	7	2.9	8	2.9	8.3	2.8	1.26	9.5	7.0
	7	4.6	8	4.5	10	4.4	9	4.4	8.5	4.5	1.29	9.8	7.2
	9	6.1	8	6.0	10	5.9	12	5.9	9.8	6.0	1.71	11.5	8.0
	12	7.6	13	7.6	16	7.5	11	7.5	13.0	7.5	2.16	15.2	10.8
	10	9.1	9	9.1	15	9.0	12	9.0	11.5	9.1	2.65	14.1	8.9
	10	10.7	13	10.6	13	10.5	12	10.5	12.0	10.6	1.41	13.4	10.6
	11	12.2	10	12.1	14	12.0	20	12.0	13.8	12.1	4.50	18.3	9.3
	10	13.7	10	13.7	12	13.6	19	13.6	12.8	13.6	4.27	17.0	8.5
	10	15.2	11	15.2	15	15.1	20	15.1	14.0	15.1	4.55	18.5	9.5

8.2 Cone and Piezocone Penetration Tests

The cone penetration test (CPT) was conducted at several locations on the site using a Hogentogler piezocone with tip cross-sectional area of 10 cm^2 and sleeve friction area of 150 cm^2; however, only the six locations (C-21, C-25, C-27, C-41, C-42, and C-43) adjacent to the soil borings were considered in finding average friction resistance values which were used in subsequent mechanical property correlations. Besides conventional cone and piezocone measurements, additional tests were performed adjacent to C-41 and C-42 using a seismic cone. The seismic CPT's were made using a Hogentogler piezocone of similar dimensions but with a geophone placed within the probe above the tip; these results are presented in Section 8.7.1.

The cone tip resistance (q_c), sleeve friction resistance (f_s), and friction ratio (R_f) values from the 6 soundings to a depth of 15 meters are shown in Figure 8.2.1, with average values as heavy lines. The average q_c values ranged from around 2,000 to 4,000 kPa with gradual increases over depth, and the f_s was fairly constant near or above 150 kPa. The R_f decreased from 8 to 4% between 1 and 15 meters, respectively. These results suggest fairly uniform conditions overall, but with lots of random spacial variability.

A plot of piezocone pore pressure measurements are shown in Figure 8.2.2 of three of the soundings mentioned above (C-41, C-42, and C-43) and three other piezocone soundings at locations shown in Figure 6.3. The porous element was located directly behind the tip (commonly referred to as the Type 2 position), and a mixture of 50% glycerine and 50% water was used to saturate the element prior to testing. As previously discussed in Section 4.2.3, different locations of the porous element will produce

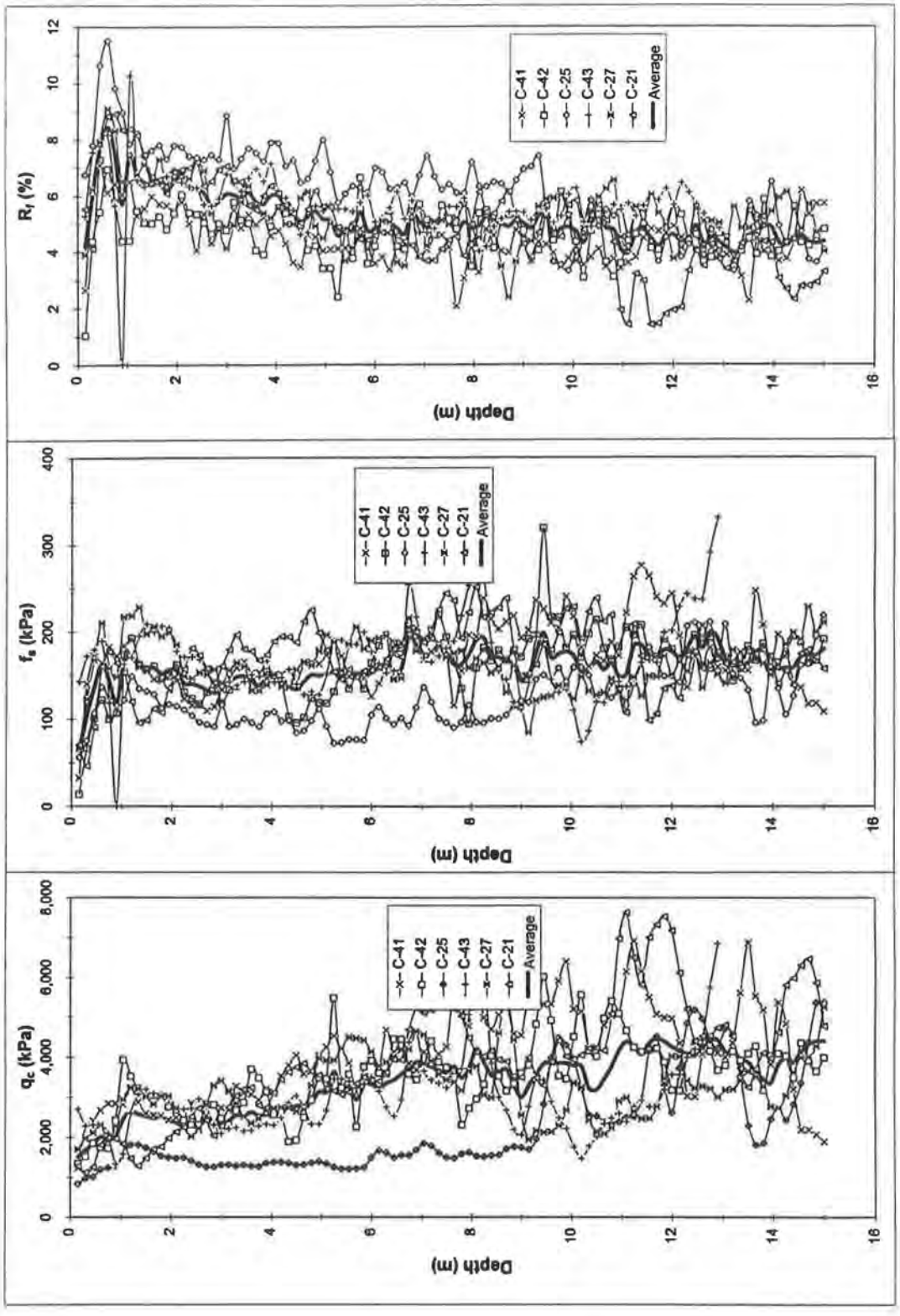

FIG. 8.2.1. - Summary of Cone Penetration Test Results.

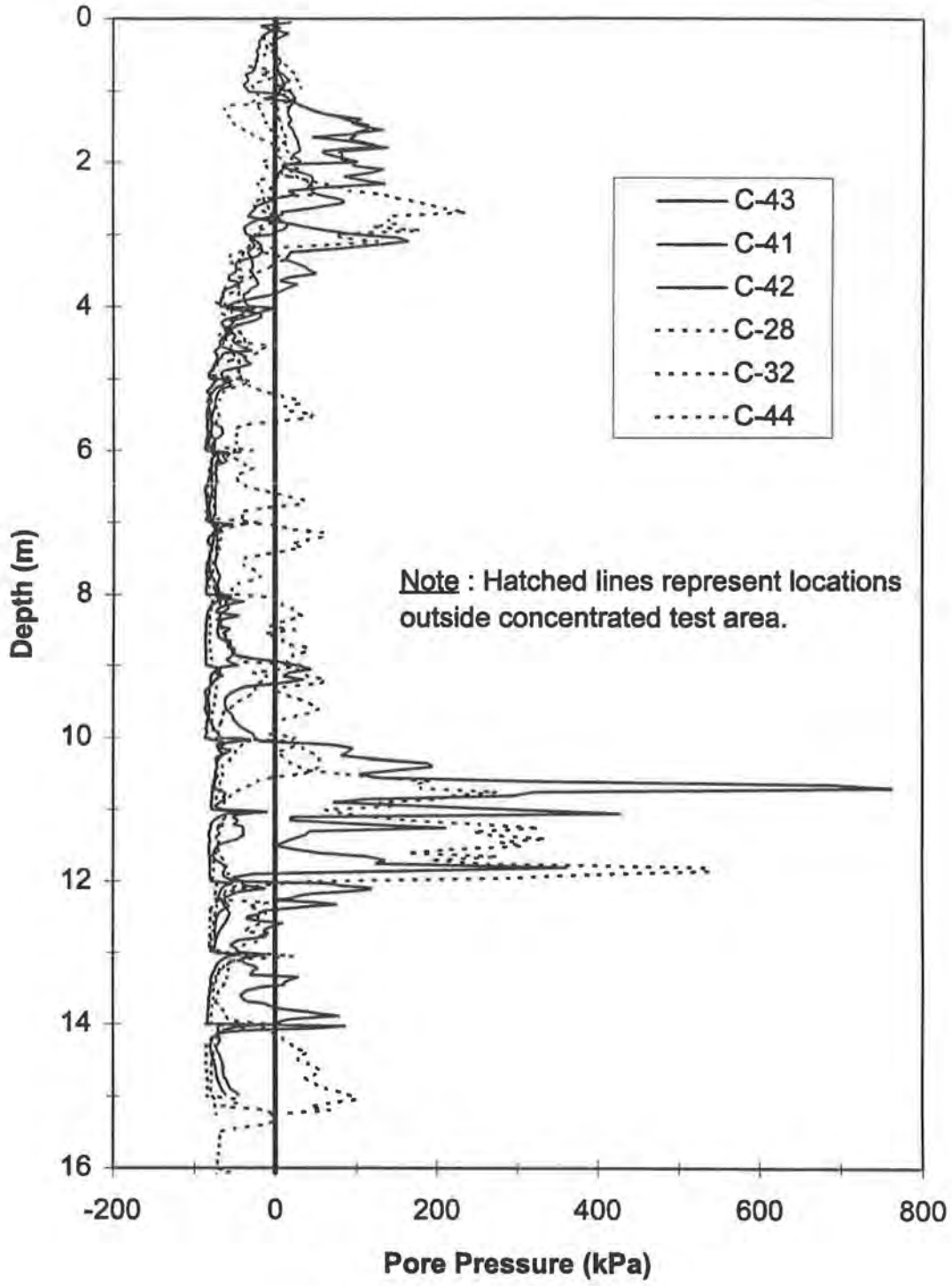

FIG. 8.2.2. - Piezocone Pore Pressures Results.

differing measures of the pore pressures during penetration. According to Mayne et al. (1995), Type 2 piezocones tend to show less detail in overconsolidated, dessicated, stiff soils prevalent in the southern U.S. than other porous element positions and that measurements may be small or even negative. The general trend at this site with the Type 2 piezocone is negative pore pressures around -100 kPa over the full depth of testing; positive pore pressures were detected, however, between depths of 1 to 3 meters and also between 10 to 12 meters. The negative pore pressure is indicative of dilatant soil behavior which may be expected of the silty sands and sandy silts at the site. Positive pressures near the upper zone may be due to the higher clay content in that zone; perhaps the positive pressures between 10 and 12 meters also occur because of the higher clay content in this zone. The grain size data on Figure 7.2.2 show that samples near the 12 meter depth have more clay-sized particles compared to those samples taken immediately above or below. Water content and Atterberg limit plots on Figure 7.2.1 also suggest that the 12 meter samples had some plasticity.

Pore pressure dissipation tests were also conducted at C-28, C-43, and C-44. These tests displayed an initial negative pore pressure which, in a matter of seconds, gradually increased until the excess pore pressures had dissipated; this behavior is indicative of the relatively high permeability of Piedmont silty sands and sandy silts compared to most sedimentary fine grained soils. The pressures stabilized at the pore pressure related to the static ground water table. The test results in C-44 are shown in Figure 8.2.3; the other dissipation profiles are included in Appendix C.

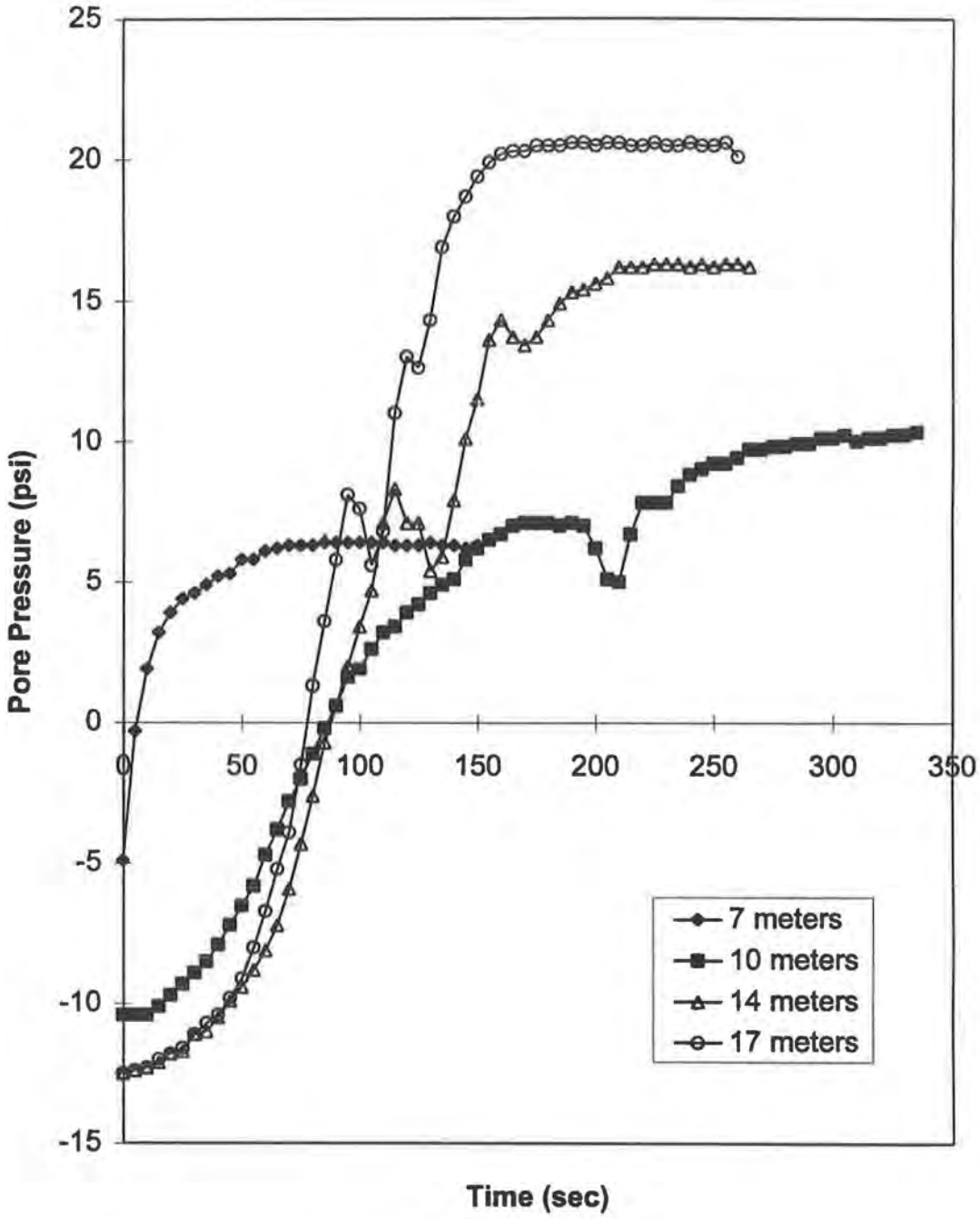

FIG. 8.2.3. - Piezocone Pore Pressure Dissipation Test Results at C-44.

8.3 Pressuremeter Test

The Menard pressuremeter tests (PMT) and cone pressuremeter tests (CPMT) were conducted at similar depths and in close proximity, as shown in Figure 6.4. The Menard pressuremeter (PM) used was a Roctest monocellular NX probe with a diameter of 70 mm, length of water and gas cells combined of 34.3 cm, and length of water cell of 22.9 cm; tests were conducted inside the cavity made by recovered shelby tube samples at various depths within borings B-2 and B-5. The cone PM was a standard PENCEL probe from Roctest; it had dimensions of 25.5 cm length and 1.73 cm radius at its center. The cone PM was positioned by hydraulically pushing a cone without friction measurements; the CPMT was performed within approximately 1 meter of the PCPT or SPCPT locations at C-41, C-42, C-43, and C-44. Also, the CPMT included an unload-reload cycle to examine small- to intermediate-strain modulus. Additional details concerning the testing procedure, data reduction, corrected loading curves or equipment of the CPMT or PMT are included in Appendix D and E, respectively.

A typical set of PM expansion curves from CPMTs and PMTs at a depth of 6 meters are shown in Figures 8.3.1 and 8.3.2, respectively. Since the CPMTs included an unload-reload cycle, an unload-reload modulus could be measured as well as initial loading PM modulus, limit pressure, and an estimate of at rest horizontal earth pressure; the PMT was conducted without an unload-reload cycle. The data presented on Figures 8.3.1 and 8.3.2 reveal the most obvious difference between the two test types. The full-displacement insertion of the CPMT causes it to be in firm contact with the soil such that the pressures on the probe have surpassed the at rest earth horizontal earth pressure and the first

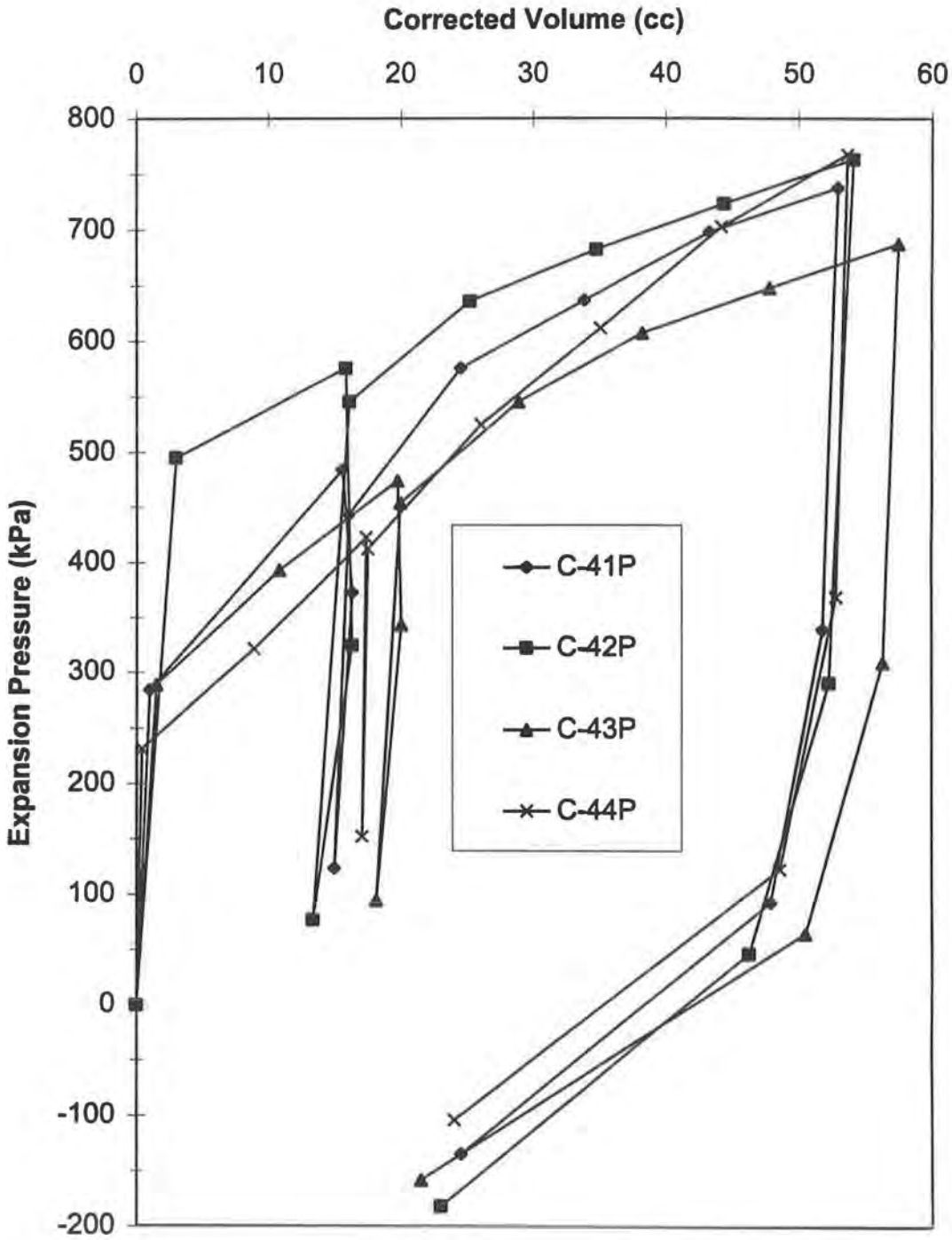

FIG. 8.3.1. - Cone Pressuremeter Curves at 6 meter Depth.

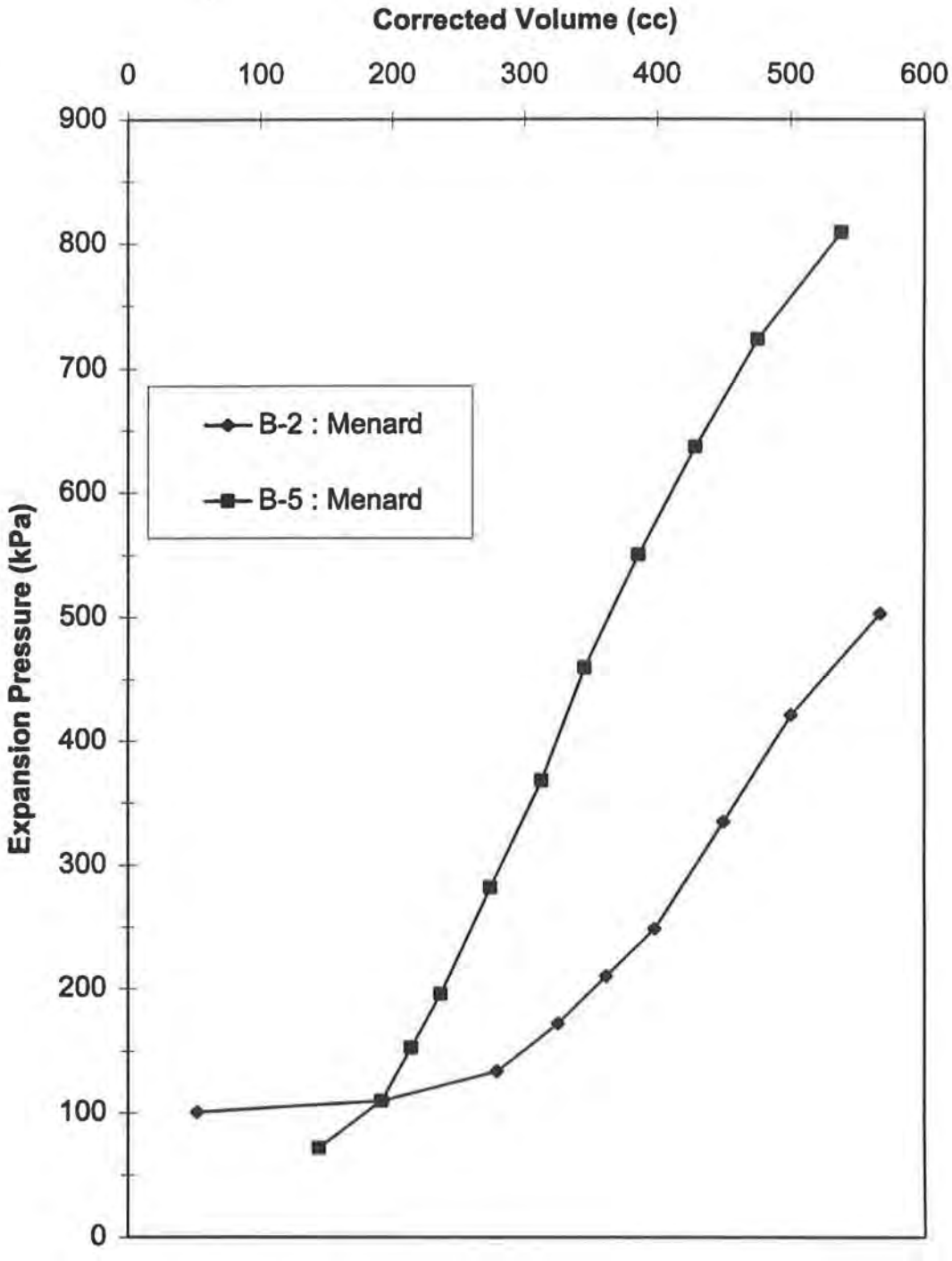

FIG. 8.3.2. - Menard Pressuremeter Curves at 6 meter Depth.

readings show great increases in expansion pressure. Conversely, the PMT curves are flat at the beginning of expansion due to the open hole causing the horizontal earth pressures to be less than the at rest pressures; the probe must expand in order to make full contact with the soil surrounding the cavity and recover the at rest horizontal earth pressure. In addition, the CPMT has a much smaller full-expansion volume than the PMT and may not be as sensitive to small changes in volume.

Both the PMT and CPMT limit and net limit pressure values are shown in Tables 8.3.1 and 8.3.2, respectively; these data are shown graphically in Figures 8.3.3 and 8.3.4. Limit pressure interpretation techniques for each PM type are described in the appropriate appendix; upon determination of total limit pressure, the interpreted total at rest earth pressure were determined in order to get net limit pressure. Although two PMTs were conducted at each testing depth, some tests did not lend themselves to reliable prediction of limit pressure and were omitted.

A fair amount of scatter was evident for both tests. Both types generally had variability at a given depth within 100 to 200 kPa. Also, location C-44 was not within the boundary of most of the other in-situ tests and borings, so the soil at this location could have different stiffness characteristics compared to the other test locations. Results at C-44 did tend to fall slightly outside of the fairly tight grouping seen at most depths for net limit pressure by the other three CPMTs. Also, it should be remembered that both limit and net limit pressures are interpretations of measured data. Even with all these factors considered, both tests displayed fairly good precision and repeatability, and except

Table 8.3.1. - Cone and Menard Pressuremeter Limit Pressures.

	Cone Pressuremeter				Menard Pressuremeter	
Location :	C-41P	C-42P	C-43P	C-44P	B-2	B-5
Depth (m)						
1	1,030	1,450	1,200	620	1,480	1,140
2	830	1,110	1,010	1,070	?	860
3	960	830	840	910	-	-
4	760	830	800	950	?	940
6	800	900	810	1,040	1,205	1,375
8	1,030	1,000	960	850	1,285	1,060
10	1,780	1,100	1,310	930	1,150	950
12	-	-	-	1,230	1,075	1,100
15	-	-	-	-	?	1,540

Note : Limit Pressures in units of [kPa].

Table 8.3.2. - Cone and Menard Pressuremeter Net Limit Pressures.

	Cone Pressuremeter				Menard Pressuremeter	
Location :	C-41P	C-42P	C-43P	C-44P	B-2	B-5
Depth (m)						
1	930	1200	1000	570	1442	1082
2	740	960	880	1020	?	783
3	880	770	750	840	-	-
4	670	770	700	860	?	825
6	680	730	660	950	1071	1250
8	840	820	810	700	1122	921
10	1610	900	1110	730	939	720
12	-	-	-	1060	864	860
15	-	-	-	-	?	1070

Note : Net Limit Pressures in units of [kPa].

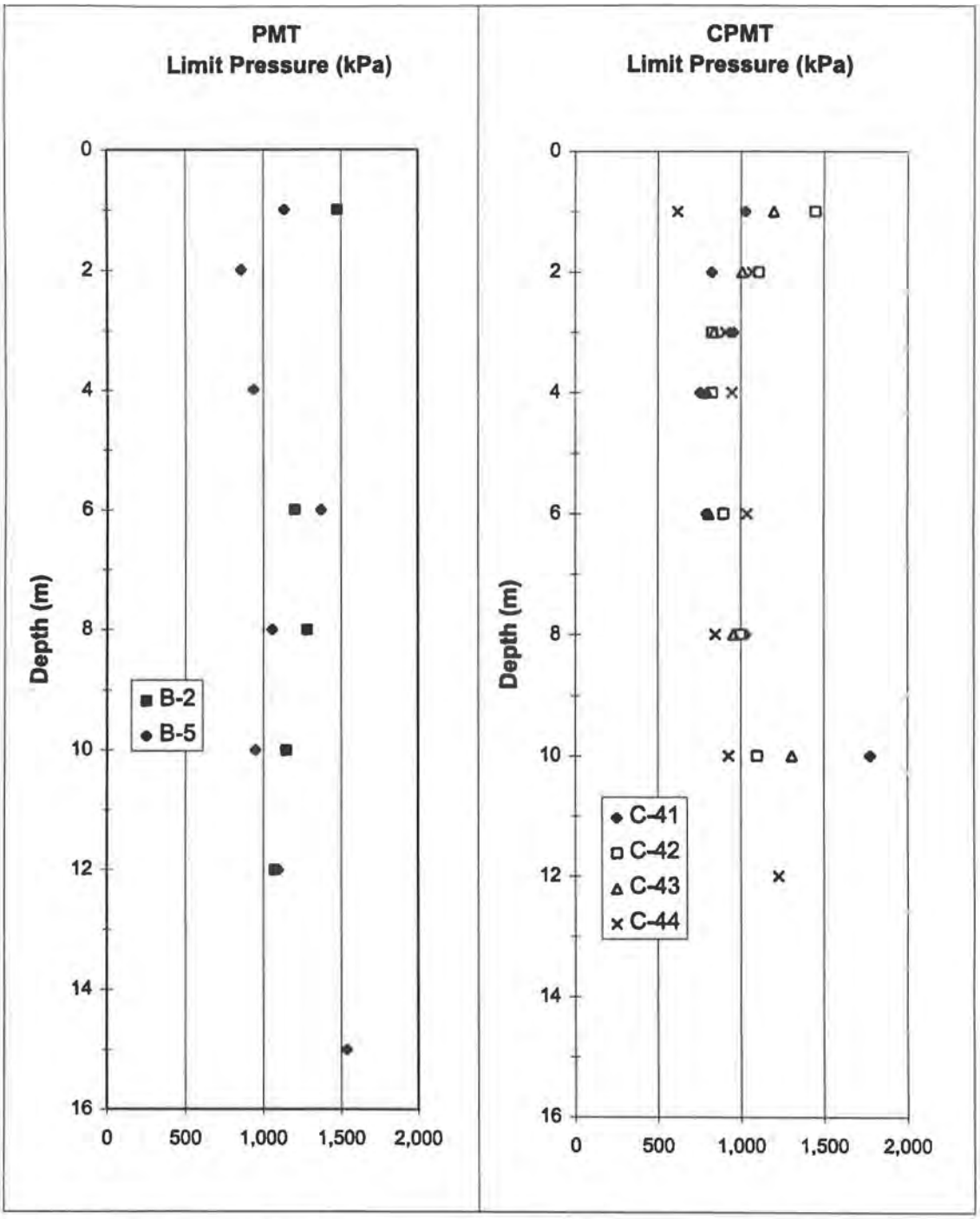

FIG. 8.3.3. - Menard and Cone Pressuremeter Limit Pressures.

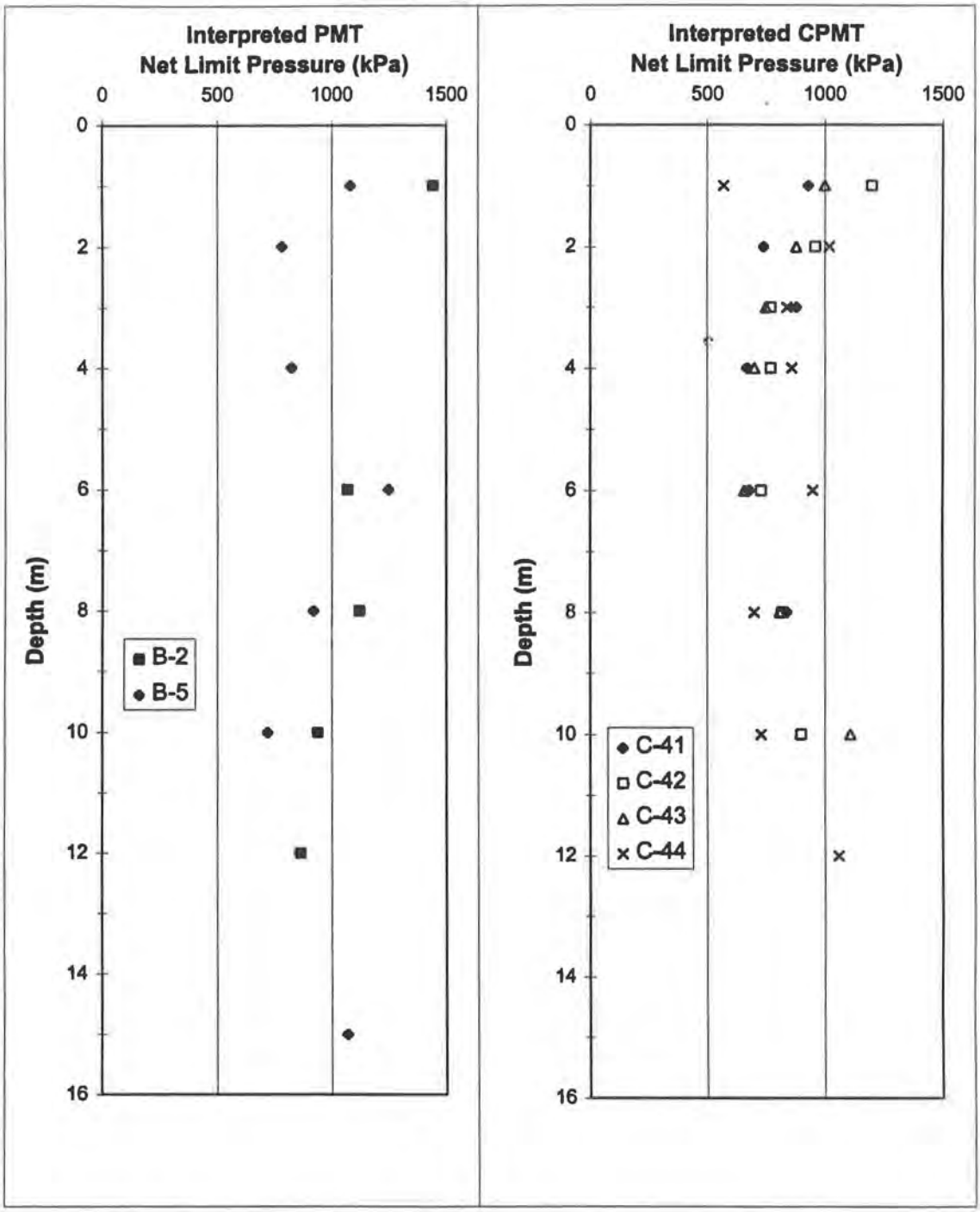

Fig. 8.3.4. - Menard and Cone Pressuremeter Net Limit Pressures.

Table 8.3.3. - Cone Pressuremeter Modulus Results.

Initial Loading Modulus Values (kPa)

Depth (m)	C-41P	C-42P	C-43P	C-44P	Average
1	14,400	18,400	23,400	5,800	15,500
2	10,100	7,400	5,900	8,900	8,100
3	9,100	4,800	3,700	4,300	5,500
4	8,000	6,300	6,800	7,800	7,200
6	7,500	3,200	5,800	5,800	5,600
8	10,500	4,300	5,900	7,900	7,100
10	17,000	4,900	8,000	3,200	8,300
12	-	-	-	12,300	12,300

Unload-Reload Modulus Values (kPa)

Depth (m)	C-41P	C-42P	C-43P	C-44P	Average
1	118,000	446,000	85,000	96,000	186,000
2	168,000	161,000	149,000	233,000	178,000
3	134,000	107,000	185,000	115,000	135,000
4	173,000	156,000	182,000	288,000	199,000
6	194,000	112,000	133,000	389,000	207,000
8	198,000	154,000	99,000	181,000	158,000
10	258,000	111,000	128,000	111,000	152,000
12	-	-	-	206,000	206,000

Table 8.3.4. Menard Pressuremeter Modulus Results.

Location : B-2 B-5

Depth (m)	E (kPa)	E (kPa)	Avg. E (kPa)
1	6,400	11,100	8,750
2	7,700	9,000	8,350
4	2,600	6,100	4,350
6	5,500	6,700	6,100
8	5,400	5,000	5,200
10	4,900	7,400	6,150
12	6,800	3,500	5,150
15	4,600	7,200	5,900

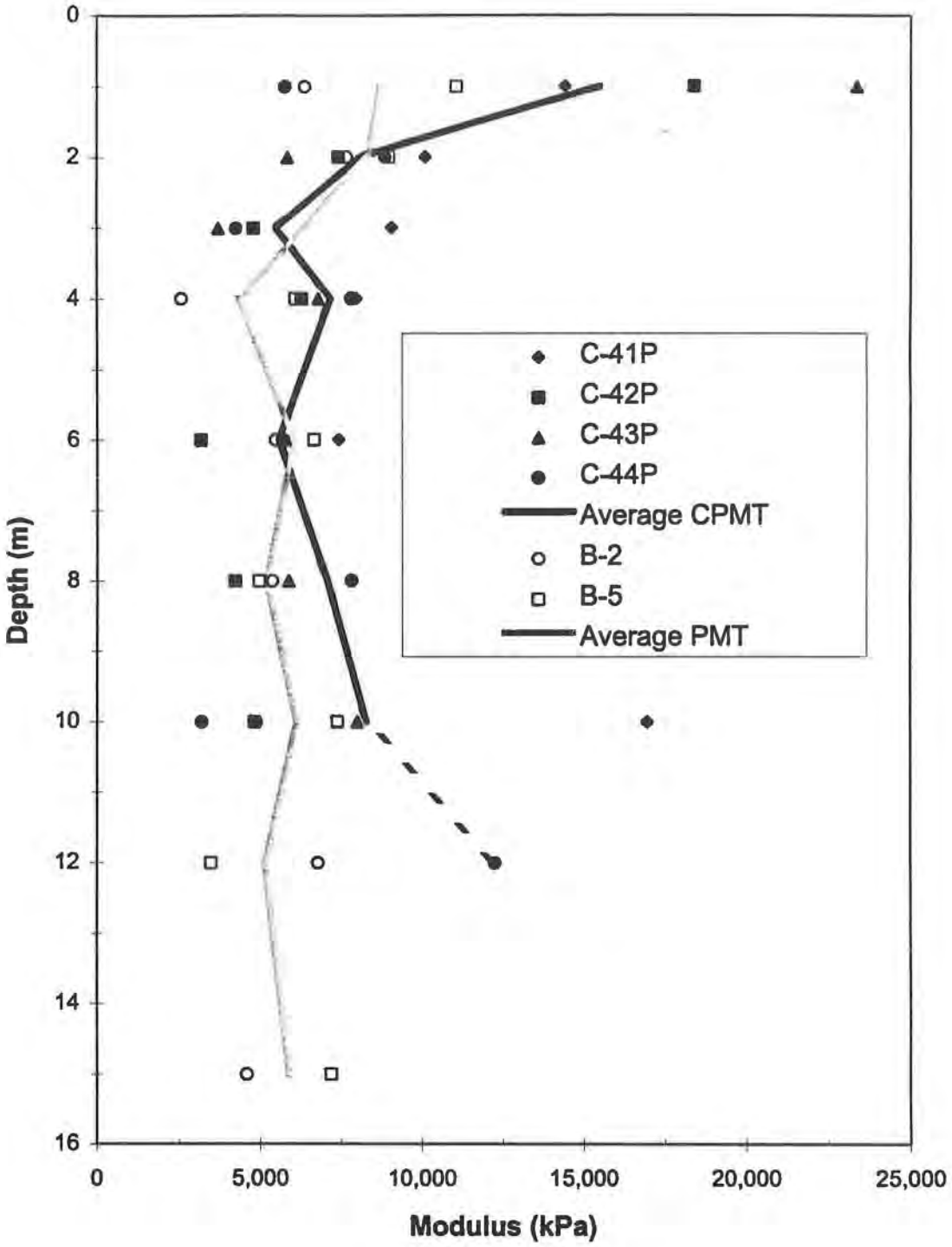

FIG. 8.3.5. - Menard and Cone Pressuremeter Moduli From Initial Loading.

for test depths at 6 and 8 meters, both tests gave similar limit pressure predictions. This difference may be due simply to the soil's spacial variability.

PM modulus values are shown in Tables 8.3.3 and 8.3.4; a comparison plot between PMT and CPMT initial loading PM modulus is shown in Figure 8.3.5. Most modulus values ranged from between 3,000 to 10,000 kPa. These are low relative to values reported by Barksdale et al. (1986) (5,500 to 28,000 kPa) and are substantially lower than the values presented by Martin (1977) (16,000 to 21,000 kPa). The average PMT modulus was generally lower than the average CPMT modulus over the depths in which comparisons can be made. This difference could be attributable to the difference in probe insertion; the CPMT assures good soil-probe contact due its nature of pushing the probe in place. Conversely, a shelby tube was pushed to create a soil cavity for the PMT; therefore, any relaxation of the soil cavity prior to the insertion and expansion of the probe would tend to soften the soil's expansion resistance. Due to the relatively rapid drainage of transient pore pressures (e.g., see Figure 8.2.3) of these soils and a shallow ground water table, it is very likely some changes in effective stress around the cavity would occur prior to performing the PMT.

The data presented on Figure 8.3.6 shows the modulus values obtained from the CPMT's unload-reload cycle. At depths of 1,4,6 and 10 meters, one value is greater than the grouping of other values. The average modulus ranged approximately between 150 and 200 MPa; this is over ten times the initial loading modulus at the same depth. This modulus would be expected to be higher since it is obtained over a much smaller strain amplitude and is measured at an increased radial stress level. The scatter in values may

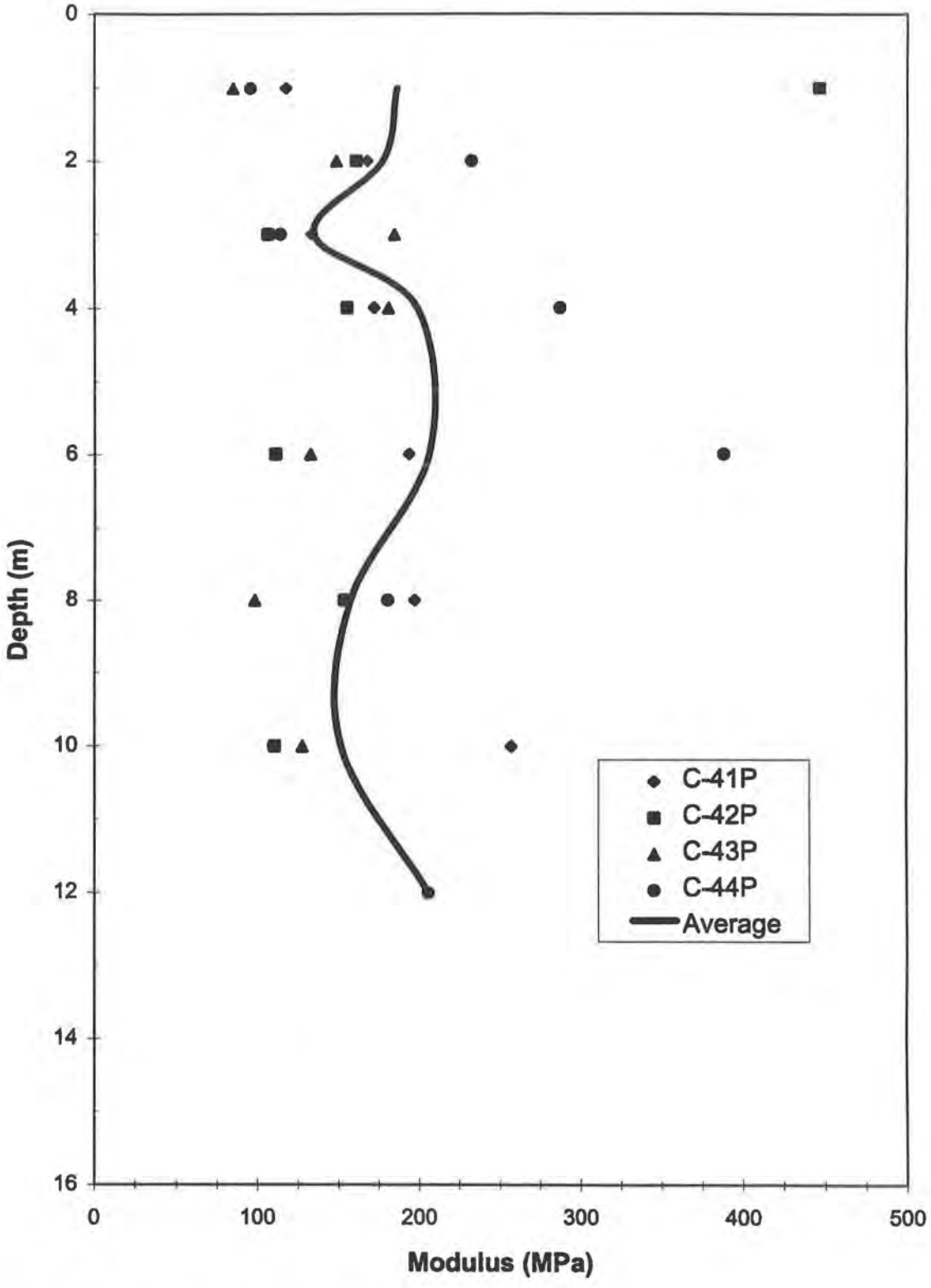

FIG. 8.3.6. - Unload-Reload CPMT Modulus Values.

be attributable to the inability of the testing equipment to measure accurately small volume changes which occur at the start of a reload cycle.

8.4 Flat Dilatometer Test

A Marchetti flat dilatometer test (DMT) was used at locations AU1, AU2, and AU3 (see Figure 6.4). In addition to the conventional DMT, a geophone receiver was attached above the probe head in order to perform downhole seismic testing; results are presented in Section 8.7 with the other seismic test results. A plot of DMT lift-off (p_o) and full-expansion (p_1) pressures vs. depth is shown in Figure 8.4.1. These pressure readings were fairly consistent between the three test locations. The p_1 pressures showed higher values in the top 2 meters and at depths below 7 meters, whereas the p_o pressures remained fairly constant over depth. Details of computations of these values from raw DMT data are described in Appendix F.

The DMT indices are presented in Figure 8.4.2. These indices include the material index (I_D), horizontal stress index (K_D), and modulus index (E_D) which are related to the prevailing grain size fraction, in-situ K_o, and soil stiffness, respectively (Marchetti 1980). These indices are derived as follows

$$I_D = (p_1 - p_o)/(p_o - u_o)$$

$$K_D = (p_o - u_o)/\sigma_v'$$

$$E_D = E/(1 - \nu^2) = 38.2(p_1 - p_o)$$

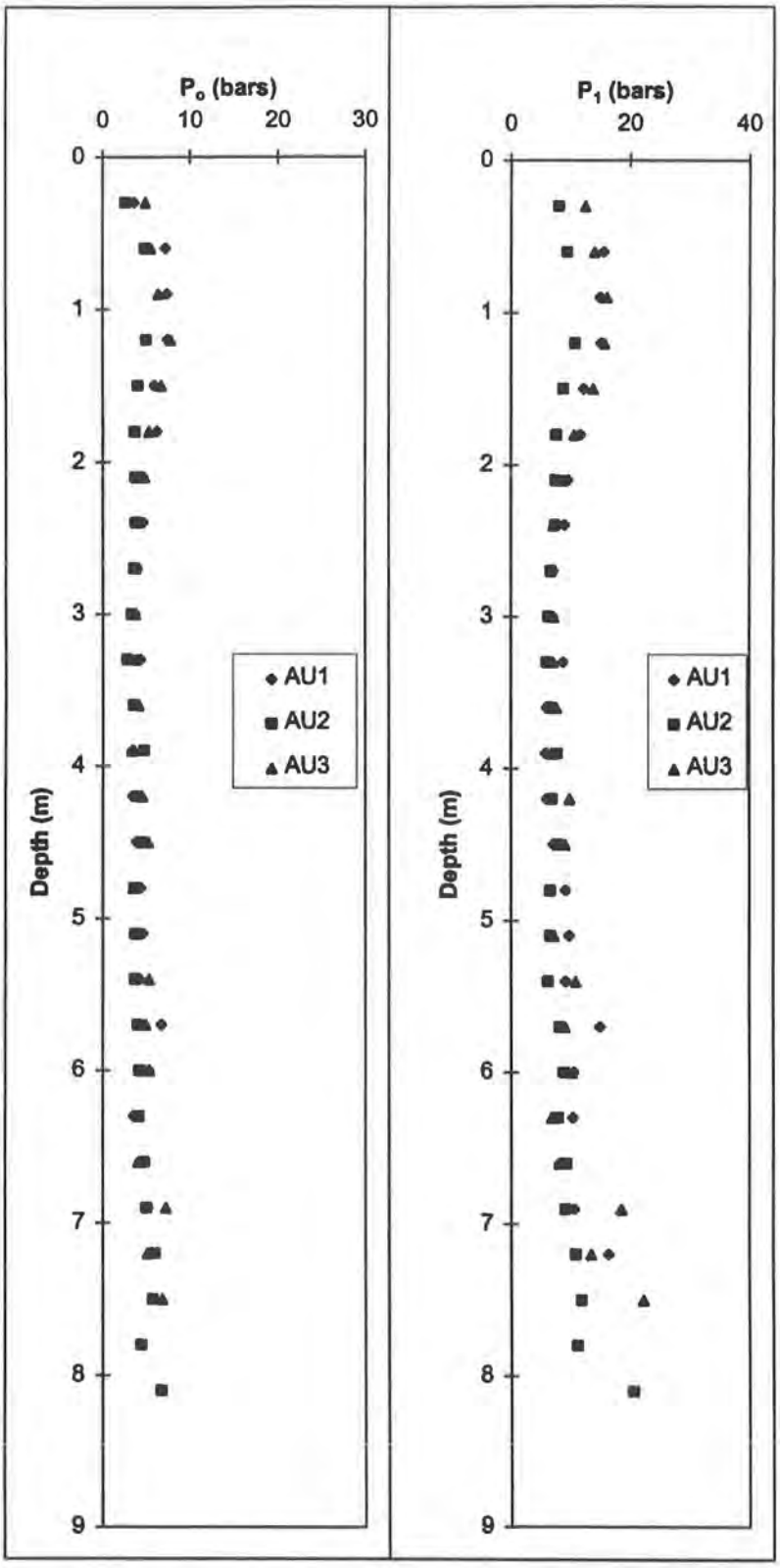

FIG. 8.4.1. - Summary of Flat Dilatometer Lift-Off (P_o) and Full-Expansion Pressures (P_1).

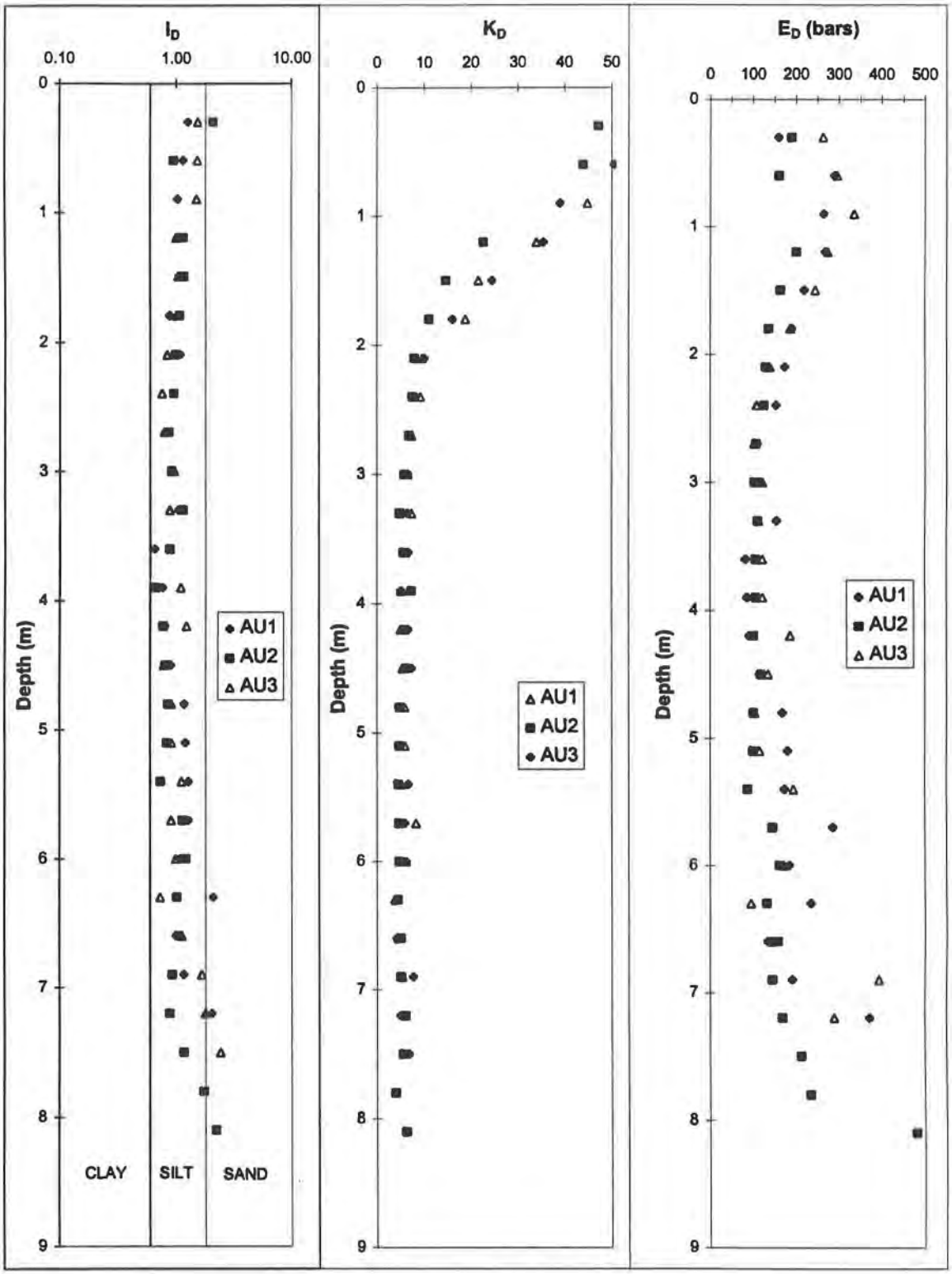

FIG. 8.4.2. - Dilatometer Index Values.

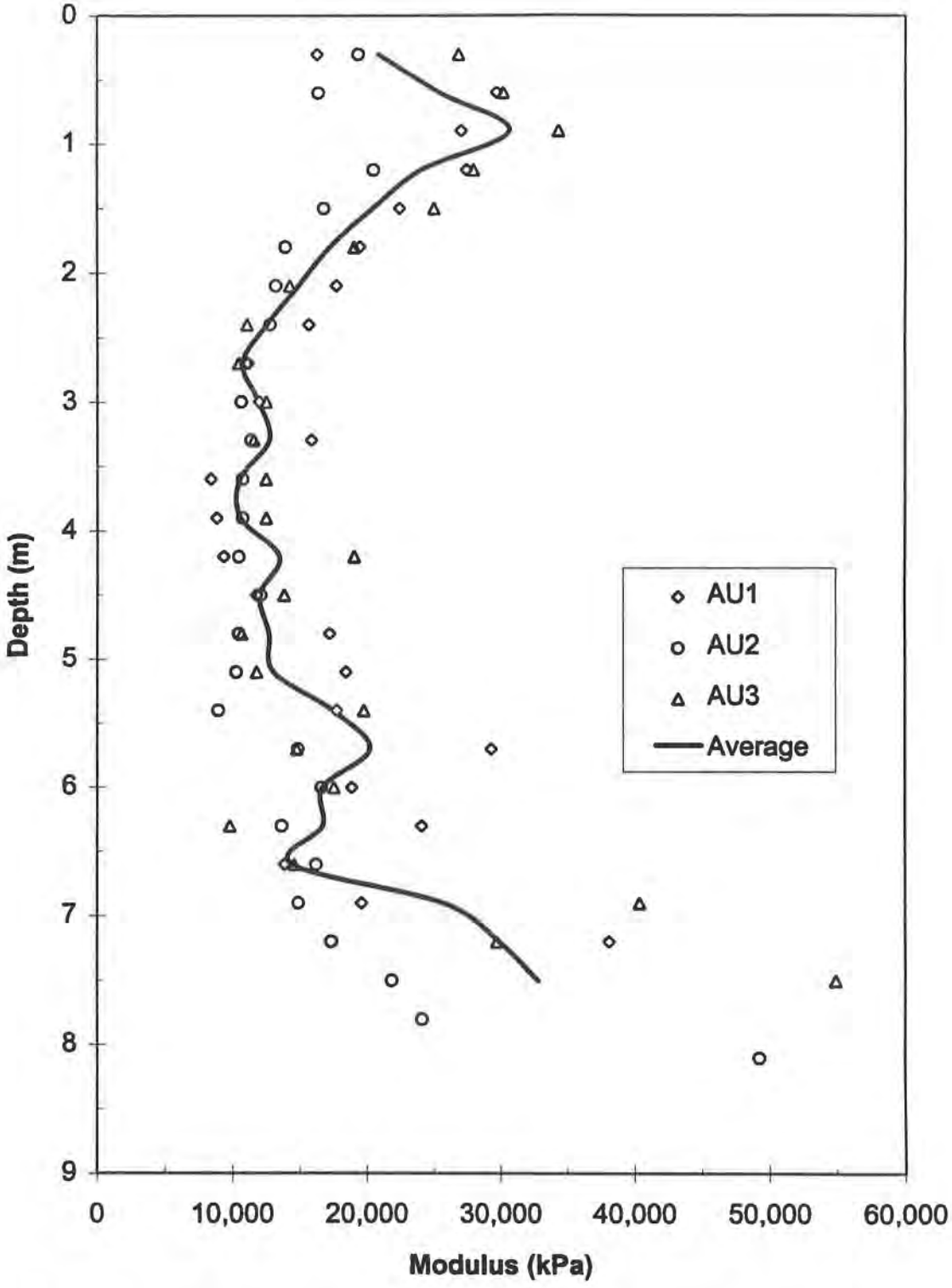

FIG. 8.4.3. - Young's Modulus from Dilatometer Modulus Index (E_D).

where u_o = pore water pressure, ν = Poisson's ratio (assumed to be 0.3 for this site), and σ_v' = vertical effective stress.

The material index (I_D) shows good agreement with the GSD analysis; the soil index predicted sandy silt to silty sand soil types over the depths tested. The horizontal stress index (K_D) was similar among the test locations and decreased to nearly constant value below a depth of 2 meters. The DMT modulus index (E_D) resembles the profile of the full-expansion pressures in Figure 8.4.1.

Young's modulus was determined from the DMT modulus values by the relationship presented above; an example calculation is shown in Appendix F. The converted average is shown in Figure 8.4.3; moduli appear to reflect overconsolidation by dessication of cohesive soils at shallow depths (less than 2 meters). Moduli were fairly constant below this crust to a depth of 7 meters, with greater scatter and larger values observed at depths greater than 7 meters.

8.5 Iowa Borehole Shear Test

Six borehole shear tests (BST) were conducted between 2 and 9 meters depth by placement of the shear head inside cavities created by shelby tube sampling. A summary of BST results including friction and cohesion values for each test are given in Table 8.5.1. These strength parameters may reflect effective stress strength; however, fully drained conditions could not be verified. Due to the quick drainage of these soils during

Table 8.5.1. - Iowa Borehole Shear Test Results.

Iowa Borehole Shear Test Results Summary						
Boring	Depth (m)	Water Table Depth (m)	No. of Points On Envelope	Regression Coefficient	Cohesion (kPa)	Friction Angle (deg)
B-8	2	3.7	5	0.9912	4	38
B-8	3	3.7	5	0.9991	0	22
B-8	4	3.7	4	0.9902	4	13
B-7	6	3.7	4	0.9988	3	27
B-8	7	3.7	5	0.9996	4	20
B-8	9	3.7	4	0.9542	7	14

other test methods, testing would be expected to represent fully drained shearing conditions.

Testing predicted rather low cohesion values between 0 and 7 kPa; friction angles varied widely between 12 to 38°. Although regression coefficients were high for defining the Mohr-Coulomb envelopes, friction angle generally appeared to be low and highly variable relative to triaxial test data. Several possibilities for the difference between triaxial and BST results include the possible stress relief of the soil after extraction of the shelby tube sample. Also, since the BST involves shearing of soil within a centimeter of the cavity wall, any remolding of this soil during shelby tube extraction or shear head insertion may cause results to reflect residual shear strength. Another factor possibly affecting results might be that the BST measures strength vertically and forces a failure plane, more or less, much like a direct shear test; the anisotropic, heterogeneous geology present at this site may have drastically differing strengths depending upon the direction of shearing.

8.6 Summary of Seismic Tests

8.6.1 Seismic CPT

The seismic piezocone penetration test (SPCPT) was performed at locations C-41 and C-42. The seismic results for these two sounding locations are presented in Figures 8.6.1 and 8.6.2, respectively. Both shear wave first arrival times vs. the distance from

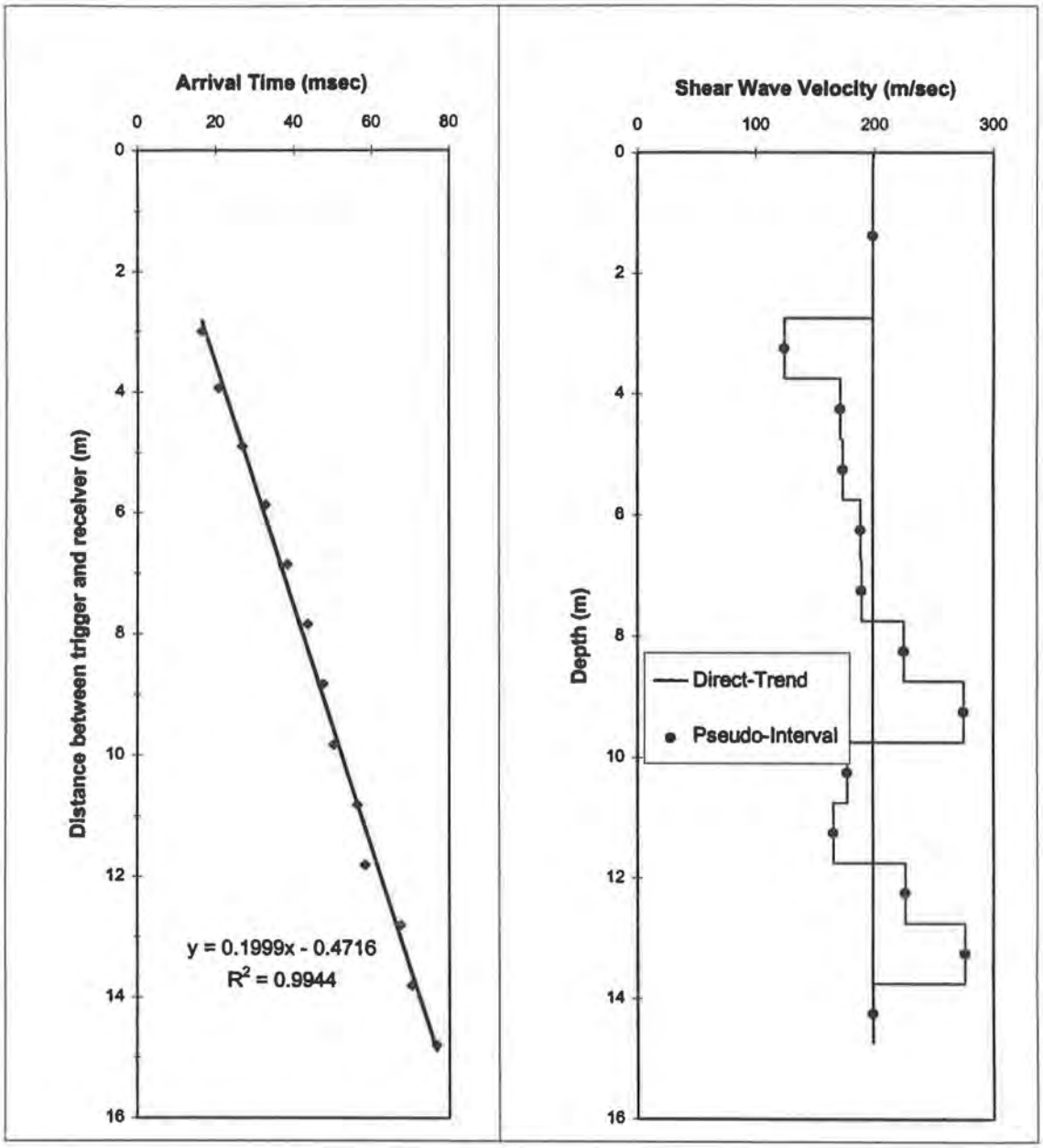

FIG. 8.6.1. - Seismic Cone Results at C-41.

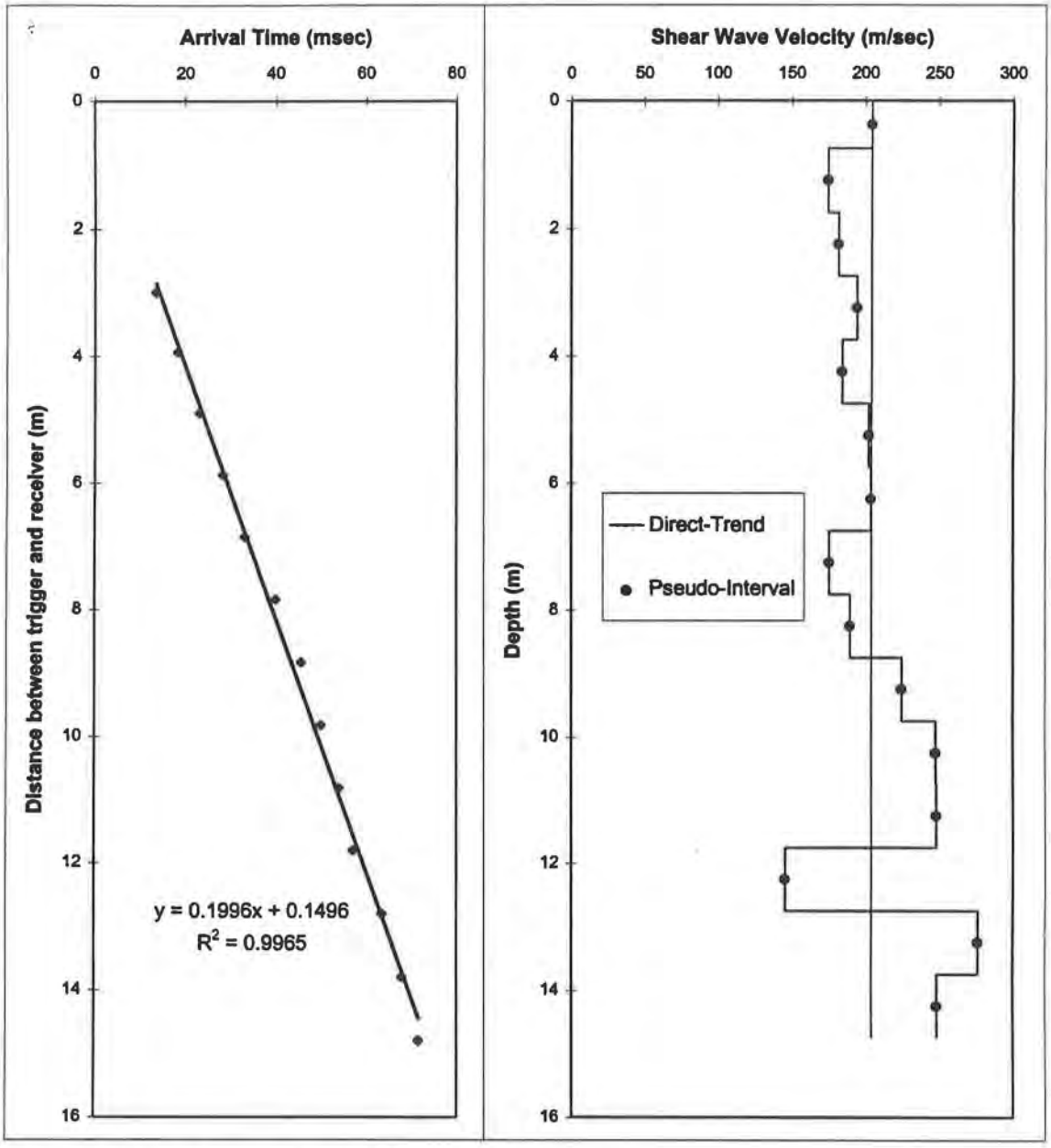

FIG. 8.6.2. - Seismic Cone Results at C-42.

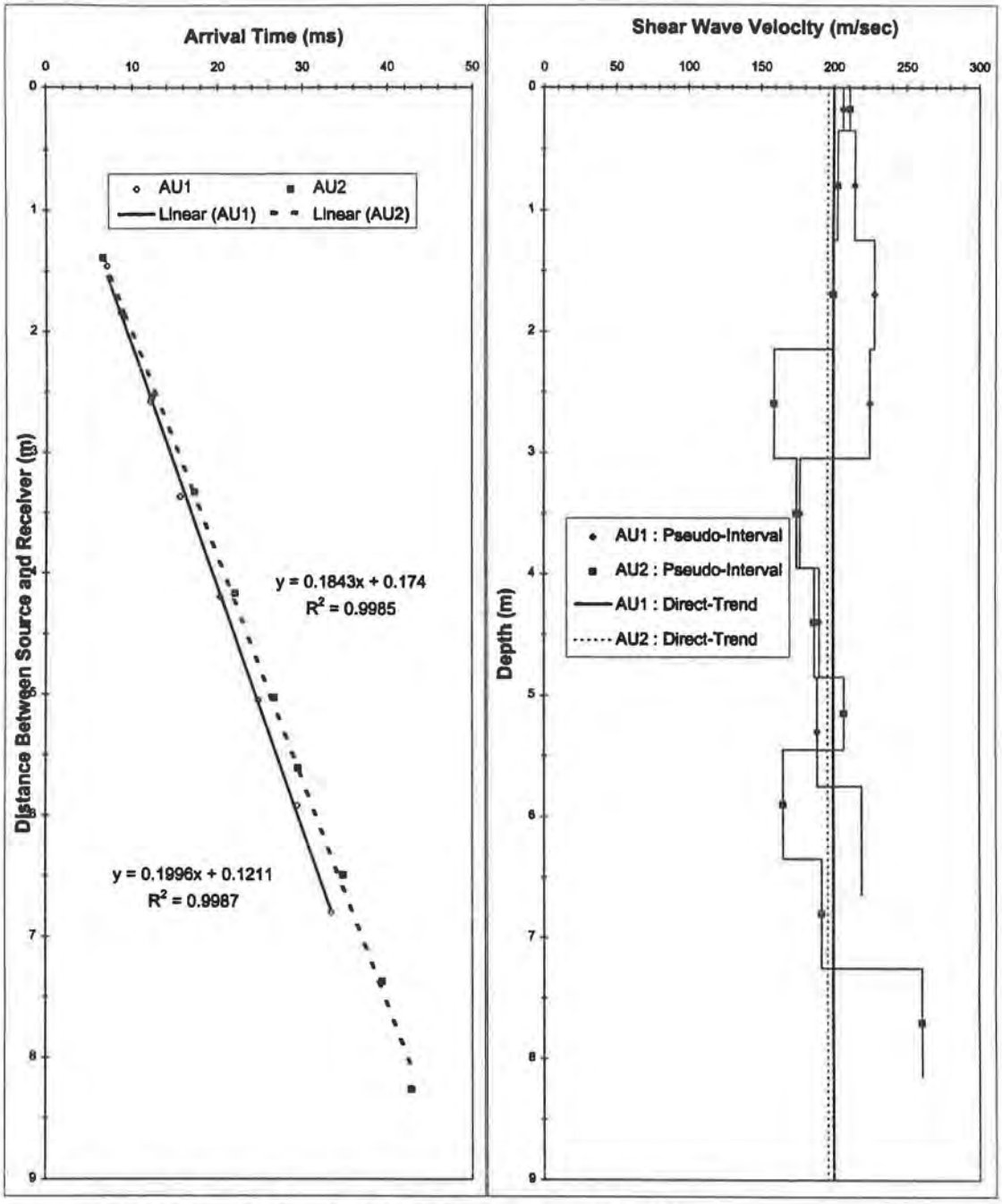

FIG. 8.6.3. - Seismic Flat Dilatometer Results.

geophone to the trigger gave very high linear regression coefficients which suggests that the soil is quite homogeneous in regard to shear wave velocity. Also included on these figures are the pseudo-interval shear wave velocity profiles; the pseudo-interval velocity, which can provide a sense of velocity variation over depth, tends to vary by up to 30% from the overall direct-trend velocity. The difference between the pseudo-interval and direct-trend velocity may be due to slight variation over depth, but it could be a product of very small timing errors since two wave measurements are used to determine a pseudo-interval velocity. Particulars of testing are included in Appendix C.

8.6.2 Seismic Flat Dilatometer Test

Seismic flat dilatometer tests (SDMT) were conducted at locations AU1, AU2, and AU3. The profile of first arrival times of the shear waves and calculated shear velocities at AU1 and AU2 is shown in Figure 8.6.3. Results from location AU3 were not included in the analysis because a cable connection to the geophone was accidentally loosened prior to testing which rendered the results from AU3 suspect. Linear regressions with high regression coefficients are also displayed; this suggests that the soil is quite uniform over depth. The pseudo-interval velocity profiles show close agreement with the direct-trend value; this closer agreement, as compared to the SCPT, could be due to differences of shear wave first arrival interpretations since the SCPT was performed by a different operator. Details of the equipment and procedure used is given in Appendix F.

8.6.3 Crosshole Seismic Test

Measured compression and shear wave velocities were made from two different arrays of cased borings. Array 1 includes borings B-1, B-2 and B-3, and Array 2 includes borings B-4, B-5 and B-6. PVC casing was grouted into place in each boring using a cement-bentonite mixture. Testing involved the use of a downhole hammer, which created a vertical shear wave (SV-wave), and two geophones; in addition, inclinometer profiling was used to evaluate the verticality of the cased holes.

Plots of compression and shear wave velocity over depth are shown on Figures 8.6.4 and 8.6.5, respectively. These plots include velocities as determined from first arrival times recorded from the source to receiver #1 (S-R1), source to receiver #2 (S-R2), and receiver #1 to receiver #2 (R1-R2). The variously predicted compression wave velocities from both arrays in Figure 8.6.4 are relatively closely spaced above the water table at values under 500 m/s, but a dramatic increase in compression wave velocities to approximately 1,500 m/s is observed at depths near where the ground water table was during testing. Although there is quite a bit of scatter, a compression wave velocity near this value would be expected below the ground water table for a saturated soil since P-wave velocity in water is around 1,525 m/s (Hoar and Stokoe 1978).

The shear wave velocities of both arrays as calculated by the different techniques mentioned above are presented on Figure 8.6.5; the average shear wave velocity is generally between 200 and 250 m/s. The scatter in velocities was fairly constant over depth. Also, the S-R2 values from both arrays were consistently near the average value

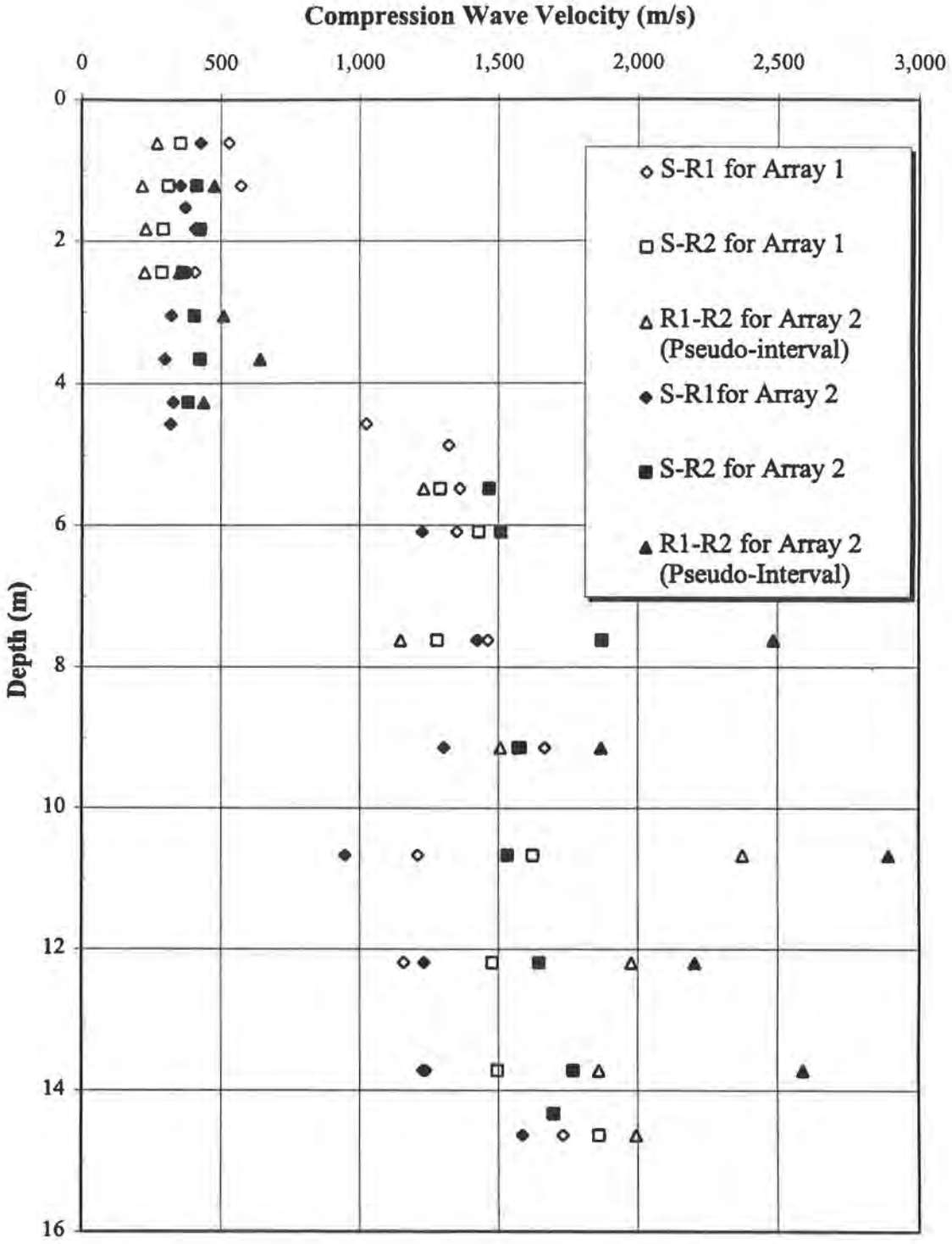

FIG. 8.6.4. - Apparent Compression Wave Velocities for Both Crosshole Seismic Test Arrays

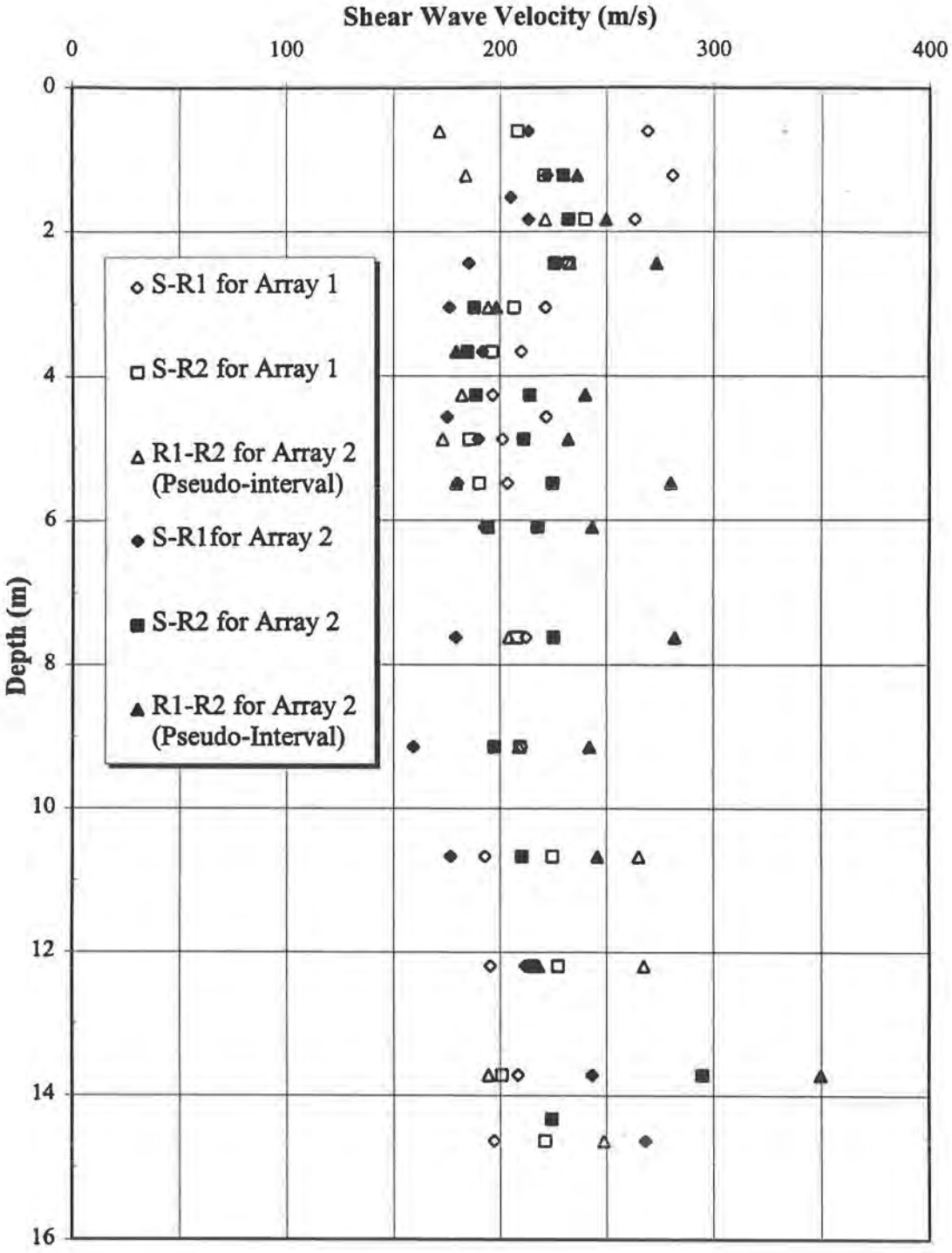

FIG. 8.6.5. - Apparent Shear Wave Velocities for Both Crosshole Seismic Test Arrays.

for each depth that was tested; therefore, an interpreted trendline used in later correlations and comparisons is shown in Figure 8.6.6.

Figure 8.6.7 shows a comparison of the overall average shear wave velocity as determined by the SCPT and SDMT to the CHT results; the downhole test velocities are lower but within 20% of the CHT values at all depths tested. This difference could be due to soil anisotropy. The CHT used a hammer which instigated vertical shear waves (SV-waves); however, the downhole techniques employed horizontal shear waves (SH-waves) through the striking of the end of a plank lying flat and in good contact with the ground. In other words, a SV-wave moves with a particle motion which varies in the vertical direction, but a SH-wave's particle motion changes in the horizontal direction. Therefore, the shear moduli measured from the SV- and SH-waves may be different because the soil stiffness is not the same in both the horizontal and vertical directions.

Figure 8.6.8 displays the CHT values compared to the SCPT and SDMT psuedo-interval shear wave velocities to better see the variation between test procedures over depth. At depths less than 7 meters, each technique gave a similar shear wave velocity measurement; however, at greater depths, the CHT shows a gradual increase in velocity over depth while the SCPT pseudo-interval shows large increases and decreases over the same depth. The SDMT was not tested beneath 8 meters depth, so comparison of this technique to the others at greater depths is not possible. Differences in SCPT pseudo-interval and CHT velocities at greater depths are quite possibly characteristic of the nature of each prediction. The SCPT evaluates vertically travelling shear wave velocity, and the CHT measures horizontally travelling waves. Therefore, the CHT measures the

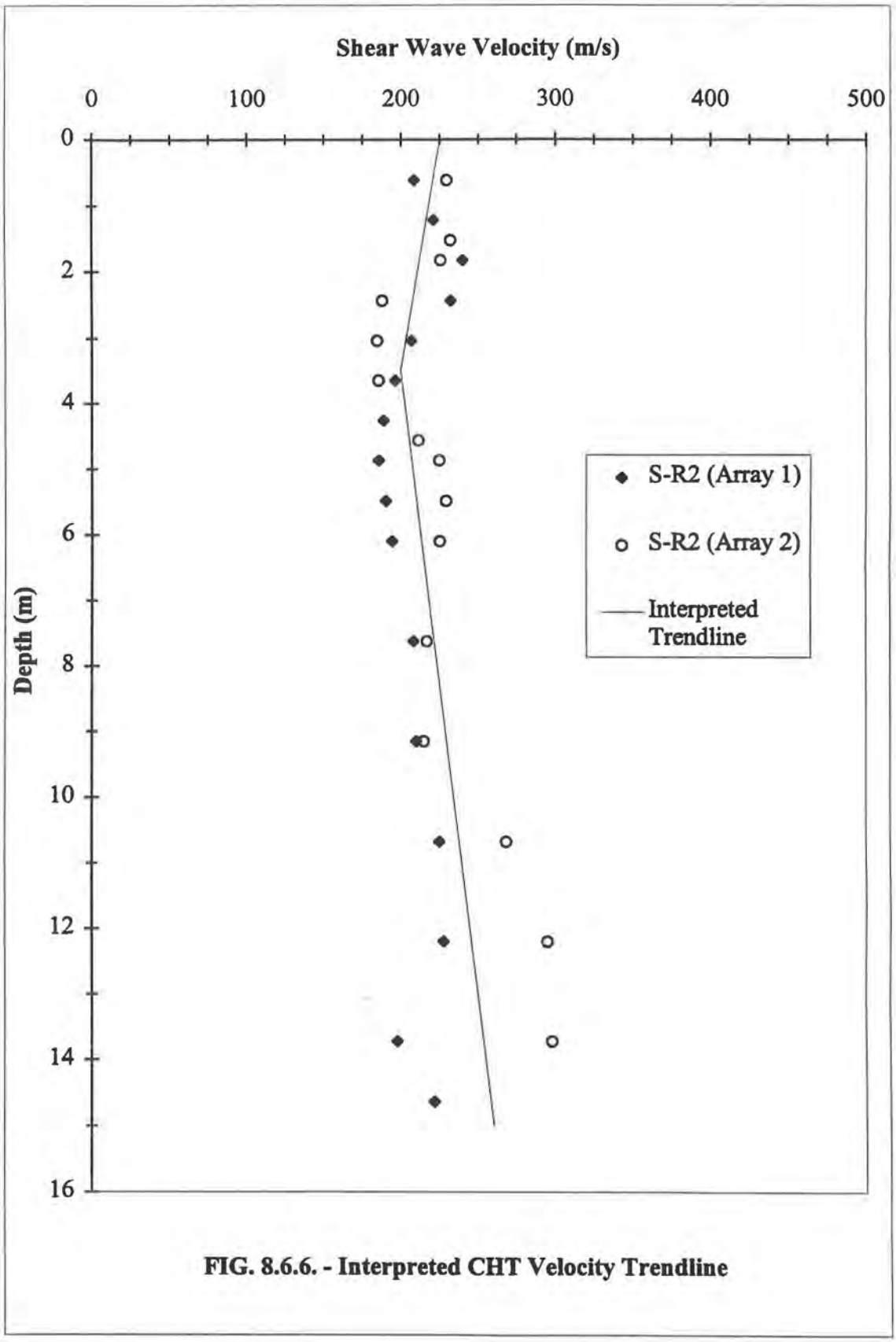

FIG. 8.6.6. - Interpreted CHT Velocity Trendline

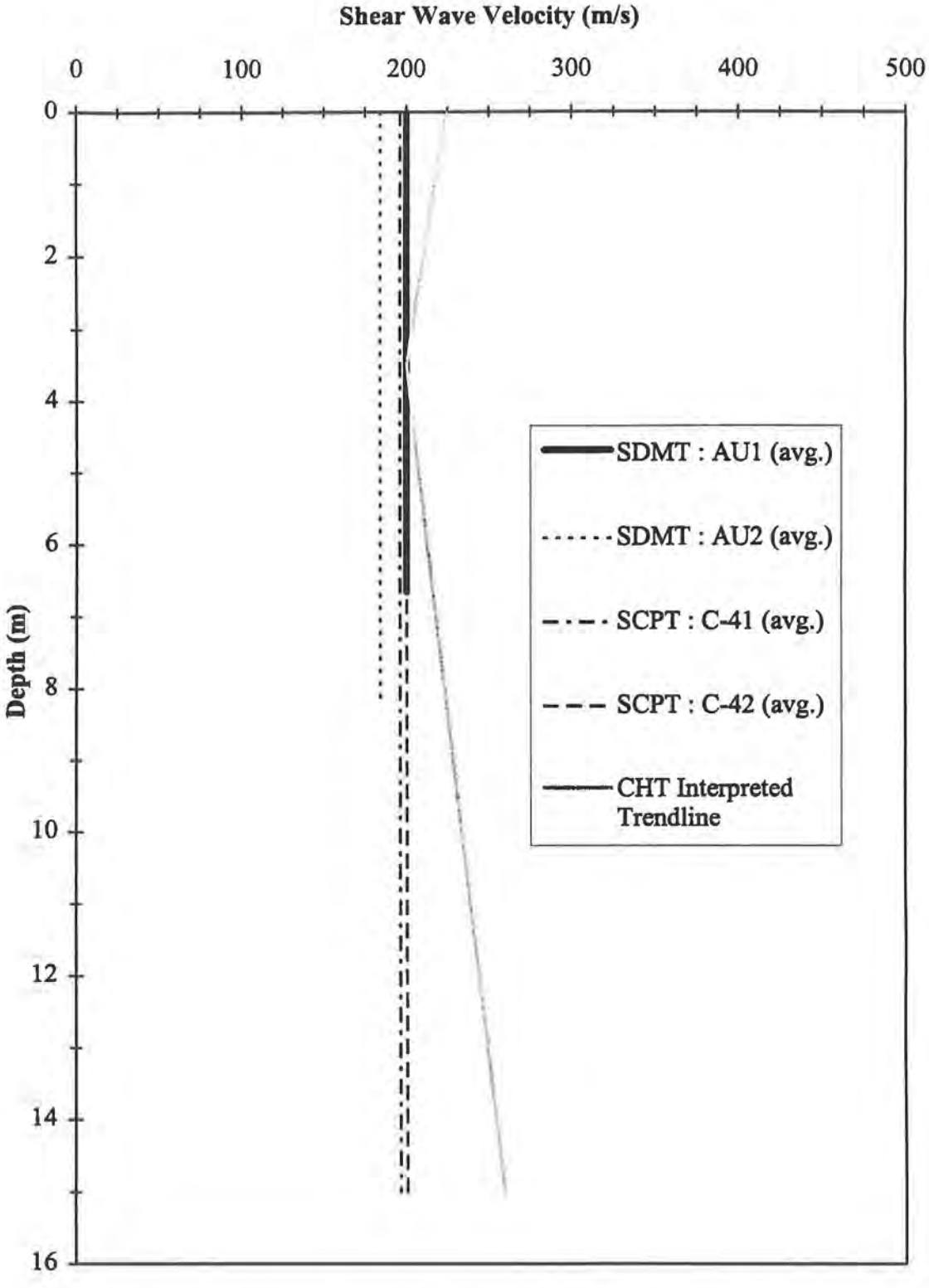

FIG. 8.6.7. - Comparison of Average Trends of Seismic Tests.

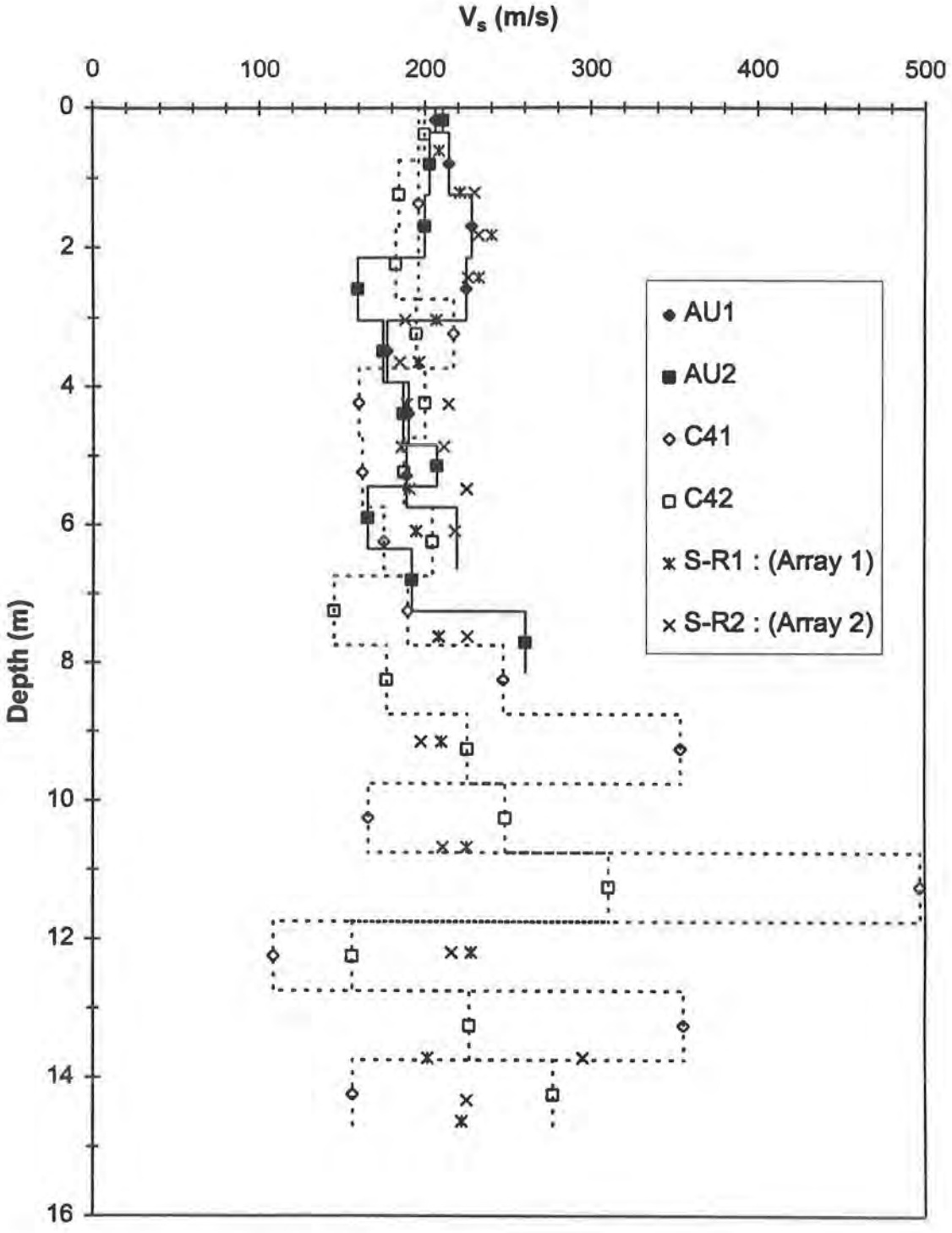

FIG. 8.6.8. - Comparison of Pseudo-Interval Shear Wave Velocities from Downhole Methods to Crosshole Method.

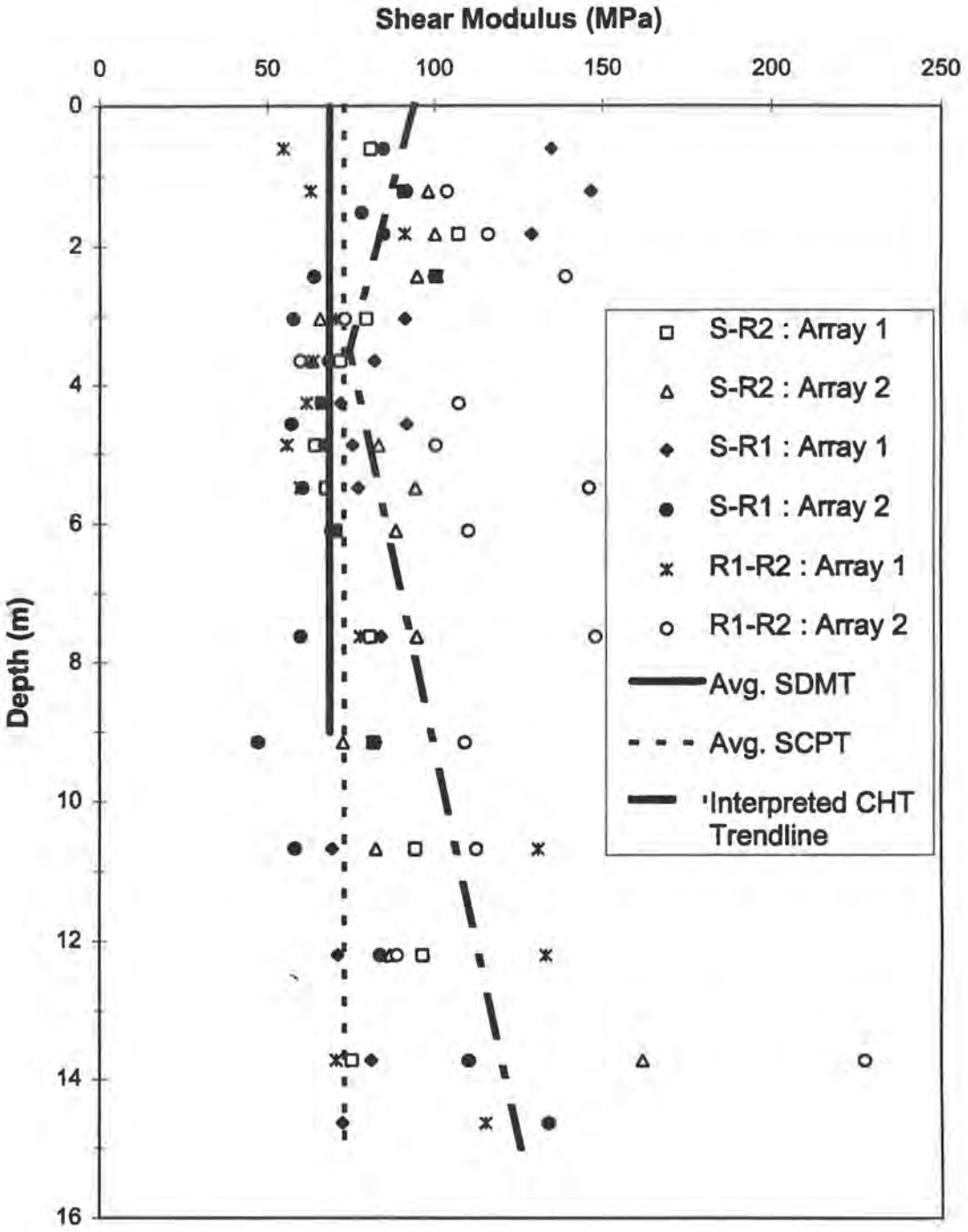

FIG. 8.6.9. - Shear Moduli from Crosshole and Downhole Seismic Test Results.

soil at a particular depth directly with one measurement rather than interpreting a difference between two measurements. This comparison may suggest that measurement error is a more significant factor with the SCPT and thus the average trend in the data is a more reliable indication of soil properties. Other than two shear wave velocities from C-41 over 8 meters depth, the SCPT and CHT predictions agree fairly well.

The shear wave velocities were converted to small strain shear modulus by the equation

$$V_s^2 = (G_{MAX})/\rho$$

where V_s = shear wave velocity, ρ = soil density (taken as 1.86 kg/m^3 for this site), and G_{MAX} = small strain shear modulus.

A plot of the average shear modulus for the SCPT and SDMT is shown in Figure 8.6.9; this figure also contains the shear modulus determined by using the different shear wave velocities generated during the CHT. The SCPT and SDMT agree quite well with the lower bound values predicted by the CHT. This figure also shows the effect of shear wave velocity on predicted shear modulus; since the velocity term is squared, the scatter in G_{MAX} is increased.

8.7 Triaxial Tests

Triaxial tests were conducted on undisturbed shelby tube samples. These samples were extruded and placed inside a mitre box to provide confinement pressure during trimming of the ends. The samples contained thin, dark bands which were inclined to

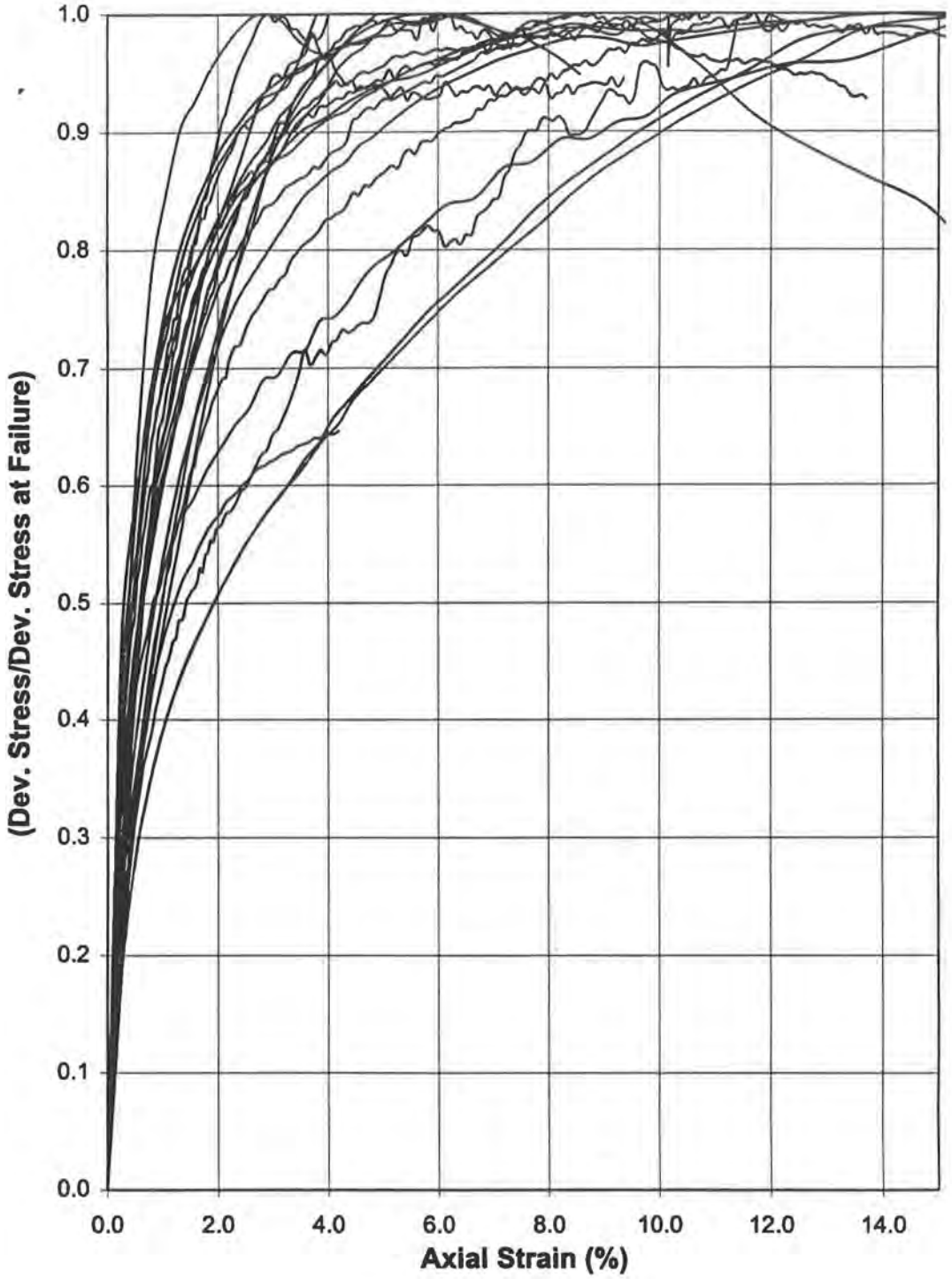

FIG. 8.7.1. - CIUC Triaxial Summary : Ratio of Deviator Stress to Failure Deviator Stress as a Function of Axial Strain (%).

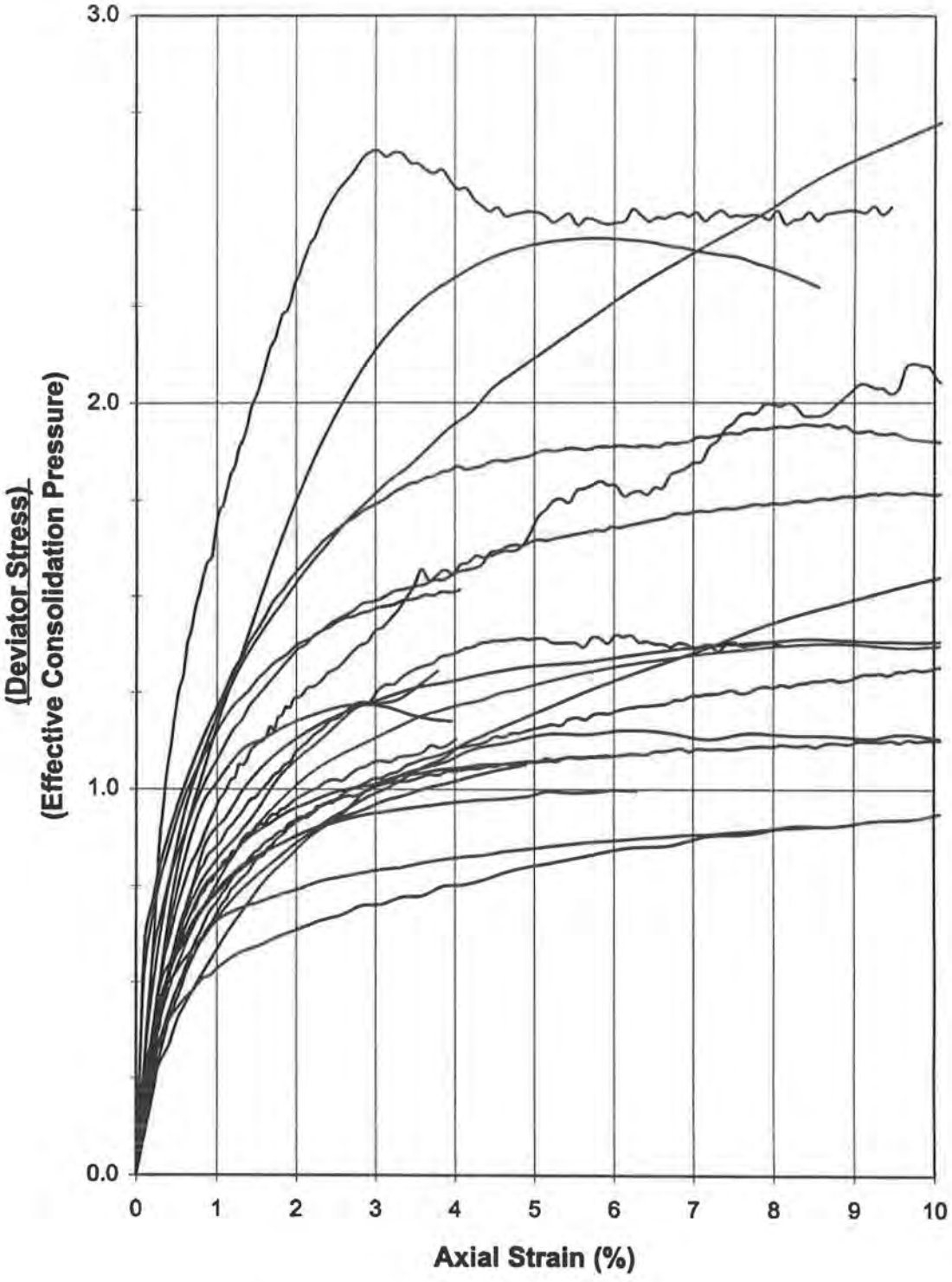

FIG. 8.7.2. - CIUC Triaxial Summary : Ratio of Deviator Stress to Effective Consolidation Pressure as a Function of Axial Strain (%).

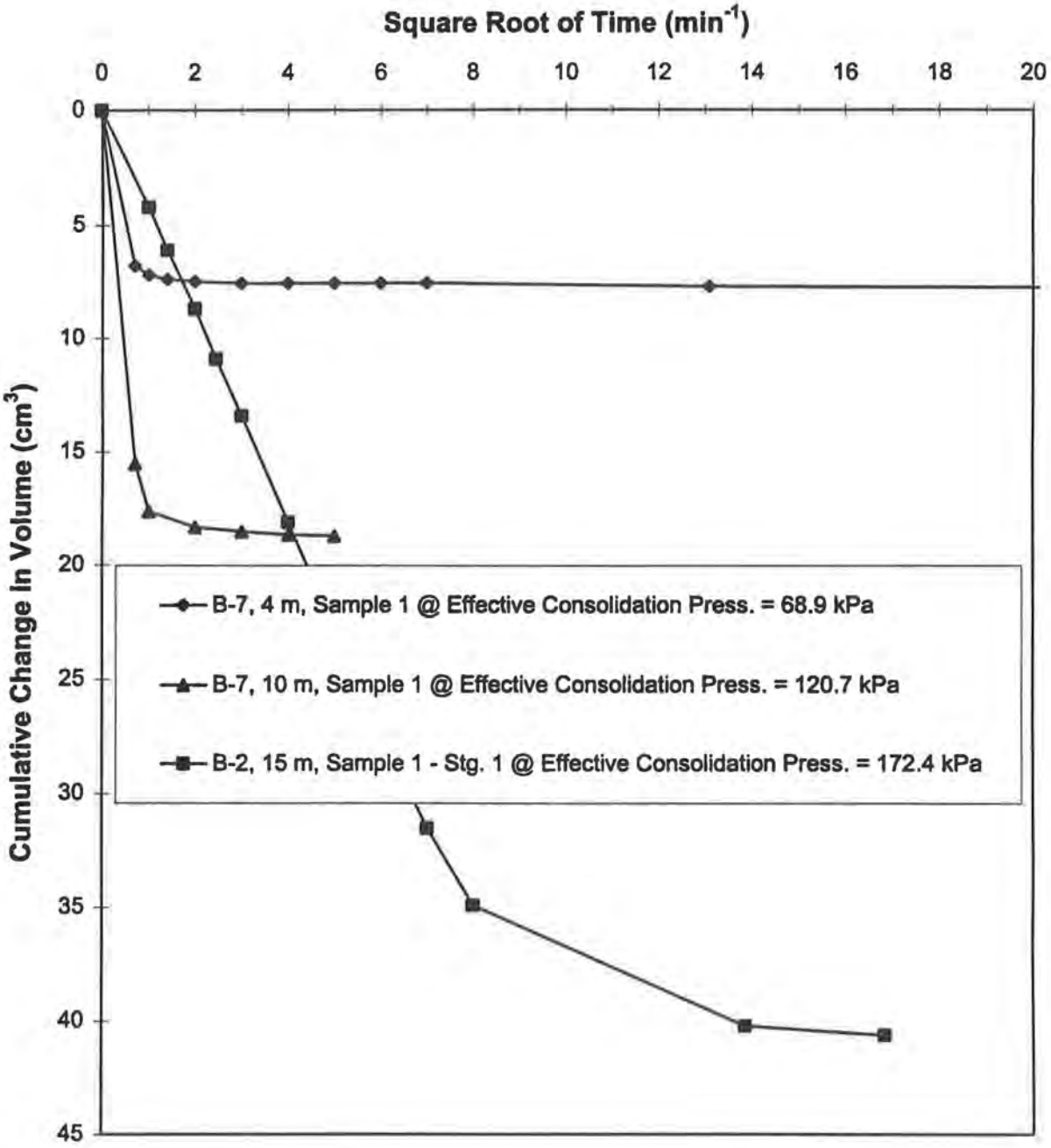

FIG. 8.7.3. - Typical Triaxial Consolidation Records.

varying degrees; quartz seams were common and oftentimes made it difficult to evenly trim the ends of the samples.

Isotropically conolidated-undrained compression (CIUC) triaxial tests were conducted on eighteen samples taken at various depths between 4 and 15 meters; four samples had two stages of loading. A summary of the stress-strain behavior from these tests are presented in Figures 8.7.1 and 8.7.2. Each test, including the second stage loading of multi-stage tests, are included in the plots.

The deviator stress vs. axial strain relationship with the deviator stress normalized by the maximum deviator stress is presented on Figure 8.7.1. Most samples reached a peak deviator stress between 6% and 8% axial strain; this is near the lower limit where multi-stage tests are recommended by Soranzo (1988) as mentioned in Section 5.5. Also, the maximum principal stress ratio of most samples was generally reached at a few percent less than that needed to reach the maximum deviator stress. Figure 8.7.2 displays these tests in another manner; in this plot, deviator stress is normalized by each test's effective consolidation pressure (σ_{3c}'). Both plots show a fair amount of scatter, although the data presented on Figure 8.7.1 does indicate less variation at small axial strains.

Figure 8.7.3 illustrates the rapid consolidation which Piedmont soils tend to exhibit; higher consolidation pressures resulted in correspondingly higher volume change. The particulars of each individual triaxial test (including B-coefficient, consolidation pressures, platen loading rate, p-q plots, and plots of deviator stress, pore pressure, and principal stress ratio vs. axial strain) are presented in Appendix I.

The p-q coordinates from each CIUC test (including second stage results for multi-stage tests) corresponding to the maximum principal stress ratio values along with the maximum p-q values from one isotropically consolidated-drained (CIDC) test were used in defining the effective stress strength envelope over the 4 to 15 meter depth range. A second CIDC test was conducted; however, since it was well above the failure trend of the other tests, it was considered an outlier and not representative of the other samples. The second CIDC test results are included in Appendix I.

These p-q values are presented on Figure 8.7.4 along with two different linear regressions. The best fit linear regression of p on q resulted in a fairly high regression coefficient which suggests an excellent correlation of these data with the $c' = 17$ kPa and $\varnothing' = 31°$ as shown; these values will be used in comparing other tests' correlations in Chapter 11. The $\varnothing'$ falls in the mid-range of reported values mentioned in Section 3.4.7 which varied from 20 to 40°; c' is near the lower end of reported values which ranged from 0 to 100 kPa (Deere and Patton 1971; Sowers 1983; Harris and Mayne 1994).

An alternative regression method noted by Handy (1981) produces a failure envelope with a lower regression coefficient, lower effective friction angle, and higher effective cohesion compared to the ordinary linear regression of p on q; however, considering the evident scatter in the data, the difference between the two regression types is probably not significant. The Handy technique attempts to account for the slope induced by multiple tests with different strengths which are tested at the same confining pressure. Using the Handy technique, the p and q axes are rotated by some angle (usually 45°) which represents the angle of the effective stress loading paths. This angle of rotation is

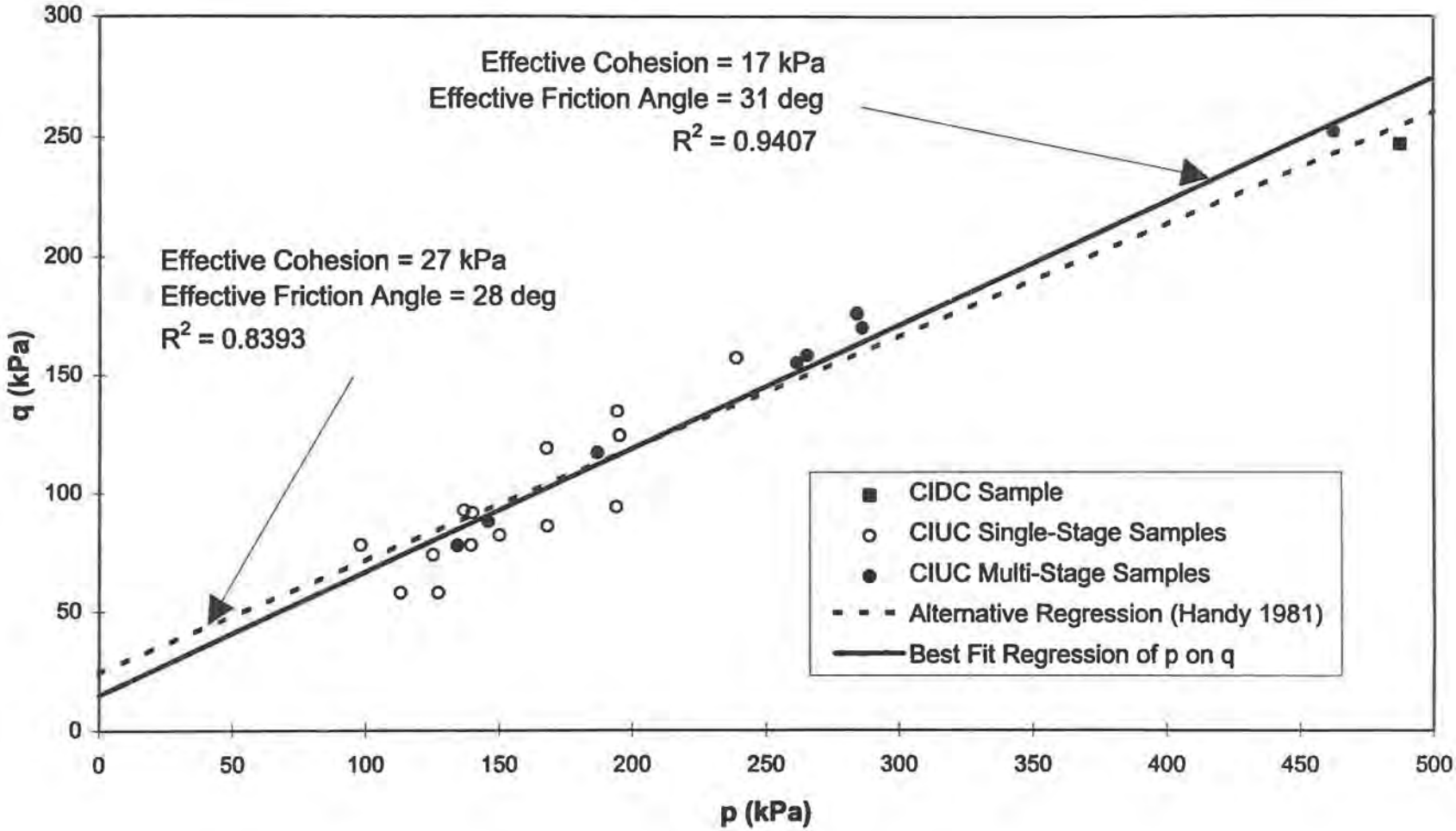

FIG. 8.7.4. - Summary p-q Plot With Linear Regressions.

definitely 45° for drained tests; however, for undrained tests, difficulty in choosing the proper angle can arise since the angle may not be the same for all tests considered. For the Handy regression shown in Figure 8.7.4, the angle was taken as 45°.

Figure 8.7.5 summarizes the complete effective stress triaxial loading paths along with upper and lower 95% probability lines for the p on q linear regression failure envelope. This narrow band, constructed as per Devore (1991), suggests a 95% probability that a future random sample would be within this range. Most CIUC samples generated a positive change in pore pressures during loading unlike the mostly negative pore pressures measured by the piezocone, but many did exhibit a dilatant shift up and right of the stress path upon contact with the yield surface. A majority of CIUC samples reached failure within 5 - 10% axial strain corrected for changes in area during loading.

A plot of the change in volume over time during shearing of the CIDC samples are presented on Figure 8.7.6. The negative cumulative volume values in this figure correspond to decreases in volume similar to that of normally consolidated clay (Holtz and Kovacs 1981). Also, the plot shows the drained tangent elastic modulus (E_t) for these samples; both gave very similar modulus estimates.

The initial tangent deformation, or elastic, modulus was also estimated from the CIUC triaxial testing. Some of the samples required back-fit estimation since the tests generally only had a few measurement readings less than 1% vertical strain. Tables 8.7.1 and 8.7.2 show the individual test's tangent modulus (E_t) along with other testing parameters such as maximum undrained shear strength (S_u) and corresponding shear modulus (G) calculated using elastic theory with a Poisson's ratio of 0.3 assumed. The

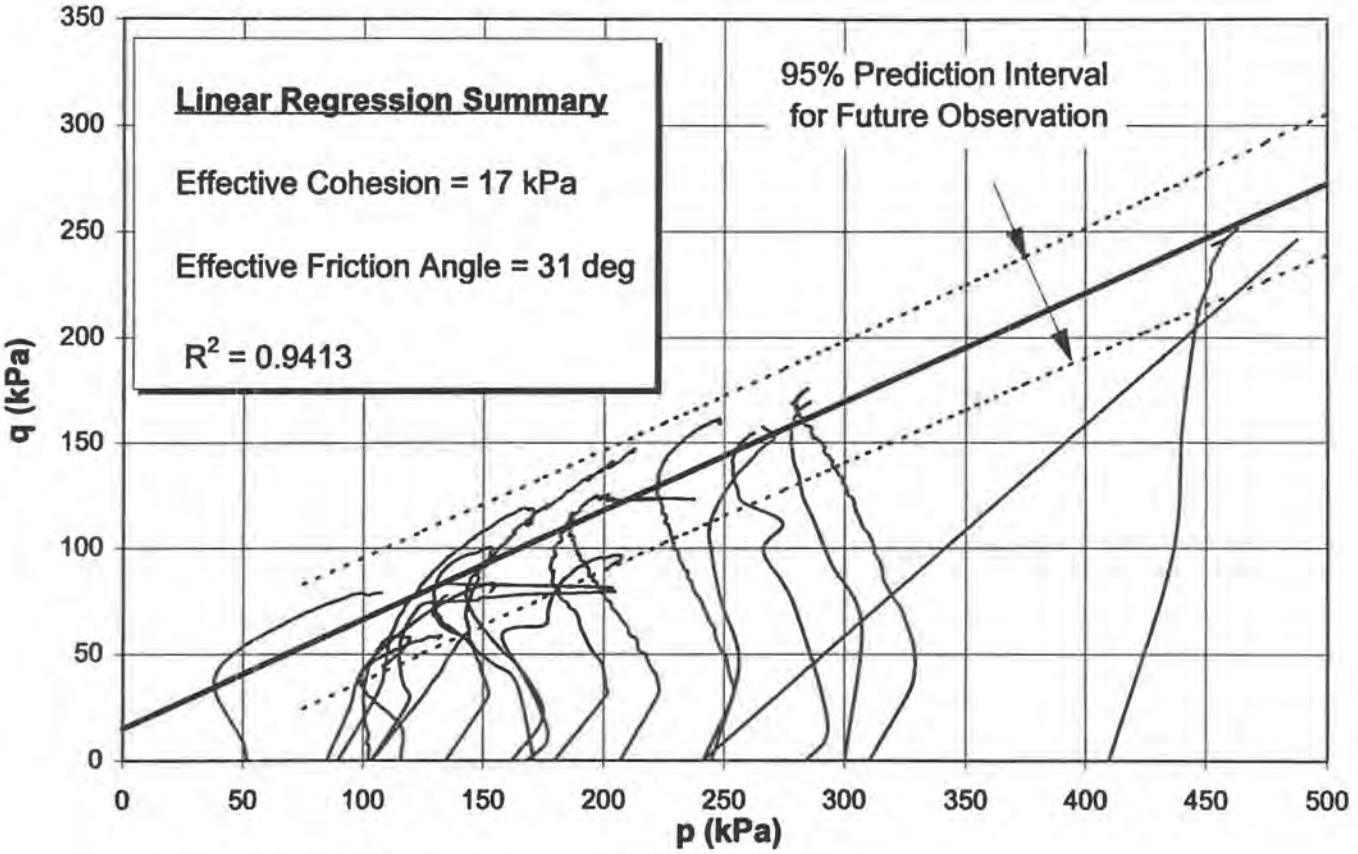

FIG. 8.7.5. - Triaxial Loading Path Summary.

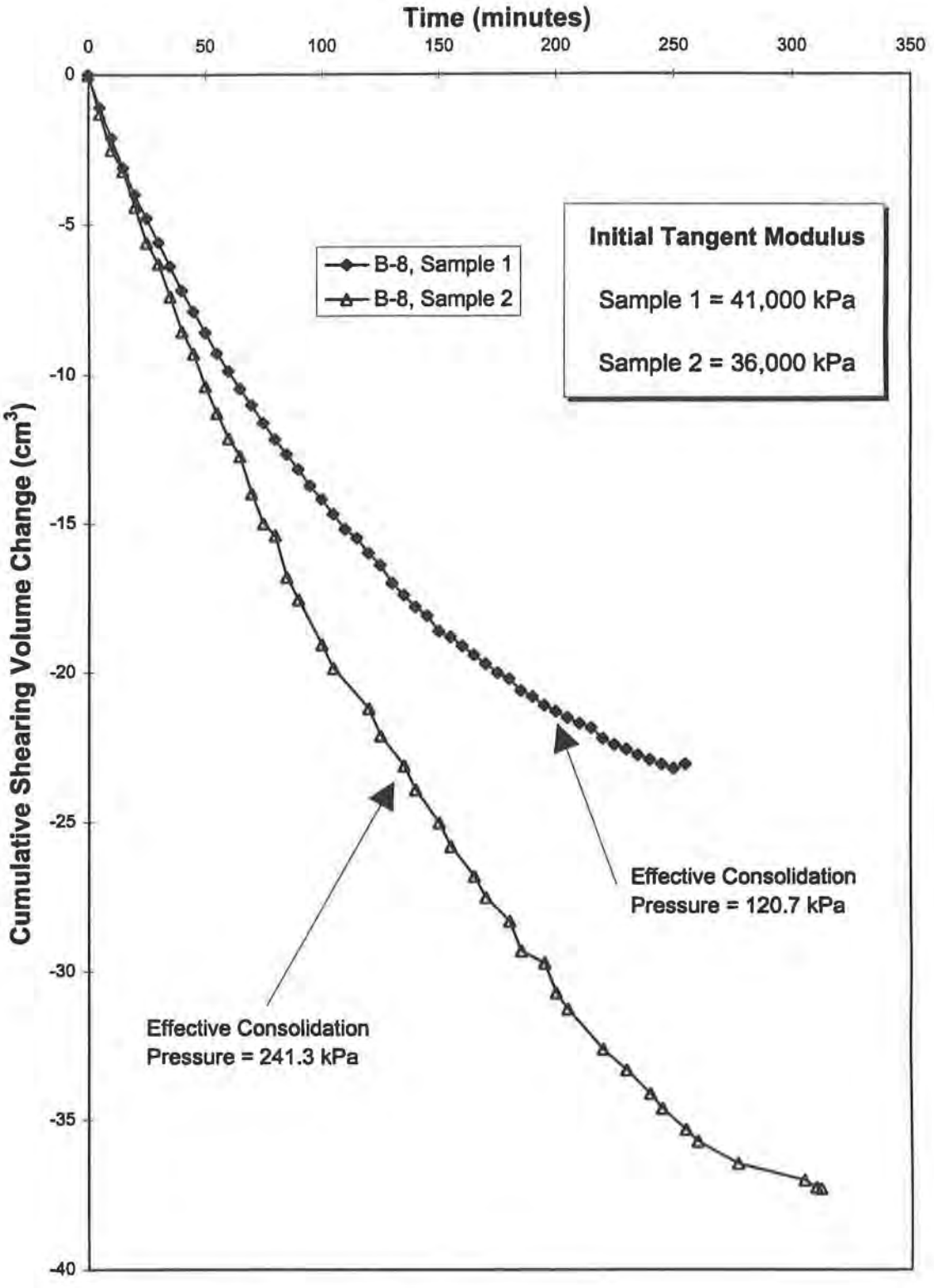

FIG. 8.7.6. - Volume Changes of CD Tests During Shearing.

Table 8.7.1. - CIUC Triaxial Samples With Effective Consolidation Equal to Effective Overburden Pressure.

Effective Consolidation Pressure Approximately Equal to P_o'

Sample ID	E (kPa)	Effective Consolidation Pressure (kPa)	Depth (m)	Maximum Undrained Shear Strength (kPa)	G (kPa)
B-7, Sample 1	13,000	68.9	4	83.5	5,000
B-5, Sample 1	14,000	52.3	4	79.1	5,400
B-7, Sample 1	37,000	89.6	6	118.2	14,200
B-7, Sample 1	32,000	103.4	8	91.6	12,300
B-2, Sample 1	14,000	99.2	8	84.1	5,400
B-7, Sample 1	30,000	120.7	10	91.6	11,500
B-7, Sample 3	32,000	103.4	10	100.5	12,300
B-2, Sample 1	23,000	116.0	12	58.7	8,800
B-5, Sample 1	32,000	127.0	12	89.0	12,300
B-5, Sample 2	20,000	102.0	12	58.8	7,700
B-5, Sample 1-Stg.1	40,000	172.4	15	91.7	15,400
B-2, Sample 1-Stg. 1	40,000	172.4	15	77.9	15,400

Table 8.7.2. - CIUC Triaxial Samples With Effective Consolidation Greater Than Effective Overburden Pressure.

Effective Consolidation Pressure > P_o'

Sample ID	E (kPa)	Effective Consolidation Pressure (kPa)	Depth (m)	Maximum Undrained Shear Strength (kPa)	G (kPa)
B-7, Sample 2	20,000	137.9	4	96.7	7,700
B-8, Sample 1	27,000	134.5	6	120.8	10,400
B-8, Sample 2	27,000	179.3	6	125.5	10,400
B-7, Sample 2-Stg. 1	31,000	206.8	8	117.0	11,900
B-7, Sample 2	38,000	241.3	10	161.7	14,600
B-5, Sample 2-Stg. 1	37,000	241.3	15	157.8	14,200

Second Stage of Multistage Test with
Effective Consolidation Pressure > P_o'

Sample ID	E (kPa)	Effective Consolidation Pressure (kPa)	Depth (m)	Maximum Undrained Shear Strength (kPa)	G (kPa)
B-7, Sample 2-Stg. 2	40,000	310.3	8	175.9	15,400
B-5, Sample 1-Stg. 2	49,000	310.3	15	169.5	18,800
B-5, Sample 2-Stg. 2	76,000	413.7	15	251.9	29,200
B-2, Sample 1-Stg. 2	40,000	310.3	15	155.0	15,400

data presented on Figure 8.7.7 of those CIUC test samples which were consolidated to approximately the vertical effective overburden pressure prior to shearing indicates that E_t varied between 14,000 to 40,000 kPa. Figure 8.7.8 presents the relationship of E_t to effective consolidation pressure (σ_3'); although a lot of scatter produces a rather low regression coefficient, a trend of increasing modulus as a function of increasing σ_3' is evident.

Nineteen UU tests were conducted on samples between 1 and 3 meters depth. The confining pressures were approximately that of vertical overburden pressure for the depth of each sample. Figure 8.7.9 is similar to Figure 8.7.1; the deviator stress is normalized by each test's maximum. Quite large scatter is evident at even small strains.

All maximum undrained shear strengths (S_u) determined from UU and CU testing are shown vs. depth in Figure 8.7.10. This figure also includes a regression of S_u with confining pressures. CU tests have an effective consolidation stress; however, UU tests are usually only partly saturated and the true effective stresses within the sample are unknown. The regression is not very good because of the large scatter evident at the UU tests' small confining pressures. Figure 8.7.11 shows the same plot of S_u vs. σ_3' but with each test denoted as CU or UU (also denoted are UU tests with zero confining pressures; i.e. unconfined compression tests). A regression computed using only CU tests, as denoted in Figure 8.7.11, gives a much higher regression coefficient than that obtained when including all S_u tests. This is probably due to the UU tests' effective confining stresses being unknown and different from the total confining stresses which were used in

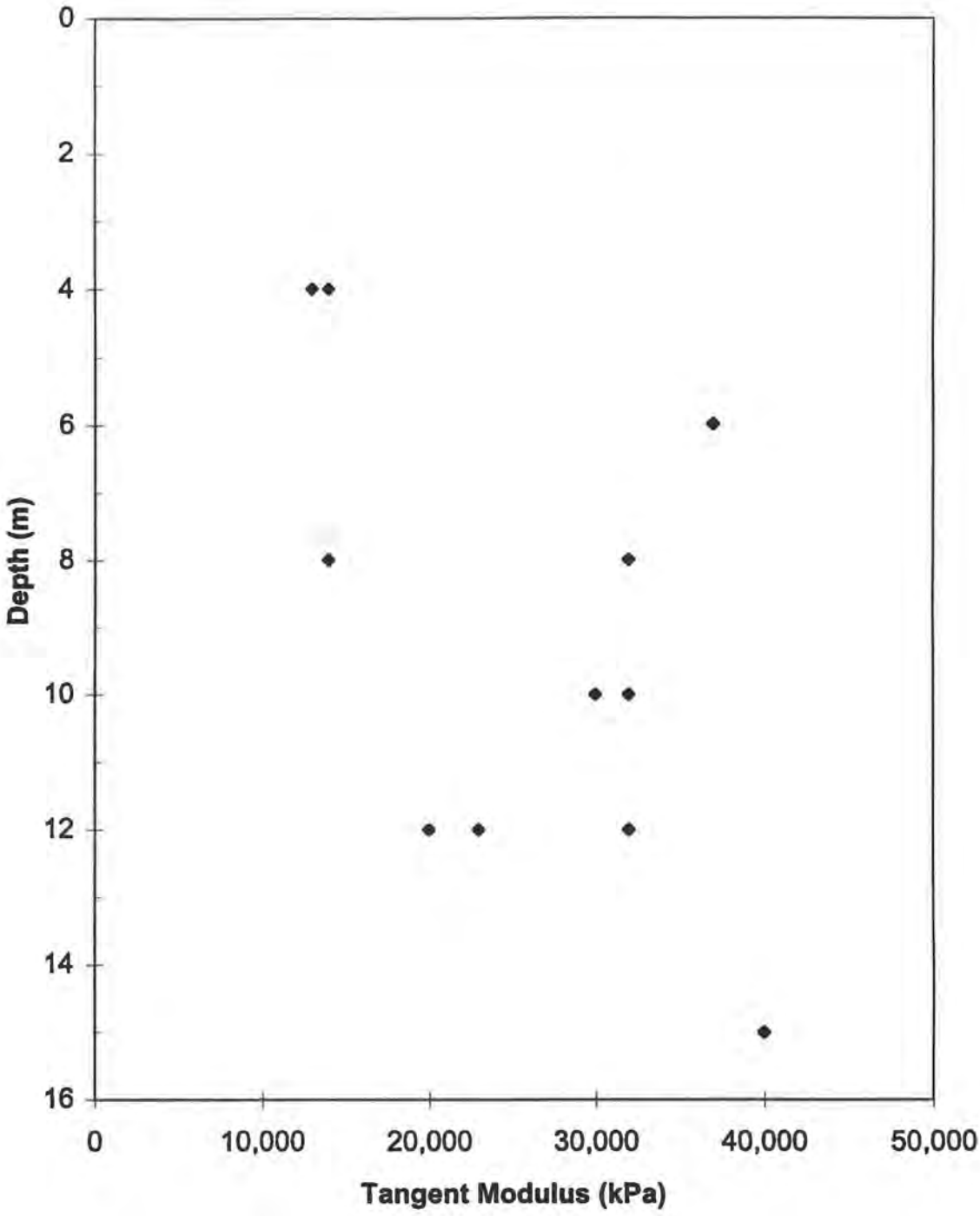

FIG. 8.7.7. - CIUC Tangent Moduli at Effective Consolidation Pressure Approximately Equal to Effective Overburden Pressure.

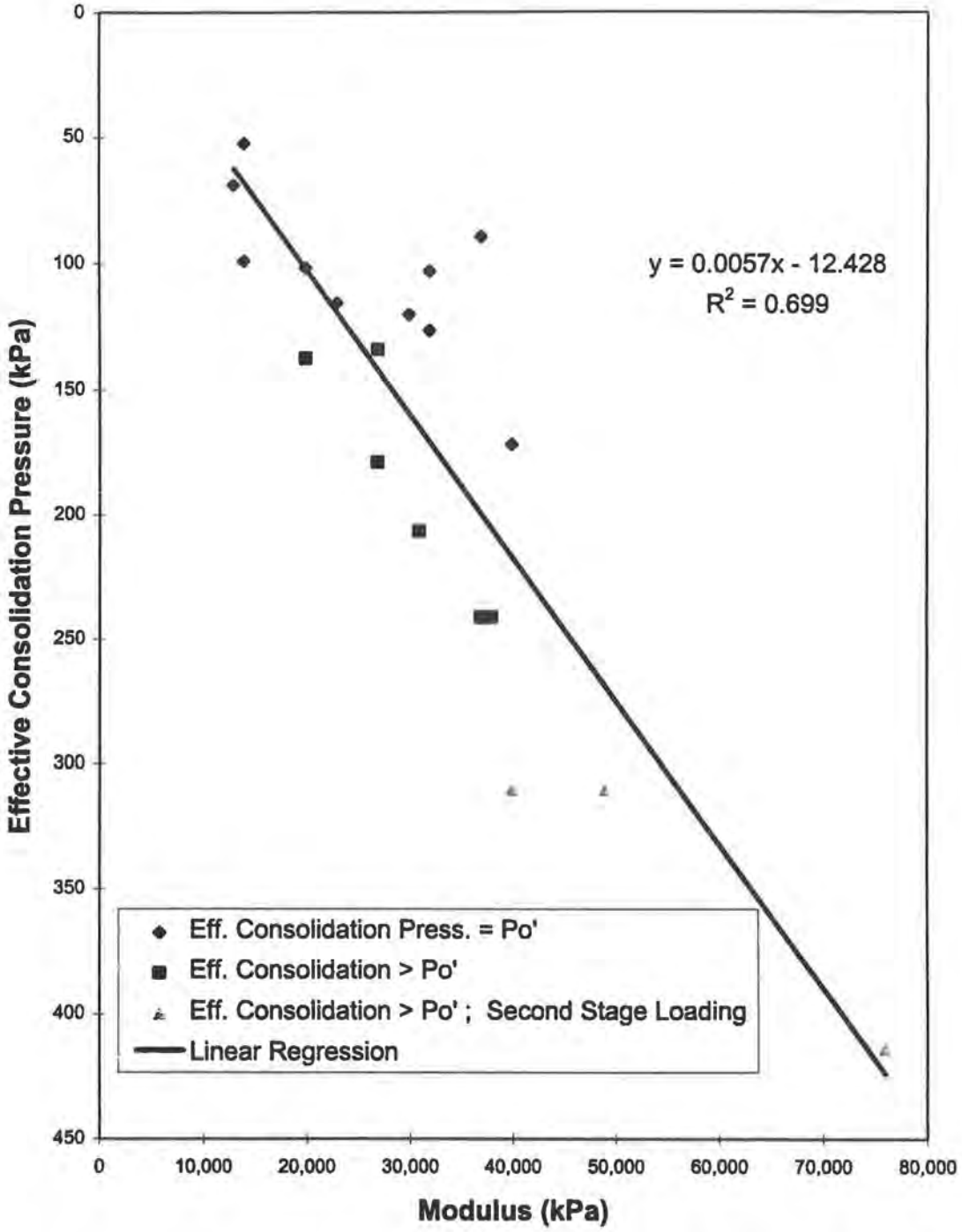

FIG. 8.7.8. - Tangent Moduli from CIUC Tests as a Function of Effective Consolidation Pressure.

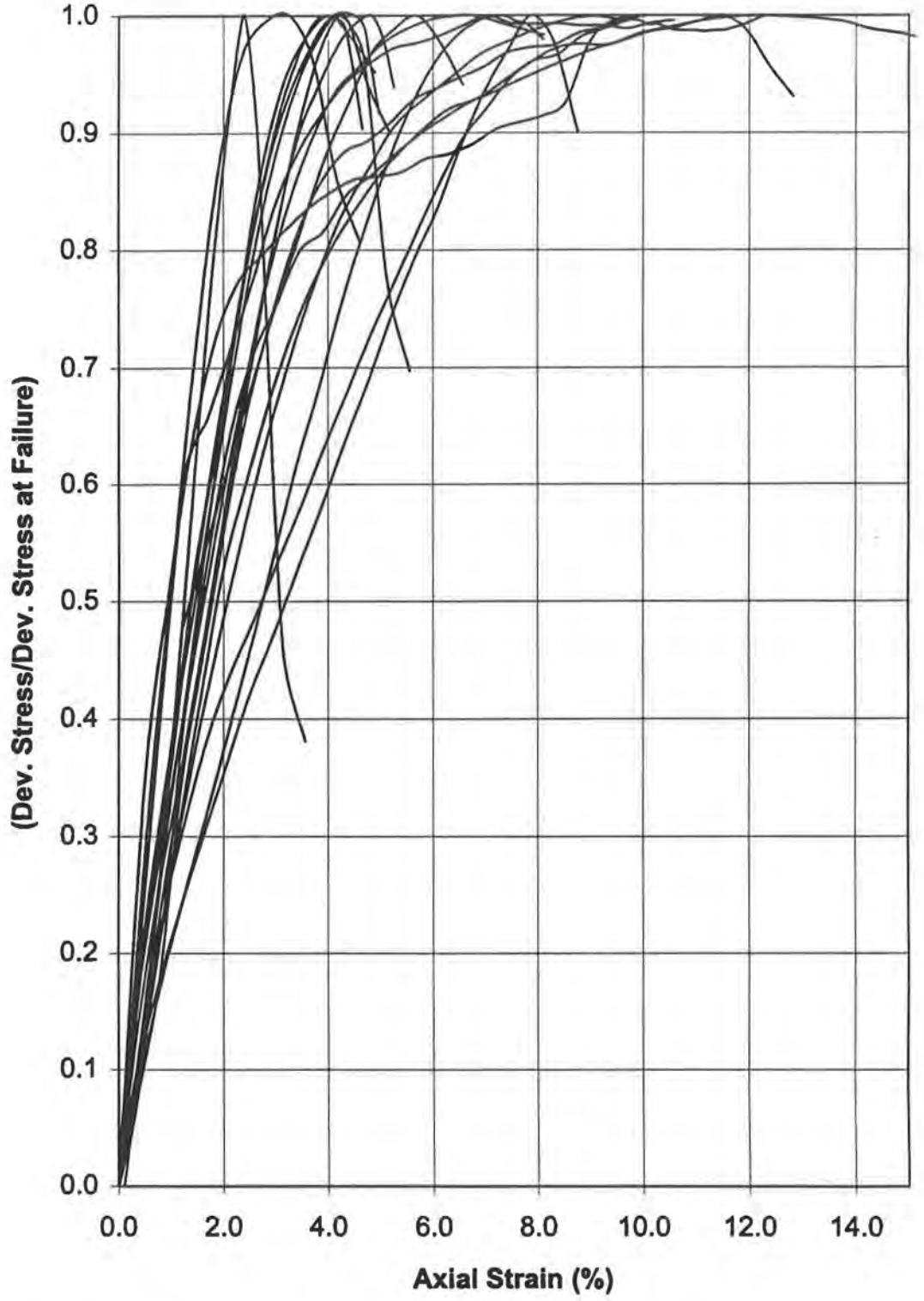

FIG. 8.7.9. - UU Triaxial Summary : Ratio of Deviator Stress to Failure Deviator Stress as a Functin of Axial Strain.

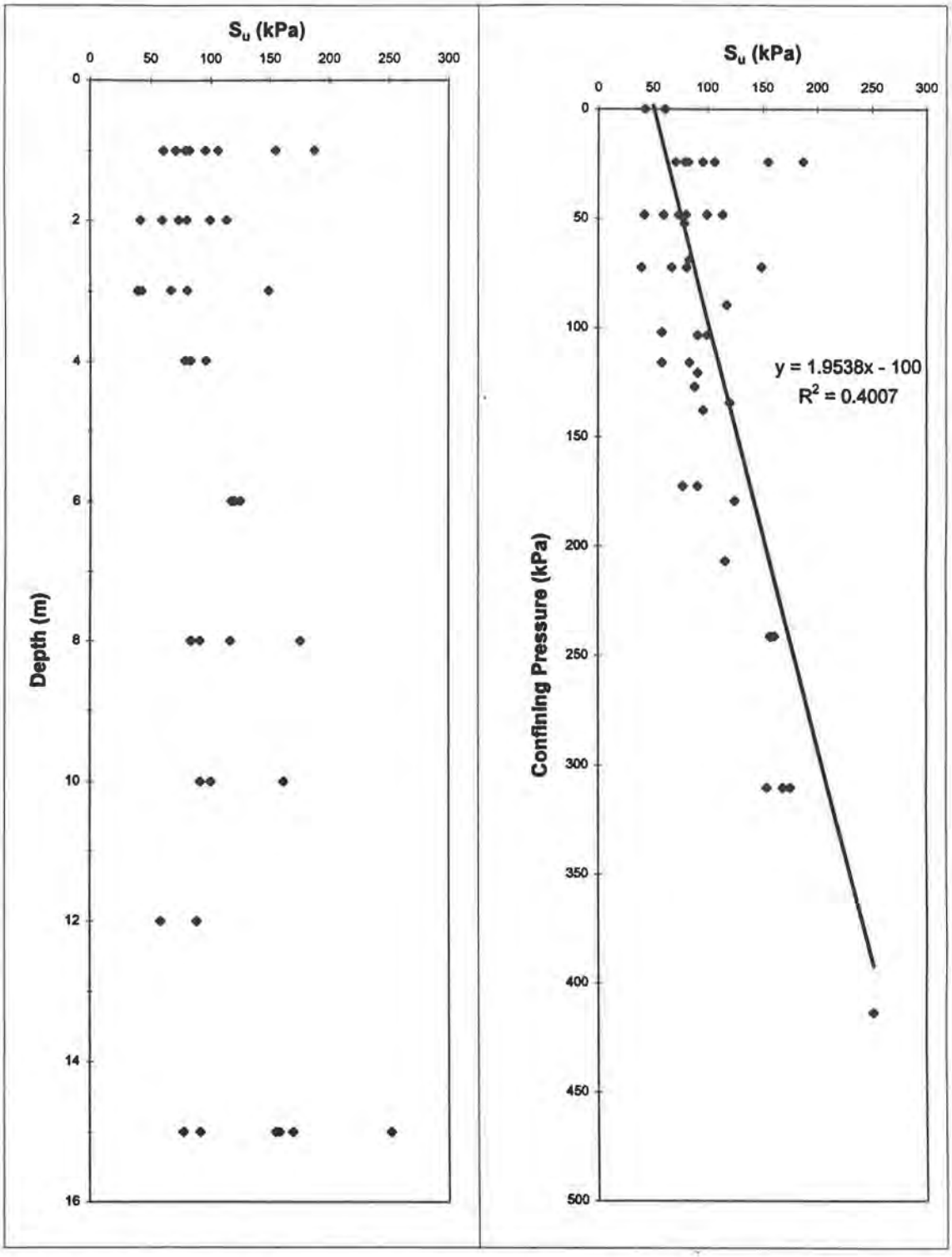

Note : Plots of all UC, UU and CU triaxial test undrained shear strength values including multistage tests regardless of confining or consolidation pressure. The plot on the right gives a linear regression of all tests.

FIG. 8.7.10. - Undrained Shear Strength Measurements from Triaxial Test

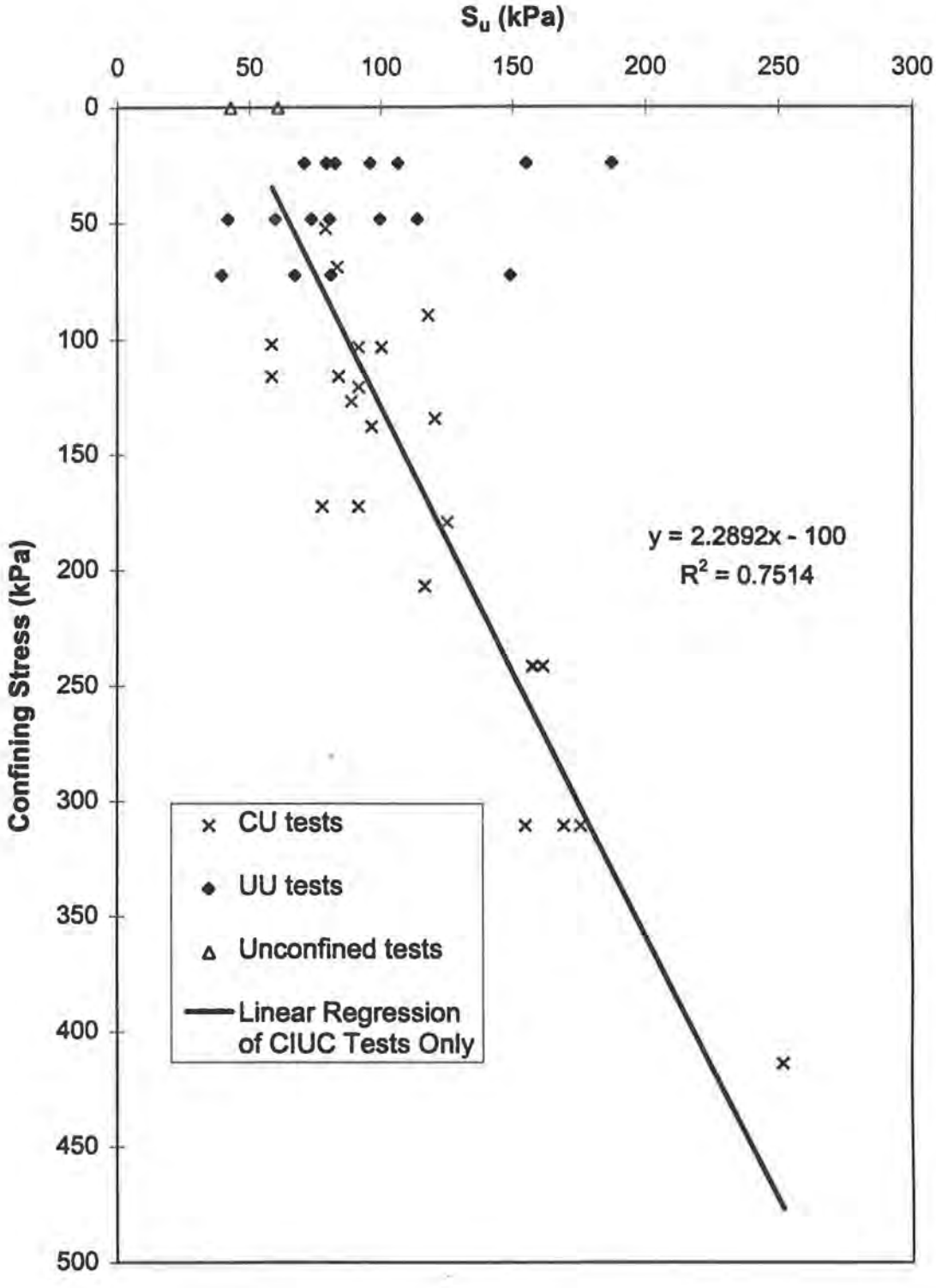

FIG. 8.7.11. - Undrained Shear Strengths by Various Triaxial Tests.

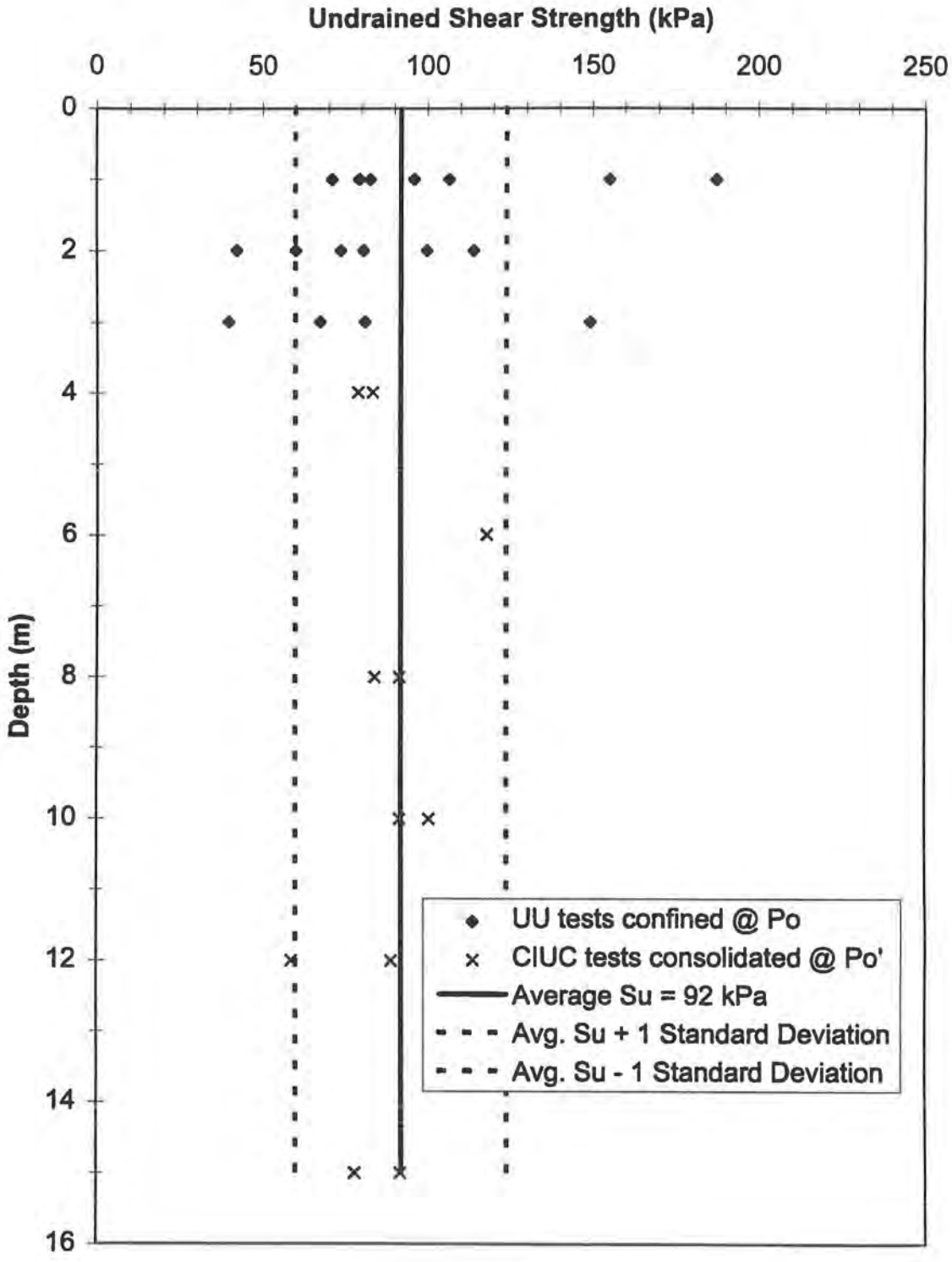

FIG. 8.7.12. - Undrained Shear Strengths at Effective Overburden.

UU testing. Also, the CU test allows reconsolidation of the sample; therefore, some of the sampling effects are overcome.

Those UU and CU tests conducted at confining pressures near the overburden pressure were plotted vs. depth; this plot is shown in Figure 8.7.12. The UU tests exhibit more scatter, but the average value is around 92 kPa. Lines representing plus or minus one standard deviation show that 22 of the 27 tests fall between 60 and 125 kPa.

CHAPTER 9

IN-SITU STRESS CONDITIONS

9.1 General

The pressure in a liquid is the same in any direction, but in natural soil deposits, it is very rare for the vertical and horizontal earth pressures to be equal. It is common for the ratio of horizontal to vertical soil pressures to be expressed as

$$\sigma_h = K\sigma_v$$

where K is termed the earth pressure coefficient. This expresses these pressures as total stresses, but since soil behavior is related to effective stress conditions and since the ground water table can fluctuate, it is convenient to express this ratio in terms of effective stresses as

$$\sigma_h' = K_o\sigma_v'$$

where K_o is called the coefficient of lateral at rest earth pressure. This ratio represents the effective stresses present at a steady state condition where no lateral straining occurs; in other words, the vertical and horizontal pressures act as principal stresses. K_o is sensitive to the overlying soil layer densities and the geologic stress history (i.e. overconsolidation ratio) (Holtz and Kovacs 1981).

9.2 Measurement of K_o

K_o is a fundamental geotechnical engineering parameter which influences bearing capacity of shallow and deep foundations, design of earth retaining structures, excavations, and liquefaction potential studies. Calculation of vertical overburden is usually quite accurate since soil densities and ground water table locations are fairly easily determined. However, measurement of horizontal earth pressure is very difficult.

Different tools can be used to get a measure of horizontal earth pressure, but in-situ devices cause disturbance during positioning which destroys the at rest pressure state they are trying to measure. Laboratory test procedures can be used, but the effects of stress relief during sampling render such tests predictions suspect at best, and some straining of the sample is required to obtain measurements. In-situ tests are considered by many to give better indications of K_o than lab testing; however, it is often justifiable to use an established correlation (e.g., Jaky 1944) to predict K_o since testing can be tedious, expensive and may not provide higher accuracy. Typical values might be assumed for rough calculations; K_o generally ranges from 0.4 to 0.6 for granular materials and from 0.5 to 0.9 for cohesive materials (Holtz and Kovacs 1981).

As mentioned in Section 3.4.6, Piedmont residual soils sometimes have horizontal stresses which are not related to the vertical stresses and can have horizontal pressures at shallow depths which exceed vertical overburden. This phenomenon is due in part to the retained tectonic stresses from previous geologic evolutions which are only partly relieved by weathering (Sowers 1985). Another theory states that volume changes due to weathering produced stress changes which are partially retained in the soil structure

(Sowers 1963). In addition, Sowers also found that Piedmont soils tend to show preconsolidation which may be unrelated to the present overburden pressure.

9.3 K_o Interpretations at Spring Villa

The various interpreted K_o values over the test depths at Spring Villa are shown in Figure 9.3.1. The Menard and cone pressuremeter tests were interpreted, as shown in Appendix D, to examine the total horizontal earth pressures; ground water table depth was accounted for in converting the total pressures to effective pressures. The values for the PMT and CPMT were averaged for each testing depth; the individual test values are shown in Tables 9.3.1 and 9.3.2, respectively. Published correlations for the DMT, CPT, and SPT are also included in Figure 9.3.1; explanations and examples of calculations are shown in the appropriate test appendix. Table 9.3.3 contains the correlation predictions of K_o involving the DMT. The correlation by Marchetti (1985) which combines CPT and DMT results is shown in Appendix E. The commonly mentioned correlation for normally consolidated, granular material by Jaky (1944) is also included in Figure 9.3.1 for comparison; an average effective friction angle value of 31 degrees was used over the depth range of effective stress strength triaxial testing for the Jaky relationship.

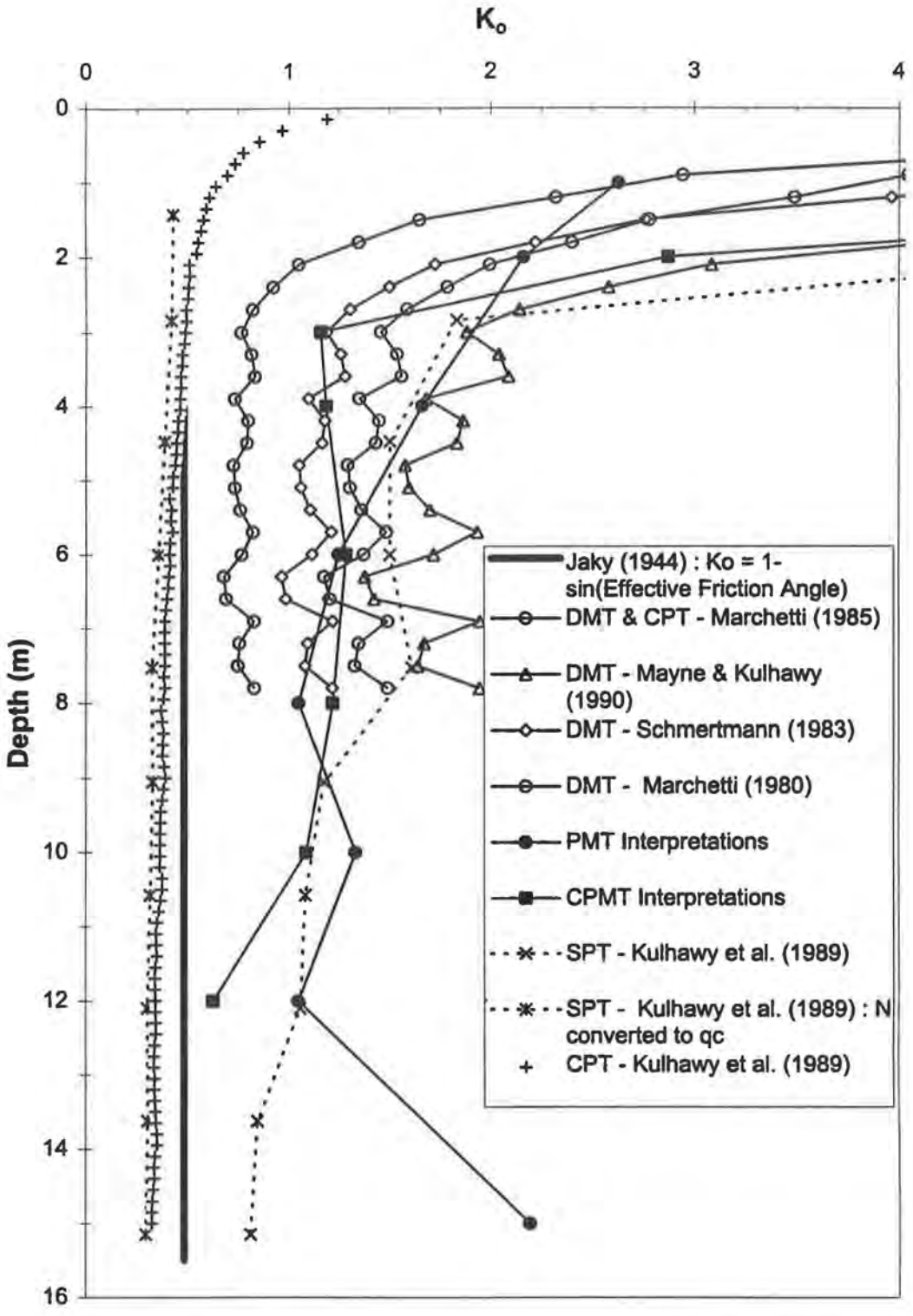

Figure 9.3.1. - Summary of K_o Estimates for Spring Villa.

Table 9.3.1. - Estimated K_o Values from Menard Pressuremeter Test.

PMT					
Location :	B-2	B-2	B-5	B-5	
Depth (m)	Horizontal Total Earth Pressure (kPa)	K_o	Horizontal Total Earth Pressure (kPa)	K_o	Average K_o
1	38	2.08	58	3.18	2.63
2	81	2.22	77	2.11	2.16
3	-	-	-	-	-
4	115	1.66	115	1.66	1.66
6	134	1.31	125	1.19	1.25
8	163	1.18	139	0.93	1.05
10	211	1.25	230	1.42	1.33
12	211	0.94	240	1.16	1.05
15	450	2.13	470	2.26	2.19

Table 9.3.2. - Estimated K_o Values from Cone Pressuremeter Test.

CPMT									
Location :	C-41P	C-41P	C-42P	C-42P	C-43P	C-43P	C-44P	C-44P	
Depth (m)	Horizontal Total Earth Pressure (kPa)	K_o	Horizontal Total Earth Pressure (kPa)	K_o	Horizontal Total Earth Pressure (kPa)	K_o	Horizontal Total Earth Pressure (kPa)	K_o	Average K_o
1	100	5.48	250	13.7	200	10.96	50	2.74	8.22
2	90	2.47	150	4.11	130	3.56	50	1.37	2.88
3	80	1.24	60	0.93	90	1.39	70	1.08	1.16
4	90	1.27	60	0.79	100	1.43	90	1.27	1.19
6	120	1.13	170	1.76	150	1.51	90	0.76	1.29
8	190	1.45	180	1.35	150	1.04	150	1.04	1.22
10	170	0.89	200	1.15	200	1.15	200	1.15	1.09
12	-	-	-	-	-	-	170	0.63	0.63
15	-	-	-	-	-	-	-	-	-

Table 9.3.3. - K_o Esimates by DMT Correlations.

Depth [m]	Effective Overburden [kN/m^3]	AU1 K_D	AU2 K_D	AU3 K_D	Average K_D	Avg. qc from CPT [kPa]	Marchetti (1980) f(K_D) Avg. K_o	Mayne & Kulhawy (1990) f(K_D) Avg. K_o	Marchetti (1985) f(K_D,q_c, P_o') Avg. K_o	Schmertmann (1983) f(K_D,phi') Avg. K_o
0.3	5.5	65.45	47.27	89.27	67.33	1,513	5.38	18.18	4.88	8.44
0.6	11.0	65.64	44.00	50.55	53.39	1,687	4.76	14.42	4.01	6.77
0.9	16.4	44.88	-	39.09	41.98	1,823	4.19	11.34	3.24	5.40
1.2	21.9	34.02	22.74	35.57	30.78	2,007	3.54	8.31	2.46	4.05
1.5	27.4	21.61	14.71	24.56	20.29	1,963	2.80	5.48	1.73	2.79
1.8	32.9	18.88	11.16	16.14	15.39	2,019	2.39	4.16	1.39	2.20
2.1	47.2	9.70	8.01	10.13	9.28	2,444	1.75	2.51	0.97	1.47
2.4	49.7	9.28	7.63	8.29	8.40	2,641	1.65	2.27	0.91	1.36
2.7	52.2	7.46	6.87	7.10	7.14	2,581	1.48	1.93	0.82	1.21
3	54.8	6.58	5.96	6.65	6.40	2,526	1.38	1.73	0.77	1.12
3.3	57.3	7.38	4.84	6.50	6.24	2,477	1.35	1.69	0.76	1.10
3.6	59.8	6.10	5.76	6.67	6.18	2,498	1.34	1.67	0.76	1.09
3.9	62.3	5.23	7.33	5.15	5.90	2,440	1.30	1.59	0.74	1.06
4.2	64.8	5.11	5.85	6.68	5.88	2,376	1.30	1.59	0.74	1.06
4.5	67.3	5.50	6.23	7.39	6.37	2,263	1.37	1.72	0.78	1.12
4.8	69.8	5.88	4.92	4.72	5.17	2,305	1.19	1.40	0.70	0.97
5.1	72.3	5.94	4.77	5.03	5.25	2,284	1.20	1.42	0.70	0.98
5.4	74.8	5.19	4.60	6.68	5.49	2,433	1.24	1.48	0.72	1.01
5.7	77.3	8.27	4.76	5.94	6.32	2,337	1.37	1.71	0.78	1.11
6	79.8	6.14	4.80	6.22	5.72	2,381	1.28	1.54	0.74	1.04
6.3	82.3	3.90	4.54	4.55	4.33	2,400	1.05	1.17	0.64	0.87
6.6	84.8	4.55	5.09	4.30	4.65	2,552	1.10	1.25	0.66	0.91
6.9	87.3	5.38	5.16	7.74	6.10	2,521	1.33	1.65	0.76	1.08
7.2	89.8	5.81	6.11	5.16	5.69	2,630	1.27	1.54	0.74	1.04
7.5	92.3	-	5.63	6.83	6.23	2,533	1.35	1.68	0.78	1.10
7.8	94.8	-	4.05	-	4.05	2,567	1.00	1.09	0.62	0.84
8.1	97.3	-	6.33	-	6.33	2,958	1.37	1.71	0.78	1.11

9.4 Comparison and Evaluation of Predictions

It is evident from Figure 9.3.1 that K_o at a given depth can vary a great deal depending on which test was used. No test methods which are considered highly accurate, such as the self-boring PM test (SBPMT), have been used to date at Spring Villa to evaluate K_o; therefore, no reference values can be used to compare with the various prediction methods.

A large K_o at depths less than 3 meters was generally predicted by most tests including pressuremeter evaluations and flat dilatometer correlations. This could be attributed to the dessicated upper zone. The upper zone contains an appreciable amount of clay particles, and the drying out of the soil could cause the soil to become overconsolidated. Holtz and Kovacs (1981) indicate increases in OCR tend to make K_o higher. The only evaluation of OCR at Spring Villa has been by DMT correlations as shown in Appendix F. These correlations show overconsolidation and that the OCR decreases with increasing depth.

The lowest K_o predictions came from the Kulhawy et al. (1989) correlation which uses CPT tip resistance (q_c) values; this correlation was established empirically on calibration chamber tests in normally and overconsolidated sands. It requires the soil's relative density; the Jamiolkowski et al. (1985) correlation, which is based on five sand sites, was used to predict the Spring Villa relative densities. The q_c and relative density values are probably not highly accurate since both correlations are based upon clean sands and not weathered silty sands and sandy silts. In addition, SPT blow counts were converted to q_c values, as shown in Appendix B, in order to use the Kulhawy et al.

correlation for sands; both SPT and CPT evaluations would probably be considered lower than the true K_o as would Jaky's relationship, which is based on sedimentary, not residual, soils.

Interpretation techniques of the pressuremeter tests show fairly good agreement between each other with most K_o values ranging between 1 and 1.5; they agree with the Marchetti (1980) and Schmertmann (1983) correlations for DMT as well. The PMT's reasonable evaluation of horizontal at rest earth pressure is dependent upon preparation of a clean, properly dimensioned hole which may be difficult below the ground water table. Also, the CPMT involves a back-fit interpretation of the loading curve since insertion of the cone causes the horizontal soil pressures to be larger than the at rest pressure from the start of testing. Even with these potential difficulties, the two PM types are seen to produce very similar average measures of K_o.

Kulhawy et al. (1989) also presented a SPT correlation from fissured and intact clays; the correlation presented by Mayne and Kulhaway (1990) for use with the DMT was also established for fissured and intact clays. These correlations produced the largest predictions at depths greater than 3 meters. Both of these correlations are probably not applicable since they were derived from clay soils. However, the SPT correlation is interestingly similar to predictions by PM testing at depths less than 12 meters.

Marchetti (1980, 1985) presented two correlations which relate the DMT's horizontal stress index, K_D, to K_o either solely or in relation with the CPT's q_c. The 1980 correlation, based solely on DMT's K_D, was established from testing of Italian insensitive clays and uncemented sands. However, the soil at Spring Villa does show varied

amounts of cementation or cohesion. The 1985 correlation involving DMT and CPT data gives K_o values at or near unity below the 2 meters depth; this correlation was based on chamber testing and field measurements of sands.

Schmertmann (1983) presented a correlation between DMT test data and effective friction angle. The correlation was developed for sandy soils with I_D values greater than 1.2; the average value of the Spring Villa soils was at or near 1.0. The average effective friction angle of 31 degrees over the range of CIUC triaxial testing was used; this angle was assumed constant for all depths considered.

9.5 Summary and Conclusions

K_o values from the various measurement techniques and correlations used at Spring Villa were scattered over a relatively large range with most at or above 1.0 within the saprolite zone (3 to 15 meters). Almost all predictions were much larger than those values of K_o predicted by the Jaky relationship or the typical ranges of K_o given by Holtz and Kovacs (1982). For residual soils, K_o is expected to be larger than that of typical sedimentary soils, especially at shallow depths, since geologic stress history affects K_o. Piedmont residual soils are reported to retain complex stress states derived from the formation of the parent rocks, to exhibit high horizontal pressures greater than the vertical overburden at shallow depths, and to possibly have weathering-induced stresses. Other factors peculiar to these soils include preconsolidation unrelated to present overburden which may cause the soil to exhibit overconsolidation. Increases in OCR suggest

increased K_o; DMT correlations predict that the Spring Villa soils are overconsolided - especially in the upper zone. The upper zone has a fairly high fines content and is probably overconsolidated because of dessication.

Although a reference K_o from the self-boring pressuremeter test at this site is not available, several observations concerning the various in-situ techniques and correlations can be made:

- All interpretations based on horizontal expansion (i.e. PMT, CPMT, and DMT) predicted K_o well above the typical range of sedimentary soils.
- The PMT and CPMT produced consistent and similar results.
- DMT interpretations varied widely, depending on soil type assumed; the Marchetti (1980) and Schmertmann (1983) correlations were most nearly consistent with the PMT and CPMT data.
- None of the interpretations using CPT were consistent with the average PMT, CPMT, or DMT measurements; these values were consistently lower possibly due to correlation with tip resistance (which may be more an evaluation of vertical and not horizontal soil conditions).
- The Kulhawy and Mayne (1989) SPT correlation developed for fissured and intact clays was generally consistent with PMT and CPMT data. Perhaps this is attributable to the saprolite exhibiting some cohesion much like a "clay"; triaxial strength testing predicted some effective, or true, cohesion in the saprolite.

CHAPTER 10

STIFFNESS PARAMETERS

10.1 General

Many construction materials tend to exhibit linear elastic behavior during initial compressive loading followed by an eventual plastic failure upon continual increases of load such as structural steel; however, soil tends to exhibit nonlinear behavior at strains well below yielding. Soil behavior is often modeled using elasticity theory for simplicity and ease of use, but a soil's stiffness resistance is curvilinear, mostly inelastic (except for that small deformation which might be regained due to particle compression rebound), and is a function of the strain level (Bowles 1996). Other factors can play a part in soil stiffness response such as stress level, time of loading, and loading frequency (Briaud 1992). Figure 10.1.1 displays the variation in secant modulus with strain range from a typical soil stress-strain plot.

Soil deformation moduli would be expected to be greater at small strains compared to larger strains. This phenomenon of modulus degradation over increasing strain amplitudes has been investigated and verified by several investigators (e.g. Seed and Idriss 1970). The rate of degradation is important in the proper design of dynamically loaded foundations, liquefaction potential estimation and other geotechnical engineering applications.

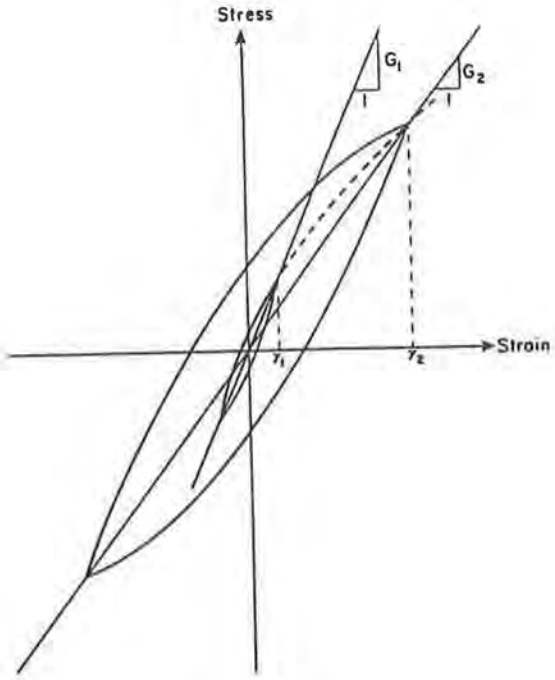

FIG. 10.1.1. - Hysteretic Stress-Strain Relationships at Different Strain Amplitudes (Stokoe et al. 1986).

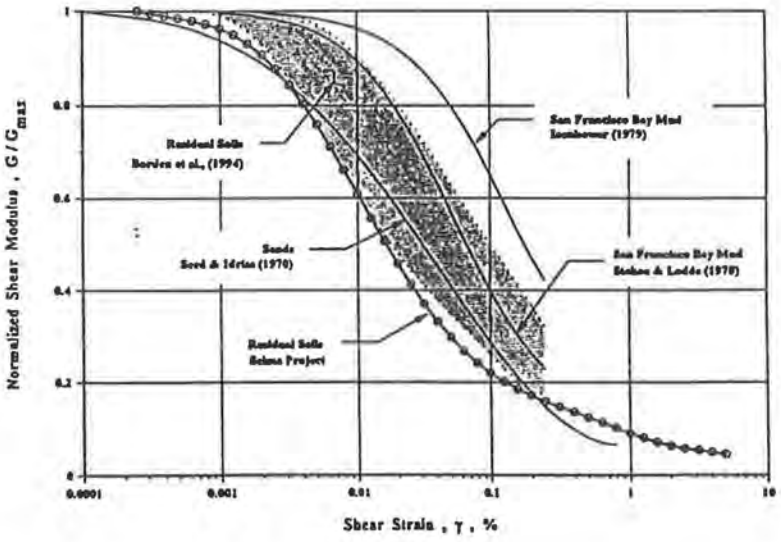

FIG. 10.1.2. - Normalized Shear Modulus as Function of Shear Strain from Published Reports (Wang and Borden 1996).

A common manner of displaying the degradation of modulus is a plot of the ratio of shear modulus to the maximum small-strain shear modulus as a function of shearing strain. Figure 10.1.2 is such a plot which displays several different soil types including Piedmont residual soils. This figure also includes a shaded region which gives a probable range for most residual soils as determined by Borden et al. (1994). Note that regardless of soil type, a maximum shear modulus is generally observed at shearing strains near or less than 0.001%. This maximum modulus value is independent of shearing strain, but the soil only exhibits this stiffness at very low strain amplitudes.

10.2 Summary of Measured Moduli

The subsequent sections in this chapter compare and contrast the various measured and correlated predictions of elastic or shear modulus. To aid in evaluation and comparison, those tests which give a measure of elastic moduli were averaged at each test depth and converted to shear modulus by using the elastic theory relationship as follows

$$G = E/(2(1 + \nu))$$

where G = shear modulus, E = Young's elastic modulus, and ν = Poisson's ratio, which was assumed to equal 0.3 for the Spring Villa soils. These shear moduli over depth are shown in Figure 10.2.1; this figure has a logarithmic abscissa in order to better illustrate the variation among the intermediate- to high-strain modulus tests. Note that all subsequent correlations are discussed along with example calculations in the appropriate test appendix.

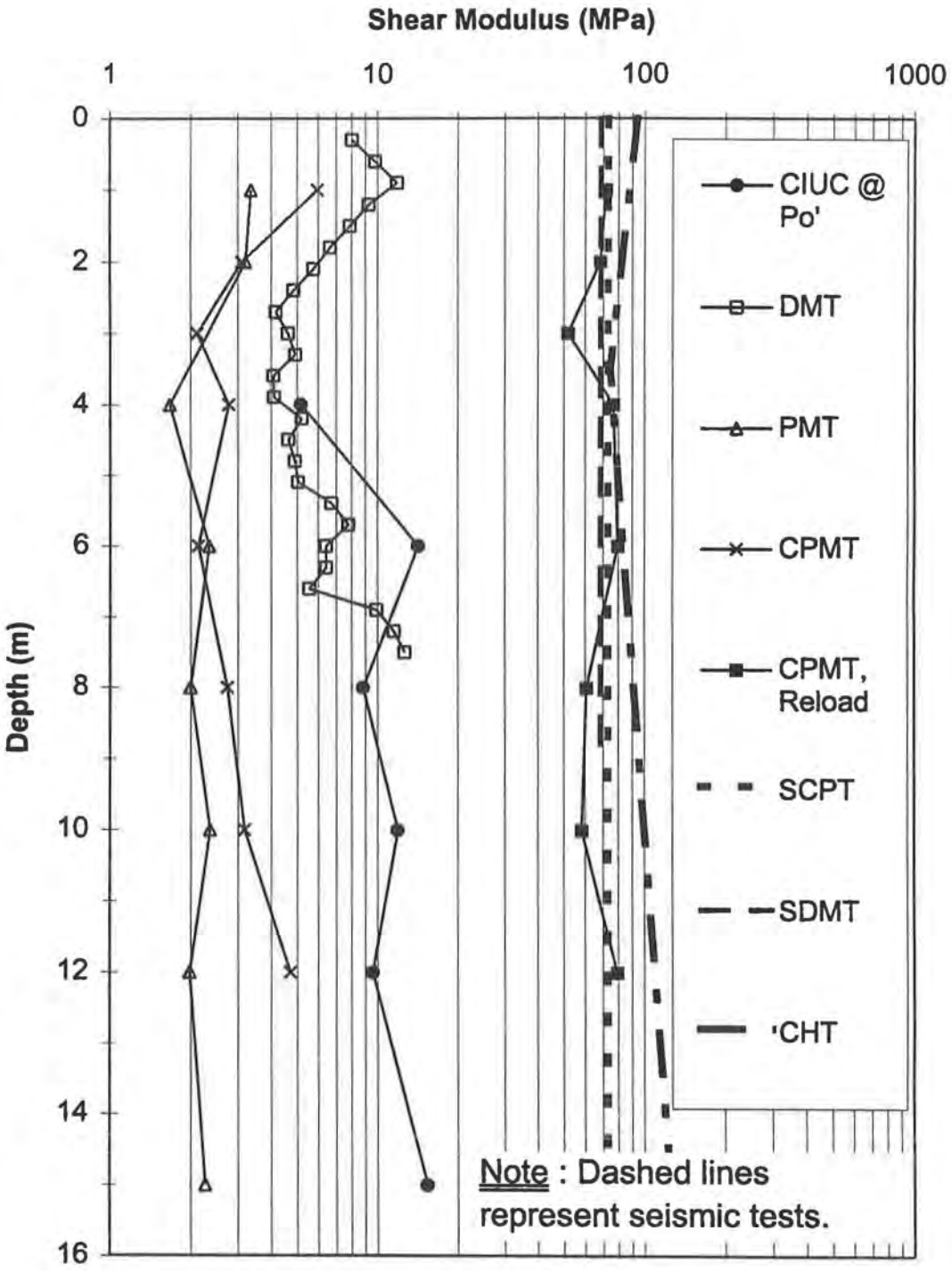

FIG. 10.2.1. - Summary of Average Measured Shear Moduli Over Depth.

From this plot, it is clearly evident that the seismic test methods generally gave shear moduli which are approximately 10 to 15 times that of most mechanically measured moduli. This is expected since the strain level of a shear wave propagating through the soil is much smaller than what most mechanical tests are able to measure; however, the unload-reload cycle of the CPMT does produce relatively high shear moduli which are approaching the seismic tests predictions.

10.3 Shear Modulus Using Shear Wave Measurements

The crosshole and downhole seismic methods measure shear wave velocities through the soil, and from these shear velocities, small-strain shear moduli can be predicted. As presented in Chapter 8, the prediction of shear wave velocities at Spring Villa showed relatively good agreement among the different seismic techniques.

As previously mentioned, the shear modulus at a shearing strain of approximately 0.001% tends to represent a near-threshold strain amplitude at which the shear modulus reaches a maximum and becomes constant over smaller strains. The shearing strain levels for the SDMT shear modulus predictions ranged from 0.001 to 0.009 % as shown in Figure 10.3.1; calculation of these shearing strains are shown in Appendix F. The shearing strain levels of the other seismic tests were assumed to be in this same general range, or lower, where a maximum shear modulus develops since results among the different techniques were relatively similar.

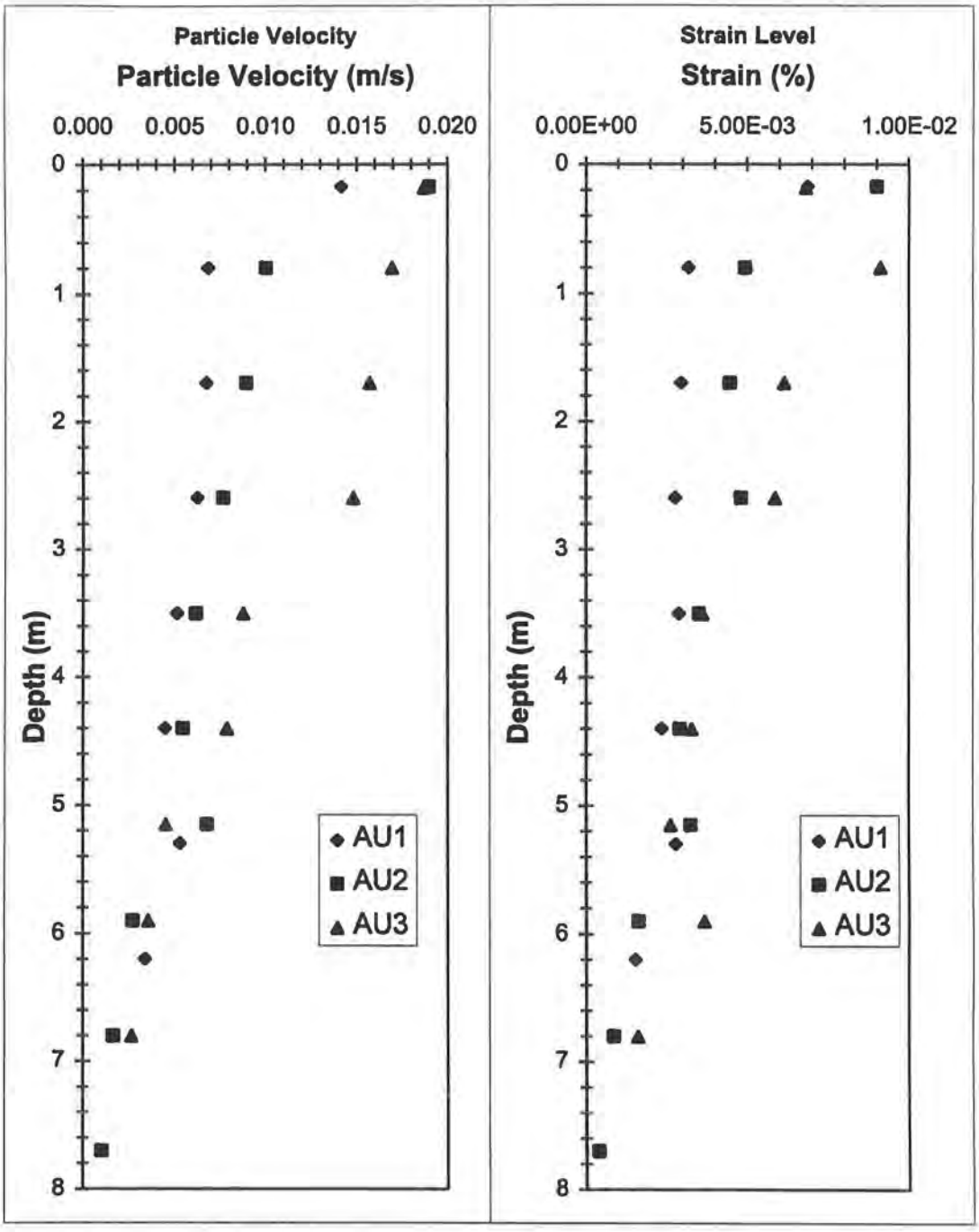

FIG. 10.3.1. - Seismic Dilatometer Test Particle Velocities and Shearing Strain Levels.

10.4 Mechanical Measures of Small- to Intermediate-Strain Shear Modulus

The CPMT unload-reload cycle produced very high modulus values compared to the other mechanical measures of modulus. The radial strain level over which this modulus is taken can be determined and converted to shearing strains by using the argument put forth by Briaud (1992) for plane strain cavity expansion around a pressuremeter probe. From plane strain theory, the principal strains are as follows

$$\varepsilon_1 = \varepsilon_r$$

$$\varepsilon_3 = \varepsilon_\theta$$

where ε_1 = major principal strain, ε_r = radial strain, ε_3 = minor principal strain, and ε_θ = circumferential tangential strain. From elasticity theory, the maximum shearing strain (γ_{MAX}) is related to these principal strains as follows

$$\gamma_{MAX} = \varepsilon_1 - \varepsilon_3$$

Radial strain can be determined by using the relationships expressed as

$$\varepsilon_r = (\Delta R/R_o)_2 - (\Delta R/R_o)_1 = ((V_o + v_c)/V_o)^{0.5} - 1$$

where $(\Delta R/R_o)$ = relative increase in probe radius, V_o = deflated volume of probe, and v_c = increase in volume of probe cavity. Further, ε_3 may approach a value as low as $-\varepsilon_r$ (i.e. tension) unless the soil cracks in tension, in which case $\varepsilon_3 = \varepsilon_\theta$ approaches zero. From evaluation of the CPMT unload-reload cycles, the radial strains were in the range of 0.1% to 0.5%; therefore, γ_{MAX} is in the range of 1 to $2\varepsilon_r$ and is expected to decrease proportional to the square of the probe radius away from the probe. So, an average γ is taken as 0.05% to 0.3%; average γ amplitude in the zone most significant in affecting modulus would be expected to near half of γ_{MAX}.

This shearing strain amplitude is much larger than that of seismic testing but smaller than most other mechanical measures; however, shear modulus values averaged approximately 75% of the small-strain shear modulus from the CHT at the same test depth. This is much larger than would be expected if all test conditions were constant among the different techniques besides γ, but it is suspected that this unload-reload cycle produces a measure of soil stiffness at higher effective stresses than the other techniques. The CPMT has displaced soil previous to the unload-reload cycle, and this displaced soil which has been consolidated to varying degrees drains quickly so that the increase in probe pressure probably means an increase in radial effective stresses. Since the modulus values were scattered and small measured volume changes during this reload cycle were near the limit of equipment capability, the similarity between the unload-reload moduli and seismic small-strain moduli may be a site-specific phenomenon.

10.5 Mechanical Measures of Intermediate- to Large-Strain Shear Modulus

The CPMT (initial load cycle), PMT, DMT, CIUC/CIDC triaxial tests consolidated isotropically to approximately effective overburden pressure (P_o'), and UU triaxial tests with confining pressure near overburden pressure (P_o) produce mechanical measures of modulus at what would be considered intermediate- to large-strains. Figure 10.5.1 gives a more detailed view of these tests' predictions of the average shear moduli over depth compared to Figure 10.2.1. All triaxial test moduli were determined by examining the

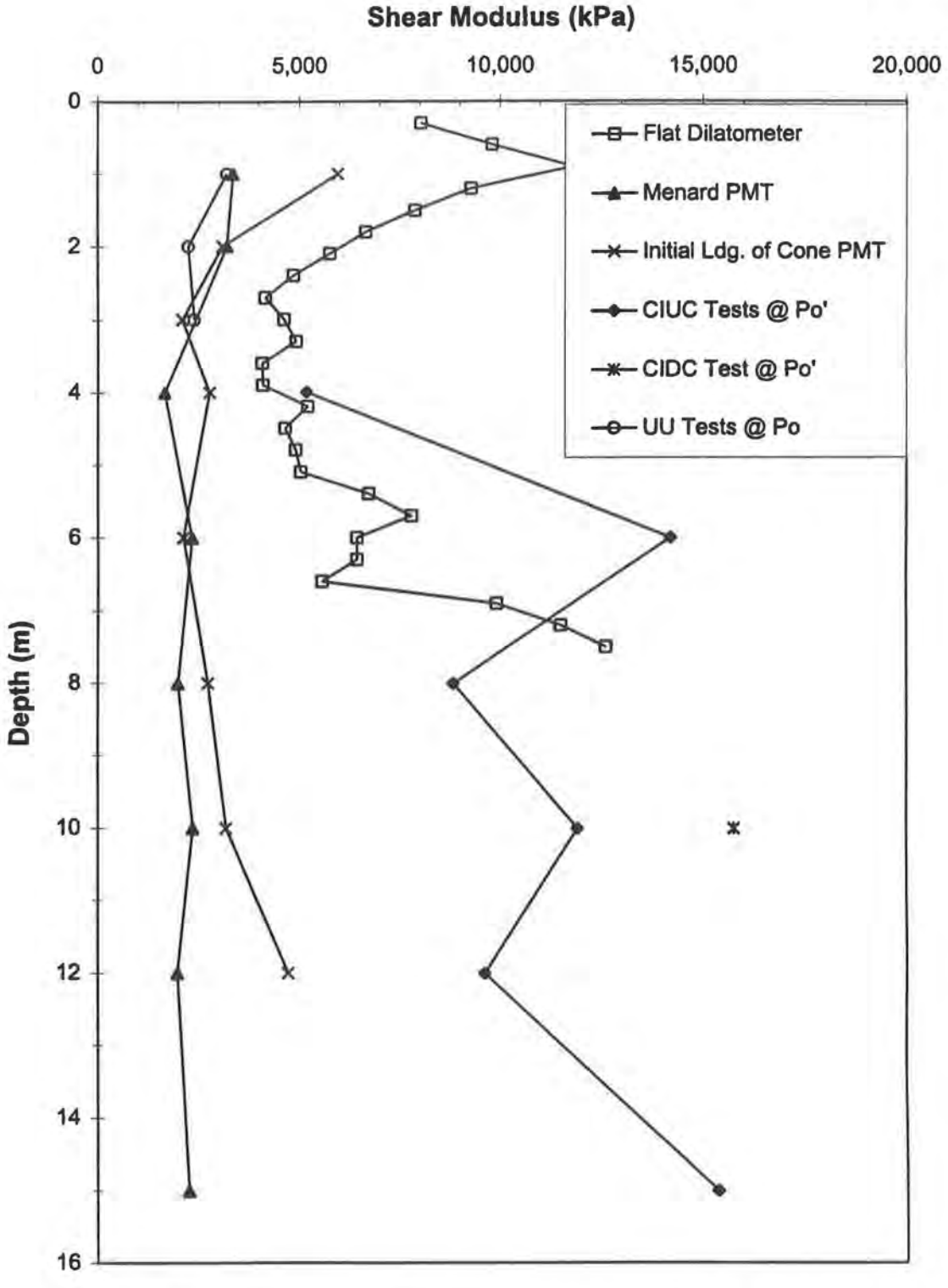

FIG. 10.5.1. - Summary of Mechanical Measures of Intermediate- to Large-Strain Shear Modulus.

tangent moduli at 0.3% to 0.5% axial compressive strain which can be related to shearing strain by the elastic theory relationship as follows

$$\gamma_{MAX} = \varepsilon_y(1 + \nu)$$

where ε_y = compressive axial strain and ν = Poisson's ratio which was assumed equal to 0.3. Therefore, since $\gamma_{MAX} \cong 0.65\%$, the average γ is taken as near 0.5%.

From this plot, it can be seen that the PMT and CPMT give similar values over depth, and the CPMT shows comparatively higher values by sometimes as much as 2,000 kPa at the 1 and 12 meter depths. Both show the general trend of little variation over depth; the CPMT does begin to show increase in modulus at the 12 meter depth. The PMT and CPMT typically have radial strains over which the initial-loading PM modulus is determined over the range of 2% to 5% (Briaud 1992). By using plane strain cavity expansion theory as discussed in Section 10.4, the average γ is considered to range from 1% to 2% for both the PMT and CPMT.

The DMT shows more variation than the PM tests at depths less than 2 meters. Values are relatively constant at about 2,000 to 3,000 kPa higher than the PMT and CPMT, but a marked increase is seen at the 7 meter depth. The DMT probably strains the soil less than the PM tests; therefore, it would be expected that moduli would be higher. In fact, using relationships presented by Poulos and Davis (1974) for distributed loads on the circular surface of a semi-infinite mass, radial shear strain is given as follows

$$\gamma_{rz} = \gamma_{zr} = p(2G_1(1 + \nu))/E = (2\tau_{rz}((1 + \nu))/E$$

where $\gamma_{rz} = \gamma_{zr}$ = vertical-radial shear strain, p = load, G_1 = function of radial and depth coordinates where γ is determined, E = Young's modulus, and τ_{rz} = vertical-radial shear stress. Also, the deflection at the center of this circular loaded area is given as

$$\rho_{z=0} = (2pa(1 + \nu^2))/E$$

where $p_{z=0}$ = deflection at center of circular loaded area and a = radius of circular area. Through rearrangement of terms, these equations become

$$\gamma_{rz}/\rho_{z=0} = G_1/((1 - \nu)a)$$

where $p_{z=0}$ = deflection at center of dilatometer's flexible circular membrane is equal to 1.1 mm at full expansion and a = radius of flexible circular membrane is 30 mm. Therefore, this relationship becomes

$$\gamma_{rz}/1.1 \text{ mm} = G_1/21 \text{ mm}$$

and since G_1 has an approximate mean of 0.2, $\gamma_{rz} \cong 0.15\%$.

The CIUC triaxial tests show agreement with the DMT between 4 and 8 meters. At greater depths, the CIUC tests have a general trend of slight increase in modulus over depth. Compared to the PM tests, CIUC moduli is sometimes 3 to 6 times as large at the same depth.

The CIDC test at 10 meters is included on Figure 10.5.1. The modulus from this test is a drained modulus, unlike the other triaxial tests. Since only one test at $\sigma_3' = P_o'$ was conducted, very few conclusions can be drawn.

In addition, the average modulus of UU tests at 1, 2 and 3 meters depth were similar to that of the PM tests. Although determined at the same strain amplitude as the CIUC tests, the lack of reconsolidating the samples may increase the effects of sample

disturbance on the moduli. No CIUC tests were conducted at these same depths for direct comparison.

Back calculation of the tangent Young's modulus (E_t) related to the undrained shear strength (S_u) of the UU and CIUC tests (confined at P_o and P_o', respectively) produced the relationships shown in Table 10.5.1. The large difference is probably attributable to the consolidation phase of the CIUC test which is not performed in the UU test. In addition, the UU tests were conducted in the upper zone while the CIUC tests were in the saprolite. However, from Chapter 11, the average S_u from UU and CIUC tests were very similar although the UU tests exhibited more scatter which may be due to the increased weathering of the upper zone.

Table 10.5.1. - Relationship of Tangent Modulus from CIUC and UU Tests with Undrained Shear Strength.

CIUC @ P_o'	UU @ P_o'
$E_t = 200S_u$	$E_t = 75S_u$

10.6 Comparison of Measured Moduli

Figure 10.6.1 presents the average shear modulus at each test depth between 3 and 12 meters from the various tests normalized by the small-strain (theoretical maximum) shear modulus from the CHT at the corresponding depths as a function of shearing strain. The CHT was assumed to have shearing strain amplitudes less than or equal to that of the SDMT that the CHT shear moduli were generally higher. The SDMT was the only seismic test for which shearing strain levels were determined. In addition, the figure also

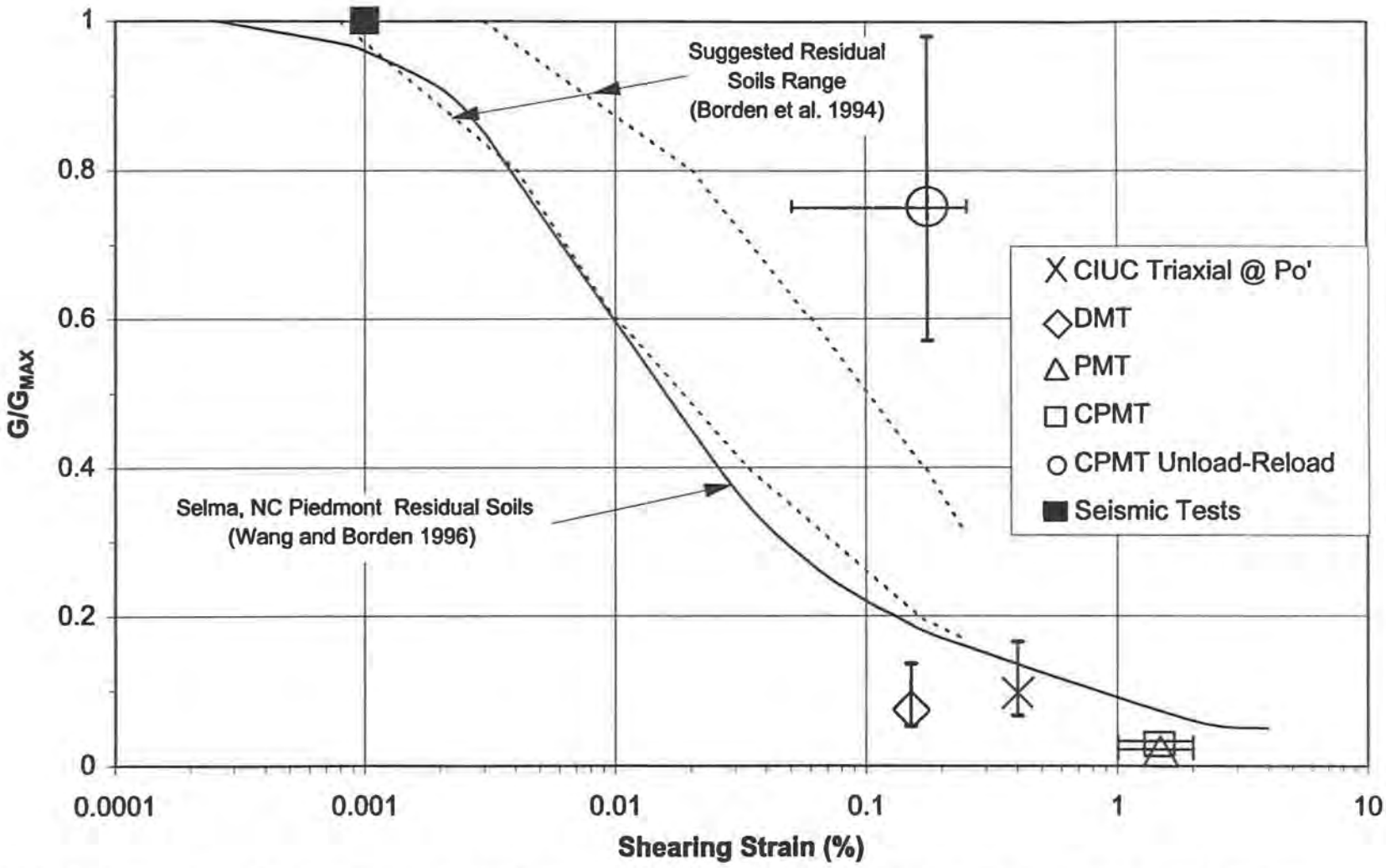

10.6.1. - Normalized Shear Modulus as a Function of Shearing Strain For Depth Range of 3 to 12 meters.

contains those published results from other soil types, including residual soils, as presented previously in Section 10.1.

The normalized shear moduli of the CIUC triaxial tests with confining pressures near effective overburden were similar to that of the DMT; however, the DMT produced moduli at slightly smaller strain levels. If shearing strain was the only variable factor, it would be expected that the DMT would produce higher moduli than the CIUC tests. Considering other factors such as unquantifiable magnitudes of sample disturbance for the CIUC tests, soil remolding during DMT probe insertion, and possible differences between vertical/horizontal stiffness due to soil anisotropy, the differences are rather small. The PMT and initial loading of the CPMT were at larger strains than either the DMT or CIUC tests; these tests results' tended to agree rather closely with one another and had normalized moduli smaller than the other tests (as would be expected based on estimated strain levels). Finally, the normalized moduli of the DMT, CIUC tests, PMT, and initial loading of CPMT tended to fall below the range of residual soils as reported by Borden et al. (1994) and Wang and Borden (1996).

Conversely, the average results of the unload-reload cycle of the CPMT plotted above the aforementioned published results of residual soils. These data were quite scattered in both strain amplitude and normalized shear modulus values. The average strain amplitude, however, is almost identical to or slightly larger than that of the DMT modulus, but these moduli are approximately 8 times that of the DMT. As mentioned in Section 10.3, it is suspected that factors other than shearing strain amplitude such as greatly increased effective stresses during the test compared to the other techniques are responsible for these larger than expected moduli.

10.7 Correlations of Small-Strain Modulus

10.7.1 Correlations Based on Effective Confining Pressure Only

Several correlations in the literature relate the effective confining pressure or the effective octahedral stress (σ_o') to small-strain shear modulus. One of the more common correlations for "sands" was presented by Seed and Idriss (1970); an often cited correlation for "clays" of moderate sensitivity was developed by Hardin and Drnevich (1972). The shear moduli from these correlations are compared to the interpreted trendline of the CHT in Figure 10.7.1.

The Seed and Idriss (1970) relationship is as follows

$$G_{max} = 1000K_{2(max)}(\sigma_o')^{0.5}$$

where $K_{2(max)}$ = dimensionless factor and $\sigma_o' = 1/3(\sigma_1' + \sigma_2' + \sigma_3')$ in units of [psf]. For these calculations, σ_o' was determined by using the average K_o values from the PMT which varied between 1.05 and 2.63,as shown in Appendix A. $K_{2(max)}$ varies between 30 for loose sands and 75 for dense sands; both boundary values are presented on Figure 10.7.1. The shear moduli found by using different $K_{2(max)}$ values on this figure indicate that $K_{2(max)} \cong 45$ agrees closely to CHT results in the saprolite range but is significantly lower in the upper 3 meters.

The Hardin and Drnevich (1972) relationship converted to SI units is given as

$$G_{max} = ((3230(2.97 - e)^2)(OCR)^K(\sigma_o')^{0.5})/(1 + e)$$

where e = void ratio determined from trimmed triaxial samples (values ranged from 0.99 to 1.29), OCR = overconsolidation ratio as determined from average DMT results (a

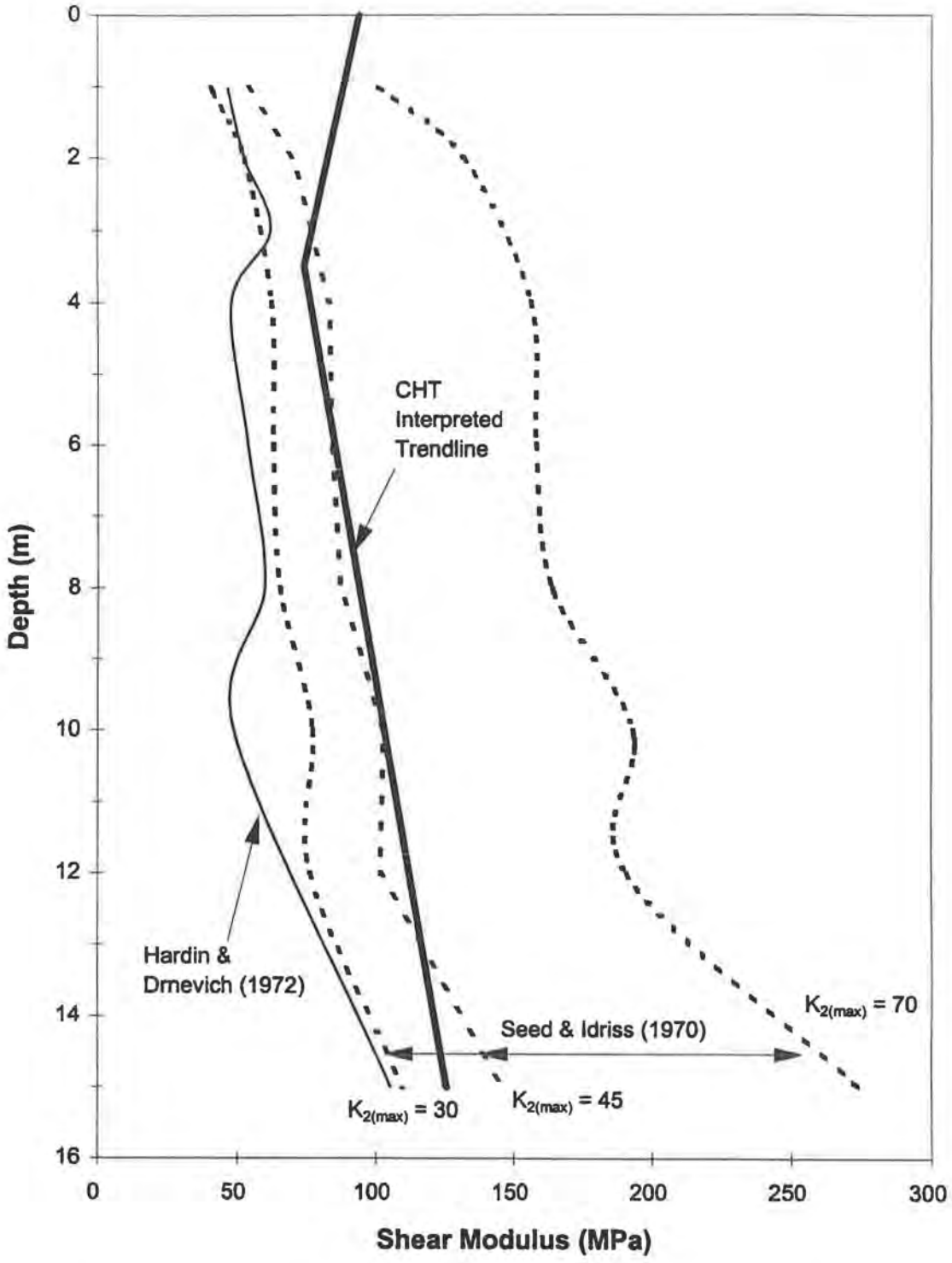

FIG. 10.7.1. - Shear Modulus Correlations Based on Effective Confining Pressure Only.

value of 2.7 was used for depths below 4 meters), K = dimensionless constant which is a function of plasticity index, and σ_o' is in units of [kN/m^2]. The explanation of assumptions and calculations is found in Appendix A. A K-value of 0.05 was chosen since these soils generally varied on average between very low plasticity and non-plasticity. The Hardin and Drnevich (1972) predictions were 15 to 50% less than the CHT results. This correlation involves determination of several factors which are difficult to assess in Piedmont residual soils because of spacial variability.

10.7.2 Standard Penetration Test

Schmertmann (1978), Imai et al. (1982) and Seed et al. (1986) introduced correlations between SPT blow count and shear wave velocity or small-strain shear modulus. The predicted shear wave velocities and shear moduli from these correlations are presented in Figure 10.7.2 and 10.7.3, respectively. These results compare well to the interpreted trendline from the CHT. Details of computations are located in Appendix B.

The Schmertmann correlation, determined from testing of a "sand" site, relates shear wave velocity (V_s) to blow count (N_{60}) by a constant (C) as follows

$$V_s = CN_{60}$$

where Schmertmann recommended C $\approx$ 15 for most soils but suggested lower constants may be appropriate for fine sands with low densities. A constant value of 12 gave the best agreement with measured shear wave velocities and is used on Figures 8.7.2 and 8.7.3. The shear wave velocities from Schmertmann (1978) were converted to shear

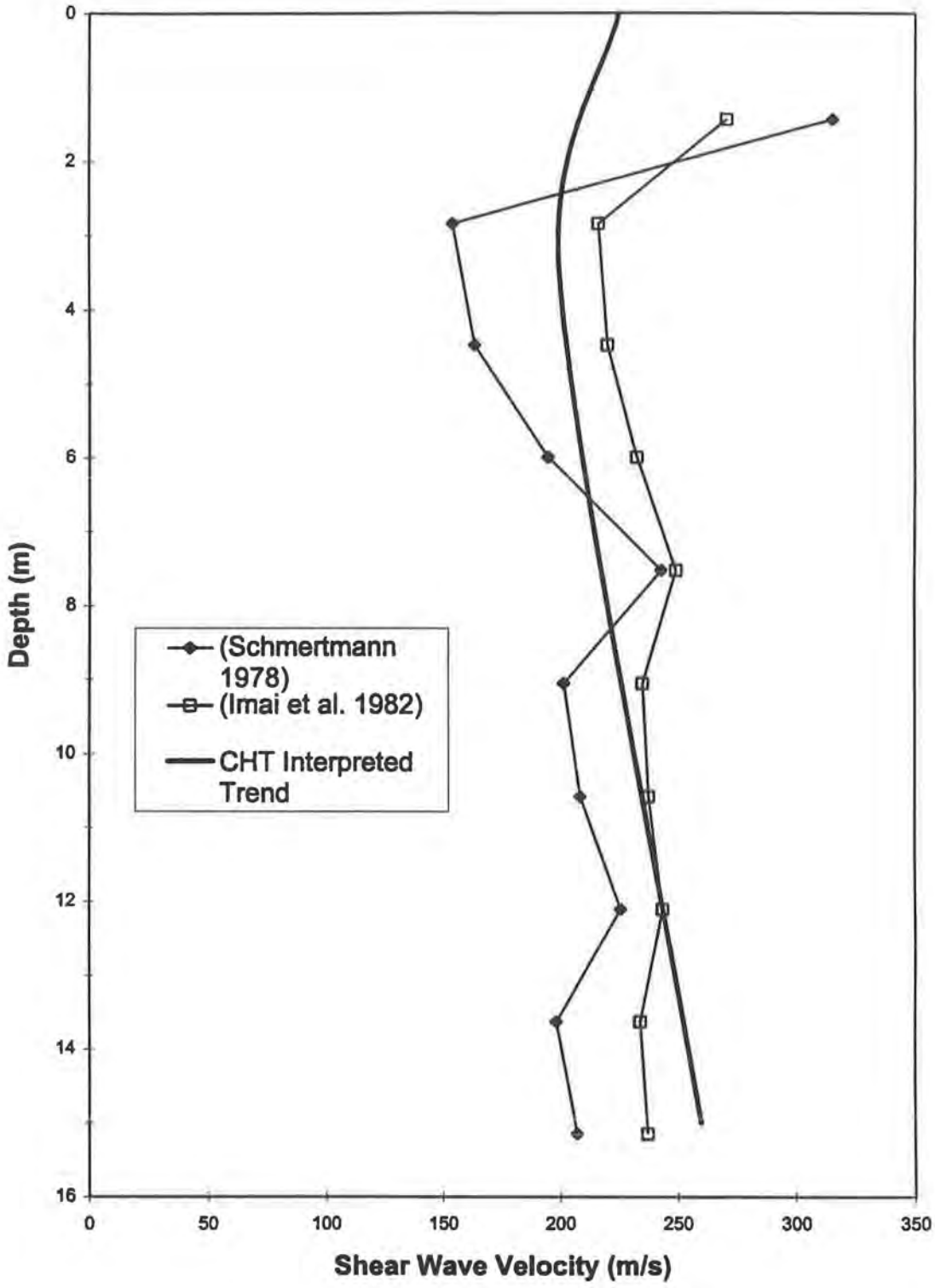

FIG. 10.7.2. - Shear Wave Velocity from SPT Correlations.

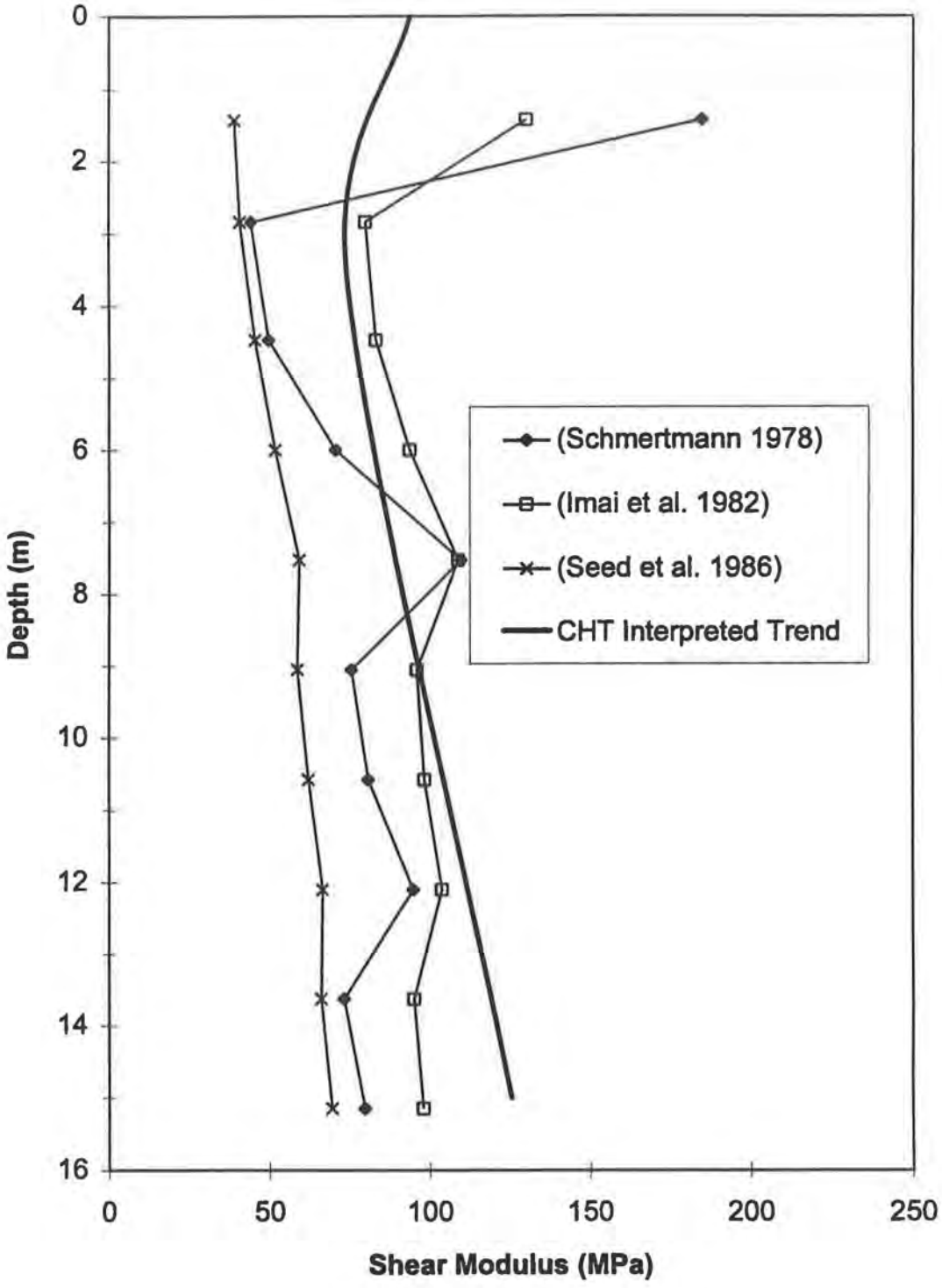

FIG. 10.7.3. - Small-Strain Shear Moduli from SPT Correlations.

moduli by the relationship of $G = \rho V_s^2$; these values are smaller than measured small-strain shear modulus except at the upper zone and 8 meter depths.

The Imai et al. (1982) correlation was established through a study of over 250 sites composed of alluvial, diluvial, and tertiary soils where V_s and SPT measurements had been made. Imai et al. related V_s and G_{max} to SPT, respectively, as:

$$V_s = 97N^{0.314} \text{ and } G_{max} = 144N^{0.680}$$

where the energy ratio for N was not stated; N_{60} was assumed to be intended. The regression coefficient for these correlations was relatively high at 0.87. The predictions were in close agreement with the CHT trendline with differences being less than or equal to 10% for V_s and 20% for G_{max} other than the SPT test depth at 2 meters.

The Seed et al. correlation given as

$$G_{max} \approx 35{,}000N_{60}^{0.34}P_o'^{0.4}$$

where P_o' = effective vertical overburden pressure in [psf]. It is noted G_{max} computed with this correlation is almost half the CHT trendline values as seen in Figure 8.7.3. This correlation was established on cohesionless deposits, but a partly cemented and a clayey sand did not show agreement. The varying amounts of cohesion exhibited at Spring Villa could be the cause for poor agreement between this correlation and measured values.

10.7.3 Cone Penetration Test

The shear wave velocity correlation values based on different soil types are presented on Figure 10.7.4; details concerning the CPT correlation computations are presented in Appendix C. These correlations were established by Hegazy and Mayne (1995) by compilation of seismic and CPT results from 61 worldwide sites. These correlations

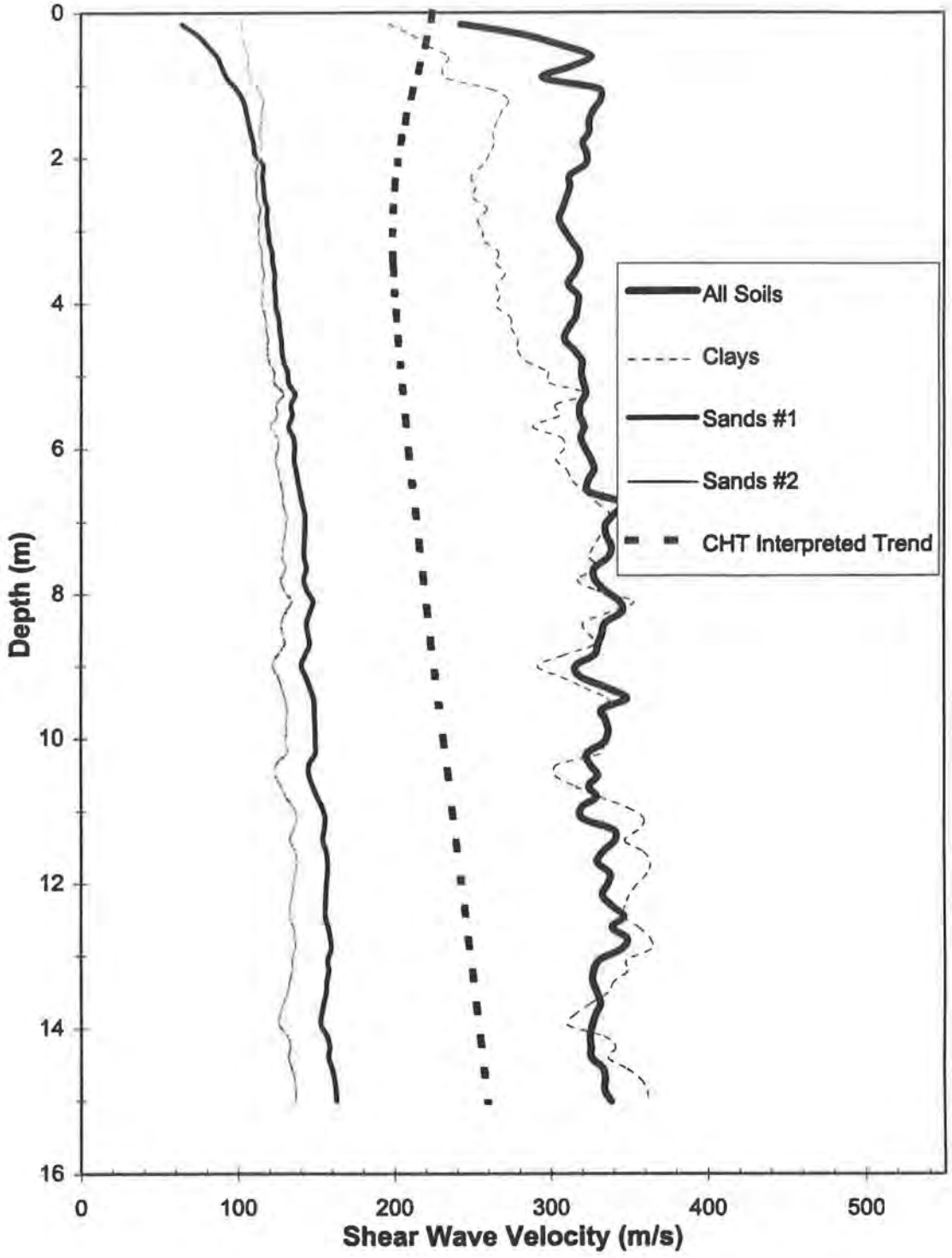

FIG. 10.7.4. - Shear Wave Velocity from CPT Correlations.

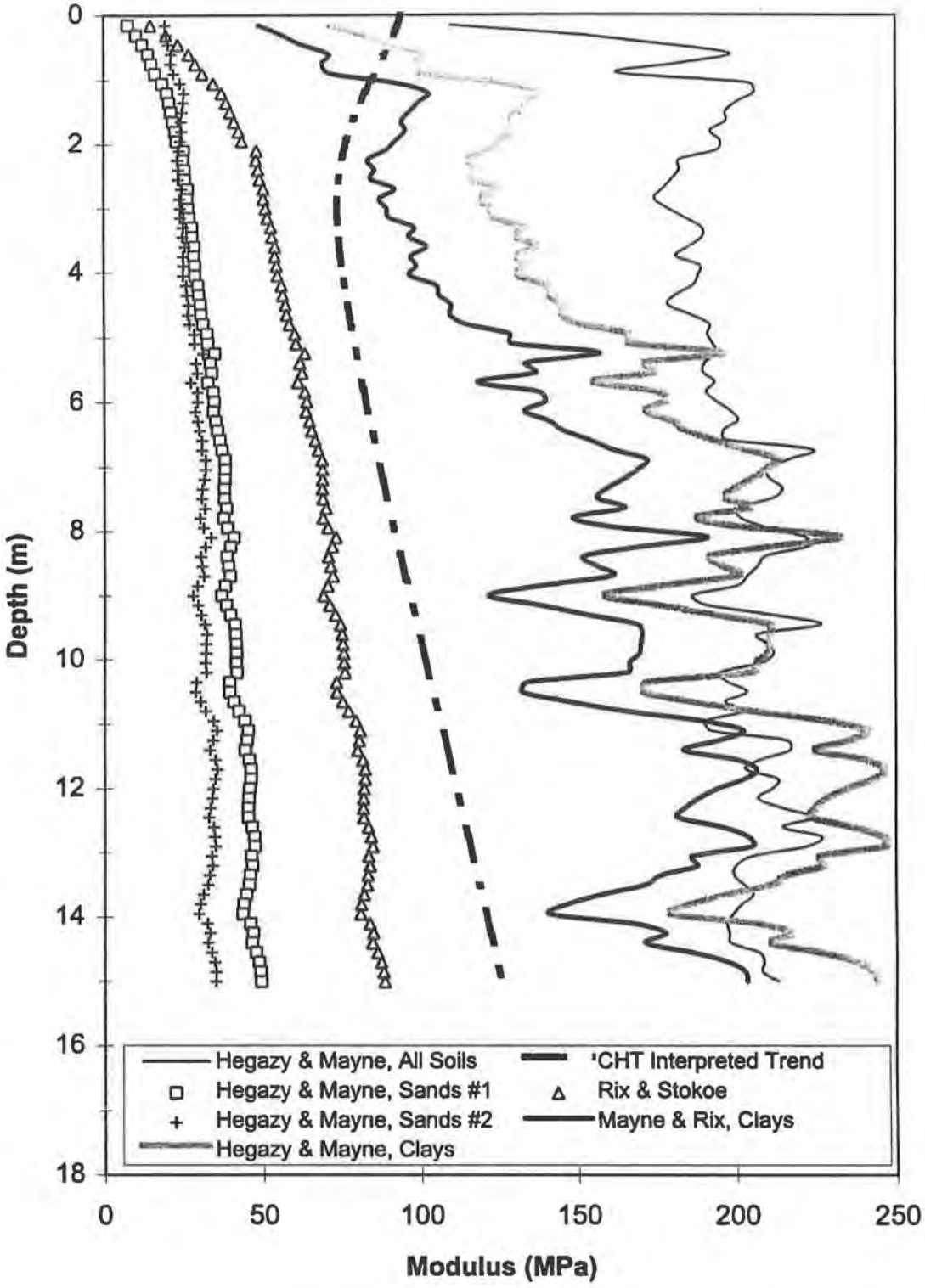

FIG. 10.7.5. - Small-Strain Shear Moduli from CPT Correlations.

relate different cone resistance parameters and/or effective overburden pressure to shear wave velocity. None of these correlations present good agreement with the seismic CHT measurements.

These shear wave velocities were converted to small-strain shear modulus and are plotted in Figure 10.7.5. The Rix and Stokoe (1991) correlation, based on q_c and P_o' of quartz sand in field and chamber tests, produced results that are in most agreement with the interpreted crosshole seismic test results; however, this correlation is at least 20 MPa less than measured values. The Mayne and Rix (1993) correlation is somewhat in agreement with measured values at shallow depths less than 3 meters but differs from measured values by almost 100% at greater depths; this is reasonable since the upper zone has relatively high clay content and this correlation was based on "clay" sites.

None of these correlations give a very good agreement with measured small-strain shear modulus values for Spring Villa. All of these correlations were established on fairly homogeneous "sands" or "clays" except for the Hegazy and Mayne (1990) correlation for "All Soils". The "All Soils" correlation attempts to relate shear wave velocity to cone tip resistance and friction ratio. These correlations do not account for such factors as void ratio and earth pressure coefficient, which can be quite high in the Piedmont for reasons discussed in Chapter 3.

10.8 Correlations of Intermediate- to Large-Strain Modulus

10.8.1 Standard Penetration Test

Table 10.8.1 contains the correlation results of intermediate- to large-strain Young's modulus, flat dilatometer (DM) modulus, and pressuremeter (PM) modulus. These moduli are plotted on Figure 10.8.1 along with average modulus values from the PMT, CPMT, DMT, and CIUC triaxial compression tests with effective confining pressure approximately equal to the effective vertical overburden. Details of computations are included in Appendix B.

The Young's modulus correlations based solely on SPT N-value include the Kulhawy et al. (1990) correlation for sands with fines and the correlation by Bowles (1996) for silts, sandy silts, or clayey silts. Each correlation presents modulus values which are nearly constant over depth, and from Figure 10.8.1, it is evident that both correlations are generally within 20% of the PMT and CPMT results.

The Mayne and Frost (1989) correlation for DM modulus in Piedmont sandy silts is included on Figure 10.8.1; this correlation is based on eight cases of back-calculated structure performance near Washington, D.C. The same general trend of modulus change over depth by the average DMT moduli is exhibited; however, measured values are nearly 5,000 kPa less than correlation predictions at the same depth. In this correlation, like many others involving blow count, the energy ratio of the hammers used to establish this correlation was not stated. This factor, along with the variability of soil properties throughout the Piedmont region, may contribute to poor correlations.

Table 10.8.1. - Intermediate- to Large-Strain Modulus Values From SPT Correlations

Note : All modulus values in units of [kPa].

Average Depth (m)	N_{60}	N_{55}	E (Kulhawy et al 1990) [sands w/fines]	E (Bowles 1996) [silts, sandy silts,or clayey silts]	E_{PM} (Ohaya et al. 1982) [sand]	E_{PM} (Barksdale et al. 1986) [Piedmont sands & silts]	E_{DM} (Mayne and Frost 1989) [Piedmont sandy silts]
1.4	26.3	28.7	13,308	10,403	7,953	16,445	32,509
2.8	12.9	14.1	6,525	6,018	4,968	9,900	18,120
4.5	13.7	14.9	6,923	6,276	5,167	10,327	19,024
6.0	16.3	17.8	8,246	7,131	5,799	11,696	21,957
7.5	20.3	22.1	10,267	8,437	6,701	13,672	26,280
9.1	16.8	18.4	8,518	7,307	5,924	11,970	22,549
10.6	17.4	19.0	8,809	7,495	6,057	12,259	23,179
12.1	18.8	20.5	9,536	7,965	6,382	12,971	24,736
13.6	16.6	18.1	8,380	7,217	5,860	11,831	22,248
15.1	17.3	18.8	8,743	7,452	6,027	12,194	23,037

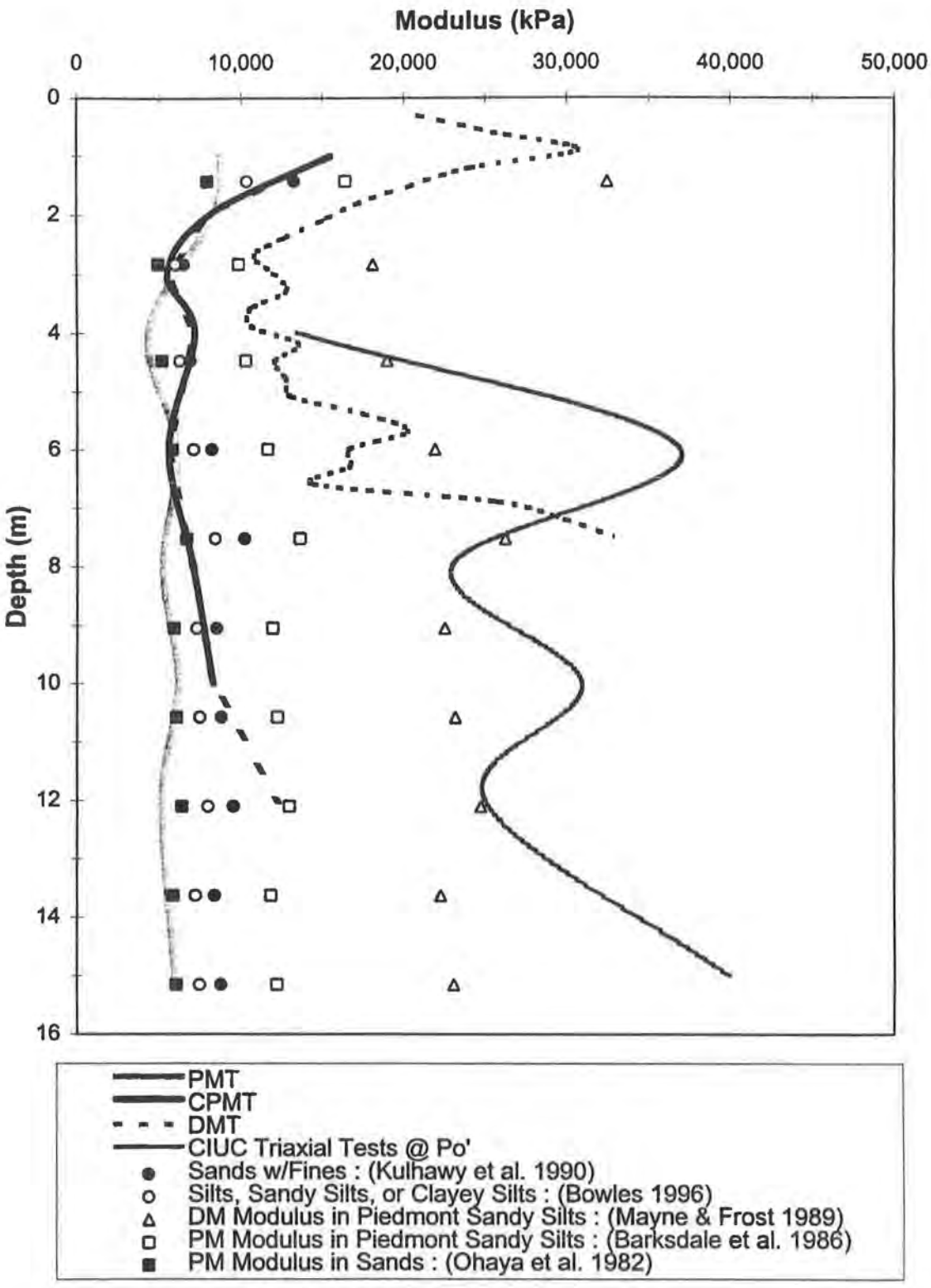

FIG. 10.8.1. - Intermediate- to Large-Strain Young's Modulus by SPT.

The predictions of PM modulus by Ohaya et al. (1982) and Barksdale et al. (1986) are presented in Figure 10.8.1; the Ohaya et al. correlation agreed rather closely between the PMT and CPMT results. The Barksdale et al. (1986) correlation, even though developed from testing in the Piedmont province, was generally almost twice that of both the measured and Ohaya et al. (1982) correlation values.

10.8.2 Cone Penetration Test

Intermediate- to large-strain Young's modulus values from CPT correlations are included on Figure 10.8.2. The in-situ and triaxial modulus data, which are considered to have a similar strain range, are included in the plot for comparison. The Senneset et al. (1988) correlation for silts, sandy silts, or clayey silts includes computation of a constrained modulus based on cone tip resistance (q_c) and then converting that modulus to an elastic Young's modulus by elastic theory. The Bowles (1996) correlation is also for silts, sandy silts, or clayey silts and is expressed as

$$E = 1.5q_c$$

The data presented on Figure 10.8.2 indicates that the Bowles correlation is in very close agreement with the PMT, but the Senneset et al. correlation is in much closer agreement to that of the CPMT. Details concerning computations and/or assumptions are discussed in Appendix C.

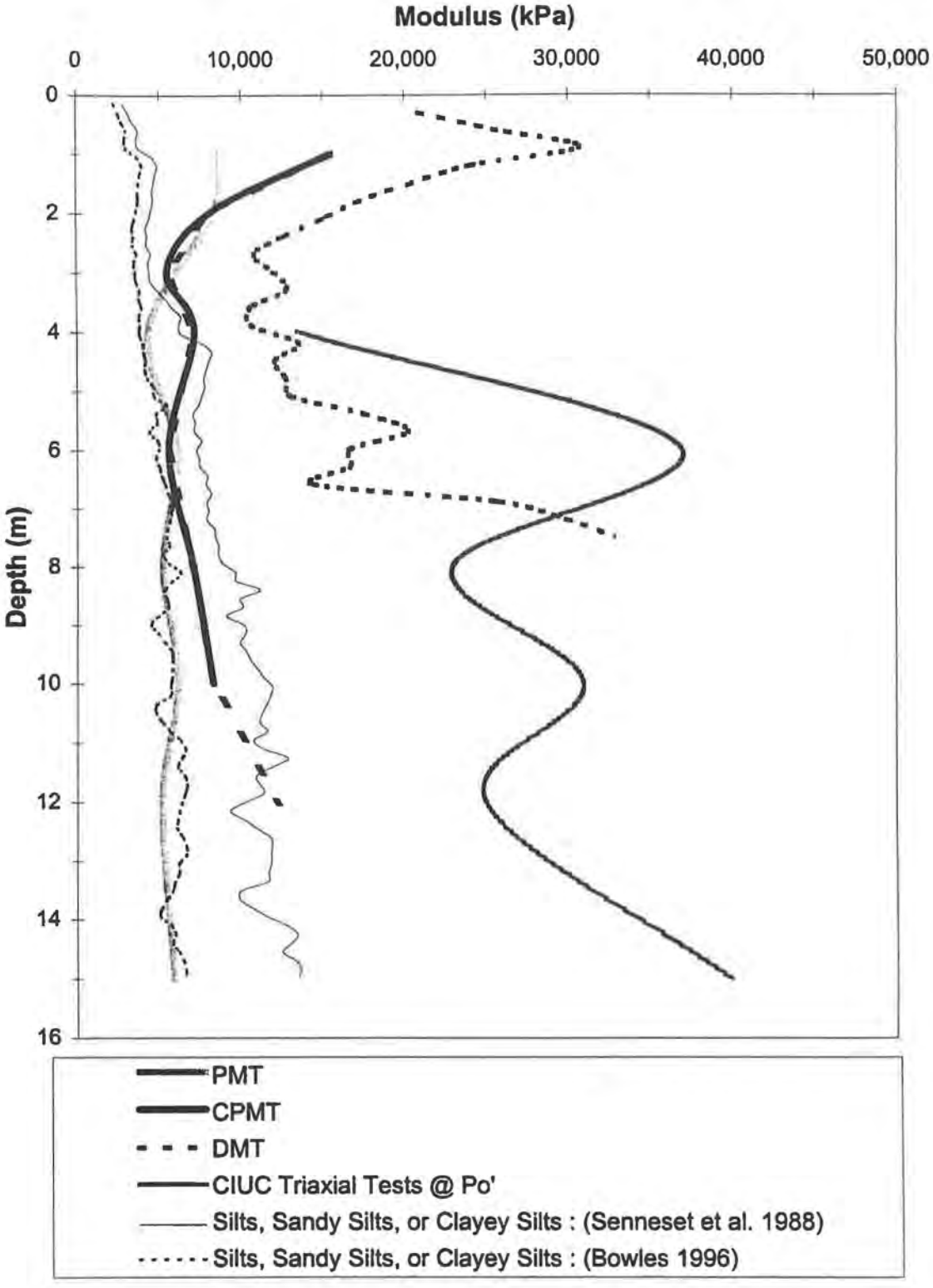

FIG. 10.8.2. - Intermediate- to Large-Strain Young's Modulus by CPT.

10.9 Summary and Conclusions

10.9.1 Measured Moduli

The following observations can be made regarding the different techniques used to gain a measure of soil stiffness:

- Seismic test moduli are approximately 10 to 15 times that of mechanical measures (except for the unload-reload cycle of the CPMT).
- Initial loading stiffness of the PMT and CPMT were in close agreement except at depths below 8 meters where the CPMT moduli tended to increase while the PMT moduli remained relatively constant.
- DMT and CIUC triaxial tests with confining pressures at effective overburden results agreed over similar test depths even though the triaxial moduli were determined over a slightly larger shearing strain amplitude.
- The CPMT unload-reload cycle produced very high moduli approaching the seismic small-strain moduli although shearing strains were approximately that of the DMT. It is suspected that factors other than shearing strain amplitude such as greatly increased effective stresses due to the initial probe expansion loading are responsible for this phenomenon.
- On a plot of average shear modulus (in the 3 to 12 meter depth range) as a function of shearing strain, the mechanical measures of modulus (except for the unload-reload cycle of the CPMT) produced values which were

lower than some published Piedmont residual soils' values at the same shearing strains.

- The relationship between undrained shear strength (S_u) and tangent modulus (E_t) was determined for the UU and CIUC triaxial tests with confining pressures approximately that of effective overburden as follows

$$E_t = 200S_u \text{ for CIUC tests}$$

$$E_t = 75S_u \text{ for UU tests}$$

These greatly different relationships are thought to occur because the UU tests were conducted in the upper zone (which was more weathered) while the CIUC tests were conducted on saprolite samples. Also, the reconsolidation phase of the CIUC test probably limits sample disturbance effects compared to the UU test.

10.9.2 Correlation Predictions of Moduli

The following observations can be made regarding the different correlations used to predict soil stiffness:

- For the correlations of small-strain shear modulus based solely on effective confining pressure, the Seed and Idriss (1970) correlation for "sands" produced the most agreeable shear moduli with $K_{2(max)} \cong 45$. The Hardin and Drnevich (1972) correlation for "clays" predicted small-strain shear moduli which were 10 to 50% less than the CHT results.
- The Schmertmann (1978) and Imai et al. (1982) SPT correlations for small-

strain shear modulus agreed fairly well with CHT results below the upper zone. The Seed et al. (1986) correlation underestimated small-strain moduli at all depths. The Schmertmann (1978) correlation provided the best agreement with a constant (C) of 12 ($G_{max} = \rho(CN_{60})^2$).

- All CPT correlations of small-strain shear modulus were poor. The best correlation appeared to be Rix and Stokoe (1991) which underestimated modulus compared to the CHT by approximately 25% at most depths.
- The SPT correlations for intermediate- to large-strain Young's modulus by Kulhawy et al. (1990) and Bowles (1996) in sands with fines and silts, sandy silts, or clayey silts, respectively, agree closely with PMT and CPMT modulus.
- The Frost and Mayne (1989) correlation of SPT with modulus from the DMT in the Piedmont province overestimated the average measured DM modulus by approximately 45%.
- The Ohaya et al. (1982) correlation of SPT with PM modulus agreed more closely to PMT and CPMT results than the Barksdale et al. (1986) correlation. The Barksdale et al. (1986) correlation, which was developed from testing in the Piedmont province, was generally 40 to 100% larger than measured values.
- The CPT correlation with intermediate- to large-strain Young's modulus by Bowles (1996) for silts, sandy silts, or clayey silts agreed most closely with

PMT and CPMT results. This correlation's moduli were approximately 50 to 80% of the Senneset (1988) correlation for the same soil type.

CHAPTER 11

SHEAR STRENGTH PARAMETERS

11.1 Total vs. Effective Stress Shear Strength

Soil shear strength can be defined as the resistance to mass deformation which can occur because of any combination of particle rolling, sliding, and crushing and can be reduced by excess pore pressures which exist/develop during particle movement (Bowles 1996). For most materials, it is commonly thought that failure occurs when shearing stress along the failure plane reaches some unique function of the normal stress on that plane (Holtz and Kovacs 1981). This assumption is expressed by the Mohr failure, or limiting stresses, envelope. This envelope is commonly constructed by determining the maximum principal stresses along the failure plane of several specimens at failure and drawing a line through their points of maximum obliquity, or maximum principal stress ratio. Mohr's failure hypothesis states that the point of tangency along this failure envelope defines the angle of the failure plane in the element or test specimen.

The Mohr-Coulomb soil shear strength criterion, which divides a soil's shearing resistance into two parameters - angle of internal friction and cohesion, was developed from the Mohr hypothesis. This criterion can be written as follows

$$\tau_{ff} = \sigma_{ff} \tan\varnothing + c$$

where τ_{ff} = shearing stress along the failure surface during failure, σ_{ff} = applied normal stress along the failure surface during failure, tan$\varnothing$ = stress-dependent component of shear strength (resistance to interparticle slip), and c = stress-independent component of shear strength (intrinsic cohesion). A linear interpretation of these data over a limited stress range would suggest that c and $\varnothing$ are constant, but a soil's true failure envelope typically has varying amounts of curvature depending upon the range of stresses. Shear strength parameters are dependent upon test type, previous stress history, and the soil's current physical state (Bowles 1996). In addition, these parameters are only applicable to the tested soil condition.

In practice, the complete Mohr-Coulomb criterion in terms of total stresses is rarely appropriate as shown in the aforementioned equation. Instead, the nature of the engineering problem and the soil type are considered in order to determine whether determination of total (short-term) and/or effective (long-term) shear strength is needed for the analysis. Since soil shear strength is ultimately a function of the effective stress strength (pore water offers zero shear resistance) in both the long term and short term loading case and drainage due to an imposed loading will eventually occur, the more correct Mohr-Coulomb criterion which takes into account pore water drainage is as follows

$$\tau_{ff} = \sigma'_{ff}\tan\varnothing' + c'$$

where σ'_{ff} = effective normal stress, $\varnothing'$ = effective internal angle of friction, c' = effective cohesion and

$$\sigma'_{ff} = \sigma - u$$

where σ = total normal stress and u = pore pressure. The only difference between short and long term strength is that transient changes in pore pressure are approximately zero for the long term case. Undrained triaxial testing can account for these transient pore pressure changes on shear strength by the aforementioned equations.

Total stress strength is sometimes used when a (typically cohesive) soil undergoes a moderately quick to fast loading. During the time of this loading, pore pressures will build, and it is assumed that no drainage will occur (i.e. zero volume change during undrained loading). The undrained triaxial test is a common method of modelling this case, and pore pressures generated during this test are assumed to be representative of field conditions. Oftentimes, the friction angle term in the Mohr-Coulomb failure criterion is assumed equal to zero for total stress conditions and the cohesion is used to express a soil's undrained shear strength as follows

$$\tau_{ff} = c = S_u$$

where S_u = maximum undrained shear strength.

Due to the curvature of true failure envelopes, the effective cohesion term is oftentimes not considered in long-term strength analysis since many soils show only an apparent cohesion due to the limited stress range over which a failure envelope is constructed (Kulhawy and Mayne 1990). This long term case is best modelled by a triaxial test with drainage allowed during shearing, but a triaxial test with pore pressure measurements made during shearing with no drainage can produce results which define the same envelope.

Because these Piedmont residual soils tend to drain relatively fast, many loading cases may be analyzed using the effective stress methods and long term pore water pressures where the change in pore pressures is approximately zero. However, for moderately quick loadings, it can sometimes be difficult to determine whether transient pore pressures may occur and where total stress analysis might be more appropriate. The very rapid drainage characteristics of Piedmont soils compared to fine-grained soils could mean that truly significant drainage may occur during measurement of strength and stiffness in-situ with such devices as the PMT, DMT, or possibly even CPT and SPT causing uncertainty in interpretation of the various tests' drainage conditions. In other words, the different tests may reflect different conditions of drainage, and none may be completely drained or undrained in the Piedmont, as is often assumed when interpreting test results in "sands" or "clays". This is an unavoidable difficulty with in-situ testing in the Piedmont. Triaxial tests, however, have known drainage conditions, and CU tests with pore pressure measurements can be interpreted either way.

11.2 Effective Stress Shear Strength Test Results

11.2.1 Triaxial Testing Results

As presented in Chapter 8, CIUC tests were performed on eighteen samples between 4 and 15 meters; four of these samples had two stages of loading. In addition, one CIDC test was used in effective stress strength characterization. The p-q coordinates

at the maximum principal stress ratio were provided on Figure 8.7.4. An ordinary linear regression of p on q indicated $c' = 17$ kPa and $\varnothing' = 31°$, with a higher regression coefficient (R^2) compared to the alternative regression performed in accordance to Handy (1981); this alternative regression involves rotating the p-q axes (typically 45°) in order to evaluate variability in both directions, and not just the q-direction.

The average effective strength parameters for the entire 4 to 15 meter depths as computed by various linear regressions are presented in Table 11.2.1. The regressions had R^2 values between 0.83 and 0.99; R^2 above 0.9 suggests good linear fit. The various regressions with R^2 above 0.9 generally indicated a $\varnothing'$ range between 31 and 34° and c' to fall between 10 and 18 kPa.

As previously mentioned, the rotated axes regression (Handy 1981) of all CU and CD tests gave a lower R^2, higher c', and lower $\varnothing'$ than the ordinary p on q linear regression, but the differences between the two regressions were relatively small considering the scatter of the data. The effect of the CD test was examined; by leaving it out of the regression, R^2 increased slightly, c' was reduced, and $\varnothing'$ increased by almost 3° compared to the ordinary p on q regression which included the CD test. The CD test has a much larger effect on the regression since it was performed at a higher confining stress compared to the majority of the CU tests.

If the failure envelope had been made using only single-stage samples and the first stage of the multi-stage samples, the data would show a poorer regression than for the other regression types; $c' \approx 0$ and $\varnothing'$ increases to around 39° compared to the values of

Table 11.2.1. - Average Effective Stress Strength Parameters from Triaxial Testing.

Regression Type	R^2	n	Effective Cohesion (kPa)	Effective Friction Angle (deg)
p on q : [CU and CD tests]	0.9128	23	17	31
Rotated Axes : [CU and CD tests]	0.8393	23	27	28
p on q : [CU tests]	0.9343	22	10	34
p on q : [single stage samples & first stage of multi-stage samples]	0.8270	18	-5	39
p on q : [first stage of multi-stage samples]	0.9913	4	0	37
p on q : [both stages of multi-stage samples]	0.9869	8	17	32

Table 11.2.2. - Effective Stress Strength Parameters by Depth Range.

Depth Range	Regression Type	R^2	n	Effective Cohesion (kPa)	Effective Friction Angle (deg)
4 to 8 meters	p on q	0.8337	10	8	36
10 to 15 meters (with CD test)	p on q	0.9639	14	14	31
10 to 15 meters (w/o CD test)	p on q	0.9641	13	6	34

$c' = 17$ kPa and $\varnothing' = 31°$ from the linear regression including all CU and CD tests. Conversely, using both stages of the multi-stage samples gave a very high R^2 and a very similar c' and $\varnothing'$ compared to the regression of all tests. Since the single-stage tests were all performed with effective consolidation pressures (σ'_3) significantly lower than the second stage of most of the multi-stage tests, it may be that the scatter over a much more limited range of confining stress leads to less reliable measurements; the R^2 of 0.83 suggests poor reliability. Also, the multi-stage tests included only four samples which were generally in the same confining stress range and which was higher than most of the single-stage CIUC tests compared to the other regressions; therefore, less material variability may result in greater reliability when these tests are included. The regression of just the first stage loading of the multi-stage samples produced a very high regression coefficient and was very similar to the regression which included all single stage (and first stage) loadings.

The data on Table 11.2.2 provide strength parameters derived from tests at different ranges of depth. The strength parameters for the different zones express the scatter which is prevalent in Piedmont soils. It is interesting to note that the regression on those samples between 4 to 8 meters produced a much lower R^2 than those between 10 to 15 meters although the failure envelopes were not that different between the two zones. The 10 to 15 meter samples include three of the four multi-stage samples; since they agreed so well with one another, this could be a major cause of the regression being better for this zone. In addition, the CD test had relatively less impact on this zone's R^2 since these tests were generally performed at higher confining stresses.

11.2.2 Multi-Stage vs. Single-Stage Triaxial Tests

Multi-stage CIUC triaxial tests were conducted on four samples. These tests involved two loading stages where the second confining pressure was approximately twice that of the first. Multi-stage test results are presented on Figure 11.2.1; the overall p on q regression results are very complementary to the overall average p on q regressions which included and excluded the multi-stage tests. In fact, R^2 was larger for the multi-stage tests' failure envelope than for the other regressions.

Table 11.2.3. - Individual Multi-Stage CIUC Test Results.

Sample ID	R^2	Effective Cohesion (kPa)	Effective Friction Angle (deg)
B-2, 15 m	N/A	-4	37
B-5, 15 m, Sample 1	N/A	4	36
B-5, 15 m, Sample 2	N/A	36	29
B-7, 8 m, Sample 2	N/A	6	37
All Multi-Stages : p on q	0.9869	17	32
All Tests : p on q	0.9128	17	31

Lambe and Heartz (1988) state that the highly variable nature of the Piedmont make multi-stage testing attractive because the same material is being tested to determine a failure envelope. Their study involved CD triaxial tests with comparison between a multi-stage test with 3 stages and 3 single-stage tests with the same confining pressures; all specimens came from the same block sample. Although results were inconclusive, it was reported that the multi-stage test gave a lower $\varnothing'$ prediction than the three single stage tests; however, the first 2 stages agreed well with their corresponding single-stage equivalents.

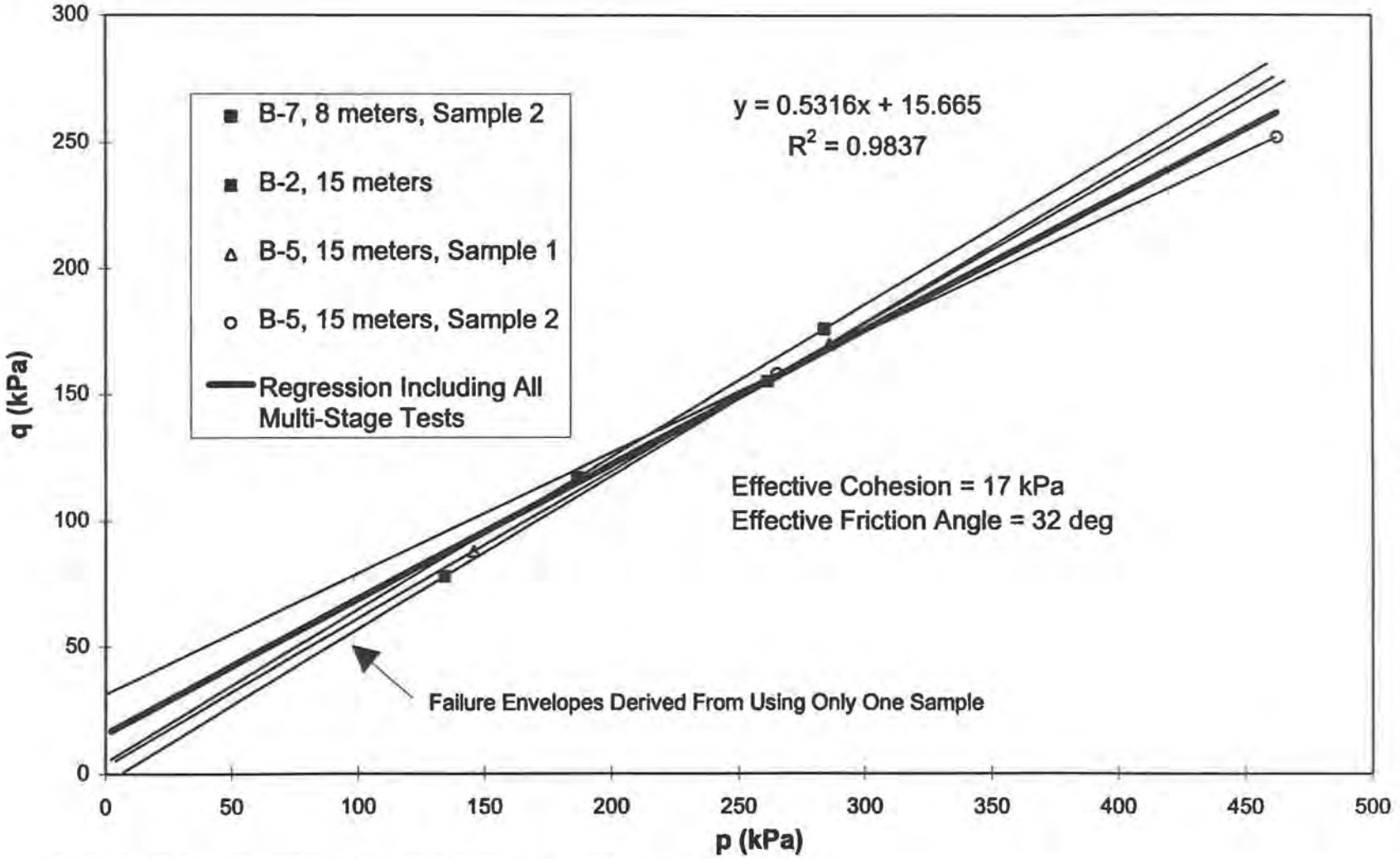

FIG. 11.2.1. - Multi-Stage CIUC Failure Envelope Summary.

Similarly, as seen in Figure 11.2.1, the first stage of Sample 2 at 15 meters depth from boring B-5 agreed very well with the second stage of loading for the other samples; unfortunately, few single-stage samples were consolidated at similar pressures to the multi-stage tests for comparison between the two. The effective stress strength parameters predicted from using each multi-stage test by itself is shown in Table 11.2.3. These tests' individual c' and $\varnothing'$ values range is quite similar to upper and lower bounds of the regressions included in Table 11.2.1; therefore, the results from this study suggest that using a few multi-stage tests may give reliable average predictions of effective stress strength parameters compared to a more extensive testing plan of just single-stage tests. The variable nature of Piedmont residual soil prohibits exact determination of strength parameters; therefore, testing should aid in determination of the range and mean of shear strength values with some confidence.

11.2.3 Iowa Borehole Shear Test Results

The failure envelopes determined from the BST conducted between 2 and 9 meter depths are presented on Figure 11.2.2. From this figure, it is evident that $\varnothing$ angles were generally much lower than that produced by triaxial testing. The soil's relatively high permeability suggest that the tests probably measured fully or nearly drained (effective stress) soil strength; however, CIUC triaxial tests exhibited positive changes in pore pressure during shearing. Therefore, the presence of excess pore pressures could be a cause for the highly variable strength measures. Another suspected reason why results were so wildly scattered and low is that, in positioning the shear head in the soil cavity

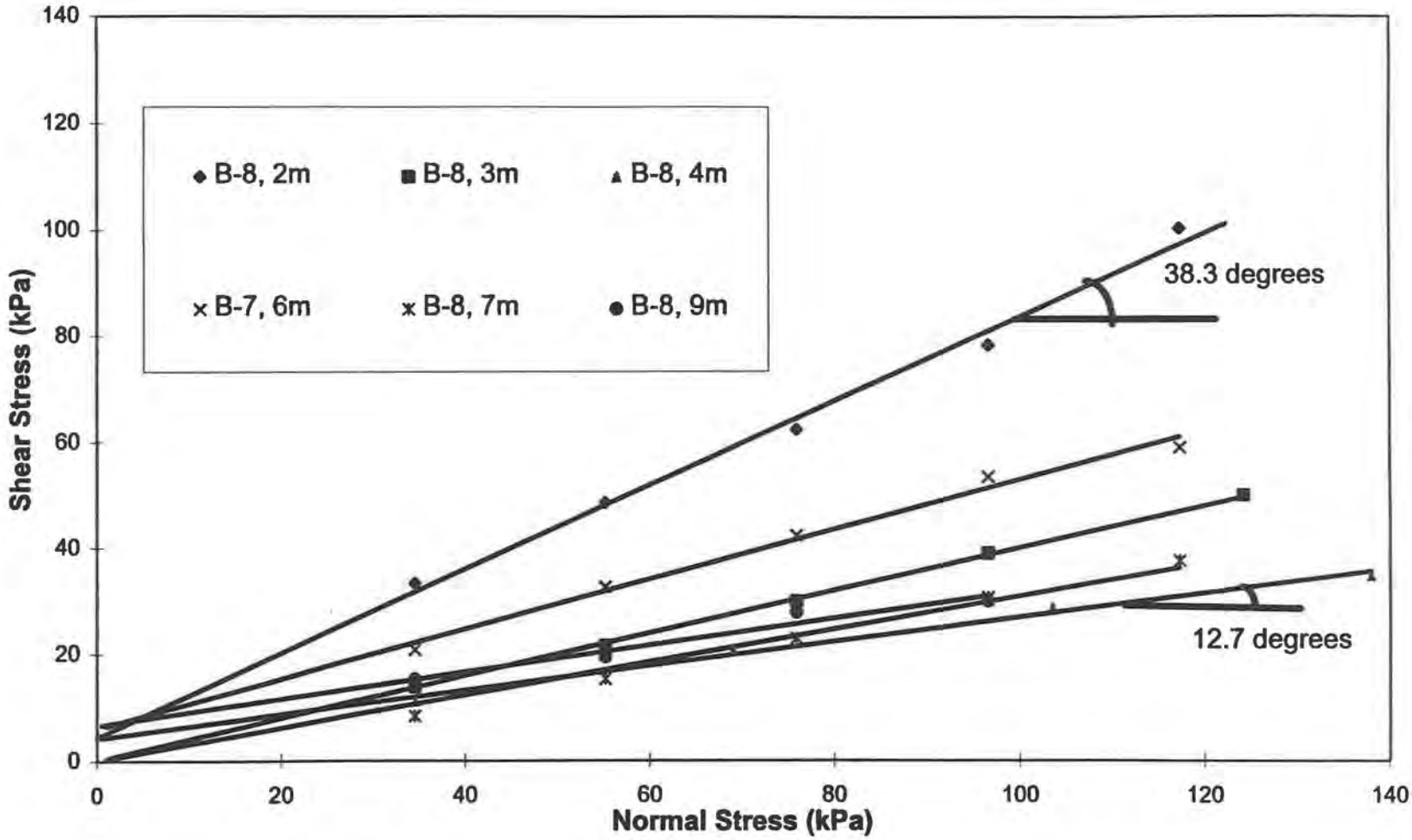

FIG. 11.2.2. - Failure Envelopes from Iowa Borehole Shear Tests.

created by a recovered Shelby tube sample, soil was loosened or disturbed at the sides of the cavity, and as a result, the shear strength of this remolded, loosened soil could affect the test. The test at 2 meters depth was above the ground water table and gave a prediction of effective stress strength comparable to triaxial testing results; it is suspected that disturbance was more significant or else only partial drainage occurred for those tests below the ground water table. Also, any seepage into the soil cavity at those test depths below the ground water table could tend to soften the soil near the cavity wall.

11.2.4 Correlations of Effective Friction Angle

In this section, various published correlations of in-situ test results with effective friction angle are presented for comparison with triaxial testing results. It should be noted that if c' is neglected (i.e. taken as zero) for the p on q regression of triaxial testing results, $\varnothing'$ will be larger than 31°.

The results of several correlations with average SPT blow count are shown in Table 11.2.4. These data are shown graphically in Figure 11.2.3. The assumptions necessary to use each of these correlations are discussed in Appendix B. Surprisingly, three of the four correlations investigated provided very good agreement with triaxial testing. The Schmertmann (1975) correlation, which is reported as oftentimes conservative, gave the largest predictions; of the correlations used, it is the only one which includes the test depth's effective vertical overburden pressure. As mentioned in Section 4.1.4, Harris and Mayne (1994) reported close agreement between CIUC triaxial tests' interpretation of $\varnothing'$ and Schmertmann's correlation.

Table 11.2.4. - Correlations of Effective Friction Angle by SPT.

Method :	Schmertmann Correlation (1975)	Shioi & Fukui Correlation 1 (1982)	Shioi & Fukui Correlation 2 (1982)	Peck, Hanson & Thornburn (1974)
Depth (m)	Effective Friction Angle (degrees)			
1.43	49.0	35.2	35.1	35.4
2.84	39.6	29.1	31.0	31.3
4.48	38.9	29.5	31.2	31.6
6.00	39.7	30.9	32.0	32.3
7.53	40.9	32.7	33.3	33.7
9.05	38.4	31.1	32.2	32.6
10.58	38.0	31.4	32.4	32.8
12.10	38.1	32.1	32.8	33.2
13.62	36.3	31.0	32.1	32.5
15.15	36.1	31.4	32.3	32.9

The $\varnothing'$ correlations seem to be fairly insensitive to blow count, and blow counts at Spring Villa varied over a rather small range. Since the triaxial test evaluation of $\varnothing'$ is fairly constant over depth at this site, it appears that a site-specific correlation between $\varnothing'$ and blow count cannot be generated. In other words, $\varnothing'$ from the triaxial test shows independence from uniform N-values at Spring Villa; the average corrected N_{70} over the 4 to 15 meters depth range of triaxial testing is 15.

Figure 11.2.3 also shows the Robertson and Campanella (1991) correlation with the DMT. Below 2 meters depth, $\varnothing'$ was predicted to be near 40° which is a significantly larger than average values reported by triaxial testing over the full depth of testing. Note that this correlation uses K_D and the K_o correlation by Marchetti (1980) which, as discussed in Chapter 9, is probably not very applicable to Piedmont residual soils.

The CPT has several available $\varnothing'$ correlations presented in the literature. As shown in Figure 11.2.4, the three widely referenced correlations used in this investigation tend to overpredict $\varnothing'$. The Kulhawy and Mayne (1990) and Robertson and Campanella (1983) correlations show close agreement between themselves; both overpredict $\varnothing'$ by a few degrees over the overall average triaxial value. The Masood and Mitchell (1993) correlation is applicable to clays and sands; however, sleeve friction is the primary factor which is used to evaluate $\varnothing'$. Sleeve friction values are relatively high at Spring Villa, thus the overprediction. As mentioned in Section 4.2.4, Harris and Mayne (1994) reported all three of these correlations to predict $\varnothing'$ less than triaxial testing by around 5°.

The PMT and CPMT can be used to predict $\varnothing'$ as well; plots showing correlation results are shown in Figures 11.2.5 and 11.2.6, respectively. Both PM tests can be

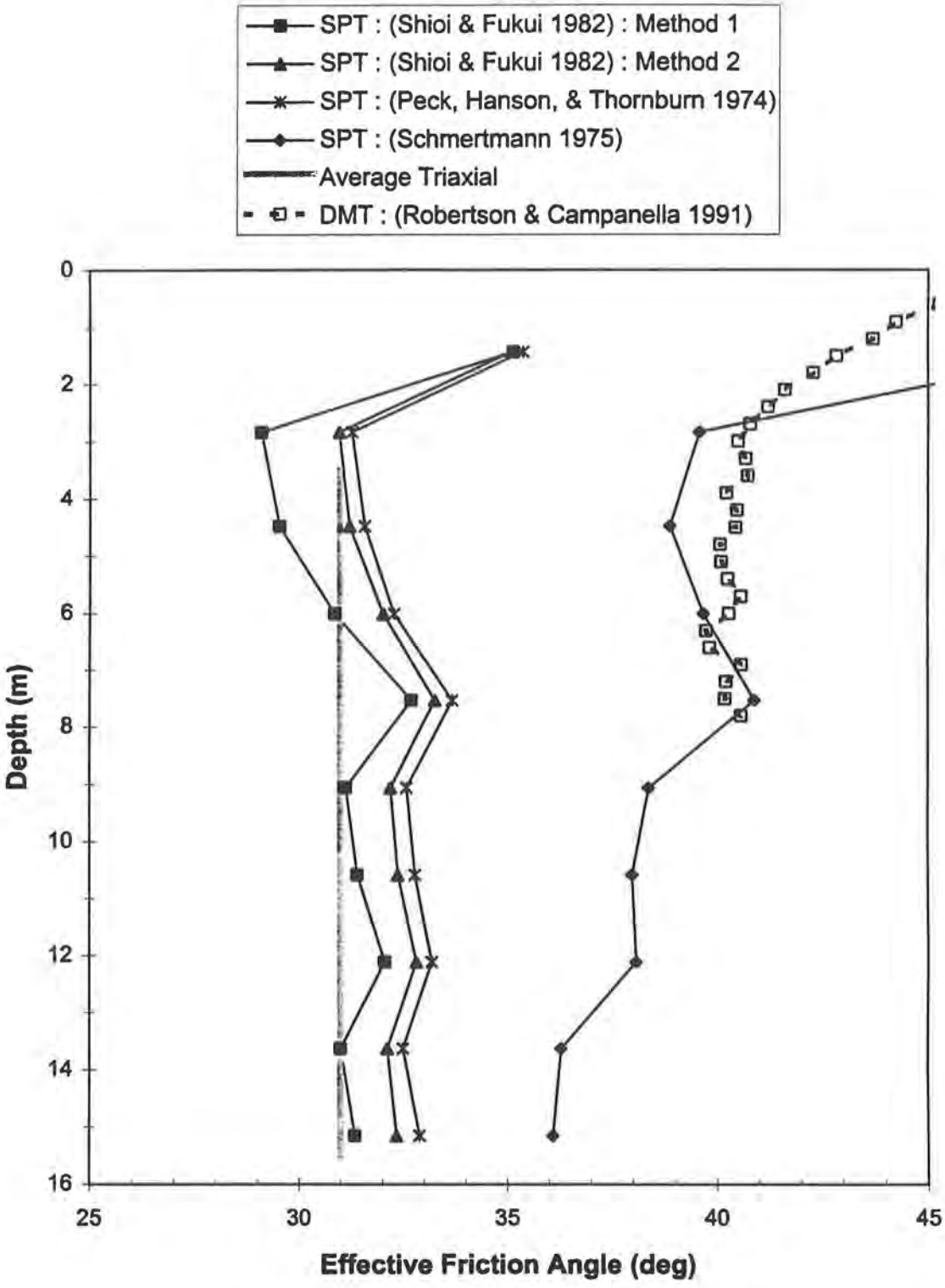

FIG. 11.2.3. - SPT and DMT Predictions of Effective Friction Angle.

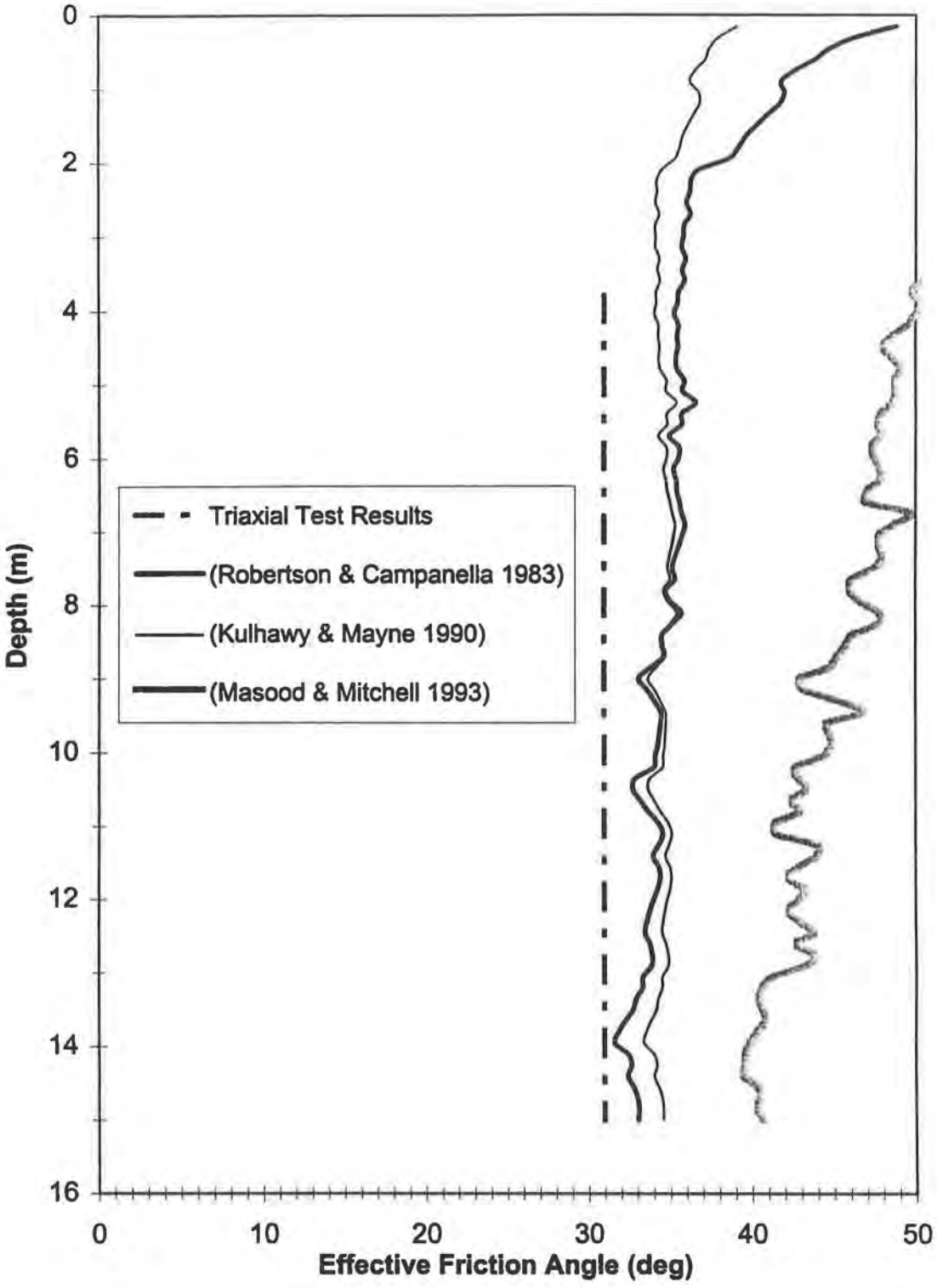

FIG. 11.2.4. - CPT Predictions of Effective Friction Angle.

FIG. 11.2.5. - Menard Pressuremeter Predictions of Effective Friction Angle.

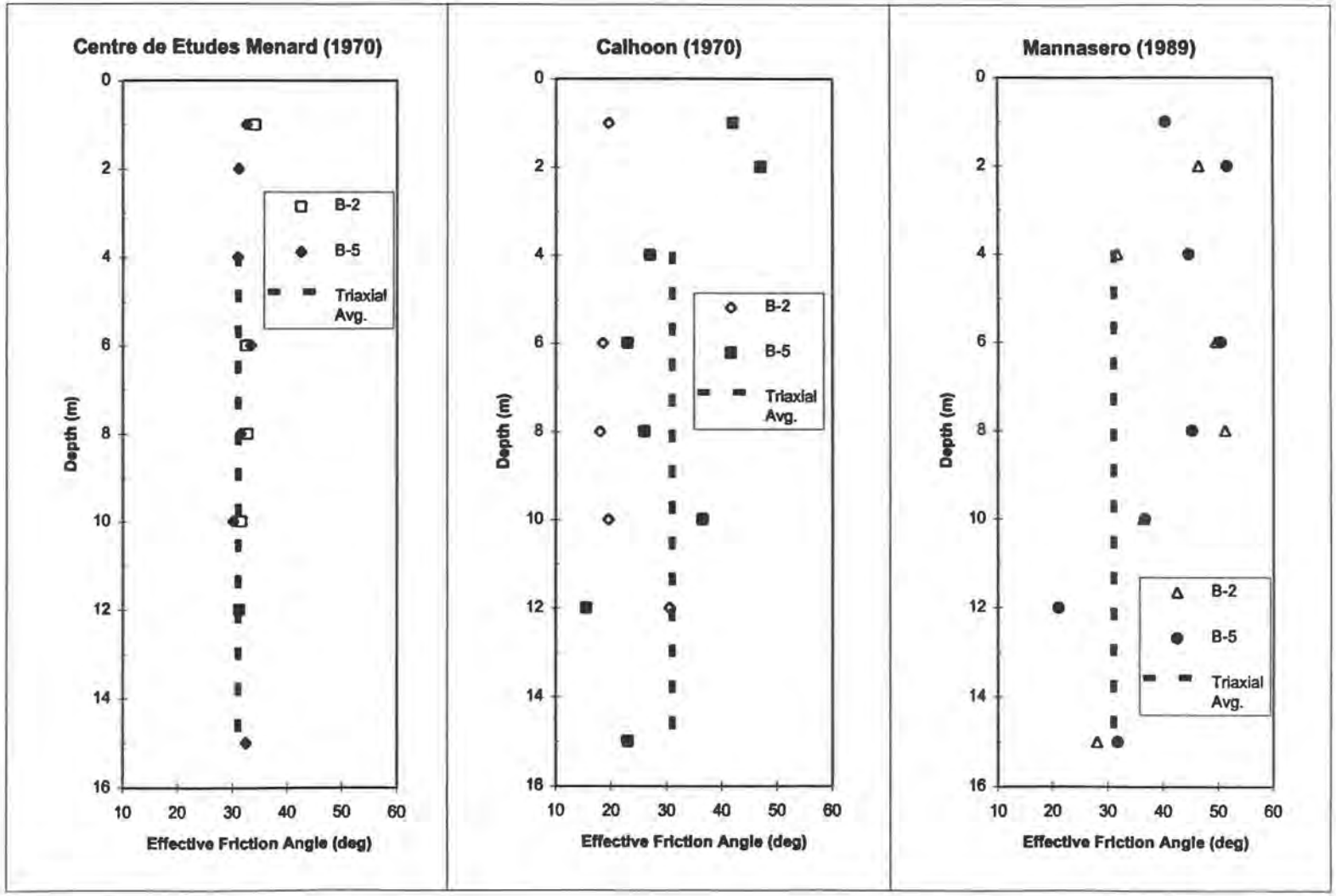

FIG. 11.2.6. - Cone Pressuremeter Predictions of Effective Friction Angle.

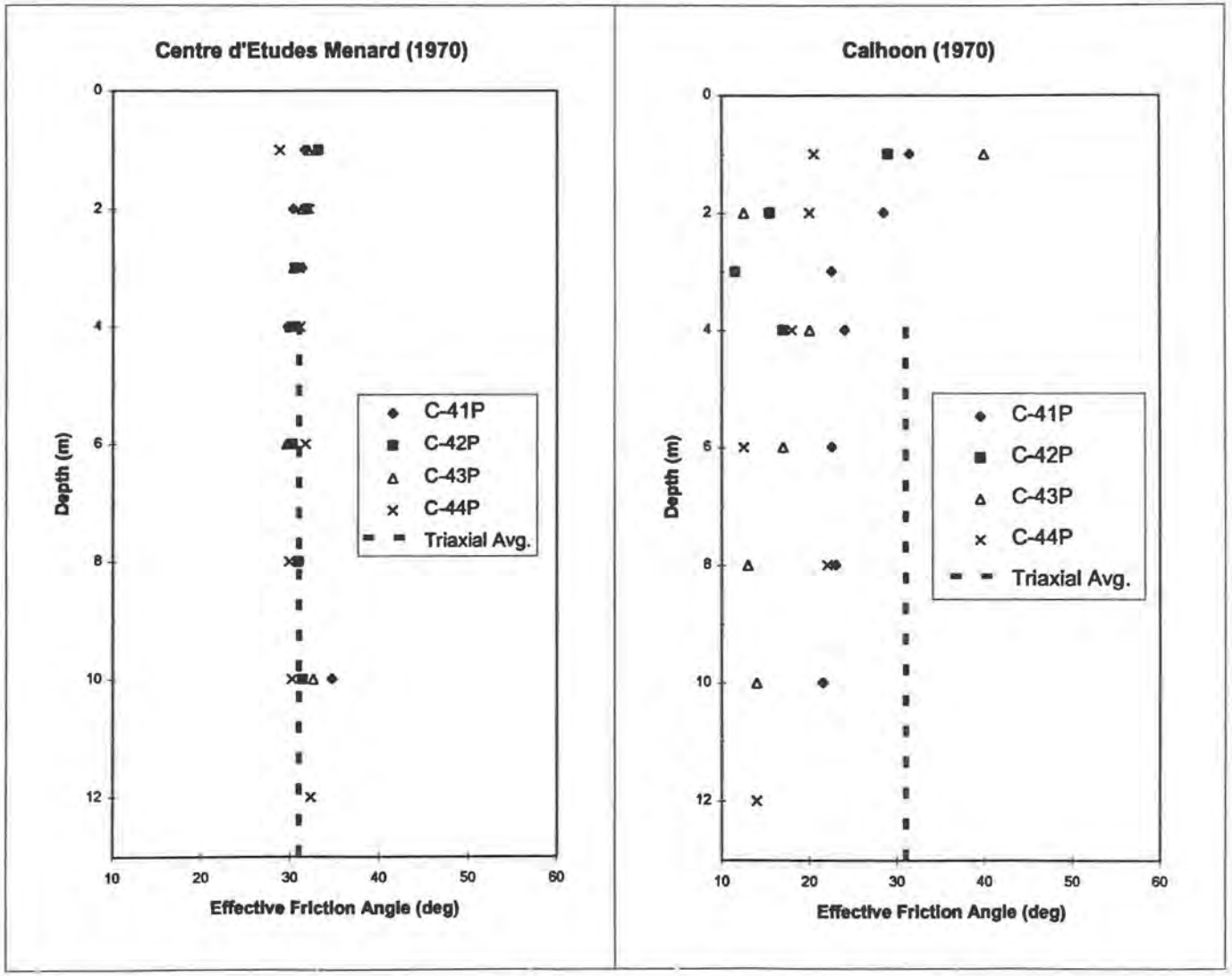

evaluated by correlations presented by the Centre d'Etudes Menard (1970) and Calhoon (1970). The first correlation is based on an empirical relationship between net limit pressure and Ø'; since net limit pressures were similar between the two PMs, Ø' predictions were also similar. Results were very near the average triaxial value. The Calhoon correlation relates limit pressure and PM modulus; this evaluation gave increasingly lower Ø' values over depth. This correlation showed very poor agreement with laboratory results possibly because the soils used to establish the interrelationship among PM modulus, limit pressure, and Ø' were not residual soils.

The PMT was also evaluated using a correlation presented by Manassero (1989) which was developed through calibration testing by self-boring PM tests in Ticino sand. This correlation makes the assumption that the ratio of volumetric to shearing strain is constant. Ø' values were much greater at most depths than those predicted by laboratory testing; however, tests at 12 and 15 meters did show agreement.

11.2.5 Comparison of Effective Friction Angle Predictions

Figure 11.2.7 presents the BST values and selected correlations of Ø' with all applicable tests which most closely agreed with laboratory determination of Ø'. The overall average Ø' triaxial test value of 31° from the p on q regression is included for comparison on the figure.

The correlations included in the figure for SPT, CPT, CPMT, and PMT show relatively good agreement and are to varying amounts higher than the triaxial value, but as noted previously, if c' is taken as zero, the Ø' will be slightly increased. The BST

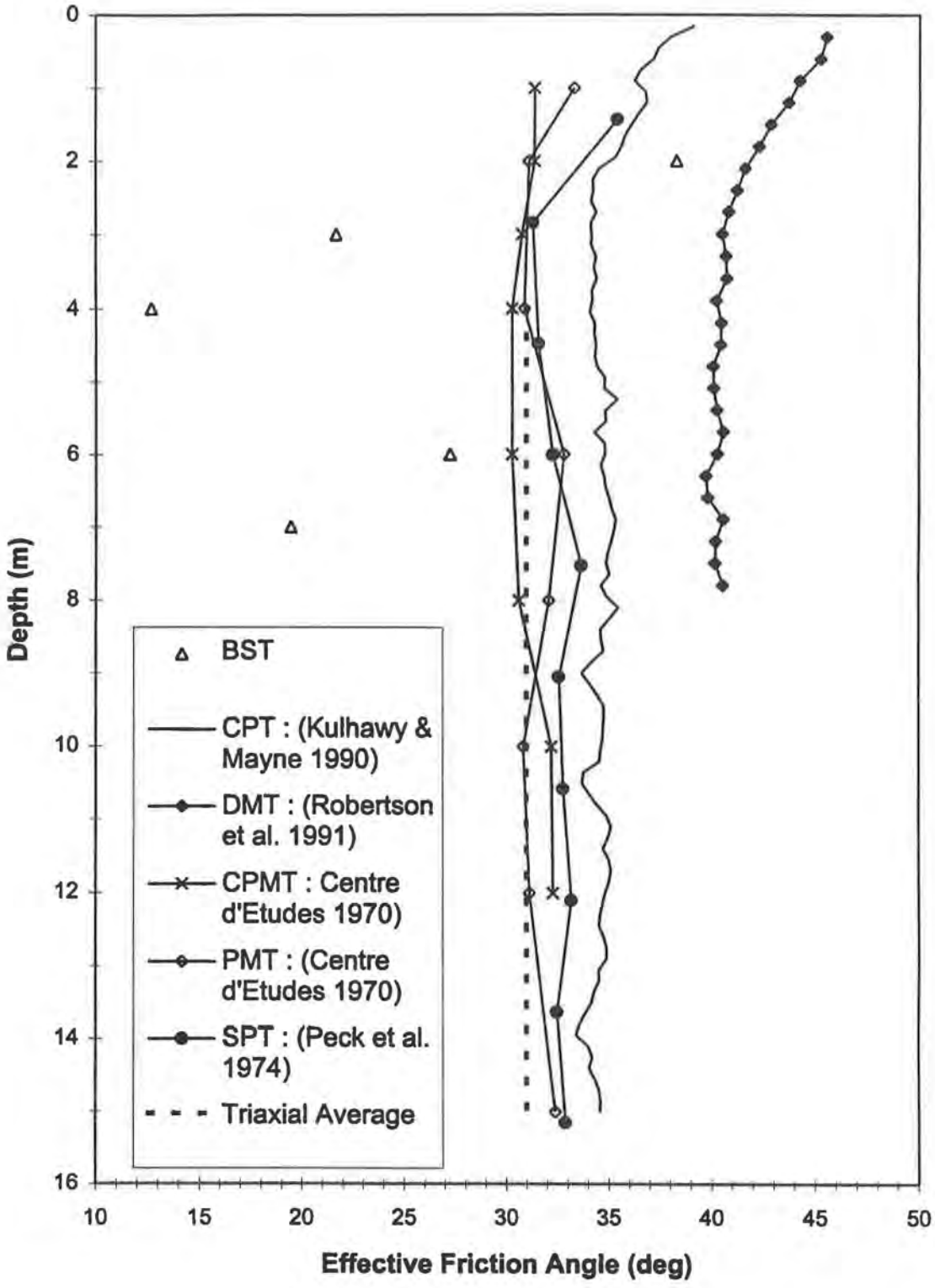

FIG. 11.2.7. - Summary of Effective Friction Angle Predictions.

results are widely scattered with most tests producing quite low $\varnothing'$ values; conversely, the DMT correlation produced the highest $\varnothing'$ values. All correlations discussed are included along with assumptions and data upon which the correlations were based in the appropriate test's appendix.

11.3 Total Stress Shear Strength Test Results

11.3.1 Triaxial Test Results

As presented in Chapter 8, nineteen UU triaxial compression tests were conducted on samples from 1 to 3 meters depth with confining pressures approximately equal to total overburden, except for two tests which were unconfined. These results are shown in Figures 8.7.10, 8.7.11, and 8.7.12 along with results of CIUC tests conducted at effective overburden. Table 11.3.1 contains a summary of UU and CU tests with confining or effective consolidation pressures, respectively, approximately equal to effective overburden.

The relationship of S_u to confining stress is given on Figures 8.7.11 and 8.7.12. From Figure 8.7.11, all triaxial tests, regardless of confinement pressure, gave a rather low overall linear regression; however, Figure 8.7.12 shows the same plot with a regression through the CU tests' S_u values. The CU regression has a much higher R^2 which suggests that S_u increases almost linearly with effective confining pressure. The scatter evident in UU testing is probably due to these samples falling in the upper zone;

the soil is more weathered in the upper 3 meters as compared to the CU test saprolite samples. Also, the difference in testing procedures probably contributes to the difference in variation between UU and CU results; CU testing involves reconsolidating the soil. Sample disturbance probably has a larger effect on S_u without reconsolidation.

Table 11.3.1. - Undrained Shear Strengths Near Effective Overburden Pressure.

Test Type	Depth (m)	n	Avg. S_u (kPa)	St. Dev. (kPa)
UU	1	7	111.2	43.7
UU	2	6	78.5	26.1
UU	3	4	84.5	46.6
CU	4	2	81.3	3.1
CU	6	1	118.2	N/A
CU	8	2	87.9	5.3
CU	10	2	96.1	6.3
CU	12	2	73.9	21.4
CU	15	2	84.8	9.8
Avg. UU	1 - 3	17	93.4	39.7
Avg. CU	4 - 15	11	87.8	14.8
Overall Avg.	1 - 15	28	91.2	32.0

11.3.2 Correlation Predictions of Undrained Shear Strength

Figure 11.3.1 shows a summary of all correlated evaluations of S_u. For comparison, the average S_u from UU and CIUC triaxial tests near the effective overburden confining pressure is included in the figure. Also, lines representing plus or minus one standard deviation of the overall average S_u of 92 kPa is included. Although each test correlation has a lot of scatter, values from all the tests fall within the band of plus or minus one standard deviation of the overall average S_u. Only the DMT correlation was taken

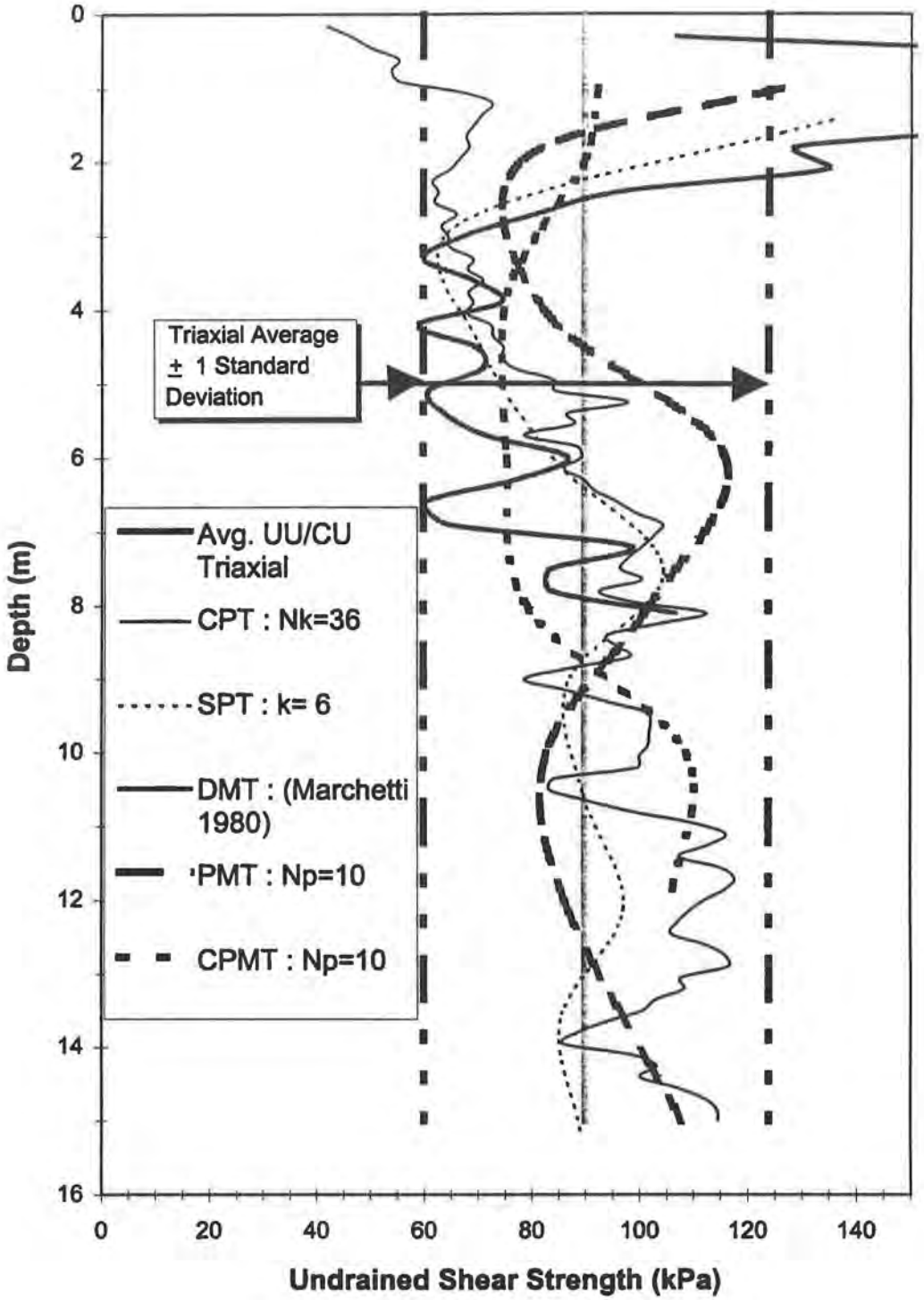

FIG. 11.3.1. - Summary of Undrained Shear Strength Correlations.

directly from the literature; all other S_u correlations presented herein are site-specific back-calculated correlations.

The DMT correlation used was presented by Marchetti (1980). This correlation is based on Italian clays with I_D values less than 1.2; however, Schmertmann (1988) suggests limiting I_D to less than 0.6. The I_D values at Spring Villa ranged between 0.6 and 1.2; therefore, the correlation would be seemingly applicable. The S_u values in the upper zone were much higher than those in the saprolite; otherwise, the DMT predictions were generally less than the overall average S_u.

SPT can been related to S_u through the relationship of blow count multiplied by a constant as follows

$$S_u = k\, N_{70}$$

where S_u = maximum undrained shear strength with units of [kPa], k = constant with units of [kPa/(blows/30cm)], and N_{70} = average corrected blow count (blows/30cm) for an SPT conducted at 70% of theoretical maximum energy. The SPT hammer used at Spring Villa was assumed to be at 90% efficiency, and N-values were scaled down to 70% efficiency for this correlation since published reports suggest that most hammers are approximately near this efficiency range. Blow counts were also corrected for overburden, borehole diameter, and rod length as presented in Appendix B. Through back-calculation, k = 6 gave the best agreement with laboratory results.

The theoretical relationship between CPT tip resistance in "clay" is as follows

$$S_u = (q_c - \sigma_{vo})/N_k$$

where S_u = maximum undrained shear strength in units of [kPa], q_c = cone tip resistance in units of [kPa], σ_{vo} = total overburden stress in units of [kPa], and N_k = dimensionless constant. N_k can vary greatly with published reports of values between 4.5 to 75 (Kulhawy and Mayne 1990); N_k values of 15 to 20 are typical. At Spring Villa, N_k = 35 to 40 gave the best agreement with laboratory testing.

For PM tests, S_u is related to limit pressure by the relationship as follows

$$S_u = (p_L - p_o)/N_p$$

where S_u = maximum undrained shear strength in units of [kPa], p_L = limit pressure in units of [kPa], p_o = interpreted total at rest horizontal stress in units of [kPa], and N_p = dimensionless constant. N_p is often between 5 to 12 , with an average of 8.5 (Kulhawy and Mayne 1990). The PMT provided a best-fit agreement with N_p = 10; the CPMT, which had similar values of p_L and p_o, also agreed well with N_p = 10.

11.4 Summary and Conclusions

11.4.1 Effective Stress Shear Strength

The following conclusions and observations are based on the various geotechnical tools and corresponding interpretations of effective stress strength utilized in this study:

- Linear regression of p on q from all single-stage and multi-stage saprolite triaxial tests (22 CIUC and 1 CIDC) between 4 and 15 meters with p-q coordinates taken at the maximum principal stress ratio produced the

following results : $c' = 17$ kPa, $\varnothing' = 31°$, and $R^2 = 0.9128$. The R^2 suggests a very good linear fit; however, due to the nonhomogeneous nature of Piedmont soils, it is conceivable that very different strength parameters may have been predicted (although probably with a low R^2) had only a small number of samples been tested.

- c' and $\varnothing'$ were fairly constant over depth, but although lower depths had similar parameters compared to greater depth ranges, the lower depths had a significantly lower R^2. This may be due to increased weathering and less homogeneous soil conditions at shallower depths.
- Four multi-stage tests with two stages of loading were conducted; the linear regression of these four samples' results agreed very closely to the overall triaxial p on q regression and had a higher R^2. Failure envelopes derived from individual samples varied similarly to that of the overall triaxial regressions; it appears that a few multi-stage samples may be able to approximately define the average and range of effective stress parameters as well as a larger number of single-stage triaxial tests.
- The BST produced very erratic results with $\varnothing'$ generally quite low at tests below the ground water table compared to triaxial results. The low friction angle predictions may be due to shearing which causes excess pore pressures, remolding of the sides of the soil cavity during shear head insertion, and possible seepage of groundwater into the soil cavity during testing.

- Three out of the four SPT correlations of N with $\varnothing'$ gave slightly higher predictions than triaxial testing. Since $\varnothing'$ was fairly constant over depth from triaxial testing and blow count varied over a small range, a site-specific correlation of N vs. $\varnothing'$ is not possible (except for one value). The average corrected N_{70} is 15 over the triaxial range of 4 to 15 meters which produced $\varnothing' = 31°$.
- The DMT correlation for $\varnothing'$ by Robertson and Campanella (1991) showed very poor agreement with triaxial results, overpredicting $\varnothing'$ significantly.
- The CPT correlations for $\varnothing'$ by Kulhawy and Mayne (1990) and Robertson and Campanella (1983) show good agreement to triaxial results with predictions generally 2 to 4° higher. The Masood and Mitchell (1993) correlation gave extremely large predictions with $\varnothing'$ at least 10° higher than the triaxial value.
- Of the PM correlations, the Centre de Etudes Menard (1970) correlation which empirically relates $\varnothing'$ to net limit pressure gave very close agreement to triaxial results. Other published correlations showed poor agreement with triaxial data.

11.4.2 Total Stress Shear Strength

The following conclusions and observations are based on the various geotechnical tools and corresponding interpretations of total stress strength utilized in this study:

- S_u increased linearly with increasing confinement regardless of sample depth or triaxial test type; this linear relationship was much more pronounced in the CU tests (4 to 15 meters depth) compared to the UU tests (upper 3 meters).
- UU or CU tests with confining pressures approximately equal to effective overburden produced an average S_u near 92 kPa over the 15 meters depth which was tested. UU tests showed much more scatter although the average S_u value from UU tests is virtually the same compared to the average of all CU tests.

- The DMT correlation by Marchetti (1980) generally predicted S_u lower than the overall average value of 92 kPa.
- All correlations, besides the Marchetti (1980) correlation for the DMT, were back-fit. Each correlation shows a lot variation over depth, but generally fall within $\pm$ one standard deviation of the overall average of measured S_u values. The constant multiplier for the SPT, CPT, PMT and CPMT which gave the best agreement with the overall average is shown below in Table 11.4.1.

Table 11.4.1. - Site-Specific Correlations With Undrained Shear Strength.

Test	Correlation Equation	Constant Value
SPT	$S_u = k\ N_{70}$	k = 6 kPa/(blows/30cm)
CPT	$S_u = (q_c - \sigma_{vo})/N_k$	N_k = 35 - 40
PMT/CPMT	$S_u = (p_L - p_o)/N_p$	N_p = 10

CHAPTER 12

CONCLUSIONS AND RECOMMENDATIONS

12.1 Nature of Piedmont Soils

Derived from in-place weathering of ancient igneous and metamorphic rock, the residual soils of the Piedmont province have several unique physical and mechanical properties. They exhibit behavior sometimes quite contradictory to that of more well understood sedimentary soils since they have not been subject to sorting and retain some of the parent rock's structure. These heterogeneous, anisotropic soils (which are usually silty sands/sandy silts) are quite difficult to characterize due to the spacial soil variability which is a result of the mineral banding caused during the parent rock's formation under extreme heat; these bands of minerals typically are of a swirled, contorted, crumpled, and/or twisted state.

The degree of weathering affects soil behavior in the Piedmont province; typically, at lesser depths, the soil has undergone greater weathering. A Piedmont residual soil profile usually consists of upper, intermediate, and partially weathered zones which overlay the parent rock formation. Each zone represents varying degrees of weathering, but zone boundaries are not discrete but gradual in nature. The upper zone is often 1-3 meters in depth and is at an advanced stage of weathering; little evidence of the parent rock can be

detected. The intermediate zone, or saprolite, retains the appearance and structure of the parent rock (e.g. mineral bonding) while being soil in texture; however, unlike the upper zone which tends to have highly variable plasticity, saprolite often has relatively high liquid limits but very low plasticity indices. The saprolite's mineralogy tends to greatly affect mechanical behavior; for example, mica content tends to have a direct bearing on void ratio (Sowers 1963). The partially weathered zone consists of alternating layers of sandy silts/silty sands and bands of relatively sound rock.

The engineering characteristics of Piedmont residual soils are often quite unique. The relatively high void ratios in these soils make them highly compressible, and they tend to exhibit rapid consolidation. Retained tectonic stresses tend to cause horizontal at rest earth pressures at shallow depths to be quite large; in other words, the coefficient of earth pressures at rest (K_o) is often higher at decreasing depths. Due to the spacial variability caused by uneven weathering or mineral banding, especially in the saprolite which is often the most critical zone to the design of foundations, shear strength and stiffness determination is usually difficult due to the scatter of testing results. Since obtaining samples for laboratory testing can be difficult or may not be representative of the soil on a macroscopic level, in-situ testing methods are often considered as more appropriate in determining the soil's degree of spacial variability. Regardless of the testing method, the lack of discrete stratification, complex in-situ stresses, and spacial variability due to weathering or mineral banding present several obstacles towards accurately assessing and characterizing the engineering properties of Piedmont residual soils.

12.2 Conclusions of Testing Measurements

12.2.1 Index Testing

Through grain size analysis and Atterberg limits determination, the soil profile of Spring Villa in the upper 15 meters was assessed; in addition, the highly variable nature of index testing in the Piedmont, as noted in the literature, was observed. The upper 2 to 3 meters of Spring Villa is composed primarily of high to low plasticity silts; this is typical of Piedmont upper zone soils. The less weathered saprolite zone below this upper zone extends to at least a depth of 15 meters. It is comprised of silty sands and sandy silts.

In-situ water contents were quite variable with values ranging between 20 and 45% at most depths. Liquid limits were relatively high at all depths with the highest value being in the upper zone at over 60%, and the lowest liquid limit was near 30% within the saprolite. Plasticity was generally quite small at all depths with almost half of the samples tested being nonplastic.

Large scatter was evident in the grain size analysis of samples at similar depths. The mean percentage of sands was just below 50%, but the standard deviation was quite large at 17%. Therefore, there could be several different soil classifications at the same depth which is characteristic of Piedmont soils. Finally, the wet unit weight was found to be relatively constant at 18.25 kN/m^3 over all depths within the upper 15 meters.

12.2.2 In-Situ Stresses

The PMT and CPMT predictions of K_o agreed fairly well with each other at most test depths, but the CPMT predictions were somewhat lower at most depths. The average K_o of both PM tests in the saprolite was approximately 1.25. Large K_o predictions in the Piedmont, especially at shallow depths, compared to sedimentary soils have been documented in the literature.

12.2.3 Stiffness Parameters

From the wide array of in-situ and laboratory techniques, both small- and large-strain moduli were determined. The following conclusions can be made regarding the different techniques used to gain a measure of soil stiffness:

- Seismic test moduli are approximately 10 to 15 times that of mechanical measures (except for the unload-reload cycle of the CPMT).
- Initial loading stiffness of the PMT and CPMT were in relatively close agreement except at depths below 8 meters where the CPMT moduli tended to increase while the PMT moduli remained relatively constant. Most techniques predicted that modulus increases over depth in the saprolite; therefore, it is suspected that the PMT moduli did not increase due to remolding of the soil cavity because of difficulty in placing the probe or soil relaxation since it took longer to withdraw the shelby tube and position the probe at these greater depths.

- DMT and CIUC triaxial tests with confining pressures near effective overburden results agreed over similar test depths even though the triaxial moduli were determined over a slightly larger shearing strain amplitude.
- The CPMT unload-reload cycle produced very high moduli approaching the seismic small-strain moduli although shearing strains were approximately that of the DMT. It is suspected that factors other than shearing strain amplitude, such as greatly increased effective stresses due to the initial probe expansion loading, are responsible for this phenomenon.
- On a plot of average shear modulus (in the 3 to 12 meter depth range) as a function of shearing strain, the mechanical measures of modulus (except for the unload-reload cycle of the CPMT) produced values which were lower than some published Piedmont residual soils' values at the same shearing strains.
- The relationship between undrained shear strength (S_u) and tangent modulus (E_t) was determined for the UU and CIUC triaxial tests with confining pressures approximately that of effective overburden as follows

$$E_t = 200S_u \text{ for CIUC tests}$$

$$E_t = 75S_u \text{ for UU tests}$$

These greatly differing relationships are thought to occur because the UU tests were conducted in the upper zone (which was more weathered) while the CIUC tests were conducted on saprolite samples. Also, the

reconsolidation phase of the CIUC test probably limits sample disturbance effects compared to the UU test.

12.2.4 Shear Strength

The shear strength at this site was measured with consolidated isotropically-undrained compression triaxial testing (CIUC) and the Iowa borehole shear test (BST). The following conclusions are based upon these tests' drained and undrained testing:

- Linear regression of p on q from all single-stage and multi-stage saprolite triaxial tests (22 CIUC and 1 CIDC) between 4 and 15 meters with p-q coordinates taken at the maximum principal stress ratio produced the following results : $c' = 17$ kPa, $\varnothing' = 31°$, and $R^2 = 0.9128$. The R^2 suggests a very good linear fit; however, due to the nonhomogeneous nature of Piedmont soils, it is conceivable that very different strength parameters may have been predicted (although probably with a low R^2) had only a small number of samples been tested.
- Triaxial values of c' and $\varnothing'$ were fairly constant over depth, but although lower depths had similar parameters compared to greater depth ranges, the lower depths had a significantly lower R^2. This may be due to increased weathering and less homogeneous soil conditions at shallower depths.
- Four multi-stage tests with two stages of loading were conducted; the linear regression of these four samples' results agreed very closely to the overall triaxial p on q regression and had a higher R^2. Failure envelopes derived from

individual samples varied similarly to that of the overall triaxial regressions; it appears that a few multi-stage samples may be able to approximately define the average and range of effective stress parameters as well as a larger number of single-stage triaxial tests.

- S_u increased linearly with increasing confinement regardless of sample depth or triaxial test type; this linear relationship was much more pronounced in the CU tests (4 to 15 meters depth) compared to the UU tests (upper 3 meters).
- UU or CU tests with confining pressures approximately equal to effective overburden produced an average S_u near 92 kPa over the 15 meters depth which was tested. UU tests showed much more scatter although the average S_u value from UU tests is virtually the same compared to the average of all CU tests.
- The BST produced very erratic results with friction angles generally quite low at tests below the ground water table compared to triaxial results. The low friction angle predictions may be due to shearing which causes excess pore pressures, remolding of the sides of the soil cavity during shear head insertion, and possible seepage of groundwater into the soil cavity during testing.

12.3 Conclusions of Correlations With Test Measurements

12.3.1 In-Situ Stresses

The range of K_o correlations was quite large with values between 0.3 to 2.0 predicted in the saprolite zone. Generally, except for the CPT correlations, predicted K_o values were well above the typical range for sedimentary soils; this was especially evident in the upper zone. The DMT interpretations varied widely, depending upon the soil type assumed, but the Marchetti (1980) and Schmertmann (1983) correlations were most nearly consistent with the PMT and CPMT data. The Kulhawy and Mayne (1989) SPT correlation developed for fissured and intact clays was also generally consistent with PM testing.

12.3.2 Stiffness Parameters

The following conclusions can be made concerning various small- and large-strain modulus correlations with different in-situ test methods:

- For the correlations of small-strain shear modulus based solely on effective confining pressure, the Seed and Idriss (1970) correlation for "sands" produced the most agreeable shear moduli with $K_{2(max)} \cong 45$. The Hardin and Drnevich (1972) correlation for "clays" predicted small-strain shear moduli which were 10 to 50% less than the CHT results.
- The Schmertmann (1978) and Imai et al. (1982) SPT correlations for small-strain shear modulus agreed fairly well with CHT results below the upper

zone. The Seed et al. (1986) correlation underestimated small-strain moduli at all depths. The Schmertmann (1978) correlation provided the best agreement with a constant (C) of 12 where $G_{max} = \rho(CN_{60})^2$.

- All CPT correlations of small-strain shear modulus were poor. The best correlation appeared to be Rix and Stokoe (1991) which underestimated modulus compared to the CHT by approximately 25% at most depths.
- The SPT correlations for intermediate- to large-strain Young's modulus by Kulhawy et al. (1990) and Bowles (1996) in sands with fines and silts, sandy silts, or clayey silts, respectively, agree closely with PMT and CPMT modulus.
- The Frost and Mayne (1989) correlation of SPT with modulus from the DMT in the Piedmont province overestimated the average measured DM modulus by approximately 45%.
- The Ohaya et al. (1982) correlation of SPT with PM modulus agreed more closely to PMT and CPMT results than the Barksdale et al. (1986) correlation. The Barksdale et al. (1986) correlation, which was developed from testing in the Piedmont province, was generally 40 to 100% larger than measured values.
- The CPT correlation with intermediate- to large-strain Young's modulus by Bowles (1996) for silts, sandy silts, or clayey silts agreed most closely with PMT and CPMT results. This correlation's moduli were approximately 50 to 80% of the Senneset (1988) correlation for the same soil type.

12.3.3 Shear Strength

The following conclusions can be made on correlations with in-situ tests and effective friction angle and undrained shear strength:

- Three out of the four SPT correlations of N with $\varnothing'$ gave slightly higher predictions than triaxial testing. Since $\varnothing'$ was fairly constant over depth from triaxial testing and blow count varied over a small range, a site-specific correlation of N vs. $\varnothing'$ is not possible (except for one value). The average corrected N_{70} is 15 over the triaxial range of 4 to 15 meters which produced $\varnothing' = 31°$.
- The DMT correlation for $\varnothing'$ by Robertson and Campanella (1991) showed very poor agreement with triaxial results, overpredicting $\varnothing'$ significantly.
- The CPT correlations for $\varnothing'$ by Kulhawy and Mayne (1990) and Robertson and Campanella (1983) show good agreement to triaxial results with predictions generally 2 to 4° higher. The Masood and Mitchell (1993) correlation gave extremely large predictions with $\varnothing'$ at least 10° higher than the triaxial value.
- Of the PM correlations, the Centre de Etudes Menard (1970) correlation which empirically relates $\varnothing'$ to net limit pressure gave very close agreement to triaxial results. Other published correlations showed poor agreement with triaxial data.

- All correlations with S_u, besides the Marchetti (1980) correlation for the DMT, were back-fit. Each correlation shows a lot variation over depth, but generally fall within $\pm$ one standard deviation of the overall average of S_u values from the triaxial test. The constant multiplier for the SPT, CPT, PMT and CPMT which gave the best agreement with the overall average is given in Table 11.4.1.

12.4 Recommendations for Future Research

The primary objective of this investigation was to characterize the Spring Villa Test Site's physical and mechanical properties through a wide array of in-situ and laboratory tests. The following is a list of suggestions for future research and areas of study :

- Examine specific gravity, mica content and void ratio as possibly being used in conjunction with the Atterberg limits and grain size analysis index tests to better distinguish and classify the various Piedmont zones which represent varying degrees of weathering. A Piedmont classification system may be appropriate since these soils tend to be inadequately characterized by Atterberg limits because results are so variable. Also, grain size analysis may classify a sample as silt and another sand even though the (-) #200 is only 1 to 5% different; many of these soils have very nearly 50% passing the #200 so small variations may mean the soil is incorrectly classified.

- Unload-reload cycle of the PMT would be of interest to see how it compares to the unload-reload CPMT results. Its results may aid in proper interpretation of the CPMT's results.
- More UU tests performed on saprolite samples and CU tests performed on upper zone samples would allow a better comparison of effect of test type on undrained shear strength predictions.
- More CU or CD tests at greater confining pressures would better define the failure envelope of the upper 15 meters; few tests were conducted at high confining pressures.
- Tangent modulus (E_t) from CD tests may be of more interest than that of CU tests since most applications are probably modeled more correctly by fully drained loading.
- More multi-stage CU tests at various depths with single-stage tests conducted at the same confining pressures and sample depths may aid in determining the viability of multi-stage testing. CD multi-stage tests would be appropriate for comparison as well.
- Resonant column or other techniques which measure modulus at shearing strains between 0.1% and that of seismic testing ($\leq 0.001\%$) would more fully define the normalized shear modulus degradation curve.
- Performance of the self-boring pressuremeter test (SBPMT) for determining the horizontal at rest earth pressure (and therefore the coefficient of at rest earth pressures - K_o) would allow for comparison of various correlations'

accuracy and possibly establishing a Piedmont correlation with simple geotechnical tools.

- Conventional consolidation and permeability testing may provide more insight into the exact nature of drainage and material compressibility.
- Different piezocone porous element locations may provide more amplified piezocone pore pressure records and more meaningful information.
- Settlement measurement of a heavily loaded footing or structure and/or measurement of dynamic foundation response would allow a back-calculation of shear modulus values suitable for design and for comparison with the various tools' measurements.

APPENDIX A

INDEX TEST RESULTS

General

1. SPT split-spoon samples and trimmings from preparation of triaxial shear samples taken from shelby tubes were used in determining in-situ water contents.

2. The average water content over all depths tested was approximately 34%.

3. Wet unit weights were determined by weighing trimmed triaxial samples with known dimensions prior to shearing.

4. Dry unit weights were determined using the average water content of 34% for all depths and the relationship of Dry Unit Wt. = Wet Unit Wt./(1 + water content).

5. Atterberg Limits were performed in accordance with AASHTO T 89-94 and AASHTO T 90-94 on all split-spoon samples and various sheared triaxial samples. Individual boring records of in-situ water contents and plasticity are included in this section.

6. Specific gravity testing was performed in accordance with AASHTO T 100-93.

7. Grain size distribution (GSD) analysis was conducted on split spoon samples and some triaxial shear samples. GSD for (+) #200 sizes was performed in accordance with AASHTO T 27-93. A Micromeritic Particle Size Analyzer, which uses x-ray absorption techniques, was used to evaluate the GSD of the (-) #200 portion of some split spoon samples. The GSD curves which follow in this section are grouped according to depth; samples are identified according to boring and to mid-height of each sample. During sampling, shelby tubes were centered at whole meter depth increments.

8. Calculation of Effective Overburden Pressure :

   a. A wet unit weight of 18.25 kN/m^3 was found to be approximately the overall average value from all triaxial samples tested and was used in calculating overburden pressure for all depths.
   b. Throughout in-situ testing, the ground water table depth varied from between 2.4 meters and 3.7 meters; a depth of 3 meters was chosen as an average value for calculations.
   c. One meter of negative pore pressure above the ground water table was assumed due to capillary effect.
   d. Sample Calculation for Depth = 2.7 meters -

$$\text{Effective Overburden} = (2.7\text{m})(18.25\ kN/m^3)-(2.7\text{m}-3\text{m})(9.807\text{m}/s^2)$$
$$= \underline{52.2\ kN/m^2}$$

9. Calculation of Small-Strain Shear Moduli from Correlations -

   a. *Hardin and Drnevich* (1972) :

   - This correlation is for "clays" of moderate sensitivity.
   - k values are recommended to be between 0.18 and 0.00 for plasticity indices less than 20%; k = 0.05 was used in these calculations.
   - The average dry unit weight of trimmed triaxial test samples at each test depth was used.
   - The average of the three specific gravity values (2.8) was assumed to be a constant over all depths.
   - Using the average dry unit weights and average specific gravity, the void ratio (e) at each depth was determined by the following equation -

   Void Ratio = ((Specific Gravity)(Unit Weight of Water)/(Dry Unit Weight)) - 1

   = ((2.8)(9.807)/(Dry Unit Weight) - 1)

   Therefore, at a 1 meter depth where the average dry unit weight is 13.8 kN/m^3, e = 0.99.

   - The overconsolidation ratio (OCR) determined from the flat dilatometer test (DMT) was used. In Appendix F, two methods of determining OCR was used, but the method denoted with an asterick (OCR*) was used to determine average values for this correlation; the values tended to be near a constant value of 2.7 in the saprolite from 3 to 8 meters depth over which the DMT was conducted. This constant value was assumed to be the same over the 8 to 15 meter range as well.
   - The effective octahedral stress is the average effective confining pressure and was determined using the average K_o values from the Menard pressuremeter test (PMT) results (see Table 9.3.1) as follows

   $$\sigma_o' = 1/3 \text{ (Effective Overburden + 2 } (K_o)(\text{Effective Overburden}))$$

   - At 1 meter depth the effective overburden pressure is 18.3 kN/m^2 and the average K_o is 2.63. Therefore, the effective octahedral stress (σ_o') is 38.1 kN/m^2; the average OCR is 30. Calculation of the small-strain shear modulus (G_{max}) follows :

   $$G_{max} = (3230(2.97 - e)^2(OCR)^k(\sigma_o')^{0.5})/(1 + e) = \underline{46,800 \text{ kPa}} = \underline{46.8 \text{ MPa}}$$

b. *Seed and Idriss* (1970) :

- This correlation is for "sands" and shearing strain amplitudes $\leq 10^{-4}\%$.
- $K_{2\,(max)}$ varies between 30 for loose sands to 75 for dense sands.
- At 1 meter depth the effective overburden pressure is 18.3 kN/m^2 and the effective octahedral stress (σ_o') is 38.1 kN/m^2. The σ_o' must be converted to [pounds/square foot] and is 795 psf. Calculation of the small-strain shear modulus using $K_{2\,(max)}$ of 30 follows as

$$G_{max} = 1000\, K_{2\,(max)}\, (\sigma_o')^{0.5} = (1000(30)(795psf)^{0.5})/(20.885\ psf/kN/m^2)$$

$$= \underline{41,500\ kPa} = \underline{41.5\ MPa}$$

Table A.1. - Index Test Results and Classifications (B-1).

	Avg. Depth :	1.4 m	3 m	4.5 m	6 m	7.5 m	10.6 m	15.2 m
Sieve Size	Opening (mm)	%Passing	%Passing	%Passing	%Passing	%Passing	%Passing	%Passing
2 "	50	100.0	100.0	100.0	100.0	100.0	100.0	100.0
1 "	25	100.0	100.0	100.0	100.0	100.0	100.0	100.0
#4	4.75	98.3	100.0	100.0	100.0	100.0	100.0	99.1
#8	2.36	90.2	98.3	99.2	100.0	99.6	100.0	98.8
#10	2	88.3	97.8	98.6	100.0	99.6	100.0	98.5
#40	0.425	66.9	90.1	91.3	98.6	97.6	92.7	97.0
#200	0.075	46.3	76.2	46.2	83.5	84.8	69.1	89.5
PC	0.002	25.3		7.9			11.9	
	Liquid Limit =	48	42	45	NP	44	54	49
	Plastic Limit =	38	38	40	NP	39	46	41
	Plasticity Index =	10	4	5	NP	5	8	8
	In Situ W/C =	22.9	30.1	35.8	34.0	26.4	44.6	46.9
	AASHTO classification	A-5 (2)	A-5 (5)	A-5 (1)	A-4 (0)	A-5 (7)	A-5 (8)	A-5 (12)
	USCS classification	SM	ML	SM	ML	ML	ML	ML

Table A.2. - Index Test Results and Classifications (B-3).

	Avg. Depth :	1.4 m	4.4 m	7.5 m	10.5 m	15.1 m
Sieve Size	Opening (mm)	%Passing	%Passing	%Passing	%Passing	%Passing
2 "	50	100.0	100.0	100.0	100.0	100.0
1 "	25	100.0	100.0	100.0	100.0	100.0
#4	4.75	100.0	100.0	100.0	100.0	98.6
#8	2.36	97.7	99.4	100.0	100.0	90.4
#10	2	96.0	99.0	100.0	100.0	88.8
#40	0.425	74.8	81.5	90.7	91.8	77.1
#200	0.075	56.0	28.5	31.2	36.4	47.7
PC	0.002	27.4	4.5	3.0	4.2	6.1
	Liquid Limit =	56	30	NP	NP	NP
	Plastic Limit =	40	26	NP	NP	NP
	Plasticity Index =	16	4	NP	NP	NP
	In Situ W/C =	24.5	24.3	27.3	25.8	35.9
	AASHTO classification	A-7-5 (8)	A-2-4 (0)	A-2-4 (0)	A-4 (0)	A-4 (0)
	USCS classification	MH	SM	SM	SM	SM

Table A.3. - Index Test Results and Classifications (B-4).

	Avg. Depth :	1.3 m	2.8 m	4.3 m	5.9 m	7.4 m	12.0 m	15.0 m
Sieve Size	Opening (mm)	%Passing	%Passing	%Passing	%Passing	%Passing	%Passing	%Passing
2 "	50	100.0	100.0	100.0	100.0	100.0	100.0	100.0
1 "	25	100.0	100.0	100.0	100.0	100.0	100.0	100.0
#4	4.75	100.0	100.0	97.6	100.0	99.3	100.0	96.5
#8	2.36	100.0	100.0	96.5	100.0	96.7	99.6	92.4
#10	2	100.0	100.0	95.8	100.0	94.1	98.9	91.1
#40	0.425	78.7	79.7	82.9	99.0	52.5	90.8	78.3
#200	0.075	45.0	50.1	42.9	90.1	29.4	74.6	64.0
PC	0.002	15.4	10.5	9.3		5.6		
	Liquid Limit =	NP	NP	40	54	40	37	NP
	Plastic Limit =	NP	NP	30	45	37	31	NP
	Plasticity Index =	NP	NP	10	9	3	6	NP
	In Situ W/C =	26.2	33.8	31.1	46.4	21.6	25.9	20.6
	AASHTO classification	A-4 (0)	A-4 (0)	A-4 (1)	A-5 (14)	A-2-4 (0)	A-4 (5)	A-4 (0)
	USCS classification	SM	ML	SM	MH	SM	ML	ML

Table A.4. - Index Test Results and Classifications (B-6).

	Avg. Depth :	2.8 m	4.3 m	5.9 m	12.0 m	15.0 m
Sieve Size	Opening (mm)	%Passing	%Passing	%Passing	%Passing	%Passing
2 "	50	100.0	100.0	100.0	100.0	100.0
1 "	25	100.0	100.0	100.0	100.0	100.0
#4	4.75	100.0	100.0	100.0	99.1	99.2
#8	2.36	100.0	100.0	100.0	99.1	93.9
#10	2	100.0	100.0	100.0	98.8	92.4
#40	0.425	75.8	92.9	82.6	93.9	68.3
#200	0.075	42.3	71.3	38.8	41.6	33.1
PC	0.002	6.3		6.5	3.7	4.7
	Liquid Limit =	NP	38	39	37	34
	Plastic Limit =	NP	35	31	34	29
	Plasticity Index =	NP	3	8	3	5
	In Situ W/C =	27.9	27	28.8	27.1	25.6
	AASHTO classification	A-4 (0)	A-4 (2)	A-4 (0)	A-4 (0)	A-2-4 (0)
	USCS classification	SM	ML	SM	SM	SM

Table A.5. - Index Test Results and Classifications (B-2 & B-5).

Grain Size Analysis : Sieve and Hydrometer
Performed by: Georgia Tech

	Boring :	B-2	
	Depth :	8 m	12 m
	Sample :	1	1
Sieve Size	Opening (mm)	%Passing	%Passing
#4	4.75	100	99
#10	2	100	97
#20	0.85	95	89
#80	0.18	55	66
#100	0.15	48	58
#200	0.075	29	40
-	0.033	18.5	35.5
-	0.026	18	32
-	0.01	14	22
PC	0.002	8	10.5

	Boring :	B-5			
	Depth :	4 m	8 m	12 m	12 m
	Sample # :	1	1	1	2
Sieve Size	Opening (mm)	%Passing	%Passing	%Passing	%Passing
#4	4.75	100	97	100	100
#10	2	99	96	96	100
#20	0.85	90	86	86	99
#80	0.18	59	49	70	75
#100	0.15	56	45	66	68
#200	0.075	37	27	56	50
-	0.033	34	25	45	39
-	0.026	28	23	44	35
-	0.01	18	14	35	27
-	0.0034	9	8	16.5	14.5
PC	0.002	7	6	13	13

Table A.6. - Index Testing Results and Classifications (B-7).

	Depth :	1 m	2 m	4 m	6 m	8 m	8 m	10 m	10 m	10 m
	Sample # :	2	1	1	1	1	2	1	2	3
Sieve Size	Opening (mm)	% Passing	% Passing	% Passing	% Passing	% Passing	% Passing	% Passing	% Passing	% Passing
2 "	50	100	100.0	100	100	100	100	100	100	100
1 "	25	100	100.0	100	100	100	100	100	100	100
0.75 "	19	100	100.0	100	100	100	100	100	100	100
0.50 "	12.5	100	100.0	100	100	100	100	100	100	100
#4	4.75	100	100.0	100	100	100	100	100	100	100
#10	2	99.5	100.0	100	100	100	100	100	100	100
#16	1.18	97.3	98.9	99	98.9	97.7	96.7	99.4	99.3	99.5
#30	0.6	94.5	96.7	96.4	92.6	93.4	88	97	97.3	98
#40	0.425	93	95.5	94.3	87.4	90	83.2	95	96.1	96.9
#50	0.3	83.7	88.1	90.6	79.1	85.8	76.5	91.5	93.9	94.9
#100	0.15	83.7	88.1	76	62.4	72.4	61.7	79.1	85.8	86.6
#200	0.075	72.6	78.4	54.5	45.1	54.1	45.3	63.3	72.1	75
	Liquid Limit =	67	57	42	NP	NP	NP	NP	NP	60
	Plastic Limit =	48	48	38	NP	NP	NP	NP	NP	50
	Plasticity Index =	19	9	4	NP	NP	NP	NP	NP	10
	In Situ W/C =	41.2	41.2	43.1	35.5	41.1	35.6	50.1	50	50.8
	AASHTO classification	A-7-5 (7)	A-5 (13)	A-5 (6)	A-4 (0)	A-4 (0)	A-4 (0)	A-4 (0)	A-4 (0)	A-5 (12)
	USCS classification	MH	MH	ML	SM	ML	SM	ML	ML	MH

Sieve Analysis in accordance with AASHTO T27-93.
Atterberg Limits in accordance with AASHTO T89-94 and AASHTO T90-94.

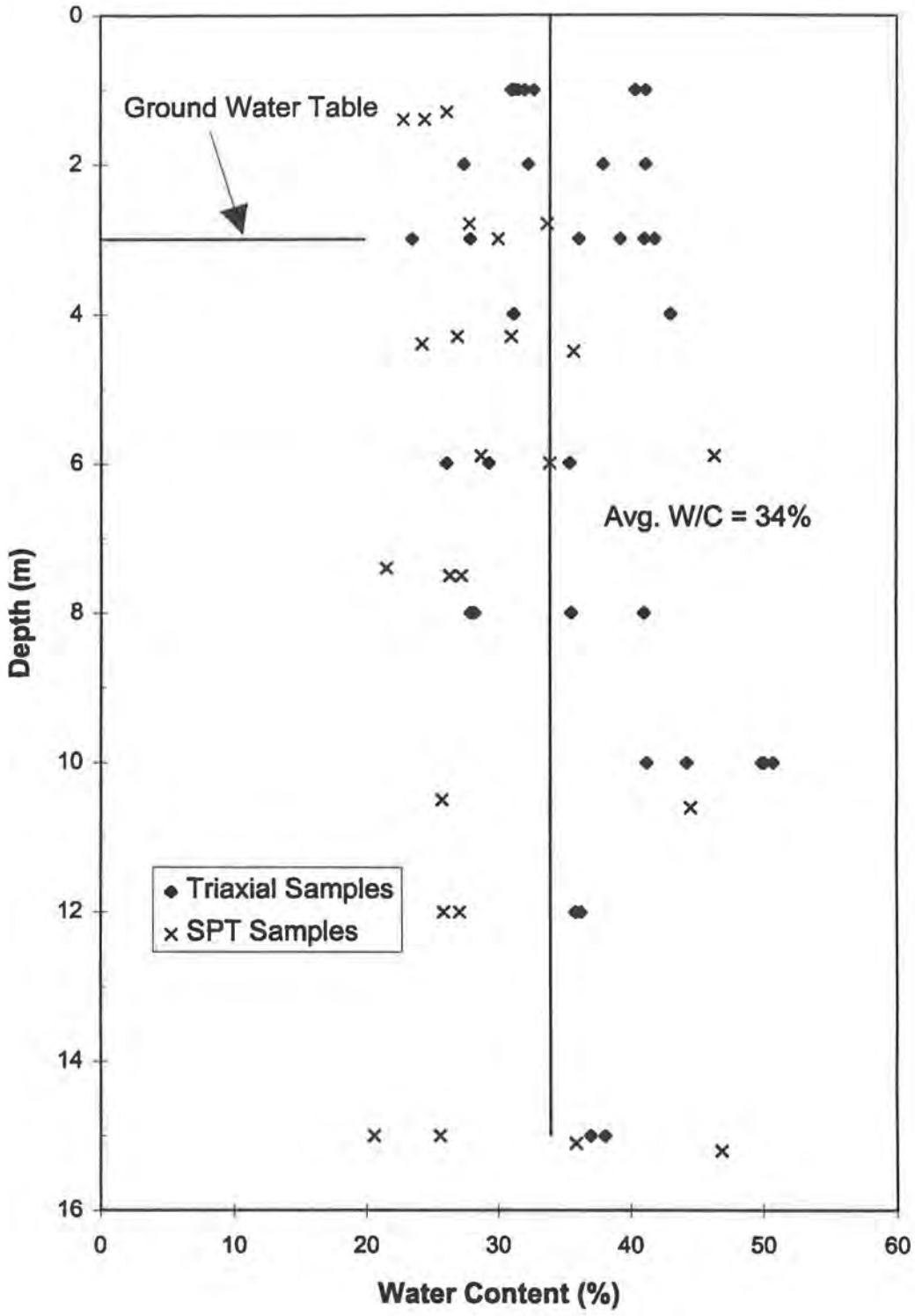

FIG. A.1. - In-Situ Water Contents

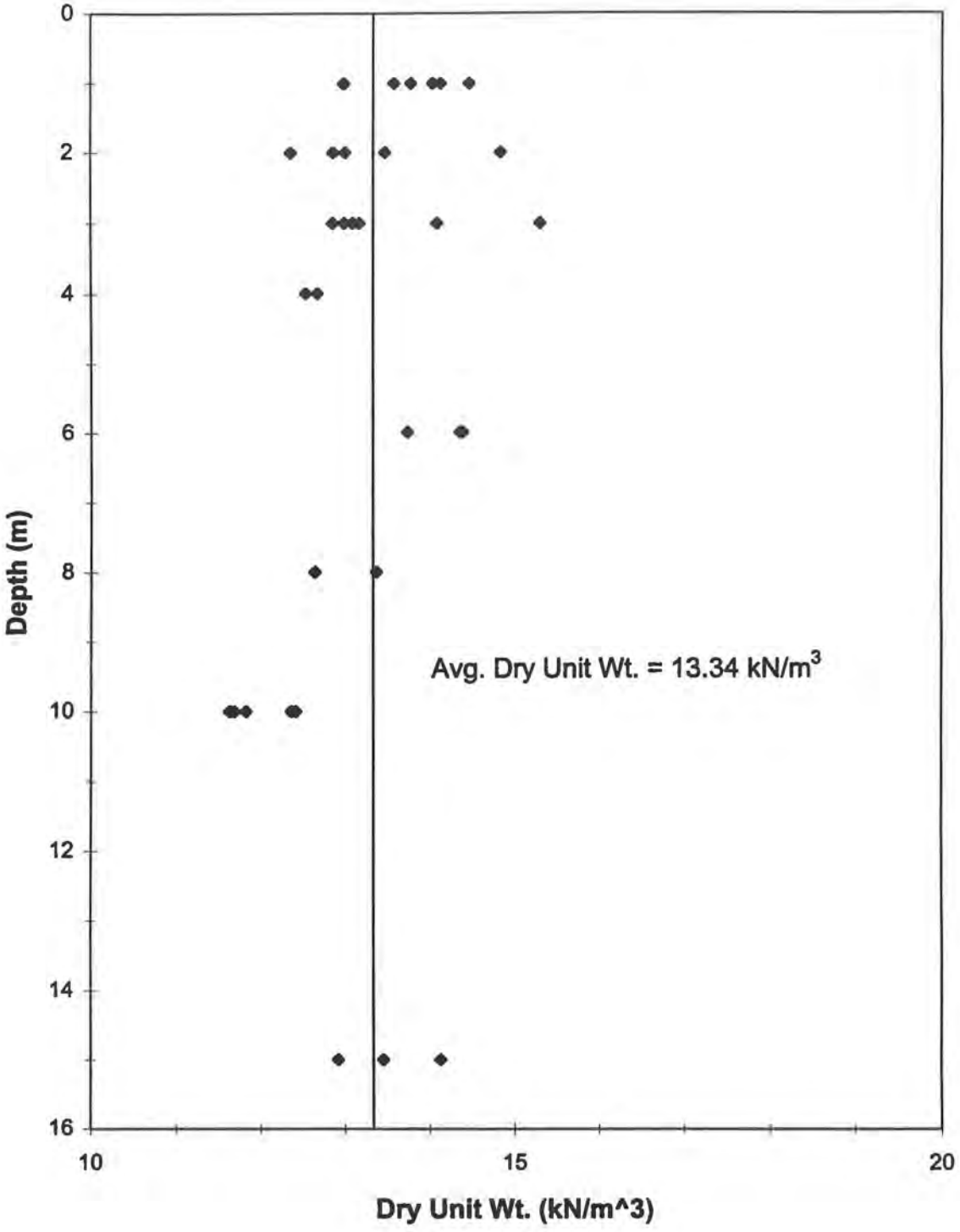

FIG. A.2. - Dry Unit Weights from Trimmed Triaxial Samples

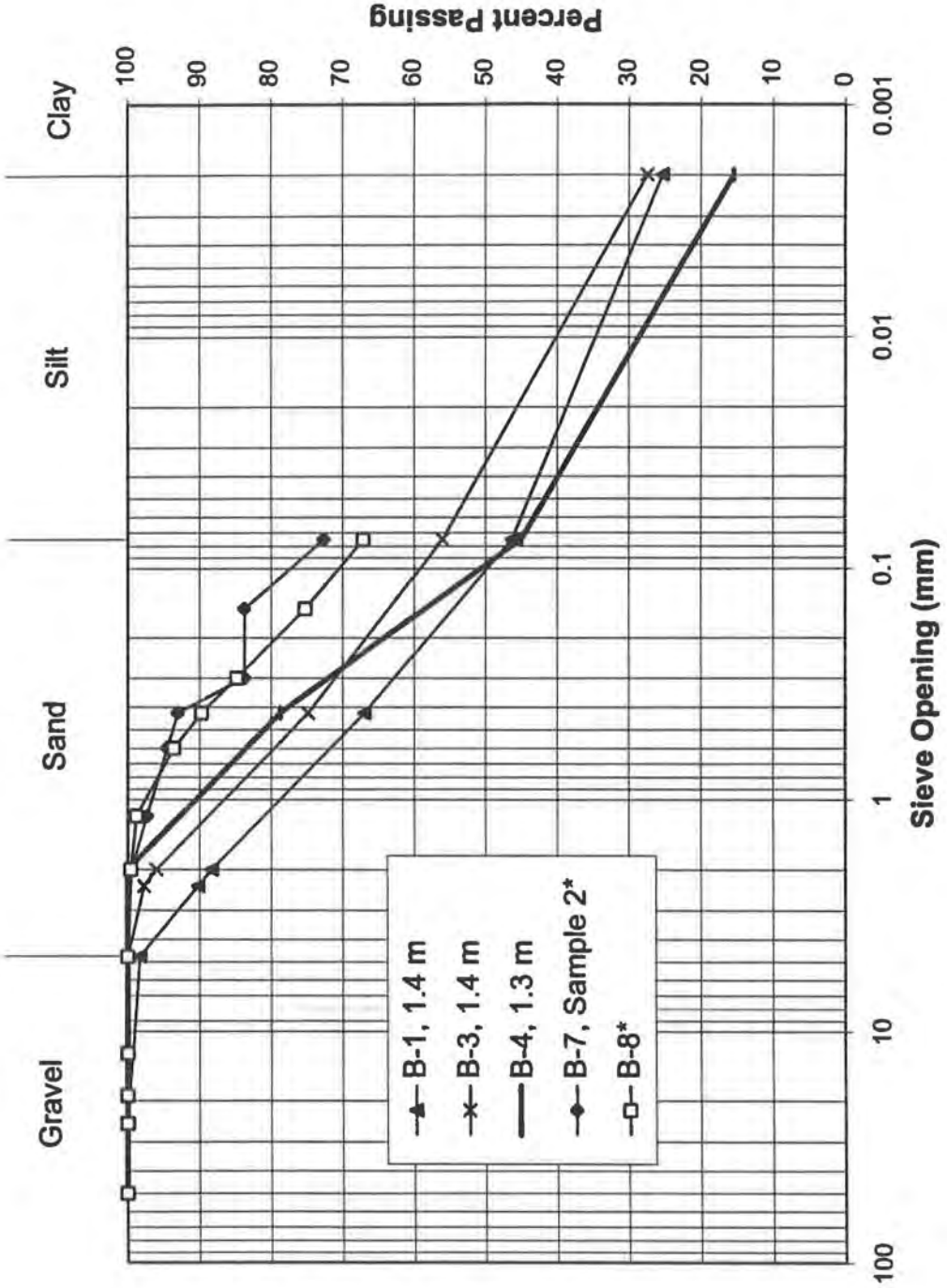

FIG. A.3. - Grain Size Distribution : Depth = 1.0 - 1.4 meters

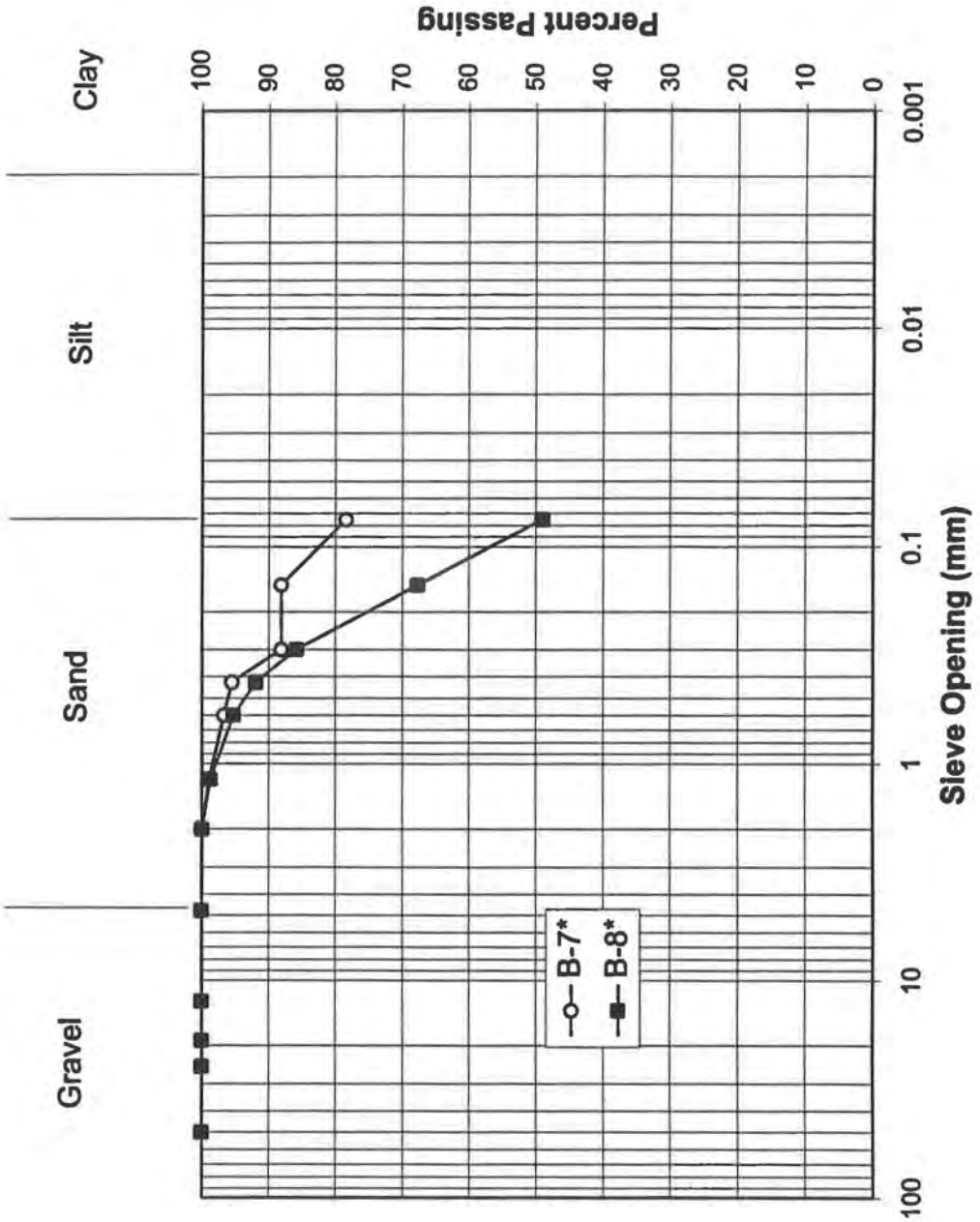

FIG. A.4. - Grain Size Distribution : Depth = 2.0 meters

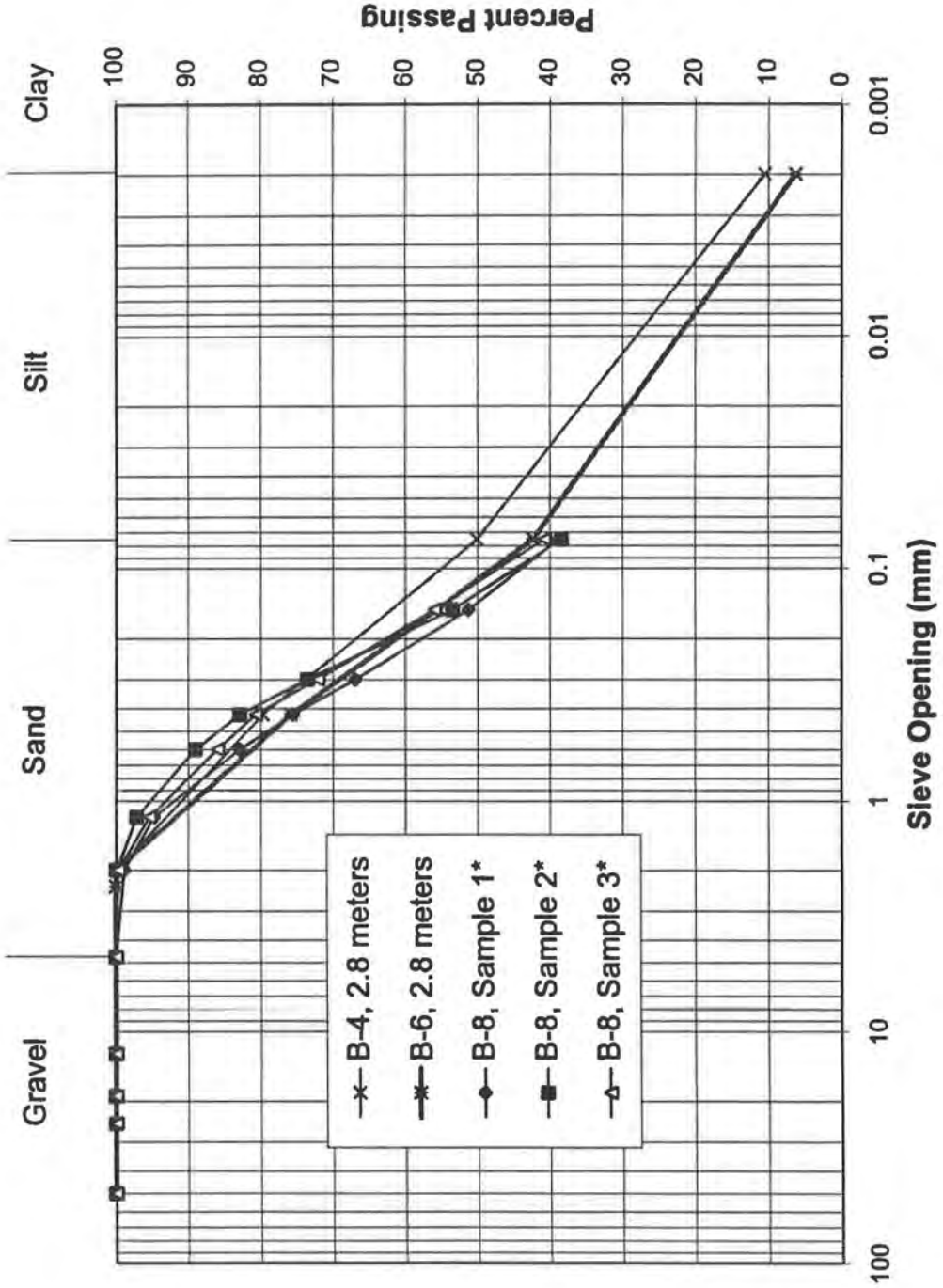

FIG. A.5. - Grain Size Distribution : Depth = 2.8 - 3.0 meters

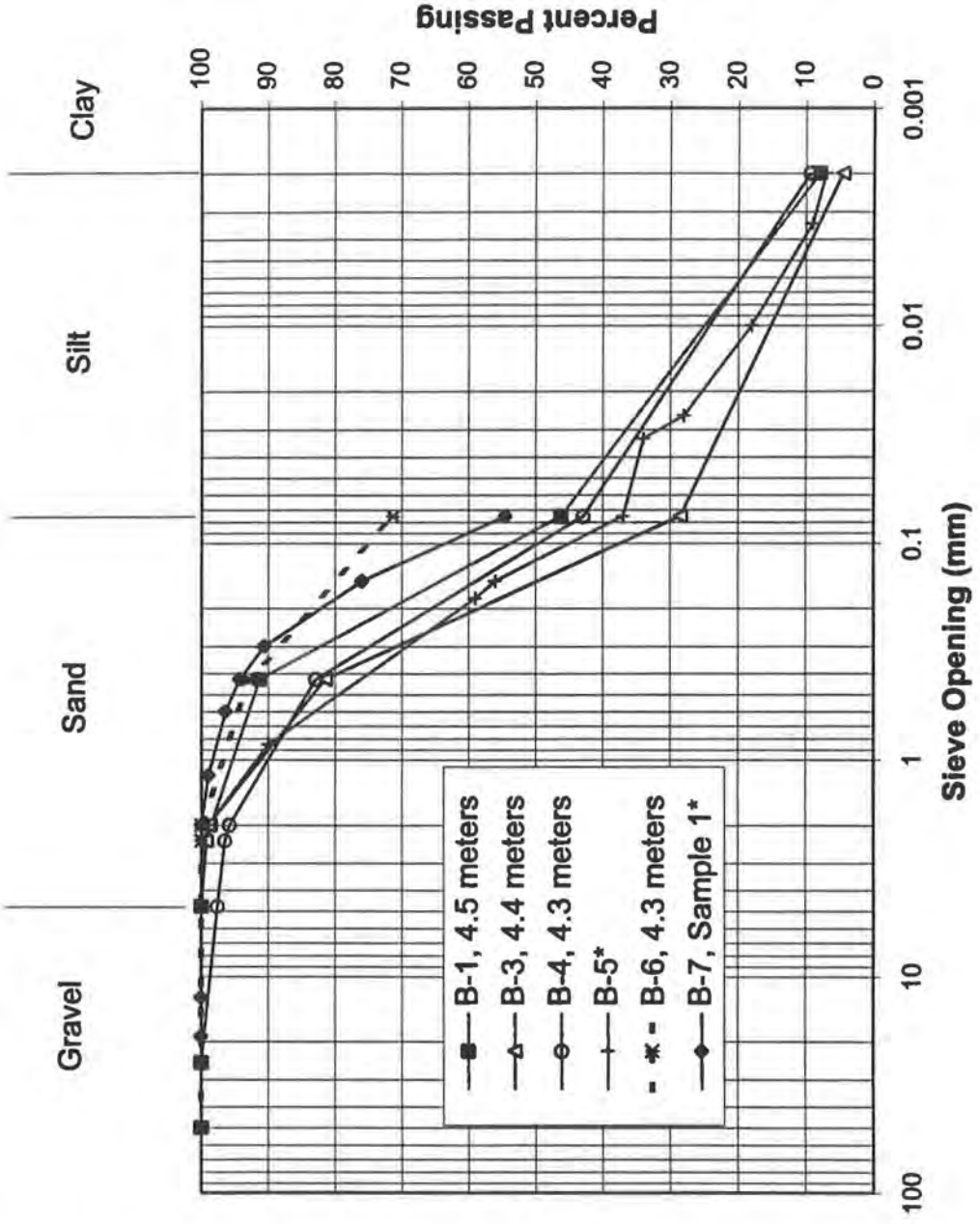

FIG. A.6. - Grain Size Distribution : Depth = 4.0 - 4.5 meters

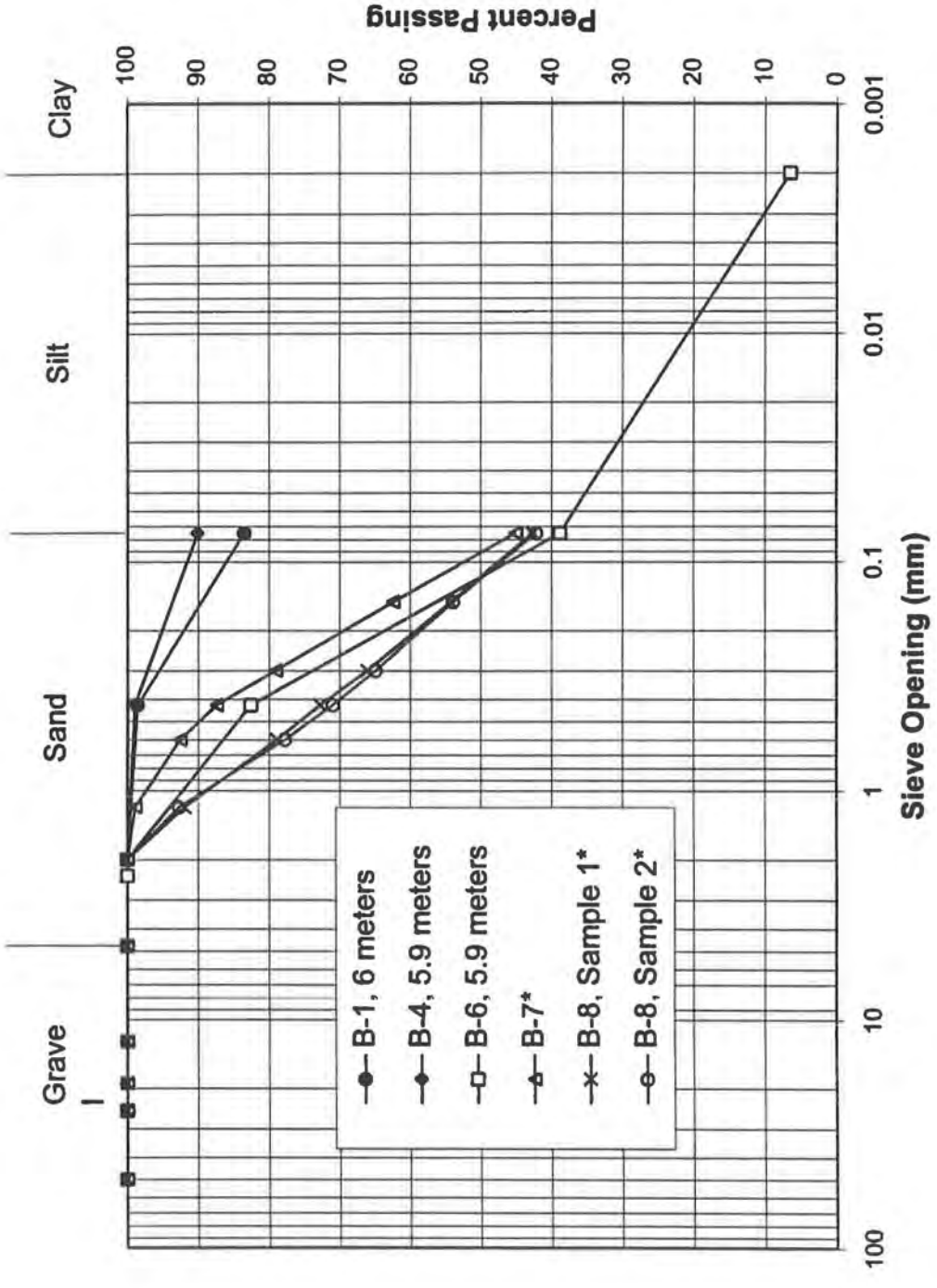

FIG. A.7. - Grain Size Distribution : Depth = 5.9 - 6.0 meters

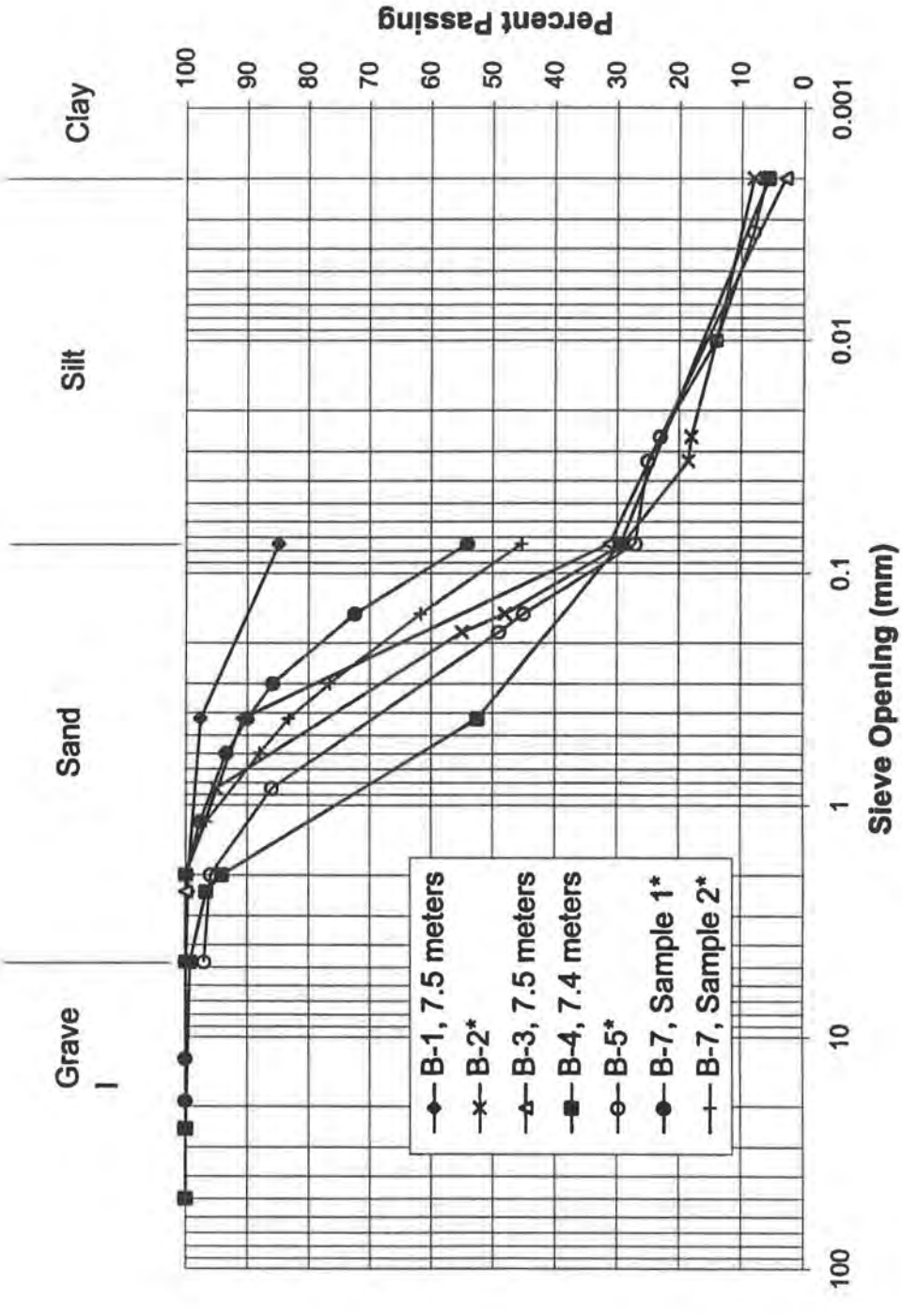

FIG. A.8. - Grain Size Distribution : Depth = 7.4 - 8.0 meters

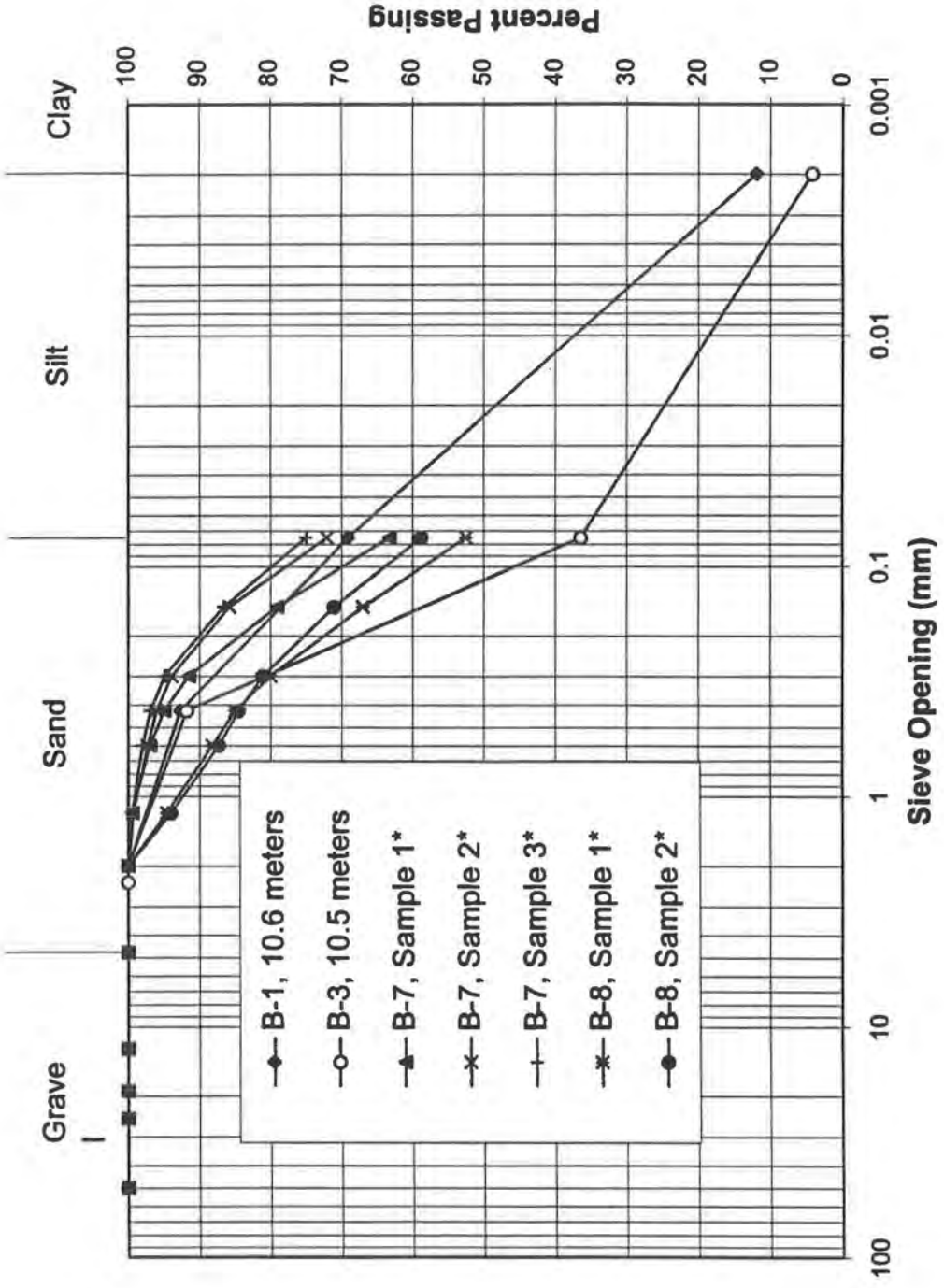

FIG. A.9. - Grain Size Distribution : Depth 10.0 - 10.6 meters

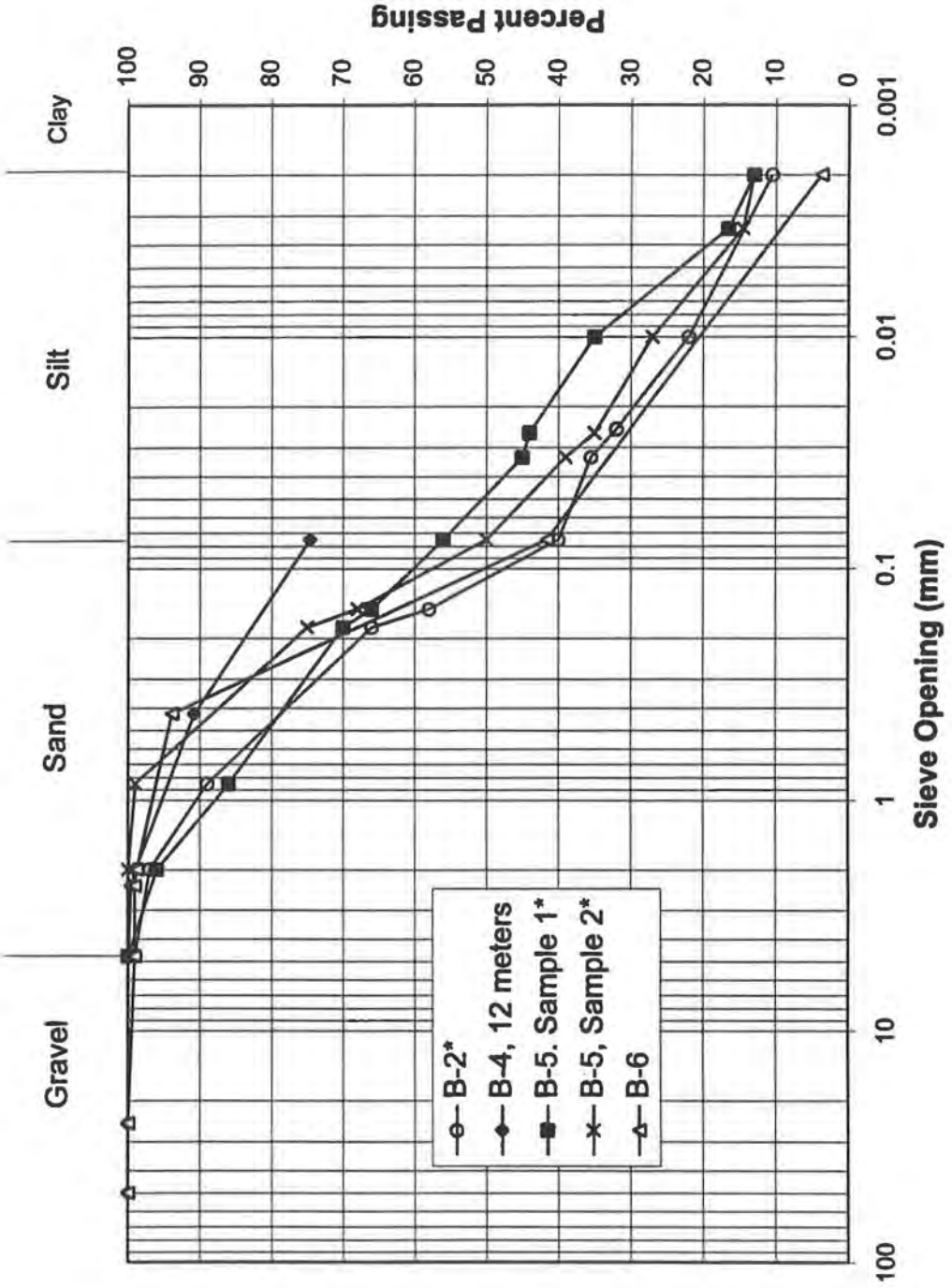

FIG. A.10. - Grain Size Distribution : Depth = 12.0 meters

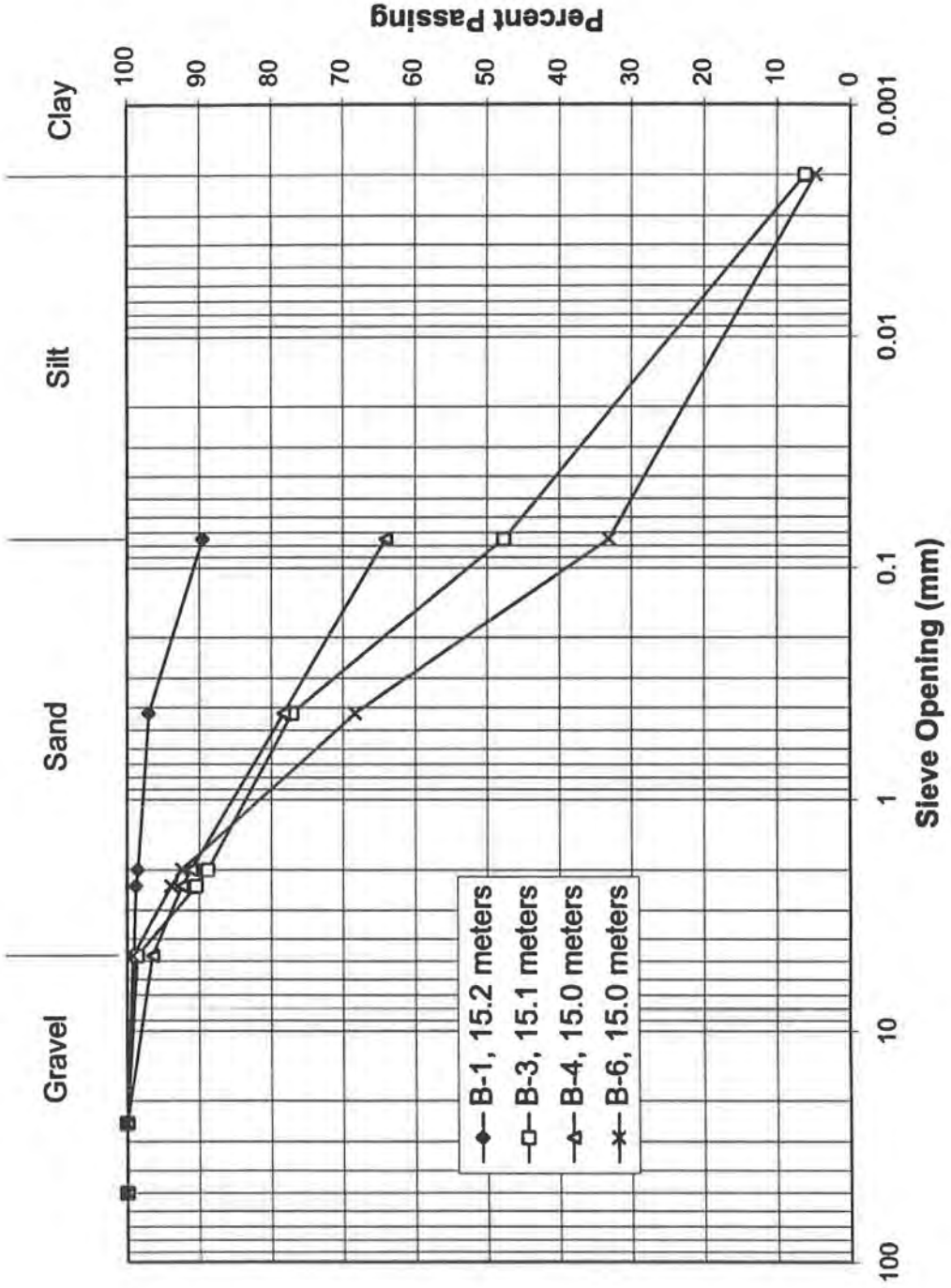

FIG. A.11. - Grain Size Distribution : Depth = 15.0 - 15.2 meters

APPENDIX B

STANDARD PENETRATION TEST RESULTS

General

1. The efficiency of the hammer was not measured. An energy ratio of 90% was assumed for this hammer; Bowles (1996) shows that typical energy ratios for automatic hammers fall within the range of 80% to 100% of the maximum theoretical energy.
2. Since each N-value was conducted at a depth within ± 0.3 meters of each of the overall average test depths, a straight average of N-values and depths was made.
3. The N-values were corrected for rod length, hole diameter, and effective overburden according to Skempton (1986). The correction factors used and corrected blow counts are shown on a following page. N-values were also adjusted for energy ratio according to the specific correlation.
4. Some correlations do not distinguish which energy ratio should be used. An energy ratio of 60% of the theoretical energy delivered by the hammer to the anvil was used for these evaluations.

Equipment

- CME 550 drill rig with 6 in. (15.2 cm) diameter hollow continuous flight augers and an automatic hammer.

Procedure

Conducted in accordance to ASTM D 1586-84.

Data Reduction

Effective Friction Angle

Peck, Hanson, and Thornburn (1974) : Correlation chart used to evaluate effective friction angle. Energy ratio of N-values not stated; N_{60} was used.

Schmertmann (1975) : Results tend to be somewhat conservative and should not be used at depths shallower than 1 to 2 meters. Energy ratio of N-values not stated; N_{60} was used.

Example : Depth = 1.43 meters, $N_{60} = 26.3$, $P_o' = 26.1$ kPa

Therefore,

$$\varnothing' = \text{ATAN}[N/(12.2+20.3\ P_o'/P_{atm})^{0.34}]$$
$$= \text{ATAN}[26.3/(12.2+20.3(26.1/101.25)]^{0.34}$$
$$= \underline{49.0 \text{ degrees}}$$

Shioi and Fukui (1982) : Two correlations from Japanese Railway Standards. Each uses a theoretical energy ratio of 70%.

Equation 1. $\varnothing = (18N_{70})^{0.5} + 15$

This equation is used in road and bridge design. Assumed that $\varnothing$ is effective friction angle.

Example : Depth = 1.43 meters, $N_{70} = 22.6$

Therefore, $\varnothing' = (18*22.6)^{0.5} + 15 = \underline{35.2 \text{ degrees}}$

Equation 2.

$$\varnothing = 0.36\ N_{70} + 27$$

This equation used for building design. Assumed that $\varnothing$ is effective friction angle

Example : Depth = 1.43 meters, $N_{70} = 22.6$

Therefore, $\varnothing' = 0.36(22.6) + 27 =$ <u>35.1 degrees</u>

<u>At-Rest Coefficient of Horizontal Soil Stress</u>

Kulhawy et al. (1989) : Effective Horizontal Pressure = H_o'

$$H_o' = (P_{atm}(q_c/P_{atm}^{1.25})/(35e^{Dr(\%)/20})$$

Empirical approach based on calibration chamber tests with electric cones in normally consolidated and overconsolidated sands. Indication that H_o' has more effect on q_c than vertical stress (P_o').

The relative density must be known in order to evaluate H_o'. Jamiolkowsky et al. (1985) was used to evaluate the relative density. This relationship is based on chamber and field tests on five different sand sites and is as follows :

$$D_r(\%) = 68[\text{Log}(q_c/((P_{atm})P_o')^{0.5})-1]$$

In order to evaluate SPT prediction by this method, the N values must be converted into equivalent q_c values. Using relationship presented by Robertson (1983), which is based on comparative study in different soils where the third parameter known for all the soils was the sieve opening of 50% passing, the average d_{50} for the test site was generally at or near 0.1 mm. This corresponds to a q_c/N_{55} ratio of 350 to get q_c in units of [kPa]. Upon conversion of N values to q_c values, the procedure used for the CPT, as mentioned above, is followed.

Example : Depth = 1.43 meters, $N_{55} = 28.7$, $P_o' = 26.1$ kPa

Equivalent $q_c = N_{55}(q_c/N_{55}) = 28.7*350 = 10{,}037$ kPa

$D_r(\%) = 68[\text{Log}(10{,}037/(101.25*26.1)^{0.5})-1] = 87.7\%$

$H_o' = (101.25(10{,}037/101.25)^{1.25})/(35e^{87.7/20}) = 11.3$ kPa

Therefore, $K_o' = 11.3/26.1 = \underline{0.43}$

Kulhawy et al. (1989) : $K_o' = 0.073(N)(P_{atm})/(P_o')$

Based on correlations with SPT and K_o' predictions for 13 intact clays and 5 fissured clays by laboratory, DMT, PMT and SBPMT tests . The number of observations was 57, and the correlation has a regression coefficient of 0.771. The N value's energy ratio is not specified; therefore, N_{60} values were used.

Example : Depth = 1.43 meters, $N_{60} = 26.3$, Po' = 26.1 kPa

Therefore, $K_o' = 0.073*26.3*101.25/26.1 = \underline{7.44}$

Undrained Shear Strength

Using the relationship of a constant mulitplied by N value (k*N), undrained shear strength (S_u) over depth can be estimated when compared to laboratory test results. Through trial and error, a k value of 6 along with N_{70} values approximately agrees with the almost constant S_u over depth as predicted by laboratory tests.

Therefore, a site specific correlation would be as follows :

$$S_u = kN_{70} = 6\ N_{70}$$

Young's Modulus

Manual for Estimating Soil Properties for Foundation Design (1990) :

$$E/(P_{atm}) = 5\ N_{60}$$

Used for initial estimate of modulus for sands with fines.

Example : Depth = 1.43 meters, N_{60} = 26.3

Therefore, E = 101.25*5*26.3 = 13,308 kPa

Bowles (1996) : $E = 500(N_{55}+15)$

Used for estimate of normally consolidated sands.

Example : Depth = 1.43 meters, N_{55} = 28.7

Therefore, E = 500(28.7 + 15) = 21,839 kPa

Bowles (1996) : $E = 300(N_{55}+6)$

Used for estimate of silts, sandy silts, or clayey silts.

Example : Depth = 1.43 meters, N_{55} = 28.7

Therefore, E = 300(28.7 + 6) = 10,403 kPa

Pressuremeter Modulus

Ohaya et al. (1982) : $E_{PMT} = 9.08(P_{atm})(N^{0.66})$

Based on 4 sand sites in Japan. A regression coefficient of 0.482 with the number of observances at 370. Standard deviation at $61.3*(P_{atm})$ means very large scatter. N_{60} used since energy ratio not specifically stated.

Example : Depth = 1.43 meters, N_{60} = 26.3

Therefore, $E_{PMT} = 9.08*101.25*26.3^{0.66}$ = 7,953 kPa

Barksdale et al. (1986) : E_{PMT} = EXP(3.509 + 0.712*LN(N))

Based on 208 pressuremeter moduli in Piedmont silty sands and sandy silts which have approximately 40% - 60% finer than the #200. Uncorrected SPT resistance values were used and assumed to be at 60% of theoretical energy. Coefficient of variation equals 0.807; modulus given in units of [kips/square feet].

Example : Depth = 1.43 meters, $N_{60} = 26.3$

Therefore, E_{PMT} = EXP(3.509 + 0.712*LN(26.3))*(48kPa/ksf)= 16,445 kPa

Dilatometer Modulus

Mayne and Frost (1989) : $E_{DMT} = 0.22(P_{atm})N^{0.82}$

Based on eight back-calculated building foundation field performance data near Washington, D.C. in sandy silts of Piedmont. . N_{60} used since energy ratio not specifically stated.

Example : Depth = 1.43 meters, $N_{60} = 26.3$

Therefore, $E_{DMT} = 0.22(101.25)(26.3)^{0.82}$

$= 32,509$ kPa

Shear Wave Velocity

Schmertmann (1978) : $V_s \approx 15\ N_{60}$ where V_s in [m/s] for a test site made up of sand and many blow counts made. It is suggested that lower constants can account for finer sand, lower density, etc.

Through trial and error, a constant multiplier of 12 gave the most accurate prediction of shear wave velocity when compared to the crosshole trend interpretation plot.

Example : Depth = 1.43 meters, N_{60} = 26.3

Therefore, $V_s = 12(26.3) = \underline{315 \text{ m/s}}$.

Imai and Tonouchi (1982) : $V_s = 97.0\ N_{60}^{0.314}$ where V_s in [m/s].

Energy ratio of N value not stated; N_{60} was chosen. Regression coefficient for shear wave velocity from the 1,654 shear wave velocity measurements is 0.868. This correlation involves different soil types (including alluvial, diluvial, and tertiary) from over 250 deposits in Japan where SPT and crosshole/downhole seismic measurements were made.

Example : Depth = 1.43 meters, N_{60} = 26.3

$V_s = 97.0(26.3)^{0.314} = \underline{271 \text{ m/s}}$

Small Strain Shear Modulus

Seed et al. (1986) : $G_{max} \approx 35{,}000 N_{60}^{0.34} P_o'^{0.4}$ where vertical effective overburden (P_o') in [psf].

Correlation for cohesionless soils; based on observations of other investigators. Six loose to very dense normally consolidated sands, which had SPT and in situ shear wave velocity measurements made, show good agreement; however, one clayey sand and one partly cemented sand do not show agreement.

Example : Depth = 1.43 meters, P_o' = 165 psf, N_{60} = 26.3

Therefore, $G_{max} \approx 35{,}000(26.3)^{0.34}(165)^{0.4}(0.04788\ kPa/psf)$

$= \underline{39{,}235\ kPa}$

Imai & Tonouchi (1982) : $G = 144N^{0.680}$ where G is in [kPa].

Energy ratio for N value was not stated; N_{60} was chosen. Regression coefficient for shear modulus from the 1,654 shear wave velocity measurements is 0.867. This correlation involves different soil types (including alluvial, diluvial, and tertiary) from over 250 deposits in Japan where SPT and crosshole/downhole seismic measurements were made.

Example : Depth = 1.43 meters, $N_{60} = 26.3$

Therefore, $G = 144(26.3)^{0.680} = \underline{130{,}454\ kPa}$

Schmertmann (1978) : Using the best fit shear wave velocity measurement, the values of shear wave velocity were plugged into the equation - G = mass density * V_s^2

Example : Depth = 1.43 meters,

V_s = 315 m/s (with N multiplier of 12 from V_s analysis)

Therefore, $G = (18.25\ kN/m^2/9.81\ m/s^2)*(315\ m/s)^2$

$= \underline{185{,}083\ kPa}$

Table B.1. - Correction of N-Values

Average Depth (m)	Average N_{90} Values	Rod Length Correction	Hole Dia. Correction	P_o' (kPa)	Overburden Correction	Energy Ratio from N_{90} to N_{60}	N_{60}	Energy Ratio from N_{90} to N_{70}	N_{70}
1.43	14	0.75	1.05	26.1	1.59	1.5	26.3	1.29	22.6
2.84	8.25	0.75	1.05	51.9	1.32	1.5	12.9	1.29	11.1
4.48	8.5	0.85	1.05	67.2	1.20	1.5	13.7	1.29	11.8
6.00	9.75	0.95	1.05	80.1	1.12	1.5	16.3	1.29	14.0
7.53	13	0.95	1.05	93.0	1.04	1.5	20.3	1.29	17.4
9.05	11.5	0.95	1.05	105.8	0.98	1.5	16.8	1.29	14.5
10.58	12	1	1.05	118.7	0.92	1.5	17.4	1.29	15.0
12.10	13.75	1	1.05	131.6	0.87	1.5	18.8	1.29	16.2
13.62	12.75	1	1.05	144.4	0.82	1.5	16.6	1.29	14.2
15.15	14	1	1.05	157.3	0.78	1.5	17.3	1.29	14.9

Sample Calculation : Conversion from N_{90} values to N_{60} values for 1.43 meters depth.

$N_{60} = (N_{90})(\text{Correction Factors}) = (14)(0.75)(1.05)(1.59)(1.5) = 26.3$

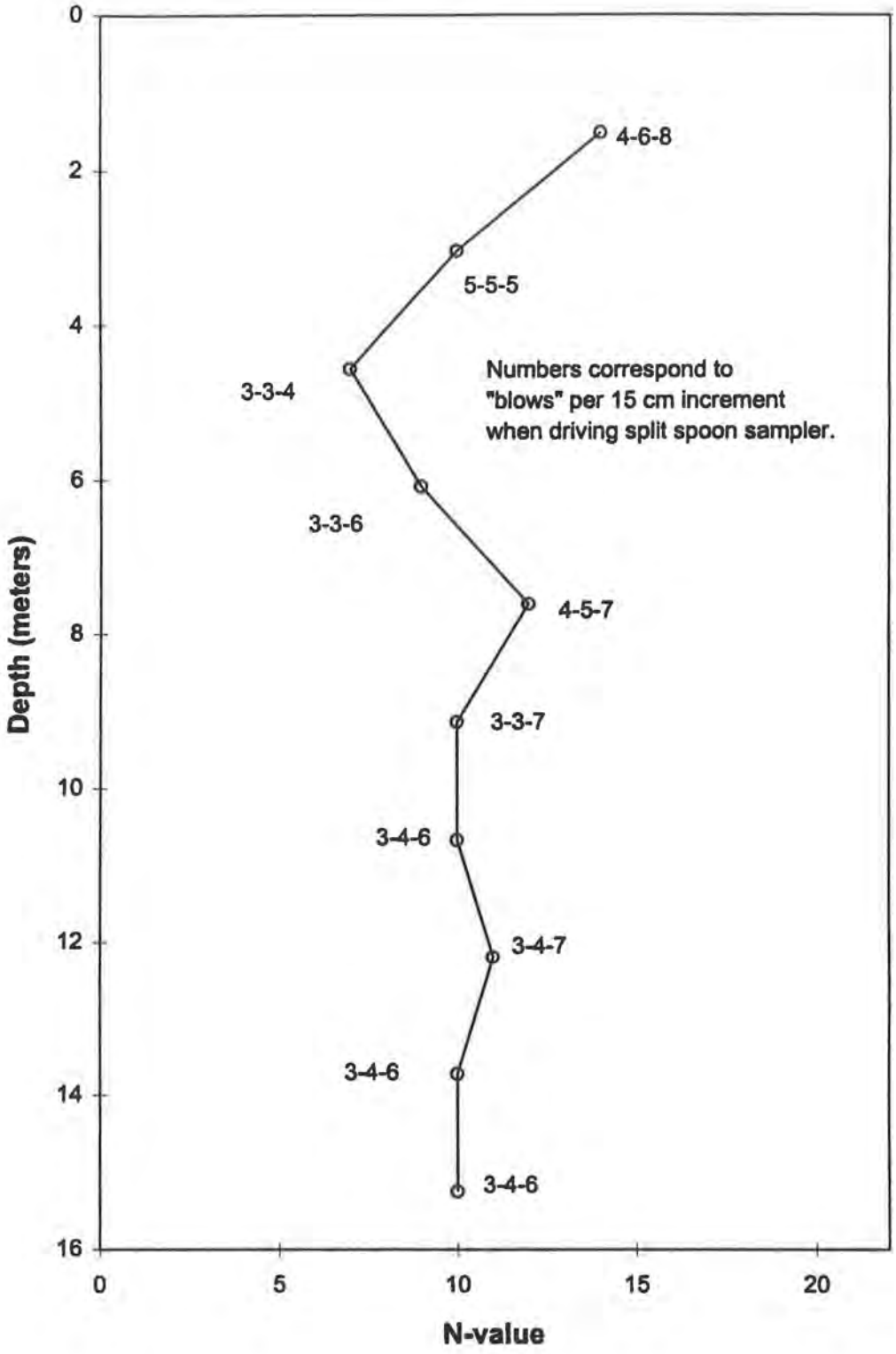

FIG. B.1. - Observed N-Values at B-1

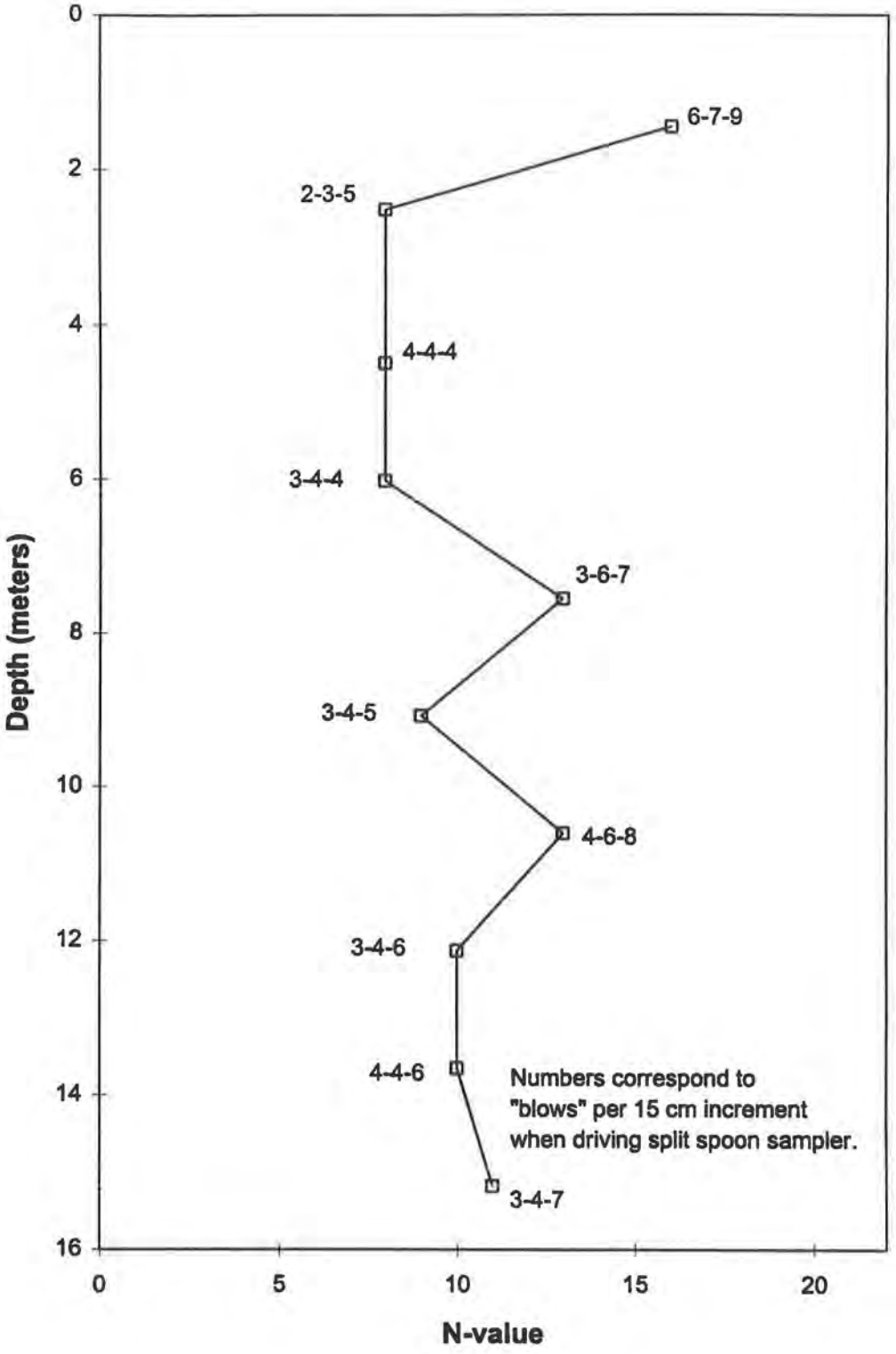

FIG. B.2. - Observed N-Values at B-3

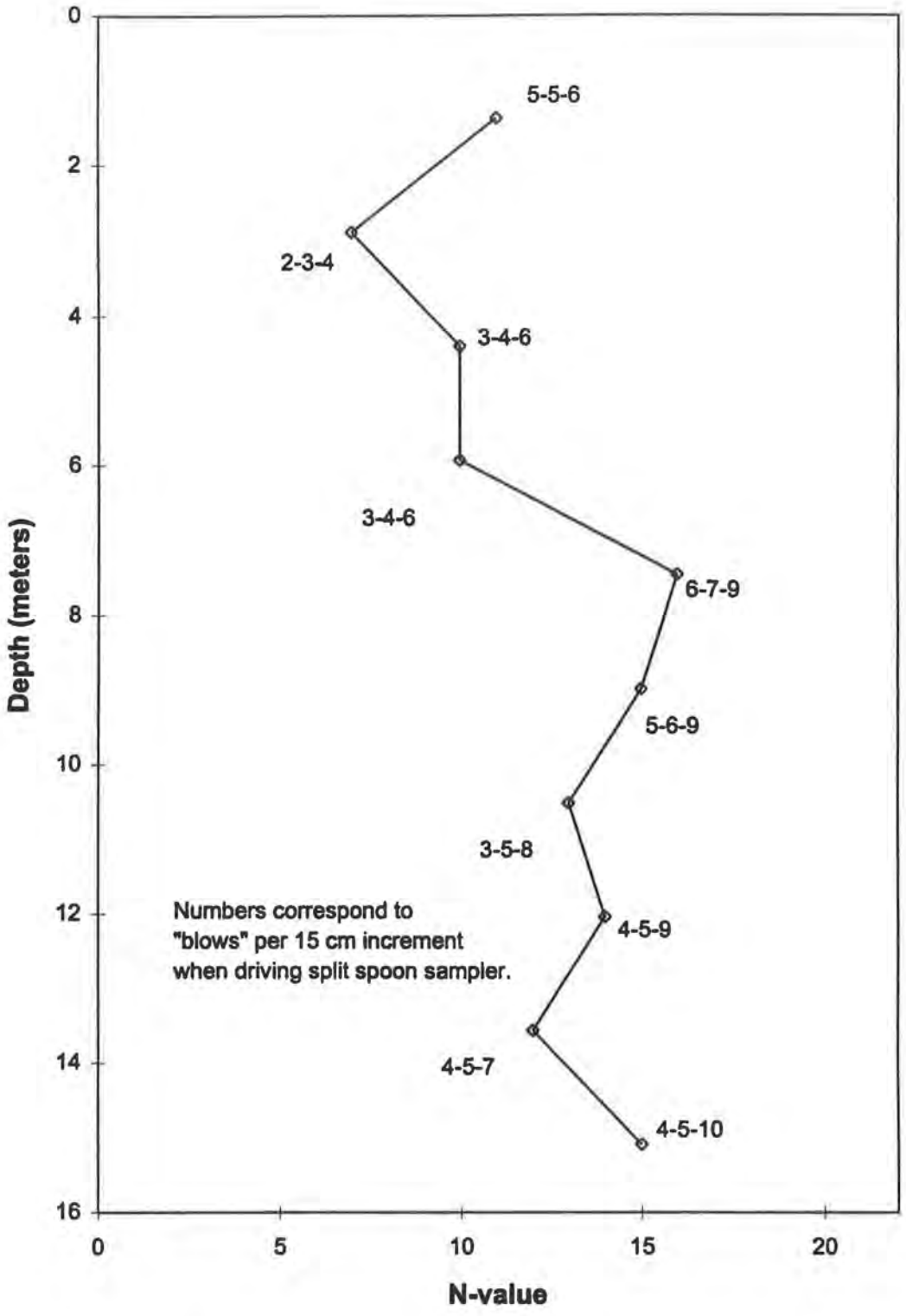

FIG. B.3. - Observed N-Values at B-4

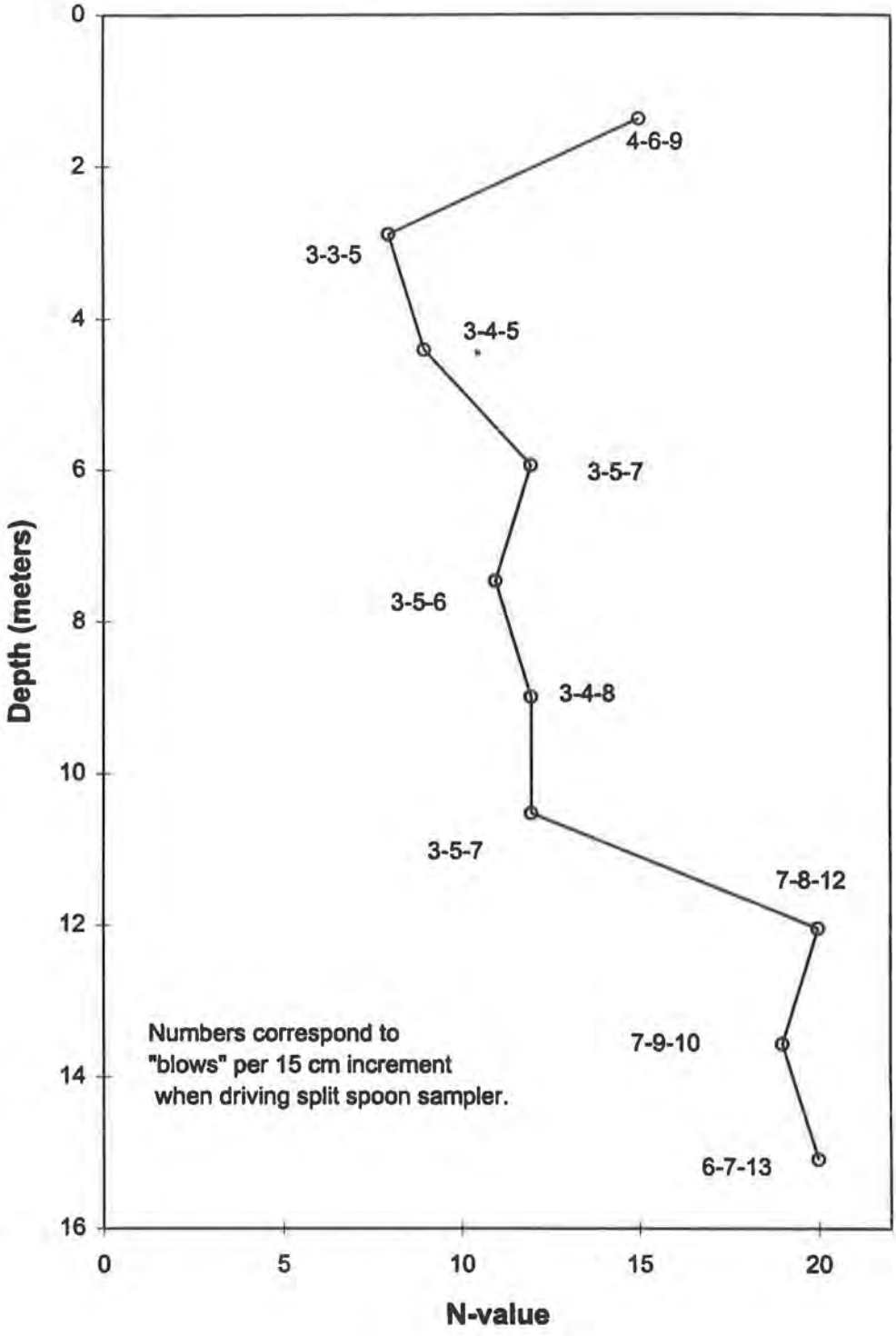

FIG. B.4. - Observed N-Values at B-6

APPENDIX C

SEISMIC-, PIEZO-, OR CONVENTIONAL CONE PENETRATION TEST RESULTS

General

1. Many cone soundings were made at the site, but only the six soundings (C-41, C-42, C-25, C-43, C-27, and C-21) which were in close proximity to the soil borings (B-1, B-2, etc.) were considered when using correlations in order to limit the effect of soil variability.

2. Cone soundings C-41 and C-42 included piezometric and seismic measurements. Also, sleeve friction (f_s) and tip resistance (q_c) were measured at a different interval from the other four; C-41 and C-42 had measurements made at approximately every 0.03 meters while the others had measurements at 0.05 meters intervals. Therefore, in order to obtain average q_c and f_s values over depth, the measured values were averaged over a range which would allow a straight average of the six soundings. In other words, C-41 and C-42 depth intervals were multiplied by 0.05 and the rest were multiplied by 0.03. Then, the average q_c and f_s of all the soundings over approximately each 0.15 meter segment were averaged to come up with a single q_c and f_s profile over depth for the site.

3. Plots of individual sounding records for q_c, f_s, friction ratio (R_f), pore pressure (u), and seismic results (where applicable) are shown on a following page.

4. The SPCPTs at C-41 and C-42 were performed using a different Hogentogler piezocone of the same features as the cone used at all other CPT locations except that it was fitted with a geophone..

Equipment

- Hogentogler piezocone (PCPT) with the following features :
  - 3.57 cm diameter
  - Tip Area = 10 cm^2
  - Sleeve Friction Area = 150 cm^2
  - pore pressure element located behind the tip (Type 2 position)
  - maximum capacity = 10 tons
  - polypropylene pore pressure element of 5 mm thickness
- Seismic Piezocone Penetration Test (SPCPT) Equipment included :
  - calibrated sledge hammer
  - geophone connected to cone
  - oscilloscope

Procedure

1. CPT conducted in accordance to ASTM D 3441 (1986).

2. Seismic testing involved momentarily halting cone penetration and striking the reaction bar under the middle of the cone truck with the calbrated hammer to create shear waves when the cone was at a depth of interest.

3. First arrival times of shear waves were monitored; with the distance between the source and receiver known, the shear wave velocity between two subsequent test depths could be could be assigned to that soil zone.

4. A 50% water/50% glycerene solution was used to saturate the pore pressure element at C-41 and C-42.

Data Reduction (Conventional CPT)

Young's Modulus

All methods considered relate Young's Modulus to the local end bearing resistance measurement (q_c).

The following examples of the methods considered will be for the 0.15 meter depth which has an average qc value of 1,513 kPa.

- Normally Consolidated Sands, Bowles (1996) $E = 3^* q_c = \underline{4,538 \text{ kPa}}$
  (A constant range of 2.5 - 3.0 was recommended.)

- Silts, Sandy Silts, or Clayey Silts, Bowles (1996) $E = 1.5^* q_c = \underline{2,269 \text{ kPa}}$

- Silts, Sandy Silts, or Clayey Silts, Senneset et al. (1988)

E' = Constrained Modulus = $2.5^* q_c$ for $q_c < 2,500$ kPa
$= 4^* q_c + 5,000$ for $2,500 \text{ kPa} < q_c < 5,000$ kPa

Since $q_c < 2,500$ kPa, use $E' = 2.5^* q_c = 3,782$ kPa.

E = Young's Modulus = $E'(1+\nu)(1-2\nu)/(1-\nu)$
where ν : Poisson's ratio of 0.3 was assumed.
$= 3,782^*(1+0.3)^*(1-2^*0.3)/(1-0.3) = \underline{2,552 \text{ kPa}}$

Coefficient of At Rest Earth Pressures

Kulhawy et al. (1989) : Effective Horizontal Pressure = H_o'

$$H_o' = (P_a(q_c/P_a)^{1.25})/(35e^{Dr(\%)/20})$$

Empirical approach based on calibration chamber tests with electric cones in normally consolidated and overconsolidated sands. Indication that H_o' has more effect on qc than vertical stress (P_o').

The relative density must be known in order to evaluate Ho'. Jamiolkowsky et al. (1985) was used to evaluate the relative density. This relationship is based on chamber and field tests on five different sand sites and is as follows :

$$D_r(\%) = 68[\text{Log}(q_c/(P_a P_o')^{0.5})-1]$$

Example : Depth = 0.15 meters, q_c = 1,513 kPa, P_o' = 2.74 kPa

$$D_r(\%) = 68[\text{Log}(1{,}513/(101.25*2.74)^{0.5})-1] = 65.2\%$$

$$Ho' = (101.25(1{,}513/101.25)^{1.25})/(35e^{65.2/20}) = 3.3 \text{ kPa}$$

Therefore, $K_o' = 3.3/2.74 = \underline{1.19}$

Effective Friction Angle

Robertson and Campanella (1983) : $\varnothing' = \text{ATAN}[0.10 + 0.38\text{Log}(q_c/P_o')]$

Developed from cone testing in NC, uncemented quartz sands with triaxial evaluations of effective friction angle.

Example : Depth = 0.15 meters, q_c = 1,513 kPa, P_o' = 2.74 kPa

Therefore, : $\varnothing' = \text{ATAN}[0.10 + 0.38\text{Log}(1{,}513/2.74)]$
$= \underline{48.8 \text{ degrees}}$

Kulhawy and Mayne (1990) : $\varnothing' = 17.6 + 11.0\text{Log}[(q_c/P_a)/(P_o'/P_a)^{0.5}]$

Determined from testing in OC and NC sands; n=633, R^2= 0.640, St. Dev. = 2.8°

Example : Depth = 0.15 meters, q_c = 1,513 kPa, P_o' = 2.74 kPa

$$\varnothing' = 17.6 + 11.0\text{Log}[(1{,}513/101.25)/(2.74/101.25)^{0.5}]$$
$$= \underline{39.1 \text{ degrees}}$$

Masood and Mitchell (1993) : $\varnothing' = 30.8[\text{Log}(f_s/P_o') + 1.26]$

Applicable to clays and sands.

Example : Depth = 0.15 meters, $P_o' = 2.74$ kPa, $f_s = 63.7$ kPa

Therefore, $\varnothing' = 30.8[\text{Log}(63.7/2.74) + 1.26]$
$= \underline{80.9 \text{ degrees}}$

Undrained Shear Strength

The theoretical relationship of undrained shear strength (S_u) with cone tip resistance (q_c) is typically shown in many references as the following equation -

$$S_u = (q_c - P_o)/N_k$$

where P_o is the total vertical overburden pressure and
N_k is the cone bearing factor.

From examining the results of UU tests with confining pressures near the effective vertical overburden pressure and CIUC tests with consolidation pressures at or near P_o', an N_k value = 36 was found to most closely correlate with the almost constant undrained strength value over depth of 90 kPa.

Shear Wave Velocity

Hegazy and Mayne (1996)

Statistical correlations from 61 sites worldwide between V_s and CPT data. Velocities were determined by either seismic cone, crosshole, downhole or spectral analysis of surface wave tests. Simple and multiple regressions were conducted to determine the most important parameter affecting V_s.

For 36 clay soil sites, q_c, f_s, void ratio, and overburden pressure were collected. Void ratio and q_c were the most significant, but an alternate correlation discounting void ratio had a regression coefficient (r^2) almost as high.

For 24 sand soil sites, effective overburden (P_o'), q_c, and f_s were considered; q_c and P_o' were most pertinent.

For a correlation considering all 61 sites, q_c, f_s, and P_o' were considered; q_c was most important. P_o' and fs were equally less important than qc.

Soil Type	Equation	n	r^2
Clays	$V_s = 3.18\ q_c^{0.549}\ f_s^{0.025}$	229	0.778
Sands #1	$V_s = 13.18\ q_c^{0.192}\ P_o'^{0.179}$	133	0.684
Sands #2	$V_s = 12.02\ q_c^{0.319}\ f_s^{-0.0466}$	92	0.574
All Soils	$V_s = (10.1 \text{Log}\ q_c - 11.4)^{1.67}(f_s / q_c * 100)^{0.3}$	323	0.695

Note : V_s units of [m/s]; q_c, f_s, and P_o' units of [kPa].

Examples : All examples use q_c = 1,513 kPa, fs = 63.7 kPa, and P_o' = 2.74 kPa for the 0.15 meter depth.

- Clay Soils : V_s = 196.4 m/s
- Sand Soils #1 : V_s = 64.4 m/s
- Sand Soils #2 : V_s = 102.4 m/s
- All Soils : V_s = 243.0 m/s

Small Strain Shear Modulus

All examples use q_c = 1,513 kPa, f_s = 63.7 kPa, and P_o' = 2.74 kPa for the 0.15 meter depth.

Rix and Stokoe (1991) : $G_{max} = 1{,}634(q_c)^{0.250}(P_o')^{0.375}$ where q_c and Po' in kPa.

Determined from two Italian sites, three U.S. sites, and one calibration chamber test on quartz sands. Assumed that q_c takes into account void ratio, overconsolidation ratio, and earth pressure coefficient.

Example : G = 14,866 kPa

Mayne and Rix (1993) : $G_{max} = 2.87\ q_c^{1.335}$ where q_c in kPa.

Determined from eight countries around the world from clay sites where Vs was measured by crosshole, downhole, seismic cone, or spectral analysis.
$n = 481$, $r^2 = 0.713$

Example : G = 48,865 kPa

Hegazy and Mayne (1996) : Shear modulus found by using the four shear velocity predictions by the relationship of G=density*Vs^2.

Examples :

- Clay - G = 71,768 kPa
- Sands #1 - G = 7,708 kPa
- Sands #2 - G = 19,492 kPa
- All Soils - G = 109,797 kPa

Data Reduction (Seismic CPT)

Shear Wave Velocity

First arrival times for each test depth were measured. The distance between the receiver and source was also determined. Therefore, the difference between two arrival times gave a pseudo-time interval for that range of soil between test depths.

Small Strain Shear Modulus

Shear Modulus = $G = \rho V_s^2$

A constant soil density over depth of 1.86 kg/m^3 was used in calculations.

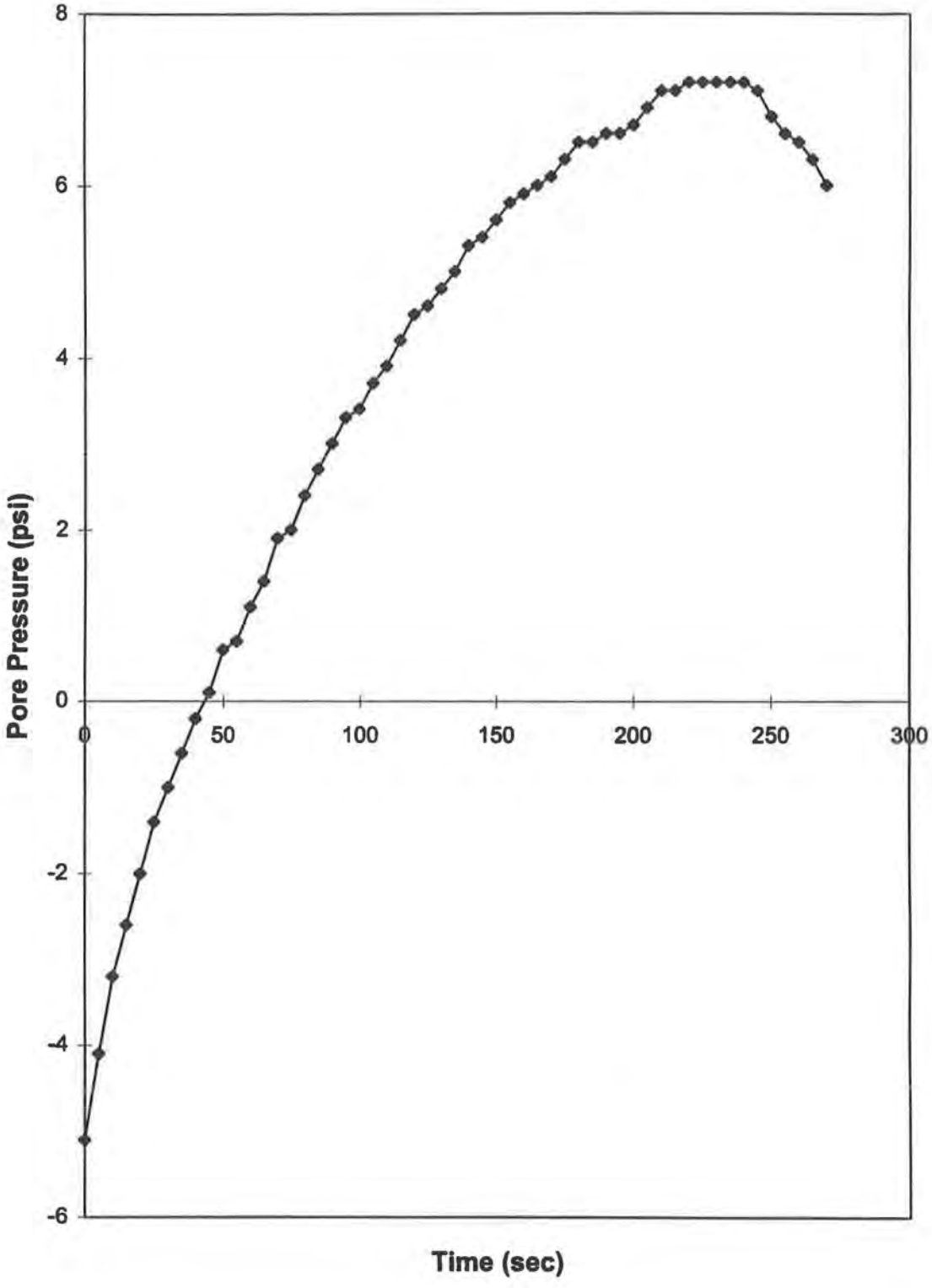

FIG. C.1. - Pore Pressure Dissipation Results : C-28

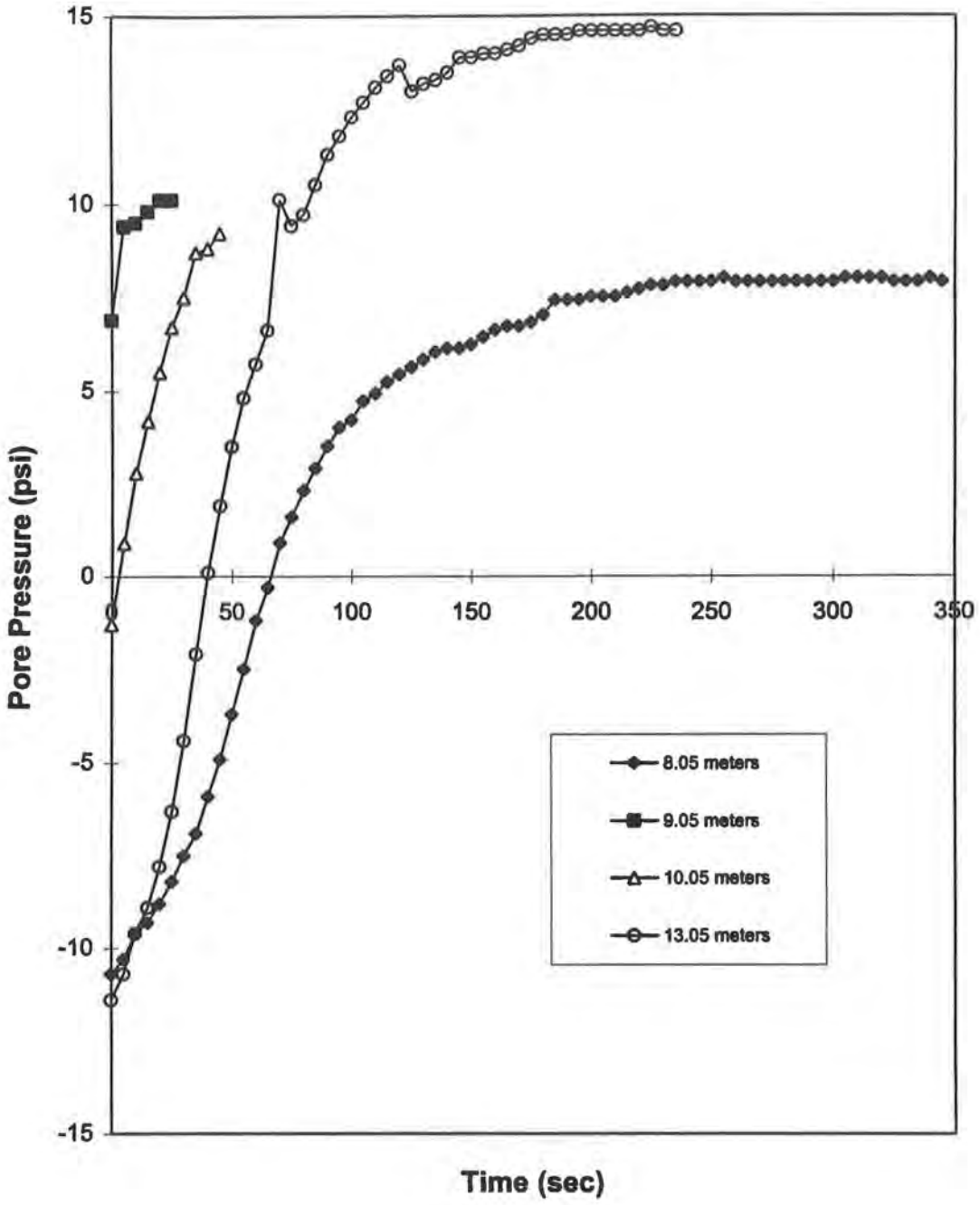

FIG. C.2. - Pore Pressure Dissipation Results : C-43

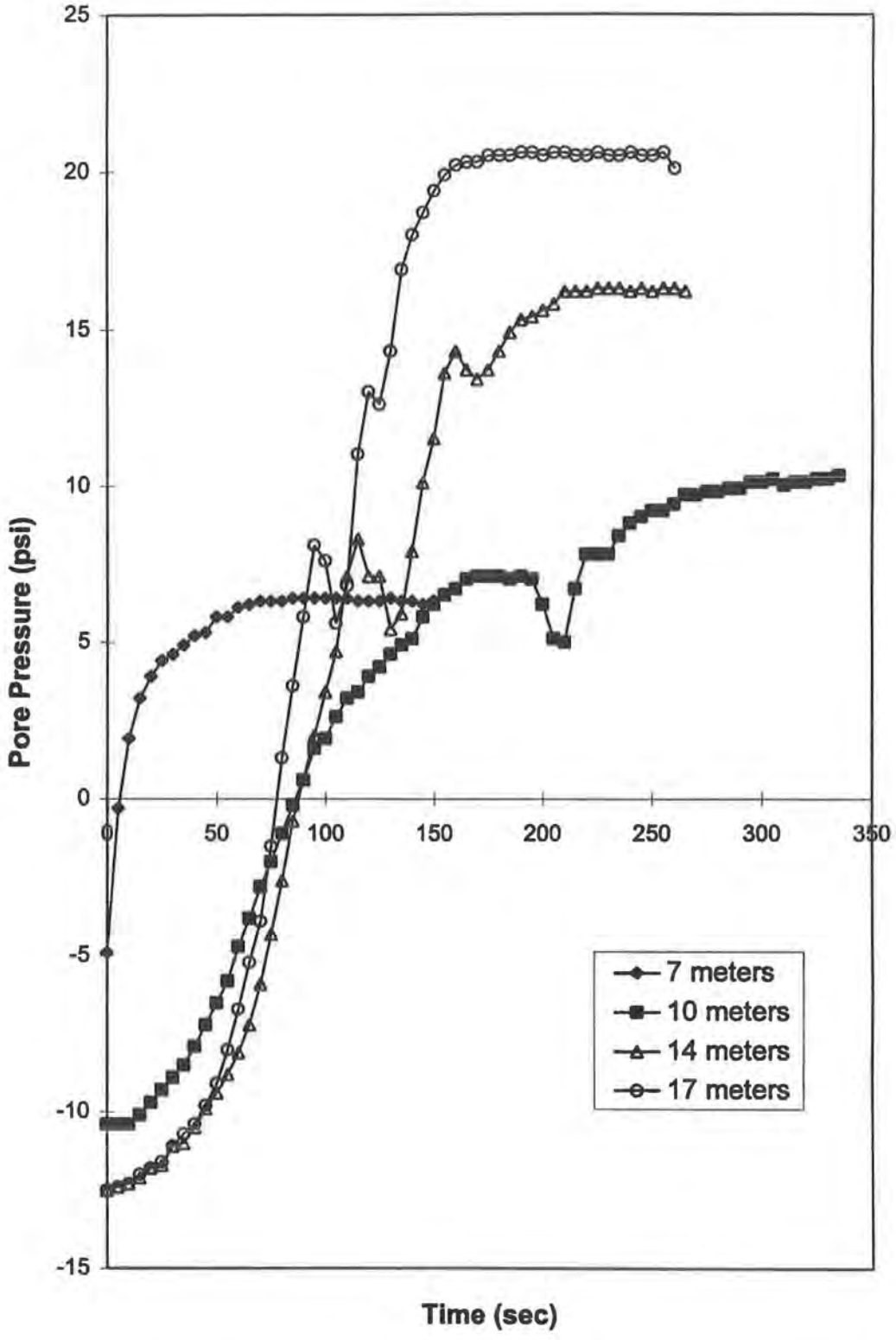

FIG. C.3. - Pore Pressure Dissipation Results : C-44

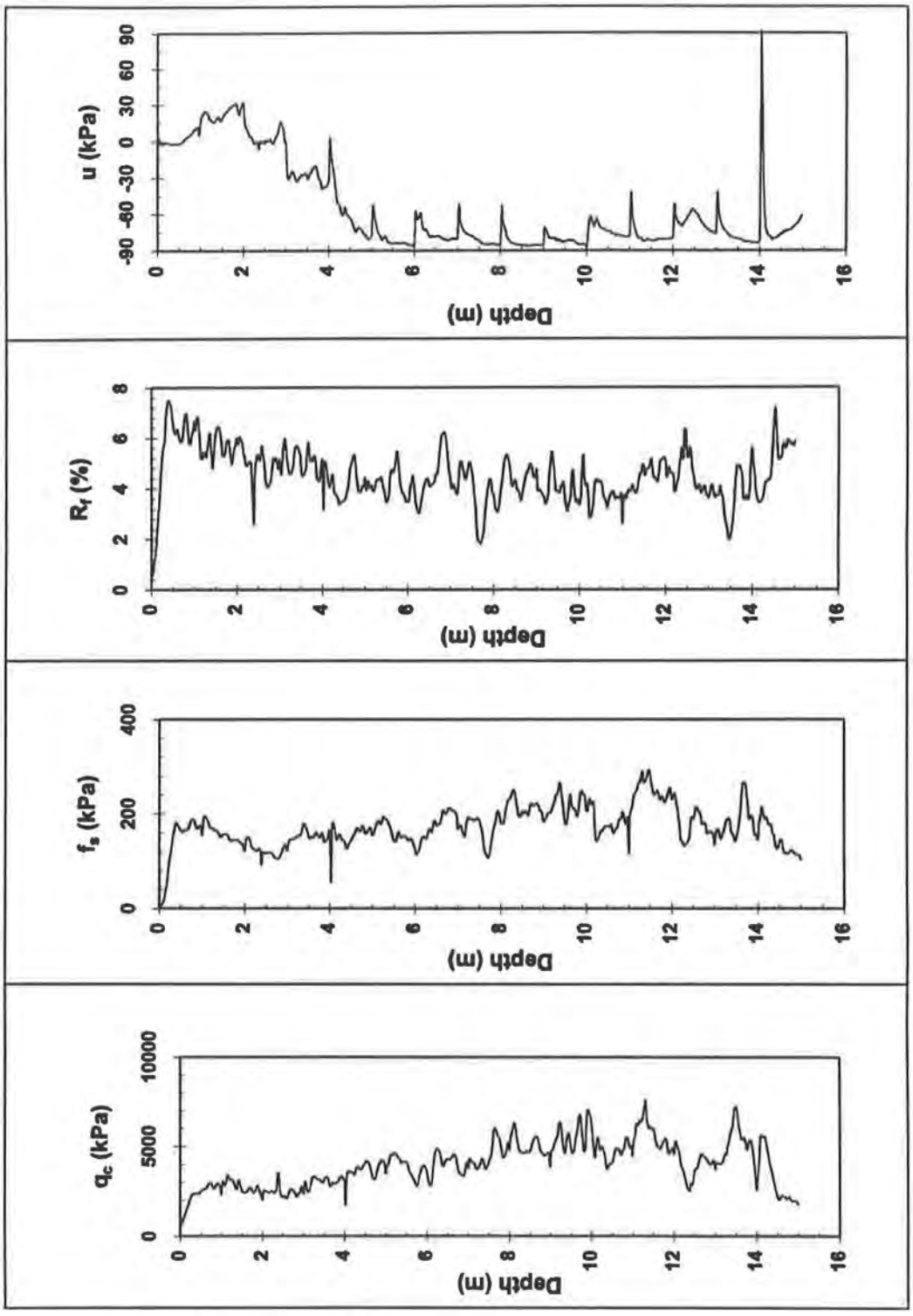

FIG. C.4. - PCPT Log : C-41

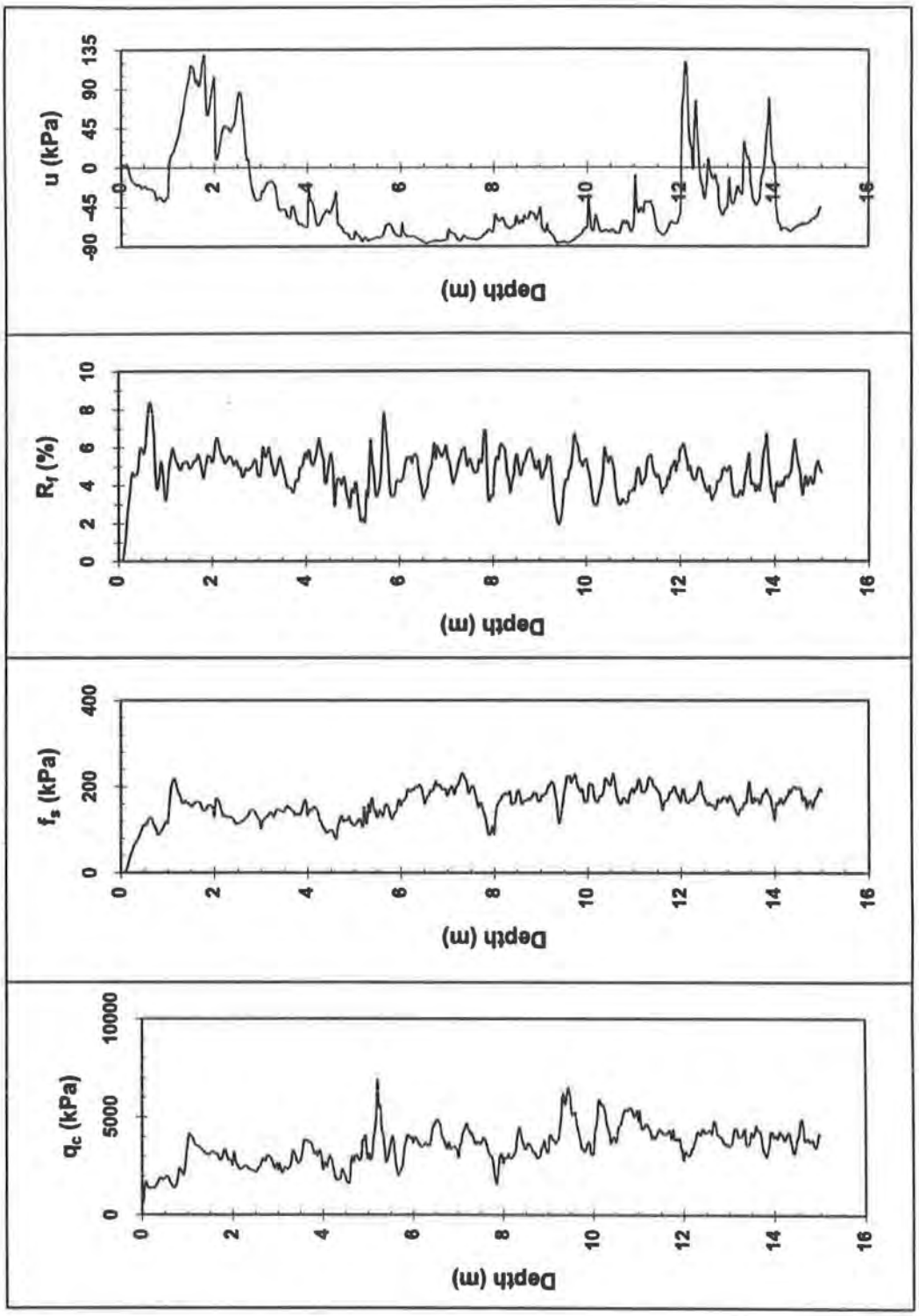

FIG. C.5. - PCPT Log : C-42

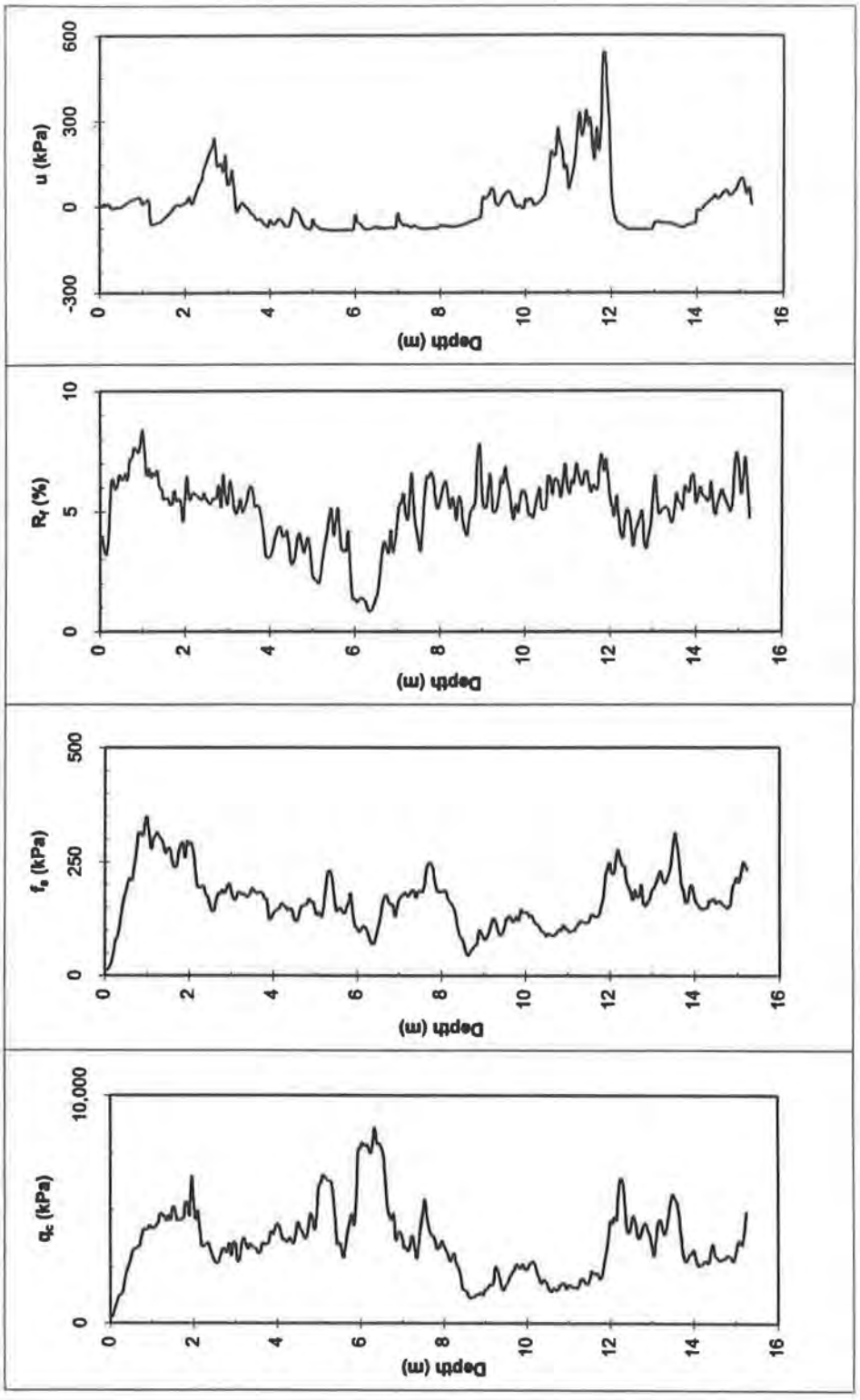

FIG. C.6. - Piezocone Sounding Record for C-28.

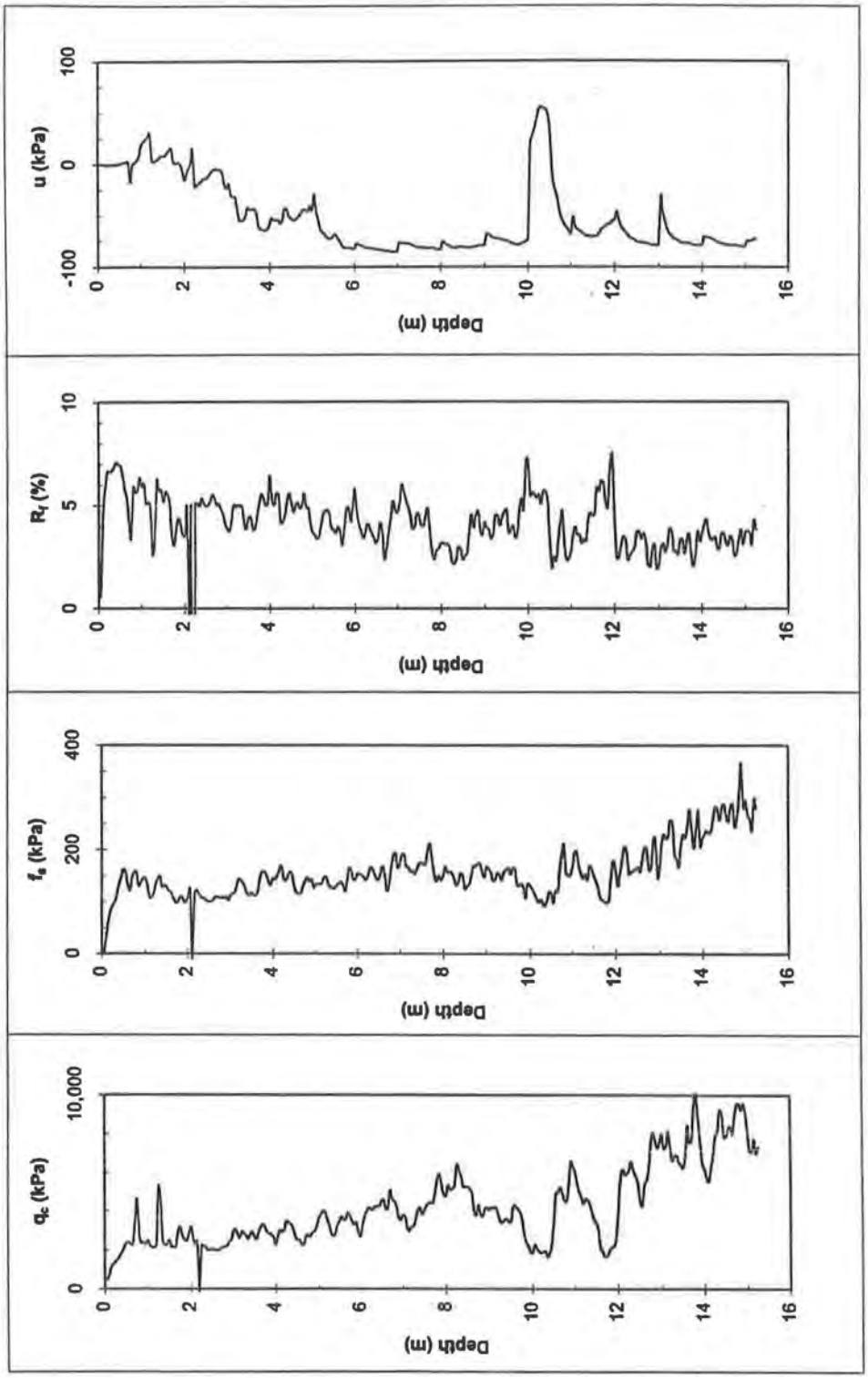

FIG. C.7. - PCPT Log : C-32 .

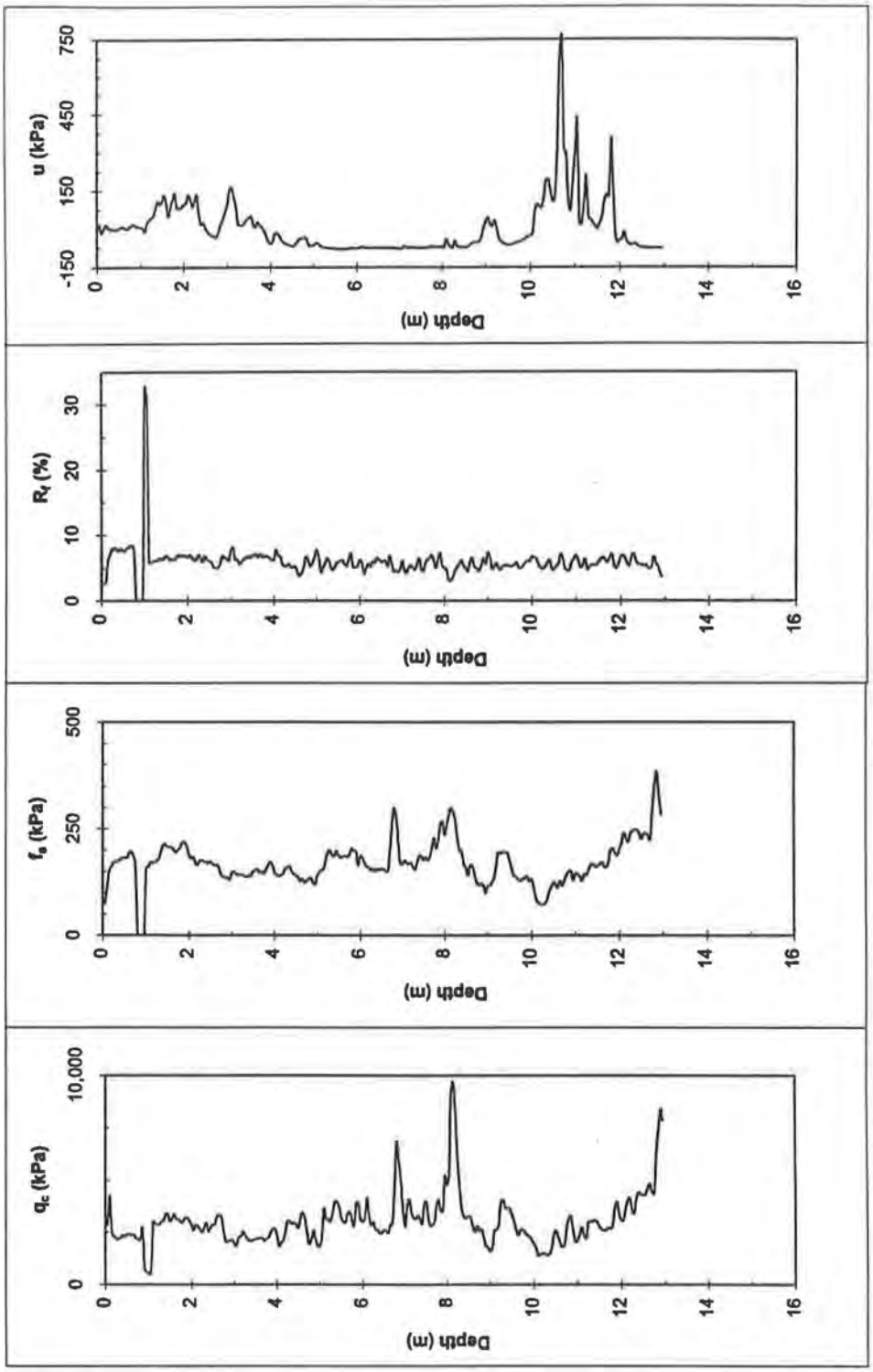

FIG. C.8. - PCPT Record : C-43.

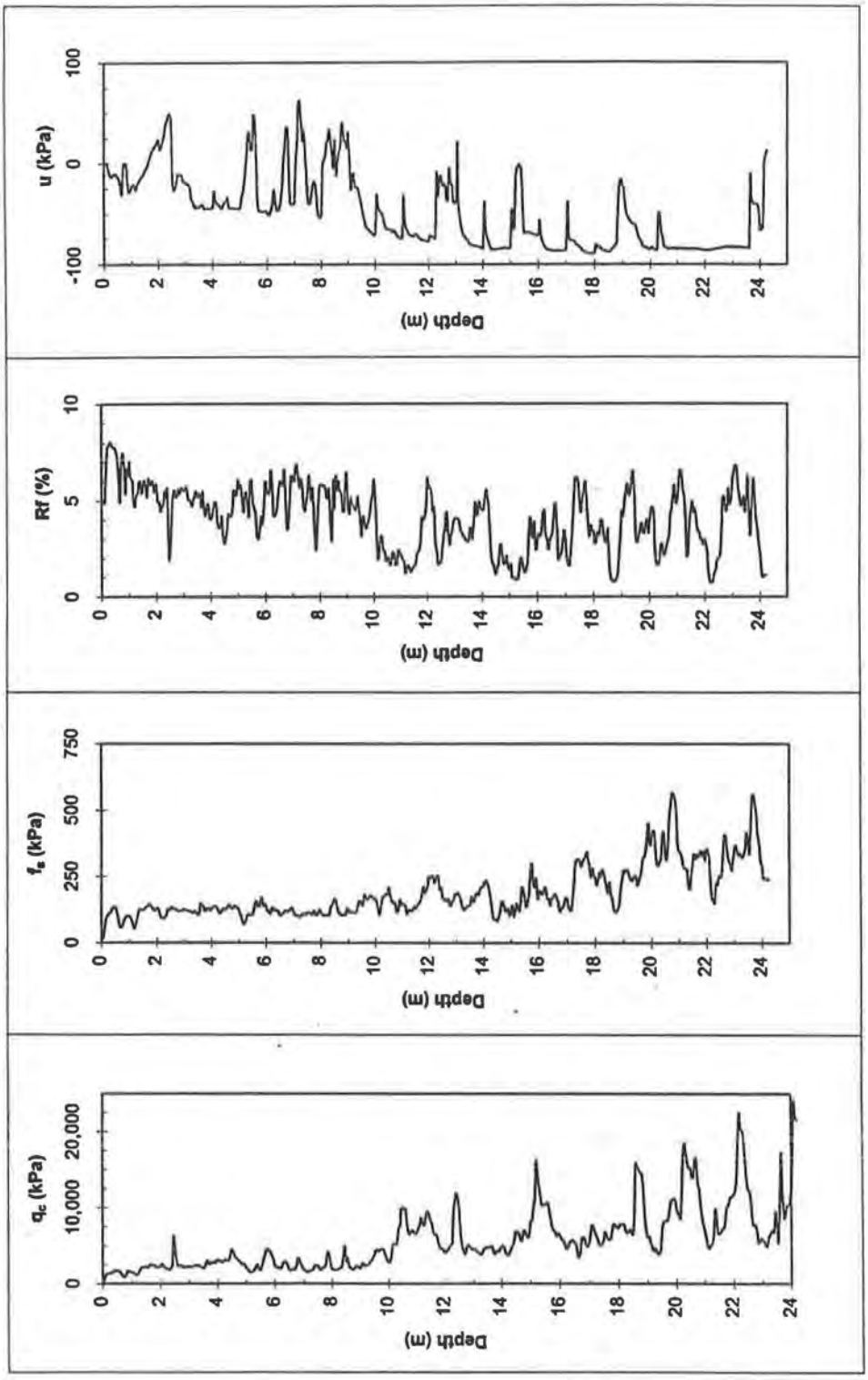

FIG. C.9. - PCPT Record : C-44.

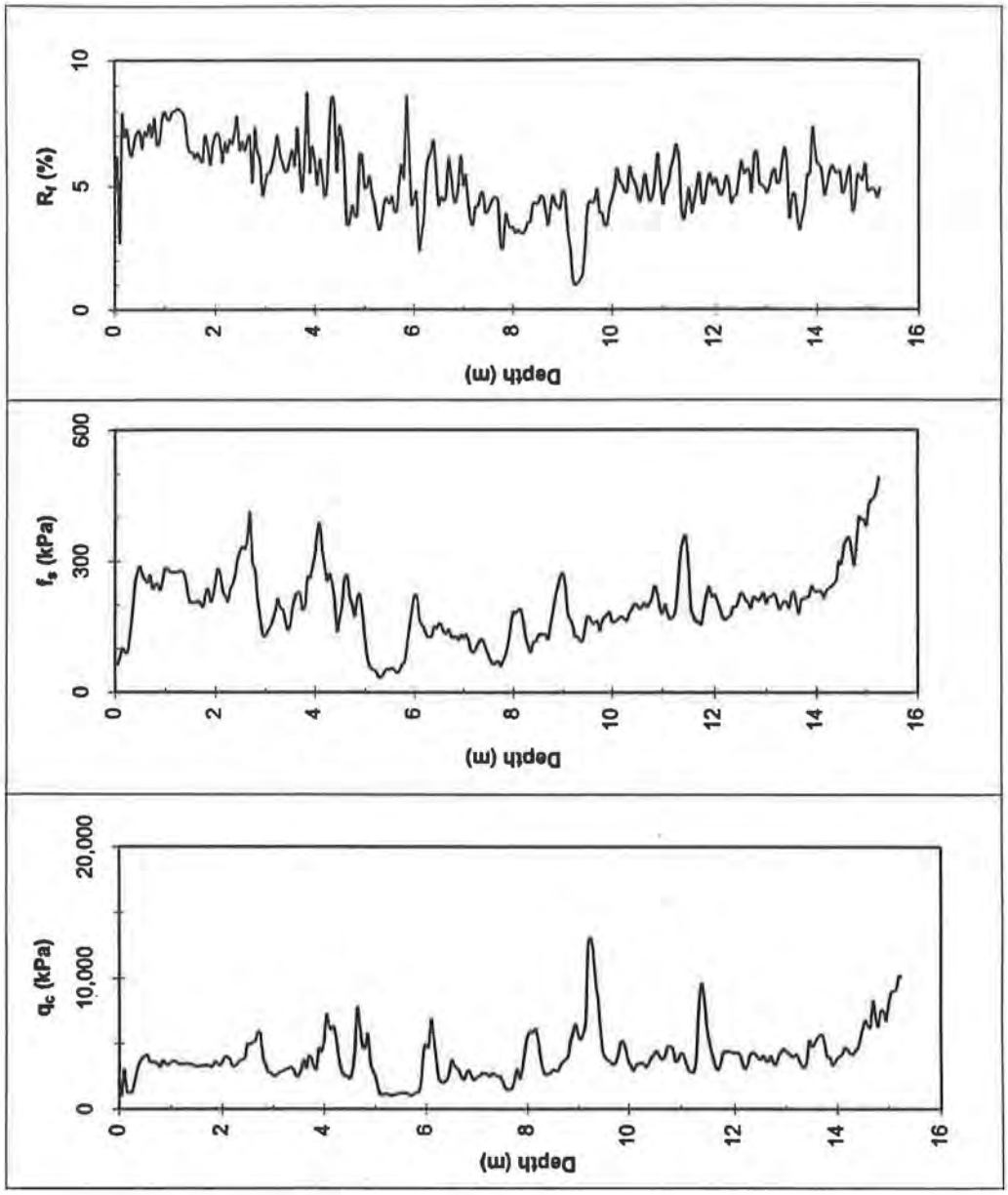

FIG. C.10. - CPT Record : C-13.

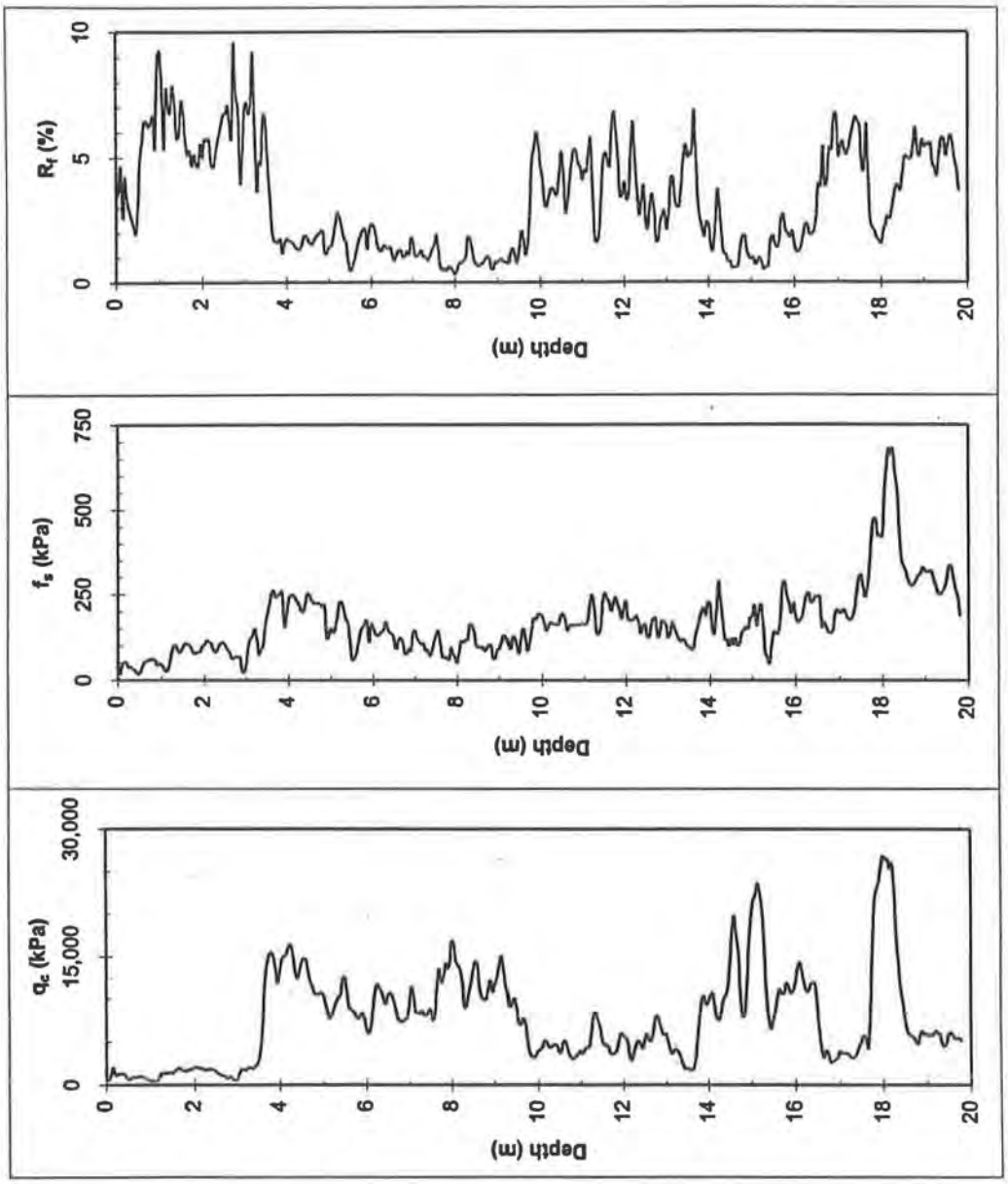

FIG. C.11. - CPT Record : C-14.

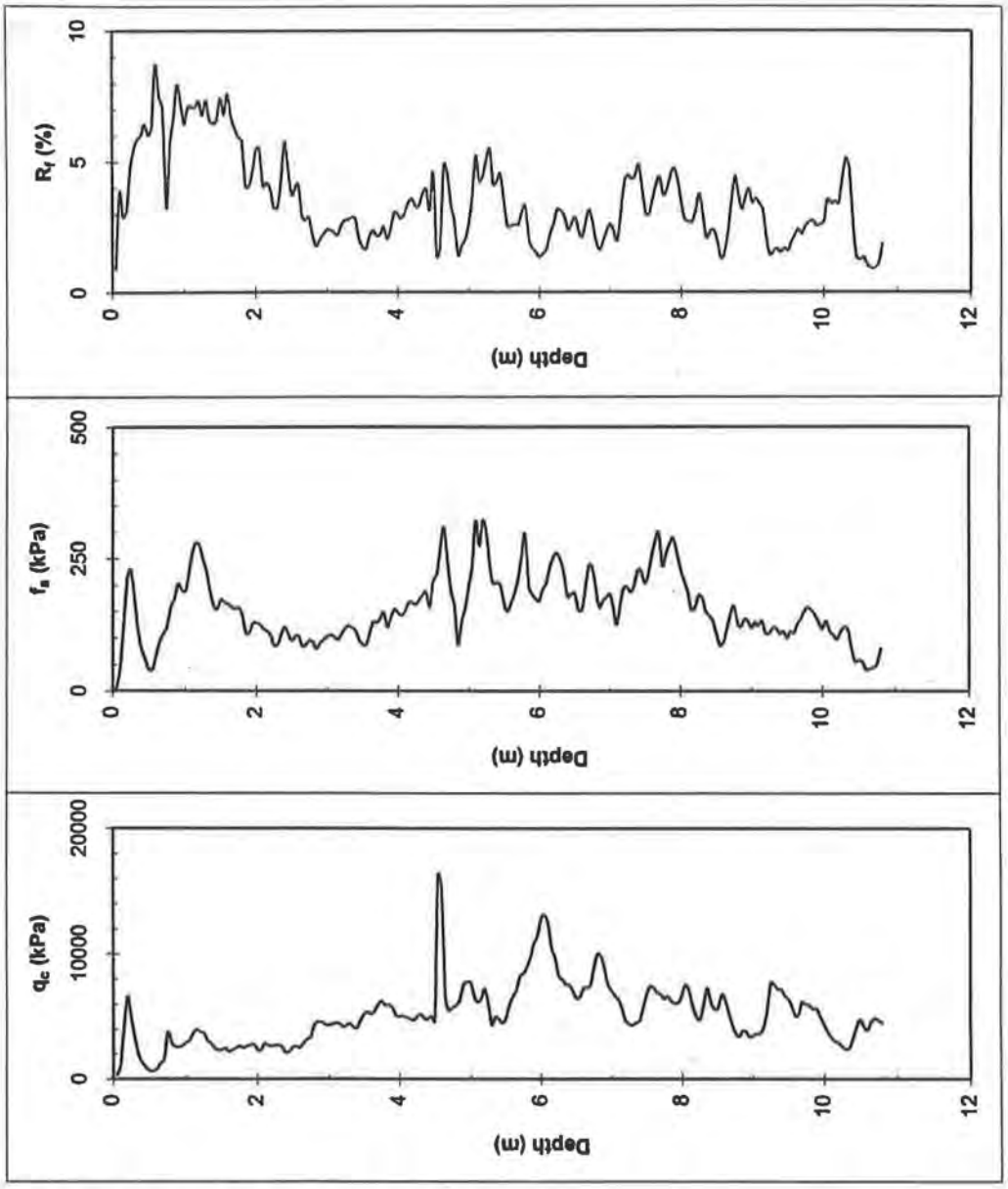

FIG. C.12. - CPT Record : C-17a.

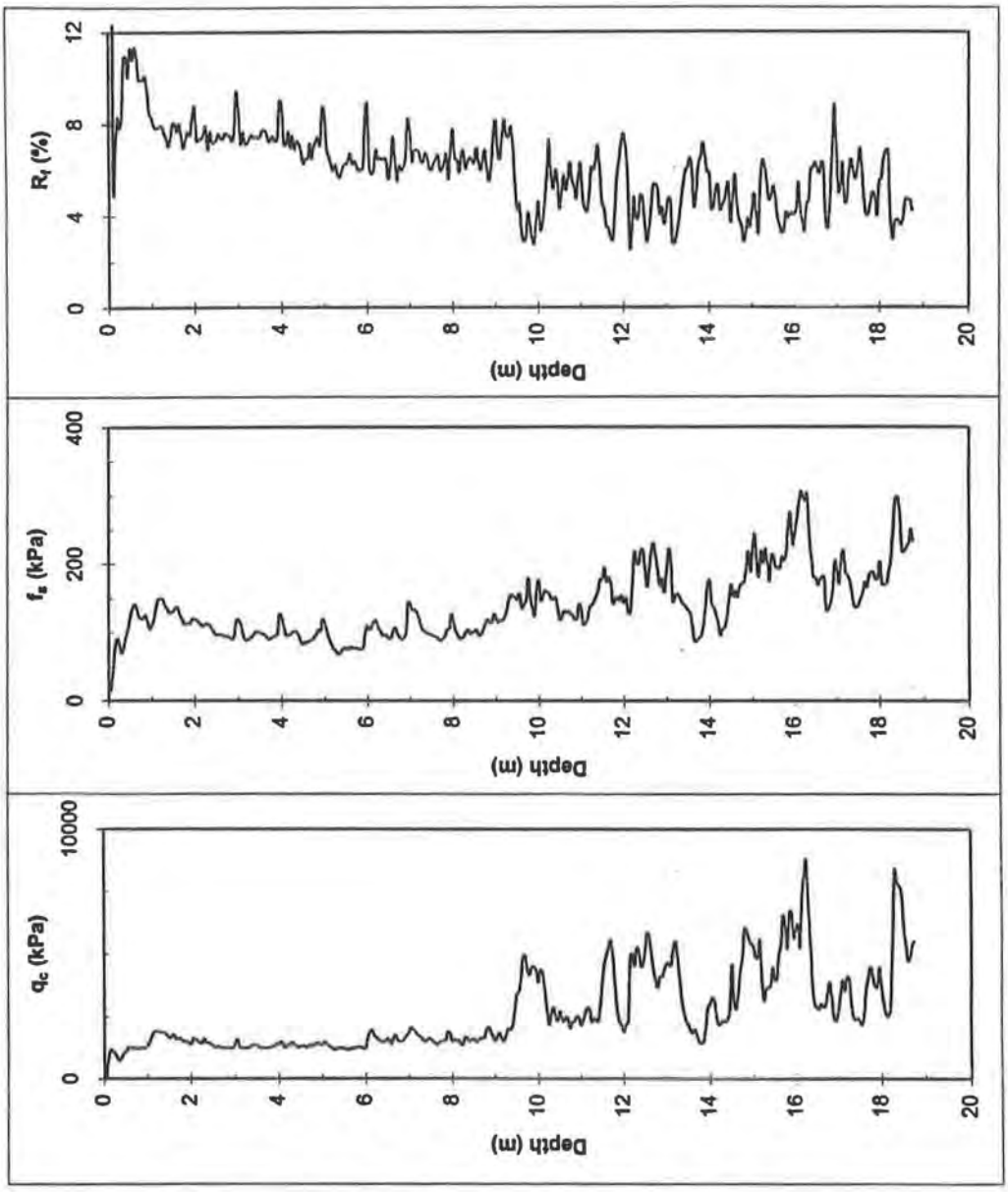

FIG. C.13. - CPT Record : C-25.

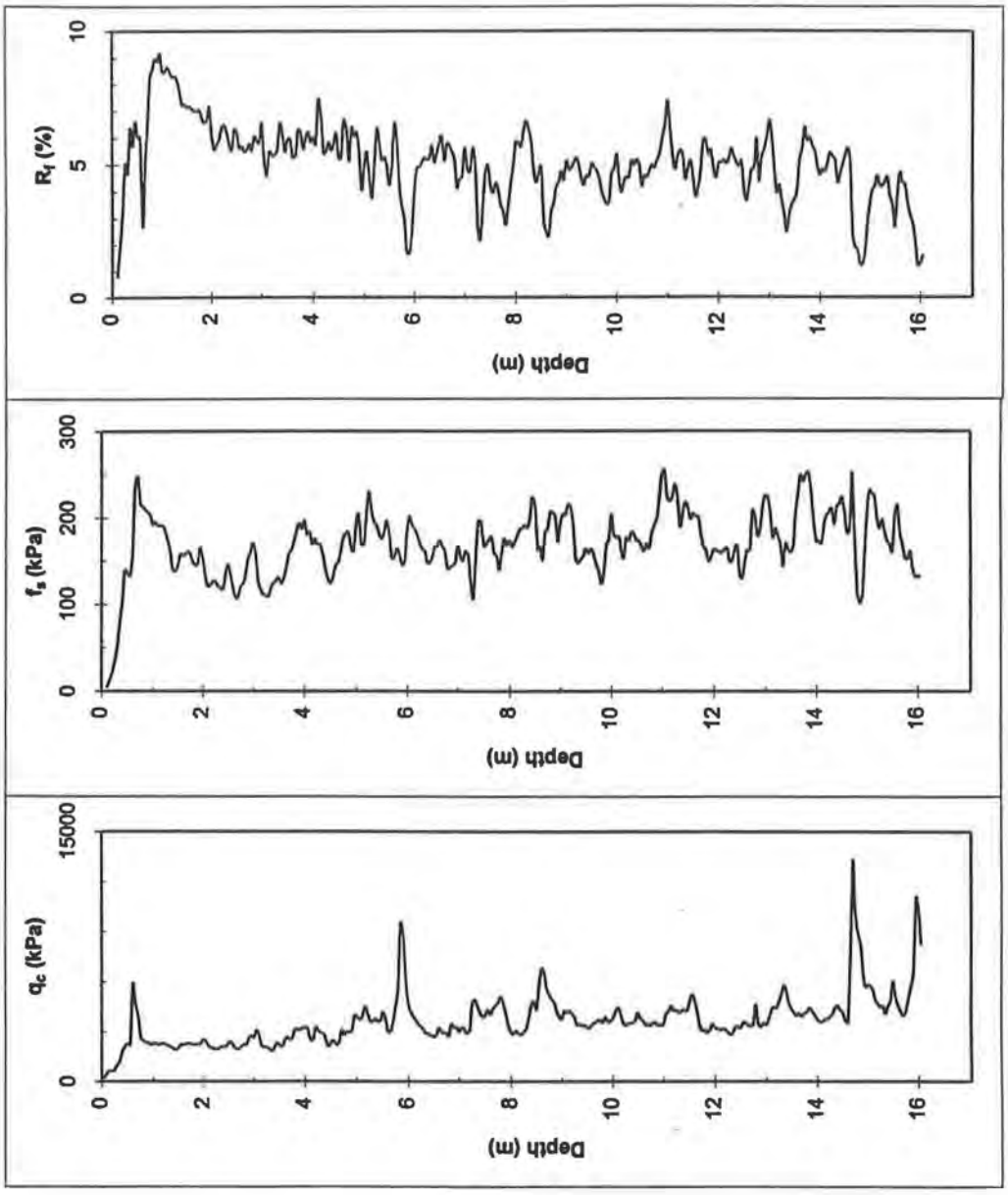

FIG. C.14. - CPT Record : C-11.

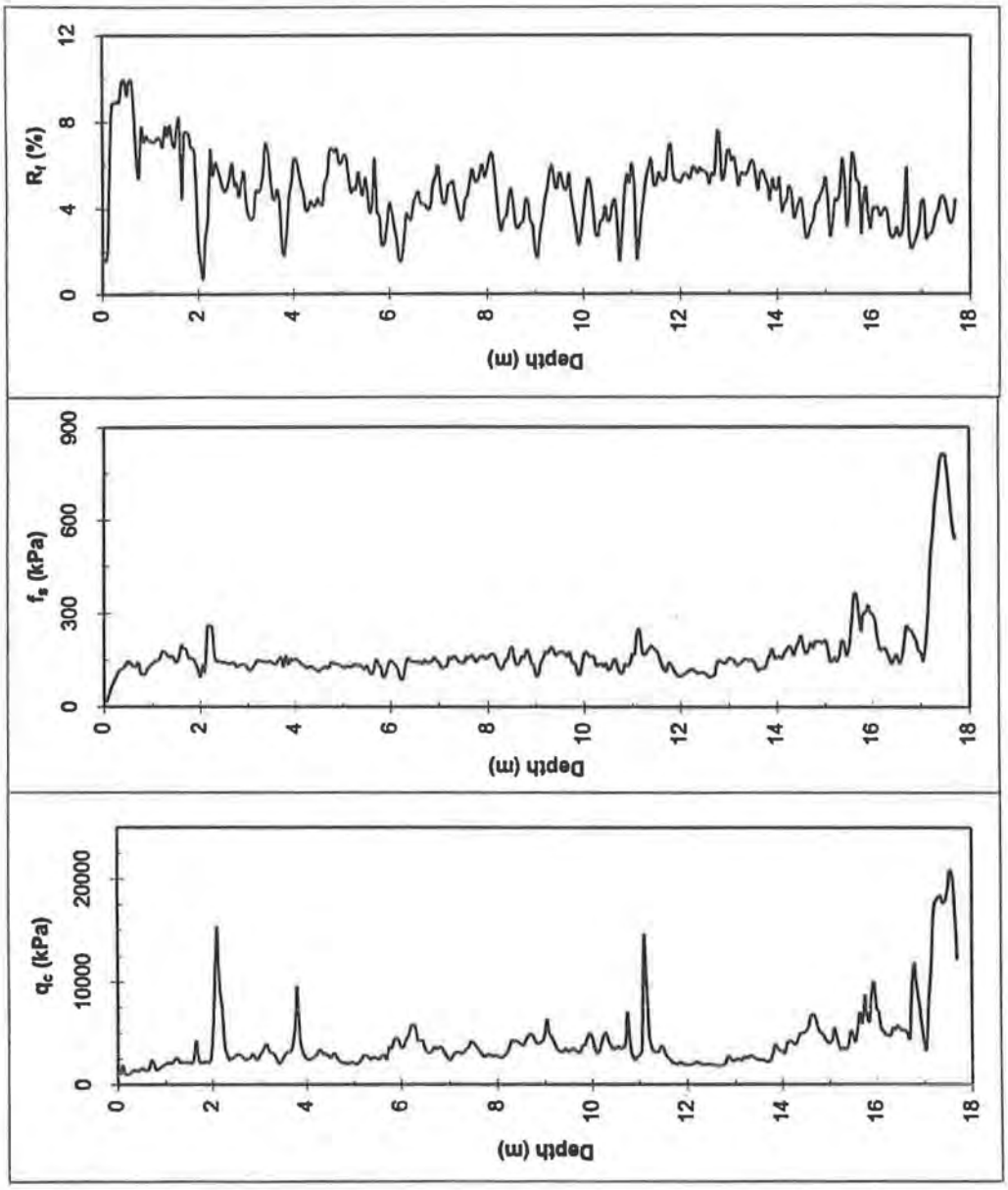

FIG. C.15. - CPT Record : C-23.

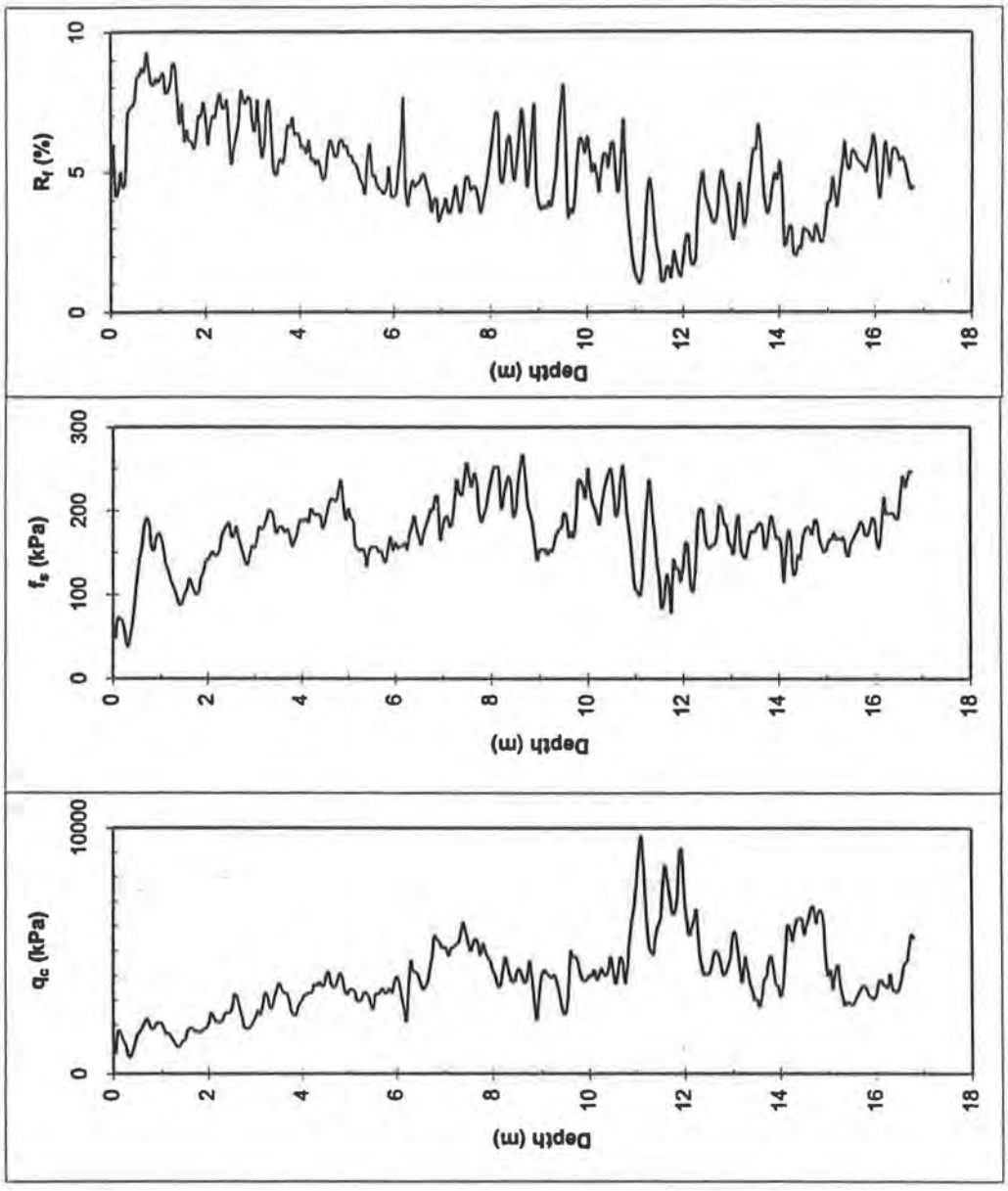

FIG. C.16. - CPT Record : C-21.

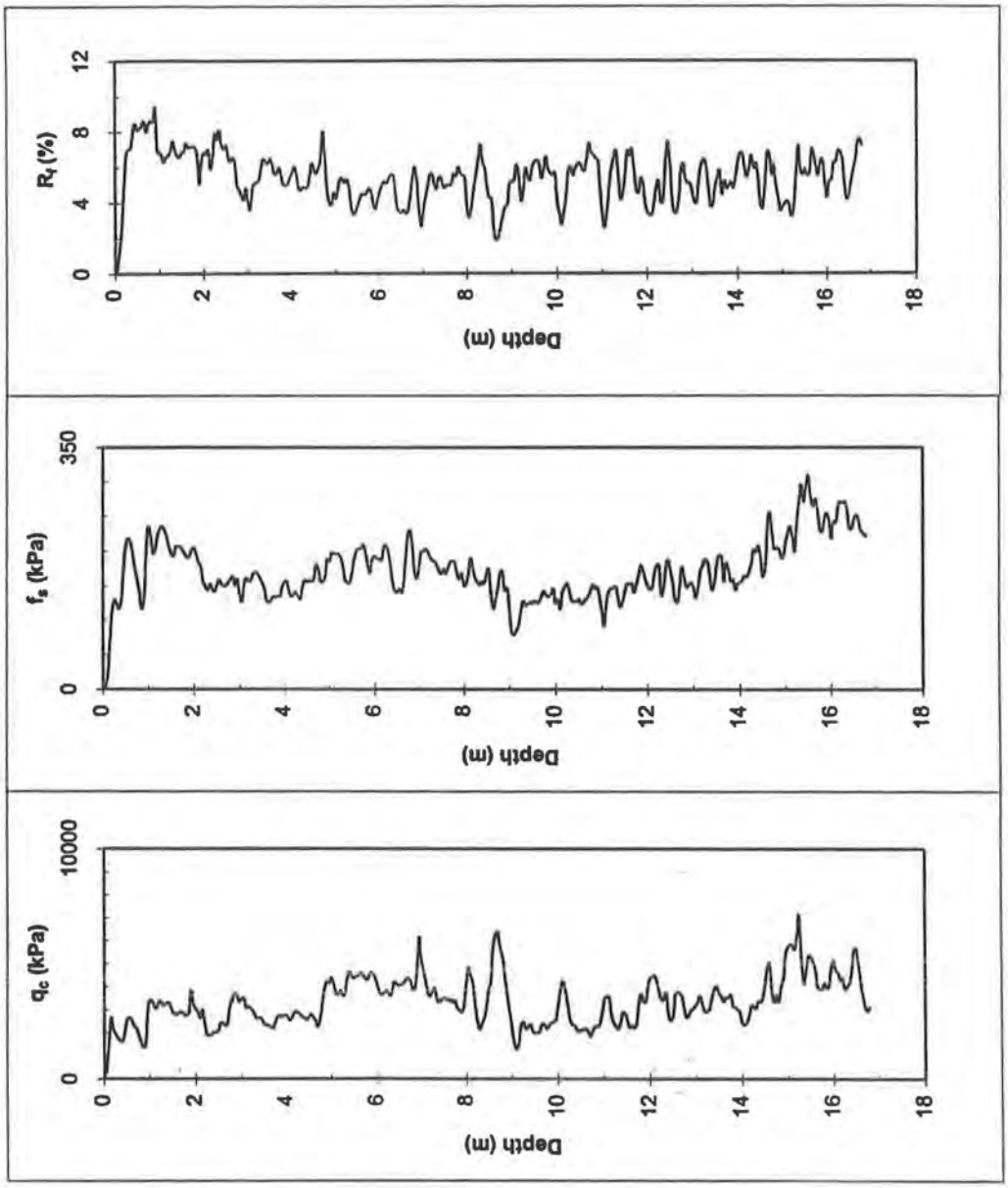

FIG. C.17. - CPT Record : C-27.

APPENDIX D

CONE PRESSUREMETER TEST RESULTS

General

1. Raw values of pressure and volume were corrected for system compressibility (volume losses) and for membrane inertia (stiffness). Hydrostatic pressure in lines was also considered in producing corrected pressure and volume readings.

2. Plots of corrected readings were further adjusted to account for the friction reducer used below the PMT to ease pushing of the rods. The friction reducer created an annulus of space between the PMT and the surrounding soil. This volume was estimated, and corresponding readings beyond this "cavity" volume were adjusted.

Equipment

- cone pressuremeter : Roctest standard PENCEL pressuremeter; 2,500 kPa capacity; 25.5 cm long, 1.73 cm radius at its center
- tubing : 6.35 mm OD, 2 mm ID
- friction reducer : 1.83 cm radius; located below PMT but above sleeve friction transducer

Procedure

1. PMT testing conducted in conjunction with standard cone penetration testing.

2. Cone pushed at standard 2-4 cm/sec rate between PMT test locations; at these depths, the cone was not pushed while the PMT probe was expanded.

3. After initial loading, the pressure was unloaded then reloaded to obtain a small strain reload modulus.

Data Reduction

Young's Modulus

Initial loading modulus was found by taking two initial points beyond the origin for the corrected curves that were translated to the origin to account for friction reducer ring. It is assumed for the calculations that linear behavior is experienced between these two points.

The unload-reload modulus was found by considering the lowest point of the unload and the next point of the reload. It is assumed for the calculations that linear behavior is experienced between these two points.

Example (Initial Loading Modulus) : From C-41P, 1 meter depth -

Volume of Cavity (V_c) = 34.67 cc
Volume of Probe w/o Applied Pressure (V_o) = 192 cc
Poisson's Ratio (ν) = 0.33
(for Initial Loading Modulus : V_2 = 10.35 cc, V_1 = 1.22 cc
P_2 = 1,150 kPa, P_1 = 832 kPa)
Average Volume Between Successive Readings (Vm)

$E = 2*(1+\nu)*(V_c+V_o+V_m)*(P_2 - P_1)/(V_2 - V_1) =$ <u>14,442 kPa</u>

Example (Unload-Reload Modulus) : From C-41P, 1 meter depth -

Volume of Cavity (V_c) = 34.67 cc
Volume of Probe w/o Applied Pressure (V_o) = 192 cc
Poisson's Ratio (ν) = 0.33
(for Initial Loading Modulus : V_2 = 15.77 cc, V_1 = 12.83 cc
P_2 = 6,160 kPa, P_1 = 99 kPa)

$E = 2*(1+\nu)*(V_c+V_o+V_m)*(P_2 - P_1)/(V_2 - V_1) =$ <u>118.065 kPa</u>

Limit Pressure

Corrected expansion curves adjusted for the "cavity" were plotted, and the curve was extended beyond the reading of maximum pressure and volume to the 100cc volume

mark. The corresponding pressure was taken as the limit pressure as recommended by the cone pressuremeter's manufacturer.

An example of extrapolation of limit pressure for C-41P at 1 meter depth is shown in Figure D.1.

Effective At-Rest Earth Pressure Ratio

Total horizontal earth pressure for each test curve was determined from back-fit estimation of the loading curve.

Effective Friction Angle

Centre d'Etudes Menard (1970) Method :

Empirical relationship between net limit pressure and Ø'.

Net Limit Pressure = $pl^* = 250*2^{((Ø'-24)/4)}$

= Limit Pressure - Total Stress Initial Horizontal Ground Pressure

Example : C-41P at 1 meter depth -

Limit Pressure = 1,030 kPa
Estimated Horizontal Ground Press. = 100 kPa
Therefore, Ø' = 31.6 degrees.

Calhoon (1970) Method :

Empirical relationship between limit pressure and Em as shown on Calhoon's graph.

Example : C-41P at 1 meter depth -

Limit Pressure = 1,030 kPa
Initial Loading Modulus from Cone Pressuremeter = 14,442 kPa
Therefore, Ø' = 31.5 degrees

Undrained Shear Strength

The average limit pressure and interpreted total horizontal pressure at each test depth were used in analysis. In 1978, Baguelin et al. suggested that, based on cavity expansion theory, the PMT can be used to evaluate Su at the limit pressure by the following relationship -

$$S_u = (P_L - P_o)/N_p$$

where P_L = Limit Pressure
P_o = Total Horizontal Earth Pressure
$N_p = 1+\ln(E_{pmt}/3S_u)$
Typical values of N_p : 5 - 12

Through trial and error, an $N_p = 11$ gave the best agreement with the average triaxial value.

Example : @ 2 meter depth, average P_L = 1,005 kPa and average P_o = 105 kPa

Therefore, for N_p =11, S_u = (1,005-105)/10 = 90.0 kPa

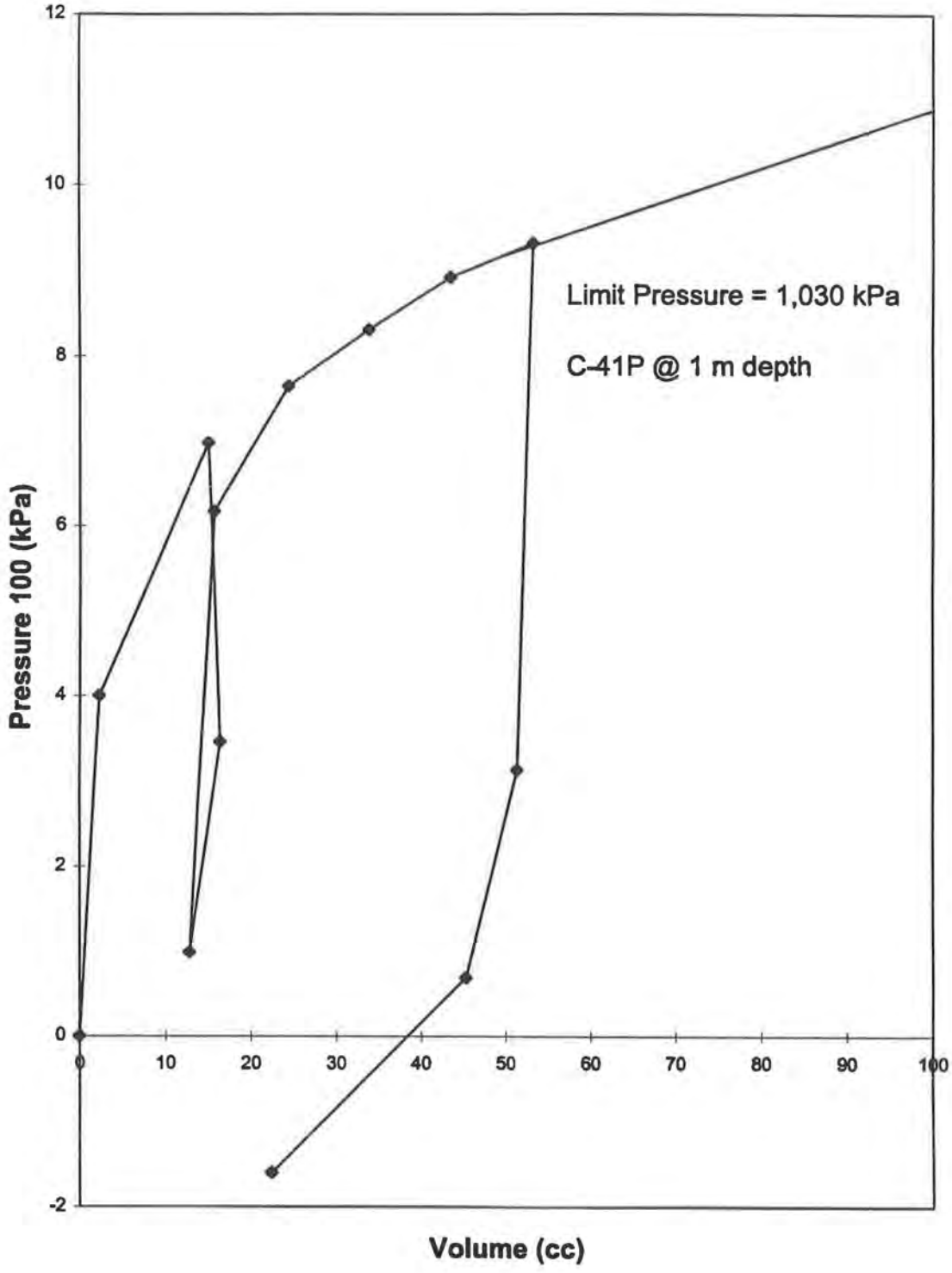

FIG. D.1. - CPMT Limit Pressure Example.

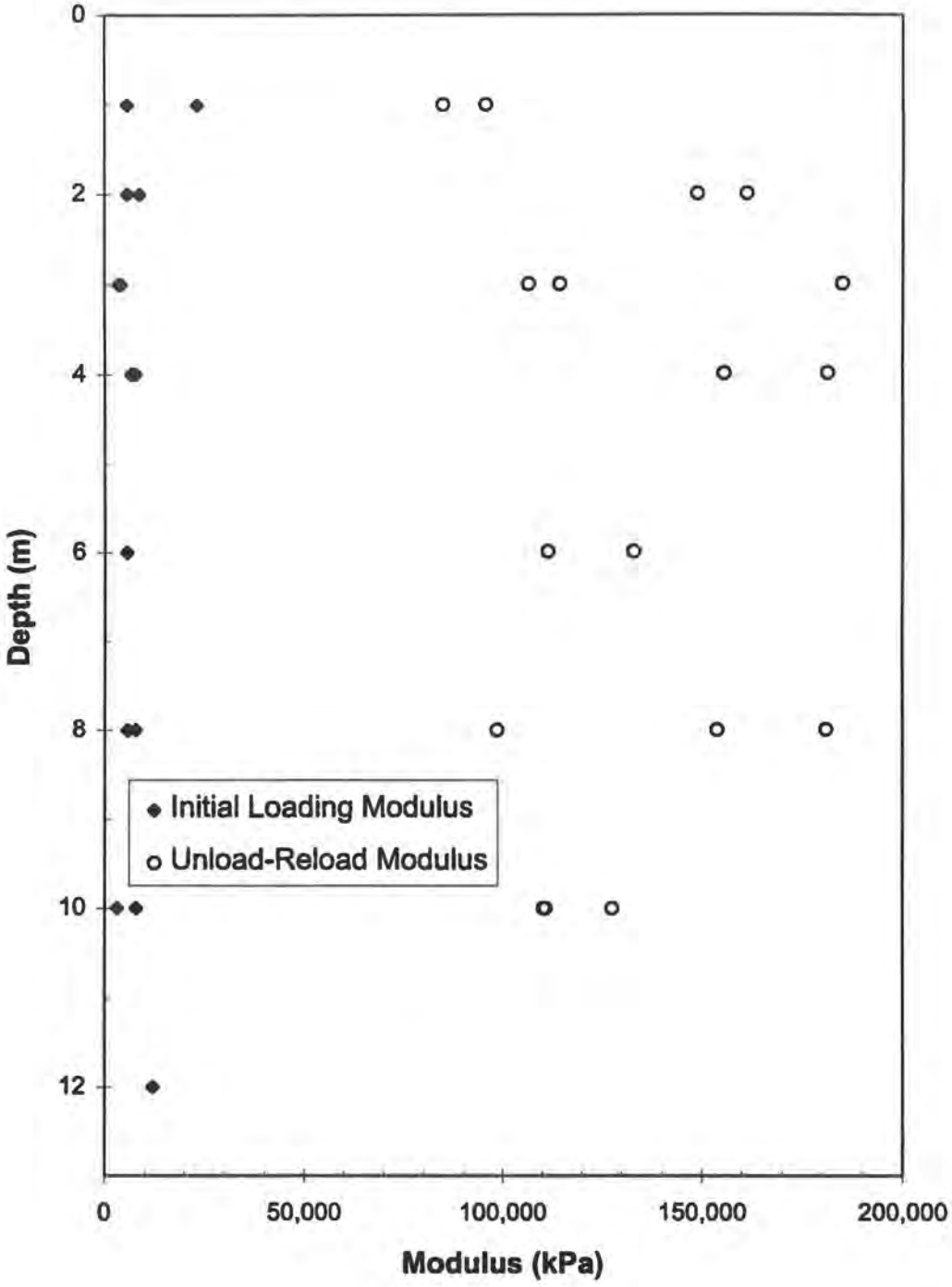

FIG. D.2. - CPMT Modulus Values.

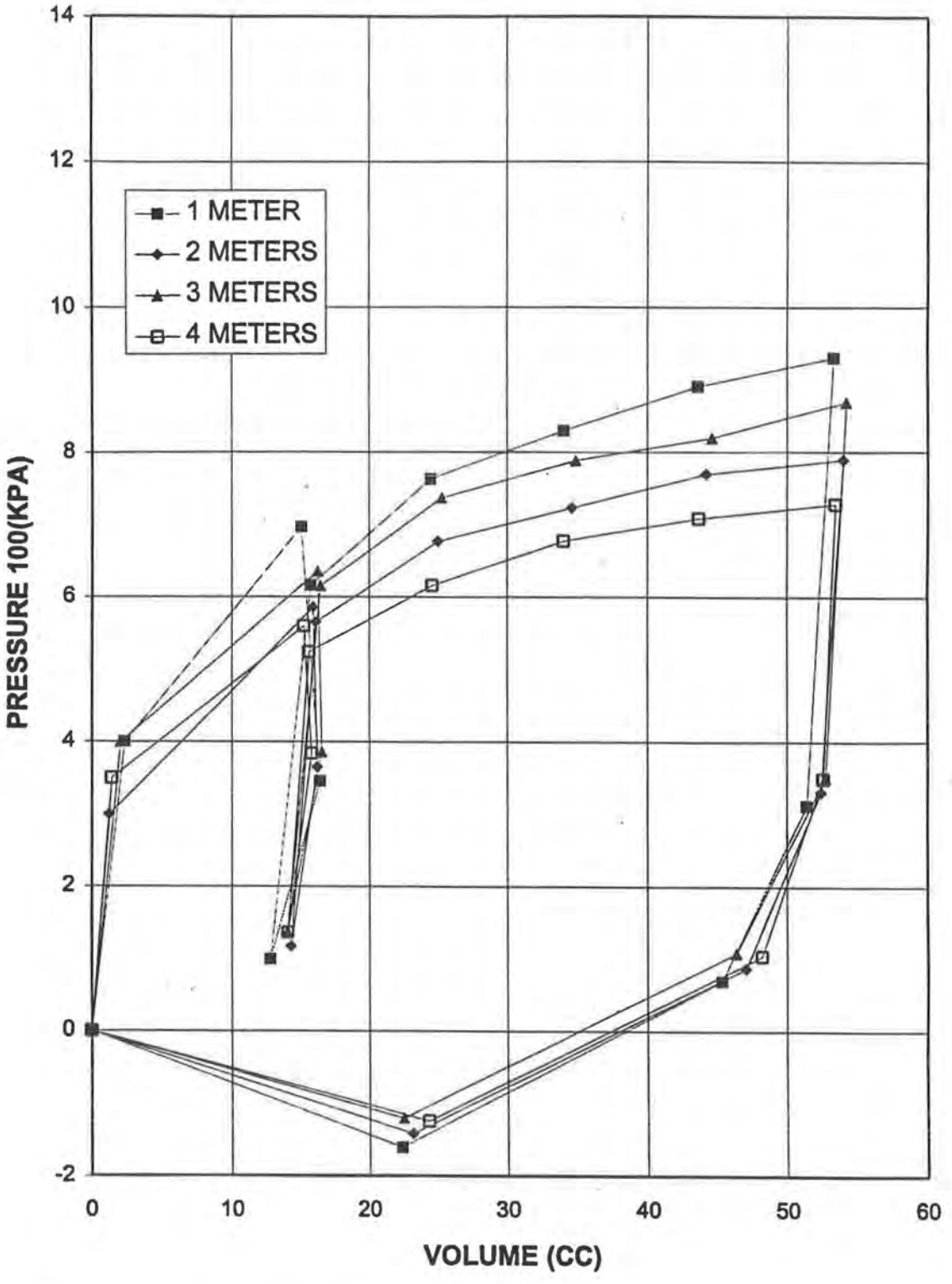

Figure D.3. - Cone Pressuremeter Results at C-41P

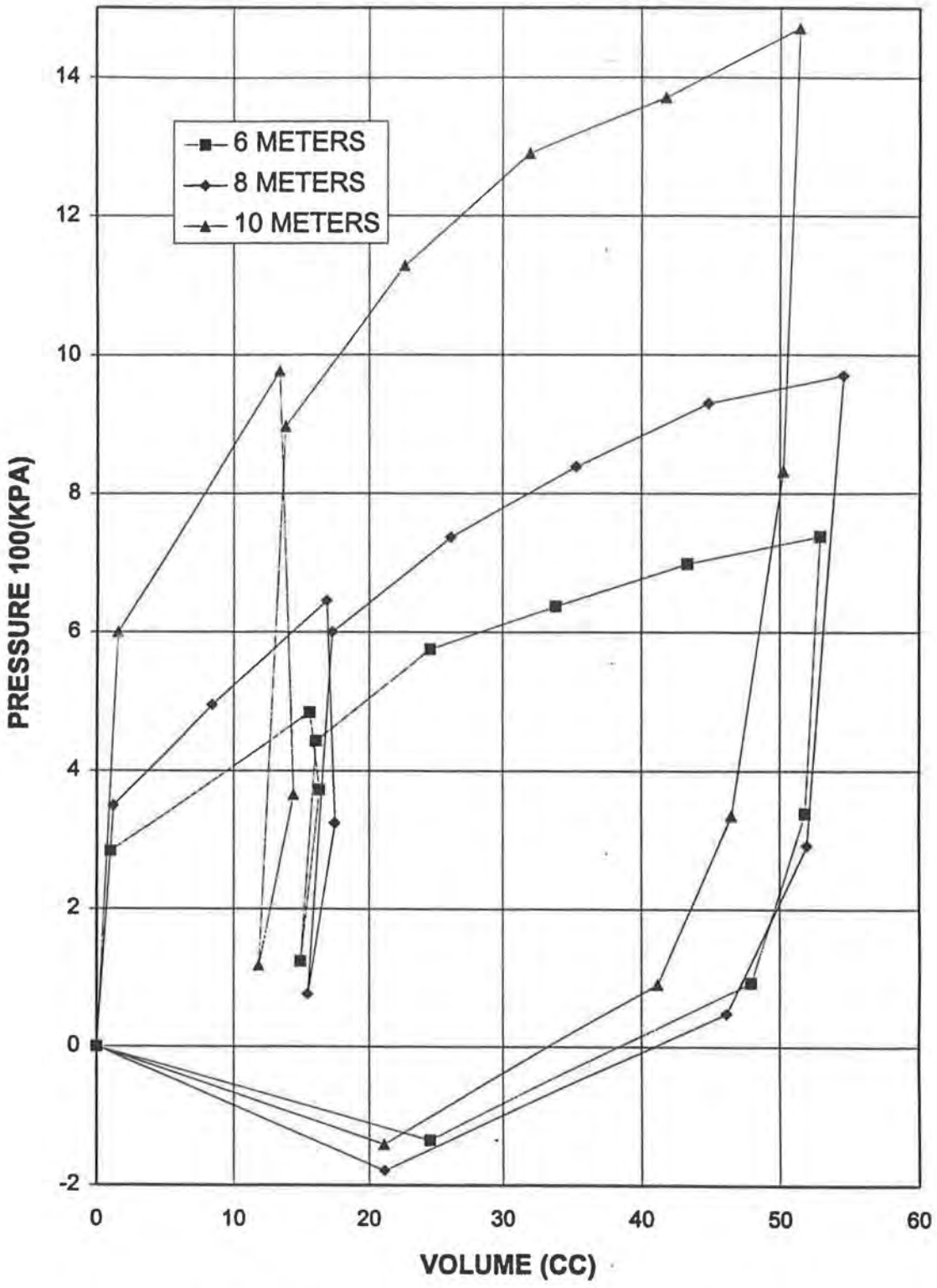

Figure D.3. - Cone Pressuremeter Results at C-41P

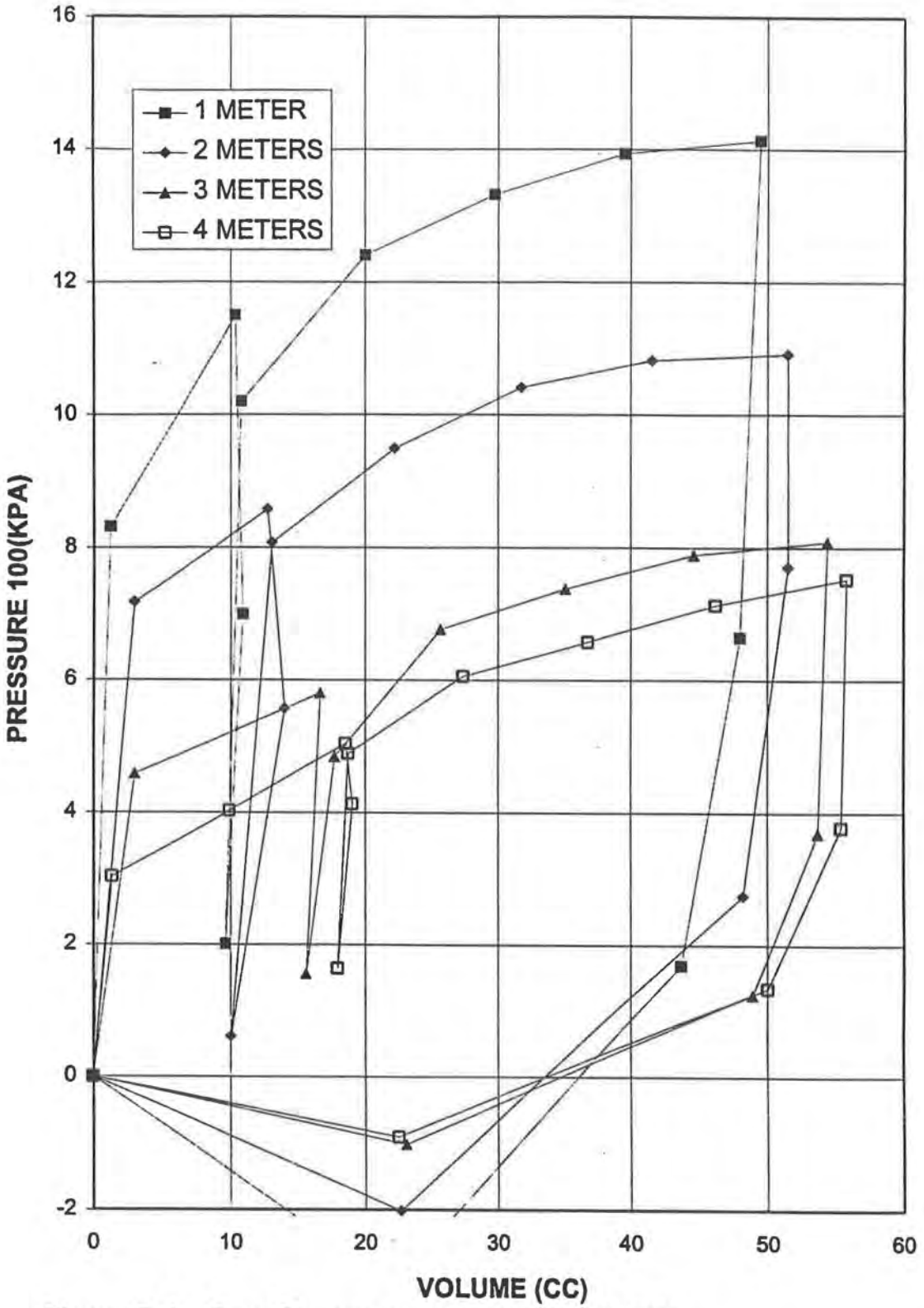

Figure D.4. - Cone Pressuremeter Results at C-42P

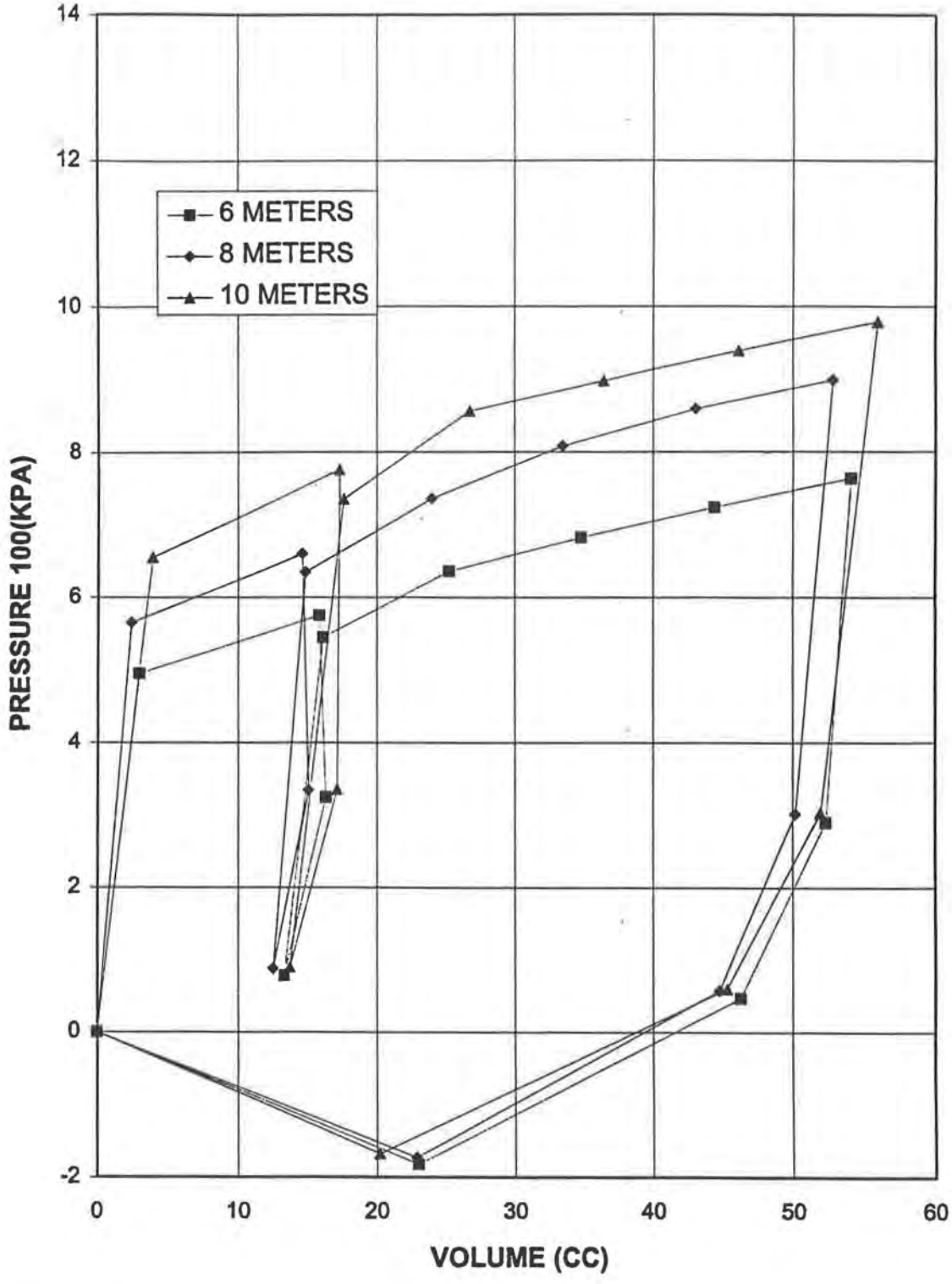

Figure D.4. - Cone Pressuremeter Results at C-42P

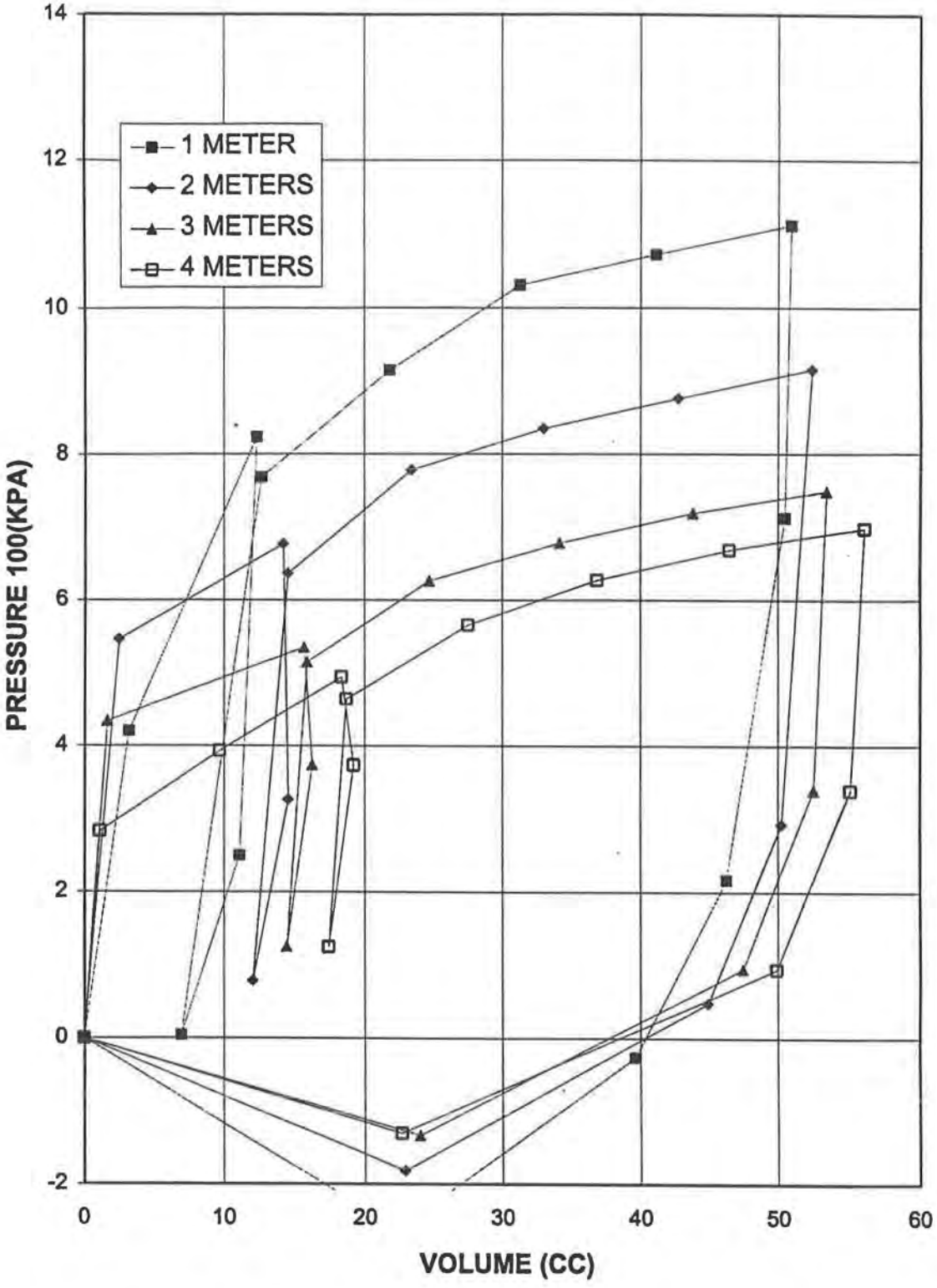

D.5. - Cone Pressuremeter Results at C-43P

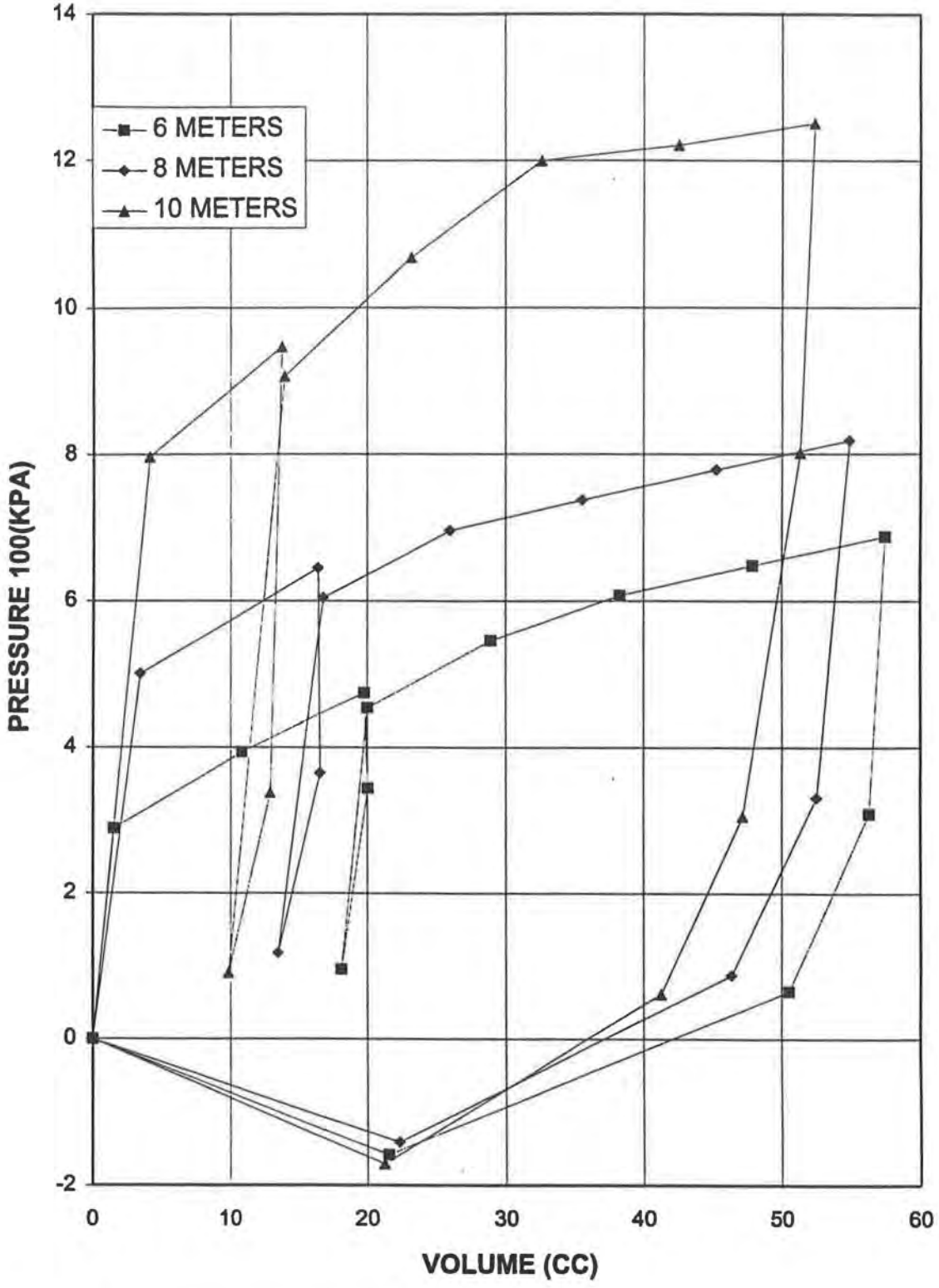

D.5. - Cone Pressuremeter Tests at C-43P

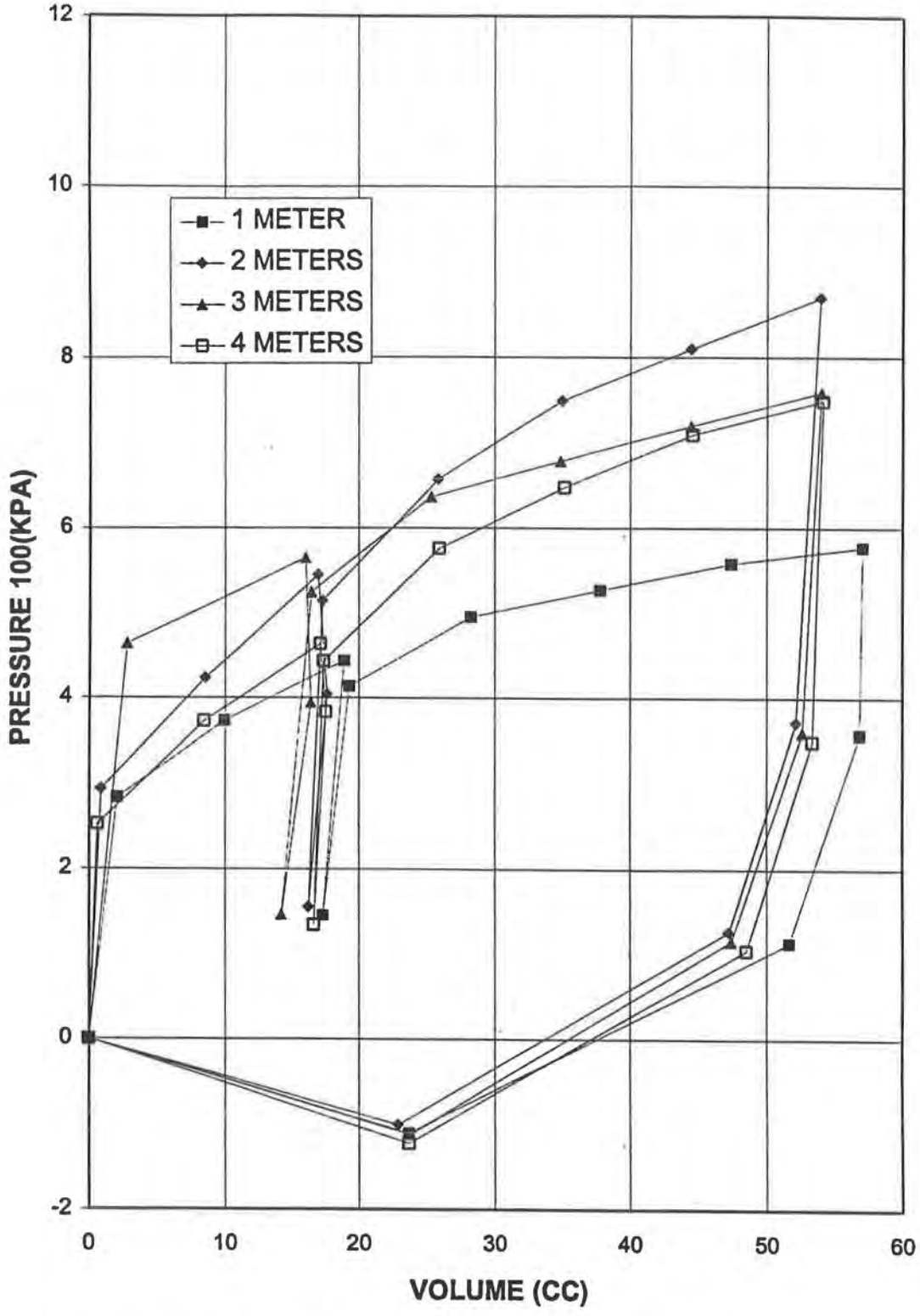

FIGURE D.6. - Cone Pressuremeter Results at C-44P

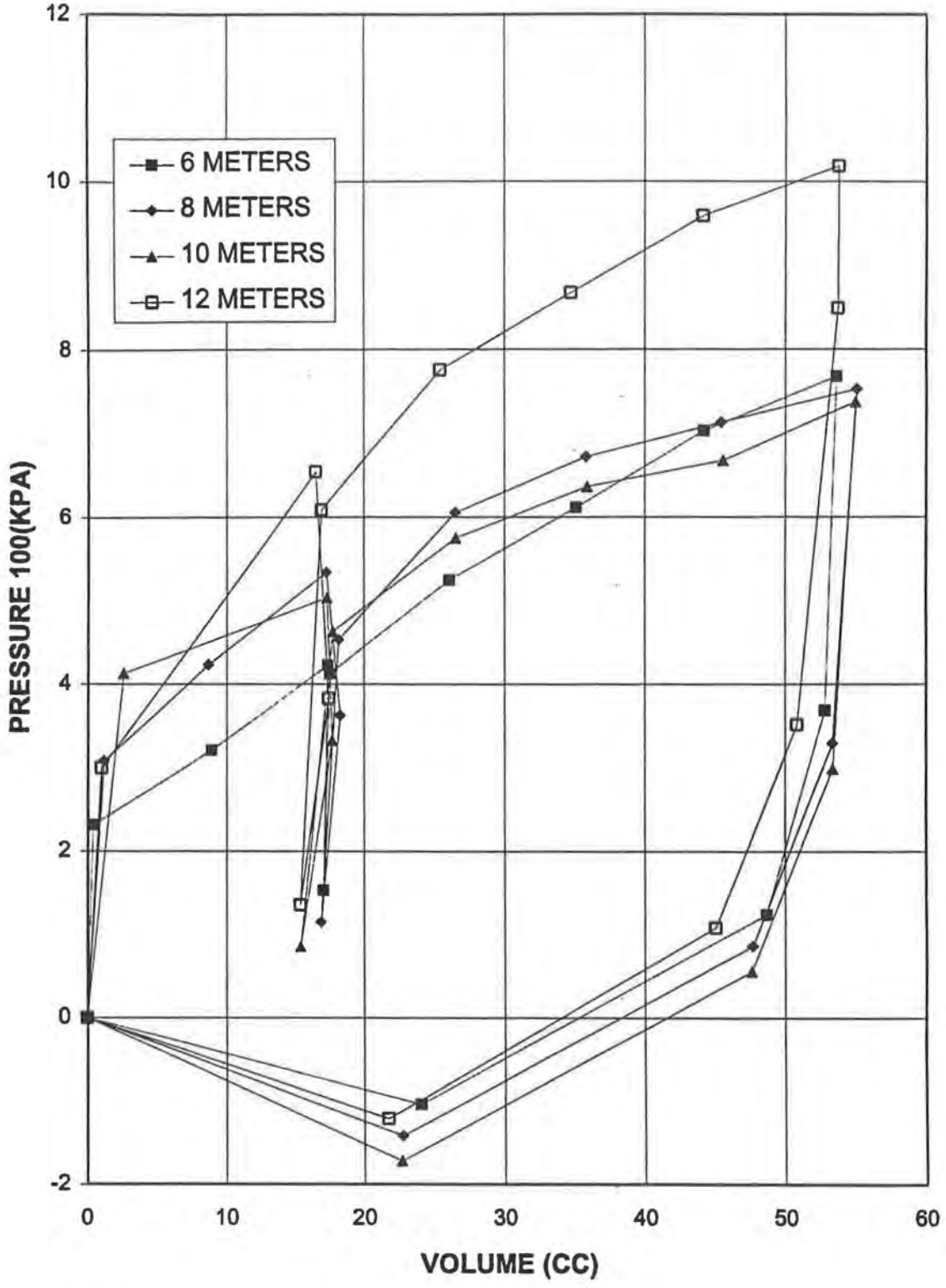

Figure D.6. - Cone Pressuremeter Results at C-44P

APPENDIX E

MENARD PRESSUREMETER TEST RESULTS

General

1. Raw values of pressure and volume were corrected for system compressibility (volume losses) and for membrane inertia (stiffness). Hydrostatic pressure in lines was also considered in producing corrected pressure and volume readings.

Equipment

- Menard-type pressuremeter probe : Roctest monocellular hydraulically inflated NX probe; diameter = 70 mm; recommended borehole diameter between 76 mm & 80 mm; length of water cell and gas cells combined = 34.29 cm; length of water cell = 22.86 cm

- volumetric/pressure measurement and control unit

Procedure

1. Boring advanced by hollow continuous flight auger to test depth.

2. Shelby tubes pushed at desired test depth; PMT probe lowered into cavity created by extraction of shelby tube.

3. Tests conducted by inflating probe's cell incrementally until near full expansion.

4. Creep vs. Pressure plots were also made by recording pressure decline over time between pressure loading increments.

5. Upon test completion at a specific depth, probe was deflated and extracted. Probe was then cleaned and prepared for next test as boring was advanced.

Data Reduction

<u>Young's Modulus</u>

The range of points to consider for calculation should fall on linear region of loading curve. Examination of creep curves aided in interpretation of which points fell

within this linear range.

Example : From B-2, 2 meter depth, Initial Loading -

Volume of Probe w/o Applied Pressure (V_o) = 790 cc
Poisson's Ratio (ν) = 0.33
(for Initial Loading Modulus : V_2 = 475.0 cc, V_1 = 364.6 cc
P_2 = 387.8 kPa, P_1 = 124.5 kPa
Average Volume Between Successive Readings (V_m)

$E = 2*(1+\nu)*(V_o+V_m)*(P_2 - P_1)/(V_2 - V_1) =$ 7,676 kPa

Limit Pressure

The log-log method presented by Jezequel et al. (1975) was used in extrapolating the limit pressures. In using this method, the corrected pressure values are plotted on the vertical axis with a log scale, and the ratio of the increase in volume of the cavity to the initial volume of the cavity as estimated from total horizontal earth pressure procedure is plotted on the horizontal log axis. The last several points should form a straight line, and this line is extended to intersect an abscissa value of one. The ordinate value of the intersection is the limit pressure. An example is shown in Figure E.1.

Total Horizontal At-Rest Earth Pressure

Total horizontal earth pressure for each test curve was determined from estimation of the lower portion of the loading curve's point of maximum curvature. (Briaud 1992). This point is denoted as A on the example of this procedure which follows. The initial volume of the soil cavity involves extending the straight line portion of curve towards the X-axis until it intersects a horizontal line extended from A. The abscissa of the intersection (point D) corresponds to the initial volume of the cavity. An example of this procedure is shown in Figure E.2.

Effective Friction Angle

Centre d'Etudes Menard (1970) Method :

Empirical relationship between net limit pressure and Ø'.

Net Limit Pressure = $pl^* = 250*2^{((Ø'-24)/4)}$

= Limit Pressure - Interpreted Total Stress Initial Horizontal Ground Pressure

Example : B-5, 2 meter depth -

Limit Pressure = 860 kPa
Estimated Horizontal Ground Press. = 77 kPa
Therefore, Ø' = 31.1 degrees.

Calhoon (1970) Method :

Empirical relationship between limit pressure and Em as shown on Calhoon's graph.

Example : B-5, 2 meter depth -

Limit Pressure = 860 kPa
Initial Loading Modulus from Menard Pressuremeter = 2,630 kPa
Therefore, Ø' = ? degrees

This test location did not fall within the allowable range of Calhoon's graph.

Manassero (1989) Method :

Method produced from self boring pressuremeter tests in a calibration chamber in Ticino sand. This method is independent of sand density. It assumes that volume decreases then increases during expansion such that the ratio of volumetric to shearing strain approaches a constant value.

The volume readings were converted to corresponding radius values in order to calculate cavity strain and current strain. A plot of current strain values are plotted on a natural log horizontal scale, and the effective applied pressure is plotted on a natural log vertical scale. The best fit linear regression produces an equation of the line. The slope of the best fit line is then related to the effective friction angle. Before a value for effective friction angle was determined, a typical value of the angle of shearing resistance at constant volume was assumed in the analysis to be 30 degrees. (Robertson and Hughes 1986)

Example : From B-2, 1 meter -

Equations and Dimensions:

Length of Membrane (L) = 20.52 cm
Volume of Probe at Atmospheric Pressure (V_o) = 790 cc
Radius of the Probe (R_o) = 3.5 cm
Radius of Cavity at Estimated Total Horizontal Press. (R_c) = 3.879 cm
Volume of the Cavity (V_c) = 180 cc
Any Radius (R_i) = Square Root ((790+V_i)/(pi*20.52))
Cavity Strain (ε_c) = (R_i-R_c)/R_c
Current Strain = $\varepsilon_c/(\varepsilon_c+1)$
$\varnothing'_{cv}$ = 30 deg

The calculations and plot for this test are shown in Figure E.3. From linear regression results, the slope of the line was 0.8069.

Manassero's relationship is as follows :

$\varnothing'$ = ASIN(slope/(1+(slope-1)*SIN$\varnothing'_{cv}$)

= 63.5 deg

Undrained Shear Strength

The average limit pressure and interpreted total horizontal pressure at each test depth were used in analysis. Baguelin et al. (1978) suggested that, based on cavity expansion theory, the PMT can be used to evaluate S_u at the limit pressure by the following relationship -

$$S_u = (P_L - P_o)/N_p$$

where P_L = Limit Pressure
P_o = Total Horizontal Earth Pressure
$N_p = 1+\ln(E_{pmt}/3S_u)$
Typical values of N_p : 5 - 12

Through trial and error, an N_p = 10 gave the best agreement with the average triaxial value.

Example : Depth = 2 meters, average P_L = 860 kPa and average P_o = 79 kPa
Therefore, using N_p =11, S_u = 78.1 kPa

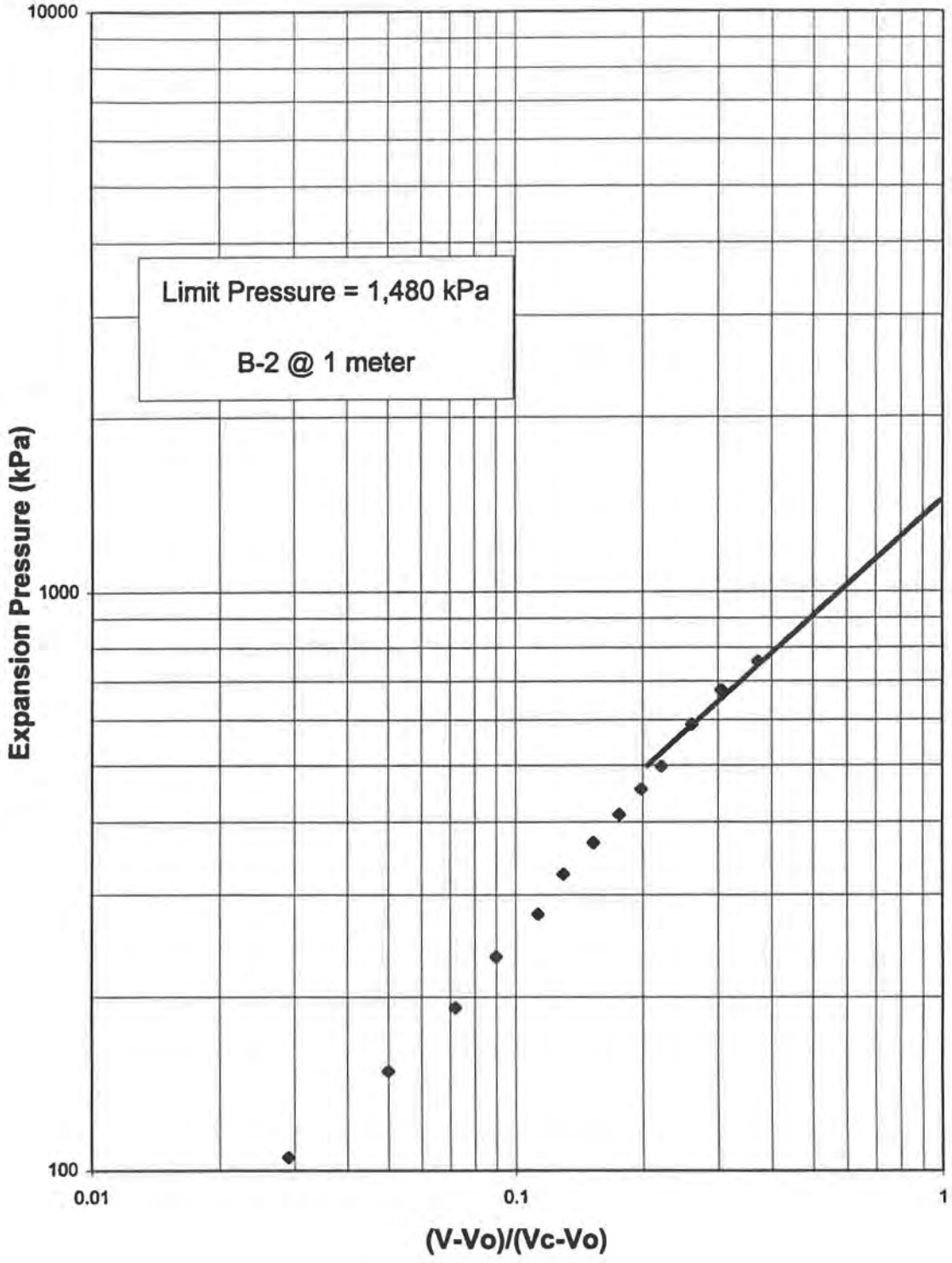

FIG. E.1. - PMT Limit Pressure Example.

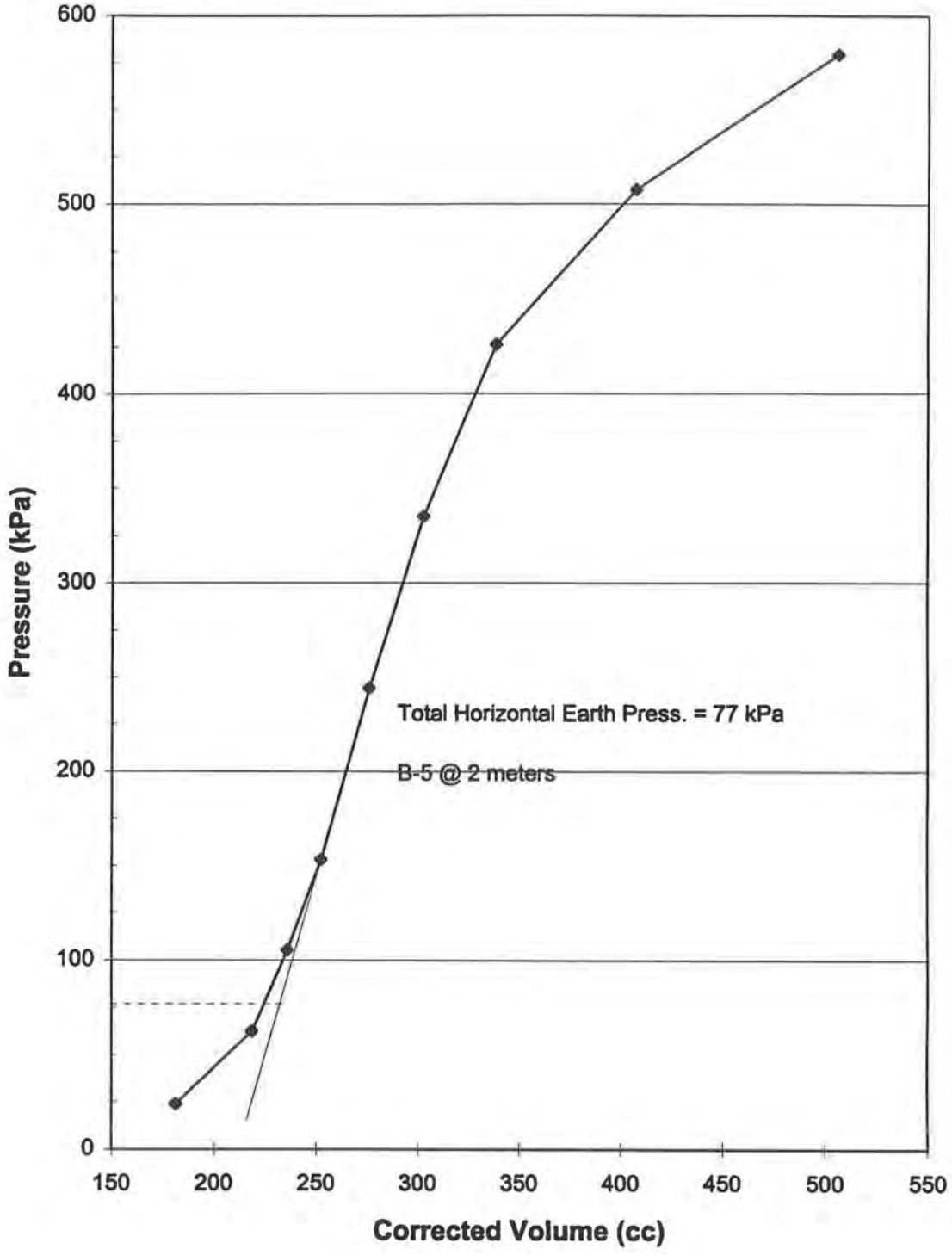

FIG. E.2. - Example of Total Horizontal Earth Pressure Interpretation.

Boring B-2

1 meter Volume (cc)	probe radius (cm)	Cavity Strain	Current Strain	Natural Log Curr. Strain	Pressure (kPa)	Effective Pressure (kPa)	Natural Log Eff. Press
116.7	3.7502				9.58		
172.4	3.8637				19.15		
191.8	3.9024	0.0060	0.0060	-5.1163	62.24	62.24	4.13
208.2	3.9349	0.0144	0.0142	-4.2547	105.34	105.34	4.66
228.6	3.9749	0.0247	0.0241	-3.7247	148.43	148.43	5.00
250	4.0164	0.0354	0.0342	-3.3752	191.52	191.52	5.25
267.4	4.0499	0.0440	0.0422	-3.1656	234.61	234.61	5.46
289.8	4.0925	0.0551	0.0522	-2.9531	277.70	277.70	5.63
306.2	4.1235	0.0630	0.0593	-2.8252	325.58	325.58	5.79
328.6	4.1654	0.0738	0.0688	-2.6771	368.68	368.68	5.91
351	4.2069	0.0845	0.0779	-2.5517	411.77	411.77	6.02
372.8	4.2469	0.0948	0.0866	-2.4461	454.86	454.86	6.12
394.6	4.2865	0.1051	0.0951	-2.3531	497.95	497.95	6.21
433.2	4.3558	0.1229	0.1095	-2.2121	588.92	588.92	6.38
476.8	4.4328	0.1428	0.1249	-2.0800	675.11	675.11	6.51
541.4	4.5444	0.1715	0.1464	-1.9213	756.50	756.50	6.63

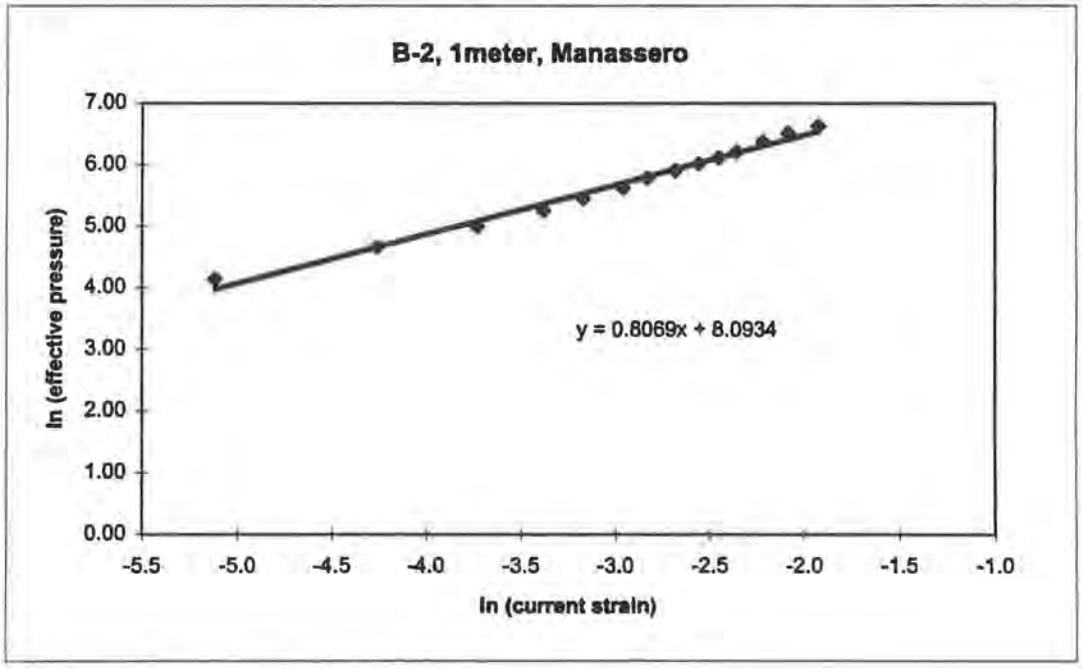

FIG E.3. - Manassero Correlation Example

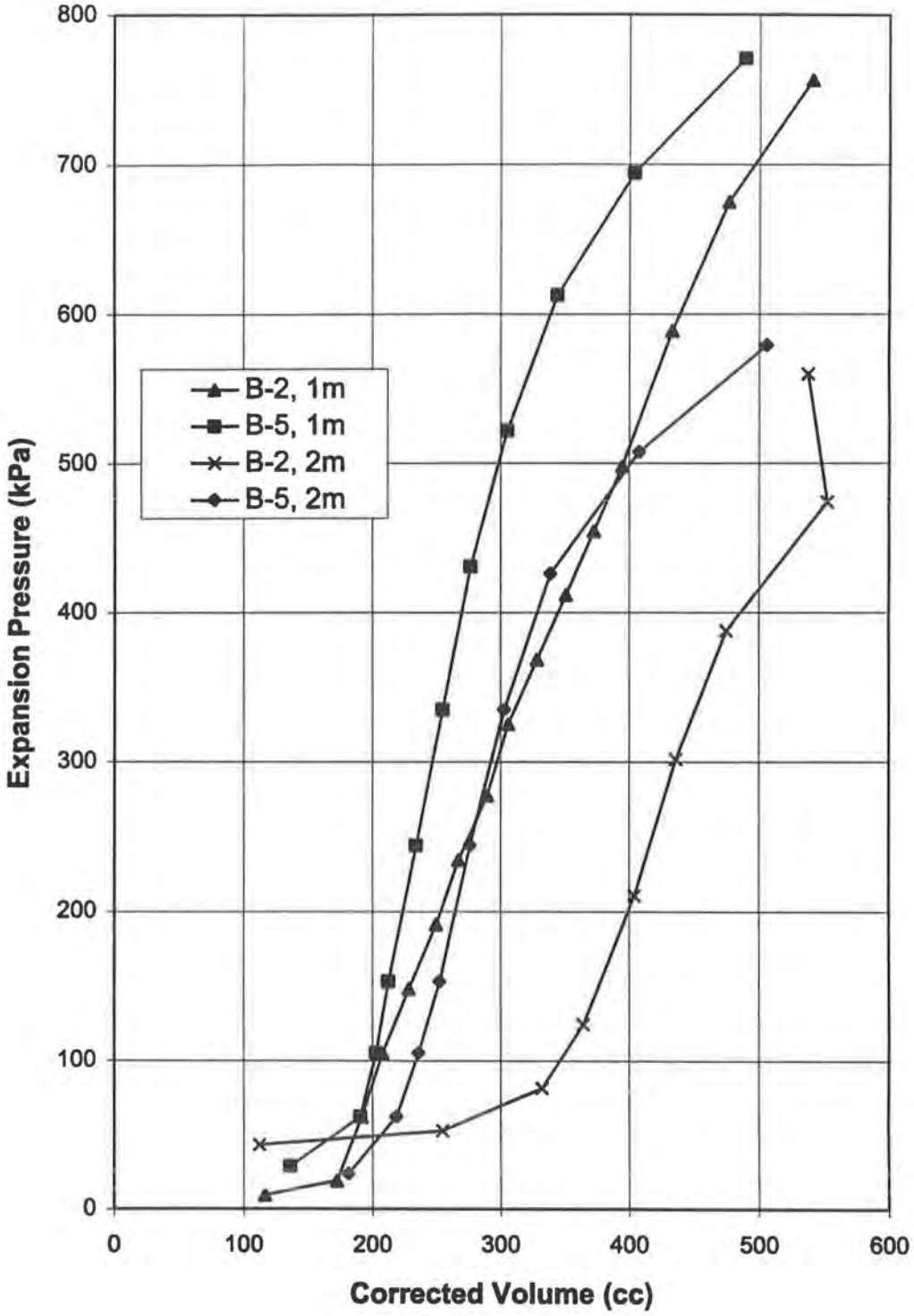

FIG. E.4. - PMT Curves : Depth 1 - 2 m

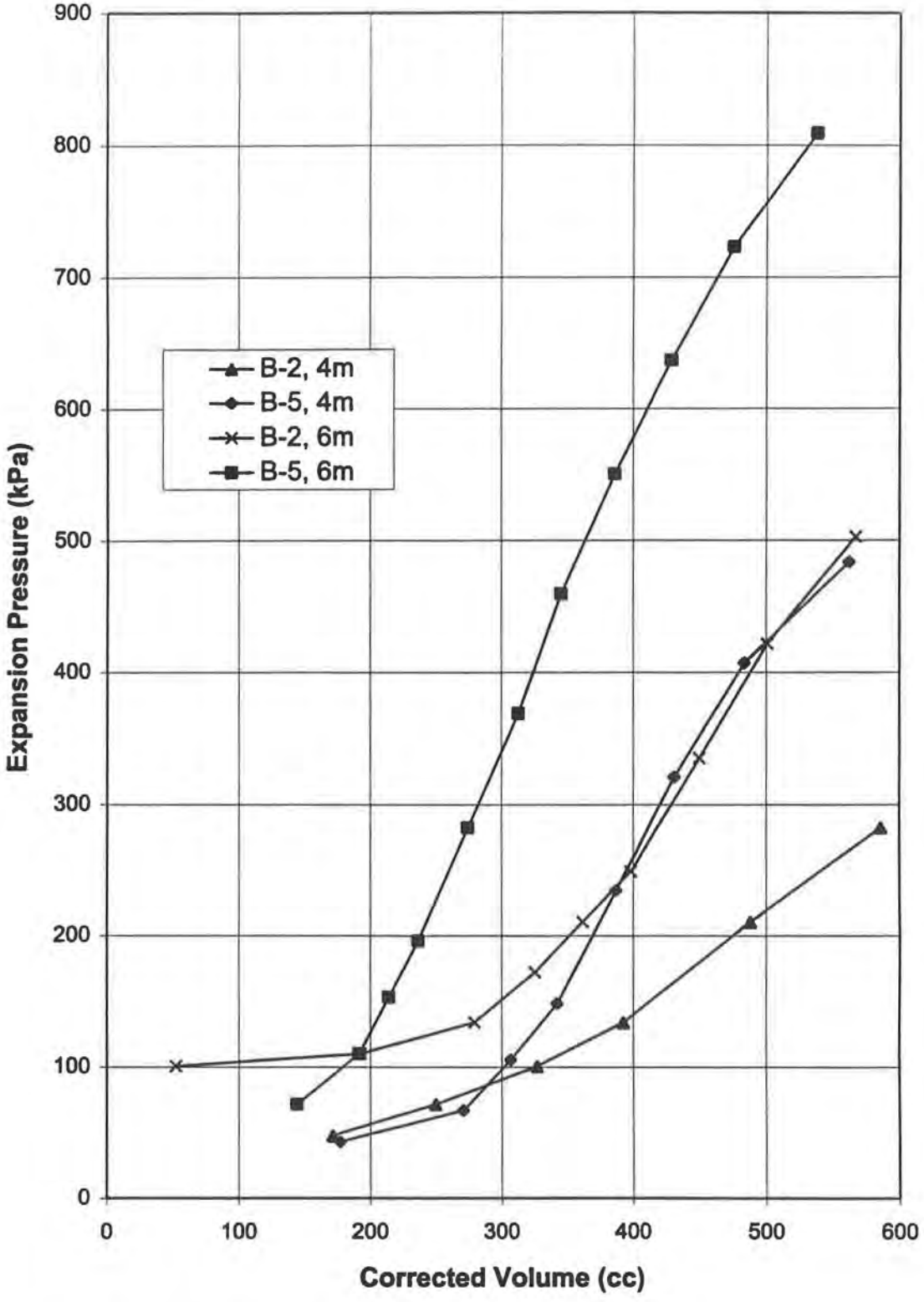

FIG. E.5. - PMT Curves : Depth 4 - 6 m.

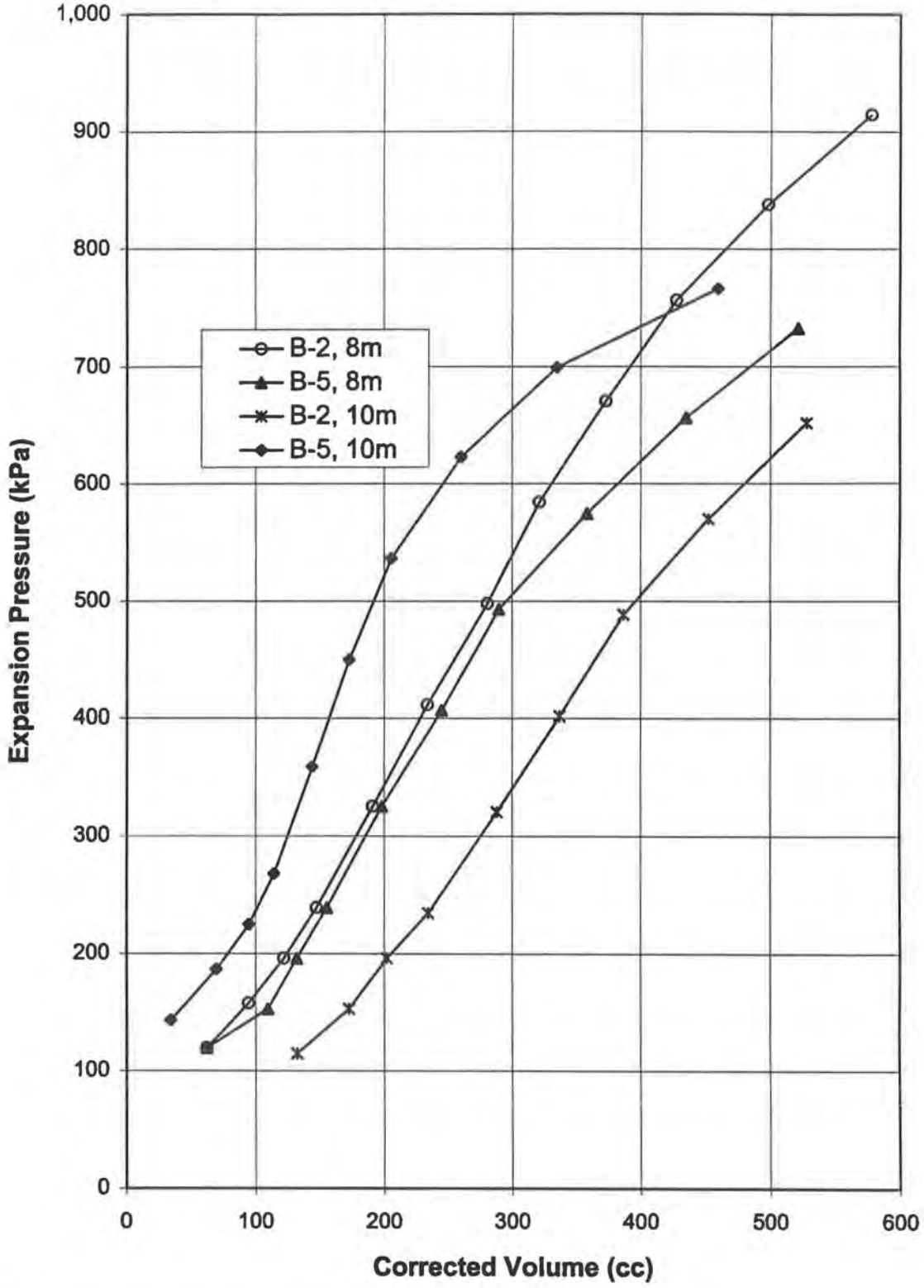

FIG. E.6. - PMT Curves : Depth 8 -10 m

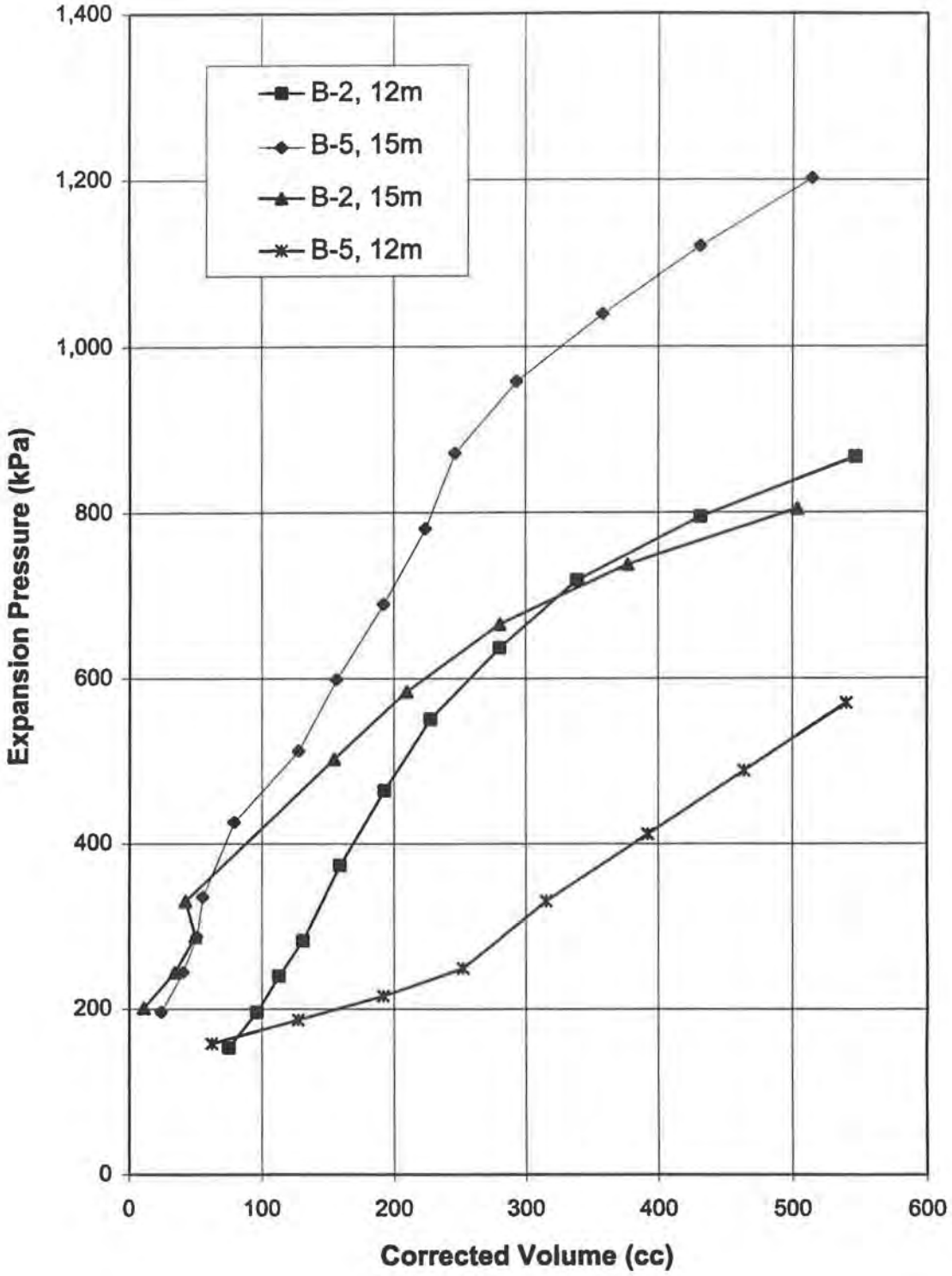

FIG. E.7. - PMT Curves : Depth 12 - 15 m.

APPENDIX F

SEISMIC FLAT DILATOMETER RESULTS

General

1. When using correlations to predict an overall property, the conventional dilatometer (DMT) value(s) used in the correlation was averaged over the three DMT locations at each test depth before using the correlation.

2. The shear wave velocity and small strain shear modulus were based on seismic dilatometer (SDMT) locations AU1 and AU2. AU3 produced suspect results because the receiver became loose upon extraction of probe from AU2 and could not be repositioned as for the other two test locations.

3. The A and B pressure readings were made in units of [bars].

4. An average wet unit weight value of 18.25 kN/m^3 was used in all calculations; all correlations or corrections are in accordance to Marchetti (1980) unless otherwise noted.

5. The thesis of Gina Kates (1996) should be consulted for further explanation on testing procedures or data reduction.

Equipment

- conventional flat Marchetti dilatometer : blade # GB-97
- receiver geophone : Geospace type 14 model L9 with a natural frequency of 28 Hz and intrinsic voltage sensitivity of 0.236 volts/cm/sec
- trigger geophone : Mark Products model L-15A with natural frequency of 14 Hz and power sensitivity of 0.87 mw/cm/sec
- oscilloscope : Hewlett Packard model 54601A

Procedure

1. Trigger geophone placed in notched section of wooden board and coupled to it with an O-ring; board placed under drill rig tire to insure good soil-to-source contact.

2. Conventional DMT testing procedure was conducted at various depths after being hydraulically pushed by wheel mounted drill rig.

3. Upon completion of a traditional DMT at a given depth, while another push rod was added, a sledge hammer was used to strike the horizontally positioned plank which was aligned perpendicular to the path to source in order to minimize compression wave interference.

4. The trigger geophone in plank used to signal start time of impulse, and receiver geophone, monitored by oscilloscope, signals shear wave arrival.

5. Travel time waves taken as difference between initial responses of each receiver from oscilloscope.

Data Reduction : Conventional Dilatometer

Pressure Reading Corrections

$p_o = 1.05(A + \Delta A)-0.05(B-\Delta B)-Zm$ = Lift-Off Pressure

$p_1 = B-\Delta B-Zm$ = Expansion Pressure

where A & B : pressure readings taken during testing

ΔA & ΔB : calibrations for membrane stiffness in air due to vacuum and inflation

Zm : zero offset of the pressure gauge

Example : Test AU1, Depth = 0.3 meters, A = 3.7 bars, B = 8.8 bars, ΔA = 0.12 bars, ΔB = 0.54 bars, Zm = 0

$p_o = 1.05(3.7+0.12)-0.05(8.8-0.54)-0 =$ 3.6 bars

$p_1 = 8.8 - 0.54 - 0 =$ 8.26 bars

Dilatometer Indices

Material Index : $I_D = (p_1 - p_o)/(p_o - u_o)$

Dilatometer Modulus : $E_D = 34.7(p_1 - p_o)$

Horizontal Stress Index : $K_D = (p_o - u_o)$/Effective Overburden

Example : Test AU1, Depth = 0.3 meters, p_o = 3.6 bars, p_1 = 8.2 bars, u_o = 0, Effective Overburden = 0.05 bars

$I_D = (p_1 - p_o)/(p_o - u_o) = (8.2-3.6)/(3.6-0) =$ 1.28

$E_D = 34.7(p_1 - p_o) = 34.7(8.2-3.6) =$ 159.6 bars

$K_D = (p_o - u_o)$/Effective Overburden = (3.6-0)/0.055 = 65.5

Young's, Shear and Constrained Modulus from DMT Modulus

E_D converted to Young's Modulus and then shear modulus by elastic theory relationships. Poisson's ratio of 0.3 was assumed for calculations.

Example : Test AU1, Depth = 0.3 meters, $E_D =$ 159.6 bars

$E = E_D / (1 - \nu^2) = 159.6/(1-0.3^2) =$ 175.4 bars = 17,540 kPa

$G = E / (2*(1+\nu)) = 175.4/(2(1+0.3)) =$ 67.5 bars = 6,750 kPa

Constrained Modulus = $M = R_m * E_D$

For soils where I_D falls between 0.6 and 3.0, use $R_m = R_m' + (2.5-R_m')\log K_D$ where $R_m' = 0.14+0.15*(I_D -0.6)$. All I_D values fell into this range.

$R_m' = 0.14+0.15(1.28-0.6) = 0.242$

$R_m' = 0.242 + (2.5-0.242)\log(65.5) = 4.36$

$M = 4.36*159.6 =$ 694 bars = 69,600 kPa

At-Rest Coefficient of Horizontal Soil Stress

Schmertmann (1983) :

$$K_o' = \frac{[40+23K_D-86K_D(1-\sin\varnothing')+152(1-\sin\varnothing')-717(1-\sin\varnothing')^2]}{[192-717(1-\sin\varnothing')]}$$

Developed for soils with a soil index (I_D) greater than 1.2.

Example : Depth = 0.3 meters, Avg. K_D=67.33,
Effective Friction Angle above 4 meter depth assumed to be equal to 31 degrees; avg. effective friction angle between 4 meters and 15 meters is 31 degrees.

Therefore, K_o' = 8.44

Marchetti (1985) : $K_o' = 0.359 + 0.071\ K_D - 0.00093(q_c/P_o')$

Based on DMT and CPT measurements in chamber tests on sand. Relationship also was modified to account for measurements made in the field.

Example : Depth = 0.3 meters, Avg. K_D = 67.33, avg. q_c = 1,513 kPa, P_o' = Effective Vertical Overburden = 5.5 kPa

Therefore, K_o' = 4.88

Marchetti (1980) : $K_o' = (K_D/1.5)^{0.47}-0.6$

Based on 8 insensitive Italian clays and 2 uncemented NC sands.

Example : Test AU1, Depth = 0.3 meters, K_D = 65.5

Therefore, $K_o' = (65.5/1.5)^{0.47}-0.6$ = 5.35

Mayne and Kulhawy (1990) : $K_o' = 0.27\ K_D$

Based on best fit linear regressions of 56 SBPMT sites of intact and fissured clays which were correlated with CPT with pore pressure measurements and DMT.

Example : Depth = 0.3 meters, Avg. $K_D = 67.33$

Therefore, $K_o' = 0.27(67.33) = \underline{18.18}$

Effective Preconsolidation Pressure and Overconsolidation Ratio

Mayne & Kulhawy (1990) : $\sigma_P' = 0.509*(p_o - u_o)$

Based on statistical analysis of 24 intact clays.

Example : Test AU1, Depth = 0.3 meters, $p_o = 3.6$ bars, $p_i = 8.2$ bars, $u_o = 0$

$\sigma_P' = 0.509*(3.6 - 0) = \underline{1.83 \text{ bars}}$

Therefore, using computed effective overburden pressure and above preconsolidation pressure, OCR can be computed.

$OCR* = 1.83/0.055 = \underline{33.32}$

OCR can also be predicted by the Marchetti (1980) relationship for soils with I_D less than 1.2; most readings were below this boundary limit.

$OCR = (0.5* K_D)^{1.56}$

$= (0.5*65.5)^{1.56} = \underline{230.8}$

Effective Friction Angle

Campanella and Robertson (1991) : $\varnothing' = 37.3[(K_D-0.8)/(K_o'+0.8)]^{0.082}$

K_o' by Marchetti (1980), which is based on cohesive soils, is suggested for use with correlation.

Example : Depth = 0.3 meters, Avg $K_D = 67.33$

Therefore, $K_o' = (67.33/1.5)^{0.47}-0.6 = 5.38$ and

$\varnothing' = 37.3[(67.33-0.8)/(5.38+0.8)]^{0.082} =$ 45.3 degrees

Undrained Shear Strength

Marchetti (1980) : $S_u = P_o'(0.22)(0.5\ K_D)^{1.25}$

Based on Italian clays with $I_D < 1.2$; however, others, such as Schmertmann (1988), suggest limiting I_D to less than 0.6.

Example : Test AU1, Depth = 0.3 meters, $P_o' = 5.5$ kPa, $K_D = 65.5$

Therefore, $S_u = (5.5)(0.22)(0.5(65.5))^{1.25}$

$=$ 0.947 bars $=$ 94.7 kPa

Soil Type & Classification

From Marchetti (1980) and based on 8 Italian clays and 2 sands. Soil type picked from range of soil index values for different soil types.

Example : Test AU1, Depth = 0.3 meters, $I_D = 1.28$

Therefore, "Sandy Silt" since soil index greater than 1.2 boundary value.

Data Reduction : Seismic Dilatometer

Shear Wave Velocity

Shear wave first arrival times for each test depth were measured. The distance between the receiver and the source were also determined. Therefore, the difference between two arrival times gave a pseudo-time interval for that range of soil between test depths. Arrival times of shear waves were interpreted; several trials were performed at each depth to insure consistent results but only one was interpreted..

Peak Particle Velocity

Particle Velocity = Amplitude/Output

Example : Location AU2, Depth = 0.175 meters

Particle Velocity = (0.4641 V) / (0.62 V/in/sec) / ((12 in/ft)*(3.28 ft/m))

= 0.019 m/s

Shear Strain

Shear Strain = Particle Velocity/Shear Velocity

Example : Location AU2, Depth = 0.175 meters, Vs = 210.8 m/s

Shear Strain =((0.019 m/s) / (210.8 m/s))*100 = 0.00902 %

Shear Modulus

Shear Modulus = $G = \rho V_s^2$

All calculations used a constant soil density over depth of 1.86 kg/m^3.

Example : Location AU2, Depth = 0.175 meters, Vs = 210.8 m/s

$G = 1.86(210.8)^2$

= 82.650 kPa

Table F.1. - DMT Results Summary : AU1.

GEORGIA INSTITUTE OF TECHNOLOGY
TEST #: AU1
LOCATION: Opelika, Alabama
DATE: 8/22/96
OPERATOR: Gina Kates

CALIBRATION INFORMATION:
BLADE #: GB-97
ΔAavg = 0.12 bars
ΔBavg = 0.54 bars
GWT Depth= 2.44 m
Zm = 0

Z (M)	A (BAR)	B (BAR)	P_0 (BAR)	P_1 (BAR)	Uo (BAR)	γ (kN/M^3)	K_D	I_D	E_D (BAR)	K_c	Sα (bars)	σvo' (BAR)	P_{ef} (BAR)	OCR	OCR*	E (BAR)	G (BAR)	M (BAR)	SOIL TYPE
0.3	3.7	8.8	3.6	8.2	0	18.25	65.5	1.28	159.6	5.30	0.947	0.055	1.83	230.8	33.32	175.41	67.5	694	SANDY SILT
0.6	7.5	16.2	7.22	15.6	0	18.25	65.6	1.16	290.8	5.31	1.901	0.110	3.67	231.8	33.41	319.55	122.9	1,269	SILT
0.9	7.6	15.6	7.36	15	0	18.25	44.9	1.04	265.1	4.34	1.762	0.164	3.75	128.1	22.84	291.33	112.0	1,060	SILT
1.2	7.7	15.8	7.45	15.2	0	18.25	34.0	1.04	268.9	3.74	1.664	0.219	3.79	83.2	17.32	295.52	113.7	1,001	SILT
1.5	6.1	12.85	5.92	12.25	0	18.25	21.6	1.07	219.7	2.90	1.161	0.274	3.01	41.0	11.00	241.37	92.8	718	SILT
1.8	6.35	12.3	6.21	11.7	0	18.25	16.9	0.88	190.5	2.69	1.197	0.329	3.16	33.2	9.61	209.34	80.5	598	CLAYEY SILT
2.1	4.7	10.2	4.58	9.6	0	18.25	9.7	1.10	174.2	1.80	0.748	0.472	2.33	11.7	4.94	191.42	73.6	430	SILT
2.4	4.7	9.65	4.61	9.05	0	18.25	9.3	0.96	154.1	1.75	0.744	0.497	2.35	11.0	4.72	169.31	65.1	374	SILT
2.7	3.95	7.7	3.92	7.1	0.026	18.25	7.5	0.82	110.3	1.53	0.595	0.522	1.98	7.8	3.80	121.26	46.6	243	CLAYEY SILT
3	3.7	7.65	3.66	7.05	0.055	18.25	6.6	0.94	117.6	1.40	0.534	0.548	1.83	6.4	3.35	129.27	49.7	245	SILT
3.3	4.4	9.4	4.31	8.8	0.084	18.25	7.4	1.06	155.8	1.51	0.644	0.573	2.15	7.7	3.75	171.21	65.9	342	SILT
3.6	3.75	6.75	3.76	6.15	0.114	18.25	6.1	0.66	82.9	1.33	0.530	0.598	1.86	5.7	3.10	91.14	35.1	165	CLAYEY SILT
3.9	3.4	6.5	3.4	5.9	0.143	18.25	5.2	0.77	86.8	1.20	0.456	0.623	1.66	4.5	2.66	95.33	36.7	160	CLAYEY SILT
4.2	3.5	6.75	3.49	6.15	0.173	18.25	5.1	0.80	92.3	1.18	0.461	0.649	1.69	4.3	2.60	101.43	39.0	168	CLAYEY SILT
4.5	3.95	7.85	3.91	7.25	0.202	18.25	5.5	0.90	115.9	1.24	0.525	0.674	1.89	4.8	2.80	127.36	49.0	220	SILT
4.8	4.45	9.8	4.34	9.2	0.232	18.25	5.9	1.18	168.6	1.30	0.592	0.699	2.09	5.4	2.99	185.32	71.3	333	SILT
5.1	4.7	10.4	4.57	9.8	0.261	18.25	5.9	1.21	181.5	1.31	0.622	0.725	2.19	5.5	3.03	199.43	76.7	360	SANDY SILT
5.4	4.3	9.8	4.18	9.2	0.29	18.25	5.2	1.29	174.2	1.19	0.543	0.750	1.98	4.4	2.64	191.42	73.6	323	SANDY SILT
5.7	7	15.6	6.73	15	0.32	18.25	8.3	1.29	287.0	1.63	1.006	0.775	3.26	9.2	4.21	315.35	121.3	664	SANDY SILT
6	5.4	11.2	5.27	10.6	0.349	18.25	6.1	1.08	185.0	1.34	0.717	0.801	2.50	5.8	3.13	203.24	78.2	373	SILT
6.3	3.8	11	3.6	10.4	0.379	18.25	3.9	2.11	236.0	0.97	0.419	0.826	1.64	2.8	1.98	259.30	99.7	383	SILTY SAND
6.6	4.35	8.8	4.28	8.2	0.408	18.25	4.5	1.01	136.0	1.08	0.523	0.851	1.97	3.6	2.32	149.48	57.5	233	SILT
6.9	5.3	11.3	5.16	10.7	0.438	18.25	5.4	1.17	192.2	1.22	0.665	0.877	2.40	4.7	2.74	211.25	81.3	363	SILT
7.2	6.1	17.05	5.71	16.45	0.467	18.25	5.8	2.05	372.7	1.29	0.753	0.902	2.67	5.3	2.96	409.54	157.5	742	SILTY SAND

Table F.2. - DMT Results Summary : AU2.

GEORGIA INSTITUTE OF TECHNOLOGY

TEST #: AU2

LOCATION: Opelika, Alabama

DATE: 8/22/96

OPERATOR: Gina Kates

CALIBRATION INFORMATION:

BLADE #: GB-97 Zm = 0

DAavg = 0.16 bars

DBavg = 0.62 bars

GWT Depth= 2.44 m

Z (M)	A (BAR)	B (BAR)	P_o (BAR)	P_1 (BAR)	Uo (BAR)	γ (kN/M^3)	K_D	I_D	E_D (BAR)	K_o	Su (bars)	σvo' (BAR)	P_o' (BAR)	OCR	OCR*	E (BAR)	G (BAR)	M (BAR)	SOIL TYPE
0.3	2.7	8.7	2.6	8.08	0	18.25	47.3	2.11	190.2	4.46	0.63	0.055	1.32	138.9	24.06	209.0	80.4	751	SILTY SAND
0.6	4.9	10.1	4.84	9.48	0	18.25	44.0	0.96	161.0	4.29	1.15	0.110	2.46	124.2	22.40	176.9	68.1	642	SILT
1.2	5.1	11.4	4.98	10.78	0	18.25	22.7	1.16	201.3	2.99	1.01	0.219	2.53	44.4	11.57	221.2	85.1	667	SILT
1.5	4.1	9.4	4.03	8.78	0	18.25	14.7	1.18	164.8	2.32	0.73	0.274	2.05	22.5	7.49	181.1	69.7	475	SILT
1.8	3.7	8.25	3.67	7.63	0	18.25	11.2	1.08	137.4	1.97	0.62	0.329	1.87	14.6	5.68	151.0	58.1	358	SILT
2.1	3.8	8.15	3.78	7.53	0	18.25	8.0	0.99	130.1	1.60	0.59	0.472	1.92	8.7	4.08	143.0	55.0	296	SILT
2.4	3.8	8.05	3.79	7.43	0	18.25	7.6	0.96	126.3	1.55	0.58	0.497	1.93	8.1	3.88	138.8	53.4	281	SILT
2.7	3.6	7.35	3.61	6.73	0.026	18.25	6.9	0.87	108.3	1.44	0.54	0.522	1.82	6.8	3.49	119.0	45.8	230	CLAYEY SILT
3	3.3	6.95	3.32	6.33	0.055	18.25	6.0	0.92	104.4	1.31	0.47	0.548	1.66	5.5	3.03	114.8	44.1	207	SILT
3.3	2.85	6.7	2.86	6.08	0.084	18.25	4.8	1.16	111.7	1.14	0.38	0.573	1.41	4.0	2.47	122.8	47.2	199	SILT
3.6	3.55	7.25	3.56	6.63	0.114	18.25	5.8	0.89	106.5	1.28	0.49	0.598	1.75	5.2	2.93	117.1	45.0	207	CLAYEY SILT
3.9	4.7	8.4	4.71	7.78	0.143	18.25	7.3	0.67	106.5	1.51	0.70	0.623	2.32	7.6	3.73	117.1	45.0	233	CLAYEY SILT
4.2	3.95	7.55	3.97	6.93	0.173	18.25	5.9	0.78	102.7	1.30	0.55	0.649	1.93	5.3	2.98	112.9	43.4	201	CLAYEY SILT
4.5	4.4	8.45	4.4	7.83	0.202	18.25	6.2	0.82	119.0	1.35	0.61	0.674	2.14	5.9	3.17	130.8	50.3	241	CLAYEY SILT
4.8	3.65	7.25	3.67	6.63	0.232	18.25	4.9	0.86	102.7	1.15	0.47	0.699	1.75	4.1	2.50	112.9	43.4	183	CLAYEY SILT
5.1	3.7	7.25	3.72	6.63	0.261	18.25	4.8	0.84	101.0	1.12	0.47	0.725	1.76	3.9	2.43	111.0	42.7	177	CLAYEY SILT
5.4	3.7	6.9	3.74	6.28	0.29	18.25	4.6	0.74	88.1	1.09	0.47	0.750	1.76	3.7	2.34	96.9	37.3	151	CLAYEY SILT
5.7	4.05	8.85	4.01	8.23	0.32	18.25	4.8	1.14	146.4	1.12	0.50	0.775	1.88	3.9	2.42	160.9	61.9	258	SILT
6	4.25	9.5	4.19	8.88	0.349	18.25	4.8	1.22	162.7	1.13	0.53	0.801	1.96	3.9	2.44	178.8	68.8	289	SANDY SILT
6.3	4.15	8.6	4.13	7.98	0.379	18.25	4.5	1.03	133.6	1.08	0.51	0.826	1.91	3.6	2.31	146.8	56.5	229	SILT
6.6	4.8	9.95	4.74	9.33	0.408	18.25	5.1	1.06	159.3	1.18	0.60	0.851	2.20	4.3	2.59	175.0	67.3	291	SILT
6.9	5	9.8	4.96	9.18	0.438	18.25	5.2	0.93	146.4	1.19	0.63	0.877	2.30	4.4	2.62	160.9	61.9	269	SILT
7.2	6.05	11.5	5.98	10.88	0.467	18.25	6.1	0.89	170.0	1.34	0.80	0.902	2.81	5.7	3.11	186.8	71.9	341	CLAYEY SILT
7.5	5.85	12.5	5.72	11.88	0.497	18.25	5.6	1.18	213.8	1.26	0.74	0.927	2.66	5.0	2.87	234.9	90.3	413	SILT
7.8	4.55	11.8	4.39	11.18	0.526	18.25	4.1	1.76	235.6	1.00	0.51	0.953	1.97	3.0	2.06	258.9	99.6	386	SANDY SILT
8.1	7.25	21.25	6.75	20.63	0.555	18.25	6.3	2.24	481.6	1.37	0.91	0.978	3.15	6.0	3.22	529.3	203.6	1001	SILTY SAND

GEORGIA INSTITUTE OF TECHNOLOGY
TEST #: AU3
LOCATION: Opelika, Alabama
DATE: 8/22/1996
OPERATOR : Gina Kates

CALIBRATION INFORMATION:
BLADE #: GB-97 Zm = 0
DAavg = 0.17 bars
DBavg = 0.7 bars
GWT Depth= 2.44

Z (M)	A (BAR)	B (BAR)	P_o (BAR)	P_1 (BAR)	Uo (BAR)	γ (kN/M^3)	K_D	I_D	E_D (BAR)	K_c	Su (bars)	σvo' (BAR)	P_o' (BAR)	OCR	OCR'	E (BAR)	G (BAR)	M (BAR)	SOIL TYPE
0.3	5.1	13.2	4.91	12.5	0	1.95	89.3	1.55	263.4	6.22	1.40	0.055	2.50	374.6	45.4	289.4	111.3	1,216	SANDY SILT
0.6	5.8	14.8	5.56	14.1	0	1.95	50.5	1.54	296.3	4.62	1.37	0.110	2.83	154.2	25.7	325.6	125.2	1,206	SANDY SILT
0.9	6.7	16.8	6.41	16.1	0	1.95	39.1	1.51	336.2	4.03	1.48	0.164	3.26	103.3	19.9	369.5	142.1	1,285	SANDY SILT
1.2	8	16.4	7.79	15.7	0	1.95	35.6	1.02	274.5	3.83	1.76	0.219	3.97	89.1	18.1	301.6	116.0	1,034	SILT
1.5	6.9	14.5	6.73	13.8	0	1.95	24.6	1.05	245.3	3.12	1.39	0.274	3.43	50.0	12.5	269.6	103.7	833	SILT
1.8	5.4	11.4	5.31	10.7	0	1.8	16.1	1.02	187.0	2.45	0.98	0.329	2.70	26.0	8.2	205.5	79.1	557	SILT
2.1	4.8	9.5	4.78	8.8	0	1.8	10.1	0.84	139.5	1.85	0.79	0.472	2.43	12.6	5.2	153.3	59.0	351	CLAYEY SILT
2.4	4.1	7.95	4.12	7.25	0	1.8	8.3	0.76	108.6	1.63	0.65	0.497	2.10	9.2	4.2	119.4	45.9	251	CLAYEY SILT
2.7	3.7	7.4	3.73	6.7	0.026	1.8	7.1	0.80	103.1	1.48	0.56	0.522	1.89	7.2	3.6	113.3	43.6	222	CLAYEY SILT
3	3.7	7.95	3.7	7.25	0.055	1.8	6.7	0.97	123.2	1.41	0.54	0.548	1.86	6.5	3.4	135.4	52.1	258	SILT
3.3	3.8	7.8	3.81	7.1	0.084	1.8	6.5	0.88	114.2	1.39	0.55	0.573	1.90	6.3	3.3	125.5	48.3	236	CLAYEY SILT
3.6	4.1	8.35	4.1	7.65	0.114	1.8	6.7	0.89	123.2	1.42	0.59	0.598	2.03	6.5	3.4	135.4	52.1	258	CLAYEY SILT
3.9	3.35	7.6	3.35	6.9	0.143	1.8	5.1	1.11	123.2	1.19	0.45	0.623	1.83	4.4	2.6	135.4	52.1	227	SILT
4.2	4.8	10.6	4.51	9.9	0.173	1.8	6.7	1.24	187.0	1.42	0.65	0.649	2.21	6.6	3.4	205.5	79.1	383	SANDY SILT
4.5	5.2	9.8	5.18	9.1	0.202	1.8	7.4	0.79	136.0	1.52	0.76	0.674	2.53	7.7	3.8	149.5	57.5	298	CLAYEY SILT
4.8	3.5	7.25	3.53	6.55	0.232	1.8	4.7	0.92	104.8	1.11	0.45	0.699	1.68	3.8	2.4	115.2	44.3	183	SILT
5.1	3.9	7.95	3.91	7.25	0.261	1.8	5.0	0.92	115.9	1.17	0.51	0.725	1.86	4.2	2.6	127.4	49.0	210	SILT
5.4	5.4	11.6	5.3	10.9	0.29	1.8	6.7	1.12	194.3	1.42	0.75	0.750	2.55	6.8	3.4	213.5	82.1	408	SILT
5.7	4.95	9.8	4.92	9.1	0.32	1.8	5.9	0.91	145.0	1.31	0.66	0.775	2.34	5.5	3.0	159.4	61.3	286	SILT
6	5.4	11	5.33	10.3	0.349	1.8	6.2	1.00	172.5	1.35	0.73	0.801	2.54	5.9	3.2	189.5	72.9	349	SILT
6.3	4.1	7.6	4.14	6.9	0.379	1.8	4.6	0.73	95.8	1.09	0.51	0.826	1.91	3.6	2.3	105.2	40.5	163	CLAYEY SILT
6.6	4.1	8.9	4.07	8.2	0.408	1.8	4.3	1.13	143.3	1.04	0.49	0.851	1.86	3.3	2.2	157.5	60.6	238	SILT
6.9	7.8	19.3	7.23	18.6	0.438	1.95	7.7	1.67	394.5	1.56	1.05	0.877	3.46	8.3	3.9	433.6	166.8	890	SANDY SILT
7.2	5.35	14.2	5.12	13.5	0.467	2	5.2	1.80	290.8	1.19	0.65	0.902	2.37	4.4	2.6	319.5	122.9	544	SILTY SAND
7.5	7.4	23	6.83	22.3	0.497	2	6.8	2.44	536.8	1.44	0.95	0.927	3.22	6.8	3.5	589.9	226.9	1,155	SILTY SAND

Table F.3. - DMT Results Summary : AU3.

DILATOMETER TEST				**SCHOOL OF CIVIL AND ENVIRONMENTAL ENGINEERING**	
DATE:	**8/22/1996**			**GEORGIA INSTITUTE OF TECHNOLOGY**	
LOCATION:	**Opelika, Alabama**				
ΔA=	0.1	bars	**TEST No:** **AU1**	**GWT:**	**2.44 m**
ΔB=	0.6	bars		**TESTED BY:**	**Gina Kates**

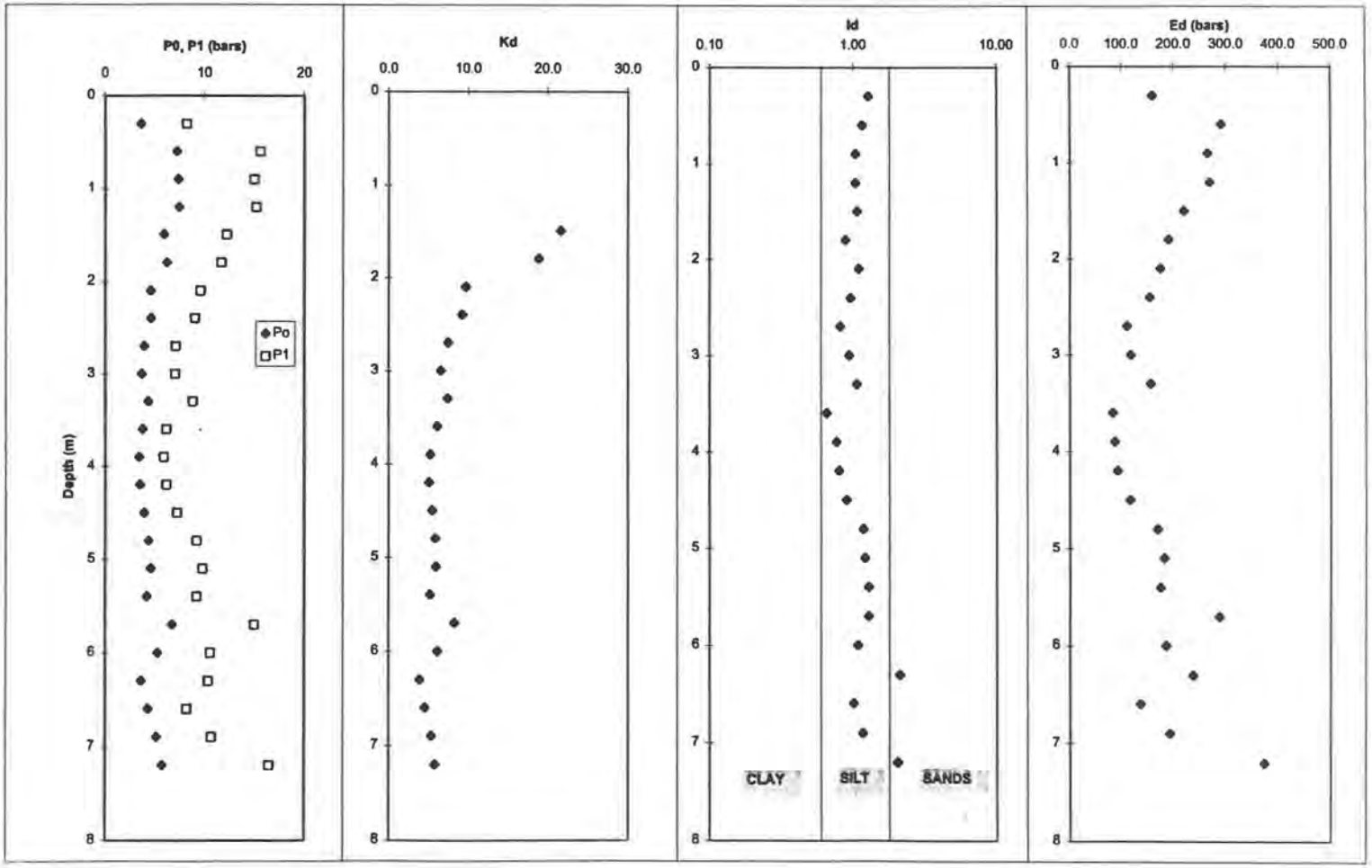

FIG. F.1. - DMT Results Summary : AU1.

DILATOMETER TEST					**SCHOOL OF CIVIL AND ENVIRONMENTAL ENGINEERING**	
DATE:	**8/22/1996**				**GEORGIA INSTITUTE OF TECHNOLOGY**	
LOCATION:	**Opelika, Alabama**					
ΔA=	0.16	bars	**TEST No:**	**AU2**	**GWT:**	**2.44 m**
ΔB=	0.62	bars			**TESTED BY:**	**Gina Kates**

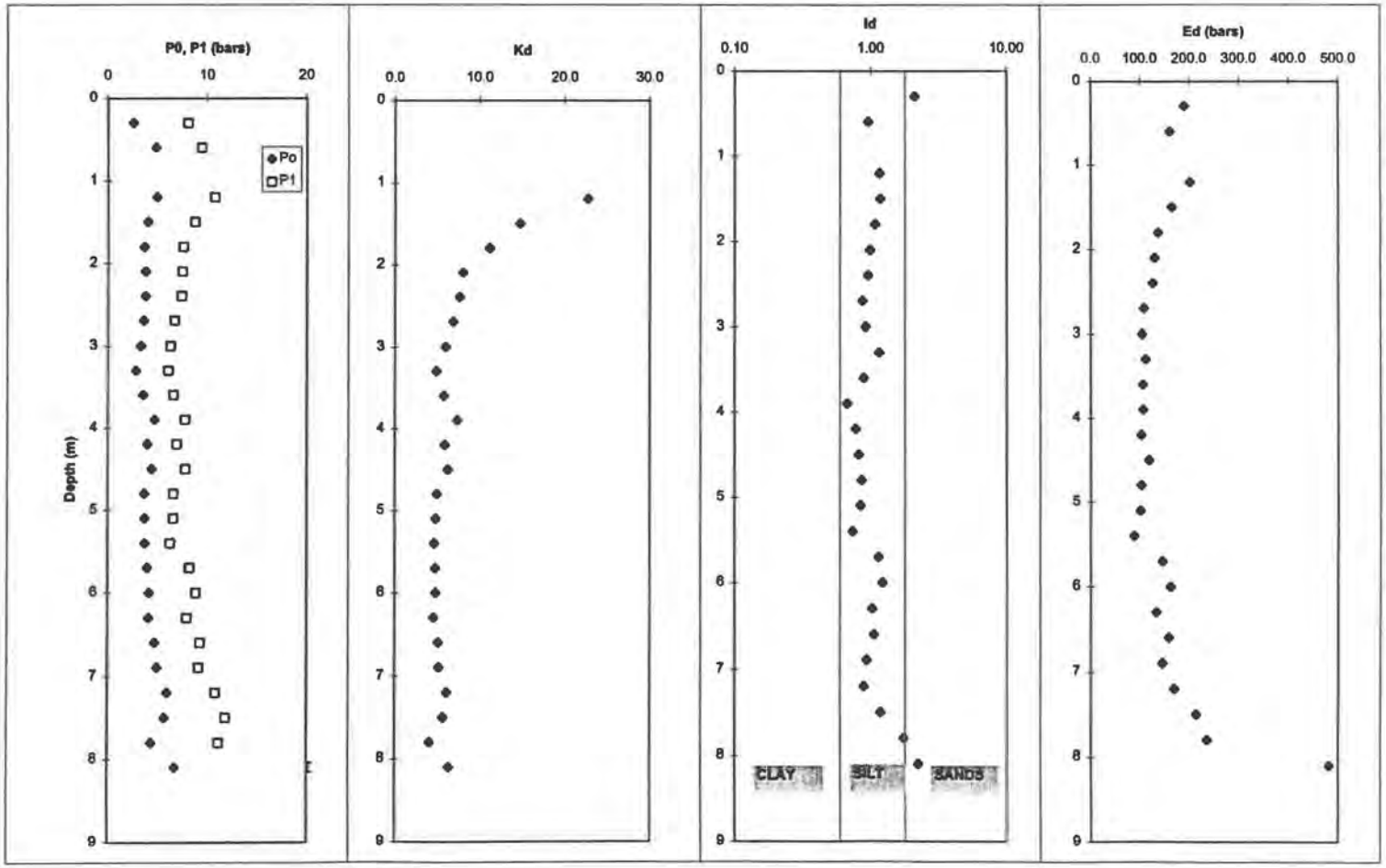

FIG. F.2. - DMT Results Summary : AU2.

FIG. F.3. - DMT Results Summary : AU3.

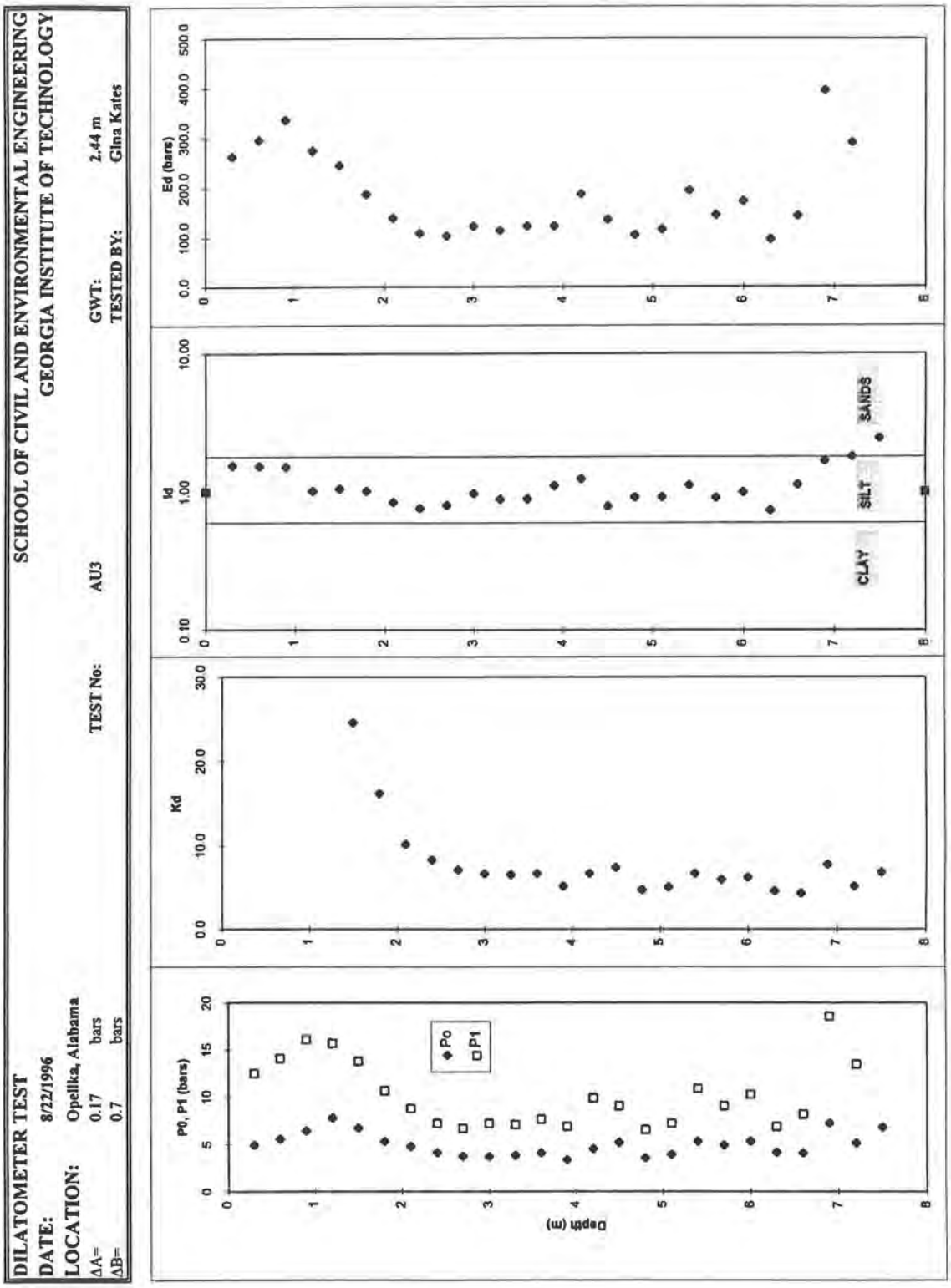

Table F.4. - Summary of SDMT Results : AU1

Depth (m)	Vs (m/s)	Amplitude (V)	Depth (m)	Frequency (hz)	Output (V/in/sec)	Particle Velocity (m/s)	Strain	Strain (%)	Gmax (MPa)
0.175	206.3	0.3681	0.175	82.70	0.66	0.014	6.87E-05	6.87E-03	79.16
0.8	214.4	0.181	0.8	76.34	0.67	0.007	3.20E-05	3.20E-03	85.50
1.7	228.1	0.1704	1.7	87.35	0.64	0.007	2.97E-05	2.97E-03	96.78
2.6	225	0.1579	2.6	74.59	0.64	0.006	2.79E-05	2.79E-03	94.16
3.5	177.2	0.1297	3.5	91.36	0.64	0.005	2.91E-05	2.91E-03	58.40
4.4	190.2	0.1203	4.4	74.10	0.68	0.004	2.36E-05	2.36E-03	67.29
5.3	188.9	0.1439	5.3	70.85	0.69	0.005	2.80E-05	2.80E-03	66.37
6.2	219.3	0.0855	6.2	91.23	0.64	0.003	1.55E-05	1.55E-03	89.45

Table F.5. - Summary of SDMT Results : AU2.

Depth (m)	Vs (m/s)	Amplitude (V)	Depth (m)	Frequency (hz)	Output (V/in/sec)	Particle Velocity (m/s)	Strain	Strain (%)	Gmax (MPa)
0.175	210.8	0.464	0.175	117.88	0.62	0.019	9.02E-05	9.02E-03	82.65
0.8	202.8	0.245	0.8	124.71	0.62	0.010	4.95E-05	4.95E-03	76.50
1.7	199.9	0.222	1.7	106.04	0.63	0.009	4.48E-05	4.48E-03	74.33
2.6	159.4	0.191	2.6	108.87	0.63	0.008	4.83E-05	4.83E-03	47.26
3.5	174.8	0.155	3.5	95.29	0.64	0.006	3.53E-05	3.53E-03	56.83
4.4	187	0.138	4.4	93.22	0.64	0.005	2.92E-05	2.92E-03	65.04
5.15	207.3	0.168	5.15	105.29	0.63	0.007	3.26E-05	3.26E-03	79.93
5.9	165.5	0.074	5.9	67.61	0.69	0.003	1.64E-05	1.64E-03	50.95
6.8	191.9	0.045	6.8	65.93	0.69	0.002	8.62E-06	8.62E-04	68.50
7.7	260.7	0.026	7.7	86.92	0.65	0.001	3.96E-06	3.96E-04	126.41

Table F.6. - Summary of SDMT Results : AU3.

Depth (m)	Vs (m/s)	Amplitud (V)	Depth (m)	Frequency (hz)	Output (V/in/sec)	Particle Velocity (m/s)	Strain	Strain (%)	Gmax (MPa)
0.18	274.5	0.471	0.18	95.16	0.64	0.019	6.817E-05	6.82E-03	140.10
0.8	185.9	0.428	0.8	94.78	0.64	0.017	9.131E-05	9.13E-03	64.24
1.7	255.4	0.384	1.7	146.26	0.62	0.016	6.161E-05	6.16E-03	121.33
2.6	252.1	0.362	2.6	110.92	0.62	0.015	5.886E-05	5.89E-03	118.22
3.5	241.5	0.214	3.5	125.86	0.62	0.009	3.633E-05	3.63E-03	108.49
4.4	240.1	0.199	4.4	92.03	0.64	0.008	3.285E-05	3.29E-03	107.23
5.15	171.3	0.110	5.15	112.85	0.62	0.005	2.638E-05	2.64E-03	54.59
5.9	231.5	0.087	5.9	113.78	0.62	0.004	1.538E-05	1.54E-03	99.69
6.8	285.4	0.066	6.8	106.75	0.63	0.003	9.27E-06	9.27E-04	151.47

APPENDIX G

IOWA BOREHOLE SHEAR TEST RESULTS

General

1. All tests were conducted as multistage tests with the standard 32.3 cm^2 shear plates as recommended by the "ASTM Suggested Method for Performing the Borehole Shear Test" presented in 1987.
2. Initial normal pressure and normal pressure increments were chosen based on the manufacturer's suggestion for a sandy/silty soil.
3. The uncorrected shear readings, readings corrected for the weight of the pull rods, normal pressure readings, individual failure envelopes, and any remarks for a specific test are shown on each test's individual data sheet.
4. The regression coefficient was found using the linear regression function in Microsoft Excel.
5. All tests conducted met the suggested minimum recommended regression coefficient of 0.95 which suggests that all the tests were probably valid.
6. All normal and shear pressures were read directly from gauges which were scaled to pounds per square inch.
7. A BST was planned for 12 m depth, but the tube sample fell out during extraction. This rendered the hole unacceptable for valid testing.

Data Reduction

Example :

Location : B-8, 7 meters -

Uncorrected Shear Gauge Reading = 2.4 psi

Pull Road Weight (Shear Gauge Reading Prior to Testing) = 1.2 psi

Corrected Shear Stress = 2.4 psi - 1.2 psi = 1.2 psi

Equipment

- Borehole Shear Tester (1988 model) from Handy Geotechnical Instruments Company, Inc.
- bottle of bone dry carbon dioxide gas used to expand shear head diaphrams
- standard shear plates (50.8 mm x 63.5 mm)
- 9.5 mm diameter, 0.8 m long pulling rods
- normal and shear pressure dial gauges factory calibrated to directly read pressure

Procedure

1. Hollow stem continuous flight auger used to advance hole to depth of interest.
2. Shelby tube sample taken below auger with auger remaining in place to case the hole.
3. Shear head lowered into cavity formed by Shelby tube sample.
4. First increment of normal pressure applied, and a consolidation time of approximately 10 minutes allowed.
5. Base plate positioned, and pull rods attached to hand crank mechanism during this time.
6. After consolidation time, hand crank turned at approximately 2 revolutions/second while observing shear stress gauge.
7. Once shear stress peaks and then decreases for approximately 40 turns, crank reversed until virtually no shear pressure applied.
8. Next increment of normal pressure applied, and consolidation time of 5 minutes allowed.
9. Steps 6.-8. Repeated until shear head was fully expanded or until a minimum of five good readings made.
10. Shear head removed, and teeth cleaned upon completion of testing at each test location.

Boring : B-8
Depth : 2 meters
Water Table Depth : 12 feet = 3.66 meters

Trial No.	1	2	3	4	5
Consolidation Time (minutes)	12	5	5	5	5
Normal Stress (psi)	5	8	11	14	17
Uncorrected Shear Stress (psi)	4.8	7.0	9.0	11.3	14.5
Tare (Pull Rods)	0	0	0	0	0
Corrected Shear Stress (psi)	4.8	7.0	9.0	11.3	14.5

Remarks : Shear stress very quickly reached a maximum value for each normal stress trial tested then remained constant for 40+ turns.

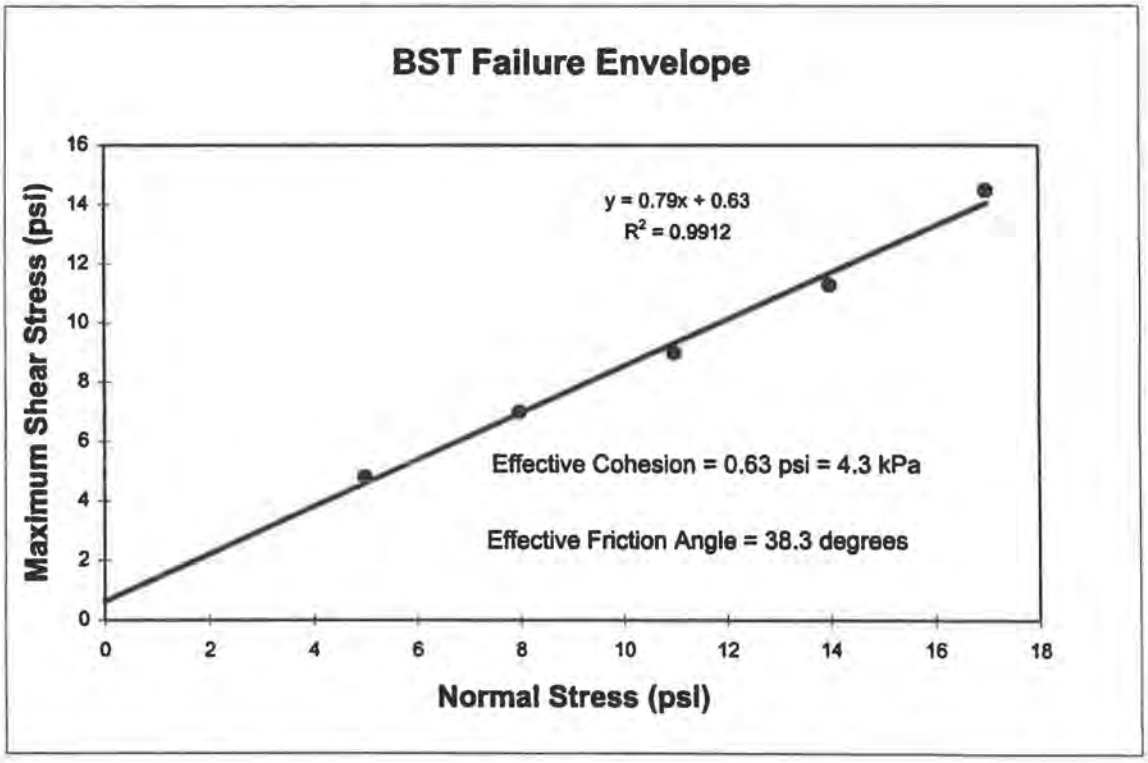

FIG. G.1. - Iowa Borehole Shear Test Results at B-8, 2 m.

Boring : B-8
Depth : 3 meters
Water Table Depth : 12 feet = 3.66 meters

Trial No.	1	2	3	4	5
Consolidation Time (minutes)	12	5.5	5	5	5
Normal Stress (psi)	5	8	11	14	18
Uncorrected Shear Stress (psi)	2.7	3.8	5.0	6.3	7.9
Tare (Pull Rods)	0.7	0.7	0.7	0.7	0.7
Corrected Shear Stress (psi)	2.0	3.1	4.3	5.6	7.2

Remarks : Each maximum shear stress remained constant through 40+ turns of crank.

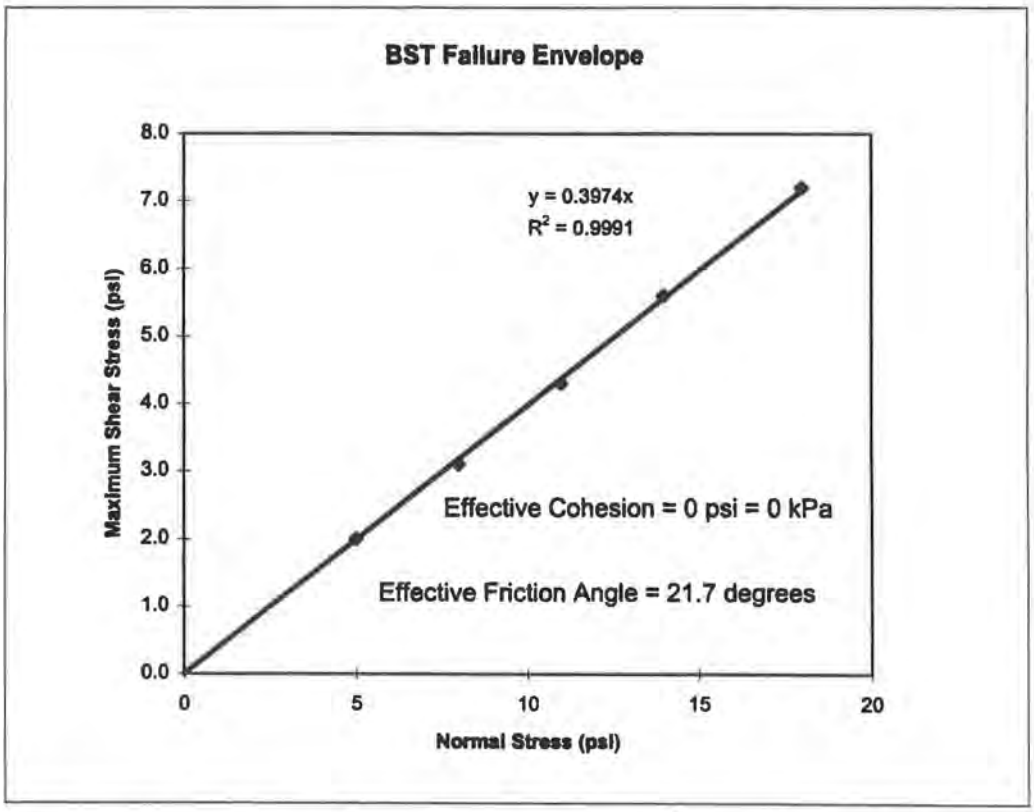

FIG. G.2. - Iowa Borehole Shear Test Results at B-8, 3 m.

Boring : B-8
Depth : 4 meters
Water Table Depth : 12 feet = 3.66 meters

Trial No.	1	2	3	4	5
Consolidation Time (minutes)	15	5	5	5	NA
Normal Stress (psi)	5	10	15	20	NA
Uncorrected Shear Stress (psi)	2.5	3.9	5.0	5.9	NA
Tare (Pull Rods)	0.9	0.9	0.9	0.9	NA
Corrected Shear Stress (psi)	1.6	3.0	4.1	5.0	NA

Remarks : Shear head reached full expansion at Trial No. 5.

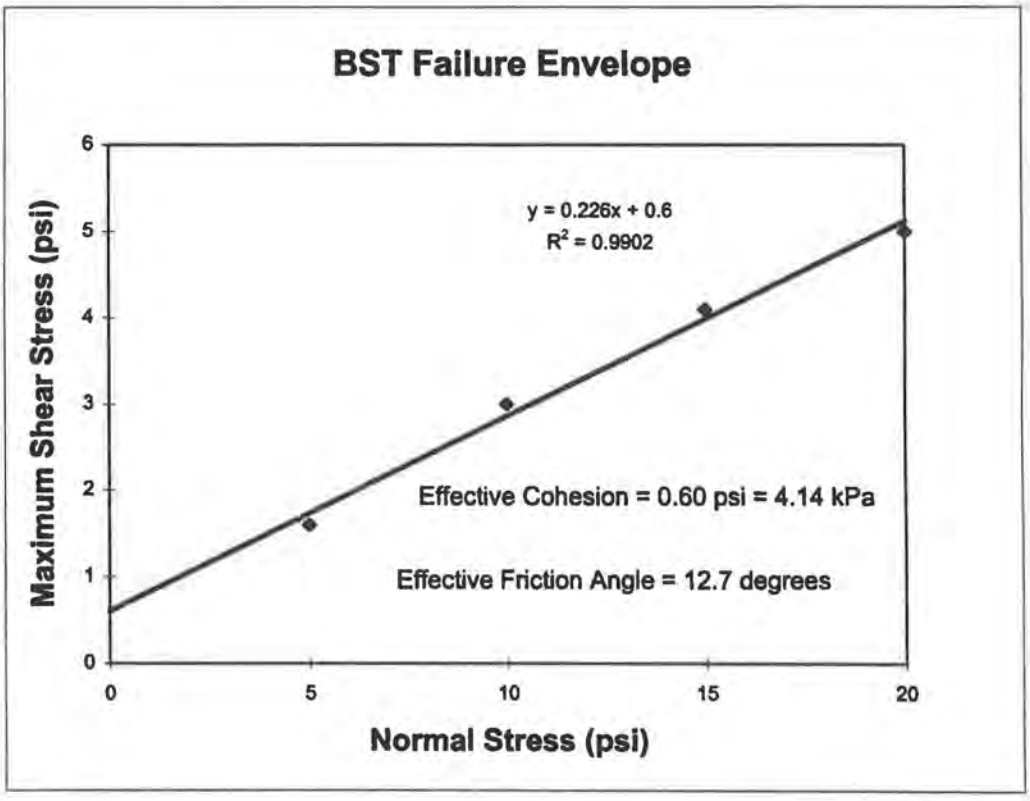

FIG. G.3. - Iowa Borehole Shear Test Results at B-8, 4 m.

Boring : B-7
Depth : 6 meters
Water Table Depth : 12 feet = 3.66 meters

Trial No.	1	2	3	4	5
Consolidation Time (minutes)	11	4	4	4	4
Normal Stress (psi)	5	8	11	14	17
Uncorrected Shear Stress (psi)	4.4	6.1	7.5	9.1	9.9
Tare (Pull Rods)	1.4	1.4	1.4	1.4	1.4
Corrected Shear Stress (psi)	3.0	4.7	6.1	7.7	8.5

Remarks : Trial No. 5 not used because full expansion of shear head suspected.

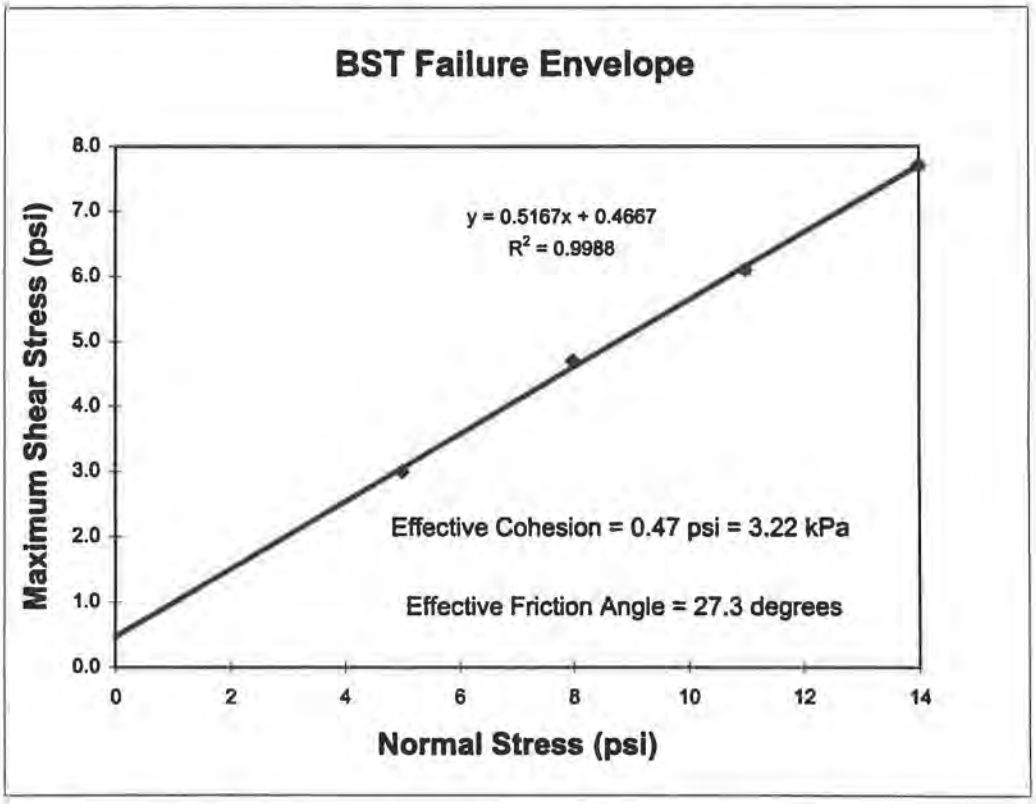

FIG. G.4. - Iowa Borehole Shear Test Results at B-7, 6 m.

Boring : B-8
Depth : 7 meters
Water Table Depth : 12 feet = 3.66 meters

Trial No.	1	2	3	4	5
Consolidation Time (minutes)	10	5	4	4	4
Normal Stress (psi)	5	8	11	14	17
Uncorrected Shear Stress (psi)	2.4	3.4	4.5	5.6	6.6
Tare (Pull Rods)	1.2	1.2	1.2	1.2	1.2
Corrected Shear Stress (psi)	1.2	2.2	3.3	4.4	5.4

Remarks : Tare reading believed to be in error. Plot below is of uncorrected values of shear stress; corrected values yield a negative cohesion value.

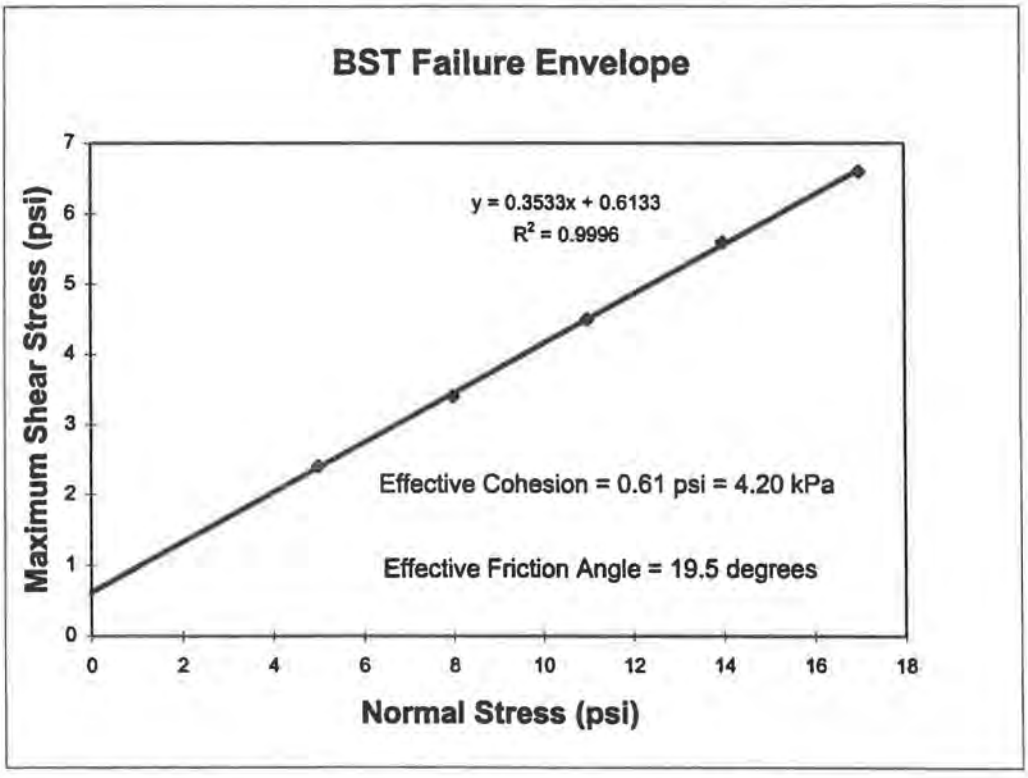

FIG. G.5. - Iowa Borehole Shear Test Results at B-8, 7 m.

Boring : B-8
Depth : 9 meters
Water Table Depth : 12 feet = 3.66 meters

Trial No.	1	2	3	4	5
Consolidation Time (minutes)	10	4	4	4	NA
Normal Stress (psi)	5	8	11	14	NA
Uncorrected Shear Stress (psi)	4.5	5.1	6.3	6.6	NA
Tare (Pull Rods)	2.3	2.3	2.3	2.3	NA
Corrected Shear Stress (psi)	2.2	2.8	4.0	4.3	NA

Remarks : Shear head reached full expansion at (or before) Trial No. 5.
Trial No. 1 may be inaccurate due to seating of shear head.

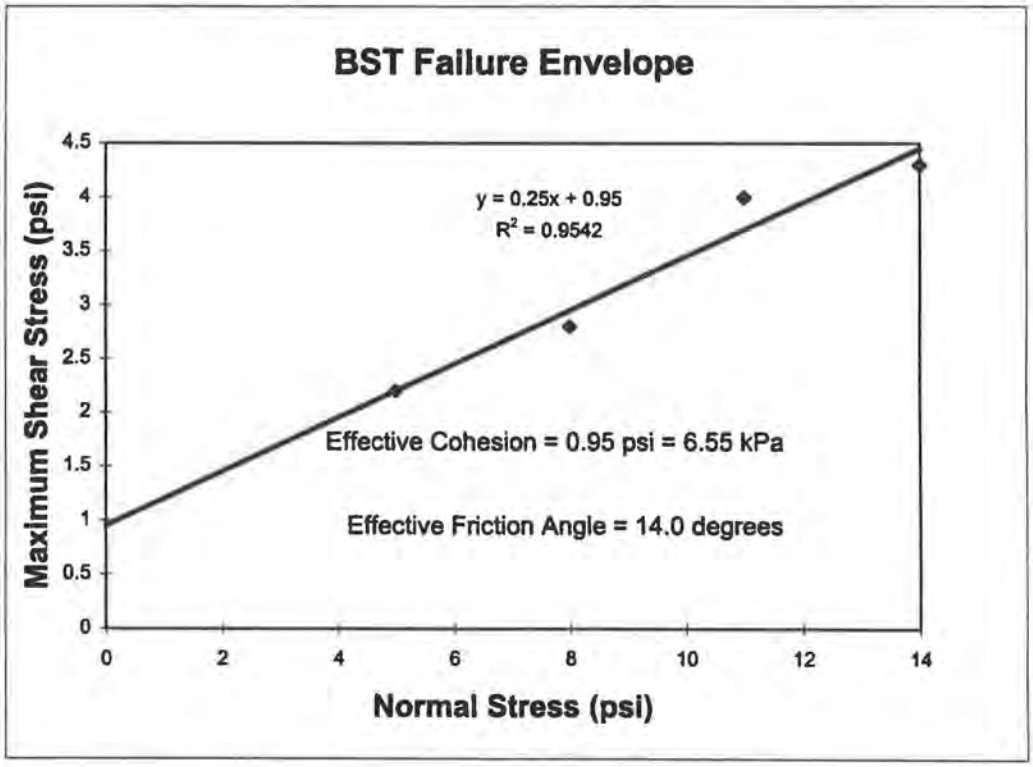

FIG. G.6. - Iowa Borehole Shear Test Results at B-8, 9 m.

APPENDIX H

CROSSHOLE SEISMIC TEST RESULTS

General

1. Several blows at each depth were made, and the resulting shear wave arrival times were averaged.

Equipment

- 4 inch (102 mm) I.D. PVC pipe
- sand/cement grout
- two geophones : manufactured by Olson Engineering of Golden, Colorado
- trigger type : downhole shear hammer manufactured by Mr. Bob Ballard
- Hewlett Packard signal analyzer

Procedure

1. Borings constructed by continuous rotary drilling with 6 in. nominal dia. auger.
2. Some augers were left in the ground overnight as remaining holes were prepared.
3. After removing augers, PVC pipe was pushed into the hole with the bottom end sealed.
4. After positioning, the PVC pipe was filled with water to keep bouyancy forces from displacing the pipe as the grout was pumped through the A-rod down the outer side of the PVC pipe.
5. Testing was conducted in accordance to ASTM D 4428 (1991).

Table H.1. - APPARENT COMPRESSION & SHEAR WAVE VELOCITIES VARYING WITH DEPTH.

Depth (m)	Array 1 (B1-B2-B3)						Array 2 (B4-B5-B6)					
	S-R1 (mps)		S-R2 (mps)		R1-R2(mps)		S-R1 (mps)		S-R2 (mps)		R1-R2(mps)	
	P	S	P	S	P	S	P	S	P	S	P	S
0.6	530.896	269.300	356.040	208.502	271.186	171.680	429.751	213.601				
1.2	573.592	280.787	311.875	221.110	217.546	183.955	356.836	222.215	414.684	229.823	477.569	236.397
1.5							374.258	205.234				
1.8	411.030	263.321	293.130	240.071	230.297	221.470	430.091	213.690	427.243	232.269	424.969	249.824
2.4	407.814	231.932	288.802	232.533	225.996	233.108	380.911	185.681	363.983	225.892	351.426	273.516
3.0		221.658		206.954		194.656	322.936	176.504	405.849	188.114	510.898	198.573
3.7		210.293		196.586		185.142	299.028	191.972	425.323	184.878	641.794	179.578
4.3		196.763		189.047		182.293	329.802	188.840	382.676	214.392	438.705	240.293
4.6	1024.635	222.149					319.224	175.605				
4.9	1322.572	201.535		185.995		173.409		190.251		211.656		232.448
5.5	1361.791	203.834	1291.325	190.628	1231.522	179.702		180.535	1467.734	225.234		280.297
6.1	1351.723	194.571	1429.882	194.679	1511.645	194.780	1226.674	192.898	1510.041	218.194	1847.747	243.453
7.6	1462.851	212.571	1280.507	208.301	1148.023	204.499	1425.502	179.544	1874.374	225.611	2485.861	282.167
9.1	1667.799	210.443	1580.450	209.798	1507.724	209.208	1305.096	159.458	1573.919	197.547	1871.246	242.169
10.7	1209.127	193.119	1624.175	224.956	2375.500	265.247	948.358	177.045	1534.109	210.512	2893.376	245.862
12.2	1159.294	195.471	1479.071	227.481	1977.649	267.520	1233.000	212.126	1648.104	215.664	2204.918	218.397
13.7	1228.922	208.587	1497.005	201.019	1862.770	194.662	1238.764	243.355	1770.272	294.985	2591.657	349.806
14.3									1700.549	224.586		
14.6	1733.446	197.2951	1862.502	221.4886	1995.31	248.75993	1588.201	268.333				

APPENDIX I

TRIAXIAL COMPRESSION TEST RESULTS

General

1. Some CIUC and all CIDC tests were performed at the laboratories of Georgia Institute of Technology; data from these tests were collected by computer acquisition systems and are denoted by analog units readings. Some CIUC and all UU tests were conducted at Auburn University; deflections, load, and pore pressures were manually recorded from a digital readout.

2. Tests from Borings B-2 and B-5 were conducted in the spring of 1996; tests from Borings B-7 and B-8 were conducted in the spring of 1997.

3. Initial portion of Deviator Stress vs. Axial Strain curves were visually back-fit to origin in order to calculate Young's Modulus for the UU and CIUC tests since there were few readings taken at less than 1% strain.

4. The average overall effective stress strength parameters were determined for a depth range of 4 to 15m by examining each CIUC and CIDC test for the maximum principal stress ratio's corresponding p' and q values. These p' and q values were plotted, and a linear regression was performed. The procedure described by Handy (1981) was also performed to analyze soil variability in both the vertical and horizontal by converting p' and q rectangular coordinates into polar coordinates, adding 45° to the angle, converting back to rectangular coordinates, and then performing a linear regression on these points.

5. The loading rate of each UU, CIUC, and CIDC test is presented with other pertinent individual test information (e.g. B-coefficient, effective consolidation pressure, etc.).

Equipment

- automated triaxial testing equipment : GEOCOMP Corp. LoadTrac unit which includes the following -
  - deflection sensors
  - microprocessor for setting test conditions and data acquisition
  - Brainard-Kilman permeability board
  - load frame

- manual triaxial equipment : Brainard-Kilman S-600 triaxial load frame and permeability board

Procedure

Unconsolidated-Undrained (UU)

Performed in accordance to ASTM D 2850 - 82 with the exception of some samples not receiving the full recommended stabilization time of 10 minutes after application of the confining pressure.

Consolidated Isotropically-Undrained Compression (CIUC)

Performed in general agreement with ASTM D 4767 - 88. A brief step-by-step procedure is as follows :

1. Shelby tube samples were extruded lengthwise horizontally, or 17 to 23 cm lengthwise segments of the dissected tube were extruded vertically.
2. The sample was then placed into a split mitre box to provide confining pressure as the ends of the sample were evenly trimmed.
3. Cuttings from the ends of the sample were used to determine the preconsolidation (in situ) water content.
4. A rubber membrane was placed around the samples, and paper filters were placed between the wetted porous stones and the sample.
5. The cell chamber was filled with deaerated water.
6. The cell pressure and back pressure were then incrementally increased with the cell pressure being 2 to 3 psi (13.8 to 20.7 kPa) larger than the back pressure.
7. The B-coefficient was checked by closing the cell pressure and back pressure lines, increasing the cell pressure by 5 psi (34.5 kPa), then opening the cell pressure line in order to observe the change in pore pressure transducer reading.
8. To increase the B-coefficient, pressures were increased and/or the sample was left under a certain pressure over an extended time period.
9. The effective confining pressure was increased to the desired testing level after an acceptable B-coefficient (generally ≥ 0.95) was obtained or until the capacity of the pressure generator was reached. B-coefficients are denoted for each individual test.
10. The back pressure lines were then opened, and volume changes in the sample were recorded over time by visually reading graduated burettes.
11. After consolidation appeared to be complete, the back pressure line was closed. An adequate shearing rate was determined, and the rate of platen travel was adjusted accordingly.
12. The loading piston was then lowered until it was just in contact with the sample.
13. Upon loading, pore pressure and load readings at different deformation intervals were taken.
14. Samples were generally loaded to near 20% strain or until the load began to drop off appreciably. After shearing to failure, some samples were removed from the cell, and a "post-test" water content was measured.

Consolidated Isotropically-Drained Compression (CIDC)

Same as for CIUC test procedure except for the following :

1. Upon completion of consolidation, the back pressure lines were left open, and the sample was then loaded.
2. During loading, the pore pressure transducer was left in-place to allow for confirmation of no excess pore pressures developing.
2. Volume changes in the sample during loading was monitored since the back pressure valve was left open upon completion of consolidation.

Data Reduction (Unconsolidated-Undrained)

Example : Boring B-6, Sample Depth = 1 meter, Sample # 1
Initial Deformation Reading = -0.003 in

- 'Zero' the Deformation Readings :

Corrected Deformation = -0.003+0.003 = 0.000

- Compute Axial Strain (%) :

Axial Strain (%) = Corrected Deformation*100/Initial Sample Height
= 0.000*100/5.6 = 0.00%

- Correct Area :

Corrected Area = Initial Area/(1-Strain)
= 6.380 in^2/(1-0.000/5.6) = 6.380 in^2

- Deviator Stress = Load Reading/Corrected Area

= 0.0/6.380 = 0.00 psi = 0.00 kPa

- Undrained Shear Strength = Deviator Stress/2

= 0.00/2 = 0.00 kPa

Data Reduction (Consolidated-Undrained)

Example : Boring B-7, Sample Depth = 10 meters, Sample #2, CIUC test type,
Observed Volume Change After Consolidation = 40.2 cm^3

- Find after-consolidation sample dimensions (assuming sample remains right circular cylinder, isotropic volumetric strains) :

Volumetric Strain = ε = Vol. Change/Initial Volume
= 40.2/(pi*(7.24^2)*14.22/4) =40.2/585.50 = <u>0.069</u>

New Sample Height = H' = Initial Height*$(1-\varepsilon)^{1/3}$
= 14.22*$(1-0.069)^{1/3}$
= <u>13.874 cm</u>

New Sample Area = A' = Initial Area*$(1-\varepsilon)^{2/3}$
= 39.73*$(1-0.069)^{2/3}$
= <u>37.821 cm^2</u>

- Convert voltage readings for load, displacement & pore pressure :

Load (analog units) = 80, Displacement (au) = 53, P.P. (au) = 741

Load = 80*conversion = 80au*0.5585499 lbs./au = <u>44.68 lbs</u>.

Displacement = 53au*0.0003176 in/au = <u>0.0168 in</u>

P.P. = 741au*0.0367405 lbs/au = <u>27.22 psi</u>

- Correct Area : Use same calculation as in UU data reduction except use H' instead original height in strain correction term and correct the A' instead of original area .

- Deviator Stress = Load/Corrected Area = <u>7.621 psi</u> = <u>52.54 kPa</u>

- Compute p, p'-q values and Principal Stress Ratio.

$p = (\sigma_1 + \sigma_3)/2$ = (Deviator Stress + 2*Eff. Confining Pressure)/2

= (52.54 kPa + 2*241.3 kPa)/2 = <u>267.9 kPa</u>

$p' = (\sigma_1' + \sigma_3')/2$ = (Deviator Stress + 2*(Cell Press.- Pore Press.))/2

= (52.54 kPa + 2*(413.7 kPa - 187.69 kPa))/2

= <u>252.27 kPa</u>

$q = (\sigma_1 - \sigma_3)/2$ = Deviator Stress/2 = 52.54/2 = <u>26.27 kPa</u>

Principal Stress Ratio = (σ_1'/σ_3')

= (Deviator Stress + (cell press.-p.p.))/(cell press. - p.p.)

= (52.54 kPa + (413.7 kPa - 187.69 kPa))/(413.7 kPa - 187.69 k
= 1.232

Table I.1. - Unconsolidated-Undrained Triaxial Test Summary.

Boring	Depth (m)	Sample #	Water Content (%)	Pre-Test Wet Unit Wt.(kN/m^3)	Confining Pressure (kPa)	Max. S_u (kPa)
B-2	1	1	32.8	19.22	0	60.9
B-2	1	2	31.6	18.17	24.1	82.7
B-5	1	1	32.8	19.22	24.1	96.0
B-6	1	1	31.3	18.45	24.1	71.1
B-6	1	2	31.1	18.60	24.1	106.7
B-7	1	1	40.4	18.20	24.1	155.3
B-7	1	2	41.2	18.35	24.1	187.5
B-8	1	1	32.1	17.94	24.1	79.4
B-2	2	1	38.0	17.77	48.3	73.8
B-2	2	2	38.0	17.92	48.3	80.7
B-5	2	1	32.4	17.86	48.3	42.2
B-5	2	2	32.4	17.86	48.3	60.1
B-7	2	1	41.2	17.45	48.3	99.9
B-8	2	1	27.5	18.90	48.3	114.1
B-7	3	1	41.9	18.45	72.4	67.5
B-7	3	2	39.3	18.28	0	43.0
B-8	3	1	36.2.	17.97	72.4	39.8
B-8	3	2	28.0	18.04	72.4	81.2
B-8	3	3	23.6	18.93	72.4	149.4

Note : All UU tests were conducted at a loading rate of 0.5% axial strain/minute (0.28 inches/minute) except B-6 @ 1 m (sample 1) which was loaded at 1.0% axial strain/minute (0.56 inches/minute).

All samples had a diameter of 7.24 cm and height of 14.22; L/D = 1.97.

TABLE I.2. - Consolidated-Undrained Triaxial Test Summary.

Boring	Depth (m)	Sample #	In-Situ Water Content (%)	Pre-Test Wet Unit Wt. (kN/m³)	σ_3' (kPa)	B-coefficient	Loading Rate (in/min)
B-7	4	1	43.1	17.92	68.9	≥ 0.92	0.0025
B-7	4	2	43.1	18.14	137.9	≥ 0.93	0.004
B-5	4	1	34.6	17.0	52.3	?	0.009
B-7	6	1	35.5	18.70	89.6	≥ 0.85	0.004
B-8	6	1	26.2	18.14	134.5	0.95	0.0013
B-8	6	2	29.4	18.63	179.3	0.96	0.0014
B-7	8	1	41.1	17.85	103.4	0.98	0.0044
B-7	8	2 - Stg 1	35.6	18.14	206.8	0.98	0.0009
B-7	8	2 - Stg 2	35.6	N/A	310.3	0.95	0.002
B-2	8	1	28.3	19.4	99.2	?	0.009
B-7	10	1	50.1	17.55	120.7	0.98	0.0024
B-7	10	2	50.0	17.75	241.3	0.96	0.0021
B-7	10	3	50.8	17.55	103.4	0.96	0.0008
B-2	12	1	36.0	17.62	116.0	?	0.009
B-5	12	1	37.5	18.62	127.0	?	0.009
B-5	12	2	35.1	16.53	102.0	?	0.009
B-2	15	1 - Stg 1	37..0	18.41	172.4	≥ 0.95	0.0028
B-2	15	1 - Stg 2	37.0	N/A	310.3	≥ 0.95	0.0028
B-5	15	1 - Stg 1	38.1	17.86	172.4	≥ 0.95	0.0028
B-5	15	1 - Stg 2	38.1	N/A	310.3	≥ 0.95	0.0028
B-5	15	2 - Stg 1	38.1	19..52	241.3	≥ 0.95	0.0028
B-5	15	2 - Stg 2	38.1	N/A	413.7	≥ 0.95	0.0028

Note : Those samples denoted with (?) were thought to near saturation, but the B-coefficient was not reported. Also, the length to diameter (L/D) ratio was approximately 2.0 for most samples, but a few were lower and ranged between 1.82 - 1.97.

Table I.3. - Consolidated-Drained Triaxial Test Summary.

Boring	Depth (m)	Sample #	In-Situ W/C (%)	σ_3' (kPa)	B-coefficient	Loading Rate (in/minute)
B-8	10	1	44.3	120.7	0.95	0.0028
B-8	10	2	41.3	241.3	0.98	0.0028

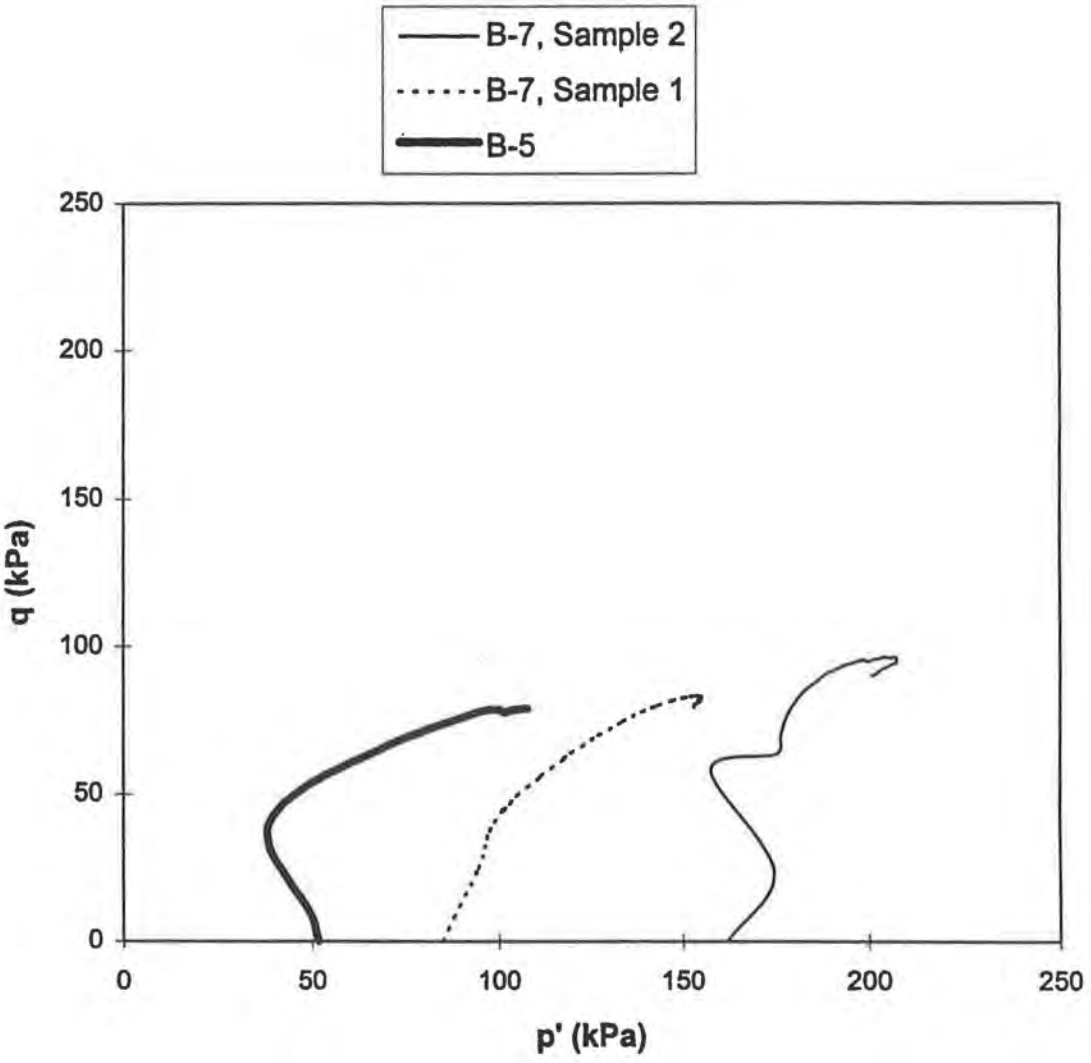

FIG. I.1. - p-q plot at 4 meters.

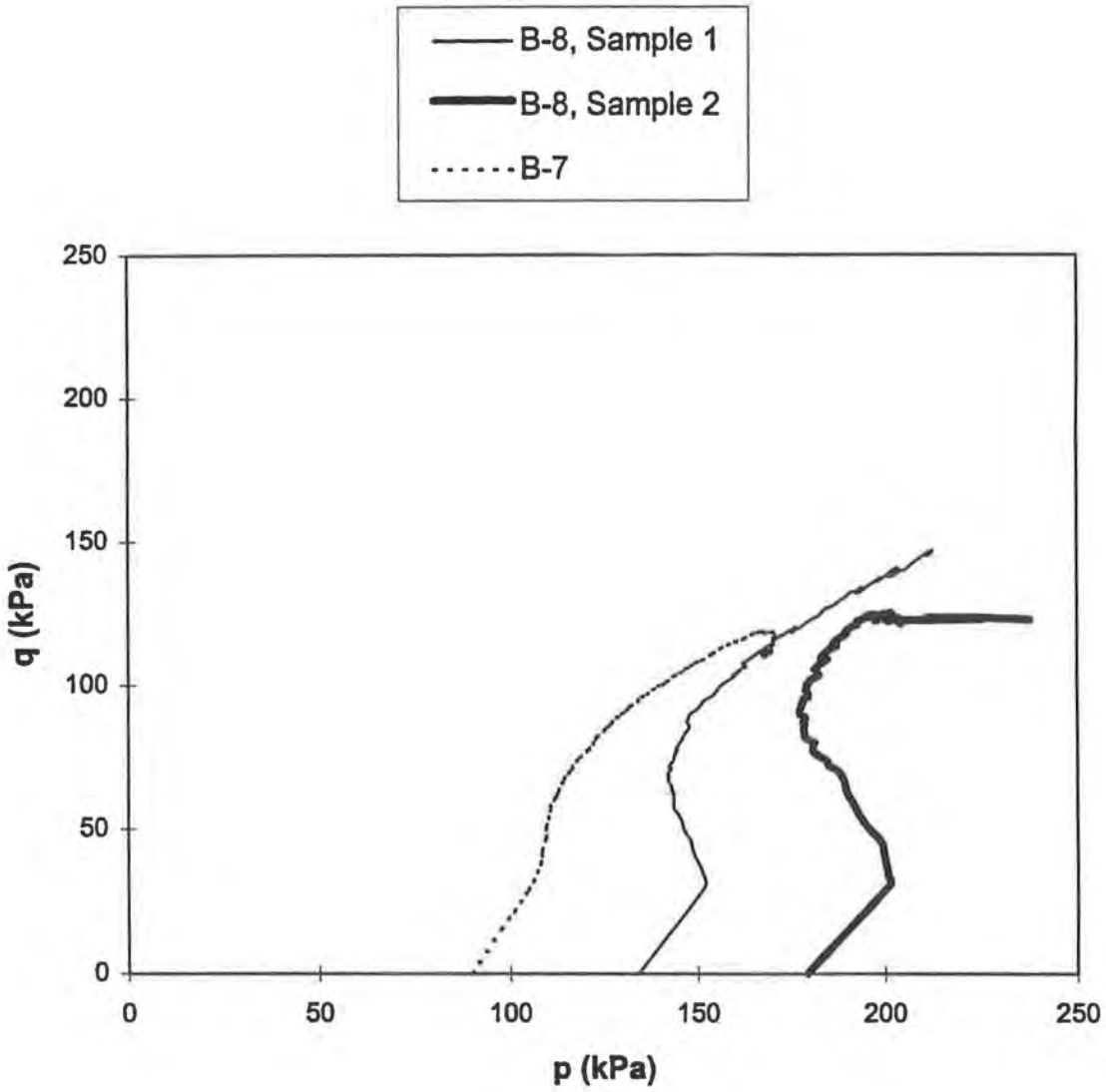

FIG. I.2. - p-q plot at 6 meters.

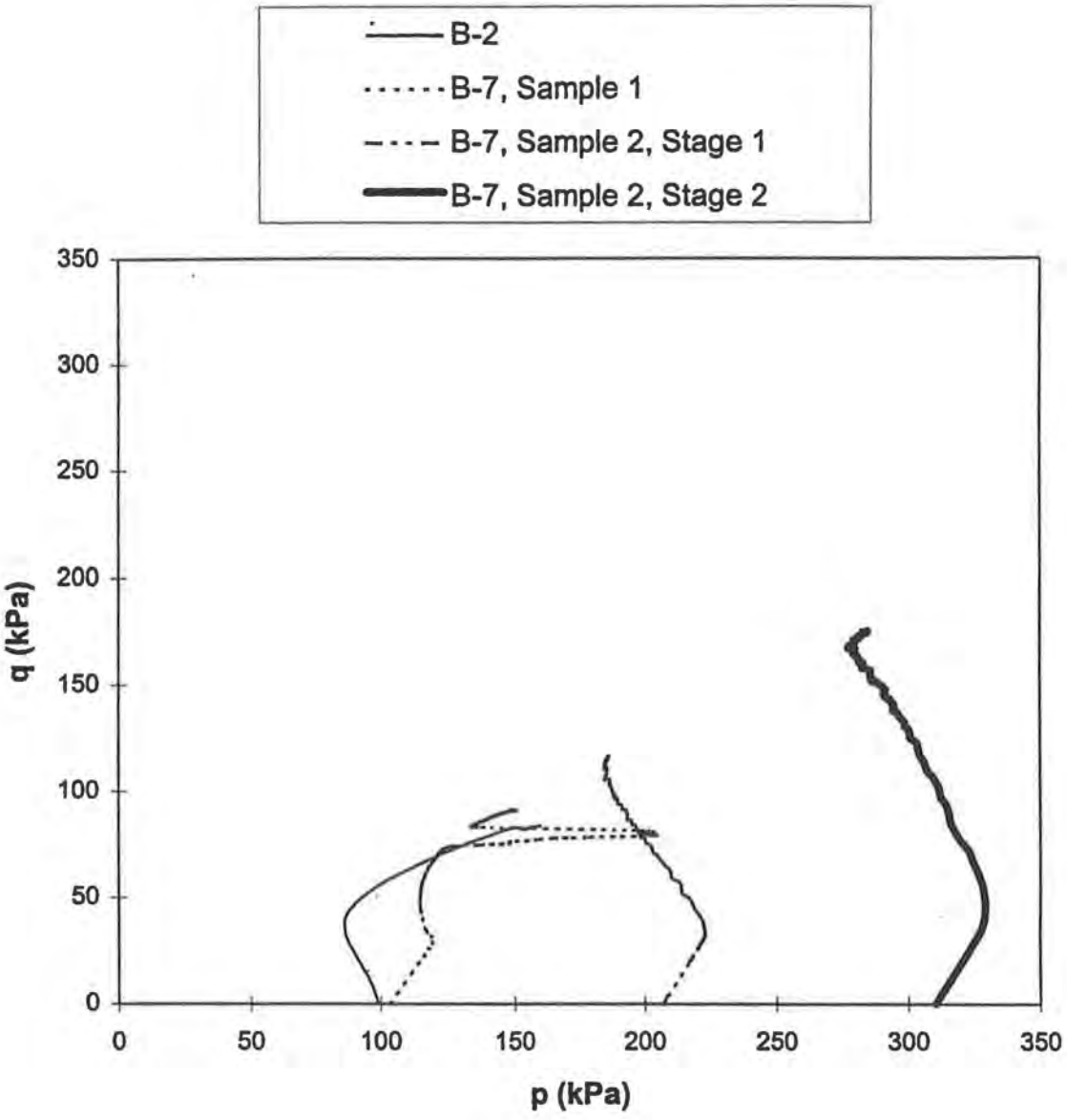

FIG. I.3. - p-q plot at 8 m.

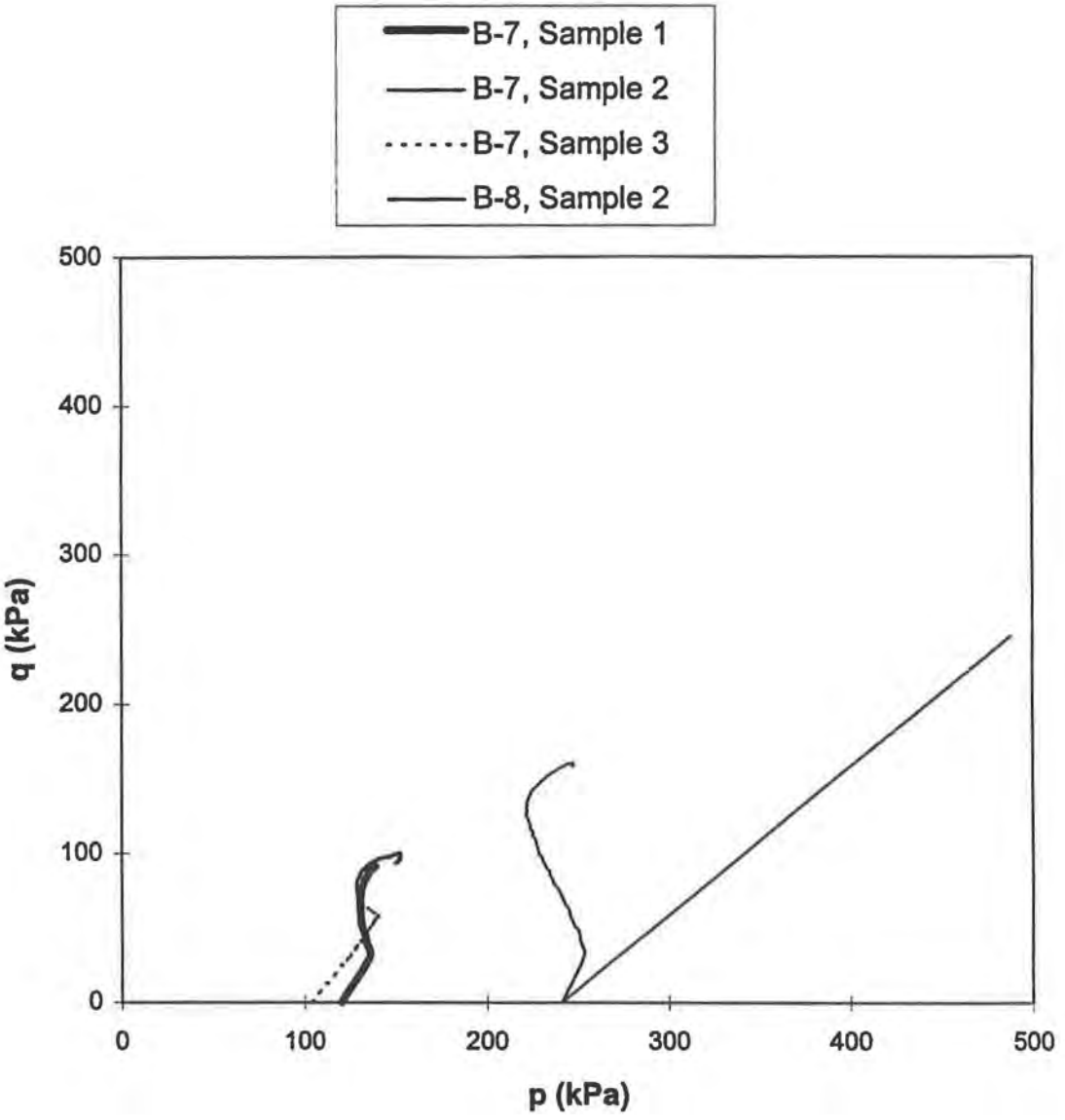

FIG. I.4. - p-q plot at 10 meters.

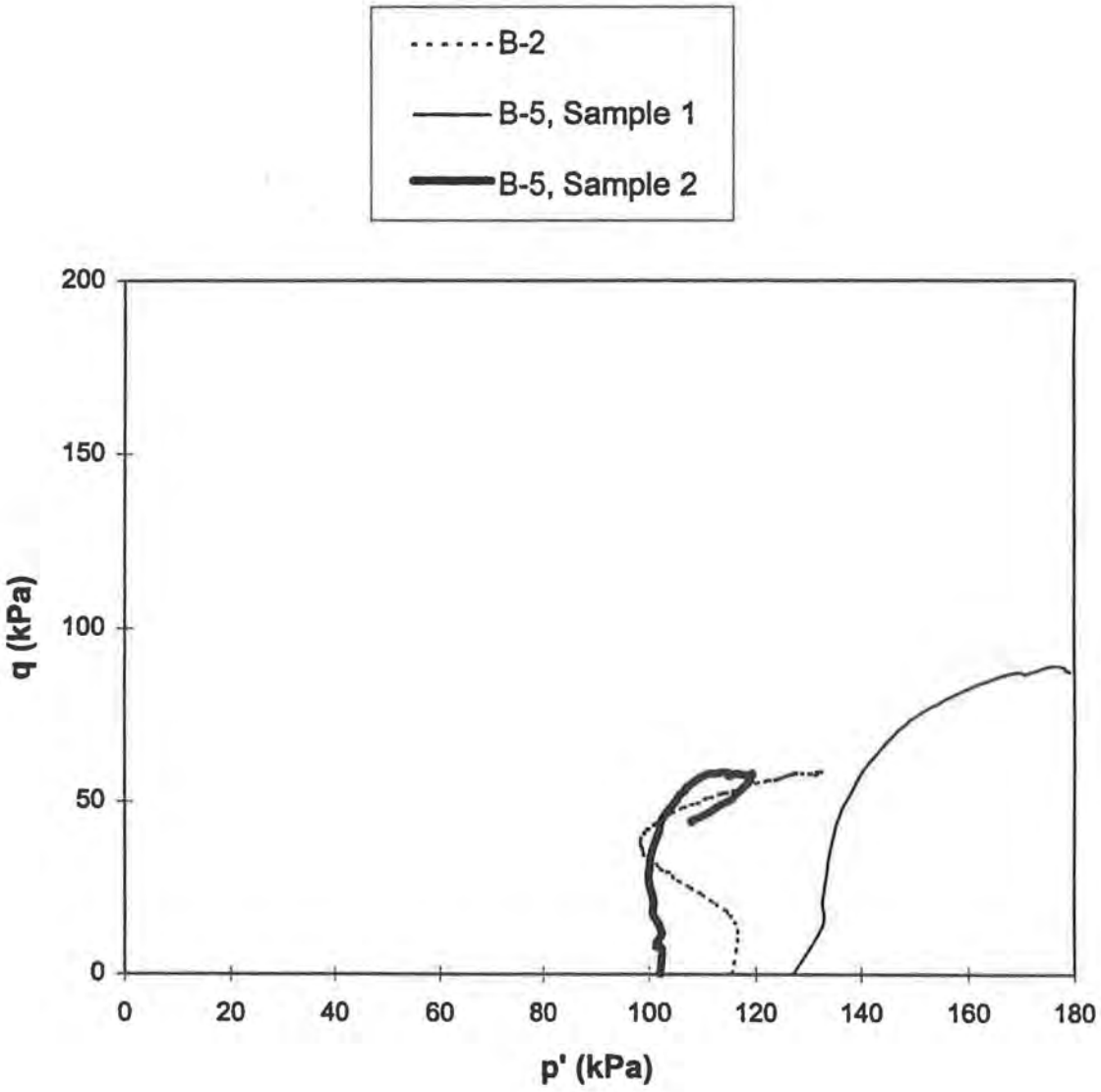

FIG. I.5. - p-q plot at 12 m.

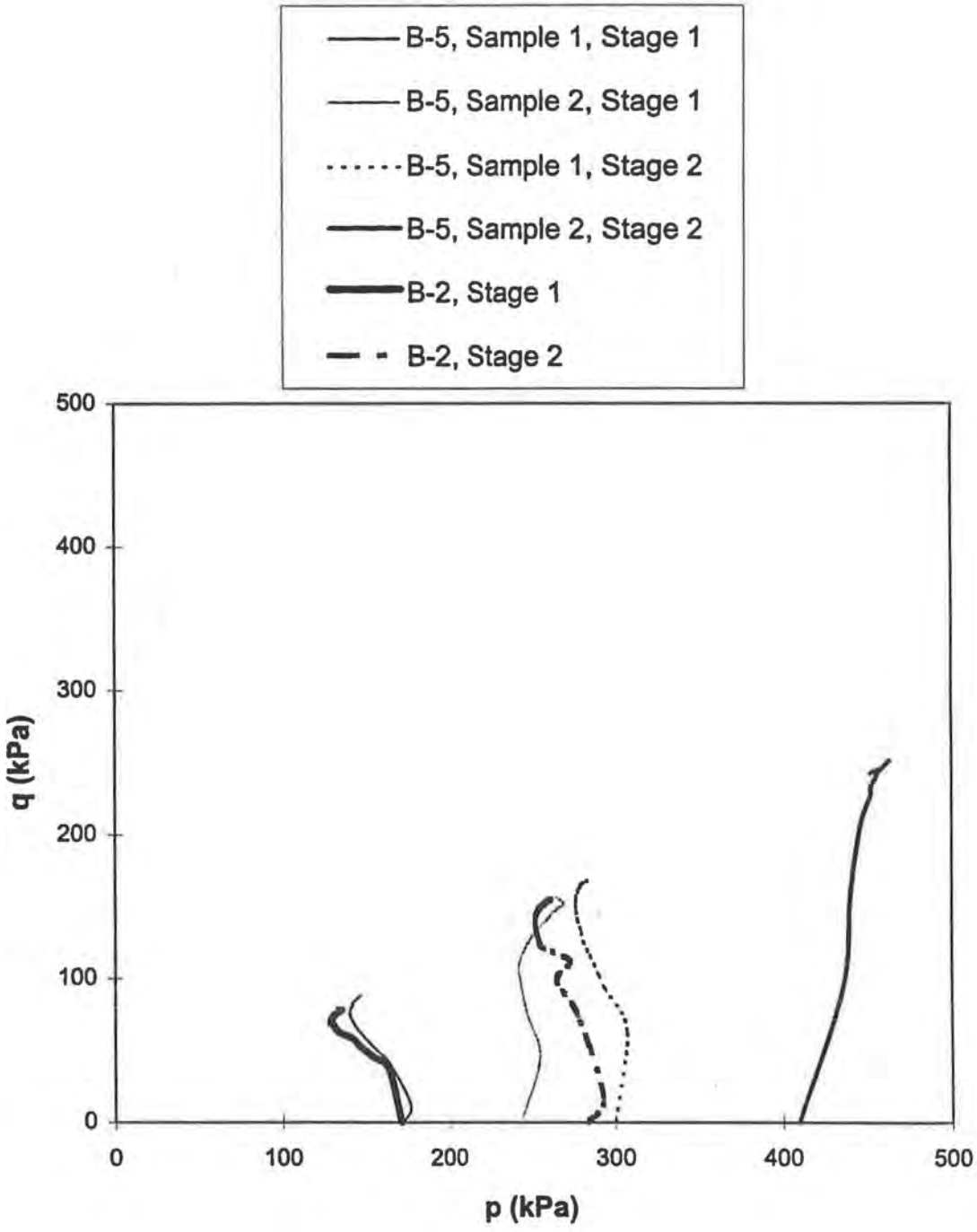

FIG. I.6. - p-q plot at 15 meters.

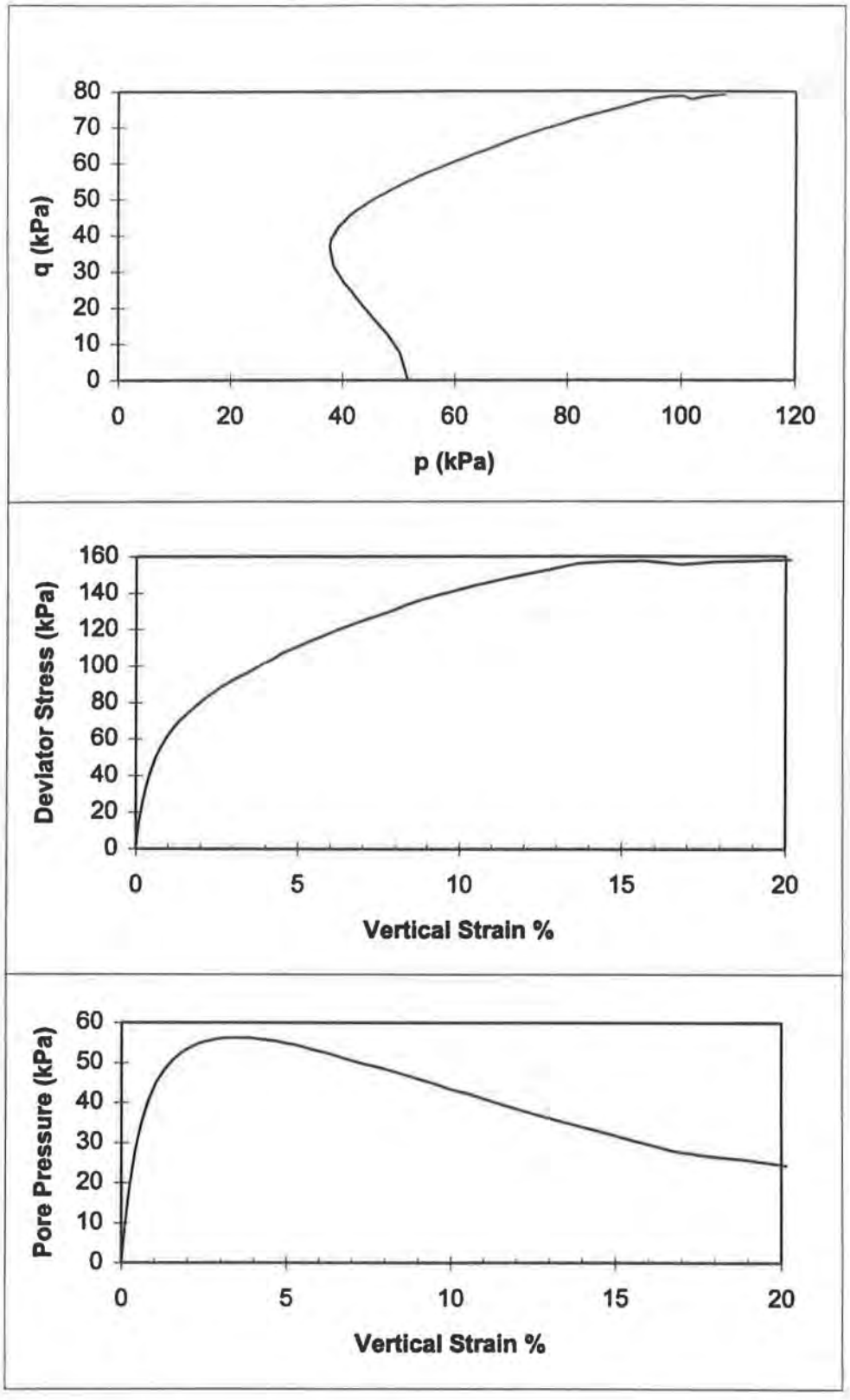

FIG. I.7. - CIUC Results : B-5 @ 4 meters, Sample 1.

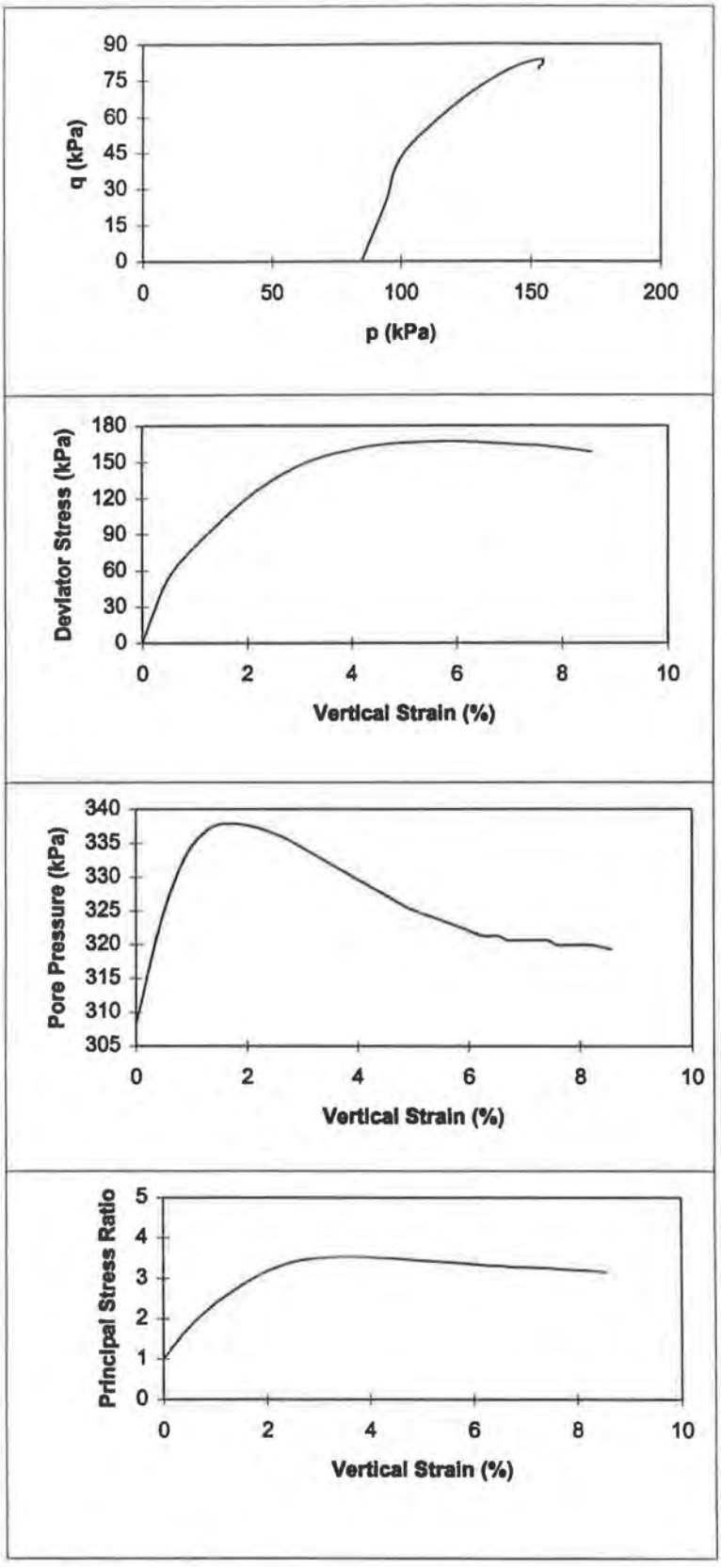

FIG. I.8. - CIUC Results : B-7 @ 4 meters, Sample 1.

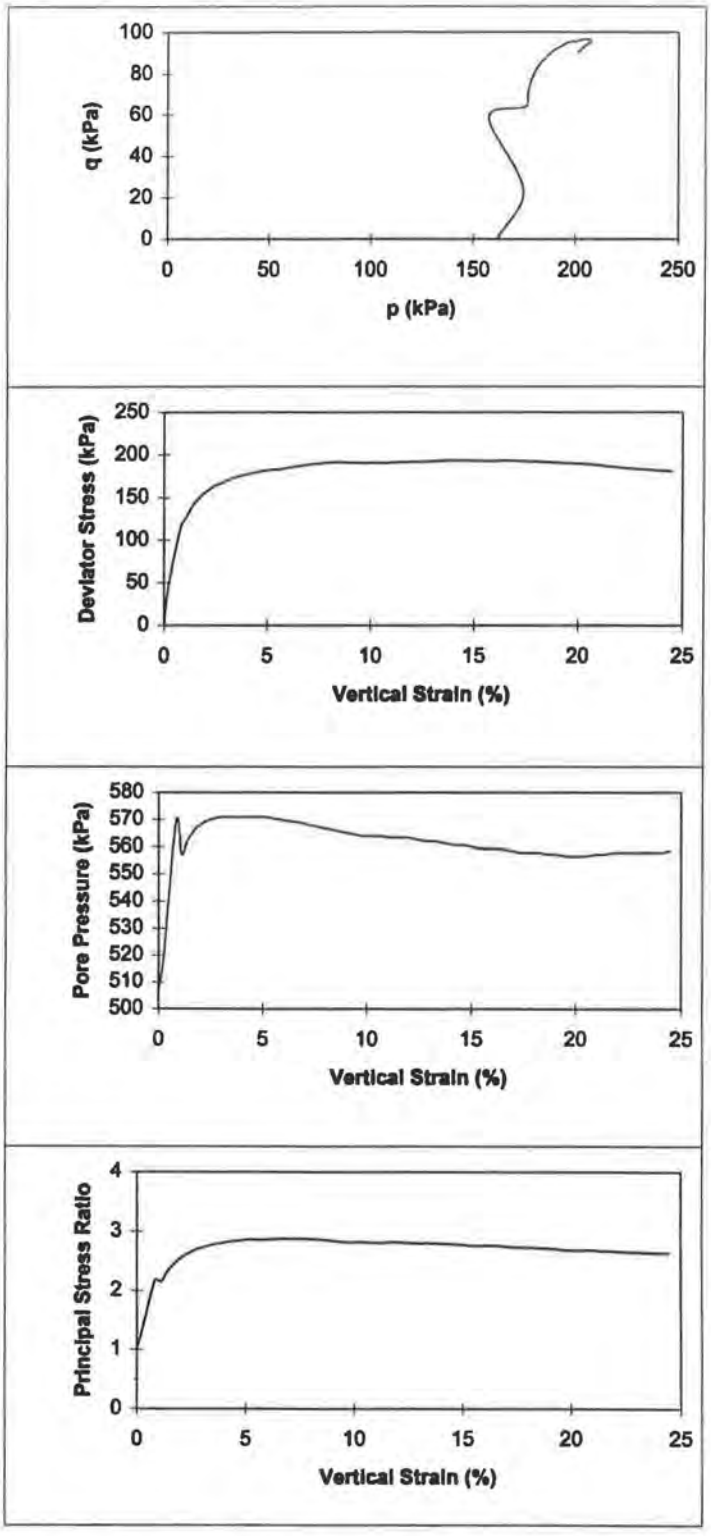

FIG. I.9. - CIUC Results : B-7 @ 4 meters, Sample 2.

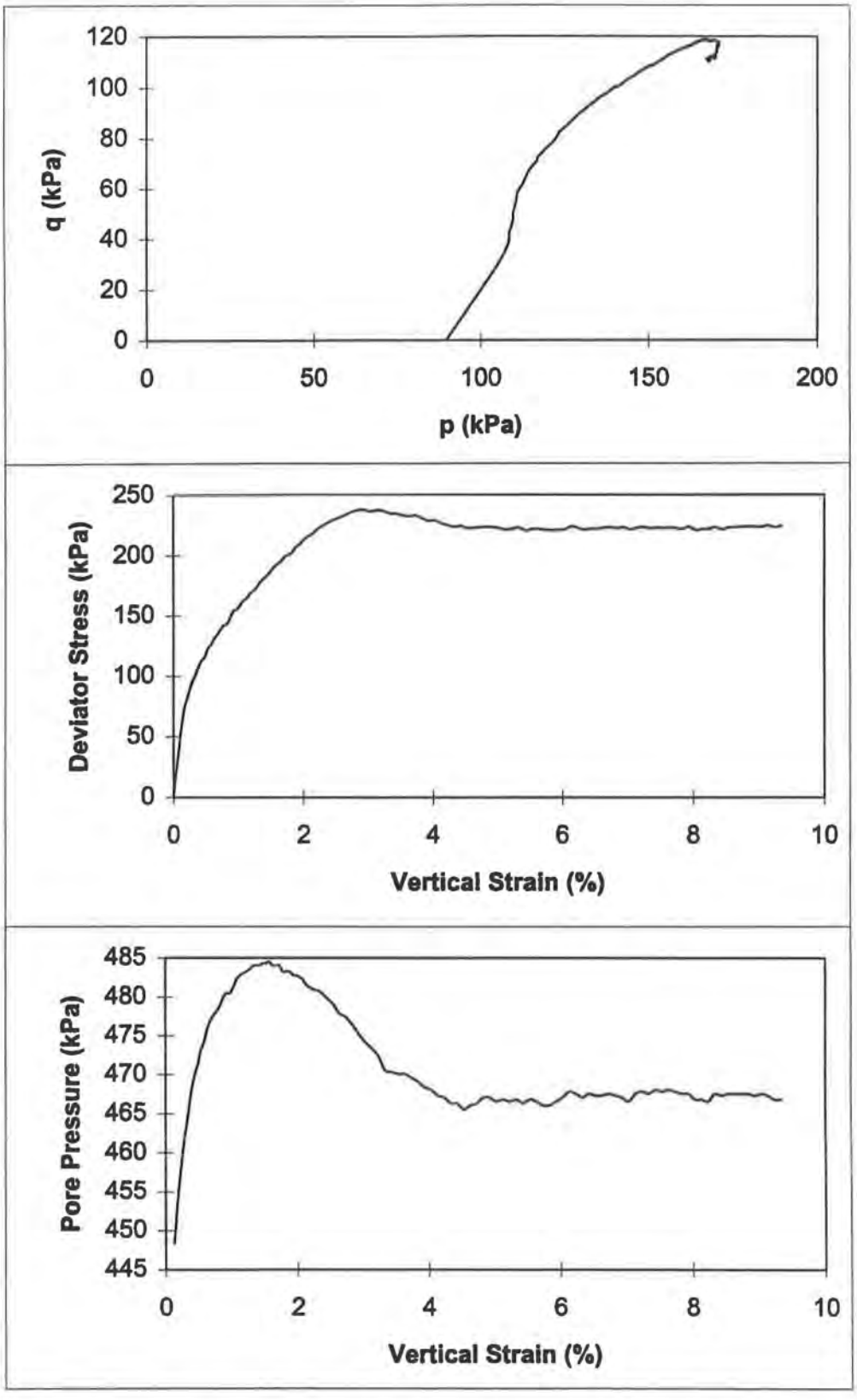

FIG. I.10. - CIUC Results : B-7 @ 6 meters, Sample 1.

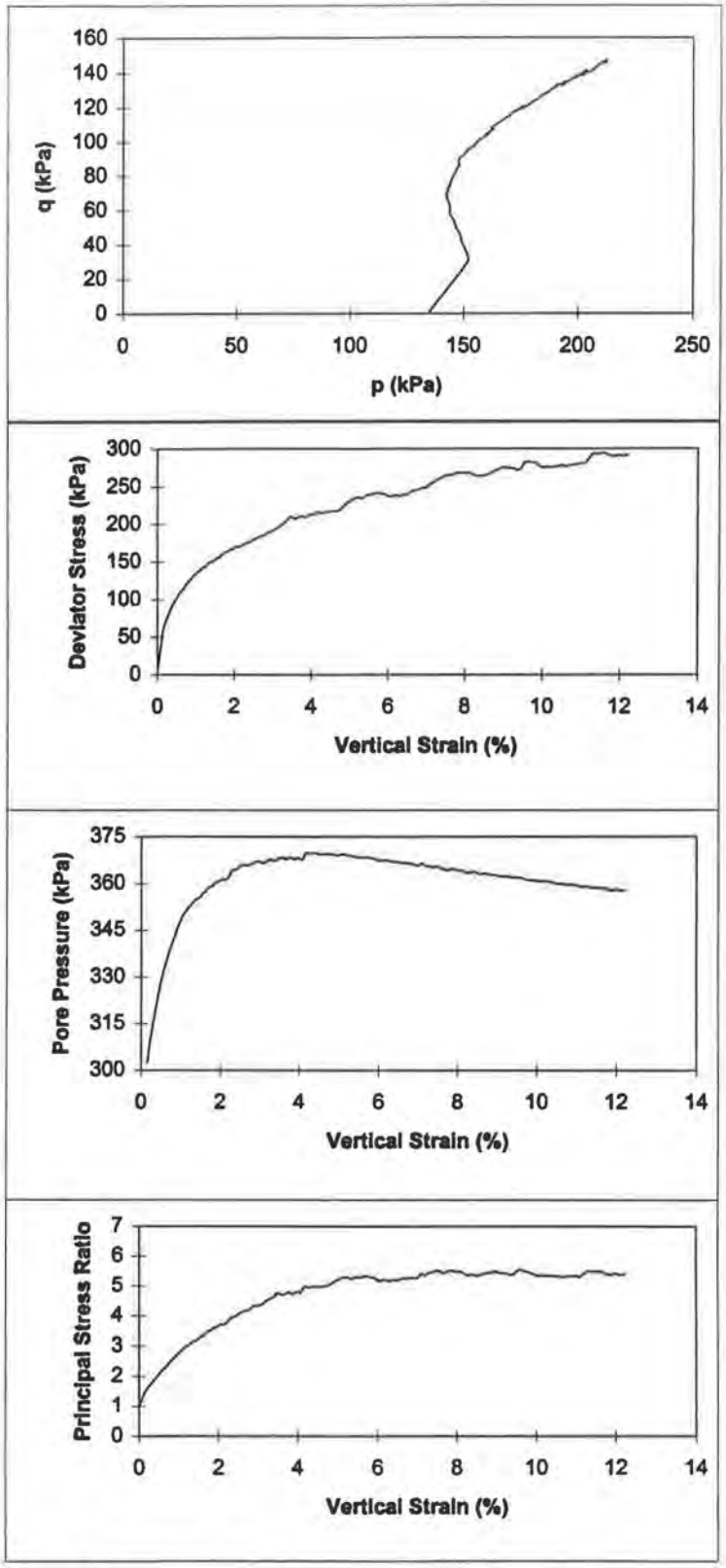

FIG. I.11. - CIUC Results : B-8 @ 6 meters, Sample 1.

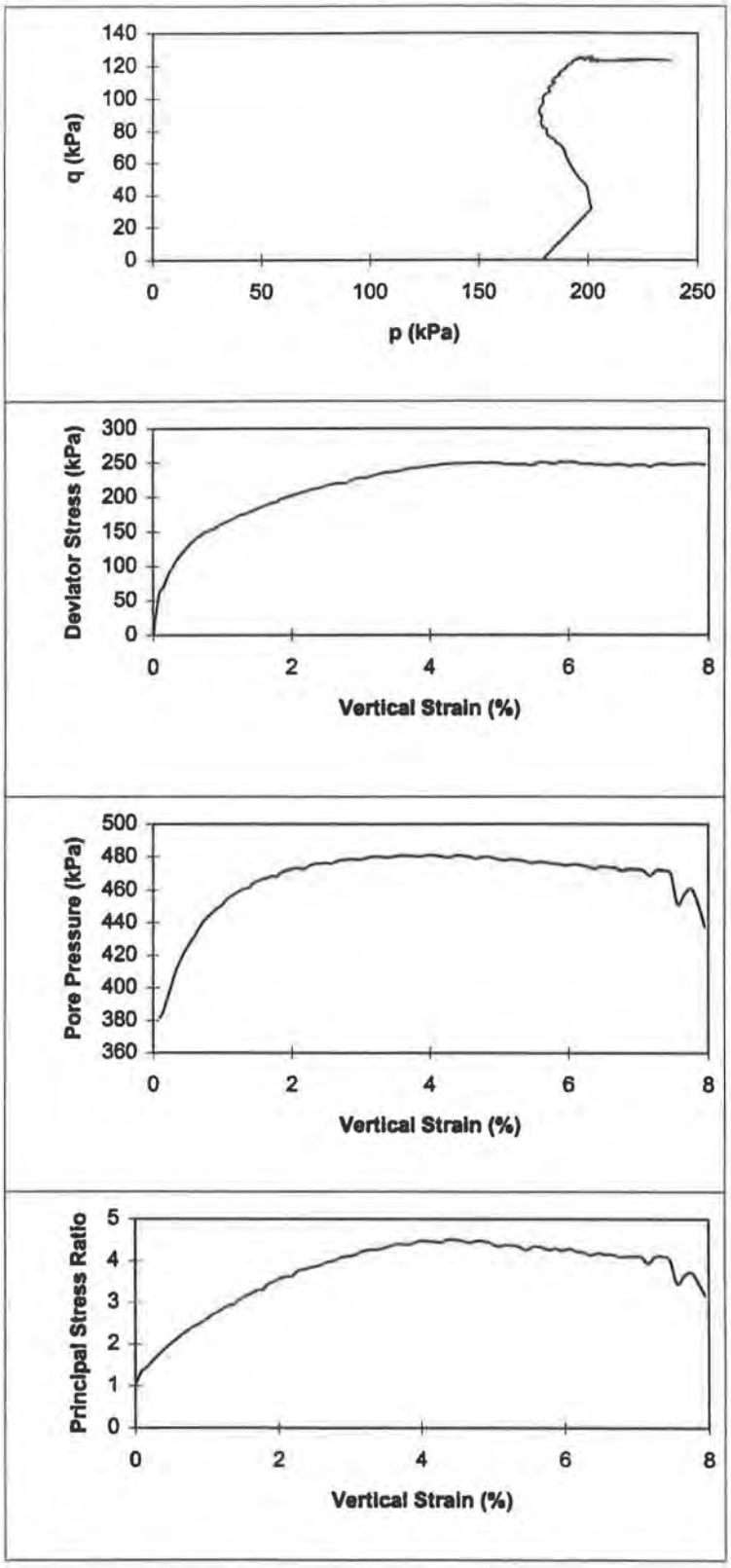

FIG. I.12. - CIUC Results : B-8 @ 6 meters, Sample 2.

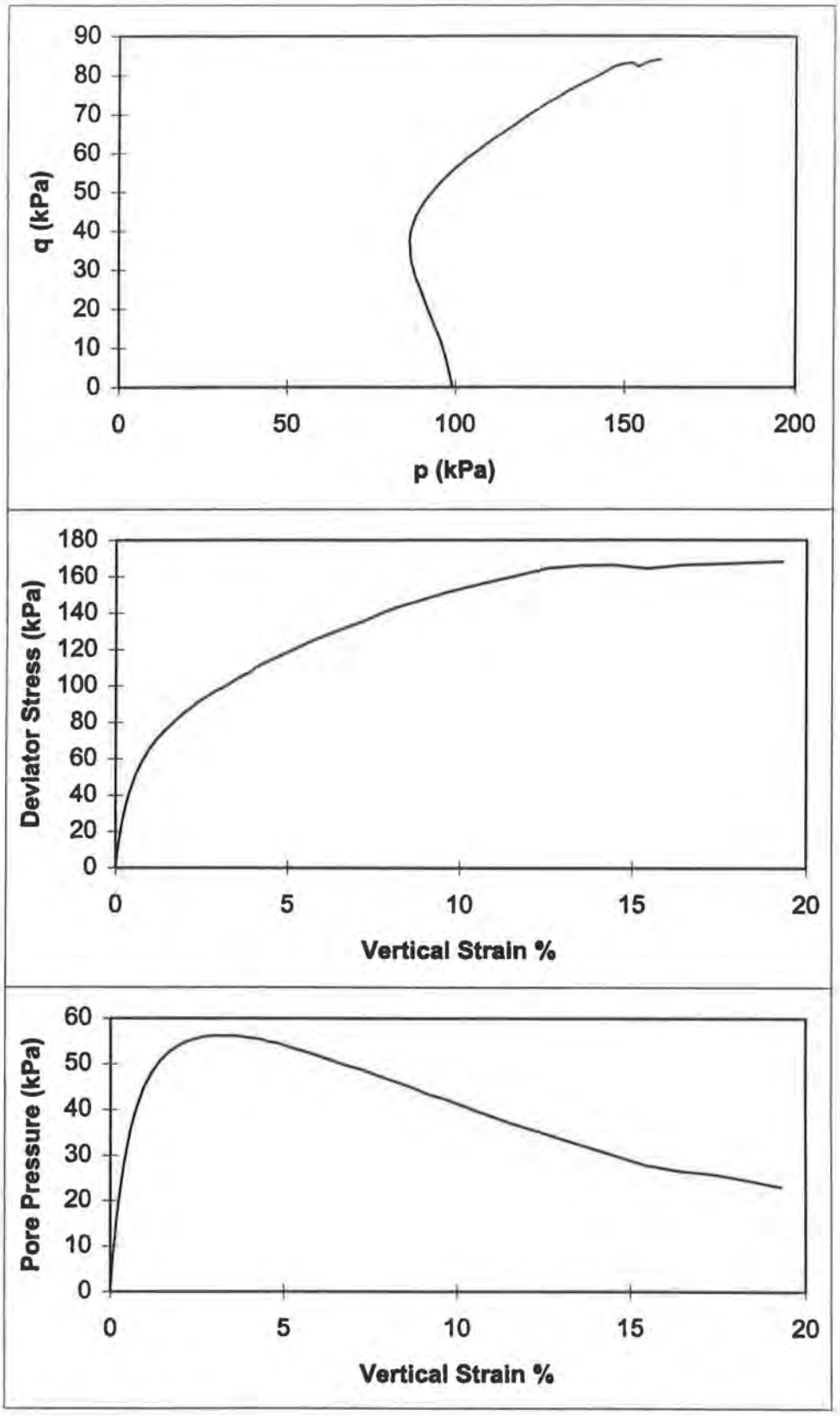

FIG. I.13. - CIUC Results : B-2 @ 8 meters, Sample 1.

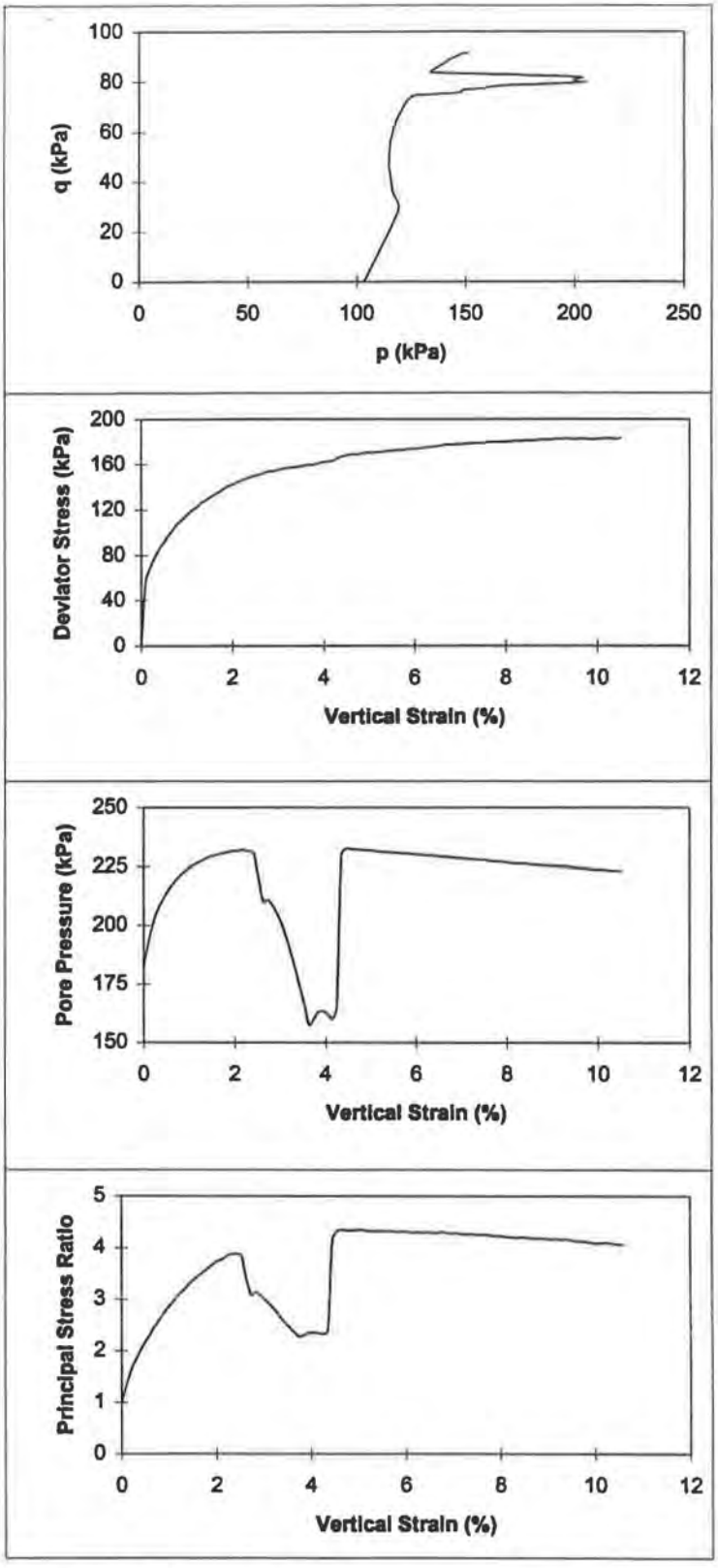

FIG. I.14. - CIUC Results : B-7 @ 8 meters, Sample 1.

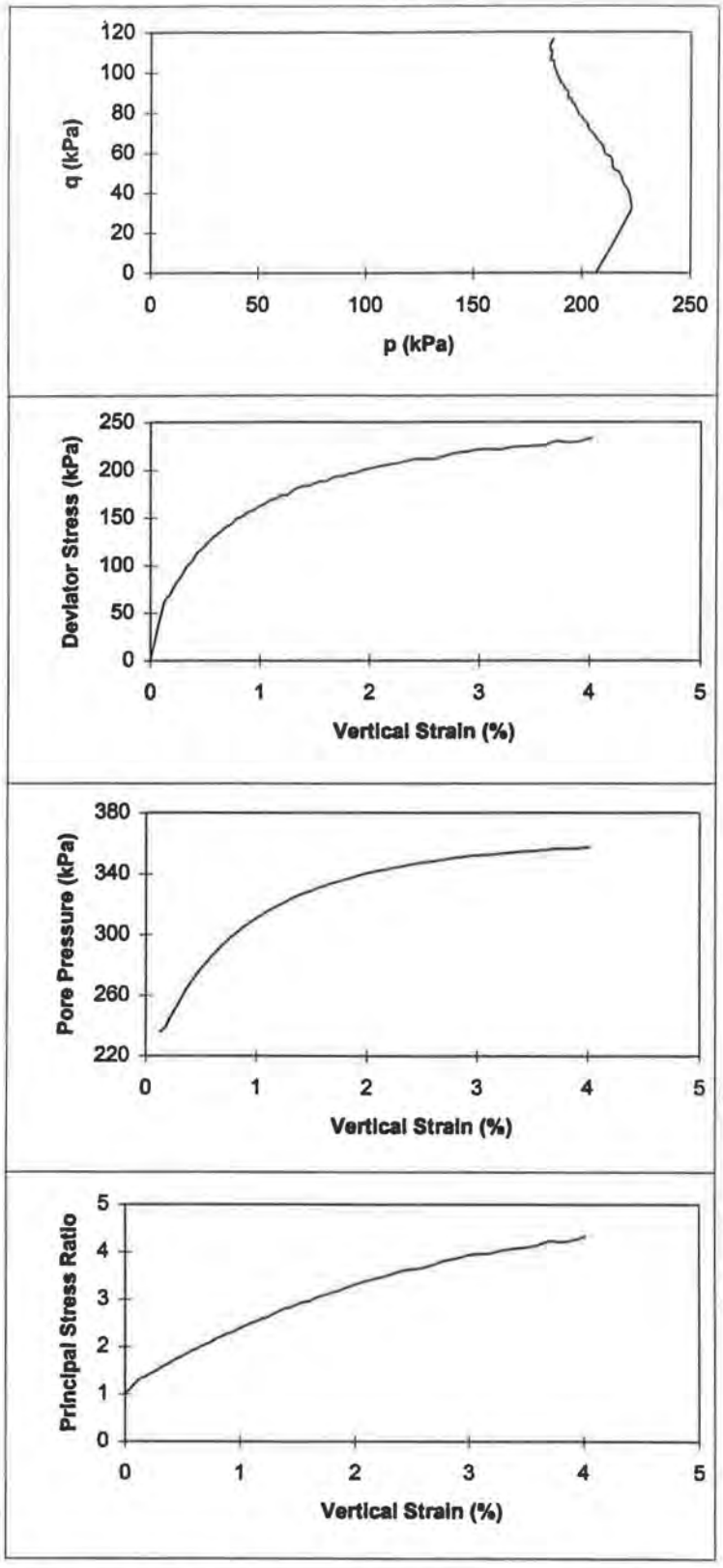

FIG. I.15. - CIUC Results : B-7 @ 8 meters, Sample 2, Stage 1.

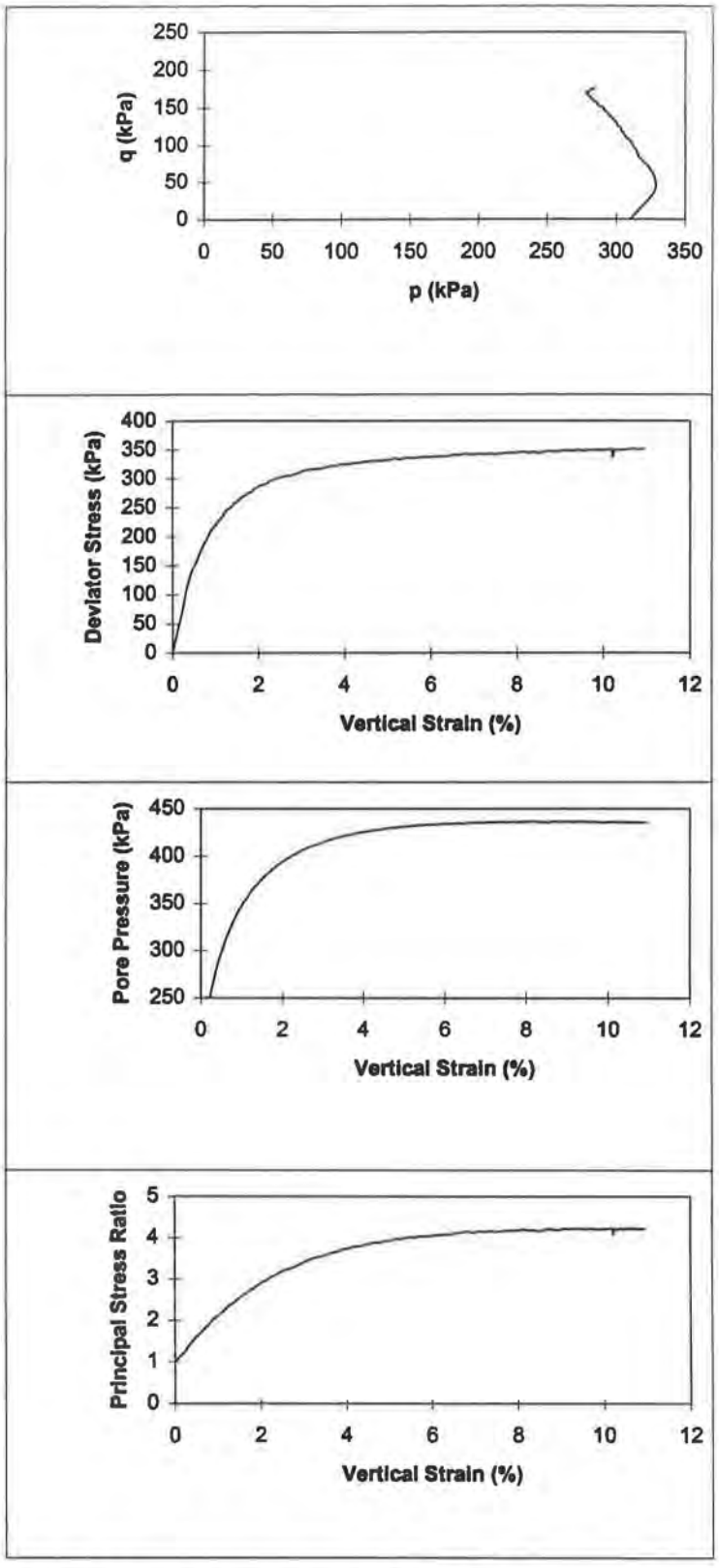

FIG. I.16. - CIUC Results : B-7 @ 8 meters, Sample 2, Stage 2.

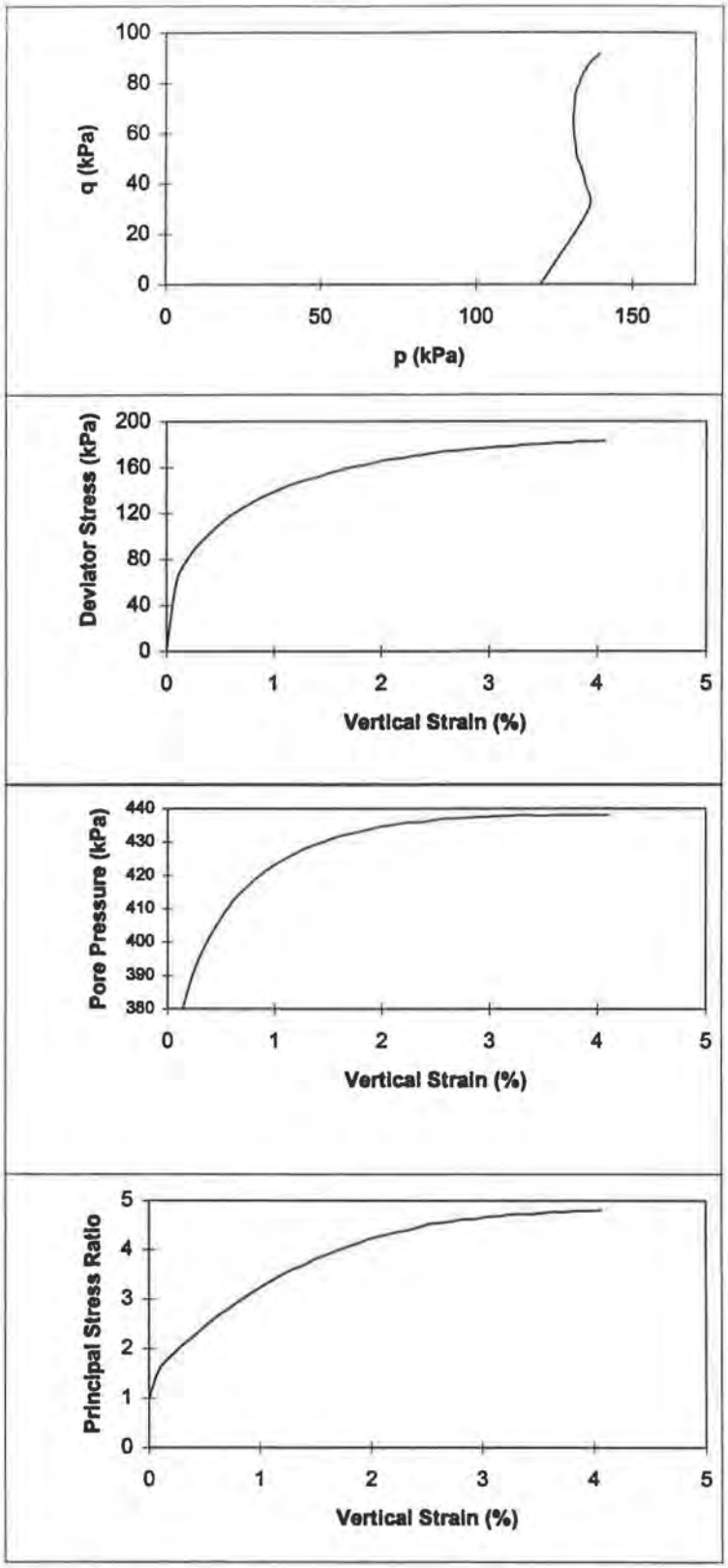

FIG. I.17. - CIUC Results : B-7 @ 10 meters, Sample 1.

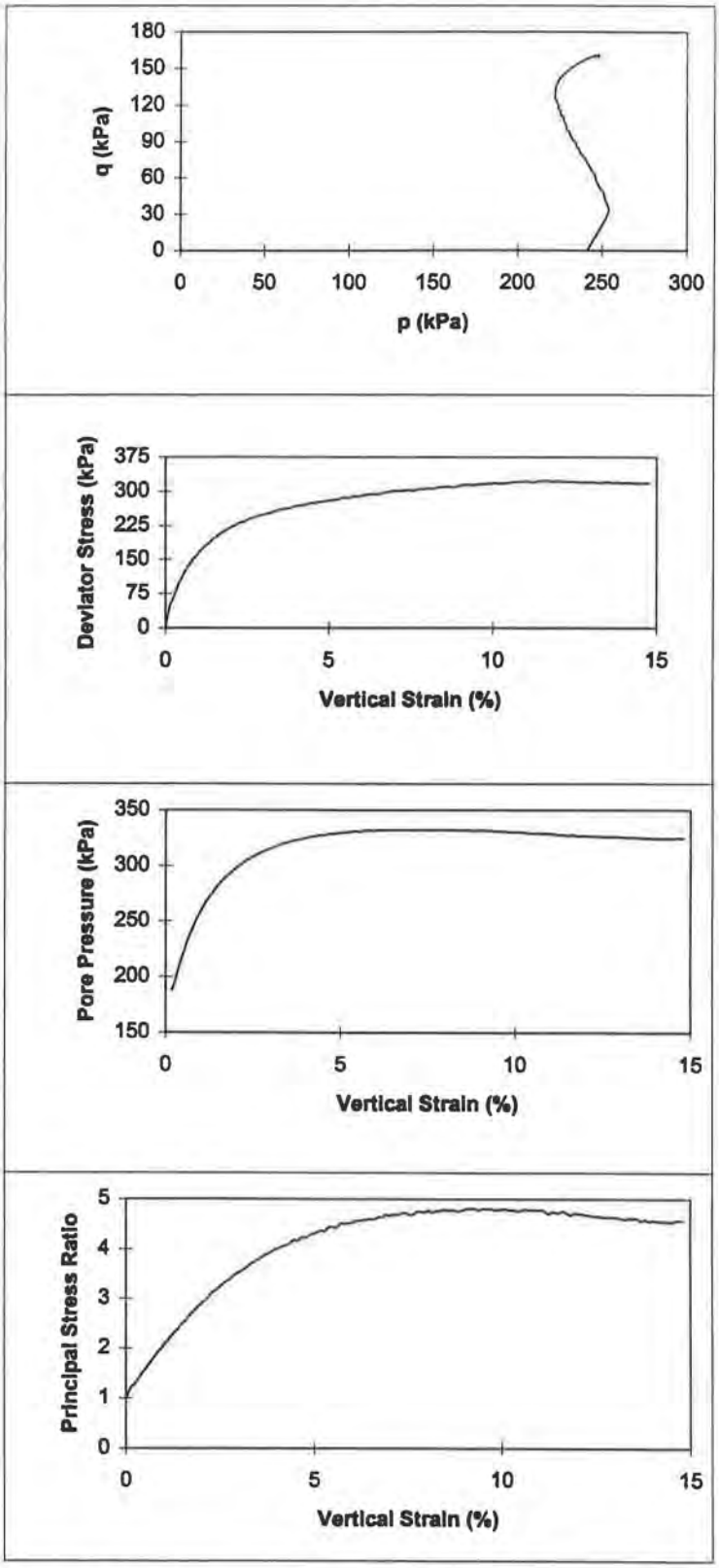

FIG. I.18. - CIUC Results : B-7 @ 10 meters, Sample 2.

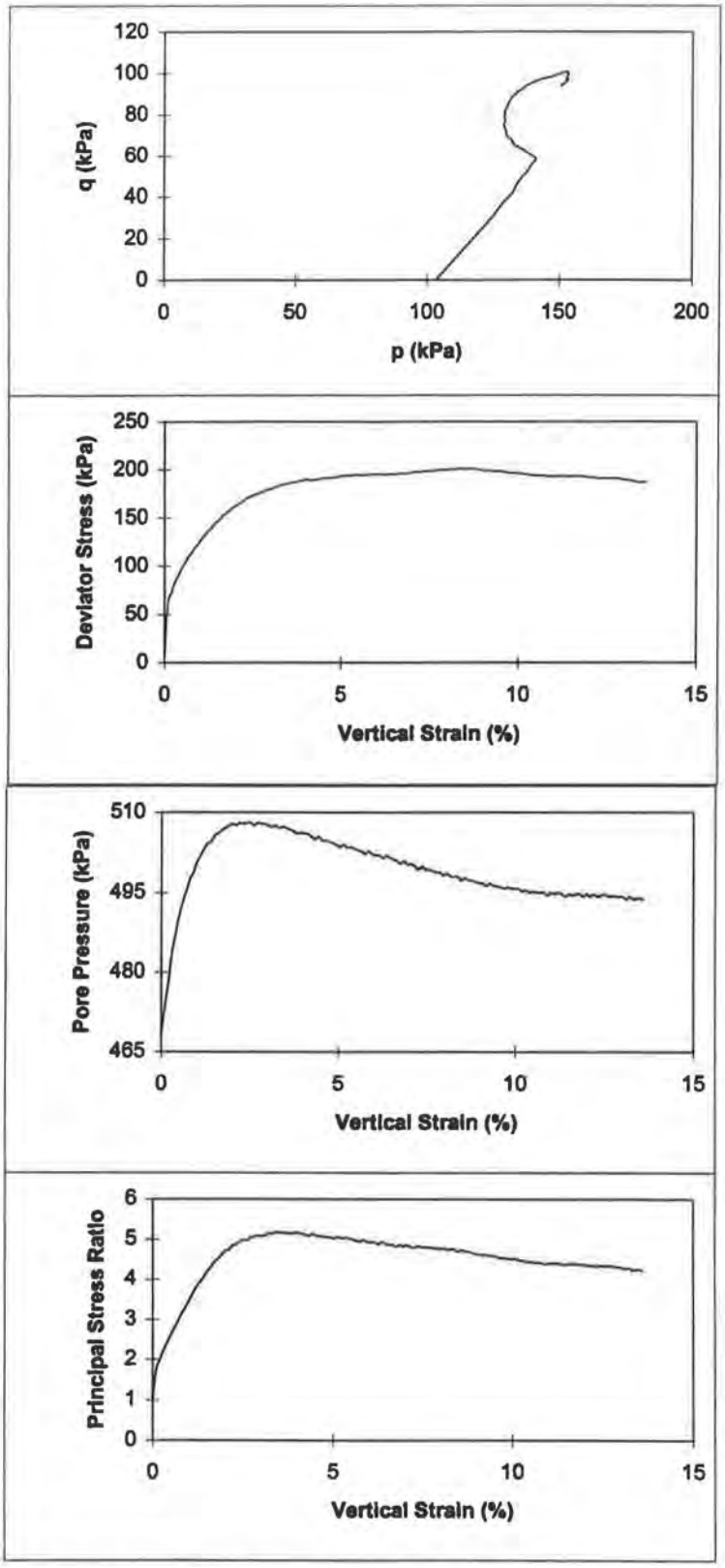

FIG. I.19. - CIUC Results : B-7 @ 10 meters, Sample 3.

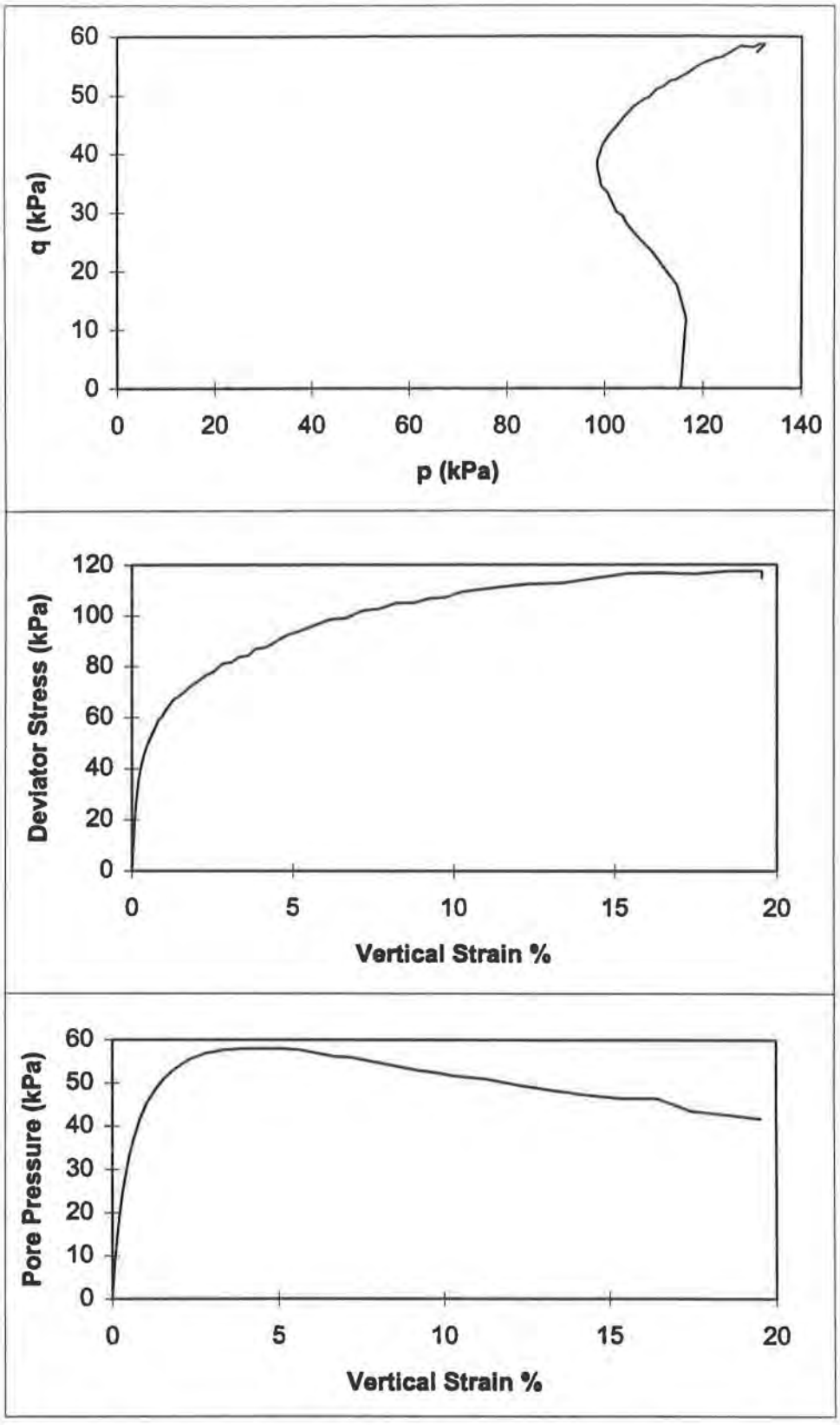

FIG. I.20. - CIUC Results : B-2 @ 12 meters, Sample 1.

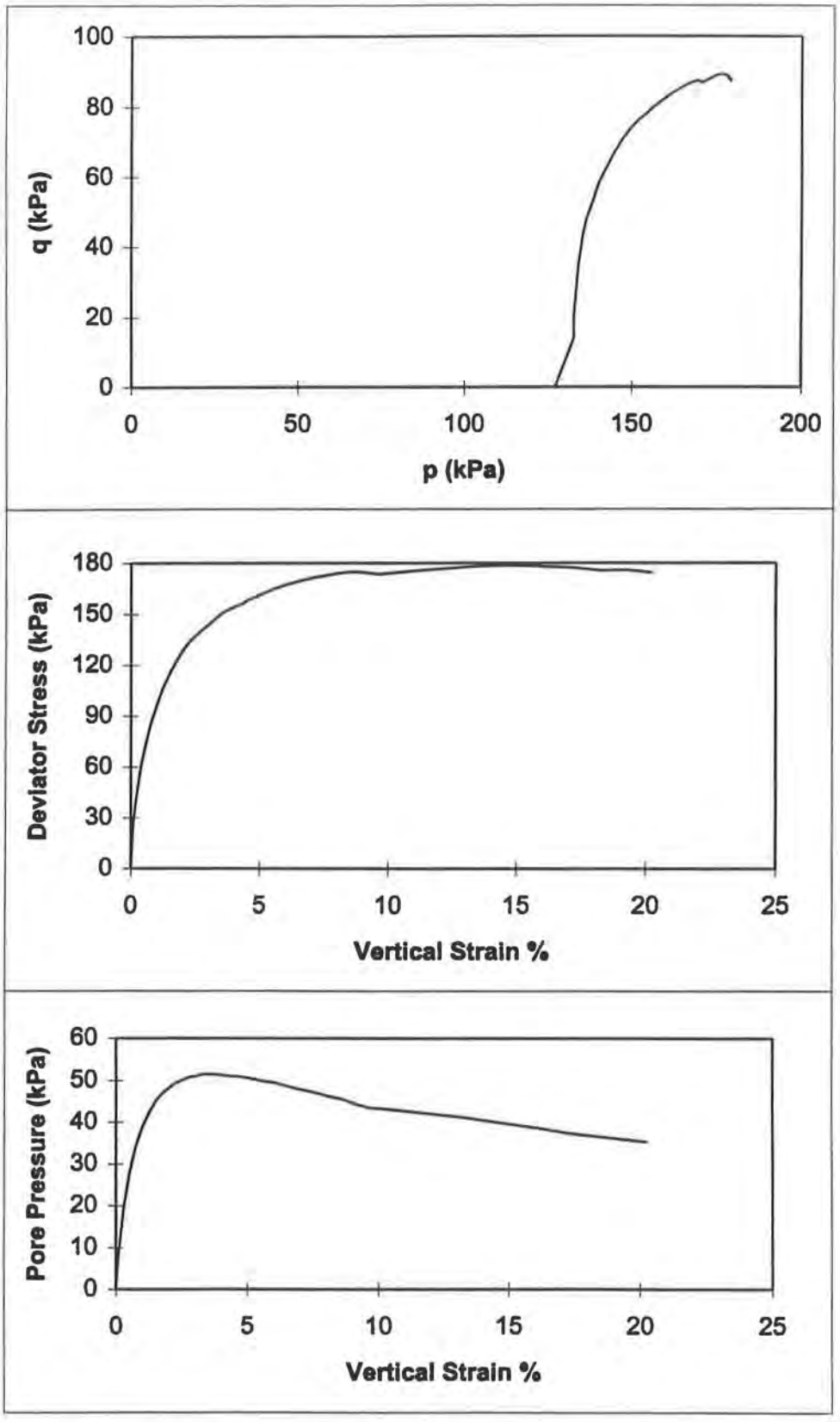

FIG. I.21. - CIUC Results : B-5 @ 12 meters, Sample 1.

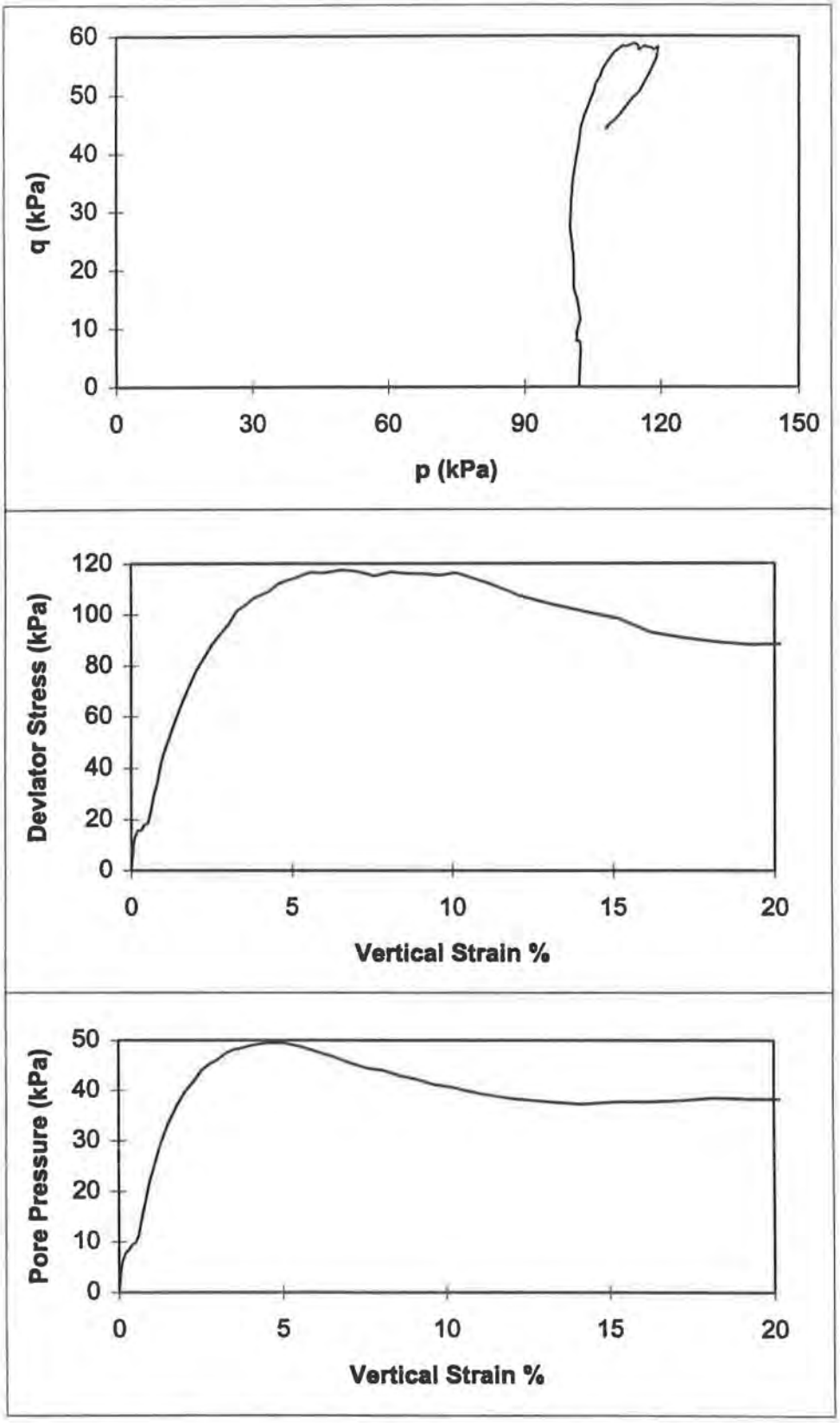

FIG. I.22. - CIUC Results : B-5 @ 12 meters, Sample 2.

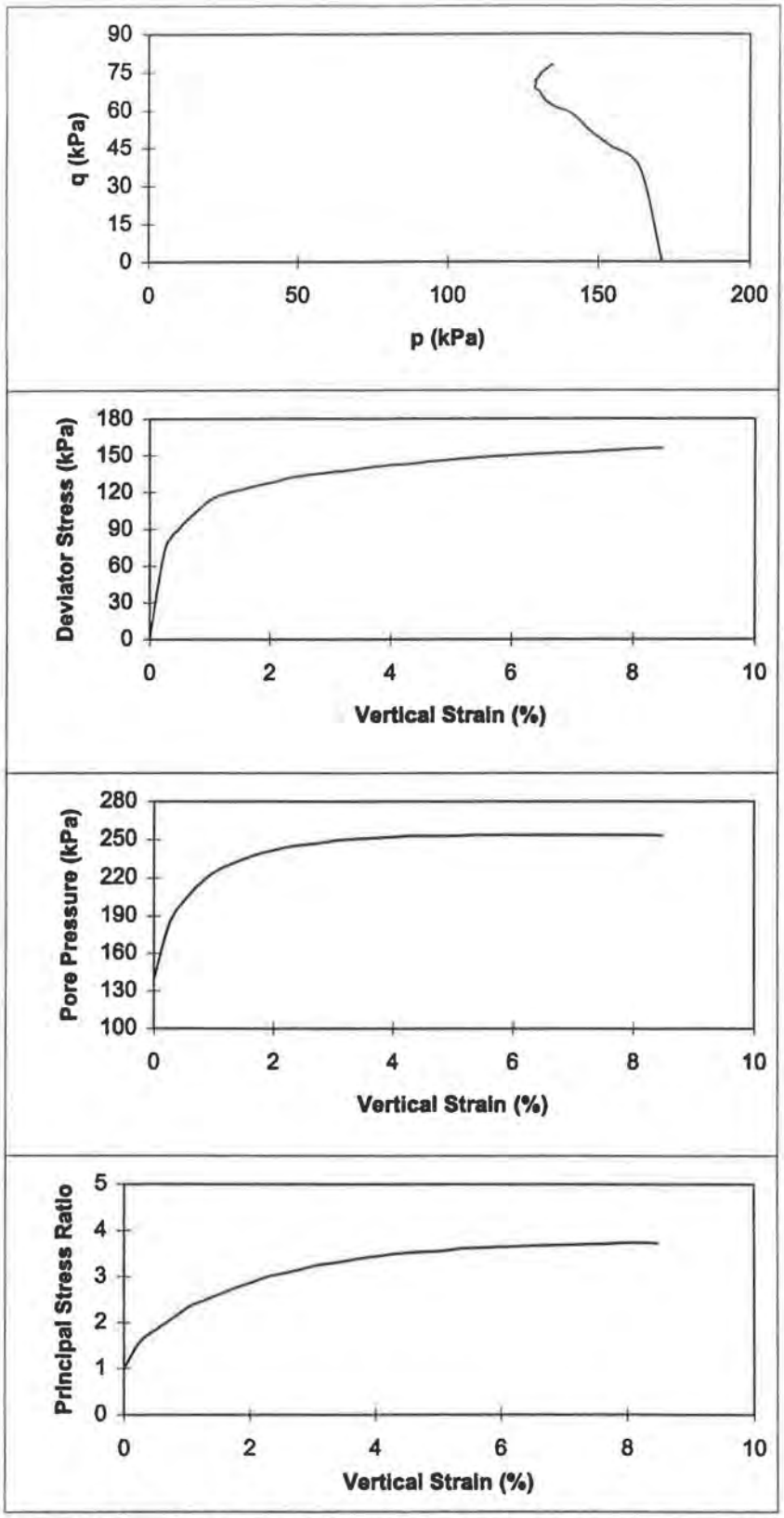

FIG. I.23. - CIUC Results : B-2 @ 15 meters, Sample 1, Stage 1.

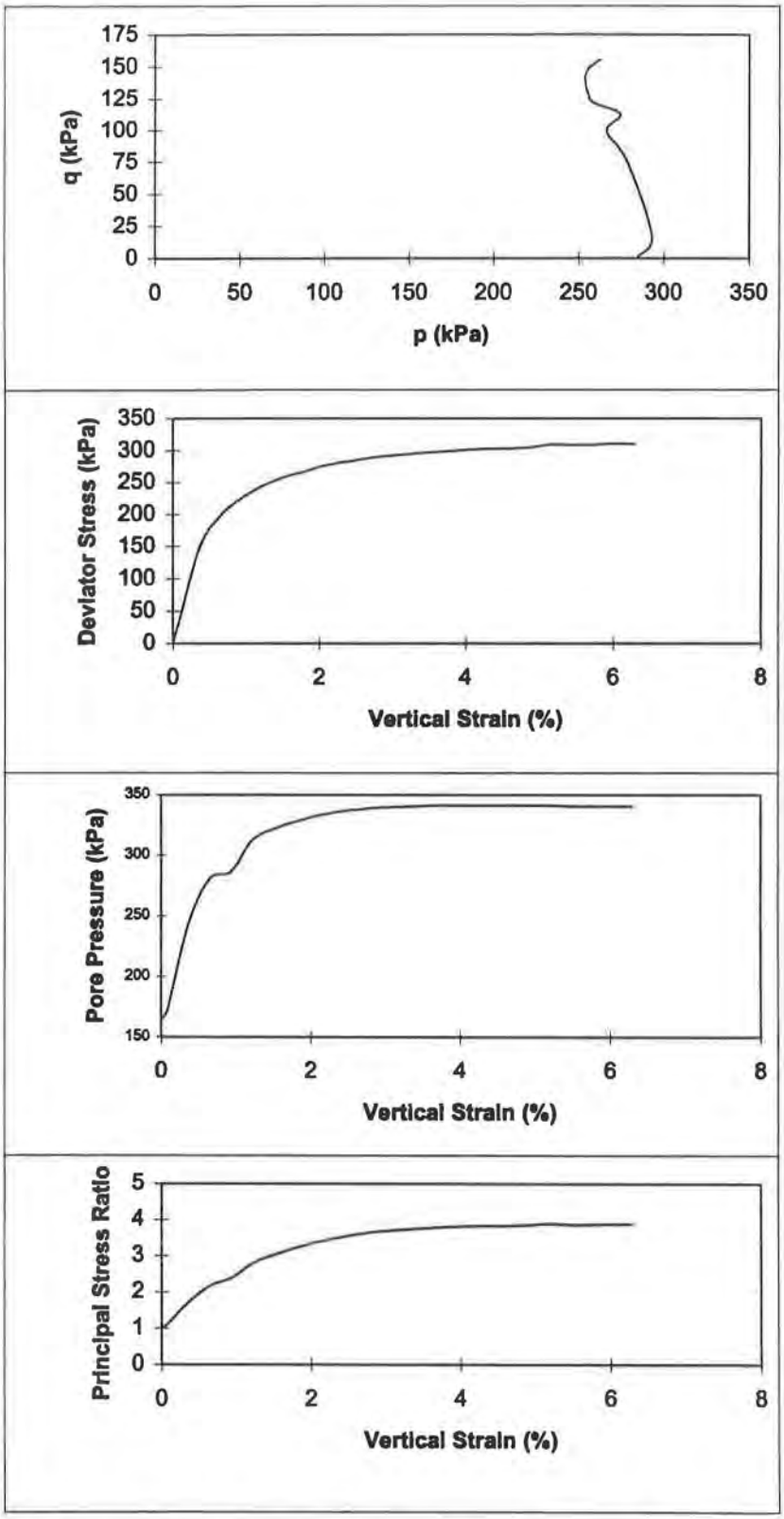

FIG. I.24. - CIUC Results : B-2 @ 15 meters, Sample Stage 2.

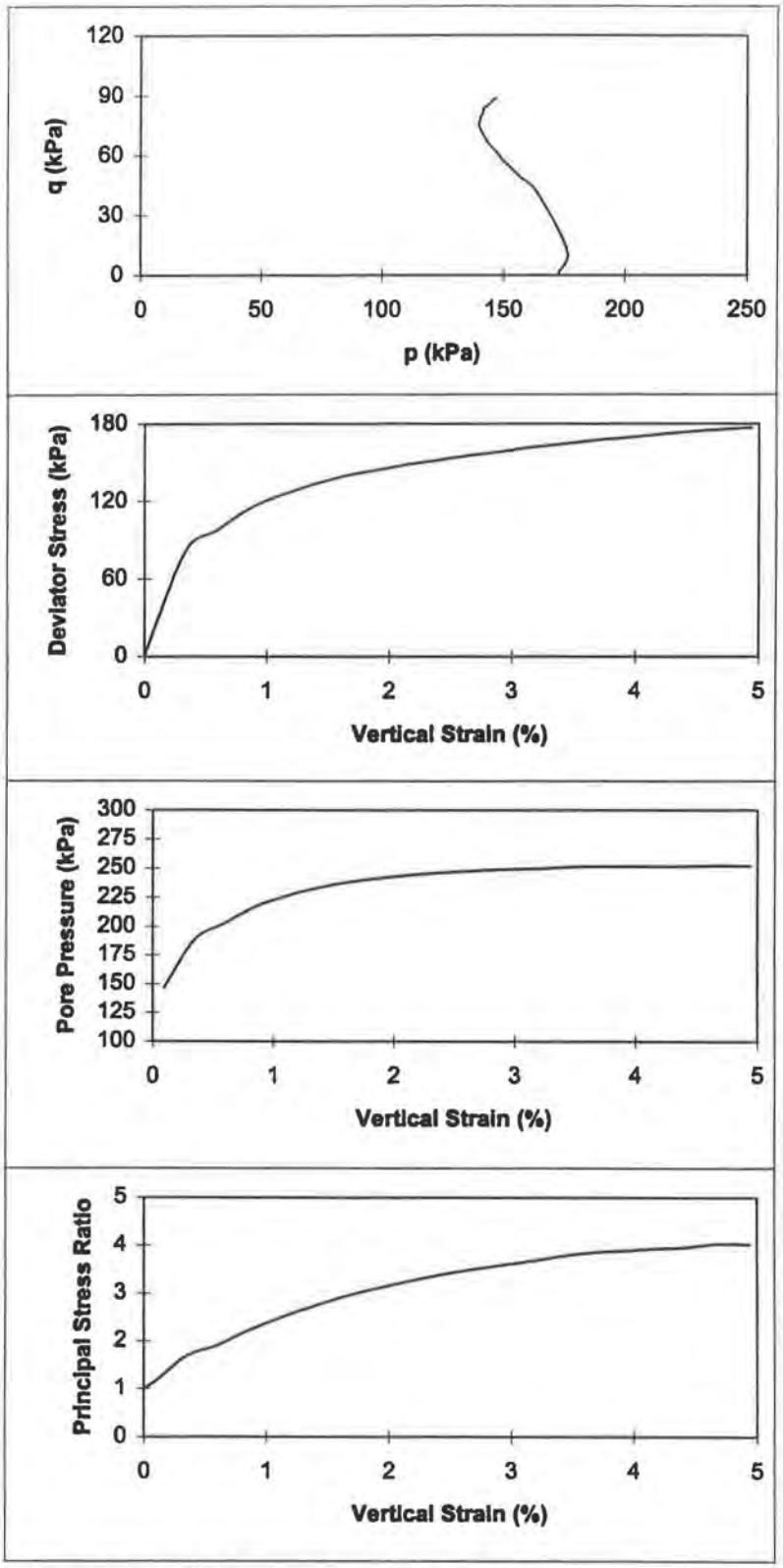

FIG. I.25. - CIUC Results : B-5 @ 15 meters, Sample Stage 1.

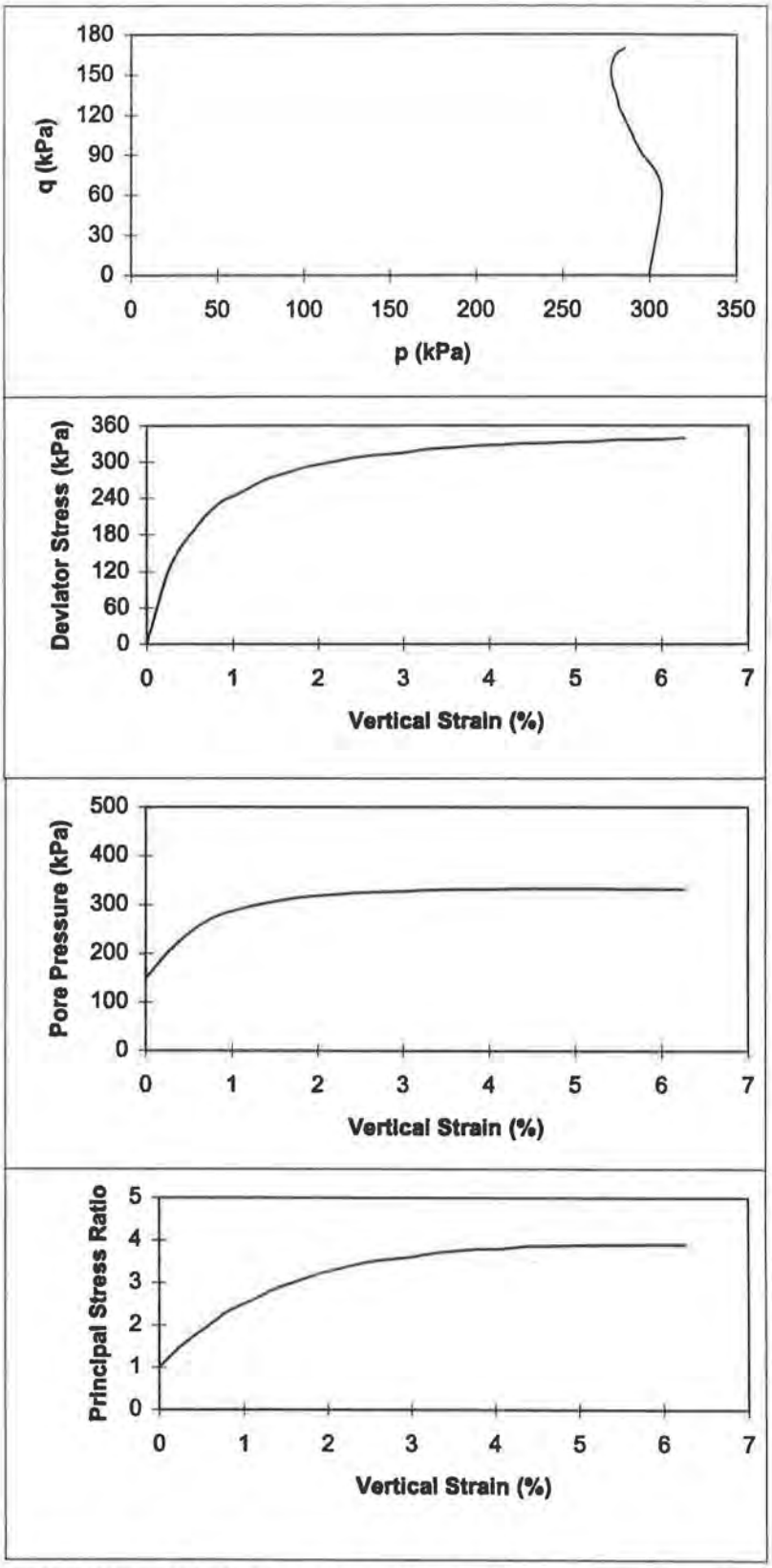

FIG. I.26. - CIUC Results : B-5 @ 15 meters, Sample Stage 2.

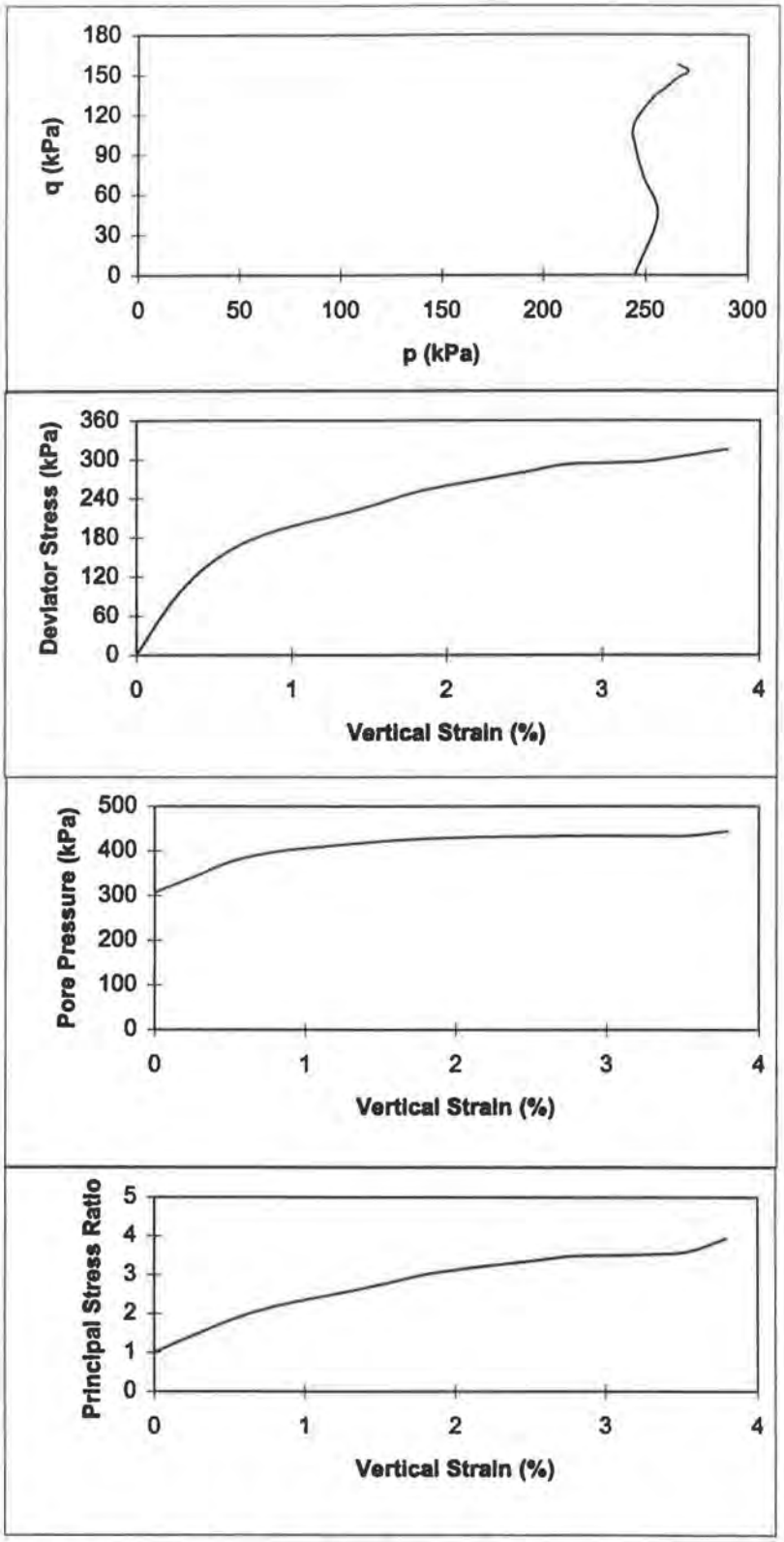

FIG. I.27. - CIUC Results : B-5 @ 15 meters, Sample Stage 1.

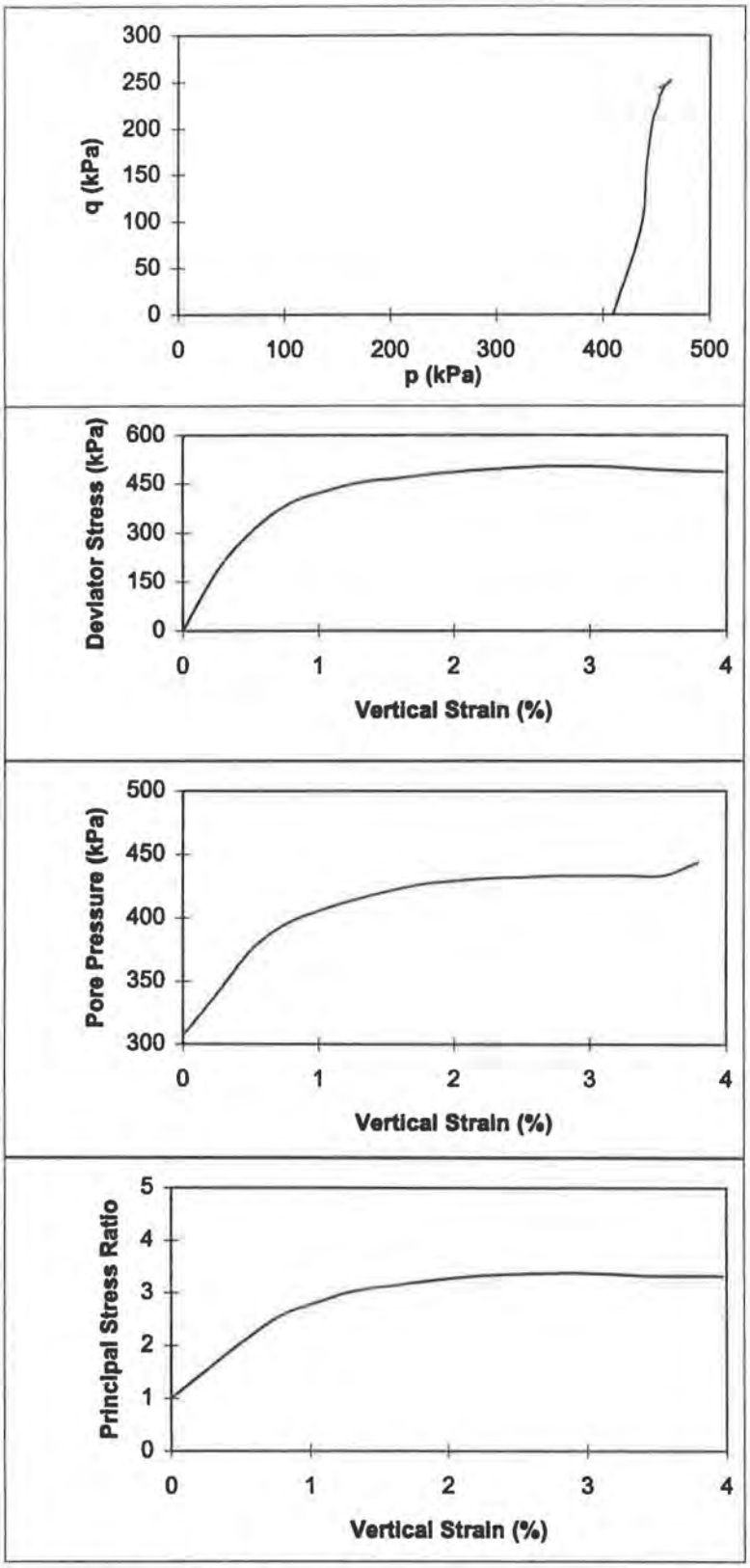

FIG. I.28. - CIUC Results : B-5 @ 15 meters, Sample Stage 2.

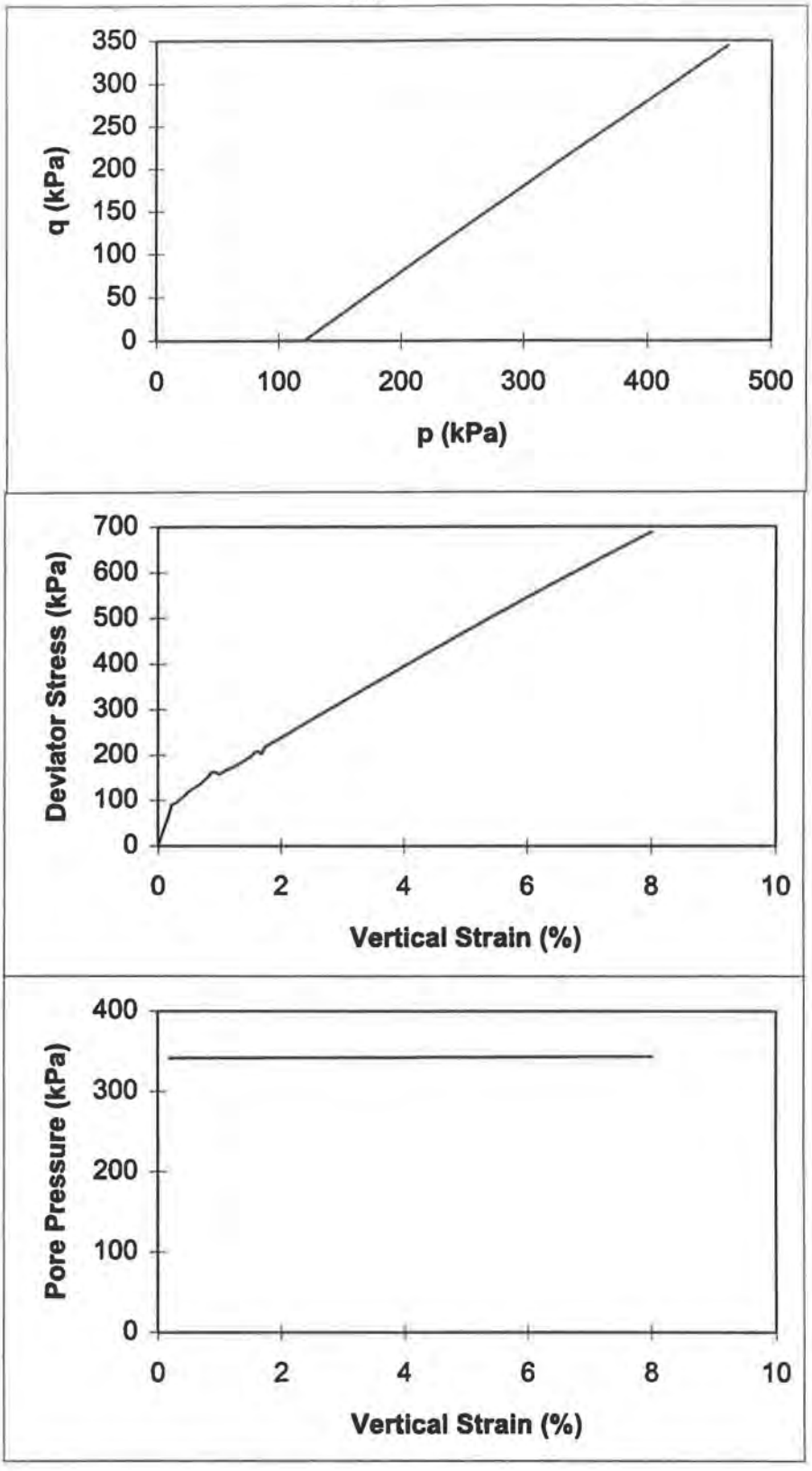

FIG. I.29. - CIDC Results : B-8 @ 10 meters, Sample 1.

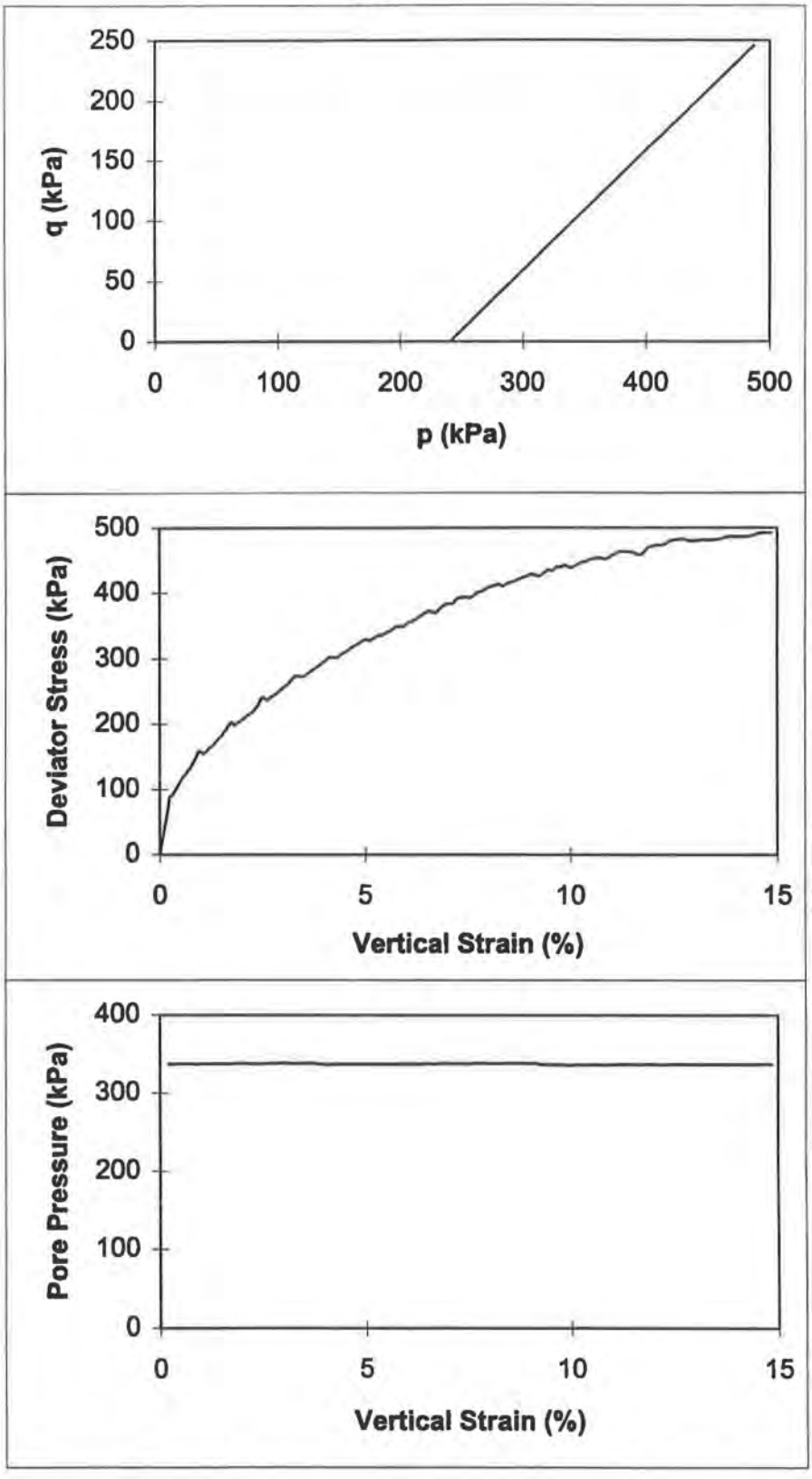

FIG. I.30. - CIDC Results : B-8 @ 10 meters, Sample 2.

REFERENCES

ASTM D 1586. (1984). *Standard Test Method for Penetration Test and Split-Barrel Sampling of Soils*. Vol. 4.08, ASTM, Philadelphia, PA, 298-304.

ASTM D 2850. (1982). *Standard Test Method for Unconsolidated, Undrained Compressive Strength of Cohesive Soils in Triaxial Compression*. Vol. 4.08, ASTM, Philadelphia, PA, 451-456.

ASTM D 3441. (1986). *Standard Test Method for Deep, Quasi-Static, Cone and Friction-Cone Penetration Tests of Soil*. Vol. 4.08, Philadelphia, PA, 470-476.

ASTM D 4428/D 4428M. (1991). *Standard Test Methods for Crosshole Seismic Testing*. Vol. 4.08, ASTM, Philadelphia, PA, 769-775.

ASTM D 4767 (1988). *Standard Test Method for Consolidated-Undrained Triaxial Compression Test on Cohesive Soils*. Vol. 4.08, ASTM, Philadelphia, PA, 926-935.

Baguelin, F., Jezequel, J.F., and Shields, D.H. (1978). *The Pressuremeter and Foundation Engineering*. Trans Tech Publications, Clausthal, Germany.

Barensten, P. (1936). "Short Description of a Field Testing Method with a Cone Shaped Sounding Apparatus." *Proceedings from the 1st International Conference on Soil Mechanics and Foundation Engineering*, Harvard University, Boston, Vol. 2, 10.

Barksdale, R.D., Ferry, C.T., and Lawrence, J.D. (1986). "Residual Soil Settlement form Pressuremeter Moduli." *Proceedings from the In Situ '86: Use of In Situ Tests Geotechnical Engineering*, Blacksburg, Virginia, 447-461.

Borden, R.H., Shao, L., and Gupta, A. (1996). "Dynamic Properties of Piedmont Residual Soils." *Journal of Geotechnical Engineering*, ASCE, 122 (10), 813-821.

Borden, R.H., Shao, L., and Gupta, A. (1994). "Construction Related Vibrations." *Report No. FHWA/NC/95-008,* Federal Highway Administration, Washington, D.C.

Bowles, J.E. (1996). *Foundation Analysis and Design, 5th Edition.* The McGraw-Hill Companies, Inc., U.S.A.

Briaud, J.-L. (1992). *The Pressuremeter*. Balkema, Rotterdam, Netherlands.

Burland, J.B. (1989). "Small is Beautiful: The Stiffness of Soils at Small Strains." *Canadian Geotechnical Journal*, 26 (4), 499-516.

Calhoon, M. (1970). "Field Testing with the Pressure-Meter." Lecture given at the University of Kansas, U.S.A. (unpublished).

Campanella, R.G., Robertson, P.K., and Gillespie, D. (1986). "Seismic Cone Penetration Tests." *Proceedings of the 11th International Conference on Soil Mechanics and Foundation Engineering*, Vol. 2, San Francisco, 849-854.

Campanella, R.G., and Robertson, P.K. (1991). "Use and Interpretation of a Research Dilatometer." *Canadian Geotechnical Journal*, 28(1), 113-126.

Centre d'Etudes Menard, (1970). "Determination de la Poussee Exercee par un Sol sur une Paroi de Soutenement." *Publication D/38/70.*

Clarke, B.G. (1995). *Pressuremeters in Geotechnical Design*. Blackie Academic and Professional, Cambridge, Great Britain.

Deere, D.U., and Patton, F.D. (1971). "Slope Stability of Residual Soils." *Proceedings of the 4th Pan American Conference on Soil Mechanics and Foundation Engineering*, San Juan, Puerto Rico, Vol. 1, 88-143.

Demartinecourt, J.P., and Bauer, G.E. (1983). "The Modified Borehole Shear Device." *Geotechnical Testing Journal*, ASTM, 6(1), 24-29.

Devore, J.L. (1991). *Probability and Statistics for Engineering and the Sciences, Third Edition*. Brooks/Cole Publishing Company, Pacific Grove, California.

Handy, R.L., and Fox, N.S. (1967). "A Soil Bore-Hole Direct-Shear Device." *Highway Research News*, 27, 42-51.

Handy, R.L. (1988). *User's Manual for the Iowa Borehole Shear Tester*. Handy Geotechnical Instruments Company, Inc., Ames, Iowa.

Hardin, B.O., and Drnevich, V.P. (1972). "Shear Modulus and Damping in Soils: Design Equations and Curves," *Journal of the Soil Mechanics and Foundations Division*, ASCE, 98 (7), 667-692.

Harris, D.E., and Mayne, P.W. (1994). *Proceedings of the International Conference on Design and Construction of Deep Foundations*, Vol. 2, Orlando, Federal Highway Administration, Washington, D.C., 352-367.

Hoar, R.J., and Stokoe, K.H. (1978). "Generation and Measurement of Shear Waves In Situ." *Dynamic Geotechnical Testing*, STP 654, ASTM, Philadelphia, 3-29.

Gazetas, G. (1991). "Foundation Virbrations." *Foundation Vibrations Handbook, 2nd Edition*, H.Y. Fang, ed., 553-593.

Hegazy, Y.A., and Mayne, P.W. (1995). "Statistical Correlations Between V_s and Cone Penetration Data for Different Soil Types." *Proceedings of the International*

Symposium on Cone Penetration Testing, CPT'95, Linkoping, Sweden, Vol. 2, 173-178.

Hepton, P. (1988). "Shear Wave Velocity Measurements During Penetration Testing." *Proceedings of Penetration Testing in the U.K.*, Birmingham, (Thomas Telford, London), 275-278.

Imai, T., and Tonouchi, K. (1982). "Correlation of N Value with S-Wave Velocity and Shear Modulus." *Proceedings of the 2nd European Symposium on Penetration Testing*, Vol. 1, Amsterdam, 67-72.

Jamiolkowski, M., Ladd, C.C., Germaine, J.T., and Lancellota, R. (1985). "New Developments in Field and Laboratory Testing of Soils." *Proceedings, 11th International Conference on Soil Mechanics and Foundation Engineering*, Vol. I, San Francisco, 57-153.

Jezequel, J.F., and Miessens, C. (1975). "In Situ Measurements of Coefficients of Permeability and Consolidation in Fine Soils." *Proceedings of the ASCE Specialty Conference on In Situ Measurement of Soil Properties*, Raleigh, North Carolina, 208-224.

Kates, G.L. (1996). "Development and Implementation of a Seismic Flat Dilatometer Test for Small- and High-Strain Soil Properties." *Master's Thesis*, Department of Civil and Environmental Engineering, Georgia Institute of Technology, Atlanta, GA.

Kulhawy, F.H., Jackson, C.S., and Mayne, P.W. (1989). "First-Order Estimation of K_o in Sands and Clays." *Foundation Engineering: Current Principles and Practices*, ASCE, New York, 121-134.

Kulhawy, F.H., and Mayne, P.W. (1990). *Manual on Estimating Soil Properties for Foundation Design*. Cornell University, Ithaca, New York.

Lambe, P.C., and Heartz, W.T. (1988). "Consolidated Drained Triaxial Testing of Piedmont Residual Soil." *Advanced Triaxial Testing of Soil and Rock, ASTM STP 977*, Robert T. Donaghe, Ronald C. Chaney, and Marshall L. Silver, Eds., American Society for Testing and Materials, Philadelphia, 311-320.

Little, W.C., Thorne, C.R., and Murphey, J.B. (1982). "Mass Bank Failure Analysis of Selected Yazoo Basin Streams." *Trans. of the American Society of Agricultural Engineers*, 25(5), 1321-1328.

Lutenegger, A.J. (1987). "Suggested Method for Performing the Borehole Shear Test." *Geotechnical Testing Journal*, 10, 19-25.

Manassero, M. (1989). "Stress-Strain Relationships from Drained Self-Boring Pressuremeter Tests in Sands." *Geotechnique*, 39 (2), 292-307.

Marchetti, S. (1980). "In-Situ Tests by Flat Dilatometer." *Journal of the Geotechnical Engineering Division*, ASCE, 106(3), 299-321.

Marchetti, S. (1985). "On the Field Determination of Ko in Sand." *Proceedings of the 11th International Conference on Soil Mechanics*, Vol. 5, San Francisco, 2667-2672.

Martin, R.E. (1977). "Estimating Foundation Settlements in Residual Soils." *Journal of the Geotechnical Engineering*, Proc. ASCE, 103 (3), 197-212.

Masood, T., and Mitchell, J.K. (1993). "Estimation of In Situ Lateral Stresses in Soils by Cone-Penetration Test." *Journal of Geotechnical Engineering*, ASCE, 119 (10), 1624-1639.

Mayne, P.W. and Frost, D.D. (1989). "Dilatometer Experience in Washington D.C. and Vicinity." *Research Record 1169*, Transportation Research Board, Washington D.C., 16-23.

Mayne, P.W., and Kulhawy, F.H. (1990). "Direct and Indirect Determinations of In Situ K_o in Clays." *Transportation Research Record 1278*, Transportation Research Board, Washington D.C., 141-149.

Mayne, P.W., and Rix, G.J. (1993). "G_{max}-q_c Relationships for Clays." *Geotechnical Testing Journal*, GTJODJ, 16 (1), 54-60.

Meigh, A.C. (1987). *Cone Penetration Testing Methods and Interpretation*. CIRIA, United Kingdom.

Ohya, S., Imai, T., and Matsubara, M. (1982). "Relationships Between N Value by SPT and LLT Pressuremeter Results," *Proceedings from the 2nd European Symposium on Penetration Testing*, Vol. I, Amsterdam, 125-130.

Szabo, M.W., Osborne, W.E., Copeland, C.W., and Neathery, T.L. (1988). "Geological Map of Alabama." Special Map 220, Geological Survey of Alabama.

Peck, R.B., Hanson, W.E., and Thornburn, T.H. (1974). *Foundation Engineering, 2nd Edition*, John Wiley and Sons, New York.

Poulos, H.G., and Davis,E.H. (1974). *Elastic Solutions for Soil and Rock Mechanics*, John Wiley and Sons, New York.

Rix, G.J., and Stokoe, K.H. (1991). "Correlation of Initial Tangent Modulus and Cone Resistance." *Calibration Chamber Testing*, Elsevier, New York, 351-362.

Robertson, P.K., and Campanella, R.G. (1983). "Interpretation of Cone Penetration Tests, Part I : Sand, Part II : Clay." *Canadian Geotechnical Journal*, 20(4), 718-745.

Robertson, P.K., Campanella, R.G., Gillespie, D., and By, T. (1986). "Seismic CPT to Measure In Situ Shear Wave Velocity." *Journal of Geotechnical Engineering*, ASCE, 112 (8), 791-803.

Schmertmann, J.H. (1975). "Measurement of In Situ Shear Strength." *Proceedings from the ASCE Specialty Conference on In Situ Measurement of Soil Properties,* Vol. 2, Raleigh, 57-138.

Schmertmann, J.H. (1978). "Use of the SPT to Measure Dynamic Soil Properties-Yes But...!" *ASTM STP No. 654*, 341-355.

Schmertmann, J.H. (1983). "Revised Procedure for Calculating Ko and OCR from DMT's with $I_D > 1.2$ and Which Incorporates the Penetration Force Measurement to Permit Calculating the Plain Strain Friction Angle." *DMT Workshop*, Schmertmann and Crapps, Inc., Gainesville, Florida.

Seed, H.B., and Idriss, I.M. (1970). "Soil Moduli and Damping Factors for Dynamic Analysis," *Report No. EERC 75-29*, Earthquake Engineering Research Center, University of California, Berkley.

Seed, H.B., Wong, R.T., Idriss, I.M., and Tokimatsu, K. (1986). "Moduli and Damping Factors for Dynamic Analyses of Cohesionless Soils." *Journal of Geotechnical Engineering Division*, ASCE, 112(11), 1016-1032.

Sennesset, K., et al. (1988). "Piezocone Tests in Silty Soils." *Proceedings from the 1st International Symposium On Penetration Testing,* Vol. 2, 955-966.

Shioi, Y., and Fukui, J. (1982). "Application of N Value to Design of Foundations in Japan." *Proceedings from the 2nd European Symposium On Penetration Testing*, Vol. I, 159-164.

Skempton, A.W. (1986). "Standard Penetration Test Procedures and the Effects in Sands of Overburden Pressure, Relative Density, Particle Size, Aging, and Overconsolidation." *Geotechnique*, 36(3), 425-447.

Solseng, R.L., and Lee, J.T. (1989). "Lake Marie Dam Evaluation and Repair." *Proceedings from the 6th ASDSO Annual Conference*, 280-295.

Sowers, G.F. (1954). "Soil Problems in the Southern Piedmont Region." *Proceedings from the ASCE*, Vol. 80, Separate 416, 1-15.

Sowers, G.F. (1963). "Engineering Properties of Residual Soil Derived From Igneous and Metamorphic Rocks." *Proceedings from the 2nd Pan American Conference on Soil Mechanics and Foundation Engineering*, Rio De Janeiro, Vol. 1, 39-61.

Sowers, G.F. (1985). "Residual Soils in the United States." *Sampling and Testing of Residual Soils*, Report of the Committee on Sampling and Testing of Residual Soils, International Symposium on Soil Mechanics and Foundation Engineering, Scorpion Press, Hong Kong, 183-191.

Sowers, G.F. (1994). "Residual Soil Settlement Related to the Weathering Profile." *Vertical and Horizontal Deformations of Foundations and Embankments*, GSP40, ASCE, New York, Vol. 1, 1689-1702.

Sowers, G.F., and Richardson, T.L. (1983). "Residual Soils of Piedmont and Blue Ridge." *Transportation Research Board, Record 919*, Transportation Research Bulletin, Washington, D.C., 10-16.

Wang, C.E., and Borden, R.H. (1996). "Deformation Characteristics of Piedmont Residual Soils." *Journal of Geotechnical Engineering*, ASCE, 122 (10), 822-830.

Wineland, J.D. (1975). "Borehole Shear Device." *Proceedings of the Conference on In Situ Measurements of Soil Properties*, ASCE, 1, 511-522.